CLATHROCHELATES: SYNTHESIS, STRUCTURE AND PROPERTIES
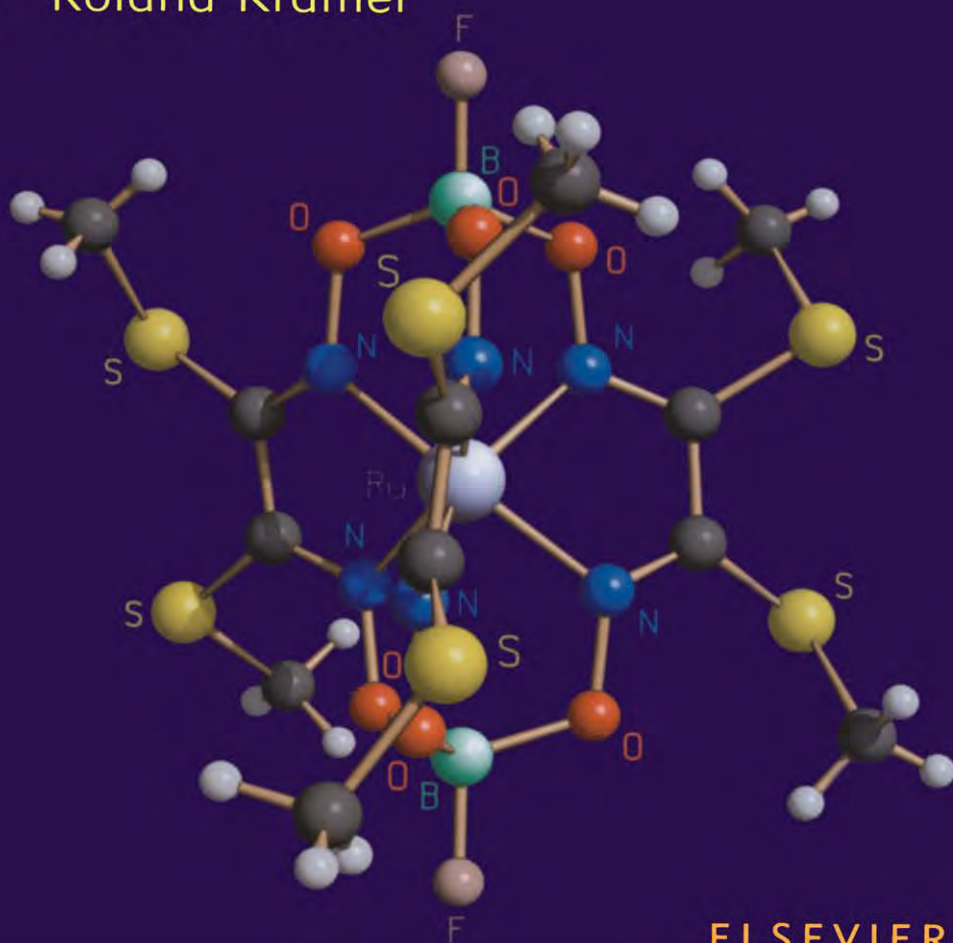
Yan Z. Voloshin

Nina A. Kostromina

Roland Krämer

Clathrochelates

Synthesis, Structure and Properties

This Page Intentionally Left Blank

Clathrochelates

Synthesis, Structure and Properties

Edited by

Yan Z. Voloshin
Karpov Institute of Physical Chemistry
Moscow, Russia

Nina A. Kostromina
Vernadskii Institute of General and Inorganic Chemistry
Kiev, Ukraine

Roland Krämer
Anorganisch-Chemisches Institut
Ruprecht-Karls-Universität
Heidelberg, Germany

2002

ELSEVIER

AMSTERDAM – BOSTON – LONDON – NEW YORK – OXFORD – PARIS
SAN DIEGO – SAN FRANCISCO – SINGAPORE – SYDNEY – TOKYO

Preface

Compounds with a metal ion encapsulated in a three-dimensional macropolycyclic ligand cavity have recently become of intense interest to scientists working in several fields of chemistry and biochemistry. This can be accounted for by the unique properties of the metal ion, completely caged by the macrobicyclic ligand and, to a great extent, isolated from environmental factors. Such complexes are suitable as membrane transporters, electron and ion carriers, models of metalloproteins and metalloenzymes, and other important biological systems (biomimetics), highly-selective and highly-sensitive analytical reagents, catalysts for photochemical and redox processes, cation and anion receptors, molecular electronic devices, and so forth.

Three-dimensional complexes with the encapsulated metal ion coordinating five or more nitrogen and/or sulphur donor atoms of not less than three macrocyclic fragments of an encapsulating ligand are named "clathrochelates." The concept of "clathrochelates" and this name itself were first proposed by D. H. Busch [1] and realized by D. R. Boston and N. J. Rose [2] for macrobicyclic cobalt(III) tris-dioximates. During the 30 years elapsed since the preparation of the first clathrochelates, several classes of such compounds (e.g., macrobicyclic tris-dioximates and tris-diiminates, sepulchrates, sarcophaginates and others), different in the capping groups, the degree of saturation, and the nature of the donor atoms, have been synthesized. Pathways of direct and directed synthesis of different types of clathrochelates, modification procedures for ligand peripheral groups, and cage framework modification reactions have been developed. The structure, chemical, and physicochemical characteristics of

clathrochelate complexes as well as relationships between them have been examined.

Special interest has focused on the redox and photochemical properties of sarcophaginates and sepulchrates, since they offer ample possibilities for the use of such compounds as sensitizers and electron carriers in photocatalytic solar energy conversion processes and in solving a variety of other practical problems. The invaluable contributions made by A. M. Sargeson and his group to the development of this trend together with some aspects of the synthesis and structure of these types of clathrochelates (see reviews [3-6]) should particularly be stressed. Undoubtedly interesting is the specific selectivity of macrobicyclic tris-dioximate formation reactions, enabling one to perform directed synthesis of analytical reagents exhibiting high selectivity together with high sensitivity.

Although clathrochelates are most closely related to thio- and aza-macrocyclic d-metal complexes, they display several specific features of their own. The number of publications is also essentially different. Numerous papers and several monographs dealing with classical macrocyclic complexes have been published [7-17], whereas the quantity of papers concerning the chemistry and physical chemistry of clathrochelates does not exceed three hundred.

For further research in this promising field of chemistry, the experimental and theoretical data on clathrochelates should be generalized and analysed. This is the aim of this monograph. Chapter 1 gives general concepts of complexes with encapsulated metal ions, discusses basic specific features of these compounds, considers and characterizes the main types of compounds with encapsulated metal ions and the main classes of clathrochelates, and includes the current nomenclature. Chapter 2 deals with the pathways of clathrochelate synthesis and the general procedures for the synthesis of macrobicyclic tris-dioximates, phosphorus-containing tris-diiminates, sepulchrates, sarcophaginates, and polyene and other types of clathrochelate complexes. Chapter 3 concerns studies of the electronic and spatial structure of clathrochelate complexes. In Chapter 4, the kinetics and mechanism of synthesis and decomposition reactions of macrobicyclic tris-dioximates, sarcophaginates, and sepulchrates in solution and gas phases are discussed. Chapter 5 considers the electrochemical, photochemical, and some other characteristics of

clathrochelates and their applications associated with these characteristics.

Finally, the practical applications of the unique properties of clathrochelates and perspectives on the synthesis of new clathrochelates are described in Chapters 6 and 7, respectively.

Yan Z. Voloshin
Karpov Institute of Physical Chemistry
Moscow, Russia

Nina A. Kostromina
Vernadskii Institute of General and Inorganic Chemistry
Kiev, Ukraine

Roland Krämer
Anorganisch-Chemisches Institut
Heidelberg, Germany

April 2002

This Page Intentionally Left Blank

A LIST OF MAIN ABBREVIATIONS

ac	– acetate ion	L	– ligand	
acac	– acetylacetone	LFSE	– ligand-field stabilization energy	
Am	– amine			
AN	– acetonitrile	LUMO	– lowest unoccupied molecular orbital	
AO	– atomic orbital(s)			
bpy	– 2,2'-bipyridine	M	– metal ion	
bpz	– 2,2'-bipyrazol	m	– multiplet	
Bs	– benzene sulphonate radical	mal	– malonate ion	
		Me	– methyl radical	
Bu	– n-butyl radical	MeIz	– N-methylimidazole	
CD	– circular dichroism	MO	– molecular orbital(s)	
cp	– cyclopentadien	mv^{2+}	– methylviologen (dication)	
CTB	– charge transfer band	NHE	– normal hydrogen electrode	
d	– doublet			
DCD	– differential circular dichroism	phen	– 1,10-phenanthroline	
		1,2pn	– 1,2-diaminopropane	
DEA	– diethylamine	1,3pn	– 1,3-diaminopropane	
DMF	– dimethylformamide	Py	– pyridine	
DMSO	– dimethylsulphoxide	q	– quartet	
EDTA	– ethylenediamine-tetraacetate ion	QS	– quadrupole splitting in Mössbauer spectra	
EFG	– electric field gradient	r_i	– physical (Shannon) ionic radius	
en	– ethylenediamine	s	– singlet	
Fc	– ferrocenyl radical	SCE	– standard calomel electrode	
Hal	– halogenide substituent	sh	– shoulder	
HOMO	– highest occupied molecular orbital	t	– triplet	
		TAP	– trigonal antiprism	
HSAB	– hard and soft acids and bases (theory)	tart	– tartrate ion	
		THF	– tetrahydrofuran	
IEC	– ion-exchange chromatography	TOF	– triethyl orthoformate	
		TP	– trigonal prism	
IS	– isomeric shift in Mössbauer spectra	tren	– tris(2-aminoethylamine)	
		Ts	– tosyl radical	
Iz	– imidazol			

This Page Intentionally Left Blank

Table of contents

Chapter 1

Fundamental concepts of complexes with encapsulated metal ions

Because the definition of metal ion encapsulation or its absence is, to a certain extent, ambiguous, we first describe the conventional criteria that we use to restrict the scope of the compounds to be considered. The major signs of complexation (formation of a complex) with an encapsulated metal ion are (a) a three-dimensional cavity (capsule, cage) produced by a macropolycyclic ligand and (b) metal ion coordinating heteroatoms in this cavity that isolate this metal ion from the environment.

The ligand capable of forming a cage must comprise at least two macrocyclic fragments (Scheme 1).

As we define them, the key difference between macrobicyclic ligands and bis-macrocyclic ones is that in the former, each of the fragments (I, II, III) is involved in the formation of two macrocycles (in contrast to bis-macrocycles) containing fourteen or more atoms in the cycle and four donor atoms, which is consistent with Melson's definition [9] of macrocycles (the number of atoms in the cycle is nine or more, and the number of donor atoms is three or more). Most encapsulating ligands contain two atoms that belong to all fragments of a macrobicyclic ligand, called ***capping*** atoms (e.g., the apical nitrogen atoms in **1**, **2**, **6**, **7**; boron, tin, germanium, etc. atoms in **8**; carbon or nitrogen atoms in **3**; phosphorous and boron atoms in **5**, Scheme 1). In ligand **4**, 1,3,5-triazacyclohexane ring acts as a capping group.

A metal ion encapsulated in the three-dimensional ligand cavity must be an acceptor bonded to the donor groups of all macrocycles forming the cage framework. This is time either when the metal ion size corresponds to the ligand cavity size or when the cavity can be transformed under the influence of the metal ion so that the distance between the central ion and the donor atoms of the cage is not over the sum of their ionic or covalent radii. In addition to the geometric parameters, the thermodynamic and kinetic stability of

| 1 | 2 | 3 | 4 |

| 5 | 6 | 7 | 8 |
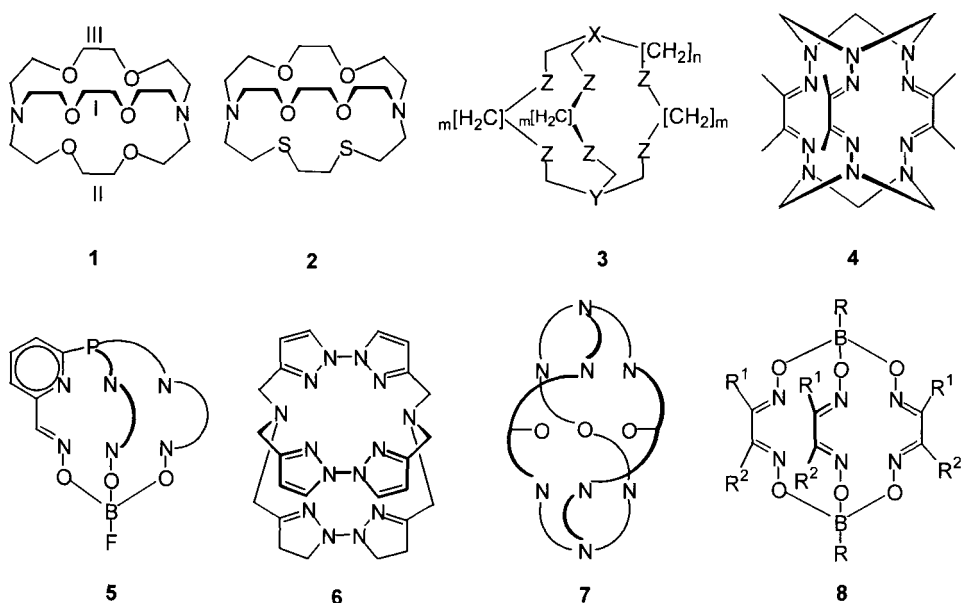
n = 0,1
m = 2,3
X,Y = CR, N, P, As
Z = S, NH, NOH, Se

Scheme 1

clathrochelate complexes is determined by the electronic structure of the encapsulated metal ion and the nature of the ligand.

1.1. CLASSIFICATION OF MACROPOLYCYCLIC LIGANDS

The nature of the donor atoms is one of the most important characteristics of macrocyclic ligands [11] and has been employed as a criterion for a classification of macrocyclic compounds. The classification of the macropolycyclic encapsulating ligands is based on the nature of the donor atoms and the type of donor groups that appear to be the best.

I. Polyazamacropolycycles. Nitrogen atoms act as donor atoms.

I.I. Macropolycyclic polyamines. Amine and/or hydroxylamine fragments act as donor groups.

I.II. Macropolycyclic tris-dioximes. Oxime groups act as donor groups.

I.III. Macropolycyclic phosphorous-containing tris-diimines. Oxime and heterocyclic nitrogen-containing fragments act as donor groups.

I.IV. Macropolycyclic polyene tris-diimines. Azomethine fragments act as donor groups.

I.V. Macropolycyclic polyaromatic tris-diimines. Heterocyclic nitrogen-containing fragments act as donor groups.

II. Polyazathiomacropolycycles. Nitrogen and sulphur atoms act as donor atoms.

III. Polyazaselenomacropolycycles. Nitrogen and selenium atoms act as donor atoms.

IV. Polythiomacropolycycles. Sulphur atoms act as donor atoms.

V. Polyoxothiomacropolycycles. Sulphur and oxygen atoms act as donor atoms.

VI. Polyazaoxothiomacropolycycles. Nitrogen, sulphur and oxygen atoms act as donor atoms.

VII. Polyazaoxomacropolycycles. Nitrogen and oxygen atoms act as donor atoms.

VIII. Polyoxomacropolycycles. Oxygen atoms act as donor atoms.

VIII.I. Macropolycyclic polyethers. Ether fragments act as donor groups.

VIII.II. Macropolycyclic tris-diols. Hydroxyl groups act as donor groups.

It is evident that this classification is incomplete, and as new data become available, more groups and subgroups of encapsulating ligands will be included.

The ligands of the first two groups form stable complexes mainly with transition metal ions. The properties of ligands belonging to these groups are close to those of synthetic polyazamacrocyclic ligands. The ligands are usually referred to as *clathrochelants* and their complexes as *clathrochelates*. However, the terms *"polyazacryptands"* and *"polyazacryptates"* also occur. Metal ions with closed electronic shells are effectively encapsulated by the ligands of groups VI and VII. The ligands of groups IV-VIII (except subgroup VIII.II) are usually called *cryptands* and their complexes *cryptates*. Cryptates have properties similar to those an oxocrown ethers. *Catenandes* are the ligands of subgroup VIII.II.

In comparison with their role in macrocyclic complexes, the role of steric factors and the correspondence of the cavity size to the metal ion size drastically increase in macrobicyclic compounds with an encapsulated metal ion. The degree of freedom in macrocyclic complexes related to the location of the metal ion outside the plane of

ligand donor atoms partly disappears in macrobicyclic complexes. The increase in the role of steric factors from monodentate to encapsulating ligands may be represented as follows [18, 19]:

Type of ligand	Degrees of freedom
Monodentate ligand	3
Bidentate, chelating ligand	2
Polydentate, macrocyclic ligand	1
Encapsulating, macropolycyclic ligand	0

In fact, steric restrictions are not rigorous, and a substantial degree of freedom can be retained due to the flexibility of the encapsulating ligand and its capacity to undergo conformational changes.

In this book, we discuss only complexes with group I and II ligands, containing nitrogen atoms or nitrogen and sulphur atoms as donor atoms, for which we adopt the name "*clathrochelates*". This term was introduced by Daryl H. Busch [1] for cage chelate complexes, and is not a direct derivative from "*clathrate*". Both these terms just have a common root from the Latin *cläthrätus*, to furnish with lattice (*Webster's Encyclopedic Unabridged Dictionary of the English Language*, Portland House, New York, 1989, P. 273).

1.2 NOMENCLATURE, ABBREVIATIONS AND CLASSIFICATION OF CLATHROCHELATES

Each of the known clathrochelates may be named according to the IUPAC regulations, but an extreme awkwardness of such name causes considerable difficulties in usage. For instance, in accordance with the IUPAC nomenclature, the clathrochelate ligand **3** (Scheme 1), when $n = m = 2$, should be called

1,3,6,8,10,13,16,19-octaazabicyclo-(6,6,6)-eicosane,

and the ligand **8**, where R = BOH and $R^1,R^2 = (CH_2)_5$, as

1,13-bis(oxybora)-2,12,14, 24,25,25-hexaoxa-3,11,15,23,26,34-hexaazapentacyclo-[11.11.11.0$^{4'10}$O$^{16'22}$O$^{27'33}$] pentatriaconta-3,10,15,22,26,33-hexaene.

The nomenclature proposed by Melson and Busch [9, 20] for monomacrocyclic compounds is not applicable to clathrochelates since

Table 1.
Symbols of the apical substituents in the capping fragments of sarcophaginates and sepulchrates.

Prefix	Group	Prefix	Group
aza	–N=	CA	–COOH
AMH	–N$^+$H$_3$	CAA	–COO-
NH$_2$OH	–N$^+$H$_2$OH	AM	–NH$_2$
MeAMH	–N$^+$H$_2$CH$_3$	NHOH	–NHOH
Me$_2$AMH	–N$^+$H(CH$_3$)$_2$	MeAM	–NHCH$_3$
Me$_3$AMH	–N$^+$(CH$_3$)$_3$	Me$_2$AM	–N(CH$_3$)$_2$
NO	–NO$_2$	EF	–COOC$_2$H$_5$
ME	–CH$_3$	Nl	–NO
HO	–OH	HM	–CH$_2$OH
AA	–NHCOCH$_3$	CN	–CN
TsAM	–NHTs	PI	–NPhth^a
SalAMH	–N$^+$H$_2$CH$_2$-2-C$_6$H$_5$OH	TerIM	–NCH-4C$_6$H$_5$CHO
BzAMH	–N$^+$H$_2$CH$_2$C$_6$H$_5$	SaIAM	–NHCH$_2$-2-C$_6$H$_5$OH
TerAMH	–N$^+$H$_2$CH$_2$-4-C$_6$H$_5$OH	BzAM	–NHCH$_2$C$_6$H$_5$
BzIM	–NCHC$_6$H$_5$	TerAM	–NHCH$_2$-4-C$_6$H$_5$OH
CL	–Cl	ClME	–CH$_2$Cl

^{a} NPhth is phthalimide

in this nomenclature the macroring is chosen as a basis, and the name incorporates abbreviations for the substituents. Each group of clathrochelates has its own system of names and symbols. The abbreviations for ligands of subgroup I.I. complexes include the symbol for the encapsulating framework with an indication of the substituents on this cage. The framework with the diamine chelate fragments and carbon atoms in the apical positions is called **sarcophagine** (*sar*), and those with nitrogen atoms in the apical positions, **sepulchrate** (*sep*) or (*diazasar*). If the clathrochelate framework is changed, its symbol is accordingly changed either by adding case letters or by giving another name to the framework (Scheme 2).

The ligand *capten* belongs to ligands of group II, but its properties are close to those of subgroup I.I.

The substituents at the carbon atoms in the apical positions and at the coordinated nitrogen atoms are denoted by placing the appropriate prefixes to framework symbol (Table 1).

Complexes with type I.II ligands are usually referred to as boron (tin, germanium, silicon, antimony)-capped macrobicyclic dioximates (oximehydrazonates, azineoximates). Their abbreviated

6

sep
diazasar

sar

oxosar

sar-2-ene

absar

1,3pnsar-S$_6$

1,3pnsar

char

sartacn

sar-N$_3$S$_3$
capten

sar-N$_5$S

sar-N$_4$S$_2$

sar-S$_6$

abcapten

mer-**1,2pnsar**

fac-**1,2pnsar**

Me$_5$tricosanesar

Me$_5$tricosatrienesar

Me$_8$tricosatrienesar

Me$_8$tricosanesar
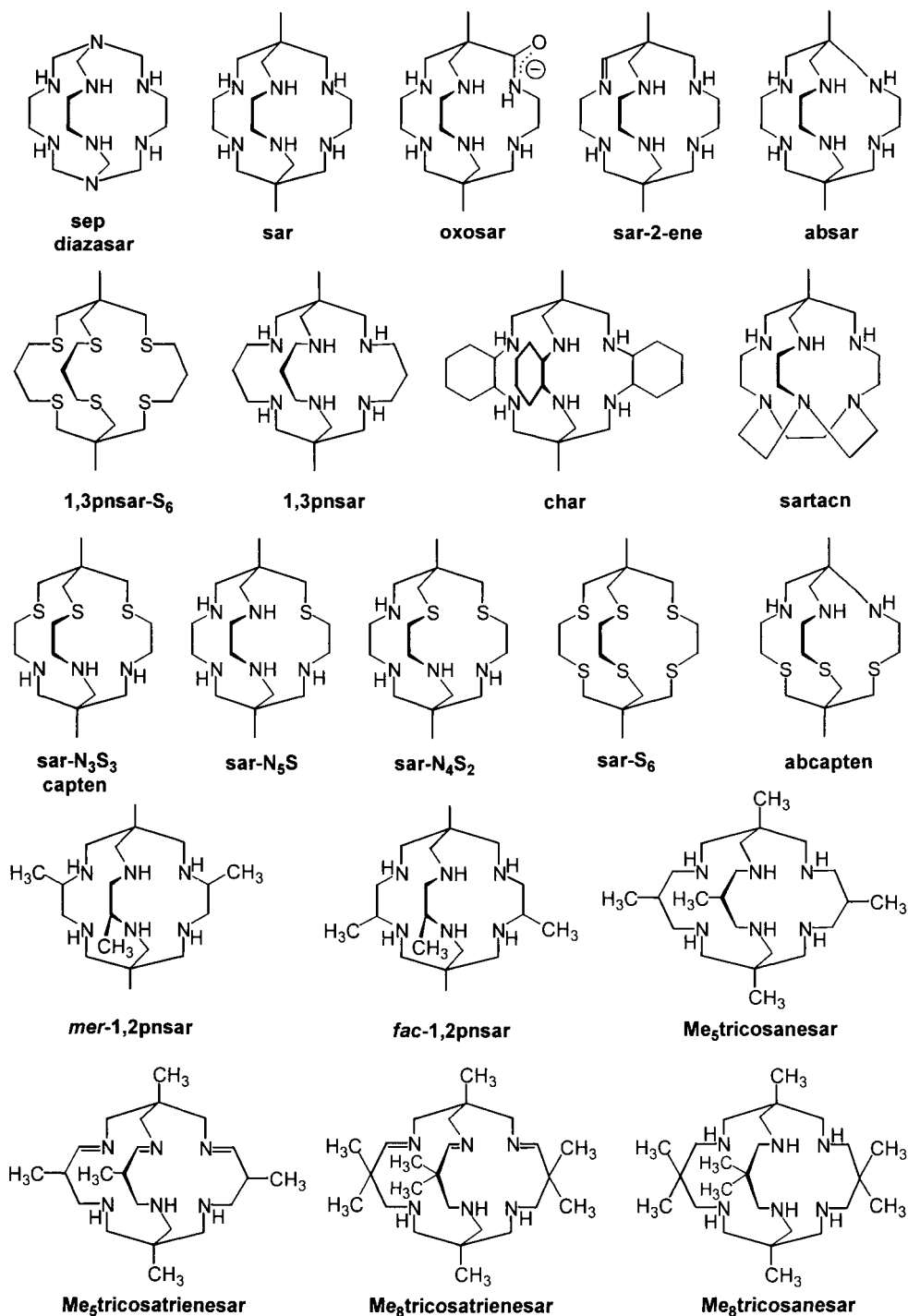
Scheme 2

name includes the conventional symbol for dioximate (or oxime-hydrazonate, or azineoximate) fragments and the capping groups, e.g. $MNx_3(BF)_2$, where Nx^{2-} is cyclohexanedione-1,2-dioxime (nioxime) dianion. The initial dioximes, oximehydrazones, and azineoximes used for the synthesis of clathrochelate complexes have the symbols given in Scheme 3.

Macrobicyclic iron(II) complexes of this type have been obtained for the aliphatic acyclic and alicyclic, aromatic dioximes as well as halogenide and functionalized ones by cross-linking with boron-containing agents of different nature (hydrogen; halogens; alkyl, aryl, hydroxyl, alkoxyl or functionalizing groups as the substituents at the boron atom) or tin-, germanium-, and antimony-containing ones (halogenide, oxygenide, perfluoroorganyl, and organyl substituents). The capping with other Lewis acids has scarcely been examined. Nevertheless, there are data available that macrobicyclic complexes may be prepared *via* a template cross-linking with compounds of most other *p*-block elements [21], in particular, bismuth, arsenic, etc.

The formation of such boron-capped compounds is less characteristic of cobalt (III); more characteristic is the formation of trihalogenotin-capped clathrochelates. Syntheses of the boron-capped cobalt(III) $CoD_3(BR)_2$ complexes have been performed under relatively rigid conditions for certain dioximes (H_2Dm, H_2Nx, H_2Bd) and with most effective capping agents ($R = F$, C_6H_5, n-C_4H_9). In this case, clathrochelate complexes are positively charged and have been isolated as salts with bulky inorganic anions. The cobalt(II) complexes have been obtained *via* reduction of cobalt(III) compounds. The trihalogenotin-capped clathrochelate cobalt(III) dianions have been isolated as salts with bulky organic cations.

Several macrobicyclic ruthenium, nickel, zinc, manganese, copper, chromium, magnesium, and lithium complexes, as well as two free macrobicyclic tris-dioximate ligands, have also been synthesized.

Clathrochelates derived from phosphorus-containing tris-diimine ligands (subgroup I.III) have been prepared for nickel, cobalt, zinc, and iron ions. These complexes are capped by the phosphorus atom bonded to the pyridine ring and by the boron atom *via* oxygen bridges. Nickel, copper, cobalt, and zinc semiclathrochelates have also been isolated. These complexes are capped by the phosphorus atom, and the three oxygen atoms of the second fragment are hydrogen-bonded by two protons.

8

glyoxime
(H2Gm)

diacetylazineoxime
(H2DAO)

nioxime
(H2Nx)

methylglyoxime
(H2Mm)

methylglyoxalazineoxime
(H2IAO)

heptoxime
(H2Gx)

dimethylglyoxime
(H2Dm)

diacetylmethylglyoxalazineoxime
(H2TMAO)

octoxime
(H2Ox)

dichloroglyoxime
(H2Cl2Gm)

phenylglyoxime
(H2Phm)

4-methylnioxime
(H24MNx)

diacetylmonooxime
hydrazone
(HDXO)

benzylacetylmonooxime
hydrazone
(HPXO)

α-furyldioxime
(H2Fd)

acetylacetonedioxime
(H2Ad)

cydohexanedione-1,2-monooxime
hydrazone
(HCXO)

α-benzyldioxime
(H2Bd)

Scheme 3

Compounds of the sarcophaginate and sepulchrate type capped by the carbon or nitrogen atom *via* methylene units have been most thoroughly studied. Complexes of numerous metals (Co, Cr, Mn, Ag, Fe, Ni, Cu, Rh, Pt, Ru, Hg, V, In, Ga, Cd, Mg) ions with various apical substituents have been synthesized with cage ligands, whose ethylenediamine fragments act as chelating groups. A predominant majority of complexes was formed with an encapsulated cobalt ion. In these complexes, capping groups are either the same or different: N and C-R, where R is a substituent listed in Table 1. Cobalt(III) complexes with 1,2- and 1,3-propanediamine, and cyclohexane-diamine chelate cycles have also been prepared.

Three classes of clathrochelates, as well as clathrochelates not included in these classes and discussed in a separate section, have the following common properties in addition to those previously mentioned:

- the geometry of all hexadentate clathrochelates is intermediate between a TP and a TAP;
- in the majority of cases, the clathrochelate ligand template forms on the metal ion matrix; the number of templates for given ligand is limited;
- the first rate-determining stage of the synthesis of clathrochelates is the formation of the corresponding semiclathrochelate;
- all clathrochelates are very stable and inert to metal ion and ligand substitution.

There are also differences that characterize each class of clathrochelates:

a) the clathrochelate ligands of types **5** and **8** (Scheme 1) in most cases exist only in complexes with metal ions and cannot be isolated in a free form. In the majority of cases, type **3** clathrochelate ligands have been obtained by demetallation of the corresponding cobalt complexes and used for the synthesis of the compounds with metal ions incapable of serving as template agents. The preliminarily synthesized macrobicyclic tris-phenantroline, tris-bipyridine, and sarcophagine-S_6 clathrochelate ligands have also been used for the synthesis of corresponding clathrochelates;

b) the formation of type **8** compounds is specially selective, and type **3** ligands are the most universal;

c) in type **8** compounds, a certain oxidation state, e.g. Fe^{2+} or Co^{3+}, is stabilized; the formation of stable compounds in two oxidation states is characteristic of type **3** compounds;

d) type **3** complexes, unlike most complexes of other types, are reactive. They undergo redox and substitution reactions involving neither capsule destruction nor a change in the central ion state, which makes it possible to synthesize a number of clathrochelate complexes of this type with different substituents in the chelating and capping fragments.

Chapter 2

Synthesis of clathrochelates

The striking results achieved in the chemistry of cryptands, synthetic ionophores, and ionic and molecular receptors are governed to a great extent by successes in developing synthetic routes that allow one the desired variations in the structure and properties of such compounds by introducing functional groups and modifying the molecule framework. Therefore, the development of methods for the synthesis of clathrochelates with the targeted geometry, symmetry, and functionality has become an extremely urgent task.

Clathrochelates may be isolated using conventional methods for the preparation of macrocyclic compounds described elsewhere in detail [7-17]. However, certain specific features observed in both the formation and the structure of these complexes drastically increase the role of template synthesis in their preparation. This is largely because some clathrochelate ligands, such as macrobicyclic tris-dioximates and phosphorus-containing tris-diiminates, in most cases are not available in the free state and can arise only from a template reaction on the metal ion. Some peculiarities of their formation are attributed to the conjugated π-bonds in α-dioxime and α-diimine fragments essentially enhancing the structural rigidity, as well as the rigidity of a capping (cross-linking) fragment that may be relatively easily detached with subsequent destruction of the whole macrobicyclic framework.

Metal ion directed (template) syntheses of the macrobicyclic complexes are effected through cyclization of the preformed tris-complexes or semiclathrochelate as well as *via* interaction of metal ion bis-complexes with cross-linking agents.

In some cases, a free clathrochelate ligand has been isolated after its template construction on the metal ion and demetallation of the resultant complexes. In particular, this has made it possible to synthesize sarcophaginates of many metals incapable of forming clathrochelates *via* direct template synthesis; they are formed from
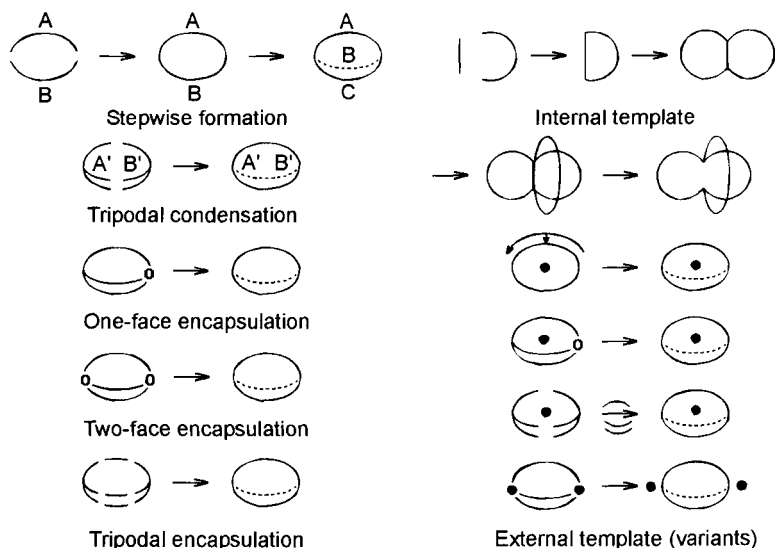
Scheme 4

the appropriate free ligands preliminarily obtained by demetallation of cobalt(III) complexes.

A number of clathrochelate ligands (Sections 2.3 and 2.4) can be preliminarily synthesized by conventional organic chemistry procedures. However, the role of the template effect can not be discounted either. In the majority of cases, alkali metal ions (most common Na^+ and Cs^+ ions) presumably act as templates that are then readily extruded from the clathrochelate ligand cavity.

The general strategy for the synthesis of macrobicyclic compounds may be represented by Scheme 4 proposed by Lehn and coworkers [22].

The clathrochelates may arise from an exchange reaction between initial complexes with labile capping fragments and an excess of a more efficient cross-linking agent (Scheme 5).

For instance, this reaction pathway has been employed for the preparation of tin-capped iron(II) tris-dioximates by the treatment of hydroxy- and alkoxyboron-capped clathrochelate complexes with

Scheme 5

excess tin tetrachloride, and, *vice versa,* fluoroboron-capped complexes have been formed by the interaction of the initial tin-capped iron(II) dioximates with an excess of boron trifluoride etherate.

The isolated free ligands may be modified and further employed for the synthesis of novel clathrochelate complexes. The latter also arise from modification reactions of complexes with reactive ligand groups (precursors). Such reactions are essential for synthesis of the sepulchrates, sarcophaginates, and apical- and ribbed-functionalized tris-dioximates. In these cases, the reactivity of peripheral ligand groups, substituents in ribbed fragments, and coordinated amino groups have been used. The redox processes involving the central metal ion and a macrobicyclic ligand also belong to the complex modification reactions.

2.1 SYNTHESIS OF MACROBICYCLIC TRIS-DIOXIMATES

In the majority of cases, the formation of macrobicyclic metal tris-dioximates is stipulated by the interaction of the reactive oxime groups in tris-dioximate complexes with Lewis acids. The most efficient capping agents have proved to be trigonal organic and inorganic boron compounds.

Christopherson and Sandell [23] suggested that the abnormally high solubility of nickel(II) $Ni(HDm)_2$ dimethylglyoximate in borate buffer is caused by substitution of the hydrogen bond protons of the dioximate fragments by boron atoms to give weak complexes. Schrauzer [24], Umland and coworkers [25, 26] have reported that the macrocyclization of nickel dimethylglyoximate yields $Ni(DmBR_2)_2$ complexes (where R is F, C_6H_5, n-C_4H_9, or CH_3). Thus, dioximate fragments in square-planar bis-dioximates have been demonstrated to be subjected to cross-linking, forming macrocyclic complexes. This route has been used by many workers engaged in the synthesis of macrocyclic d-metal bis-dioximates [27-37]. Moreover, the fact that the tris-dioximate complexes can be capped with boron-containing agents facilitates the synthesis of macrobicyclic compounds with an encapsulated metal ion.

Cobalt complexes of this type were initially isolated by Boston and Rose [2] and independently by Umland and coworkers [38]. Boron-capped iron(II) and cobalt(III) tris-dioximates have been obtained by two main routes: a direct template reaction on the metal ion and the

cross-linking of the initial nonmacrocyclic tris-dioximates (Reaction 1).

$$Fe^{2+}[Co^{2+}+1/4O_2] + 3H_2D + 2BR_3[RB(OH)_2] \xrightarrow{R'OH}$$

$$[Fe(H_2D)_3]^{2+}[CoD_3]^{3-} + 2BR_3[RB(OH)_2] \xrightarrow{solv}$$

(1)

M = Fe(II), Co(III)
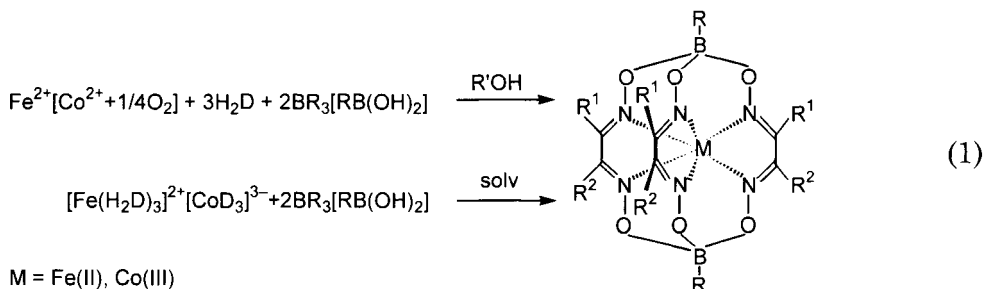
The first route proved to be the most universal one. Owing to a shift in the equilibrium brought about by the formation of a clathrochelate complex, it permits one to prepare a number of compounds in relatively high summary yields. The second pathway, which is carried out in aprotic media, offers higher yields than the first one. However, a low yield of the nonmacrocyclic tris-complex at the first stage imposes restrictions on the scope of this method.

The yields of desired products have been improved by the azeotropic distillation of water from the reaction mixture and the resultant H^+ ion neutralization.

The synthesis of boron-capped iron(II) tris-dioximates has also been implemented using two other methods: the rearrangement of the Tchugaev type $Fe(HD)_2Am_2$ bis-dioximates in the presence of boron-containing Lewis acids:

$$Fe(HD)_2Am_2 + \text{excess } BR_3[RB(OH)_2] \xrightarrow[-Am, -Fe^{2+}]{R'OH} FeD_3(BR)_2$$

(2)
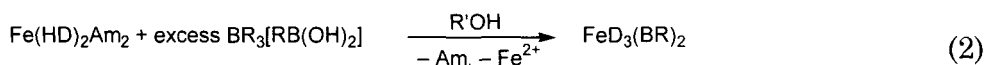
and by a capping group exchange (re-metallation) reaction:

$$+ \text{ excess } BR_3[RB(OH)_2] \xrightarrow[-SnHal_3^+]{R'OH} FeD_3(BR)_2$$

(3)
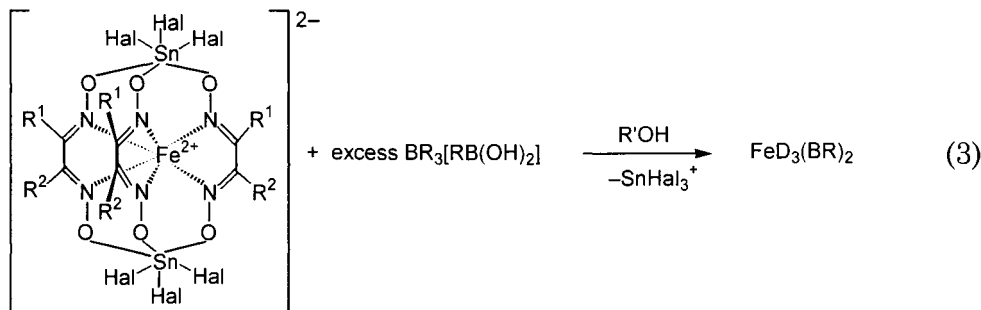
Reactions 2 and 3 take place only in the presence of strong Lewis acids, e.g., BF_3, which is the most efficient agent among boron-

containing Lewis acids. The fact that alkyl- and arylboron-capped compounds have easily been produced *via* Reaction 1 is due to a relatively high energy of their crystal lattice (as a result compounds precipitate) as well as to decrease in the decomposition reaction rate, which leads to an equilibrium shift in the direction of their formation.

The proposed schemes for the synthesis of macrobicyclic tris-dioximates have most readily been realized in high yields for alicyclic dioximes, having a *cis*-conformation both in crystals and in solutions. The change of the acyclic dioxime conformation from *trans* to *cis* during complexation decreases the stability of the compounds formed.

For the first time, a preformed nonmacrocyclic cobalt(III) tris-dimethylglyoximate was cross-linked with boron trifluoride in diethyl ether [2]:

$$K_3CoDm_3 + 6BF_3 \xrightarrow{(C_2H_5)_2O} \left[\text{CoDm}_3(\text{BF})_2 \right]^+ BF_4^- + 3KBF_4 \qquad (4)$$
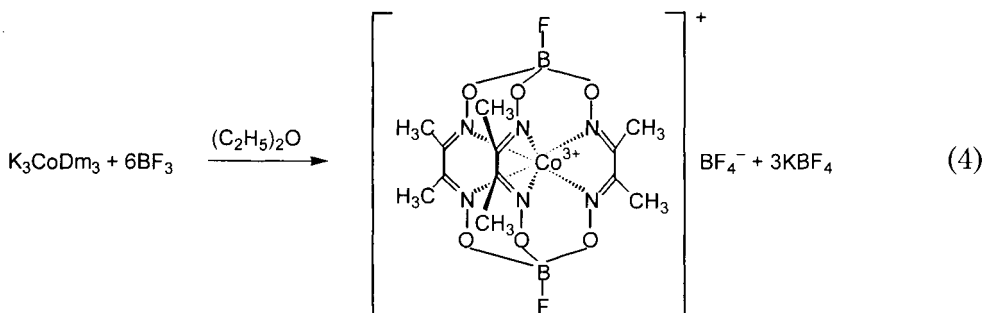
The preparation of the $[CoDm_3(BF)_2](BF_4)$ complex was described in detail [39]. Its disadvantage is a low (13%) yield of an intermediate K_3CoDm_3 product. A more facile and efficient Reaction 5 requires no isolation of an intermediate nonmacrocyclic tris-dioximate [40]:

$$2CoCl_2 + 6H_2Dm + 10\,OH^- + 1/2O_2 + 12BF_3 \xrightarrow[BF_3 \cdot (C_2H_5)_2O]{n\text{-}C_4H_9OH}$$

$$\xrightarrow{\qquad} 2[CoDm_3(BF)_2]^+ + 11H_2O + 8BF_4^- + 4Cl^- \qquad (5)$$
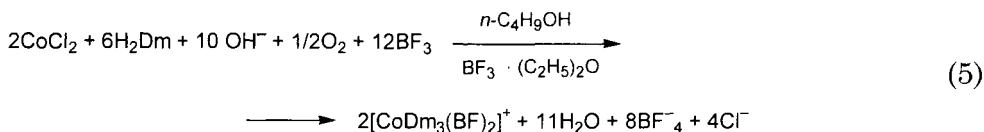
The BF_4^- anion in the clathrochelate $[CoDm_3(BF)_2](BF_4)$ complex can readily be replaced by another large inorganic anion (e.g. PF_6^-) *via* an exchange reaction occurring in aqueous-acetonitrile solution in the presence of a great excess of the substituting anion salt [39]. The reduction of the $[CoDm_3(BF)_2](BF_4)$ clathrochelate with NaI solution in acetone yielded a macrobicyclic cobalt(II) $CoDm_3(BF)_2$ complex. The synthesis of the latter *via* a template condensation on the Co^{2+} ion was not yet successful.

A template condensation on the Co^{3+} ion proved to be the most efficient approach to the preparation of such cobalt compounds. A similar route was employed for the synthesis of a macrobicyclic cobalt(III) $[CoNx_3(BF)_2](BF_4)$ and $[CoBd_3(BF)_2](BF_4)$, $[CoBd_3(BC_6H_5)_2](BF_4)$ nioximates and α-benzyldioximates, when boron trifluoride and phenylboronic acid were used as cross-linking agents [41, 42]. The $[CoNx_3(BF)_2](BF_4)$ complex was also synthesized *via* capping of the nonmacrocyclic K_3CoNx_3 complex with boron fluoride [41]. This procedure was used to prepare $[CoDm_3(BC_6H_5)_2](BF_4)$, $[CoNx_3(BC_6H_5)_2](BF_4)$, $[CoDm_3(Bn-C_4H_9)_2](BF_4)$, and $[CoNx_3(Bn-C_4H_9)_2](BF_4)$ clathrochelates by cross-linking of the analogous tris-complexes with a reactive boron-containing agent ($C_6H_5BCl_2$ or $n-C_4H_9BCl_2$) in methylene chloride, accompanied by replacement of the Cl^- anion by the BF_4^- anion on an ion-exchange column.

The reduction of cobalt(III) complexes with NaI solution in acetone yielded analogous macrobicyclic cobalt(II) $CoBd_3(BF)_2$ and $CoNx_3(BF)_2$ complexes [42]. The formation of these complexes, as well as $CoDm_3(BC_6H_5)_2$, $CoDm_3(Bn-C_4H_9)_2$, $CoNx_3(BC_6H_5)_2$, $CoNx_3(Bn-C_4H_9)_2$, and $CoBd_3(BC_6H_5)_2$ clathrochelates in acetonitrile solution *via* reduction of the corresponding cobalt(III) clathrochelates with ferrocene was studied in research reported in Ref. 41, but their isolation as solids was not described.

In the synthesis of the boron-capped cobalt(II) tris-dioximates, ferrocenylboronic acid was also used as a capping agent [43]. Reaction of this Lewis acid with anhydrous $CoCl_2$ and dioximes in oxygen-free methanol gave clathrochelate $CoNx_3(BFc)_2$ and $CoDm_3(BFc)_2$ complexes:

$$Co^{2+} + 3H_2D + 2FcB(OH)_2 \longrightarrow \qquad (6)$$

R = CH$_3$, (R,R) = (CH$_2$)$_4$
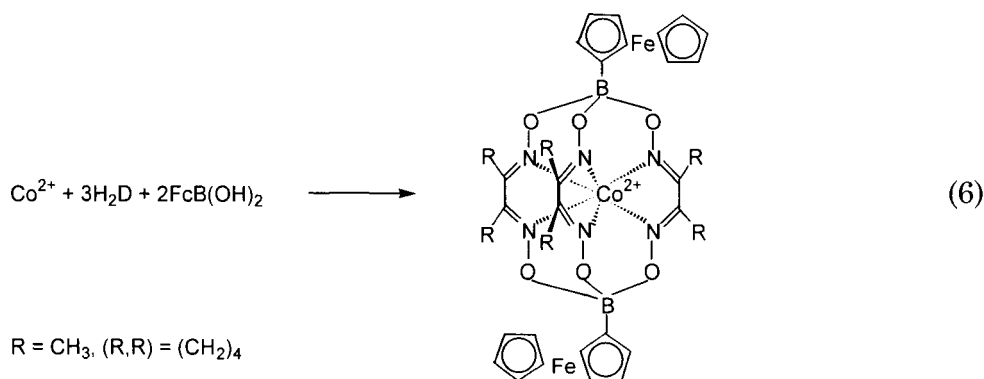
Cobalt(III) tris-dioximates were also cross-linked with other Lewis acids, such as $SnCl_4$ and $SiCl_4$ [39]. Reaction of K_3CoDm_3 in methylene chloride with anhydrous $SnCl_4$ resulted in the macrobicyclic $[CoDm_3(SnCl_3)_2]^-$ anion, which was isolated as an ionic associate with a bulky $(n\text{-}C_3H_7)_4N^+$ cation [39].

Attempts to use tin(IV) tetraalkylates and trialkylhalogenides as capping agents met with failure just like those undertaken with cobalt(III) tris-dioximates and tin tetrafluoride as a capping agent. The latter appears to be explained by the difficulties encountered in the detachment of the fluoride ion bonded to the tin atom and the formation of by-products (cobalt(III) and tin(IV) bis-dioximates). It is evident that in this case steric factors are negligible because the fluorine substituent is small [44].

For tin(IV) bromide, the halogenide ion detachment apparently takes place much more readily compared with that of SnF_4. However, the bulky bromine atom causes steric hindrances due to its interaction with the substituents at the α-dioxime fragments. In particular, attempts to obtain clathrochelate tribromotin-capped cobalt(III) α-benzyldioximate and α-furyldioximate were not successful, whereas the corresponding trichlorotin-capped complexes were obtained [45].

Tin-capped clathrochelate cobalt(III) tris-dioximates were synthesized by a procedure similar to Reaction 1 in the presence of organic bases (amines or tetra-n-butylammonium hydroxide):

$$Co^{2+} + 1/4O_2 + 3H_2D \quad \diagdown \atop \diagup \quad + \ SnHal_4 \xrightarrow[(CH_3)_2CO,\ C_6H_6]{ROH} [CoD_3(SnHal_3)_2]^-$$
$$Co(HD)_3$$

(7)
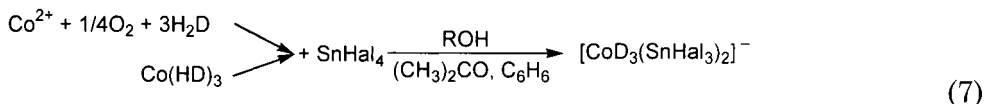
Hal $= Cl, Br$
$H_2D = H_2Gm, H_2Mm, H_2Dm, H_2Bd, H_2Nx$

A number of compounds of this type were obtained and isolated as complex acids or salts with organic cations when tin(IV) tetrachloride and tetrabromide were used as the capping agents [44, 45].

Certain α-dioximate $H[CoD_3(SnHal_3)_2]$ complex acids were isolated at the first stage without the addition of amine or with its addition in small amounts. The subsequent addition of amines resulted in the formation of the corresponding ionic associates.

A similar reaction of K_3CoDm_3 with $SiCl_4$ in boiling THF enabled one to prepare a macrobicyclic $[CoDm_3(SiO)_2]\cdot HPF_6$ complex [39]:

$$K_3CoDm_3 + 2SiCl_4 \xrightarrow[t°]{THF} [CoDm_3(SiCl_2)_2] \xrightarrow[CH_3OH + H_2O]{NaPF_6;\ H^+} [CoDm_3(SiO)_2] \cdot HPF_6 \tag{8}$$
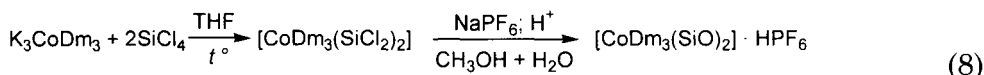
This compound was isolated as a polymeric gel. Macrobicyclic fragments in the polymer chain are linked by Si–O–Si bridging fragments. It was claimed [39] that this clathrochelate may be either a low-spin cobalt(II) compound or a mixture of cobalt(II) and cobalt(III) compounds. However, taking into account the polymeric nature of the complex and the difficulties encountered in its isolation and investigation, one may conclude that the data reported [39] are not sufficient for its unambiguous identification.

Transition metal aqua ions and their complexes with amines have also been utilized as capping agents in the synthesis of macrobicyclic cobalt tris-dioximates [46]. The reactions of nonmacrocyclic K_3CoDm_3 tris-dimethylglyoximate with dienCrCl$_3$, dienCoCl$_3$, and tameCo(NO$_3$)$_3$ complexes (where *dien* is diethylenetriamine and *tame* is 1,1,1-tris(aminomethyl)ethane) and Li_3CoDm_3 with $[Zn(H_2O)_6]^{2+}$ and $[Ni(H_2O)_6]^{2+}$ aqua ions resulted in the formation of the corresponding clathrochelate $[CoDm_3(dienCr)_2](PF_6)_3 \cdot C_2H_5OH$, $[CoDm_3(dienCo)_2](PF_6)_3 \cdot CH_3OH$, $[CoDm_3(Ni(H_2O)_3)_2](PF_6) \cdot 4H_2O$, and $[CoDm_3(Zn(H_2O)_3)_2](PF_6) \cdot 3H_2O$ complexes. The interaction between the two last compounds and free *dien* ligand permitted one to obtain the $[CoDm_3(dienNi)_2](PF_6) \cdot 4H_2O$ and $[CoDm_3(dienZn)_2](PF_6) \cdot 2H_2O$ clathrochelates [46].

Synthesis of macrobicyclic $MDm_3(BR)_2$ complexes (where M is nickel (paramagnetic), iron and cobalt ions; R is C_6H_5 and n-C_4H_9) was reported by Umland and coworkers [38]. However, the formation of nickel complexes of this type was not further confirmed.

A series of boron-capped iron(II) tris-dimethylglyoximates was obtained in high yield by direct template reactions [47, 48]. Iron ions serve an "organizational role" by providing a template on which three dimethylglyoxime fragments become bound *prioro* to the reaction with boron-containing agents either in alcohol or water (Reactions 9 and 10).

$$Fe^{2+} + 3H_2Dm + 5OH^- \xrightarrow[n\text{-}C_4H_9OH]{BF_3 \cdot (C_2H_5)_2O} FeDm_3(BF)_2 + H^+ + 4BF_4^- \tag{9}$$

$$Fe^{2+} + 3H_2Dm + 2H_3BO_3 \xrightarrow{ROH} FeDm_3(BOR)_2 + 2H^+ + 6H_2O \tag{10}$$

R = H, CH$_3$, C$_2$H$_5$, *iso*-C$_3$H$_7$, n-C$_4$H$_9$
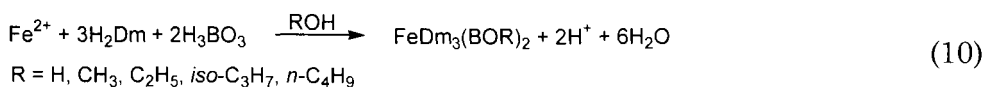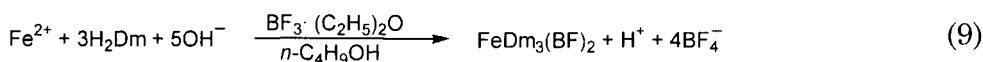
It was noted that the base must be slowly added to the iron(II) salt, dimethylglyoxime, and boron trifluoride etherate solution in n-

butanol. The reaction mixture must be slightly acidic; otherwise, the by-products formed contaminate the resultant complex and reduce its yield. If no base is added, the product is formed over a period of days [47]. The process was accelerated by reaction mixture refluxing for several minutes [49, 50]. The fluoroboron-capped complexes, prepared in the absence of the base, have the advantage that they are free of by-products.

An iron(II) salt can be replaced by an iron(III) salt or metallic iron in the synthesis of the $FeDm_3(BF)_2$ and $FeDm_3(BOR)_2$ complexes. The reduction of iron(III) ions to iron(II) ions takes place in the first case and gaseous hydrogen is released in the second case. Attempts to prepare a clathrochelate iron(III) complex *via* oxidation of $FeDm_3(BF)_2$ clathrochelate with bromine, iodine, hydrogen peroxide, oxygen, cerium(IV), and copper(II) led either to obvious decomposition of the complex or to no reaction [47]. The macrobicyclic $FeDm_3(BF)_2$ complex was also obtained by the interaction of the initial Tchugaev type $Fe(HDm)_2Py_2$ bis-dimethylglyoximate with an excess boron trifluoride etherate in *n*-butanol [50]:

$$Fe(HDm)_2Py_2 + \text{excess } BF_3 \cdot (C_2H_5)_2O \xrightarrow{\; -Fe^{2+} \;} FeDm_3(BF)_2 \qquad (11)$$
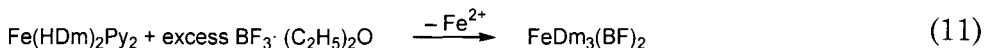
Acidic medium is also needed for efficient synthesis of $FeDm_3(BOR)_2$ complexes by Reaction 10. Therefore, $Na_2B_4O_7 \cdot 10H_2O$ and sodium and ammonium acetates, used for neutralization of the reaction mixture, were added in small amounts to increase the product yield. The use of $Na_2B_4O_7 \cdot 10H_2O$ as a capping agent instead of boric acid leads to no desired complexes [47].

The macrocyclization has been accelerated by heating the reaction mixture in a flask fitted with a reflux condenser. With alkoxy-containing complexes, care must be taken since upon inefficient cooling low-boiling boric acid esters can be distilled off, whereby the product yield is drastically reduced. In some cases, an appreciable effect has been observed when the water from the reaction mixture has been distilled off as azeotrope [47]. The preformed $FeDm_3(BOH)_2$ complex has undergone esterification in alcohol medium to give alkoxyboron-capped macrobicyclic compounds. Compounds of this type can also arise from transesterification of preformed complexes (Scheme 6) [47].

Transesterification of alkoxy-groups in macrobicyclic tris-dioximates is a modification reaction whereby the compounds that cannot be readily prepared by conventional methods may be

$$\text{FeDm}_3(\text{BOR})_2 + 2\text{R'OH} \xrightleftharpoons{\text{H}^+} \text{FeDm}_3(\text{BOR'})_2 + 2\text{ROH}$$

R		R'
OH	$\longrightarrow$	CH_3, C_2H_5, $n\text{-C}_4\text{H}_9$,
CH_3	$\longrightarrow$	H, C_2H_5, $iso\text{-C}_3\text{H}_7$, $n\text{-C}_4\text{H}_9$,
C_2H_5	$\longrightarrow$	H, CH_3, $n\text{-C}_4\text{H}_9$,
$iso\text{-C}_3\text{H}_7$	$\longrightarrow$	H, C_2H_5, $n\text{-C}_4\text{H}_9$,
$n\text{-C}_4\text{H}_9$	$\not\longrightarrow$	H, CH_3, C_2H_5, $iso\text{-C}_3\text{H}_7$
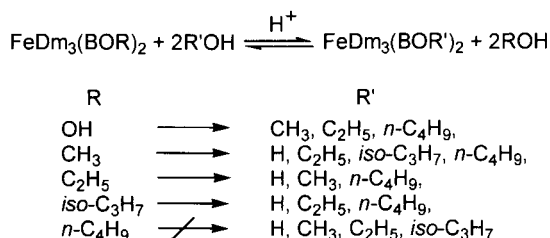
Scheme 6

synthesized. Thus, a clathrochelate $\text{FeNx}_3(\text{BOC}_6\text{H}_5)_2$ resulted from esterification of an initial $\text{FeNx}_3(\text{BOH})_2$ complex in boiling phenol [49].

A route similar to Reaction 10 was utilized to prepare alkoxyboron-capped macrobicyclic $\text{FeAd}_3(\text{BOR})_2$ and $\text{FeBd}_3(\text{BOR})_2$ acetylacetonedioximates and α-benzyldioximates [51].

When phenylboronic acid was employed as a capping agent, a template condensation in methanol yielded an insoluble macrobicyclic $\text{FeDm}_3(\text{BC}_6\text{H}_5)_2$ dimethylglyoximate [52].

Attempts to synthesize $\text{FeDm}_3(\text{BCl})_2$ and $\text{FeDm}_3(\text{BBr})_2$ complexes were not successful, presumably due to reactions of capping BCl_3 and BBr_3 agents with the solvent [52]. It is rather intriguing that sodium borohydride has been used for preparation of hydride-containing tris-dioximate complexes. A prolonged reaction of iron(II) bromide, dimethylglyoxime, and NaBH_4 in anhydrous acetonitrile followed by recrystallization resulted in a macrobicyclic $\text{FeDm}_3(\text{BH})_2$ complex containing a non-reactive B–H bond [52].

A methylboron-capped $\text{FeBd}_3(\text{BCH}_3)_2$ α-benzyldioximate was obtained *via* a direct reaction between iron(II) salt, α-benzyldioxime, and methylboronic acid in boiling n-butanol [52]. The fluoroboron-capped $\text{FeBd}_3(\text{BF})_2$ α-benzyldioximate has been prepared both by a template condensation on the Fe^{2+} ion [50] and *via* reaction of the preformed $\text{Fe}(\text{HBd})_2(\text{Melz})_2$ and $\text{Fe}(\text{HBd})_2\text{Py}_2$ bis-dioximates with $\text{BF}_3\cdot(\text{C}_2\text{H}_5)_2\text{O}$ in diethyl ether or n-butanol [50, 53]. Reaction of the iron(II) bis-α-benzyldioximate with phenylboronic acid was also employed for the synthesis of a $\text{FeBd}_3(\text{BC}_6\text{H}_5)_2$ complex. The preparation of the tetragonal boron-containing iron(II) dioximates is possible with suitable (e.g., diarylsubstituted) boron-containing cross-linking reagents (Scheme 7) [53]. When diphenylboron bromide has been used as a reagent, boron-containing tetragonal bis-dioximates

Tetragonal H-containing iron(II) dioximate

BF$_3$·(C$_2$H$_5$)$_2$O

(C$_6$H$_5$)B(OH)$_2$

(C$_6$H$_5$)$_2$BBr   Melz

clathro-compaund   clathro-compaund   "pre-clathro" compaund   "pre-clathro" compaund

Melz   Melz   Melz

no reaction   no reaction   tetragonal boron-containing
iron(II) dioximate

A   ‖ – A

adduct of tetragonal boron-containing
iron(II) dioximate
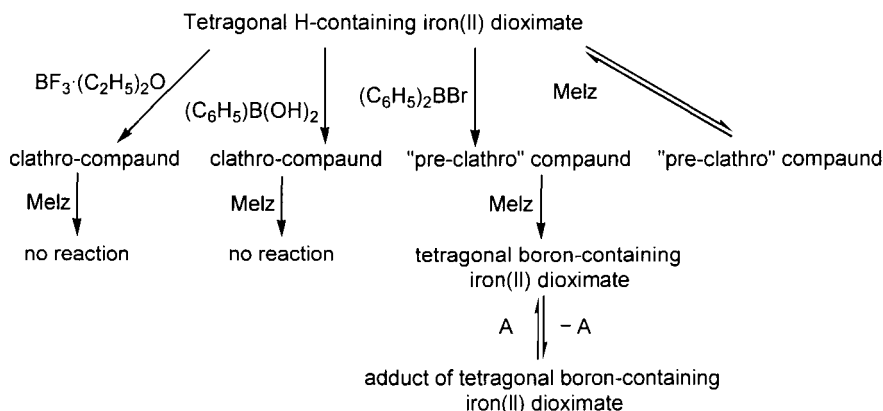
Scheme 7

have been formed through "pre-clathro" intermediates that show a tendency to rearrange into a clathrochelates after a prolonged time. The "pre-clathro" compounds were isolated only in the case of weak cross-linking agents (e.g., (C$_6$H$_5$)$_2$BBr and (CH$_3$)$_2$BBr) [53].

When macrobicyclic iron(II) dimethylglyoximates and α-benzyldioximates are studied in detail, for acyclic dioximes such as glyoxime, methylglyoxime, phenylglyoxime, and α-furyldioxime, only fluoroboron-, alkylboron-, and arylboron-capped complexes have been obtained by direct template condensation on the Fe^{2+} ion and by interaction of the corresponding Fe(HD)$_2$Py$_2$ bis-dioximates with BF$_3$·(C$_2$H$_5$)$_2$O in n-butanol [21, 50].

Clathrochelate iron(II) complexes derived from alicyclic dioximes (nioxime, heptoxime, 4-methylnioxime, and octoxime) are of particular interest. The first clathrochelate FeNx$_3$(BOH)$_2$ and FeNx$_3$(BF)$_2$ compounds of this type, prepared by template cross-linking of three dioxime molecules on the Fe^{2+} ion with a boric acid in water and BF$_3$·(C$_2$H$_5$)$_2$O in n-butanol, respectively, were described in Ref. 40. The syntheses with alicyclic dioximes have been realized for a number of boron-containing cross-linking agents in many cases, in a quantitative yield, and in dilute solutions well [49, 54-61].

Synthesis of the clathrochelate with hydridoboron capping groups *via* template condensation in dry acetonitrile occurs by Reaction 12:

$$FeBr_2 + 3H_2Nx + 2NaBH_4 \xrightarrow{\text{AN}} FeNx_3(BH)_2 + 2NaBr + 6H_2 \tag{12}$$
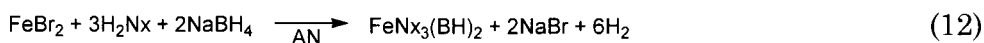
to give a chromatographically isolated FeNx$_3$(BH)$_2$ complex [52, 58]. A nonmacrocyclic protonated [Fe(H$_2$Nx)$_3$]Br$_2$ tris-complex was obtained as an intermediate in the synthesis of this hydride-containing

clathrochelate. Interaction of this intermediate with $NaBH_4$ in THF also led to the formation of a clathrochelate $FeNx_3(BH)_2$ compound with a non-reactive B–H fragment. In contrast to tris(*iso*-propoxy)borane, this clathrochelate complex is inert in acetone even upon boiling for 16 h. Although acetoacetate is formed in some amount upon heating for 67 h in glacial acetic acid, the B–H fragments are partly retained. A similar result was obtained after 16 h treatment with concentrated hydrochloric acid at room temperature [58]. The use of substituted boron hydride, e.g., cyanboron hydride or sodium acetoanilidotrihydroborate instead of $NaBH_4$ in Reaction 12, resulted in no new compounds [52].

The alicyclic clathrochelate $Fe(4MNx)_3(BR)_2$ (where R is CH_3, *n*-C_4H_9, C_6H_5, OH, O*iso*-C_3H_7, O*n*-C_4H_9, O*sec*-C_4H_9, F); and $FeGx_3(BR)_2$ and $FeOx_3(BR)_2$ (where R is CH_3, *n*-C_4H_9, C_6H_5, OH, OCH_3, O*n*-C_4H_9, and F) tris-dioximates have been synthesized in the same manner as the corresponding nioximates [59-61]. Since alkoxyboron-capped iron(II) 4-methylnioximates do not readily crystallize from organic solvents, with lower alcohols (CH_3OH and C_2H_5OH) the alkoxyde complexes were not isolated as solids [59].

With the majority of alicyclic boron-capped iron(II) dioximates, neither template condensation nor recrystallization from organic solvents gave crystals suitable for X-ray analysis. A rate-controlled template condensation within several days yielded $FeGx_3(BOH)_2 \cdot 3H_2O$ monocrystals, since the synthesis of this clathrochelate compound proceeds much more slowly than that of analogous complexes with nioxime and 4-methylnioxime [62, 63].

In most cases, the synthesis of macrobicyclic iron(II) tris-dioximates occurs *via* a one-step procedure, enabling one to obtain only complexes with identical dioxime fragments and capping groups. It is not expedient to utilize mixtures of dioximes or capping agents with similar properties in these processes to produce meridional (C_3) and axial (C_2) nonsymmetric compounds, respectively, because of the formation of a mixture of products that is close to a statistical one. The predominant formation of the symmetric complexes has been observed even when the dioximes and capping agents used differ significantly in their properties. In the case of dioximes, this can be accounted for by the difference in the stability constants of nonmacrocyclic tris-dioximates as first intermediates (for example, $\beta_3^{[Fe(H_2D)_3]^{2+}} \gg \beta_3^{[Fe(H_2D)_2(H_2D')]^{2+}}$, see Chapter 4). The predominantly formed symmetric $[Fe(H_2D)_3]^{2+}$ complex reacts with cross-linking

agents owing to the symmetric clathrochelate product. Similarly, in the case of capping agents, when the capping agents display an essentially different activity, a second (semiclathrochelate) intermediate, will be formed preferentially by the more efficient agents and will presumably be capped in a statistical ratio, since the second capping is not a rate-controlling step (see Chapter 4). Additionally, a higher crystal lattice energy of symmetric compounds compared with that of nonsymmetric ones is observed: in most cases clathrochelates are obtained as solids in the course of the reaction, and, therefore, an increase in the crystal lattice energy leads to a shift in equilibrium in the direction of the symmetric product. When C_2-nonsymmetric dioximes such as phenylglyoxime or methylglyoxime are employed as the initial ligand, a mixture of *fac*- and *mer*-isomers has been formed. In spite of the fact that clathrochelates are produced by a multistage mechanism through the formation of a semiclathrochelate in all cases except one (see below), the semiclathrochelates have not been isolated because of their lability. At the same time, a directed synthesis of clathrochelates containing different dioximate fragments and capping agents allows one to produce reactive precursors suitable for further functionalization, as well as to vary rather finely the physicochemical properties of the products obtained [64].

C_3-nonsymmetric iron(II) clathrochelates have been obtained by the cycloaddition of α-dioximes to initial square-planar macrocyclic iron (II) bis-dioximates by the Reaction 13:

$$[FeD_2(BF_2)_2AN_2] + H_2D' \longrightarrow FeD_2D'(BF)_2 + 2\,HF \tag{13}$$
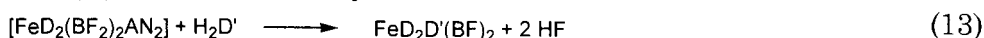
It is obvious that this reaction is favored by binding the HF acid released during its course, i.e., in the presence of H^+ and F^- ion acceptors. A weakly coordinating sterically hindered N,N-di(*iso*-propyl)ethyl amine and boron trifluoride etherate have been used as H^+ ion acceptor and electrophilic agent to remove F^- ions, respectively. In addition, $BF_3 \cdot O(C_2H_5)_2$ has prevented the side fluoroboron caps elimination reaction (Scheme 8).

The cycloaddition reaction proceeds under more rigid conditions and takes more time than a direct template condensation on the iron(II) ion. This can be explained by the fact that the overall mechanism of clathrochelate synthesis involves an intermediate tris-complex formation step. It is evident that macrocyclic square-planar iron(II) bis-dioximates are relatively kinetically stable, and the
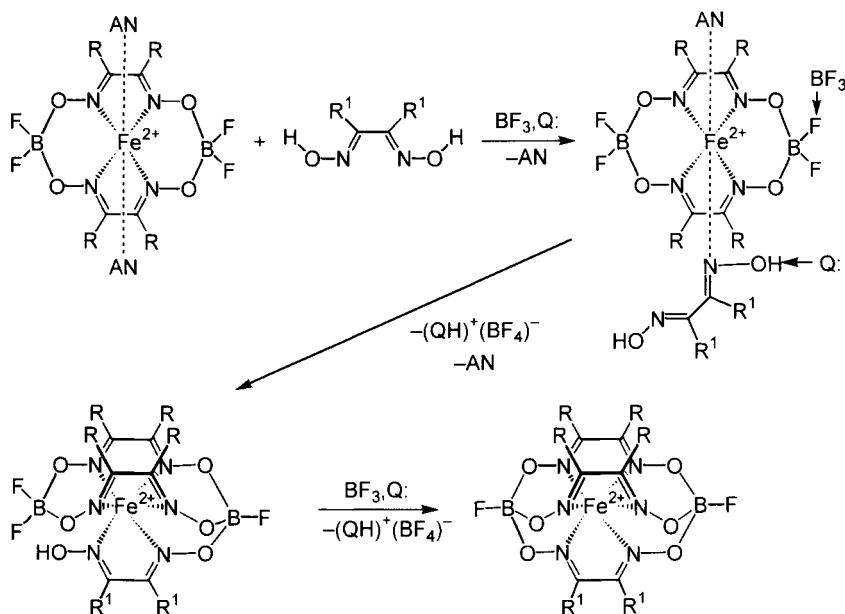
Scheme 8

addition of a third dioxime molecule involves not only detachment of an axially coordinated solvate molecules, but also considerable changes in the iron(II) ion coordination arrangement.

In the absence of F^- ion acceptors, a clathrochelate is not formed and the reaction completed at a stage of *cis*-addition of the protonated dioxime to a square-planar macrocycle. With certain dioximes (H_2Nx and H_2Dm), in the absence of the base the reaction yields a mixture of symmetric clathrochelates. In other cases, only a mixture of decomposition products has been formed [64].

A direct synthesis of C_2-nonsymmetric tris-dioximate iron (II) clathrochelates *via* the formation of semiclathrochelate complex **2** cannot be realized even with a great excess of complex **1**, since compound **2** readily disproportionates to give **1** and **3** (Scheme 9).

A C_2-nonsymmetric $FeNx_3(BC_6H_5)(BF)$ complex was obtained *via* a "re-boronating" reaction from the initial $FeNx_3(BC_6H_5)_2$ clathrochelate attacked by triethyloxonium boron fluoride, and the complex obtained was chromatographically isolated (Scheme 10).

However, this is not a general method; attempts to prepare the $FeDm_3(BC_6H_5)(BF)$ complex by an analogous scheme have not been
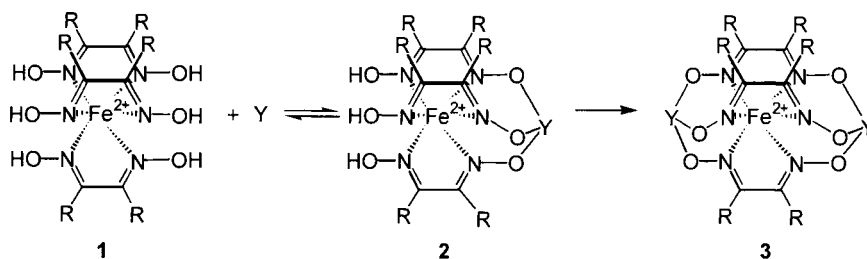
Scheme 9

Scheme 10

Scheme 11

Y,Z = Lewis acids
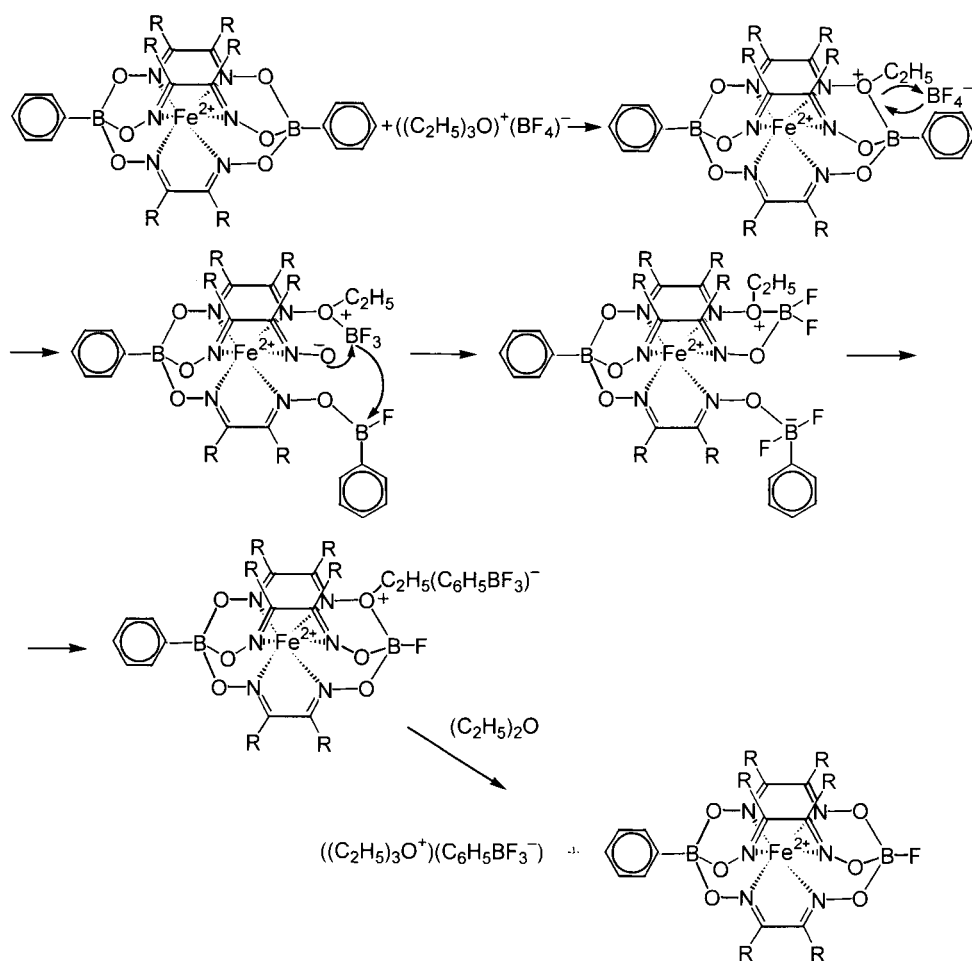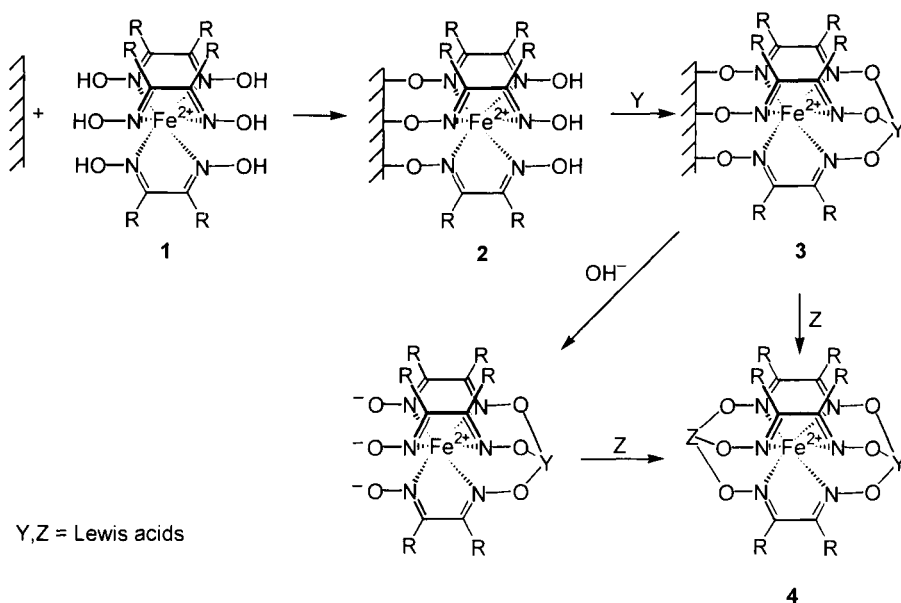
successful (only a symmetric FeDm₃(BF)₂ complex has been formed) [64].

The synthesis of C_2-nonsymmetric clathrochelate iron(II) dioximates was realized through a stepwise "assembling" on the sorbent surface (Scheme 11).

A chemical immobilization of a nonmacrocyclic tris-complex **1** on the matrix surface has enabled one to protect one of the two triangular planes formed by the oxime group (**2**) and to obtain the immobilized semiclathrochelate **3** *via* cross-linking with Lewis acids. The desorption of these semiclathrochelates with the help of another capping agent leads to the formation of C_2-nonsymmetric clathrochelate **4**. The success of the synthesis carried out by this procedure is governed by a sorbent aptitude for a specific binding of the initial tris-complex **1** and the subsequent desorption of a semiclathrochelate **3** affected by cross-linking agents.

The best results were obtained with aluminium hydroxide resulting from hydrolysis of aluminium(III) *iso*-propylate. A high sorption capacity (*ca* 10%) of compound **2**, a high degree of desorption of complex **3**, and the purity of the resulted clathrochelate **4** make aluminium(III) hydroxide the most suitable matrix for the synthesis of targeted compounds [64].

The unique properties of a metal ion encapsulated in the cage of a macropolycyclic ligand and isolated from the influence of external factors have allowed the use of clathrochelates as models of important biological systems, electron carriers, and catalysts of photochemical and redox processes (see above). However, the low reactivity of the majority of the clathrochelates impedes their modification and hence the possibility of their utilization for the solution of these problems.

An apical functionalization of clathrochelates enables one to obtain complexes with improved chemical, physicochemical, biomimetic, and bioactive properties and characteristics that are primary governed by functionalized groups [65]. The possibility of an apical modification of macrobicyclic α-dioximates and oximehydrazonates is indicated by the relative availability of functionalized boron-containing Lewis acids as efficient capping agents.

Ferrocenylboron-capped macrobicyclic iron(II) acyclic, alicyclic and aromatic dioximates as potential electron carriers were synthesized by direct template reactions using ferrocenylboronic acid as the cross-linking agent [66].

$$Fe^{2+} + 3H_2D + 2FcB(OH)_2 \xrightarrow[R^1OH]{t^\circ} \qquad (14)$$

R = CH$_3$, (R,R) = (CH$_2$)$_4$
    H   (CH$_2$)$_5$
    C$_6$H$_5$ CH$_3$CH(CH$_2$)$_3$
    C$_4$H$_4$O
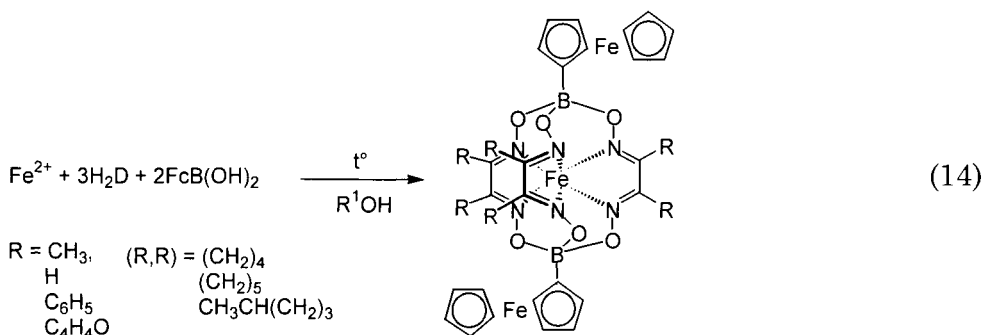
The introduction of lipophilic substituents is of interest for producing surface-active compounds (surfactants) and liquid-crystal systems. The complexes with allyl substituents at the apical boron atoms are precursors for the synthesis of linear and netlike polymeric clathrochelates.

Clathrochelate iron(II) tris-dioximates with hexadecylboron capping groups were synthesized by direct template condensation of acyclic and alicyclic dioximes with the corresponding n-C$_{16}$H$_{33}$B(OH)$_2$ boronic acid (denoted as HdB(OH)$_2$) on iron(II) ion in methanol:

$$Fe^{2+} + 3H_2D + 2RB(OH)_2[excess\ BR_3] \xrightarrow[\begin{array}{c}R^2OH\\ [-2C_3H_8]\end{array}]{}$$

$$R^1 = H;\ CH_3,$$
$$(R^1,R^1) = (CH_2)_4;$$
$$R = n\text{-}C_{16}H_{33}\ (Hd);\ CH_2\text{-}CH=CH_2\ (Allyl)$$

(15)
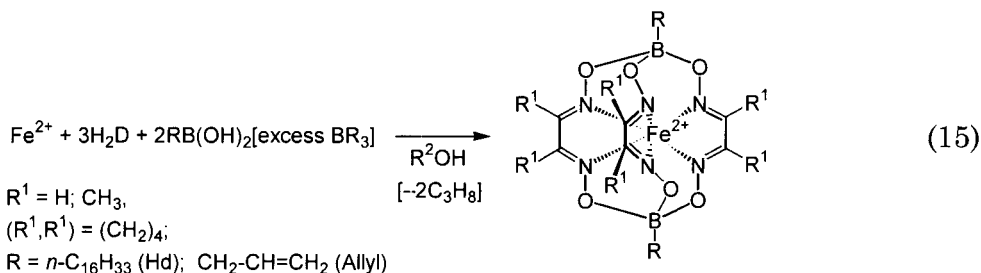
Allylboron-capped compounds were prepared similarly in *n*-butanol using triallylborane BAllyl$_3$ instead of HdB(OH)$_2$. Under these reaction conditions, two of the three B–C bonds in BAllyl$_3$ are cleaved by *n*-butanol or water to form AllylB(OH)$_2$ and propane [67].

The mutual electronic influence of the apical substituents and the clathrochelate framework (and, therefore, the encapsulated ion) is negligible. The steric effects of apical substituents are also small. The substituents in chelating (ribbed) fragments of polyene clathrochelates have much greater steric and electronic effects on the coordination polyhedron geometry and the central metal ion properties because of the direct interaction of the π-system of a ligand and the π- and σ-system of a substituent. As a result, one has an opportunity to use such substituents in order to change the central metal ion characteristics; conversely, one can change the central metal ion configuration *via* a redox transition to affect the electronic characteristics of substituents. From this point of view, the synthesis of ribbed-functionalized clathrochelates with substituents apt to coordinate a metal ion to produce polynuclear complexes with interaction through the clathrochelate framework metal centers is of particular interest: polynucleating ligand systems and polynuclear complexes of *d*-metals derived from them are actively being investigated as models of metalloproteins and metalloenzymes and other important biological systems (biomimetics), efficient catalysts for chemical reactions, and promising materials for molecular electronics (molecular magnets, switches, transistors, and wires) [65].

The most feasible Routes I-III for the synthesis of triribbed-functionalized α-dioximate clathrochelates (Scheme 12) were proposed in Ref. 65. The halogen-carbon bonds are reasonably active in nucleophilic substitution reactions, and the dihalogenoxime complexes are relatively stable (unlike dihalogenoximes, these complexes are available and undergo no intramolecular conversions
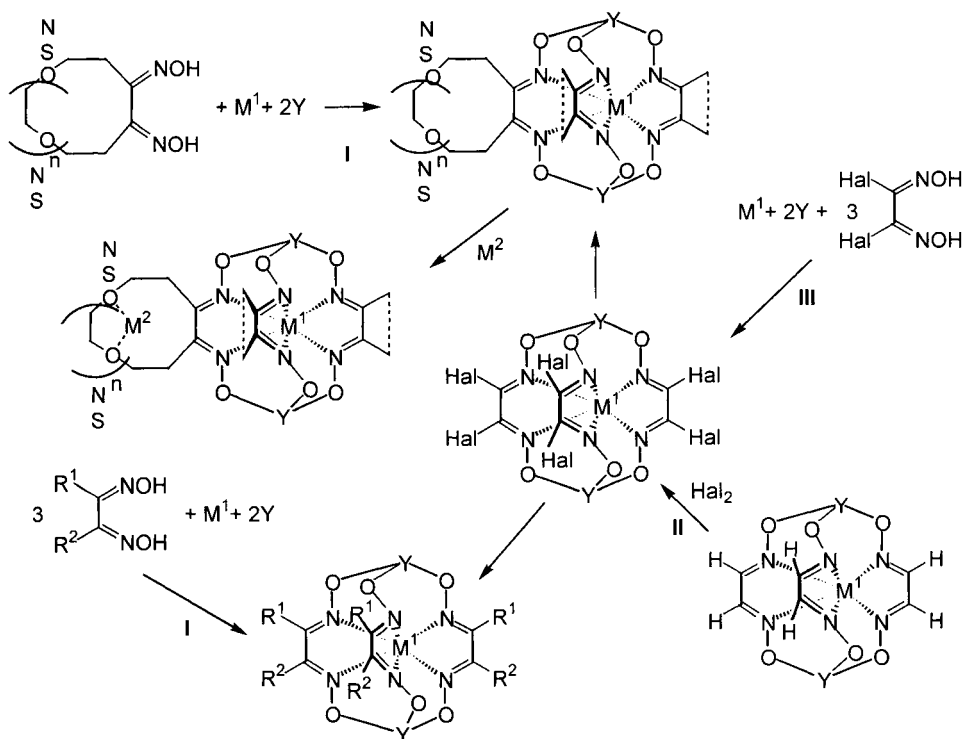
R^1, R^2 = PAlk$_2$(Ar$_2$), NHAlk(Ar), NAlk$_2$(Ar$_2$), oxo- and thiocrown ether, Fc,

SAlk(Ar), cp, CN, OAlk(Ar), PO(OH)$_2$

Y = Lewis acid

Scheme 12

that could complicate modification reactions). It is rather complicated to use the preliminarily functionalized α-dioximes (Route I) in the synthesis of clathrochelates to obtain partially substituted compounds and complexes with redox-active coordinating groups. In the course of a template condensation on the metal ion, the preliminarily functionalized α-dioximes can react not only with oxime groups but also with functionalizing substituents. Side reactions of these groups can markedly reduce the yield of the desired products and hinder their isolation. Consequently, Routes II and III (Scheme 12) were chosen for the synthesis of the ribbed-functionalized clathrochelates. Route II has been regarded as the most promising procedure since modern methods for the synthesis of the initial glyoximate clathrochelates with yields of 70 to 80% are

developed. However, attempts to implement a complete halogenation of dioximate fragments of such complexes and to isolate hexahalogenide precursors of triribbed-functionalized clathrochelates has met with failure. A mixture of partial substitution products, largely containing trihalogen-substituted compounds, was obtained. In addition, in the case of a phenylboronic $FeGm_3(BC_6H_5)_2$ glyoximate the halogenation side reactions of the aromatic substituents at apical boron atoms were observed [65].

The use of Route III presented problems because the attempts to obtain hexahalogenide precursors from initial dihalogendioximes by the standard procedures of synthesis of such clathrochelates have not been successful. Nevertheless, the conditions under which the yield of these complexes was 60-90 % were selected in Ref. 65: nitromethane was as a solvent, and acetonitrile $FeAN_4Cl_2$ solvato-complex as a source of Fe^{2+} ions, and the water was removed from the reaction mixture. The three hexachloride precursors with phenylboronic, n-butylboronic, and fluoroboronic capping groups (Scheme 13) were obtained [65].

Hexachloride precursors interacted with excess thiophenol in the presence of potassium carbonate under soft conditions to yield hexathiophenol clathrochelates (Scheme 13).

The reaction with an excess of methylmercaptan in the presence of potassium carbonate at room temperature led to the formation of partially substituted products only, mainly trisubstituted clathrochelates. Therefore, a more active potassium methylmercaptanate was used in the synthesis of the hexasubstituted product, and the reaction readily proceeded in a high yield [65].

The thioalkyl-containing macrobicyclic complexes have been dealkylated and realkylated easily under the action of potassium thiolates in aprotic media (Scheme 14). The products of de- and realkylation reactions were detected by PD and FAB mass spectrometry. In this respect the thioalkyl-containing clathrochelates are close to the aryl alkyl sulfides. In the course of thioalkyl derivative synthesis with an excess of potassium thiolate, a mixture of dealkylated products was obtained in addition to the desired hexathioalkyl clathrochelates. The addition of corresponding alkyl iodide and potassium carbonate to the reaction mixture in the final stage of reaction led to an increase in yields by alkylation of HS groups, resulting in the side dealkylation process [65].
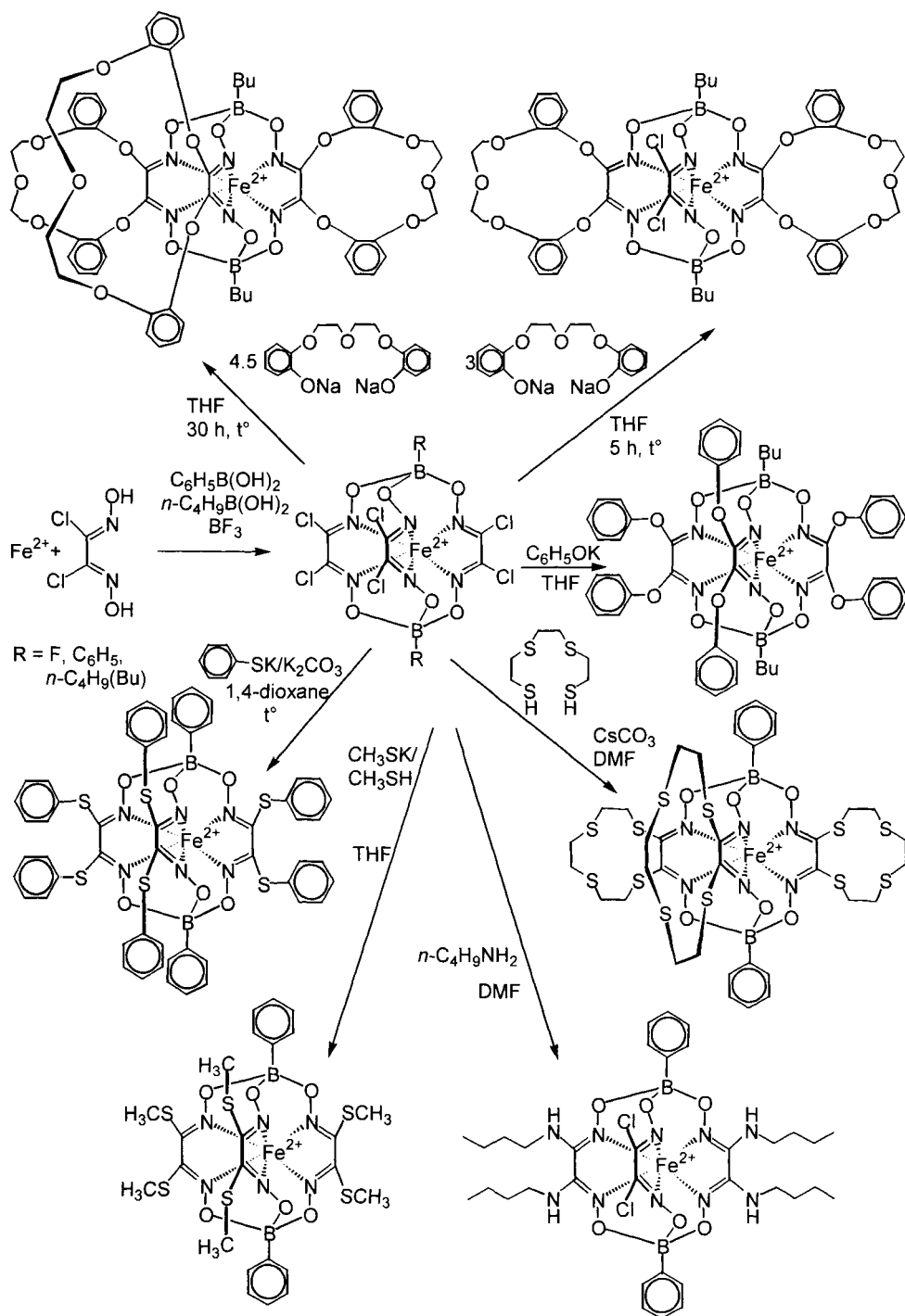
Scheme 13
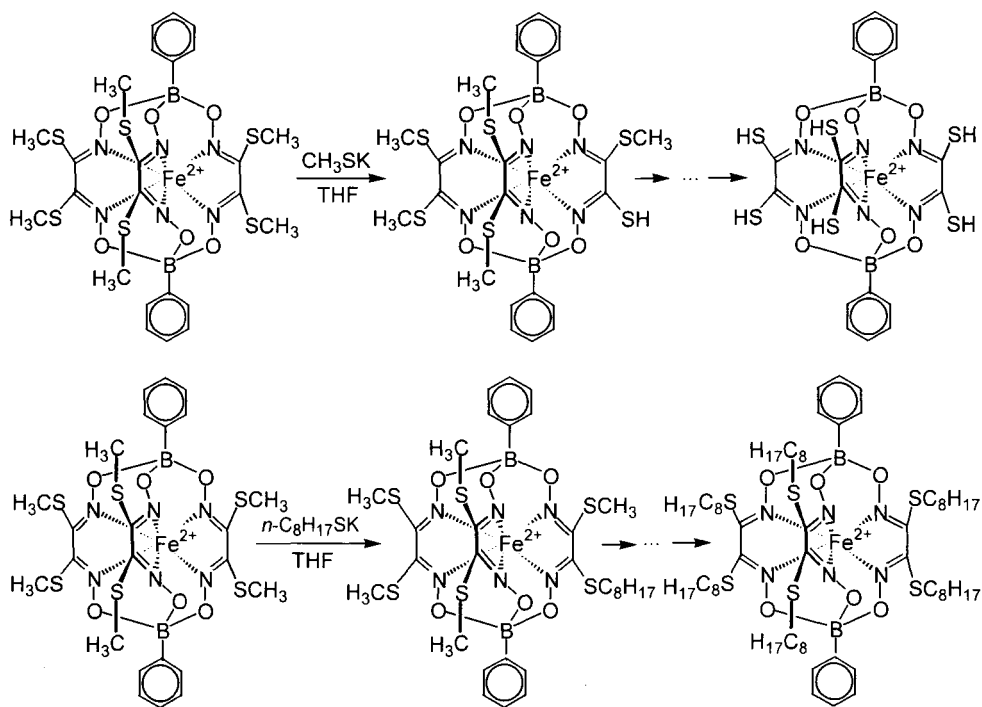
Scheme 14

The reaction of a *n*-butylboronic precursor with potassium phenolate led to the formation of hexaphenol Fe((C₆H₅O)2Gm)₃(B*n*-C₄H₉)₂ complex (Scheme 13). Attempts to obtain of the *n*- and *t*-butoxy-containing clathrochelates met with failure because of the destruction of precursors.

The well-known synthetic procedures for crown ethers and their analogs allowed one to synthesize clathrochelates with dioximate fragments of the oxo- and thioether crown type (Scheme 13). The interaction of phenylboronic and *n*-butylboronic precursors with 3 mols of the sodium salt of bis-(2-(*o*-oxyphenoxy))diethyl ether for 5 h in THF at 50-60° led largely to the formation of C_3-nonsymmetric tworibbed-substituted products (Scheme 13). The reactions of *n*-butylboronic precursor were studied in more detail. The use of a 30% excess of the sodium salt of bis-(2-(*o*-oxyphenoxy))diethyl ether and an increase in the reaction time up to 30 h permits one to isolate a tricrown ether clathrochelate (Scheme 13). Tetrabutylammonium salt ((*n*-C₄H₉)₄N)Cl was used as an interphase catalyst for the

condensation reaction. The by-products of this reaction mainly resulted from the condensation reaction of one of the two deprotonated oxy groups of bis-(2-(o-oxyphenoxy))diethyl ether and the dichloroglyoximate fragments of the precursor. Such open-chain compounds are readily soluble in methanol. Attempt to use the sodium triflate at a high concentration and to create the appropriate conditions for a template condensation on the sodium ion through orientation of the terminal oxygen atoms met with failure [65].

The template condensation of n-butylboronic precursor with 3,5-dithiaoctane-1,8-dithiol in the presence of Cs_2CO_3 allowed to obtain in a low yield tris-(12-an-S_4)-containing clathrochelate as a representative of a promising series of models of "blue" proteins [65].

The appropriate conditions for the synthesis of tris-azamacrocyclic clathrochelates containing dioximate fragments in polyazamacrocyclic rings were not selected. Attempts to use open-chain polyamines, as well as their complexes with transition metals, primarily Ni^{2+}, gave no desired results.

The reaction of a phenylboronic precursor with an excess of n-butylamine unexpectedly led to the preferential formation of the tetrasubstituted clathrochelate by the modification of two of the three dichloroglyoximate fragments (Scheme 13). A similar product was also obtained in the case of cyclohexylamine. Attempts to obtain a hexa-n-butylamine clathrochelate were not successful. The interaction of precursors with aniline and its derivatives has resulted in the formation of a mixture of di- and trisubstituted products, which failed to be isolated as individual compounds [65].

Clathrochelate ribbed-functionalized tris-dioximates have attracted interest because they offer scope for the synthesis of polynuclear complexes with targeted structural parameters and physicochemical properties (see above). In most instances, it is not necessary to functionalize all α-dioximate fragments, and it appears to be sufficient to modify only one of the three ribs in the clathrochelate framework to alter the properties significantly. Several feasible synthetic routes to clathrochelate monoribbed-functionalized tris-dioximates have been proposed in Ref. 68. A direct template condensation of the mixture of α-dioximes with Lewis acids on a metal ion (Scheme 15, Route I) leads to the formation of a poorly separable mixture of nonsymmetric and symmetric products, in which the latter predominate. Halogenation of the initial clathrochelate
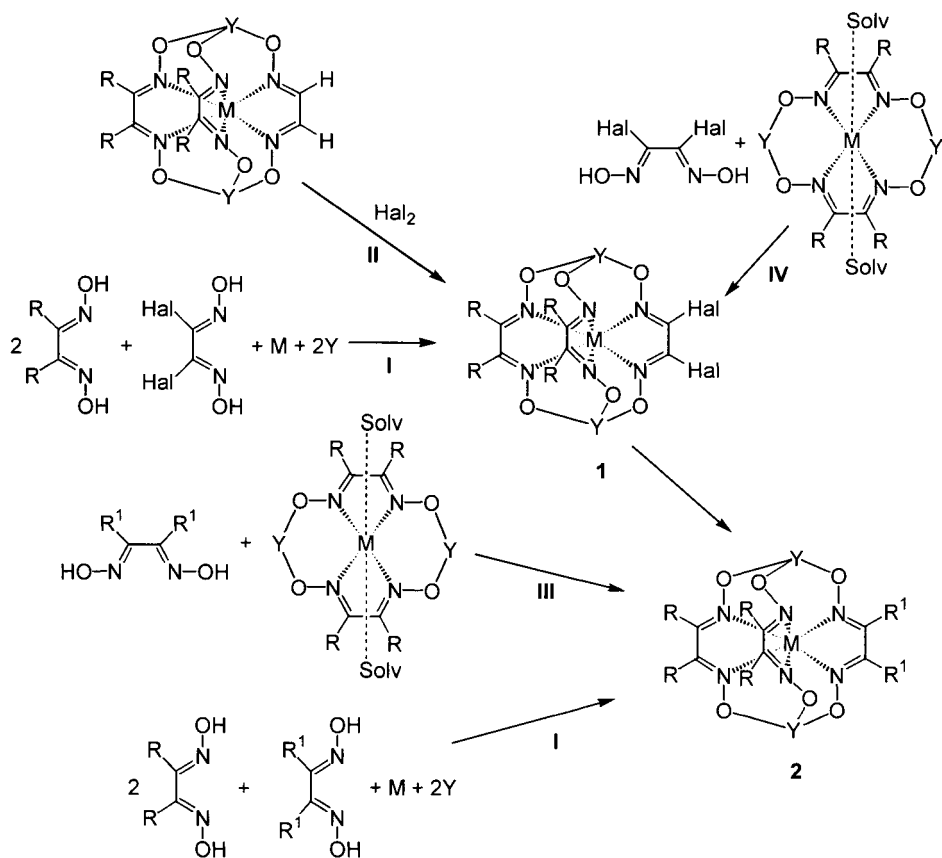
R=aliphatic or aromatic substituent; (R,R)=alicyclic fragment

R^1=functionalizing substituent; (R^1,R^1)=crown etheric or another macrocyclic fragment

Y=Lewis acid

Scheme 15

monoglyoximate (Scheme 15, Route II) is complicated, since by-products are readily generated from partial halogenation of a glyoximate moiety and aliphatic and aromatic substituents in two other dioximate fragments as well. The methods of preparation developed for C_3-nonsymmetric clathrochelates (see above) may be used for the synthesis of desired tris-dioximates 1 and 2 from square-planar macrocyclic bis-dioximates and are thought to be the most promising ones (Scheme 15, Routes III and IV). Route III makes use of the condensation of the functionalized α-dioxime with the macrocyclic bis-dioximate. However, the appearance of additional coordinating groups and side reactions associated with

functionalising substituents drastically reduces the desired product yield. Route IV at the first stage produces a reactive dihalogenide precursor that readily undergoes modification by well-known procedures (Scheme 16). This route was chosen for the synthesis of a series of monoribbed-functionalized clathrochelate iron(II) dioximates [68]. The synthesis of the dichloride precursor was implemented from dichloroglyoxime and macrocyclic iron(II) $FeBd_2(BF)_2)_2AN_2$ bis-α-benzyldioximate. Last complex was chosen as the starting compound because of its availability and relative stability to a side reaction of disproportionation to yield a symmetric $FeBd_3(BF)_2$ clathrochelate as by-product [68].

The dichloride precursor readily reacted with sterically unhindered primary amines to form disubstituted products (Scheme 16).

Secondary amines underwent a reaction that involved the substitution of only one of the two chlorine atoms. The reaction of precursor $FeBd_2(Cl2Gm)(BF)_2$ with an excess of *aza-18-C-6* and diethylamine resulted in the formation of the monocrown-substituted $FeBd_2((aza-18-C-6)ClGm)(BF)_2$ clathrochelate and the monodiethyl-amine-containing $FeBd_2(((C_2H_5)_2N)ClGm)(BF)_2$ complex. An attempt to isolate the corresponding disubstituted complexes was not successful. These monofunctionalized complexes may undergo further functionalization, especially with primary aliphatic amines. The use of primary aliphatic diamines allows one to obtain the functionalized spacer-containing $FeBd_2(((C_2H_5)_2N)(NH(CH_2)_5NH_2)Gm)(BF)_2$ clathro-chelate and $(FeBd_2(((C_2H_5)_2N)Gm)(BF)_2)_2(NH(CH_2)_5NH)$ bis-clathro-chelate [68].

The synthesis of the functionalized macrobicyclic $FeBd_2(CwGm)(BF)_2$ compound containing one crown ether dioximate fragment was carried out using the approach proposed for triribbed-functionalized clathrochelates (see above).

Reaction of the $FeBd_2(Cl2Gm)(BF)_2$ precursor with potassium aliphatic thiolates such as CH_3SK and $n\text{-}C_8H_{17}SK$ was complicated by side reactions of stepwise dealkylation of the resulting products in an excess of the thiolate ion. For the methylthiol $FeBd_2((CH_3S)2Gm)_2(BF)_2$ complex, this process occurred most readily.

This clathrochelate also readily underwent de- and realkylation, especially with *n*-octylthiolate ion in DMF (Scheme 17) like the triribbed-functionalized clathrochelates. The purification can be improved and the yield of the desired product increased by the
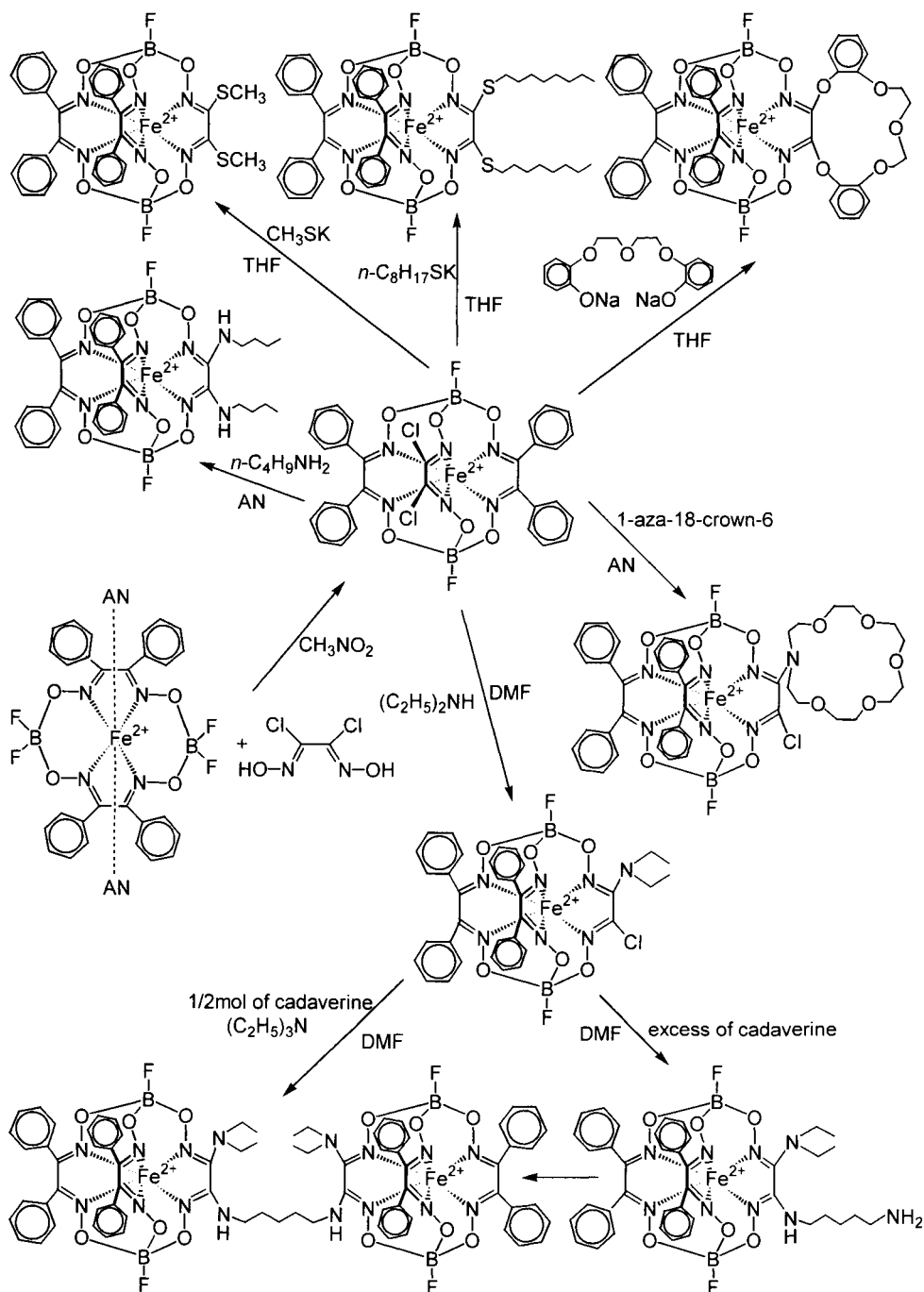
Scheme 16
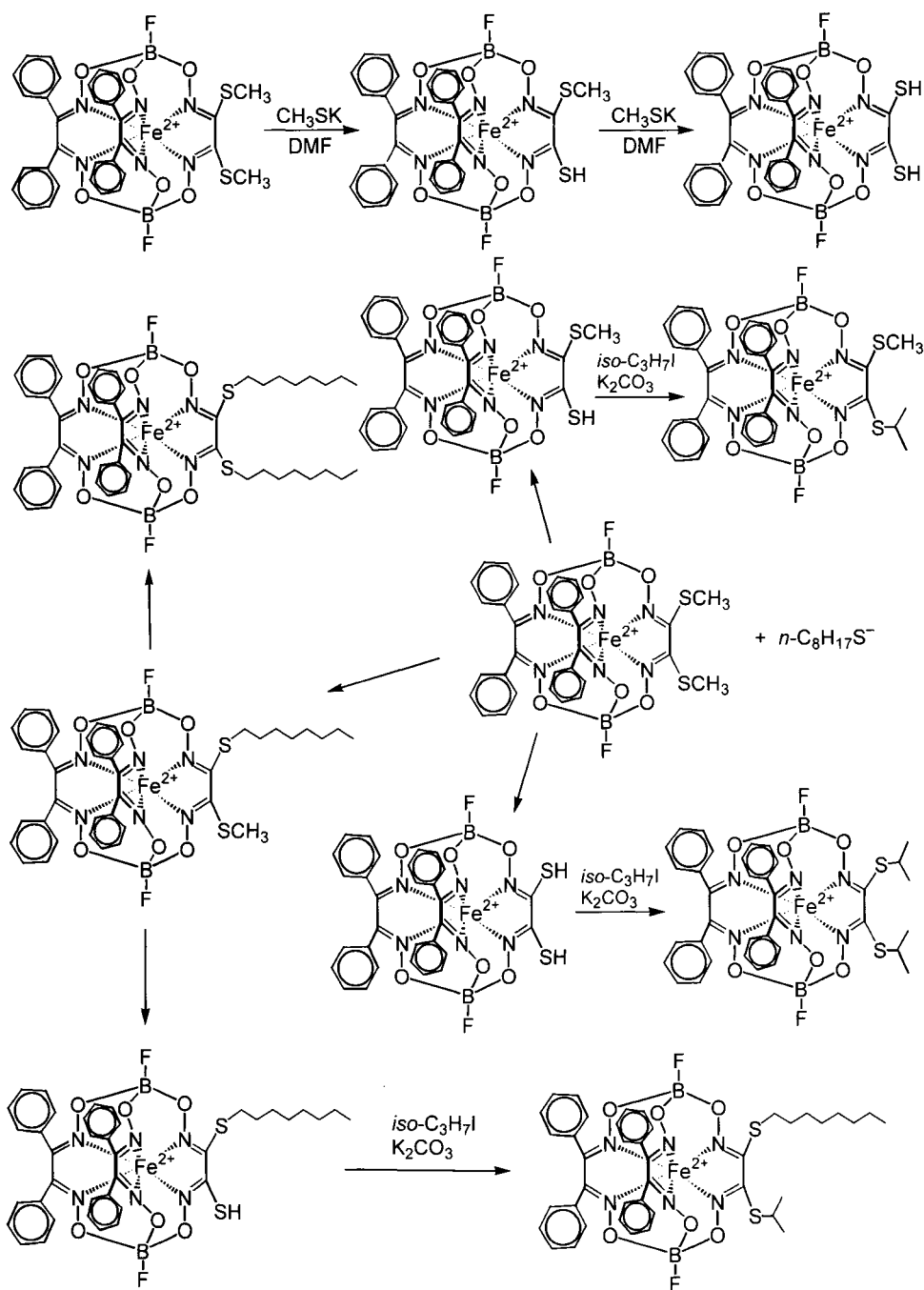
Scheme 17

addition of the corresponding alkyl iodide at the final stage of this process [68].

A systematic study of the effect of both aliphatic amines and the nature of the solvent on the products of reactions with reactive di- and hexachloride clathrochelates was performed [69].

The reactions of phenyl-, n-butyl- and fluoroboron-capped hexachloride iron(II) precursors with aliphatic amines proceeded under steady-state conditions of the solvent, temperature, and reaction time to produce clathrochelates of only one type irrespective of the nature of the substituent at the boron atom (Scheme 18). Therefore, the reactions of the phenylboronic $Fe(Cl2Gm)_3(BC_6H_5)_2$ precursor were studied. The reaction of precursor with n-butylamine in DMF, benzene, THF, and n-butylamine as the solvent led to the formation of only tetrasubstituted clathrochelate, whereas the reaction in chloroform unexpectedly resulted in trisubstituted clathrochelate, which underwent further functionalization in DMF with n-butylamine and cyclohexylamine but did not react with diethylamine (Scheme 18).

The reaction of phenylboronic precursor with primary alicyclic cyclohexylamine in DMF and $CHCl_3$ also led to the formation of tetra- and trisubstituted clathrochelates, respectively (Scheme 19). Trisubstituted clathrochelate underwent further functionalization in DMF with an excess of n-butylamine and aliphatic diamine (cadaverine). Thus, the overall reaction pathway in the previously mentioned reactions with primary sterically unhindered aliphatic amines involved a stepwise substitution in two of the three dichloroglyoximate fragments of hexachloride clathrochelates [69].

In the case of a sterically unhindered secondary aliphatic amine, in particular diethylamine, and of a sterically hindered t-butylamine, the reaction proceeded via a different pathway (Schemes 20 and 21). First, the reaction stopped at an earlier stage: trisubstituted and disubstituted clathrochelates were formed in DMF and $CHCl_3$, respectively. Second, in the case of t-butylamine, the reactions in chloroform and DMF gave di- and trisubstituted clathrochelates, respectively, with the substitution in two of the three dichloroglyoximate fragments (Scheme 20). But in the case of t-butylamine trisubstituted complex, together with substitution products in two of the three dioximate moieties, fac- and mer-isomers of this complex with t-butylamine substituents in three dioximate fragments were identified (Scheme 21). In the case of diethylamine,
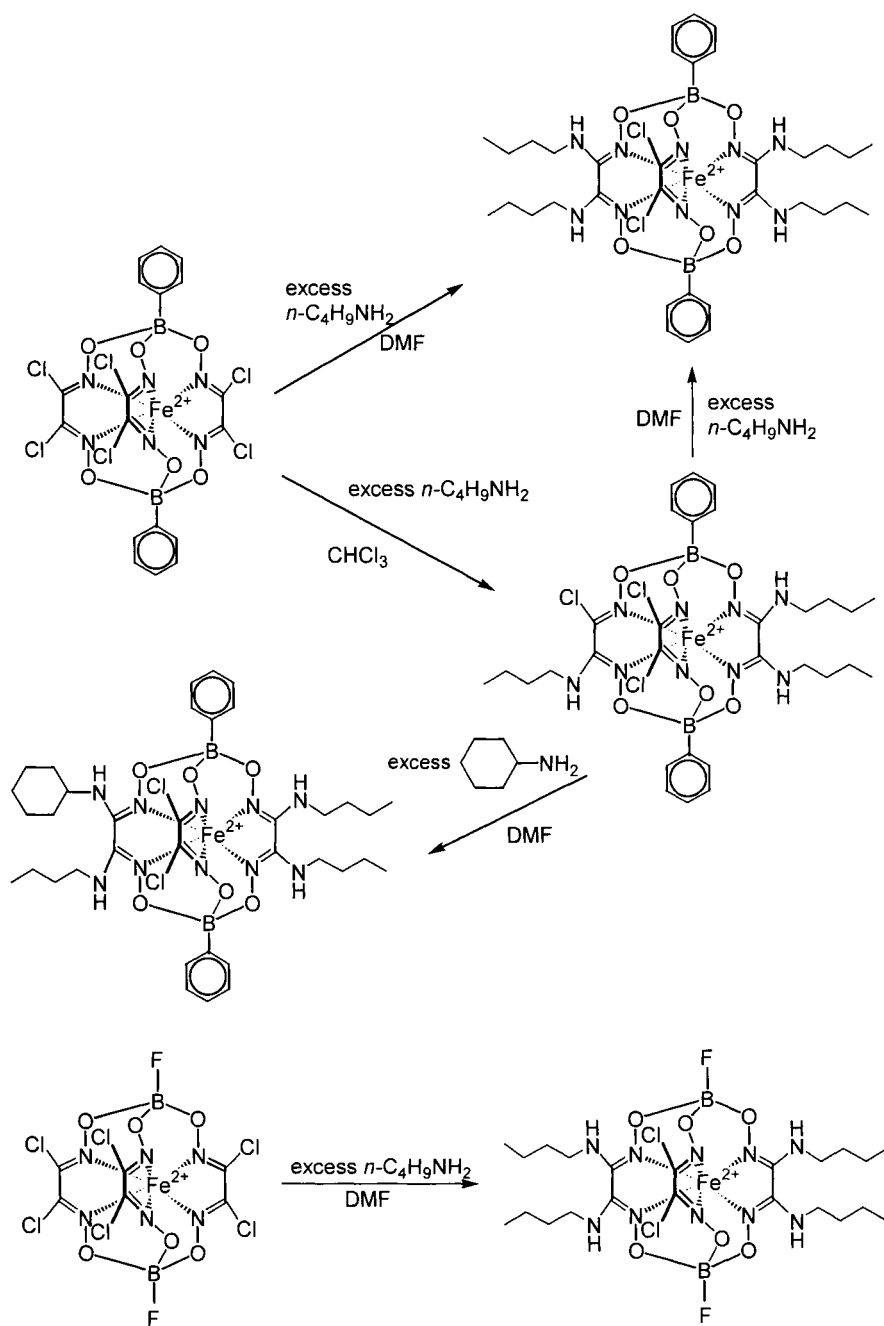
Scheme 18
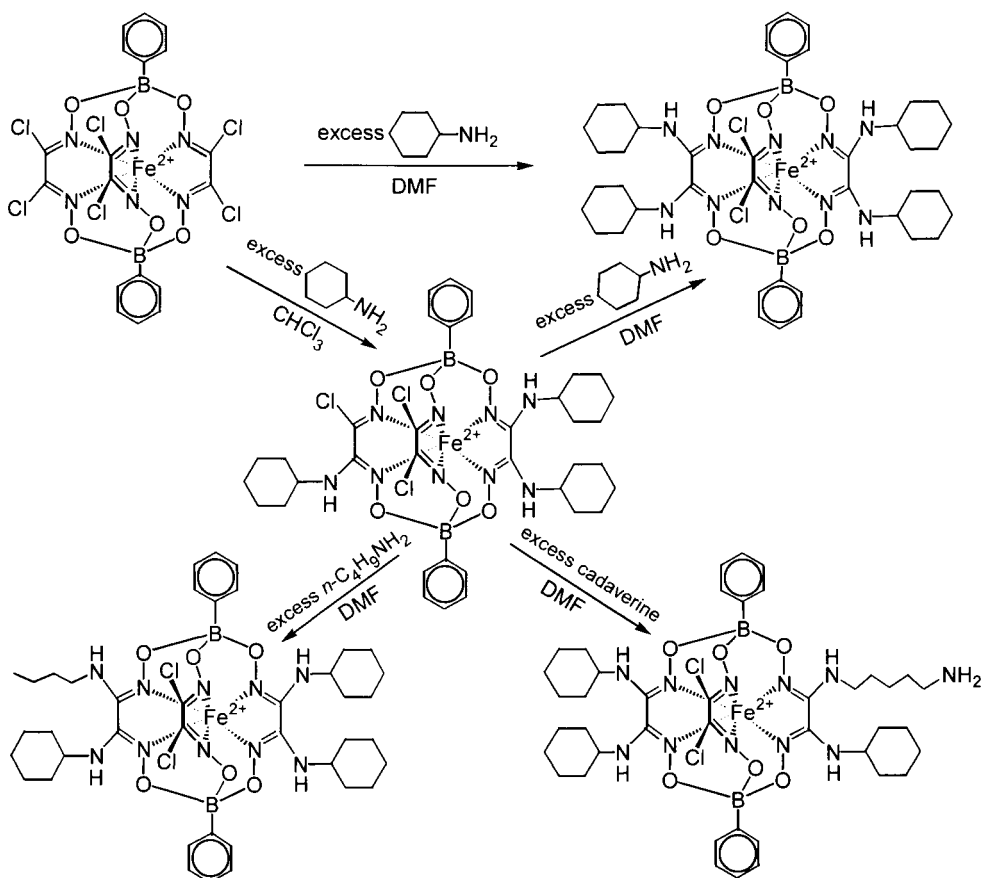
Scheme 19

only a *mer*-isomer of trifunctionalized clathrochelate with substitution in the three dioximate fragments was obtained (Scheme 20). The resultant clathrochelates underwent further modification with a more reactive amines (Schemes 20 and 21). Analogous trisubstituted clathrochelates were also obtained *via* the reaction of phenylboronic precursor with dimethylamine and morpholine in DMF, 1,4-dioxane, and THF [69].

Dichloride FeBd$_2$(Cl2Gm)(BF)$_2$ precursor readily reacted with aliphatic primary amines of different natures in the DMF and THF to produce disubstituted clathrochelates (Scheme 22). The secondary amines react with dichloride precursor to substitute one of the two reactive chlorine atoms, and this permits one to obtain spacer-containing clathrochelate and bis-clathrochelate (Scheme 23). An alternative pathway for the synthesis of bis-clathrochelates uses
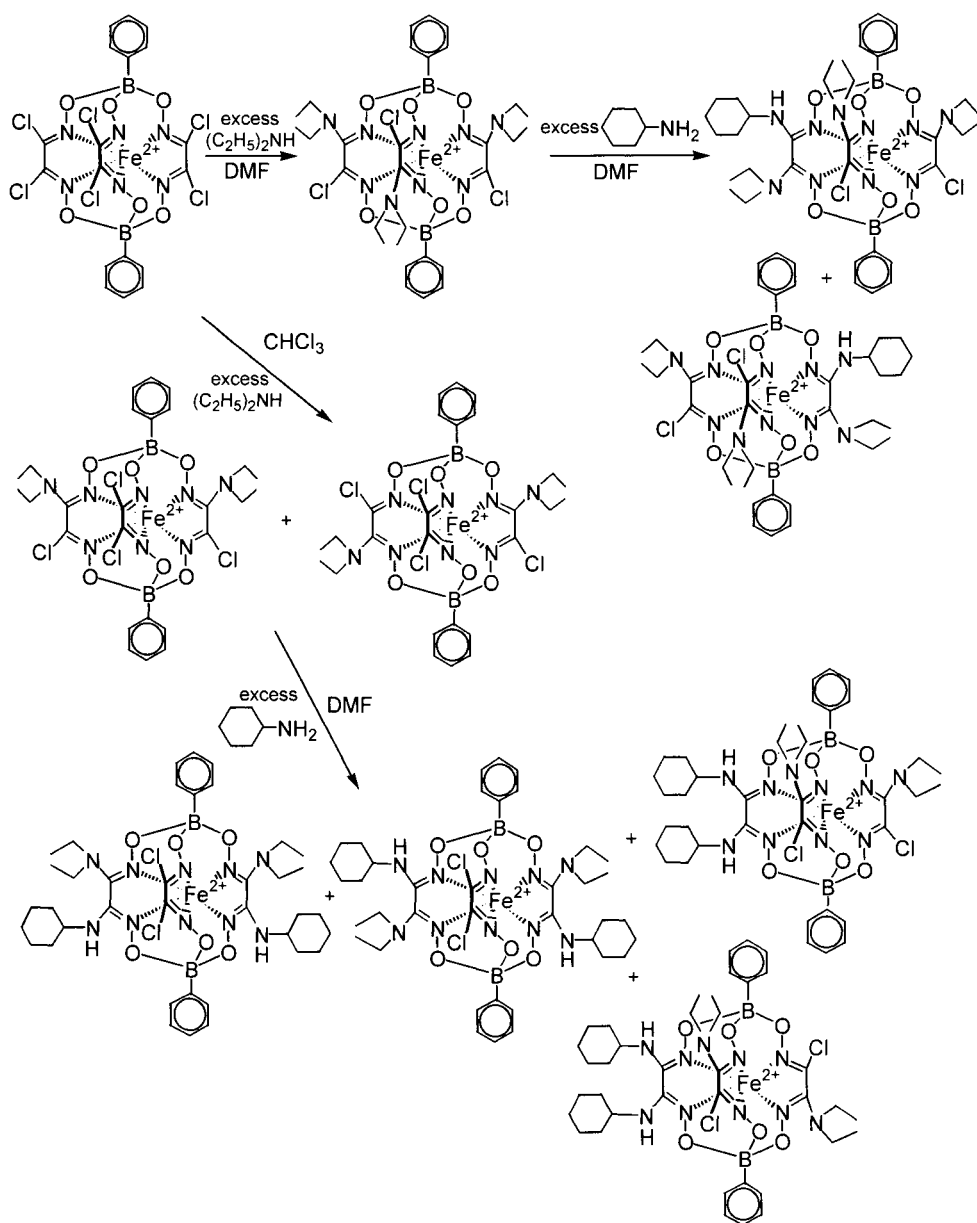
Scheme 20

secondary diamines, in particular piperazine (Scheme 23). In this case, monosubstituted bis-clathrochelate has been formed in both DMF and chloroform.

The causes of such unexpected influences of the nature of both amines and solvents on the reaction products are discussed in Ref. 69.

42
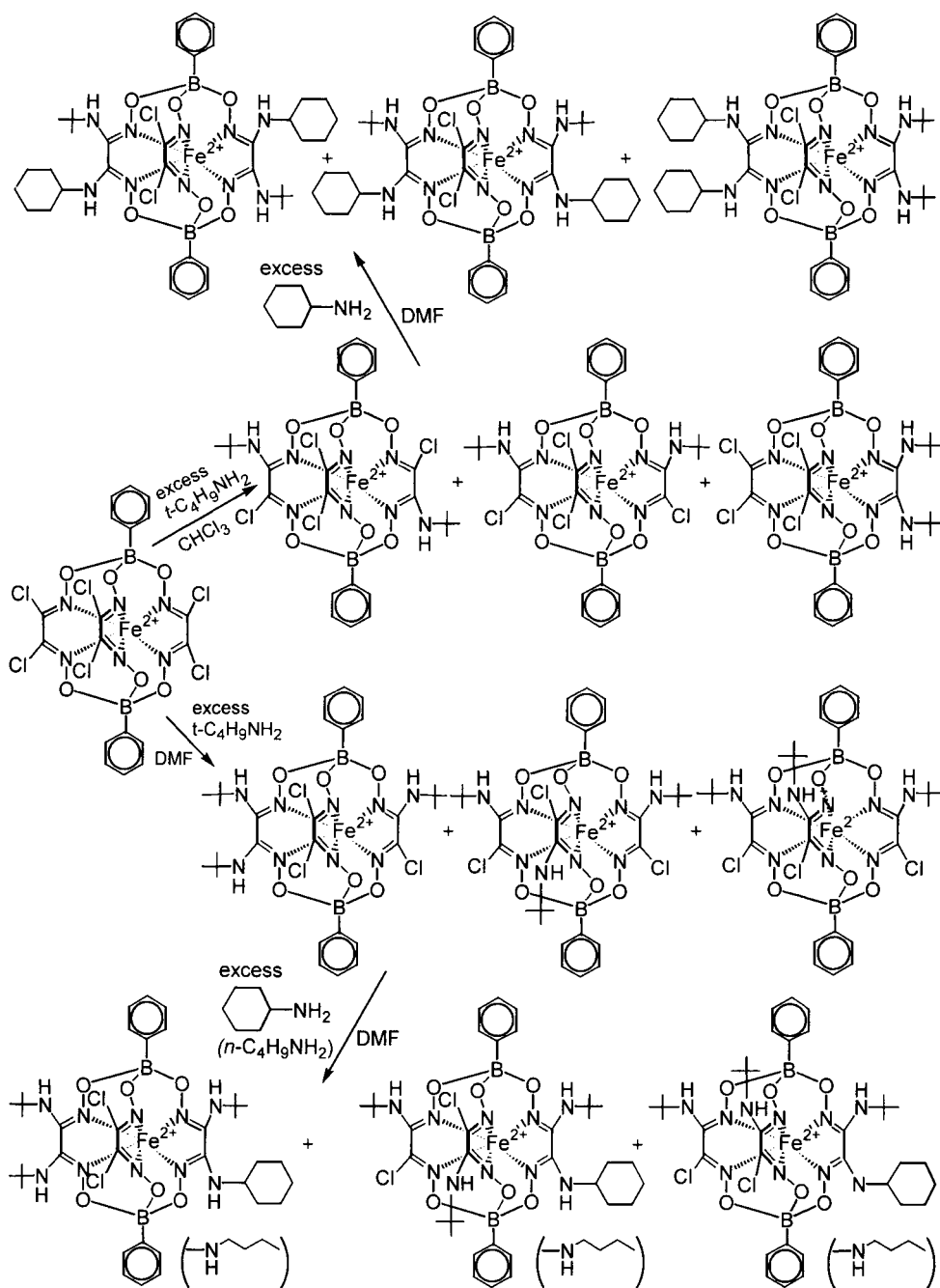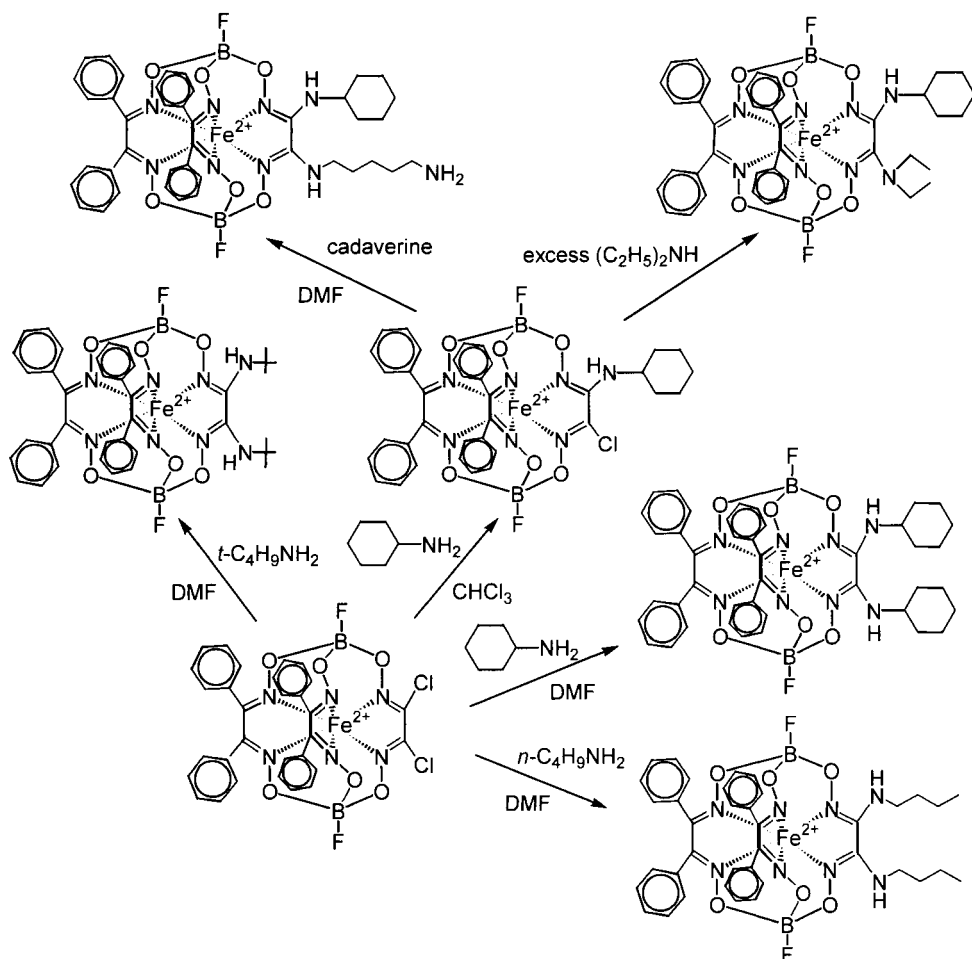
Scheme 21

Scheme 22

The nucleophilic substitution of the reactive chlorine atoms in hexa- and dichloride clathrochelates by a series of aliphatic amines is very sensitive to the effects of the medium (primary, the solvent employed), and the trend of the reaction is determined to a great extent by the donor properties of the amines and the steric accessibility of the nucleophilic centre. The subsequent substitution reaction course and feasible reaction products in the case of hexachloride precursors are presented in Scheme 24. The stepwise-formed clathrochelate complexes are denoted according to the degree of the substitution of chlorine atoms by amine groups:
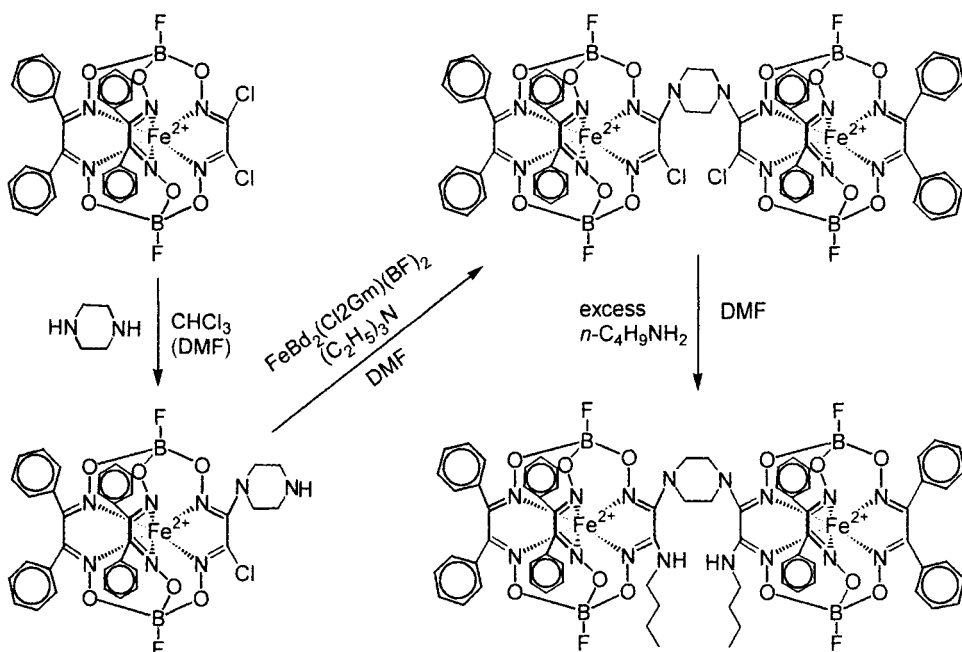
Scheme 23
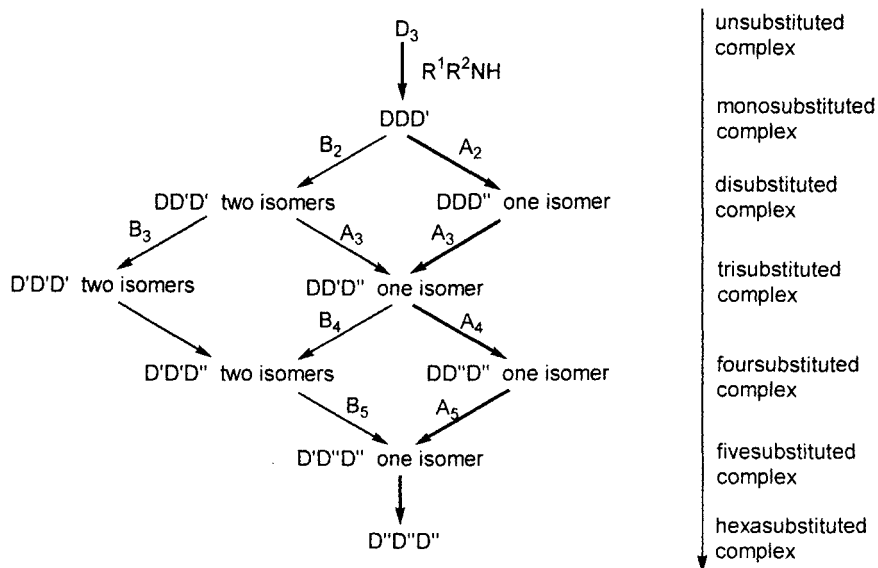
Scheme 24

- D stands for a dichloroglyoximate fragment, $Cl2Gm^{2-}$;
- D' corresponds to a monosubstituted dioximate fragment, $(R^1R^2N)ClGm^{2-}$;
- D" denotes a diamine fragment, $(R^1R^2N)2Gm^{2-}$.

According to Scheme 24, 12 reaction products can be formed. The following results were established:

1. The reactivity of partially substituted iron(II) clathrochelates is essentially dependent on the degree of substitution with primary sterically unhindered aliphatic amines in donor solvents. In the case of hexachloride precursors, a tetrasubstituted product is formed and is inert to further actions of amines.

2. Different chlorine-substituted fragments in partially substituted complexes have similar reactivities, and the direction of the reaction is not determined by the electron density on the carbon atoms (i.e., their electrophilic properties) but by more specific effects: an intramolecular activation *via* hydrogen bonds in the case of sterically unhindered primary amines and sterical hindrances in the case of secondary and sterically hindered primary amines. The reaction with sterically unhindered primary amines occurs *via* the route A_n through the substitution of a halogen atom from an already monofunctionalized fragment. In the case of secondary and sterically hindered primary aliphatic amines, the reaction proceeds *via* the route B_n with sterically controlled substitution.

3. The reactions of nucleophilic substitution with participation of reactive clathrochelates are very sensitive to the donor properties of an attacking amine. With aromatic amines, as well as secondary and primary sterically hindered amines in acceptor solvents, and hexachloride precursors, the reaction stops with the formation of disubstituted products. When secondary and sterically hindered primary aliphatic amines are used in donor solvents and sterically unhindered primary aliphatic amines in acceptor solvents, the reaction terminates at trisubstituted products. In the case of sterically unhindered aliphatic amines, tetrasubstituted clathrochelates are formed. With dichloride precursor $FeBd_2(Cl2Gm)(BF)_2$, the primary aliphatic amines in donor solvents form diamine clathrochelates, whereas the secondary amines (diethylamine or piperazine) give only monoamine complexes both in acceptor and donor solvents.

In the case of primary aliphatic amines, the reaction products are dramatically affected by the solvent employed. For instance, in the presence of solvents apt to produce a specific solvation of amines (chloroform, and an amine chlorohydrate solution in methylene dichloride), the reaction with hexachloride precursors terminates to yield the trisubstituted product DD'D" formed *via* route **A**. At the same time, the use of some other solvents (such as benzene, 1,4-dioxane, THF, methylene dichloride, DMF, and alcohols, or the corresponding amine media) led to the formation of the sole tetrasubstituted product (DD"D"). In addition, in the case of sterically unhindered primary amines an alternative isomer (D'D'D") is not isolated, which indicates reaction route **A** and a specific control of the tie reaction in the transition state by solvation interactions and intramolecular hydrogen bonds. In the case of the dichloride $FeBd_2(Cl2Gm)(BF)_2$ precursor, with both primary (cyclohexylamine) and secondary (diethylamine and piperazine) aliphatic amines, only a monosubstituted product of the Bd_2D' type is formed in chloroform, whereas in some other solvents, a diamine clathrochelate of the $Bd_2D"$ type is obtained with both sterically hindered and unhindered primary aliphatic amines.

4. A kinetic control of the reaction in the transition state was suggested in Ref. 69, since the reactions of trisubstituted DD'D" complexes with primary and secondary amines, as well as complexes of the DD'D' type with primary amines in donor solvent, yielded "regular" tetrasubstituted clathrochelates DD"D" or $DD_1"D_2"$. Accordingly, monosubstituted complexes of the Bd_2D' type in donor solvents have interacted with primary amines to produce C_2-symmetric or C_2-nonsymmetric $Bd_2D"$ clathrochelates depending on the nature of amine. The secondary aliphatic amines in the donor solvents have interacted exclusively with complexes of the Bd_2D' type formed by primary amines only.

Thus, one can state that an inductive effect of the substituents is distributed uniformly throughout the whole macrobicyclic system, and, unlike the well-studied substitution in aromatic systems, there is no pronounced *ortho, para*, and *meta* effects of the substituents in clathrochelates. A key role in the transfer of electromeric interactions in a clathrochelate molecule is played by the encapsulated central metal ion, rather than a σ, π-bond system. Therefore, the electron interactions in the clathrochelate molecule are distributed isotropically rather than alternately [69].

As a result, thermodynamic control of the reactivity of a clathrochelate is affected by the sum of the partial effects of the substituents introduced, whereas kinetic control in the transition state is determined by steric factors, solvation, and orientation effects. Most unexpected proved to be a preferential orientation of the second amine substituent in the *vic*-position relative to the first introduced. This phenomenon is explained by the orientation effects of a hydrogen bond in the transition state (Scheme 25). The necessary transition state is facilitated by the occurrence of a hydrogen bond with the amino group involved. This determines the trend of the reaction *via* the route **A**. As for the use of solvents, hydrogen bond acceptors ($CHCl_3$ and $CH_2Cl_2/RNH_2^+Cl^-$) lead to a decrease in the nucleophilic properties of the solvated amine and hamper the orientation of the reacting species in the transition state. As a result, the reaction stops at an earlier stage: trisubstituted products in the case of hexachloride precursors and monoamine clathrochelates in the case of dichloride precursors are formed in the reaction with primary sterically unhindered aliphatic amines [69].

The synthesis of boron-capped clathrochelate iron(II) tris-dioximates has been realized for wide range of substituents at the boron atom. The attempts to obtain analogous trialkyl- and triaryl-tin-capped iron(II) compounds have not been successful. In the some cases, polymeric clathrochelate compounds have been formed, especially when reactions proceed under basic conditions. With tin(IV) iodide, the primarily formed soluble green complexes also readily transform into polymeric red compounds that are presumably associated with the detachment of iodide ions because of steric hindrance between substituents in dioxime fragments and the bulky iodide atoms of capping groups [70].

Attempts to use other tin halogenides (preferentially tin(IV) tetrachloride) as capping agents have turned out to be more
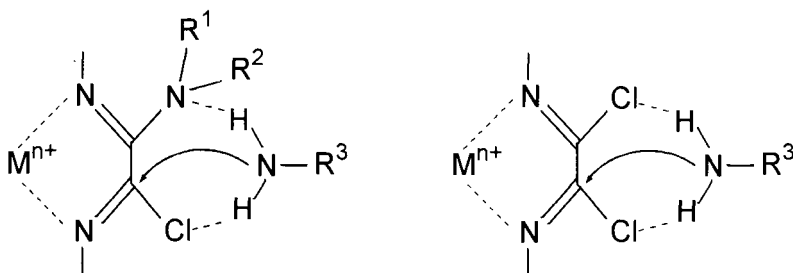
Scheme 25

successful. In the case of acyclic and alicyclic α-dioximates, tribromotin-capped complexes, like their trichlorotin-capped analogs, have also readily formed. Contrariwise, aromatic dioximes with bulky substituents as a phenyl or furyl radicals did not formed tribromotin-capped clathrochelates because of steric hindrances. In the case of SnF_4, reactions proceed with greater difficulties. A relatively high yield was obtained for the complex with nioxime, which has a *cis*-configuration that implies a higher stability of the resultant complex. As for acyclic dioximes, the reaction with SnF_4 in the presence of Fe^{2+} ion was carried out only for dimethylglyoxime and methylglyoxime. Unlike the germanium-capped clathrochelates, the corresponding complexes with other acyclic α-dioximes have failed to arise by a remetallation reaction [70]. In particular, an attempt to employ the reaction between alkoxyboron-capped $FeBd_3(BOCH_3)_2$ complex and an excess of SnF_4 in ethanol for the preparation of the corresponding trifluorotin-capped macrobicyclic complex met with failure. It appears that the difficulties encountered in the formation of trifluorotin-capped complexes are accounted for by the rupture of a strong Sn–F bond and the detachment of the fluoride ion. Besides, the fluoride anion is capable of removing SnF_4 from the reaction, and it favours the occurrence of side reactions.

Unlike the synthesis of $(HAm)_2[FeD_3(SnCl_3)_2]$ compounds, the reactions carried out with SnF_4 and $SnBr_4$ require a prolonged refluxing at the first stage; otherwise, semiclathrochelate complexes might be formed. It was noted that when the initial iron(II) salt with a halogen different from that in tin(IV) tetrahalogenide was used, a mixture of products with various state of substitution of one halogenide ion by another in the capping group (as seen from ^{119}Sn NMR spectra) resulted [70].

$$Fe^{2+} + 3H_2D + 2SnCl_4 + 6DEA \longrightarrow (HDEA)_2[\ldots] + 2Cl^- + 4HDEA^+ \quad (16)$$
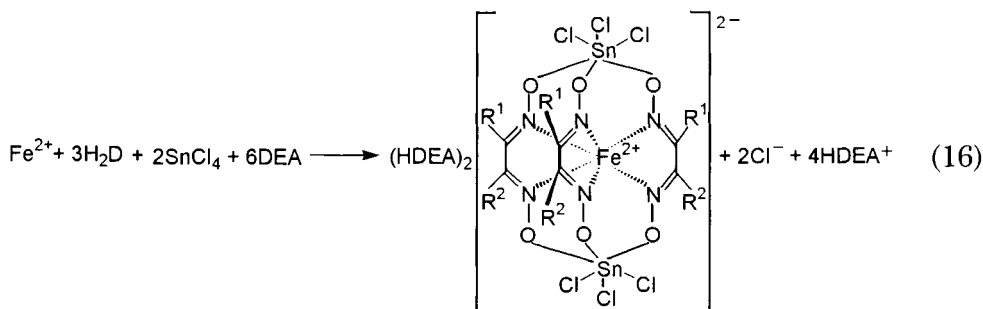
Diethylamine and tetra-*n*-butylammomium salts of the clathrochelate $[FeD_3(SnCl_3)_2]^{2-}$ dianion were obtained by template

condensation of a variety of acyclic, aromatic and alicyclic dioximes (H_2Gm, H_2Mm, H_2Dm, H_2Bd, H_2Fd, H_2Nx, H_24MNx and H_2Ox) with tin(IV) tetrachloride on the Fe^{2+} ion in *iso*-propanol [71] (Reaction 16).

The nioximate dianion was also isolated as a salt with a HPy^+ cation.

Clathrochelate $(HAm)_2[FeD_3(SnCl_3)_2]$ complexes were also formed by cross-linking of the initial nonmacrocyclic iron(II) tris-dioximates with tin(IV) tetrachloride either in acetone or in an acetone-benzene mixture with subsequent addition of amine [71]:

$$[Fe(H_2D)_3]^{2+} + 2SnCl_4 + 6Am \longrightarrow (HAm)_2[FeD_3(SnCl_3)_2] + 2Cl^- + 4HAm^+ \tag{17}$$
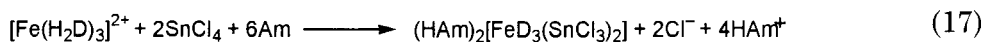
Direct Reaction 16 is likely to proceed *via* an intermediate step, i.e., the formation of a protonated tris-complex. Although the product yield of Reaction 17 is higher, Reaction 16 is preferred because of the difficulties encountered in the isolation of nonmacrocyclic iron(II) tris-dioximates. Tin-capped complexes also arise from the interaction of the Tchugaev type $Fe(HD)_2Am_2$ bis-dioximates with tin(IV) tetrachloride, and from the labile boron-capped $FeD_3(BOR)_2$ complexes with a great excess of $SnCl_4$.

The cross-linking of iron(II) tris-dioximates with germanium tetrachloride occurs *via* a somewhat unexpected pathway: instead of the expected formation of the clathrochelate $[FeD_3(GeCl_3)_2]^{2-}$ dianion, in the case of certain dioximes (H_2Nx, H_2Dm and H_2Mm) the direct reaction in the alcohol medium yielded polymeric $[FeD_3(Ge_2O_3) \cdot xSolv]_n$ complexes. Deep red-coloured clathrochelate $[FeD_3(GeCl_3)_2]^{2-}$ dianions have been observed in both DMF and DMSO media. However, attempts to isolate monomeric $(HAm)_2[FeD_3(GeCl_3)_2]$ complexes from such solutions were not successful. In all cases, only polymeric compounds were obtained. The germanic acid, formed upon dissolution of GeO_2 in water, can also serve as the capping agent that favours the formation of such polymeric compounds. It appears that germanium(IV) alcoholates can also act as capping agents; however, the formation of monomeric compounds in this case is impossible since these alcoholates are apt to hydrolyze. The cross-linking of the nonmacrocyclic iron(II) tris-dioximates implemented for nioximate turned out to be more efficient than a direct template reaction [72].

A direct template synthesis has failed for α-benzyldioxime and glyoxime, for which germanium-capped clathrochelate complexes were prepared by remetallation (capping group exchange) reactions.

$n(Fe^{2+} + 3H_2D + 2GeCl_4[H_2GeO_3])$

$n([Fe(H_2D)_3]^{2+} + 2GeCl_4[H_2GeO_3])$

$n(FeD_3Y_2 + excess\ GeCl_4)$ $\xrightarrow{R^2OH}$

$Y = BOR;\ SnHal_3$
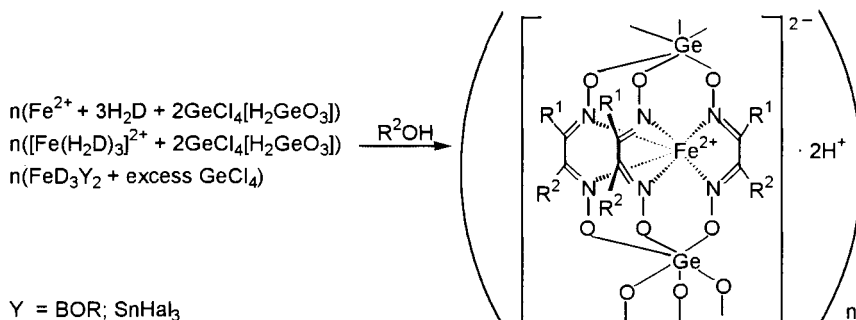
Scheme 26

In this case, a two-stage detachment of the capping groups of the initial clathrochelate complex presumably takes place with the simultaneous cyclization with another capping agent (Scheme 26).

The high stability of the complexes formed in the acidic medium was emphasized. This stability may account for the formation of certain polymeric structure upon capping with germanium tetrachloride accompanied by the detachment of H^+ ions. The formation of polymeric clathrochelate compounds has also been observed when $(HAm)_2[FeD_3(SnHal_3)]$ compounds in water or Fe^{2+}-H_2D-$SnHal_2$ systems in methanol have been treated with strong bases (e.g., NaOH and C_2H_5ONa). In the second case, tin(II) ion has been oxidized by air oxygen to a tin(IV) ion that acts as the capping agent. However, in the case of tin-capped compounds, brightly colored clathrochelate complexes partly retain in the aqueous solution [1].

The use of electron-accepting perfluoroalkyl substituents instead of the electron-donating alkyl ones increases the Lewis acidity of the corresponding cross-linking agents. It was suggested that $IGe(CF_3)_3$ may be a promising capping agent in the synthesis of monomeric germanium(IV) compounds. Trifluoromethyl substituents form one of the two triangular bases of the resultant octahedral coordination polyhedron of the capping germanium atom and, since the Ge–C bond is inert in substitution reactions, impede the polymerization reactions, which are typical for germanium halides and alcoholates. Thus, the perfluoroalkyl groups have proved to be protecting and activating at the same time [73].

---

[1] The known analytical reaction for a qualitative determination of microamounts of iron with dioximes after reduction with tin(II) chloride responsible for the intense coloring of the solution is, in our opinion, caused by the formation of such clathrochelate complexes.

The first monomeric tris(trifluoromethyl)germanium-capped clathrochelate was prepared by template condensation of nioxime and $IGe(CF_3)_3$ on a Fe^{2+} ion:

$$Fe^{2+} + 3H_2Nx \xrightarrow[\substack{H_2O \\ CaCO_3}]{IGe(CF_3)_3} \left[\ \right]^{2-} \ ((n\text{-}C_4H_9)_4N)^+ \longrightarrow ((n\text{-}C_4H_9)_4N)_2[FeNx_3(Ge(CF_3)_3)_2] \quad (18)$$
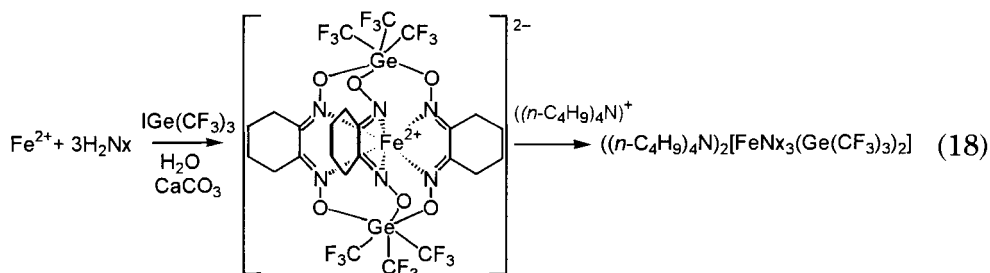
The nonmacrocyclic iron(II) tris-complex (an intermediate product in the synthesis of clathrochelates, see Chapter 4) have readily reacted with two molecules of $IGe(CF_3)_3$ in aqueous solution. In this case $IGe(CF_3)_3$ formed dianionic octahedral capping groups. The H^+ ions released in the course of the reaction were neutralized by calcium carbonate. The resultant clathrochelate $[FeNx_3(Ge(CF_3)_3)_2]^{2-}$ dianion was isolated as a salt with a bulky organic $(n\text{-}C_4H_9)_4N^+$ cation [73].

The synthesis of clathrochelates resulting from capping with antimony(V) compounds was realized for the first time as described in Ref. 74. With antimony(V) halogenides, only polymeric complexes were isolated, but antimony(V) triorganyles, unlike tin(IV) triorganyles, readily form nioximate iron(II) clathrochelates by Reaction 19.

$$Fe^{2+} + 3H_2Nx + 2R_3Sb(OH)_2[R_3SbBr_2] \xrightarrow[{[CaCO_3]}]{C_2H_5OH} \quad (19)$$

$R=C_6H_5, \ CH=CH_2, \ C_2H_5$
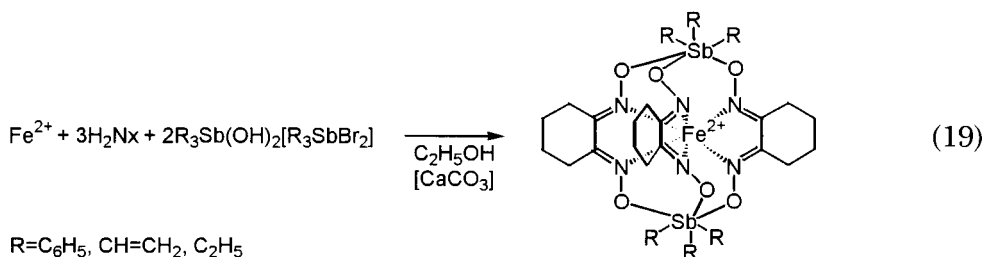
Reaction 19 was carried out in dry ethanol by the interaction of $FeCl_2 \cdot 4H_2O$ and nioxime with triphenylantimony(V) dihydroxide, and trivinylantimony and triethylantimony(V) dibromides. In the cases of dibromides, an excess of $CaCO_3$ was added [74].

As described above, the C_2-nonsymmetric boron- and boron-tin-capped clathrochelate compounds can be prepared by a solid-phase synthesis on the element oxide surface that serves as both a matrix

and a topochemical protecting group. At the same time, such a synthetic route is rather complicated, and it may be applied to only a limited number of compounds. Alternative methods for directed synthesis of C_2-nonsymmetric clathrochelates and polyclathrochelates from the preliminarily prepared semiclathrochelates and modification reactions of the apical capping fragments were proposed in Ref. 75. The lability of antimony-capped iron(II) semiclathrochelates and clathrochelates and the fact that one (targeted) complex can be isolated from several possible products in the course of reaction have determinated a successful synthesis of C_2-nonsymmetric mono- and bis-clathrochelates. Antimony-capped complexes proved to be far more labile than their boron- and tin-capped analogs, for which a remetallation (a capping group exchange) reaction has first been observed [70]. The chemical behaviour of such antimony-capped complexes occupied an intermediate position between that of the clathrochelate and that of molecular adducts, and a considerable "onic" contribution to their geometry cannot be excluded (Scheme 27).

The determination of the conditions under which the $[Fe(HNx)_3(Sb(C_6H_5)_3)](ClO_4)$ semiclathrochelate forms and can be isolated seems to be very important, since semiclathrochelate tris-dioximates except this one have readily undergone disproportionation (see Scheme 9) to yield more kinetically and thermodynamically stable clathrochelates. Even in the case of a triethylantimony derivatives with similar geometry and properties, the simultaneous occurrence of capping and disproportionation reactions could not be avoided, and, therefore, the $[Fe(HNx)_3(Sb(C_6H_5)_3)](ClO_4)$ complex proved to be the first tris-dioximate semiclathrochelate that was isolated and characterized [75]. The reaction of the $[Fe(HNx)_3(Sb(C_6H_5)_3)](ClO_4)$ semiclathrochelate with mono- and bifunctional capping agents (Lewis acids) other than $(C_6H_5)_3Sb(OH)_2$
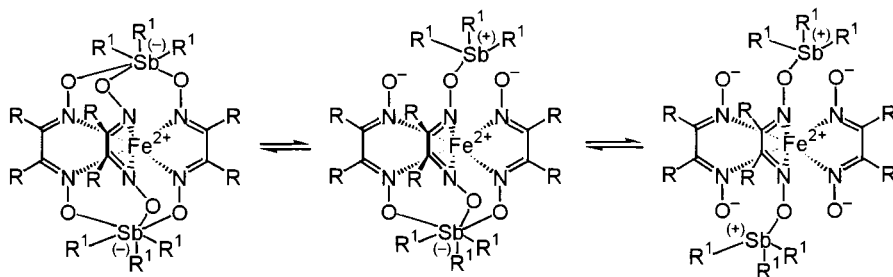
Scheme 27
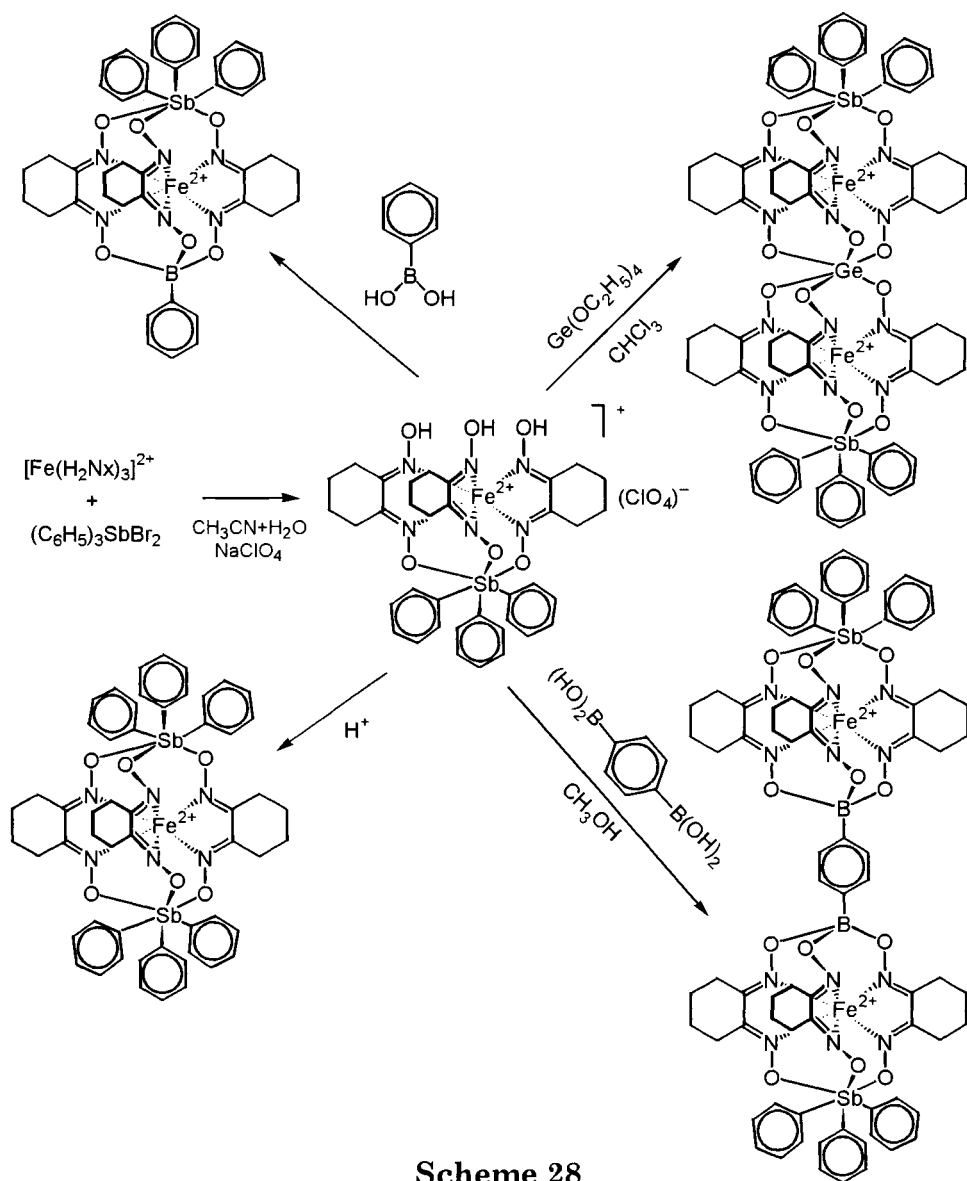
Scheme 28

and its derivatives led to the formation of C_2-nonsymmetric mono-
and bis-clathrochelates (Scheme 28).

The clathrochelates with a labile triethylantimony capping group
have undergone remetallation in the presence of silicon dioxide as a
catalyst. The reaction did not occur under mild conditions in the
absence of SiO_2, and under hard conditions it yielded a mixture of

products. The first stage leads to the formation of a surface-immobilized antimony-silicon-capped clathrochelate, which is desorbed from the surface with another capping agent to give a C_2-nonsymmetric mono- or bis-clathrochelate depending on the nature of this agent (Scheme 29).

The fact that antimony-containing Lewis acids, unlike boron-containing cross-linking agent, are apt to form semiclathrochelate (lacunar) complexes permits one to obtain a great variety of C_2-nonsymmetric mono- and polyclathrochelates and to employ them as syntones. An appreciable change in the stability to capping group dissociation in the series Sb_2-cap << SbB-cap << B_2-cap complexes allows one to employ them for the directed synthesis of polynuclear boron-capped complexes with stepwise preparation of chainlike clathrochelates (Scheme 30), the triorganylantimony capping groups of which can be regarded as protecting groups [75].

For the first time, a macrobicyclic ruthenium (II) tris-dioximate was obtained by refluxing of $RuCl_3 \cdot 3H_2O$ and nioxime in dry ethanol under argon with subsequent cooling to room temperature and treatment with phenylboronic acid [76].

Ruthenium(II) clathrochelates have also been synthesized *via* interaction of $RuDMSO_4Cl_2$ solvato-complex and nioxime, α-benzyldioxime, and dimethylglyoxime with different boron-containing capping agents in THF. The use of this solvato-complex as an initial ruthenium(II) salt substantially increases the yield of clathrochelates. For instance, in the preparation of $RuNx_3(BC_6H_5)_2$, the use of $RuDMSO_4Cl_2$ solvato-complex instead of $RuCl_3 \cdot 3H_2O$ salt enhances the yield from 12.5 to 45%. The majority of macrobicyclic ruthenium(II) $RuNx_3(BR)_2$ tris-dioximates (where R is F, CH_3, C_6H_5, n-C_4H_9, OCH_3, OC_2H_5, On-C_3H_7, *iso*-C_3H_7, On-C_4H_9, On-C_5H_{11} and On-$C_{10}H_{21}$) were obtained in high yields with nioxime. Acyclic dioximate $RuBd_3(Bn$-$C_4H_9)_2$, $RuBd_3(BOCH_3)_2$, $RuDm_3(Bn$-$C_4H_{10})_2$, and $RuDm_3(BOCH_3)_2$ clathrochelates were isolated in much lower yields [77].

A keen recent interest in polyimine ruthenium(II) complexes (tris-bipyridinates, tris-phenanthrolinates, and their analogues) has largely been evoked by the ample scope they offer as selective DNA-cleaving agents and probes in biochemistry. Such ruthenium(II) complexes, as well as their photophysics, are of particular interest in creating the devices for molecular electronics (e.g., systems of the "light-switch" type) and in analytical detection of metal ions as well.

Scheme 29

$$\text{FeD}_3(\text{Sb}(\text{C}_2\text{H}_5)_3)_2 \xrightarrow{\text{R}^2\text{B}(\text{OH})_2} (\text{R}^2\text{B})\text{FeD}_3(\text{Sb}(\text{C}_2\text{H}_5)_3) \xrightarrow{\text{R}^3(\text{B}(\text{OH})_2)_2}$$

$$(\text{R}^2\text{B})\text{FeD}_3(\text{R}^3\text{B})\text{FeD'}_3(\text{Sb}(\text{C}_2\text{H}_5)_3) \xleftarrow{\text{FeD'}_3(\text{Sb}(\text{C}_2\text{H}_5)_3)_2} (\text{R}^2\text{B})\text{FeD}_3(\text{BR}^3\text{B}(\text{OH})_2)$$

$$\xrightarrow{\text{R}^4(\text{B}(\text{OH})_2)_2} (\text{R}^2\text{B})\text{FeD}_3(\text{BR}^3\text{B})\text{FeD'}_3(\text{BR}^4\text{B}(\text{OH})_2) \longrightarrow \ldots$$

Scheme 30

In the majority of research performed, the chelating ligands have preliminarily been functionalized, and this has permitted one to obtain ruthenium(II) complexes with improved chemical and physicochemical properties. Through a highly conjugated aromatic system, both the medium (solvent and acidity) and functionalizing substituents influence the energy of the central metal ion d orbitals and ligand π,π^*-orbitals. An electronic effect of aliphatic and aromatic substituents in the dioximate fragments in the series of the above described boron-capped ruthenium(II) clathrochelates is substantially lower. Such substituents exhibit low reactivity, and their modification with variations in physicochemical parameters (and, consequently, in the corresponding characteristics of the clathrochelates itself) is rather complicated. The several procedures for the synthesis of ribbed-functionalized macrobicyclic ruthenium(II) complexes starting from the reactive chloride clathrochelates were proposed in Ref. 78.

Several pathways for the synthesis of ribbed-functionalized tris-dioximate clathrochelate complexes (i.e., clathrochelates with functionalizing substituents in α-dioximate fragments) have been thoroughly analyzed above. The optimal synthetic route is based on a preliminary isolation of a reactive halogenide precursor and its further functionalization *via* nucleophilic substitution reactions so well known in organic chemistry. The syntheses of ruthenium(II) clathrochelates are complicated by a kinetic inertness of the initial ruthenium solvato-complexes in the reactions of coordinated ligand substitution, as well as by the ability of ruthenium complexes to form intra- and intermolecular redox reactions, frequently with participation of coordinated ligands. Moreover, the Ru^{3+} ion is apt to form stable square-planar bis-dioximates. Therefore, an attempt to extend the procedures of the precursor synthesis, described above for iron(II), to ruthenium(II) ion without any modification met with failure. The poor donor ability displayed by the dichloroglyoxime does not permit one to obtain clathrochelate ruthenium(II) precursors

starting from RuDMSO$_4$Cl$_2$ solvato-complex in the manner described above for boron-capped ruthenium(II) clathrochelates with aromatic, alicyclic, and acyclic dioximes. The syntheses of hexachloride ruthenium(II) precursors were realized under hard conditions (in particular, a mixture of nitromethane and SbCl$_3$, or boiling TFA, or boiling BF$_3$·O(C$_2$H$_5$)$_2$ were used as a reaction media) with much lower yields compared with reactions with iron(II) ion [78].

The approach employed was highly successful because of the low basicity and high protolytic stability of the dichloroglyoxime. In most cases, the Ru^{2+} ion generated *in situ* during the reduction of oxychloride ruthenium compounds in the higher oxidation states with metallic lead in the presence of electron-accepting SbCl$_3$-type ligands also favored the elimination of chloride ions from the inner coordination sphere of ruthenium ions. As a result, the Ru(Cl2Cm)$_3$(BF)$_2$ and Ru(Cl2Gm)$_3$(Bn-C$_4$H$_9$)$_2$ precursors were obtained with reasonable yields. However, the hard conditions required for the activation of the Ru^{2+} ions in the reaction with poorly coordinating dichloroglyoxime impose restrictions on the use of the previously proposed synthetic routes. Such methods can be employed only when capping agents (in particular, BF$_3$, alkylboronic acids, and their derivatives) are stable to protolytic dissociation. When arylboronic acids and their derivatives (especially phenylboronic acid), which are more apt to protolytic dissociation and transmetallation, were employed as capping agents, one could observe an abrupt decrease in the desired product yield induced by the destruction of the capping agent. Thus, the reaction involved two competitive processes: the formation of a clathrochelate, which precipitates from the reaction mixture because of its low solubility (this shift the equilibrium in the desired direction), and a protolytic dissociation of the capping agent. Consequently, one should determine the optimal conditions for a synthetic procedure (time and temperature) that make it possible on the one hand to achieve a maximal formation of the desired complex, and one the another hand to avoid a significant decomposition of the capping agent, which can eventually lead to the decomposition of the already-formed complex. To avoid such negative phenomena during the synthesis, the capping agent must be added periodically in excess [78].

The reactivity of hexachloride ruthenium(II) precursors in the reactions of nucleophilic substitution is somewhat lower than that of their analogs with an encapsulated iron(II) ion. The hexathiophenol

clathrochelate was obtained when potassium thiophenolate (not the C_6H_5SH/K_2CO_3 system) was used.

The reaction of $Ru(Cl2Gm)_3(BC_6H_5)_2$ precursor with a 15% excess of *n*-butylamine (calculated from a tetrasubstituted clathrochelate) in DMF at 0°C for 2 h resulted solely in trisubstituted clathrochelate, and the substitution took place in two of the three dioximate fragments (Scheme 31). To produce tetrasubstituted product, a twofold excess of *n*-butylamine was used, and the reaction mixture was stirred for 10 h at room temperature. An unexpected result was obtained when DMF was replaced by chloroform: the interaction of $Ru(Cl2Gm)_3(BC_6H_5)_2$ with *n*-butylamine both at room temperature and with a prolonged stirring at 50÷60°C yielded only one trisubstituted product [78].

As with iron(II) complexes, the di- and tricrown ether ruthenium(II) clathrochelates were isolated depending on the molar ratio precursor/salt of (bis-(2-(*o*-oxyphenoxy))diethyl ether and on the reaction time [78].

Drago and Elias's idea [46] to employ tridentate amines for protection of one of the two triangular bases of hexacoordinate *d*-metal ions coordination polyhedron (in case the latter act as capping agents) from polymerization has successfully been developed by P. Chaudhuri and K. Wieghardt for the synthesis of linear homo- and heterotrinuclear macrobicyclic complexes with tris-dioximate bridging ligands.

The first $[M^{II}Dm_3(ttnFe)_2](ClO_4)_2$ complexes of this type were obtained [79] by the interaction of iron(II) acetate and copper, zinc, nickel, cobalt, and manganese acetates with dimethylglyoxime and 1,4,7-trimethyl-1,4,7-triazacyclononane (*ttn*) in methanol in the presence of triethylamine (Reaction 20). In this case, a triazamacrocycle served as the protecting group in the octahedral capping $ttnFe^{III}O_3$ fragment.

$$M^{2+} + H_2Dm + \quad + Fe^{2+}[ttnFeCl_3] \xrightarrow[CH_3OH]{(C_2H_5)_3N} \qquad\qquad (20)$$

M = Co, Mn, Zn, Ni, Fe, Cu(II)
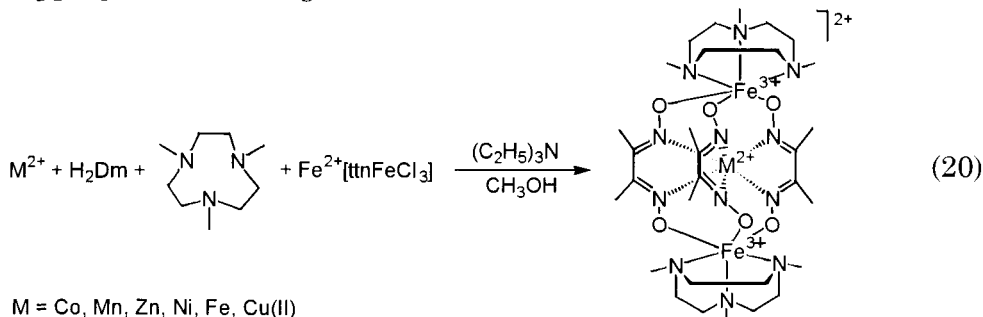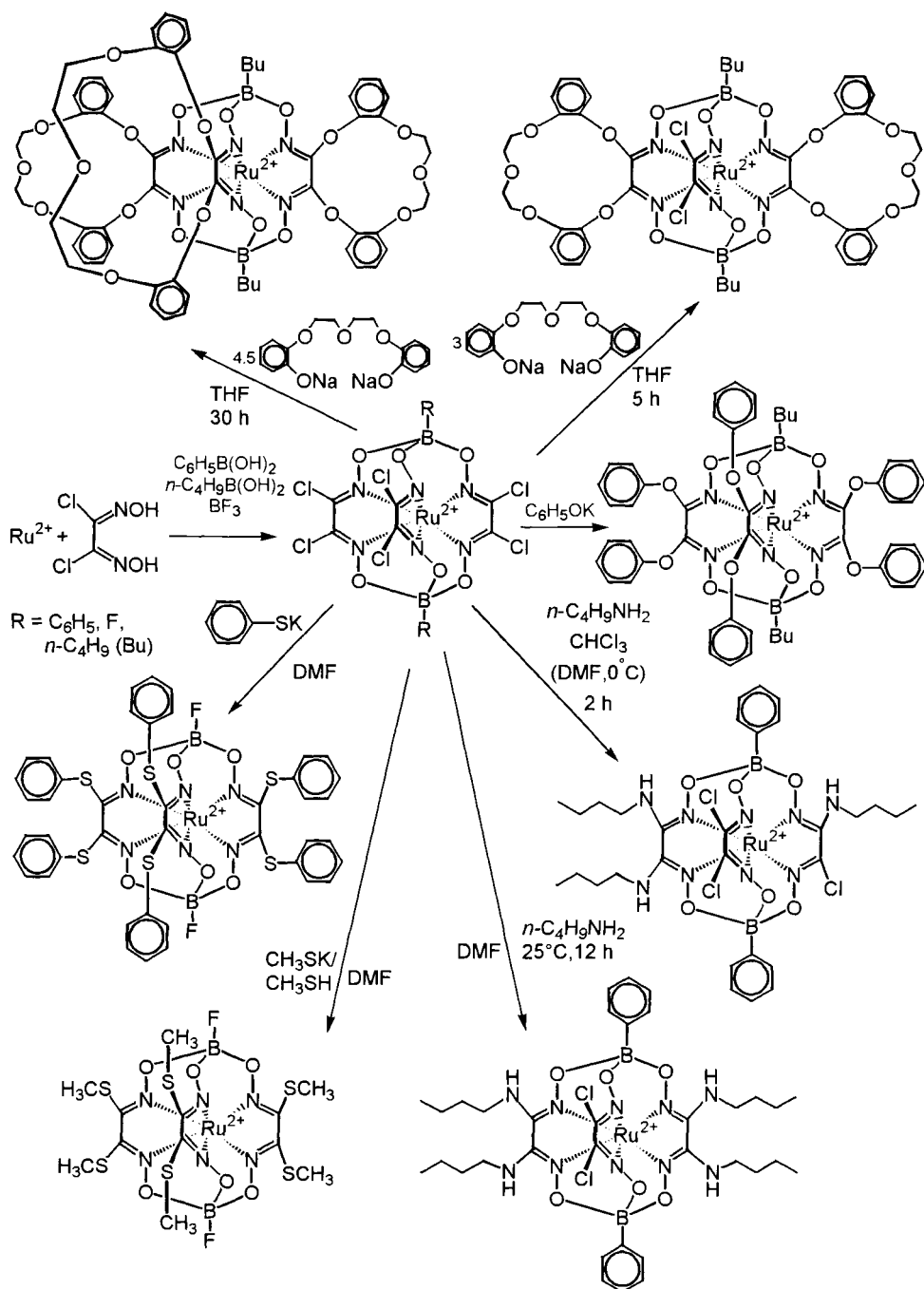
Scheme 31

The template synthesis with ttnFe^{3+} cation as capping agent (Reaction 20) has also made it possible to isolate the clathrochelate nickel(II) [NiDm$_3$(ttnFe)$_2$](ClO$_4$)$_2$ and [NiDm$_3$(ttnFe)$_2$](PF$_6$)$_2$· 0.5CH$_3$OH tris-dioximates arising from the interaction of either Fe^{3+} ions, *ttn*, and nonmacrocyclic nickel(II) tris-dimethylglyoximate (formed under basic conditions with the action of triethylamine), or Ni^{2+} ions and dimethylglyoxime in the presence of ttnFeCl$_3$ complex in methanol [80].

Manganese-capped [M^{II}Dm$_3$(ttnMn^{III})$_2$](ClO$_4$)$_2$ tris-dimethylgly-oximates were first synthesized [81] by an analogous procedure (Reaction 21). The oxidation of manganese-containing capping groups with nitrosyl ions led the formation of the [M^{II}Dm$_3$(ttnMn^{IV})$_2$](ClO$_4$)$_2$ clathrochelates with a capping manganese(IV) atoms. The synthetic procedures for these complexes were described more thoroughly in Ref. 82.

$$M^{2+} + H_2Dm + \quad + Mn^{3+} \xrightarrow[CH_3OH]{(C_2H_5)_3N} \quad \xrightarrow[AN]{NOBF_4} \quad (21)$$

M = Zn, Cu, Ni, Mn (*hs*), Ni(II)
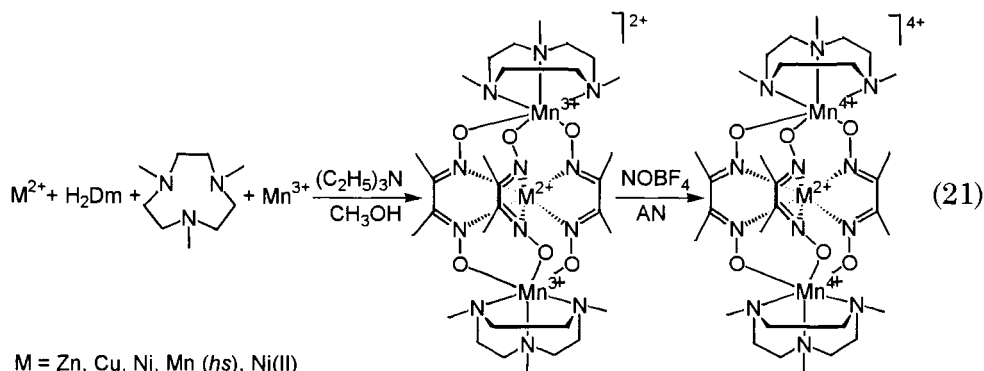
The manganese(III)-capped tris-nioximate macrobicycles, also oxidized to manganese(IV)-capped clathrochelates, were obtained in higher yields [83]:

$$M^{2+} + H_2Nx + \quad + Mn^{3+} \rightarrow \quad \xrightarrow[AN]{NOBF_4} \quad (22)$$

M = Zn, Cu, Mn(II)
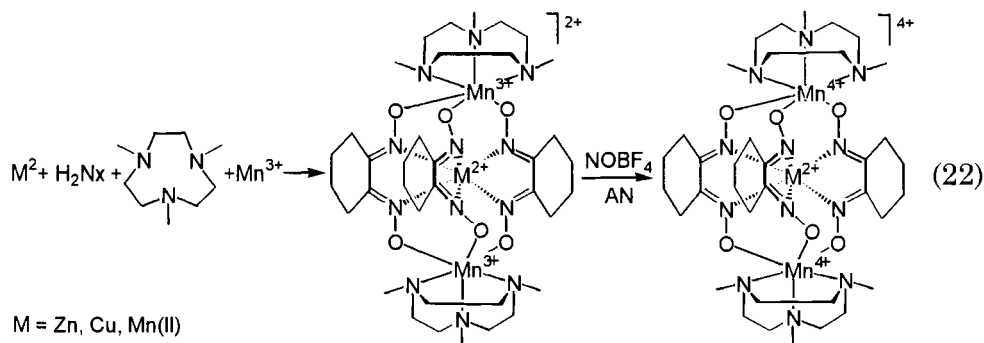
An attempt to use Cr^{3+} ions as capping agents produced unexpected results. The prolonged refluxing of $ttnCrBr_3$ complex, dimethylglyoxime, and triethylamine in methanol resulted in first doubly protonated free macrobicyclic $[H_2Dm_3(ttnCr^{III})_2](ClO_4)_2$ ligand *via* Reaction 23 [84].

$$H_2Dm + ttnCrBr_3 \xrightarrow[CH_3OH]{(C_2H_5)_3N}$$

(23)
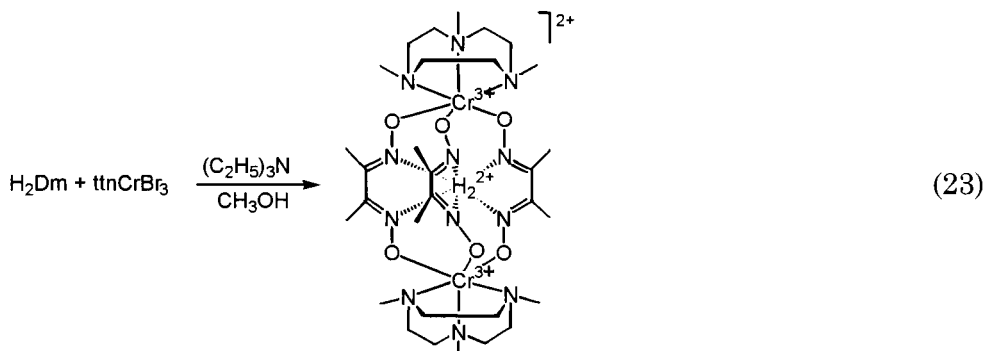
This free clathrochelate ligand has been employed for the synthesis of nonprotonated and tetraprotonated free cages using tetra-*n*-butylammonium hydroxide and $HClO_4$, respectively, as well as chromium(III)-capped magnesium, manganese(II) and lithium clathrochelates (Scheme 32) [85].

Chromium(III)-capped clathrochelate complexes were also obtained by a direct reaction in the presence of Cu^{2+}, Ni^{2+}, Fe^{2+} and Co^{2+} ions (Scheme 33). In the latter case the central ion underwent oxidation in the course of the reaction, and a cobalt(III) clathrochelates was isolated.

An analogous zinc-containing clathrochelate resulted from capping with an initial $ttnCrBr_3$ compex [86]. The encapsulated nickel and iron(II) ions were oxidized with nitrosyl perchlorate to nickel(IV) and iron(III) ions in acetonitrile (Scheme 33) [85].

Attempts to isolate clathrochelate technetium(III) tris-dioximates *via* template cross-linking three dioxime molecules with alkylboronic acid have not been successful. Only semiclathrochelate $TcNx(HNx)_2(BR^2)Hal$ and $TcDm(HDm)_2(BR^2)Hal$ complexes (where Hal^- is Cl^-, Br^-; R^2 is CH_3 and n-C_4H_9) were prepared [87, 88].

The tin-capped $^{99}Tc(HDm)_2(H_2Dm)(\mu-OH)(SnCl_3)$ and $^{99}Tc(HNx)_2(H_2Nx)(\mu-OH)(SnCl_3)$ complexes were obtained by the reduction of NH_4TcO_4 with $SnCl_2$ in the presence of α-dioxime in aqueous/alcohol HCl solution (Scheme 34) [89, 90].
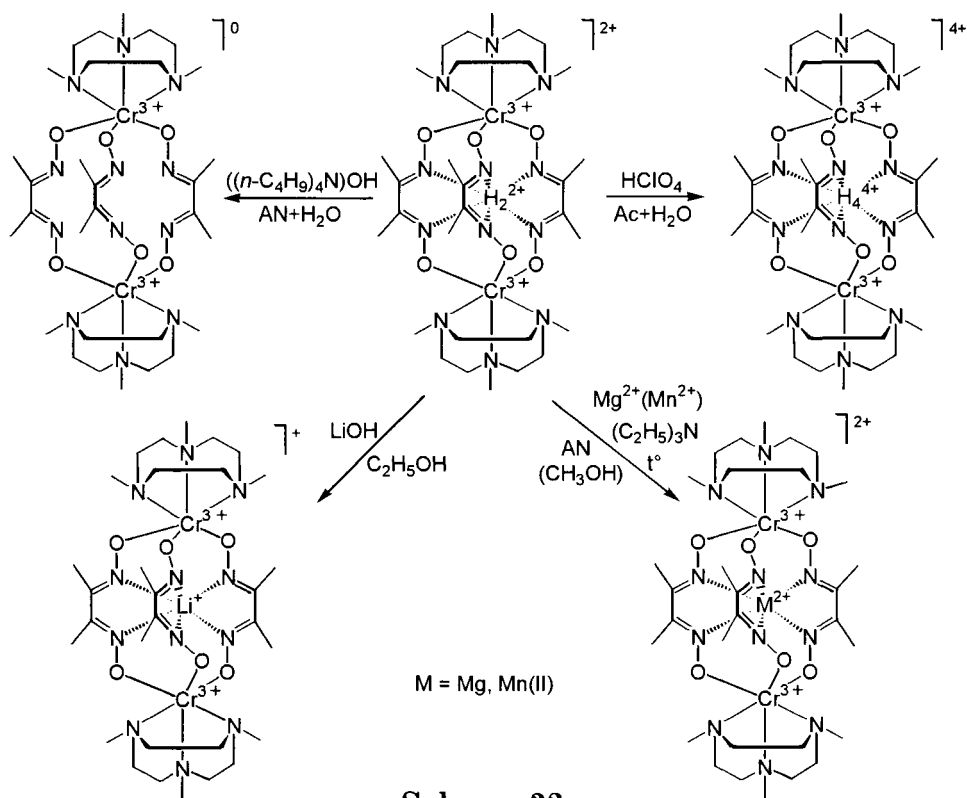
Scheme 32
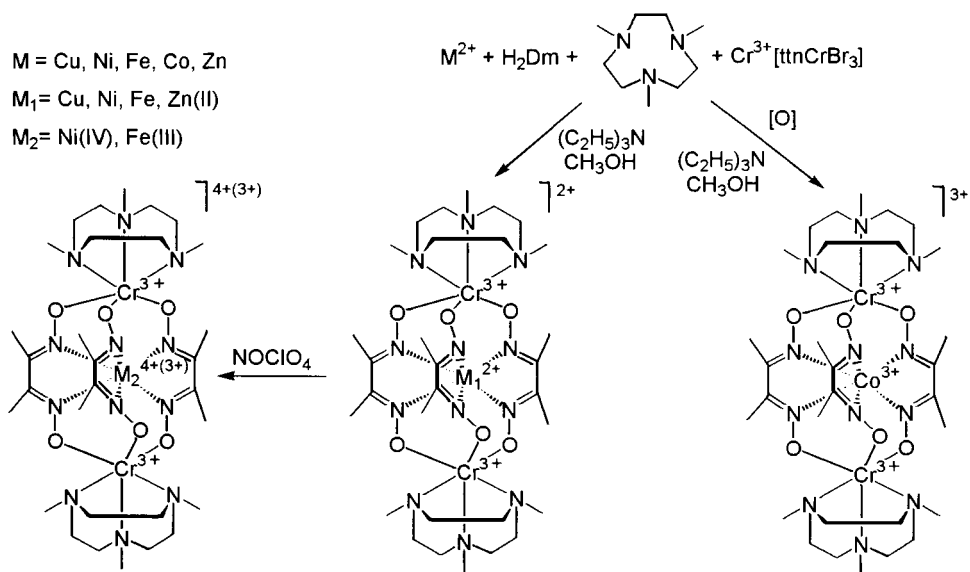
Scheme 33
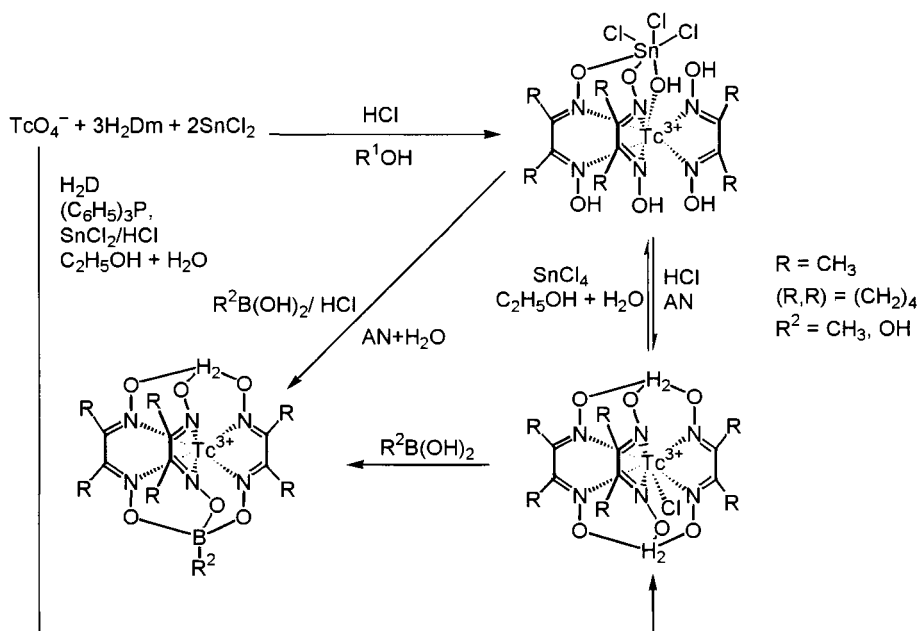
Scheme 34

The addition of HCl to a solution of the complexes obtained caused the formation of non-capped Tc(H₂Dm)(HDm)₂Cl and Tc(H₂Nx)(HNx)₂Cl compounds. These compounds have reacted with SnCl₄ to reform the initial tin-capped complexes.

Both non-capped and tin-capped products were cross-linked with an excess of the boric and methylboronic acids to form the corresponding semiclathrochelate [TcD(HD)₂(BR²)]⁺ cations [89, 90].

2.2 SYNTHESIS OF MACROBICYCLIC PHOSPHORUS-CONTAINING *d*-METAL TRIS-DIIMINATES

Clathrochelates of this type were synthesized starting from semiclathrochelate phosphorus-containing tris-diimine ligand, which was obtained by Scheme 35.

The resultant ligand readily formed semiclathrochelate [M(P(Hpox)₂(pox))]⁺ complexes (where M is nickel, copper, cobalt, or zinc(II) ions) by the interaction of metal salts, e.g., perchlorates, with *P(Hpox)₃* ligand either in dry ethanol or in acetonitrile. Attempts to isolate analogous iron(II) and manganese(II) complexes gave no desired results [91, 92]. Direct synthesis of the macrobicyclic
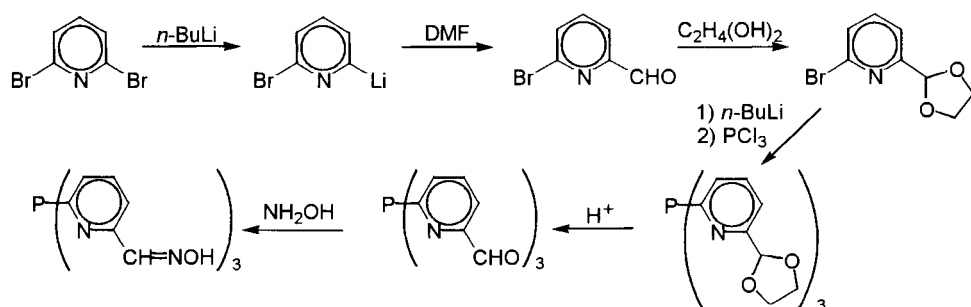
Scheme 35

complexes (without the isolation of semiclathrochelate products) was realized *via* interaction between a tetrafluoroborate $M(BF_4)_2 \cdot 6H_2O$ salt (where M is iron, cobalt, nickel, and zinc(II) ions) and *P(Hpox)*$_3$ ligand in acetonitrile followed by capping with boron trifluoride etherate [92]. [CoPcc(BF)](BF$_4$) and [NiPcc(BF)](BF$_4$) complexes were also synthesized by capping of the semiclathrochelate [Ni(P(Hpox)$_2$(pox))](ClO$_4$) and [Co(P(Hpox)$_2$(pox))](ClO$_4$) compounds with BF$_3 \cdot$O(C$_2$H$_5$)$_2$. This is evidence in favour of the synthesis of macrobicyclic complexes occurring through the formation of a semiclathrochelate compound intermediate step (Scheme 36).

In an attempt to isolate the [M(P(Hpox)$_2$(pox))] (BF$_4$) complexes, it was revealed [92] that the BF$_4^-$ anion cross-linked a semiclathrochelate complex yielding the corresponding [MPcc(BF)](BF$_4$) clathrochelates. This made it possible to synthesize [MPcc(BF)](BF$_4$) complexes by an alternative pathway using NaBF$_4$ as a capping agent. Boiling of the corresponding salt $M(BF_4)_2 \cdot 6H_2O$, *P(Hpox)*$_3$ ligand, and NaBF$_4$ in acetonitrile for several hours followed by treatment with water yielded complexes identical to those obtained by the above procedure [92].

P(Hpox)$_3$ [M(P(Hpox)$_2$(pox))]$^+$ [MPcc(BF)]$^+$
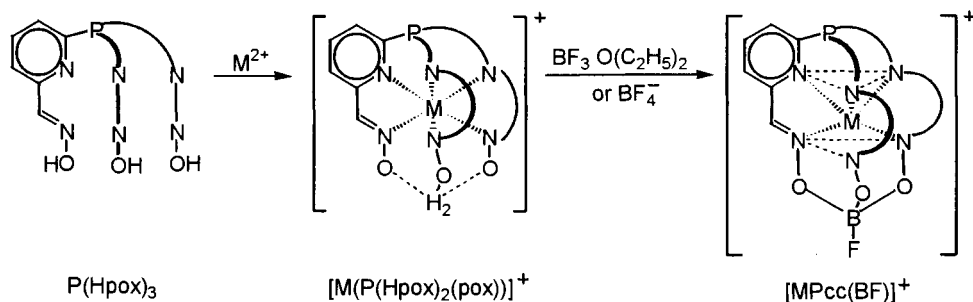
Scheme 36

A similar reaction pathway was also employed to prepare the nickel(II) complex with a macrobicyclic *4-MePcc(BF)* ligand [93]. Attempts to obtained macrobicyclic manganese(II) and copper(II) complexes of this type from the corresponding semiclathrochelate complexes have not been successful [92].

2.3 SYNTHESIS OF SEPULCHRATES AND SARCOPHAGINATES

A template synthesis of macrobicyclic ligand is, as in the cases considered, also most important pathway for the preparation of sepulchrates and sarcophaginates. However, modification reactions of free ligands and complexes, as well as synthesis from the free ligands (preformed by template condensation on the metal ion followed by demetallation or synthesized by other methods) are of particular importance in the preparation of these types of clathrochelates. The specific features observed in the synthesis of sepulchrates and sarcophaginates are accounted for by the fact that their structural peculiarities distinguishes them from other clathrochelates. First, these ligands have a specific flexibility that allows the synthesis of complexes with metal ions of a different nature and in various oxidation states, as well as allowing the free ligands to be obtained by demetallation of preformed clathrochelate complexes. Second, a considerable number of stereoisomers that fairly readily convert to each other can be obtained. Numerous reactive sites provide a wide range of modification reactions of ligands and complexes for the preparation of sepulchrates and sarcophaginates. These complexes seem also to be obtained by metal ion substitution.

Sepulchrates and sarcophaginates have primarily been synthesized *via* template macrocyclization of the preformed metal tris-diaminates with capping agents, which is regarded as being the most significant approach to the synthesis of these compounds. Sargeson and coworkers first prepared the cobalt(III), platinum(IV), and rhodium(III) sepulchrates and sarcophaginates as well as the corresponding cobalt(II) complexes [94, 95].

The [Co(sep)]Cl$_3$ complex is obtained from Reaction 24 between cobalt(III) [Co(en)$_3$]Cl$_3$ tris-ethylenediaminate and dilute aqueous solutions of ammonia and formaldehyde in the presence of lithium carbonate with subsequent isolation of the product by IEC [94-96]:

$$[Co(en)_3]^{3+} \xrightarrow[NH_3]{CH_2O} [Co(sep)]^{3+} \tag{24}$$
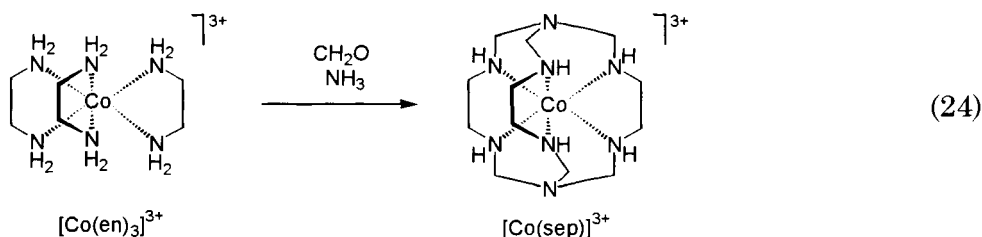
Several variants of the first-developed procedure have been reported [97-100].

The corresponding macrobicyclic cobalt(II) [Co(sep)](ZnCl$_4$)·H$_2$O complex was prepared by reduction of the [Co(sep)]Cl$_3$ complex with zinc dust in aqueous HCl [95]. A similar procedure was used for the synthesis of the dithionate [Co(sep)](S$_2$O$_6$) salt in the presence of Li$_2$S$_2$O$_6$ [99]. The optically active *R*- and *S*-isomers of cobalt sepulchrate were obtained from the optically active parent Δ-[Co(en)$_3$]Cl$_3$ and Λ-[Co(en)$_3$]Cl$_3$ complexes [94-95].

The use of nitromethane instead of ammonia has resulted in the formation of the [Co(diNOsar)]Cl$_3$·H$_2$O sarcophaginate [94, 101].

$$[Co(en)_3]^{3+} \xrightarrow[CH_2O]{CH_3NO_2} [Co(diNOsar)]^{3+} \tag{25}$$
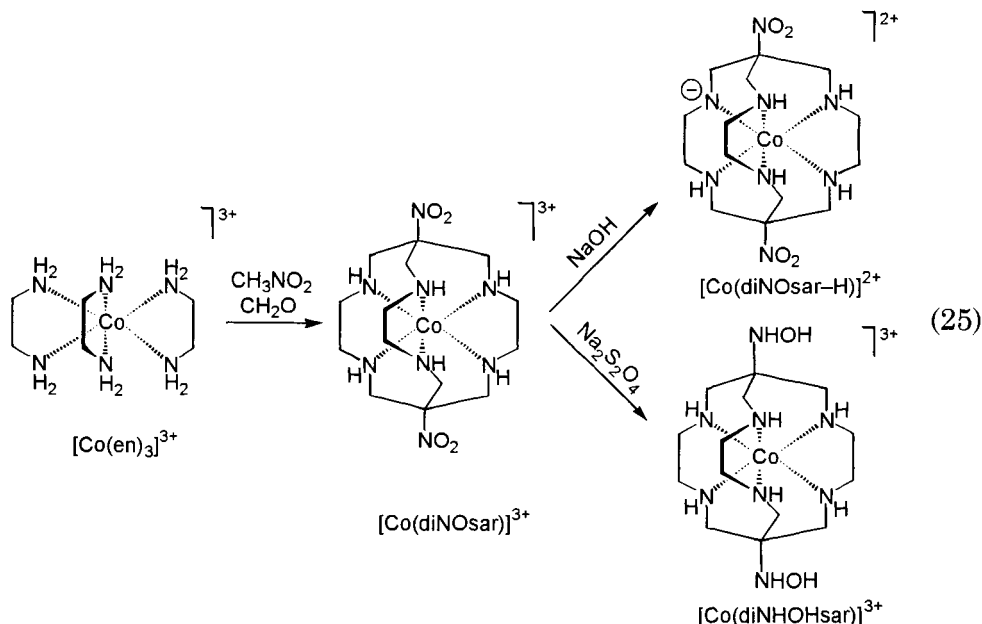
A similar procedure was employed to obtain the [Co(diNOsar)]$^{3+}$ cation optically active isomers and salts of other anions [101]. A more rational approach to the synthesis of this clathrochelate was reported in Ref. 102.

Monoimine, N-methylated, and semiclathrochelate complexes have been isolated and identified as by-products of sarcophaginate synthesis to gain a deeper insight into the reaction mechanism. The addition of sodium hydroxide to an aqueous solution of [Co(diNOsar)](ClO$_4$)$_3$ complex leads to a change in the colour of the solution from orange to violet. The violet crystals of the deprotonated [Co(diNOsar–H)](ClO$_4$)$_2$ compound were isolated [101].

Partial reduction of [Co(diNOsar)]Cl$_3$·H$_2$O complex with Na$_2$S$_2$O$_4$ in slightly acidic medium yielded a sarcophaginate containing hydroxylamine groups in apical fragments [103]. This complex was also prepared using organic radicals as reductant [104].

The [Co(diNOsar)](ClO$_4$)$_3$ sarcophaginate easily reduces with zinc dust in neutral aqueous solution to the corresponding cobalt(II) compound. To avoid the reduction of the nitro groups, the reaction must proceed quickly. The resulting [Co(diNOsar)](ClO$_4$)$_2$ complex is unstable and on storage decomposes because of intramolecular redox processes [94, 101].

The reaction of the [Co(diNOsar)]$^{3+}$ cation with zinc dust in acidic medium has proceeded to the reduction of nitro groups to amino groups, which are protonated and, therefore, not affected by treatment with hydrogen peroxide. As a result, the [Co(diAMsar)]Cl$_3$·2HCl and [Co(diAMHsar)]Cl$_5$ diaminosarcophaginates were isolated, which makes it possible to synthesize sarcophaginates with different substituents in the capping group [101]. It was also observed that cobalt(II) and cobalt(III) aminosarcophaginates resulted from a catalytic hydrogenation of cobalt(III) dinitrosarcophaginate [105].

Nitrosation of [Co(diAMsar)]$^{3+}$ cation in the presence of chloride anion led to the formation of cobalt dichlorosarcophaginate, the reduction of which with zinc dust and subsequent treatment with H$_2$O$_2$ and HCl gave the simplest [Co(sar)]Cl$_3$ sarcophaginate [94, 101]:

$$\text{(26)}$$
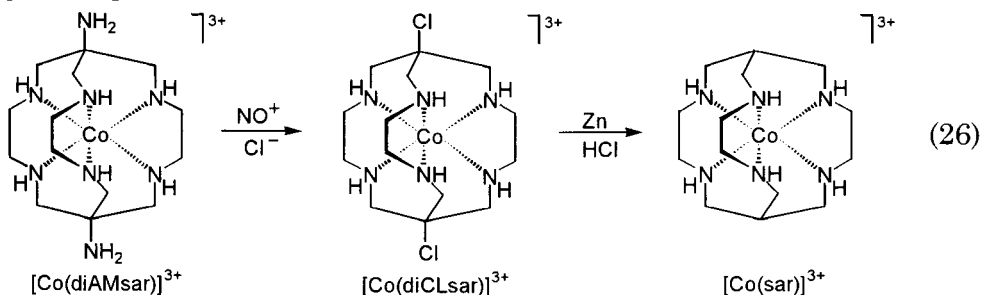
An intermediate [Co(CLsar)]Cl₃ monochlorosarcophaginate has also been formed. In addition to clathrochelate [Co(diCLsar)]³⁺ cation, nine compounds were isolated from two main fractions ("orange" and "yellow") of the nitrosation products by IEC [101]. The first one contained unreacted [Co(diNOsar)]Cl₃ (3%), [Co(CLNOsar)]Cl₃ (18%), [Co(HONOsar)]Cl₃ (7.5%), [Co(HOCLsar)]Cl₃ (26%), [Co(diHOsar)]Cl₃ (1.5%) and the expected [Co(diCLsar)]Cl₃ (44%) sarcophaginates. The second fraction was a mixture of complexes of a contracted *absar* ligand that arose from intramolecular rearrangement:

$$(27)$$
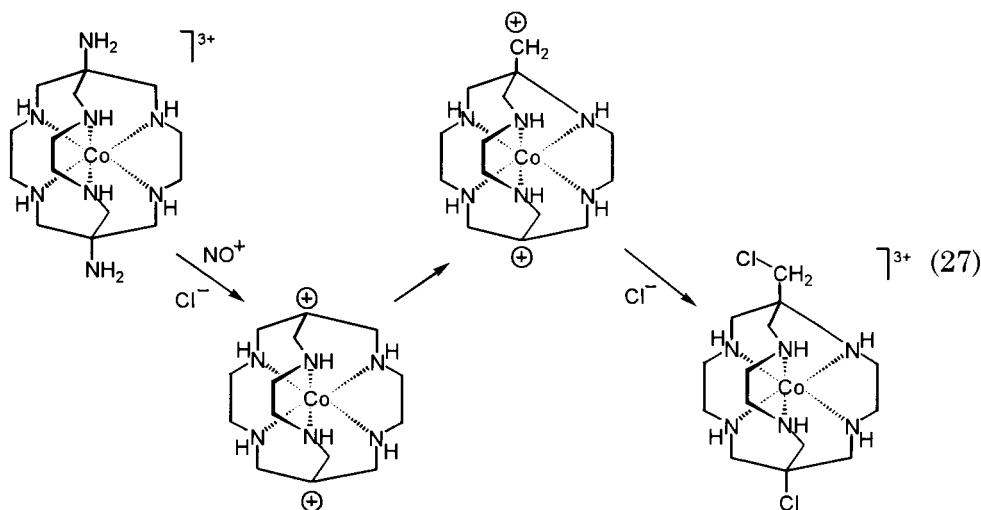
The contracted [Co((ClME)CLabsar)]Cl₃ (60%), [Co((ClME)NOabsar)]Cl₃ (20%), [Co((ClME)HOabsar)]Cl₃ (17%), and [Co(AMH(ClME)absar)]Cl₄ (3%) sarcophaginates were isolated from the "yellow" fraction by IEC.

Thus, apart from the expected [Co(diCLsar)]Cl₃ complex, the nitrosation of [Co(diAMsar)]³⁺ diaminosarcophaginate yielded four regular sarcophaginates and four contracted *absar* ligand complexes [101].

The rearrangement mechanism of a cobalt(III) nitrosarcophaginate in the basic conditions to yield a contracted N₆-cage, as well as the intermediate reaction products are described in Ref. 106 (see Chapter 4).

The hydrolytic stability of the [Co(diCLsar)]³⁺ cation toward conversion to the [Co(diHOsar)]³⁺ dihydroxysarcophaginate is due to the difficulty of forming a carbocation at a planar bridgehead position. It was noted that the nitrosation of [Co(diAMsar)]³⁺ sarcophaginate occurring without rearrangement involves compe-

tition of all nucleophiles in solution, whereas its nitrosation with rearrangement appears to involve chlorine anion selectively [101].

The ethylenediaminate fragments of the sarcophaginate frameworks exhibit certain flexibility, which enables them to have conformations from the λ (the Δ-C_3lel_3 form) to δ (the Δ-D_3ob_3 form). Conformations *"lel"* and *"ob"* define the parallel and oblique orientation of the C–C bond of the ethylenediaminate moiety relative to the C_3 axis, respectively. The existence of intermediate forms as energetically stable conformations is also possible [107]. Theoretical interpretation of the $Co^{2+/3+}$ electron transfer and electrochemical and chiroptical properties is hampered by the need to consider several accessible conformations of the cobalt(II) and cobalt(III) sarcophaginates and sepulchrates.

Application of the template encapsulation procedure to the rigid cyclohexanediaminate lel_3-[Co(chxn)$_3$]$^{3+}$ cation has yielded a high symmetric cage systems [107]. For the synthesis of the diaminocyclohexane sarcophaginates, the condensation procedure was modified (pH 11÷12 and elevated temperatures) compared with that for ethylenediamine sarcophaginates.

The resolved (+)-(S,S)- and (–)-(R,R)-*trans*-1,2-cyclohexanediamine isomers reacted with a cobalt(II) salt in methanol upon air bubbling to yield Λ-lel_3-[Co(chxn)$_3$]Cl$_3$·4H$_2$O and Δ-lel_3-[Co(chxn)$_3$]Cl$_3$·4H$_2$O tris-diaminates, respectively. Capping of these tris-complexes in aqueous solution at pH 11.5 with a great excess of nitromethane and formaldehyde upon heating to 55°C gave Λ-lel_3-[Co(diNOchar)]Cl$_3$·3H$_2$O and Δ-lel_3-[Co(diNOchar)]Cl$_3$·3H$_2$O sarcophaginates in 50% yield. Nitromethane (16-fold excess) and formaldehyde (10-fold excess) were added in portions, and readjustment of the solution to pH 11.5 was periodically carried out. The products obtained were isolated by IEC [107]. Only lel_3-[Co(NOsemichar)]Cl$_3$·5H$_2$O semiclathrochelate has been formed at room temperature.

Reduction of the Δ-lel_3-[Co(diNOsar)]Cl$_3$·3H$_2$O sarcophaginate with zinc dust followed by treatment with concentrated aqueous NaClO$_4$ yielded the cobalt(II) Δ-lel_3-[Co(diNOchar)](ClO$_4$)$_2$·2H$_2$O clathrochelate. The Δ- and Λ-lel_3-[Co(diAMHchar)]Cl$_5$·6H$_2$O diamino-sarcophaginates were obtained by reduction of the reaction mixture with zinc dust in aqueous HCl after template encapsulation at 50°C without isolation of the dinitrosarcophaginates (Scheme 37). At room temperature, reduction of these dinitrosarcophaginates gave the [Co(AMHNOchar)]Cl$_4$·6H$_2$O semiproduct. Reduction of the

cobalt(III) Δ-*lel*₃- diaminosarcophaginate with zinc dust and subsequent treatment of the reaction mixture with Li₂ZnCl₄ resulted in the cobalt(II) Δ-*lel*₃-[Co(diAMchar)](ZnCl₄)·2H₂O sarcophaginate (Scheme 37) [107].

The clathrochelate cyclohexanediamine complexes display a high chemical stability. For instance, heating a cyclohexanediamine cobalt (III) sarcophaginate in 5 molar NaOH at 200°C and a cobalt(II) sarcophaginate in a sealed ampule with concentrated hydrochloric acid at 270°C for 24 h leads to only slight decomposition of the complex. No change from the *lel* sarcophaginate isomer to its *ob* form was observed. Attempts to cross-link the preformed *ob*₃-[Co(chxn)₃]³⁺ cation resulting in the *ob*₃-[Co(diNOsar)]³⁺ sarcophaginate have also failed. However, the *ob* and *lel* forms of such complexes were
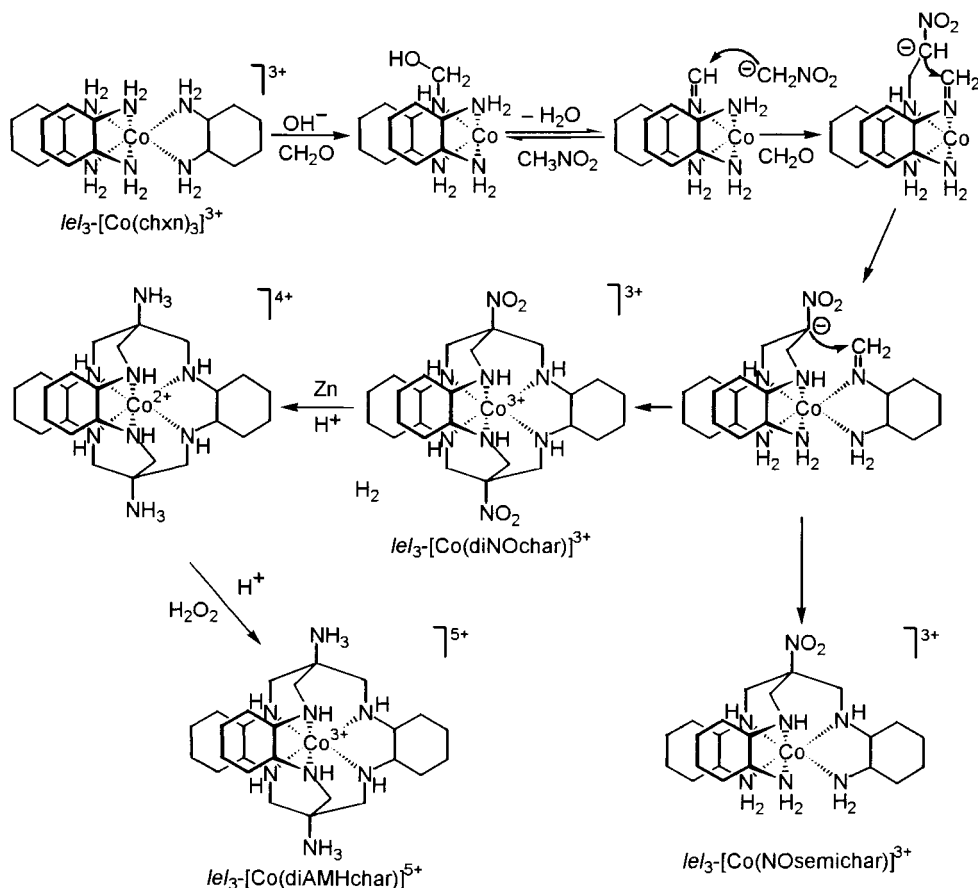
Scheme 37

synthesized by capping the meridional (*mer*-) and facial (*fac*-) *lel*₃-[Co(1,2pn)₃]³⁺ cation isomers. The Co³⁺ ion was then removed from the chiral cage and recoordinated. Under these conditions a small quantities of the *ob* isomer were obtained and separated from the *lel* form by IEC [5].

Several novel clathrochelate complexes have also been prepared *via* the oxidation of preformed sarcophaginates. The cyclohexane-diamine fragments of *char* sarcophaginate underwent oxidation with mercury(II) acetate in acetic acid to give the diamide complex (Reaction 28). In addition, one of the cyclohexane rings has also been aromatized:

(28)
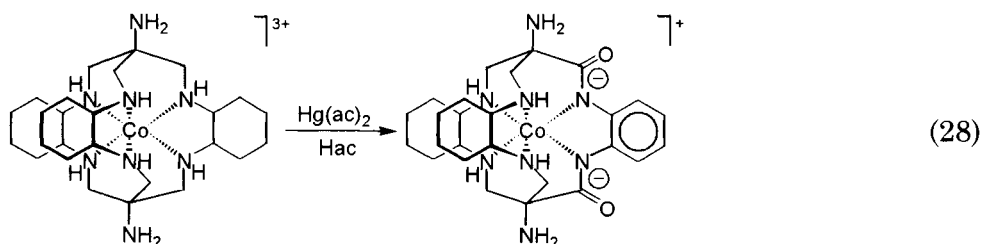
The resultant sarcophaginate may be oxidized by a two-electron mechanism to the *o*-benzoquinonediimine derivative. Reduction of the latter by a three-electron mechanism carried the cage complex back to an aromatic cobalt(II) derivative:

(29)
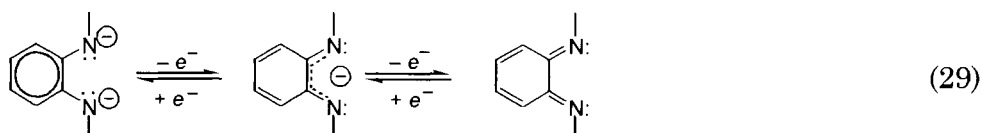
Cerium(III) or tin(II) ions were chosen as a reductant [5]. Application of redox processes is promising for the synthesis of novel sarcophaginates with higher stability and a small cavity size. The reactivity of sarcophaginate ligands may also be employed to prepare imine-, hydroxylamine-, and amide-containing systems not only with cyclohexanediamine derivatives, but with simpler clathrochelates as well.

A mixture of [Co(diNO1,2pnsar)]³⁺ diastereoisomers was obtained by capping of [Co(*R,S*-1,2pn)₃]³⁺ tris-diaminate (containing *lel*₃ (36%), *lel₂ob* (42%), *ob₂lel* (18%), and *ob₃* (4%) conformers) with formaldehyde and nitromethane under basic conditions followed by reduction with zinc dust in aqueous HCl. The resultant mixture was

separated by IEC. Alongside *fac-* and *mer-* isomers of the *lel₃*-[Co(diAMl,2pnsar)]³⁺ complex (in 23% yield), four products were recovered and identified as one *fac* and three *mer* isomers of the *lel₂ob* conformers of this sarcophaginate (the total yield is *ca* 11%). The *ob₂lel* and *ob₃* isomers were prepared in a similar manner, i.e. by demetallation of three *lel₂ob*-[Co(diAMl,2pnsar)]²⁺ isomers with concentrated NaCN aqueous solution and subsequent interaction between the resultant free clathrochelate ligands and *trans*-[CoPy₄Cl₂]Cl complex in 2-methoxyethanol. In this case *ca* 10% of the *(S₂,R)-lel₂ob* cage has been inverted to the *(S₂,R)-ob₂lel* conformer (Scheme 38) [5].

Reaction of the [Co(diCLsar)]³⁺ cation with hydrogen peroxide under basic conditions yielded the monohydroxylamine [Co(diCLsar·NOH)]³⁺ complex even with an excess of the oxidant. The hydroxylamine group is stable toward strong oxidants (Cr₂O₇²⁻, Ce⁴⁺) but is reduced with zinc powder as well as Cr²⁺, Eu²⁺, and V²⁺ ions to a secondary amine [5, 108]. Only one of the six coordinated secondary amino groups of the cobalt dichlorosarcophaginate is oxidized to the hydroxylamine group, whereas in the case of cobalt dinitrosarcophaginate, two or three of groups undergo such oxidation because the first complex exhibits higher basicity (pK$_a$ = 10.36) than the second (pK$_a$ = 9.87). In the majority of
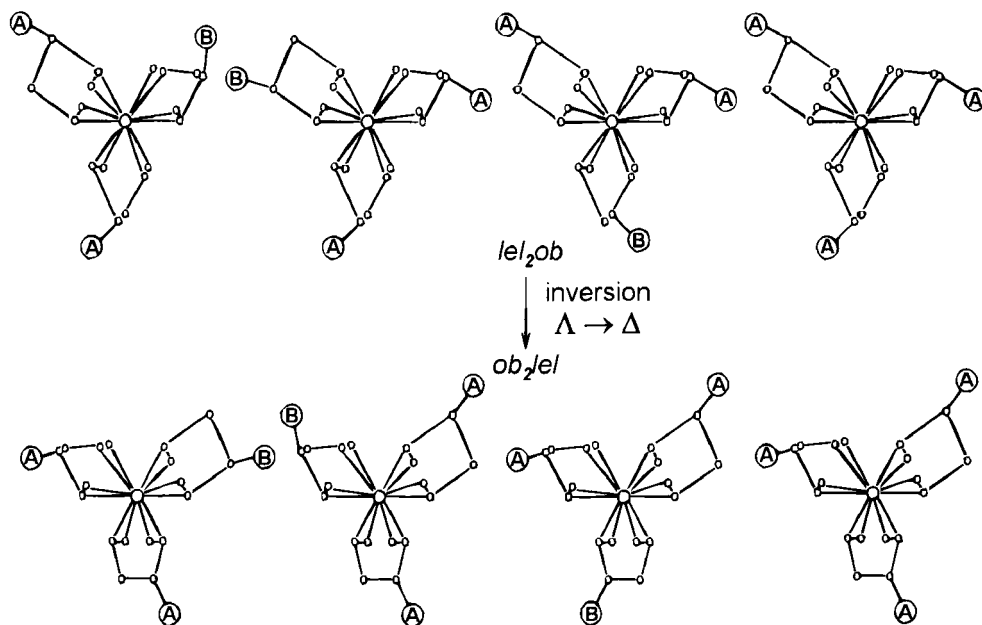
Scheme 38
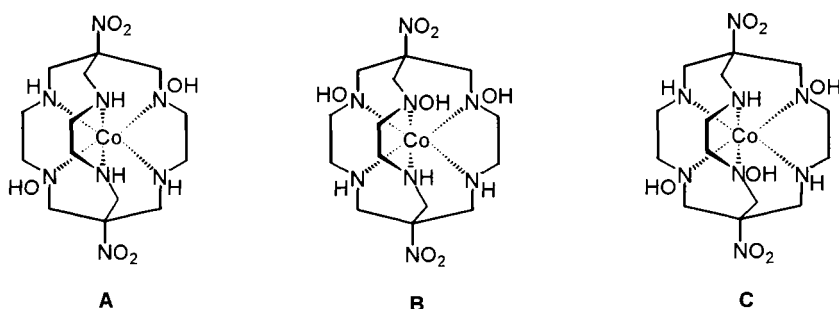
Scheme 39

cases, coordinated amino groups are too basic (pK$_a$ = 14) to deprotonate readily in aqueous solutions. As a consequence, they cannot be attacked by electrophilic H$_2$O$_2$ and oxidized [108].

Addition of hydrogen peroxide and base in equimolar amount to the [Co(diNOsar)]$^{3+}$ cation aqueous solution led to the formation of a monohydroxylamine [Co(diNOsar·NOH)]Cl$_3$·3H$_2$O complex. The treatment of the [Co(diNOsar)]$^{3+}$ cation with a large excess of H$_2$O$_2$ and base gave the product mixture. Three different complexes were isolated by IEC: a dihydroxylaminosarcophaginate **A** and trihydroxyl-aminosarcophaginates **B** and **C** (Scheme 39).

These complexes are less stable than the initial sarcophaginates, and their stability decreases in basic conditions. The hydroxylamine groups in these compounds demonstrated no reducing ability because the macrobicyclic ligand stabilises itself. Their further oxidation caused destruction of the clathrochelate framework [108].

Cobalt(II) sarcophaginates were oxidized to imines and amides. In the presence of activated carbon, oxygen, and cobalt(II) ions at pH 8.5, the [Co(diAMsar)]$^{3+}$ cation was oxidized first to imine and then through carbinolamine and amide to diamide sarcophaginate:

(30)
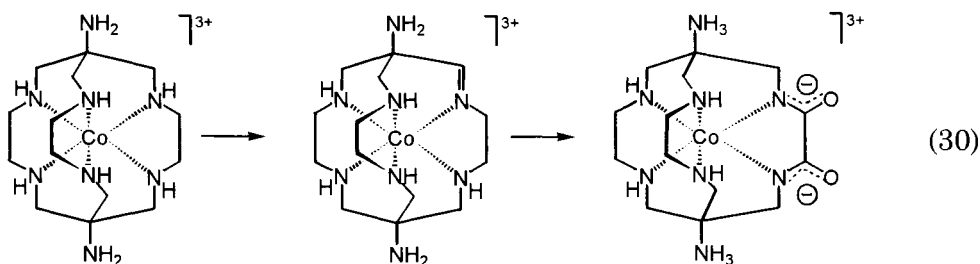
The same type of oxidation was also realized by mercury(II) acetate in acetic acid [5].

The relatively low nucleophilicity of the apical amino substituent in cobalt(III) diaminosarcophaginate has been used in acylation and alkylation reactions leading to a variety of apical functionalized cobalt(III) sarcophaginates with apical pendant aromatic and heteroaromatic substituents [109].

Attempts to react [Co(diAMsar)]$^{3+}$ cation with benzoyl chloride in aqueous solution resulted in mono- and dibenzoylated sarcophaginates in very low yields, and this reaction in other solvents such as AN, DMSO, and Py was even less successful, except in the cases of dimethylacetamide (DMA) and DMF. In last case, the benzoylated products along with formamidino-appended sarcophaginates were obtained in moderate yields by varying the reaction conditions (Scheme 40). The phthaloylation of cobalt(III) diaminosarcophaginates in both glacial acetic acid and DMA led to the formation of bis(phthalamic acid) derivative. The reductive alkylation of the [Co(diAMsar)]$^{3+}$ and [Co(AMMEsar)]$^{3+}$ cations with aromatic carbaldehydes resulted in mono- and 1,8-difunctionalized products (Scheme 40) in acceptable yields. As in the case of macrobicyclic tris-dioximates, the apical substitution of a sarcophaginate does not significantly modify the properties of the cage unit, and, correspondingly, the properties of the pendant groups do not appear to be substantially modified by the presence of the nearly clathrochelate cationic centre [109].

The reactivity of apical amino groups has been used in the synthesis of surface-active sarcophaginates (surfactants) [110]:

$$(31)$$
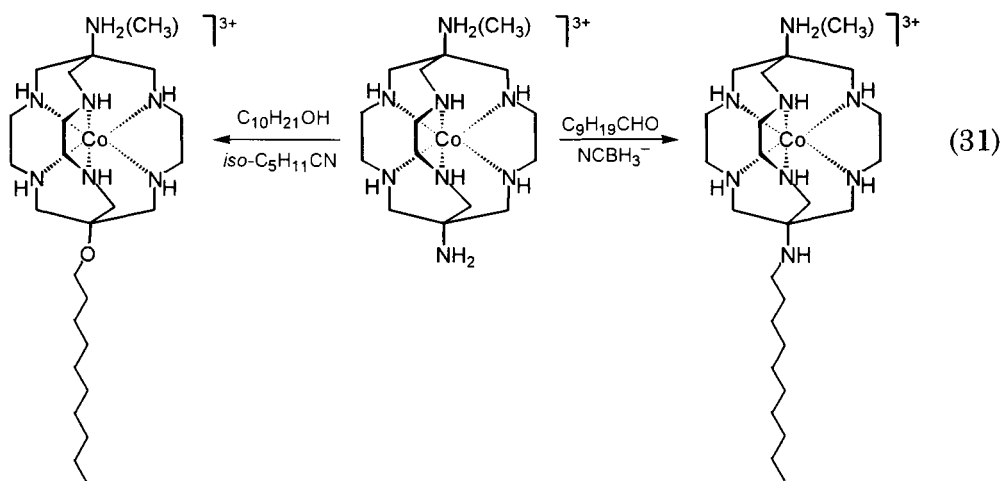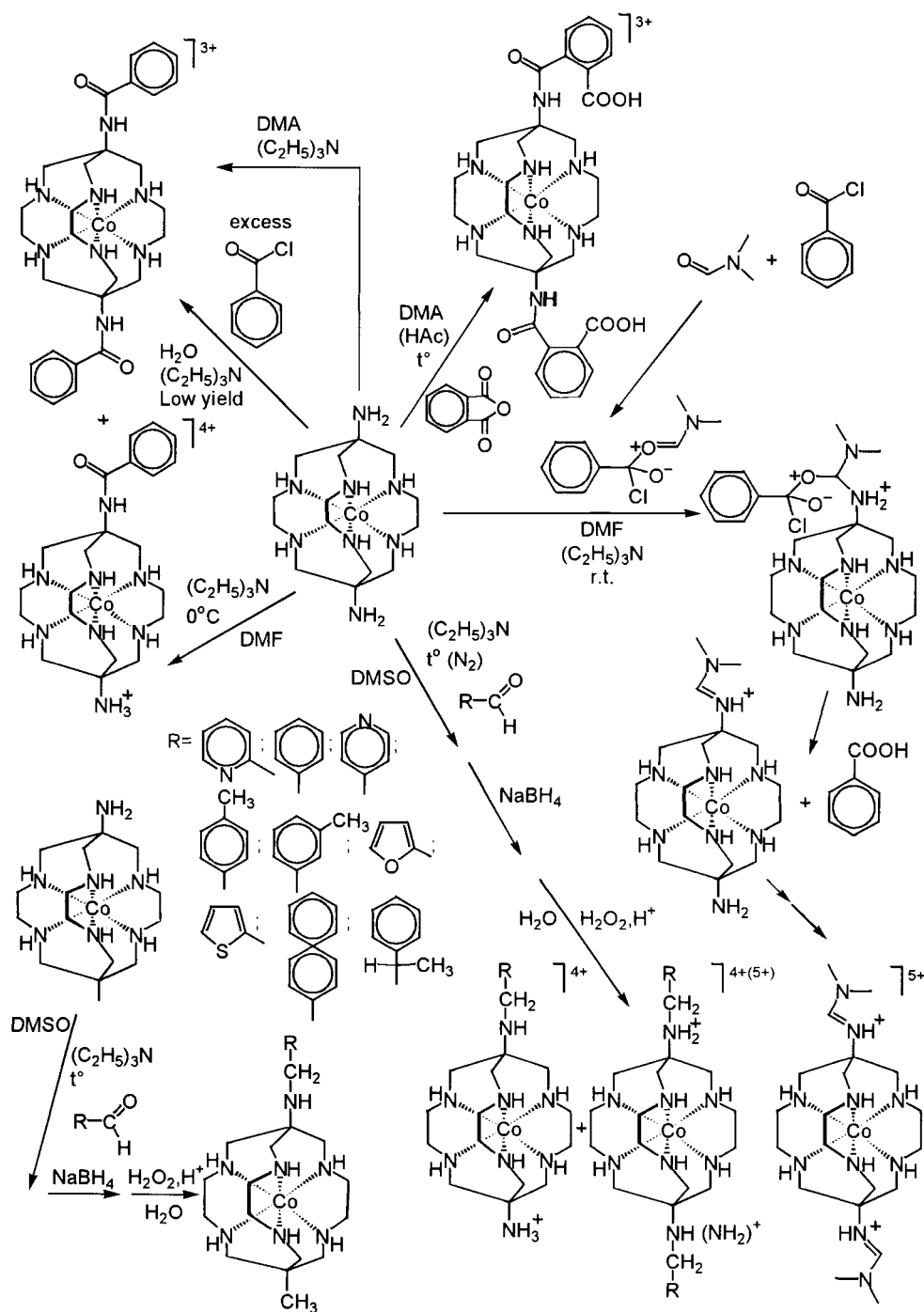
Scheme 40

Oxidation of the [Co(MEAMsar)]$^{3+}$ cation apical amino groups resulted in the bis-sarcophaginate:

$$(32)$$
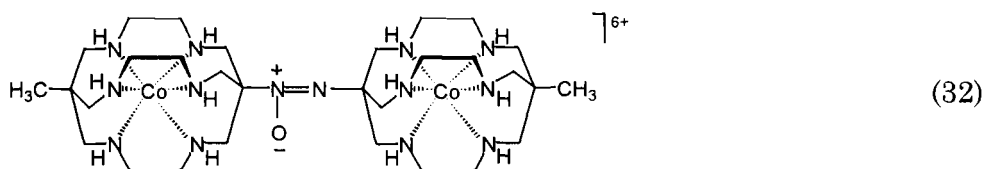
The synthesis of the cobalt cage complex with pendant pyridylmethyl arms (Scheme 41) was performed in excellent yield [111].

It is undoubtedly of interest that the substituents in the clathrochelate framework and in apical groups affect the structure and properties of macrobicyclic complexes. In particular, it was noted that N-methylation of the complexes must stabilize the lowest oxidation states of the encapsulated metal ion. In this case, one should take into account the steric effects of substituents whose introduction influences the dissociation kinetics of the sarcophaginates [112].

The copper and nickel(II) complexes of penta-, hexa-, and hepta-N-methylated sarcophaginate ligands showed tetradentate coordination of the metal ions, unlike the hexadentate coordination in regular sarcophaginates [113-115]. Exhaustive methylation of free *sar* ligand produced the highly lipophilic, hexatertiary base hexamethyl-sarcophagine [115].
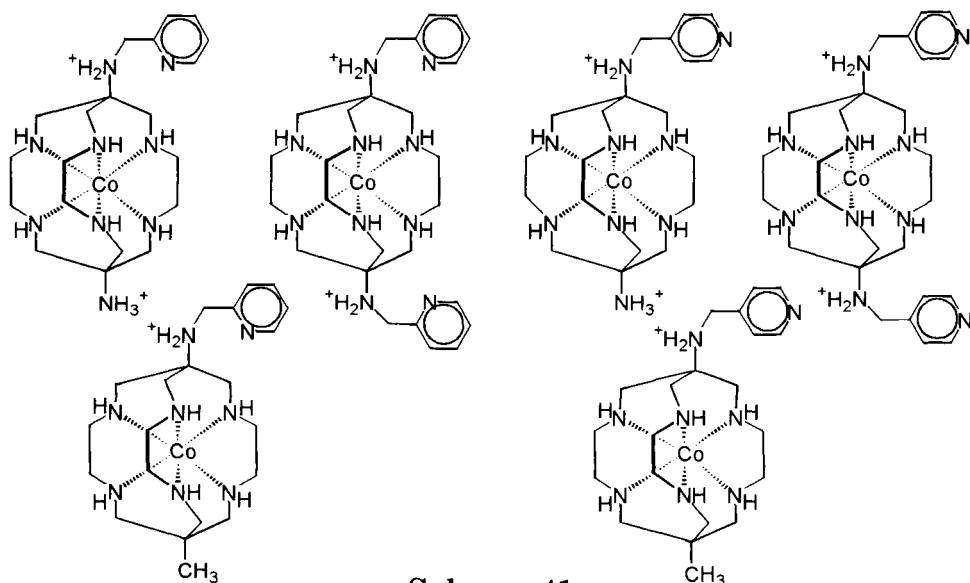
Scheme 41

Stepwise methylation of apical amino substituents in cobalt(III) sarcophaginate make it possible to obtained a tris-N-methylated complex with conformational inversions in the ethylenediamine moieties from mainly a *lel₃*-conformation in $[Co(diAMsar)]^{3+}$ cation to an *ob₃* conformation in $[Co(diMe_3AMHsar)]^{3+}$ sarcophaginate both in the solid state and in solution [116].

$$(33)$$
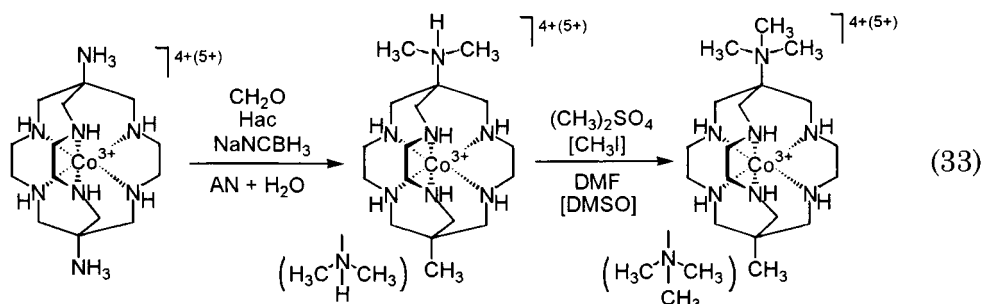
Free sarcophagines and their complexes were also modified by N-carboxymethylation with chloroacetate controlled by an encapsulated metal ion.

The reaction of a free diaminosarcophagine with an excess of chloroacetate under basic conditions led to a mixture of mono- and dicarboxymethylsarcophagines with substitution at the secondary nitrogen atoms; these were isolated as complexes with a cobalt(III) ion (Scheme 42) [117].

In the case of cobalt(III) diaminosarcophaginate, the Reaction 34 proceeded by an alternative pathway: only primary amino groups were involved to form apical mono- and difunctionalized sarcophaginates (in the latter case, only the symmetric product was obtained).

$$(34)$$
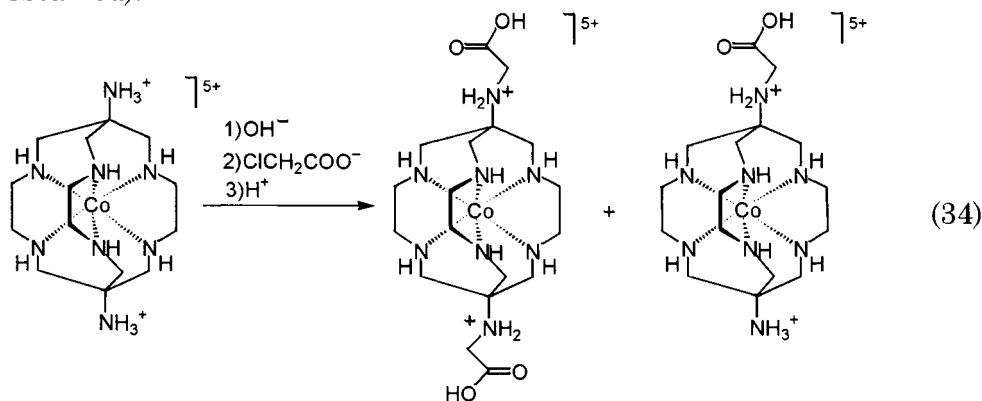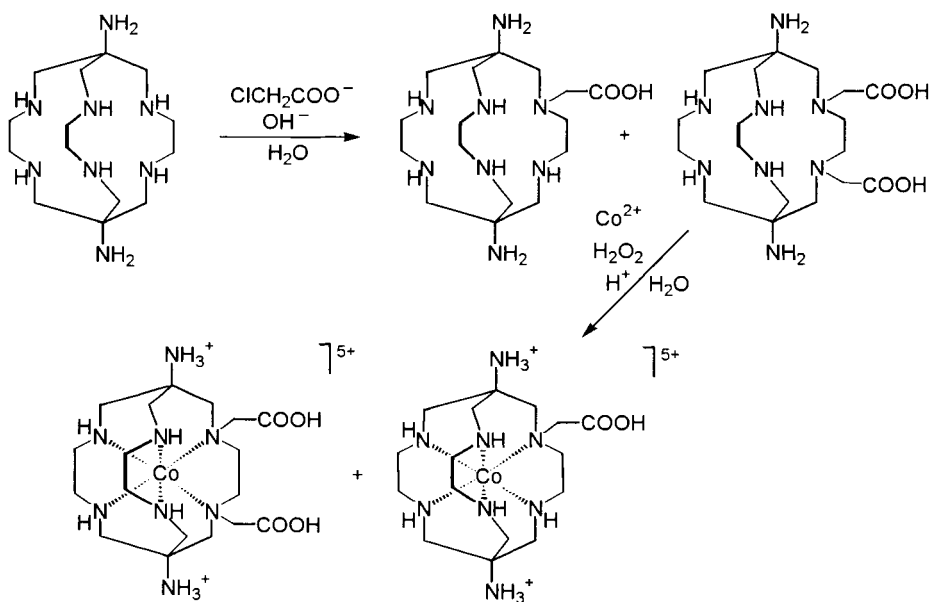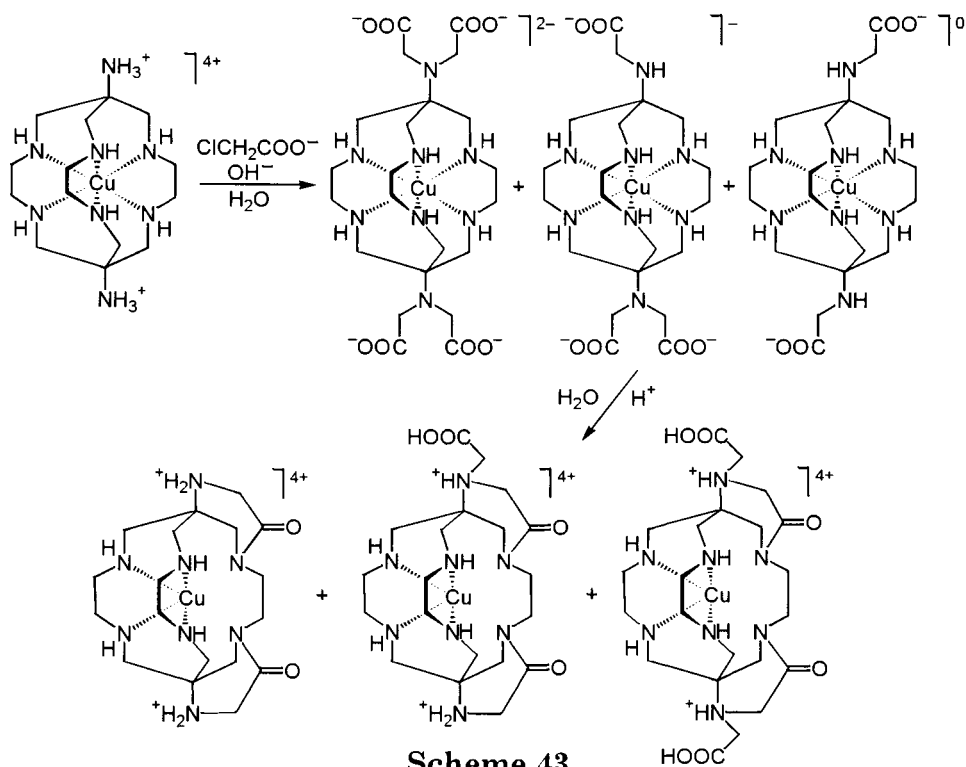
Scheme 42

Scheme 43

The reaction of a copper(II) diaminosarcophaginate with chloroacetate made it possible to isolate complexes containing up to four functionalizing substituents in the apical fragment that undergo an intramolecular condensation to give lactam units in neutral and acidic media. The condensation involves one of the three ethylene-diaminate fragments, and the copper(II) ion assumes a square-planar coordination (Scheme 43). A higher degree of carboxymethylation in the case of the copper(II) sarcophaginate was accounted for by the lower charge of the latter compared with that of a cobalt(III) complex. This caused a lesser reduction of the nucleophilicity of the uncoordinated primary nitrogen atoms [117].

The use of the preformed semiclathrochelate ligands, first proposed in Ref. 94, is an alternative (and supplementary) approach to the synthesis of the sarcophaginates and sepulchrates. A semi-clathrochelate *sen* ligand was employed to obtain sarcophaginates by template reaction of the [Co(sen)]Cl$_3$ complex with formaldehyde and ammonia to yield the [Co(MEazasar)]Cl$_3$ clathrochelate. A [Co(N-sen)]Cl$_3$·2H$_2$O complex was isolated as a by-product [96]. The resolution of [Co(MEazasar)]$^{3+}$ cation into its *S*- and *R*-isomers was achieved by IEC (aqueous sodium-antimony (+)-tartrate was used as an eluent). (+)-Co[(MEazasar)]Cl$_3$ sarcophaginate resulted from the (+)-[Co(sen)]Cl$_3$ semiclathrochelate as the initial compound [94]:

(35)
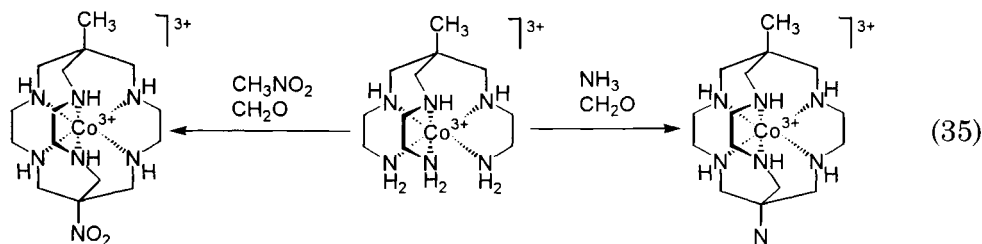
The reduction of [Co(MEazasar)]Cl$_3$ complex with a large excess of zinc dust in aqueous solution followed by treatment with hydrochloric acid and a Li$_2$ZnCl$_4$ solution yielded the cobalt(II) [Co(MEazasar)](ZnCl$_4$)·H$_2$O sarcophaginate [96].

Cross-linking of [Co(sen)]Cl$_3$ semisarcophaginate with nitro-methane and formaldehyde led to the formation of the [Co(NOMEsar)]Cl$_3$ complex readily reducible to [Co(AMMEsar)]Cl$_3$ sarcophaginate. A detailed procedure for the preparation of [Co(NOMEsar)]Cl$_3$ complex was reported in Refs. 101 and 118. Nitrosation of [Co(AMMEsar)]Cl$_3$ clathrochelate accompanied by reduction with zinc dust resulted in the [Co(MEsar)]Cl$_3$ complex [94]:

$$(36)$$
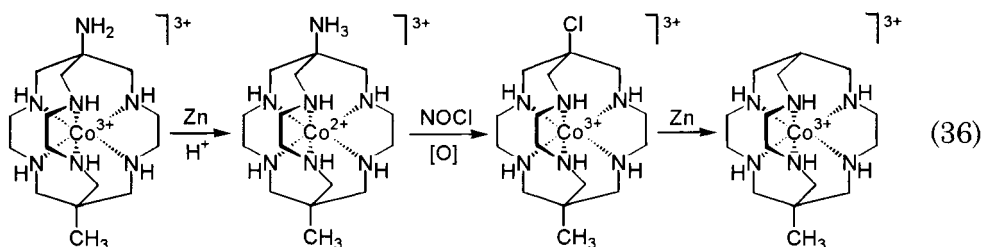
As with [Co(diAMsar)]³⁺ cation, nitrosation of the [Co(AMMEsar)]³⁺ cation led to the formation of "orange" and "yellow" fractions separated by IEC. The orange fraction contained the products of nucleophilic addition to carbanion without rearrangement (expected [Co(ClMEsar)]Cl₃ (*ca* 70%) and [Co(HOMEsar)]Cl₃ (*ca* 20%)sarcophaginates). The yellow fraction contained the product of nucleophilic addition to carbocation with rearrangement – [Co((ClME)MEabsar)]Cl₃ clathrochelate (*ca* 10%) [101].

The isolation of both regular and contracted cobalt(III) [Co(MEOHsar)]Cl₃ and [Co(MEOHabsar)]Cl₃ hydroxysarcophaginates, as well as their analogs with an encapsulated cobalt(II) ion, obtained by reduction with zinc dust (Scheme 44), is described in Ref. 106.

The synthesis of [Co(NOazasar)]³⁺ sarcophaginate was realized by two pathways starting from [Co(NOsen)]³⁺ and [Co(azasen)]³⁺ semiclathrochelates [119].
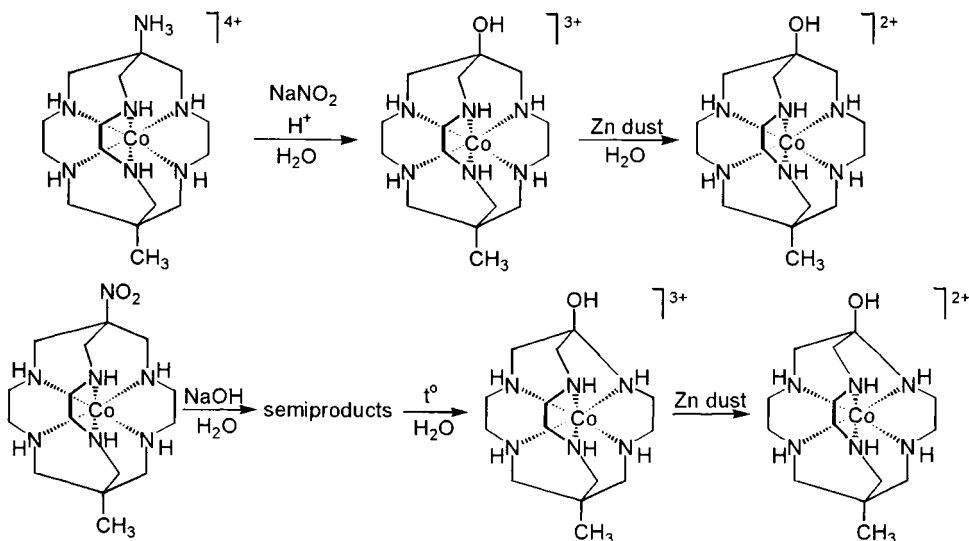
Scheme 44
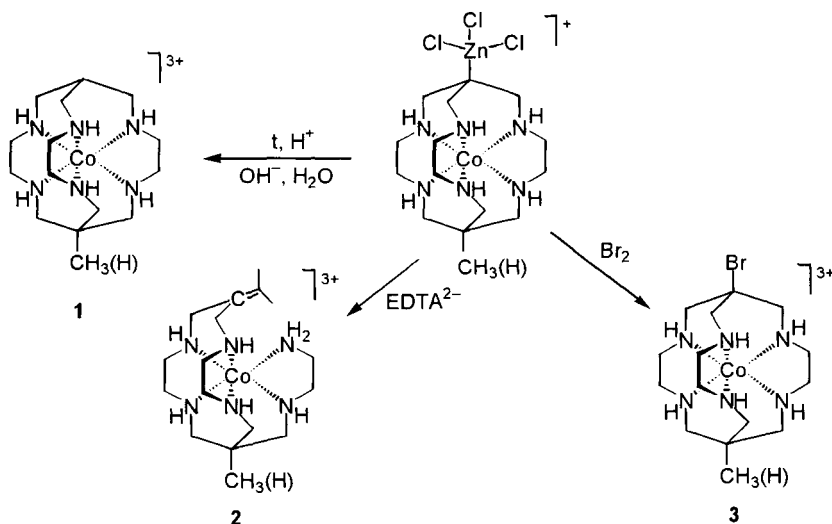
Scheme 45

During the synthesis of the methyne-capped cobalt(II) sarcophaginate *via* reduction of the chlorosarcophaginate complex with zinc dust in water (Scheme 45), an alkylzinc clathrochelate stable even in 6 molar hydrochloric acid was isolated [120].

Prolonged heating of the alkylzinc complex in acidic, neutral, or basic media resulted in the clathrochelate **1**. In the presence of Na_2EDTA, the rate of Zn–C bond cleavage is significantly faster because zinc ion forms a very stable complex with $EDTA^{2-}$ dianion. In addition to the initial sarcophaginate, olefin **2** was isolated. A bridgehead carbanion formed by the loss of zinc(II) ion can either capture a proton from the solvent (or any other additional electrophilic species including halogens, complex **3**) or rearrange to the olefin [120]. The unusual stability of the alkylzinc sarcophaginates also implies the possibility to synthesize relatively stable analogous magnesium, cadmium, aluminium, titanium, copper, cobalt, and nickel alkyl complexes [120].

The use of a semiclathrochelate hexadentate ligand is promising for the synthesis of sarcophaginates with different donor atoms, e.g. for the synthesis of N_3S_3-complexes. The N_3S_3–semisarcophaginate ligands were preliminarily synthesized in a high yield by refluxing 1,1,1-tris(mercaptomethyl)ethane and cyclohexane-1,3,5-trithiol with ethylene imine (Scheme 46) [121, 122].

The preformed semiclathrochelate $[Co(ten)]Cl_2(ClO_4) \cdot H_2O$ complex was capped with ammonia and formaldehyde in the presence of

Scheme 46

lithium carbonate to give a [Co(azacapten)](ClO$_4$)$_3$·2H$_2$O sarcophaginate, separated by IEC. The aqueous ammonium (+)-tartarate resolved the entantiomeric forms of this clathrochelate. The entantiomeric forms of the [Co(ten)]Cl$_2$(ClO$_4$)·H$_2$O complex were separated by the same technique.

Capping of [Co(ten)]$^{3+}$ cation with nitromethane and formaldehyde in aqueous solution in the presence of sodium carbonate gave the [Co(NOcapten)]Cl$_2$(ClO$_4$)·3/2H$_2$O complex. The reduction of the latter with zinc dust in aqueous HCl followed by treatment with hydrogen peroxide yielded a [Co(AMcapten)]Cl$_3$·5/2H$_2$O sarcophaginate. Cobalt(II) compounds were readily obtained by reduction of the corresponding cobalt(III) complexes with amalgamated zinc [121].

The reactivity of the protonated amino group in the [Co(AMHcapten)]$^{4+}$ aminosarcophaginate was used in the diazotization reaction [123], permitting to obtain the numerous N$_3$S$_3$-sarcophaginates with various apical substituents by analogy with N$_6$-sarcophaginates [94, 101] and also synthesize the *abcapten* type complexes with a contracted cavity (Scheme 46).

The capping of N$_3$S$_3$-semiclathrochelate [Co(ten)]$^{3+}$ cation *via* a template-assisted mixed aldehyde (formaldehyde/propanal) condensation (Scheme 47) made it possible to obtain N$_3$S$_3$-sarcophaginates with both regular and contracted cavities in fairly high yield, as well as to isolate the corresponding free ligands [124].

At the first stage, the semisarcophaginate ligand coordinated amino groups react with more active formaldehyde (two groups in the case of a "regular" cap, and one group in the case of a "contracted" cap), and the di- and monoimine products obtained are then attacked by a propanal carbanion to form monoimine sarcophaginates with regular and contracted cavities. A subsequent reduction with sodium borohydride leads to the [Co(diMEcapten)]$^{3+}$ and [Co(diMEabcapten)]$^{3+}$ sarcophaginates, respectively. It was stressed that the complexes obtained, unlike N$_6$-sarcophaginates, undergo facile reduction to low-spin cobalt(II) clathrochelates and after the reduction smoothly demetallate in the presence of cyanide anion.

This was attributed to a higher polarizability of thioether groups compared with that of amino groups, which leads to a decrease in the donor-acceptor interaction of thioether donors with first-row transition metals [124].

The cobalt(III) N$_3$S$_3$-oxosarcophaginates were obtained from [Co(ten)]$^{3+}$ semiclathrochelate with diethylmalonate (Scheme 48)
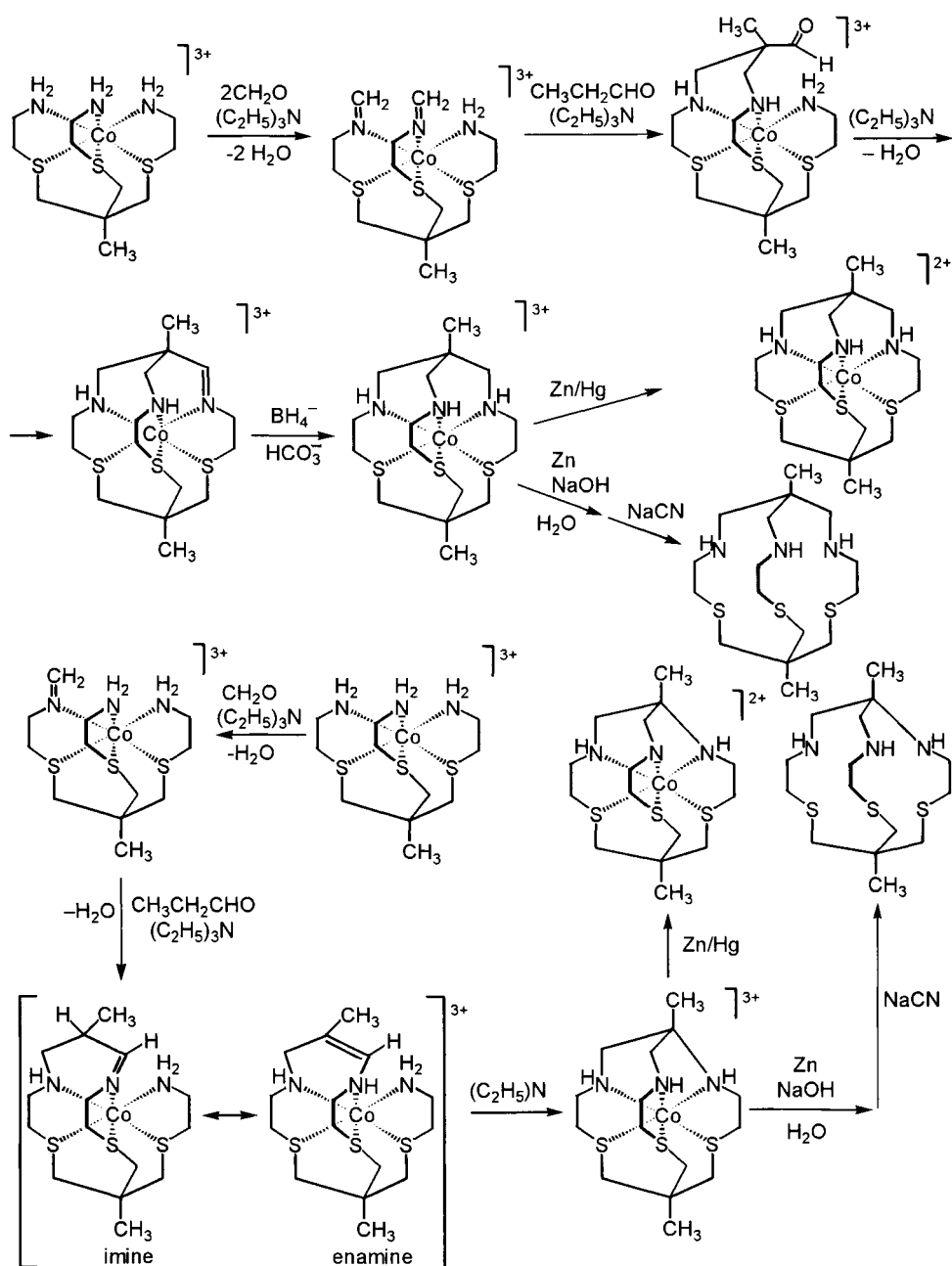
Scheme 47
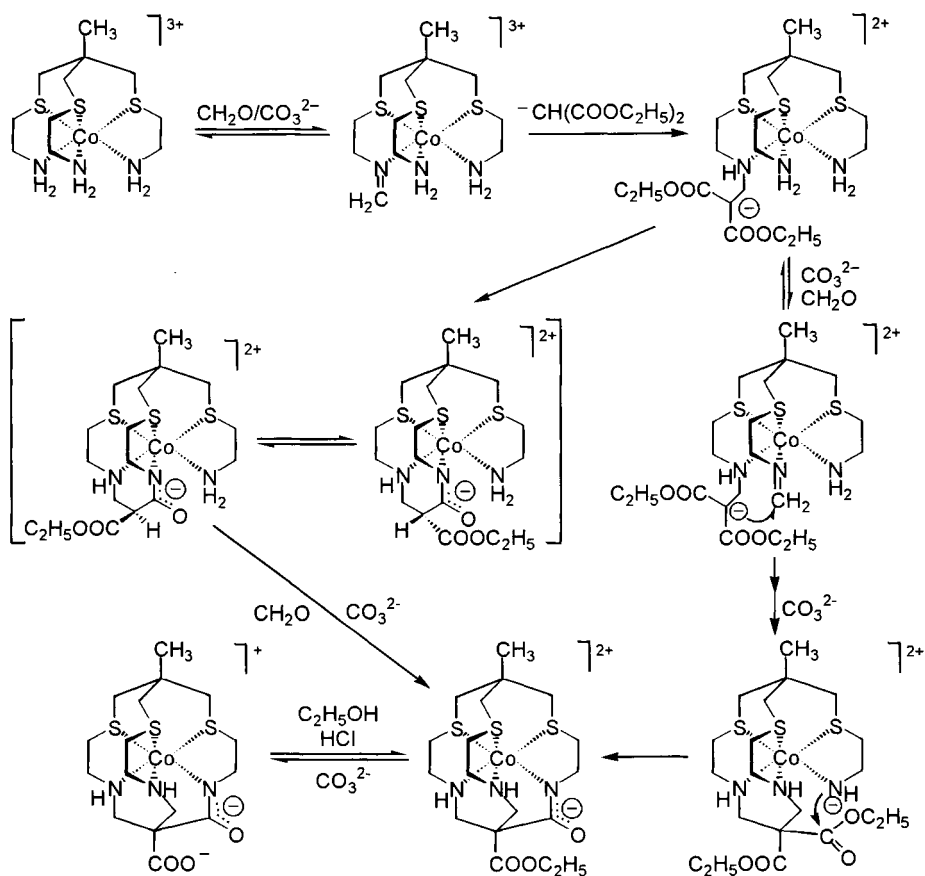
Scheme 48

[123]. As with N_6-complexes [94, 101], other N_3S_3-oxosarcophaginates can also be synthesized using reactive amino groups of the $[Co(AMoxocapten)]^{2+}$ cation.

The first selenium donor atoms incorporating sarcophaginate was obtained starting from the initial cobalt(III) N_3Se_3-semiclathrochelate by condensation with nitromethane and formaldehyde in water (Reaction 37).
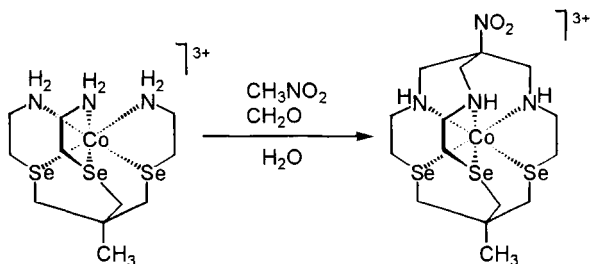
(37)

The following IEC separation (hydrochloric acid was used as eluent) and the vapor diffusion of ethanol into an aqueous solution of the cobalt(III) N_3Se_3-sarcophaginate led to the formation of $[Co(MENOsar-N_3Se_3)]Cl_3 \cdot 5H_2O$ crystals [125].

In the synthesis of amidine-functionalized cobalt(III) N_3S_3-sarcophaginates, malononitrile was used as a bifunctional carbon acid. The interaction of its pendant nitrile with the coordinated amino group of the $[Co(ten)]^{3+}$ semiclathrochelate led to the formation of an amidine N_3S_3-cage with an amide apical substituent.

This sarcophaginate originated from the nitriloamidine sarcophaginates, obtained at the first stage by a rapid intermolecular basic hydrolysis. The hydrolysis reaction was promoted by coordination to cobalt(III) ions. The resulting amide-substituted amidine sarcophaginates reacted with formaldehyde under basic conditions. The formaldehyde joined *exo*-nitrogen and the imine obtained then reacted with a neighboring deprotonated amide fragment forming a heterocycle (Scheme 49) [126].
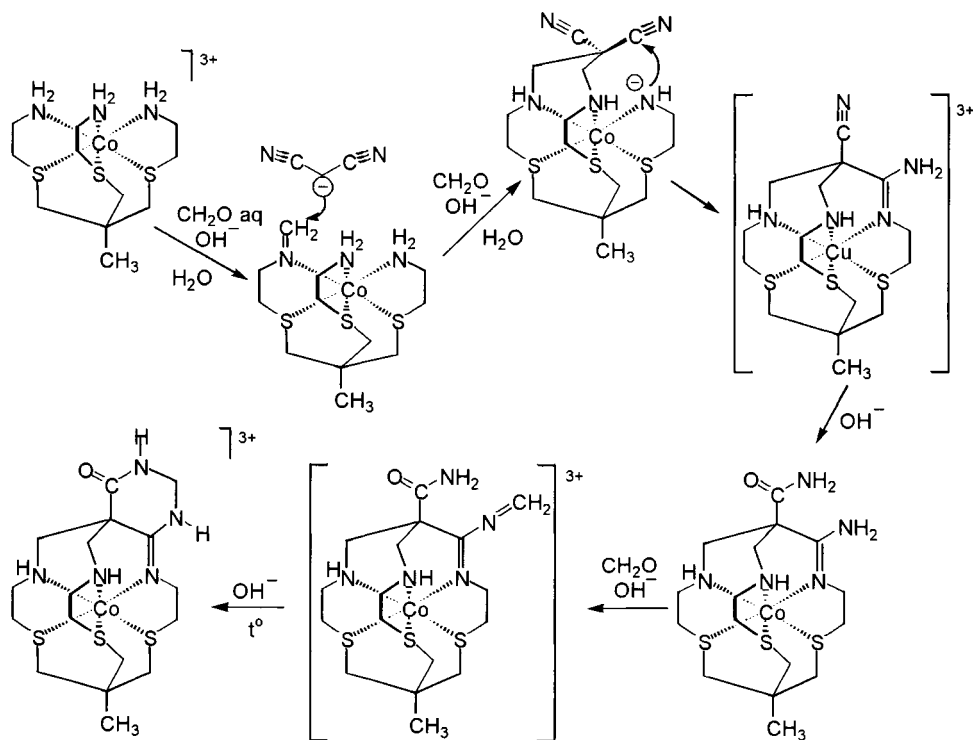
Scheme 49
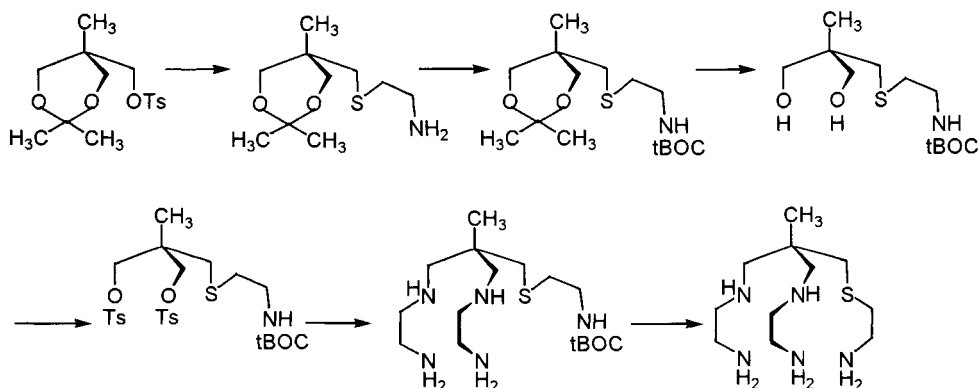
Scheme 50

The N5S-semiclathrochelate ligand was prepared [127] according to Scheme 50. The interaction of this ligand with Co^{2+} ions in methanol during oxidation by air oxygen and subsequent cross-linking with nitromethane and formaldehyde led to the formation of the $[Co(MENOsar-N_5S)](ClO_4)_3 \cdot H_2O$ sarcophaginate. The reduction of the latter by analogy with that for N6-dinitrosarcophaginate resulted in the formation of the $[Co(MEAMHsar-N_5S)]Br_1 \cdot H_2O$ N5S-sarcophaginate [127].

The analogous Scheme 51 was used for N4S2-sarcophaginate synthesis [128]. The mixture of the resultant $[Co(MENOsar-N_4S_2)]^{3+}$ and $[Co(MENOcapten)]^{3+}$ sarcophaginates was chromatographically separated. The reduction of the apical nitro group to a protonated amino group and subsequent diazotization reaction to produce $[Co(MECLsar-N_4S_2)](ClO_4)_3 \cdot 3H_2O$ and $[Co(MEsar-N_4S_2)](ClO_4)_3$ complexes were achieved. Free *AMMEsar*-N4S2 ligand was isolated after cobalt(II) complex reaction with cyanide anion and used for the synthesis of other ion complexes [128].

The first representatives of a new type of N3S3-sarcophaginates capped with *d*-metal ions were obtained starting from a trinuclear $[Co(Co(aet)_3)_2]^{3+}$ derivative of the 2-aminoethanethiol (Scheme 52). In this case, the kinetically inert central cobalt(III) ion served as a bifunctional capping agent. Both *rac*- and *meso*-forms of the initial complex were preliminarily isolated by IEC.

An attempt to carry out routine capping procedures with the NH_3/CH_2O and CH_3NO_2/CH_2O systems under basic conditions failed because of the occurrence of side reactions. Therefore, a stepwise
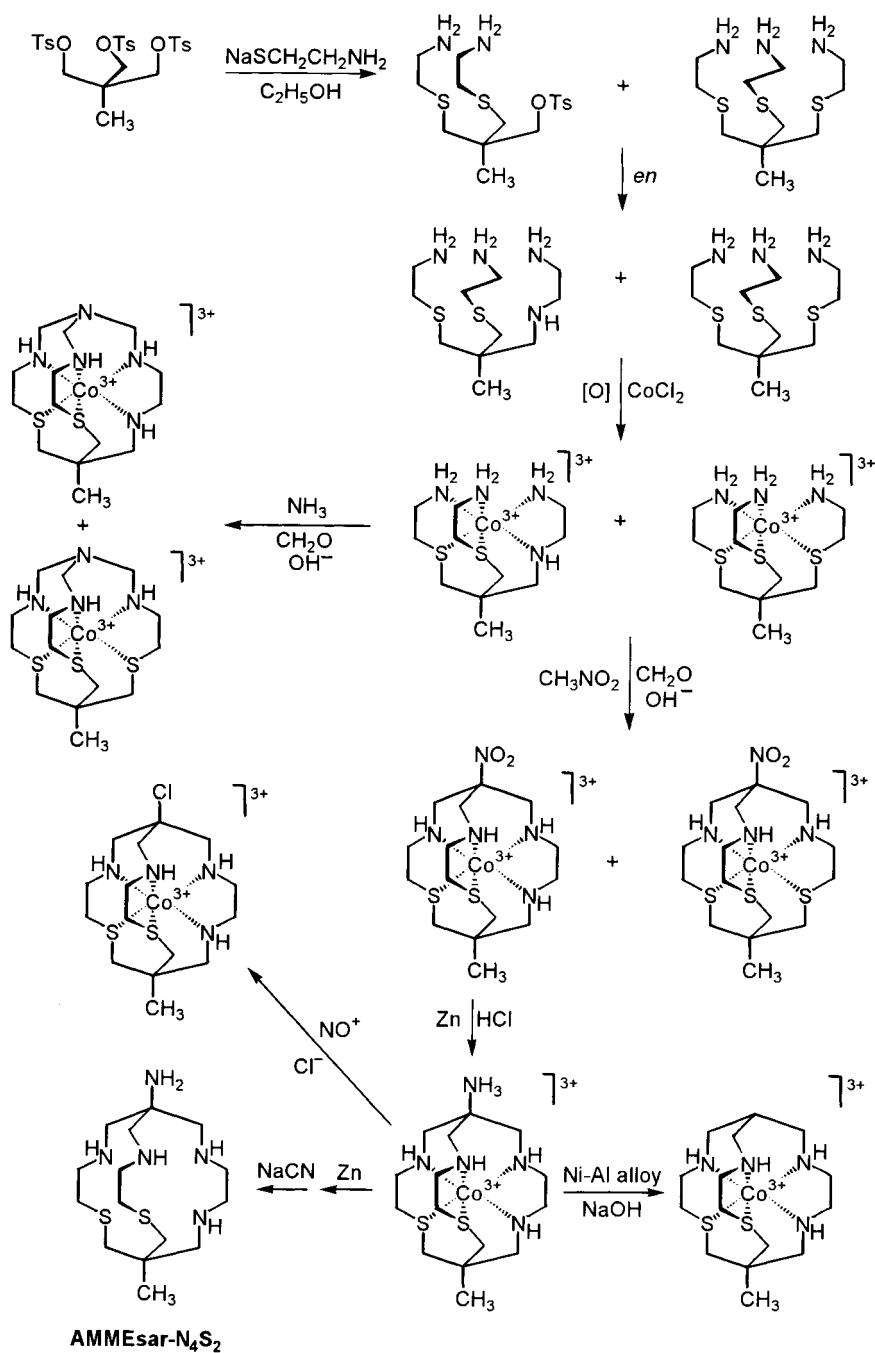
Scheme 51

Scheme 52

Scheme 53
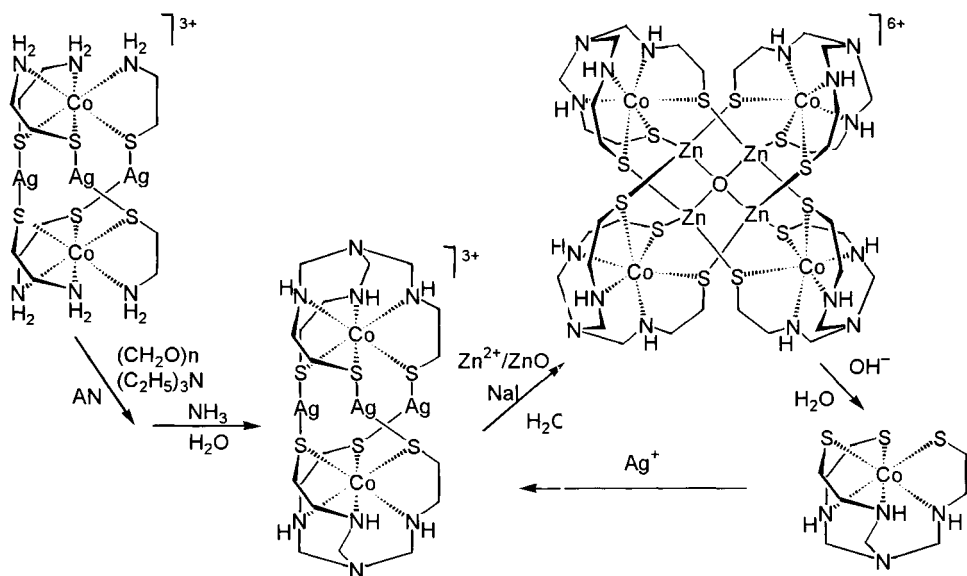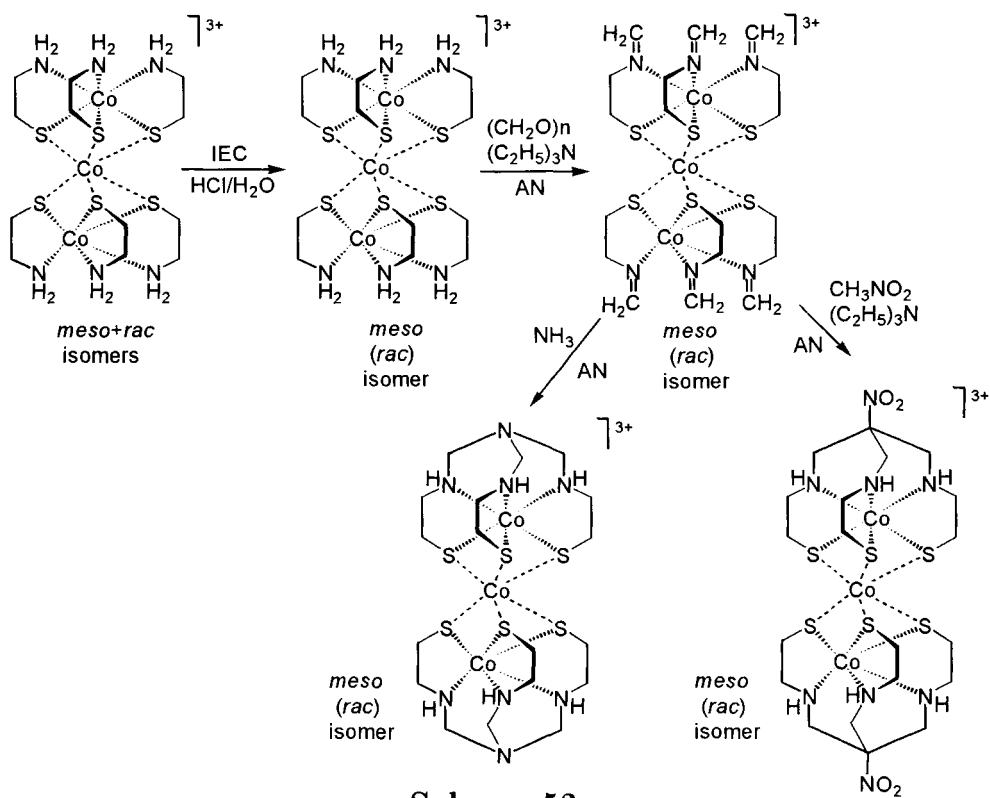
synthesis of bis-sarcophaginates was implemented. At the first stage, the interaction of the $[Co(Co(aet)_3)_2]^{3+}$ cation with paraformaldehyde in the presence of triethylamine led to the hexaimine bis-semi-clathrochelate. Then the compound obtained underwent capping with ammonia or nitromethane in the presence of triethylamine in catalytic amounts. In this case, the resulting clathrochelates retained the initial (*rac-* or *meso-*) configuration [129].

A similar strategy was employed to obtain mixed pentanuclear cobalt(III) and silver(I) N_6S_6-bis-sarcophaginates. The preliminarily synthesized $[Ag_3(Co(aet)_3)_2]^{3+}$ bis-semiclathrochelate [130] underwent condensation with paraformaldehyde in acetonitrile in the presence of triethylamine. A subsequent addition of aqueous ammonia led to the formation of a pentanuclear cobalt(III) bis-azasarcophaginate in high yield (Scheme 53) [131]. It was emphasized that the latter complex can also be obtained in a low yield by a routine procedure in aqueous solution. The resultant pentanuclear cobalt(III) bis-azasarcopha-ginate, when treated with zinc nitrate and oxide in water in the presence of NaI, formed an octanuclear Zn_1Co_4 aza-capped complex. This complex gave a cobalt(III) N_3S_3-semisarcophaginate under basic conditions [131].

In addition to ammonia and nitromethane, some other compounds containing active hydrogen atoms, such as bis-ethylenediamine cobalt(III) pyruvate, can be employed as capping agents for the synthesis of sarcophaginates [132]. The interaction of the trifluoromethanesulphonate salt of bis-ethylenediamine cobalt(III) pyruvate and $[Co(sen)]^{3+}$ semisarcophaginate with paraformaldehyde in acetonitrile in the presence of diisopropylethylamine gave a sarcophaginate containing bis-ethylenediamine cobalt(II) pyruvate in the apical position:

$$(38)$$
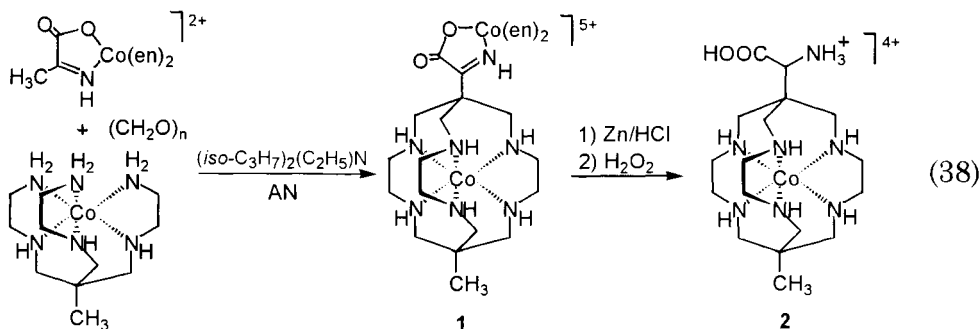
Reduction of complex **1** with zinc dust in aqueous hydrochloric acid followed by oxidation with hydrogen peroxide led to the formation of sarcophaginate **2**.

When diethylmalonate or cyanoacetate have been used instead of bis-ethylenediamine cobalt(III) pyruvate, the cobalt(III) oxoaza- and oxosarcophaginates were isolated by analogy with the previous scheme [133]. The semiclathrochelate [Co(azasen)]Cl$_3$ and [Co(sen)]Br$_3$ complexes, respectively, were used as initial compounds.

The interaction of [Co(sen)]Br$_3$ semiclathrochelate with formaldehyde and diethylmalonate in aqueous solution resulted in the [Co(EFMEoxosar–H)](ClO$_4$)$_2$ sarcophaginate **1**. The modify- cation reactions of this complex resulted in clathrochelates **2-5** (Scheme 54). When the (+)- or (–)-isomer of [Co(sen)]Br$_3$ semisarco- phaginate was used as initial complex, the corresponding [Co(EFMEoxosar–H)](ClO$_4$)$_2$ optical isomers were obtained. The reduction of [Co(EFMEoxosar–H)](ClO$_4$)$_2$ complex with zinc amalgam in aqueous solution led to the formation of the corresponding cobalt(II) complex [133].
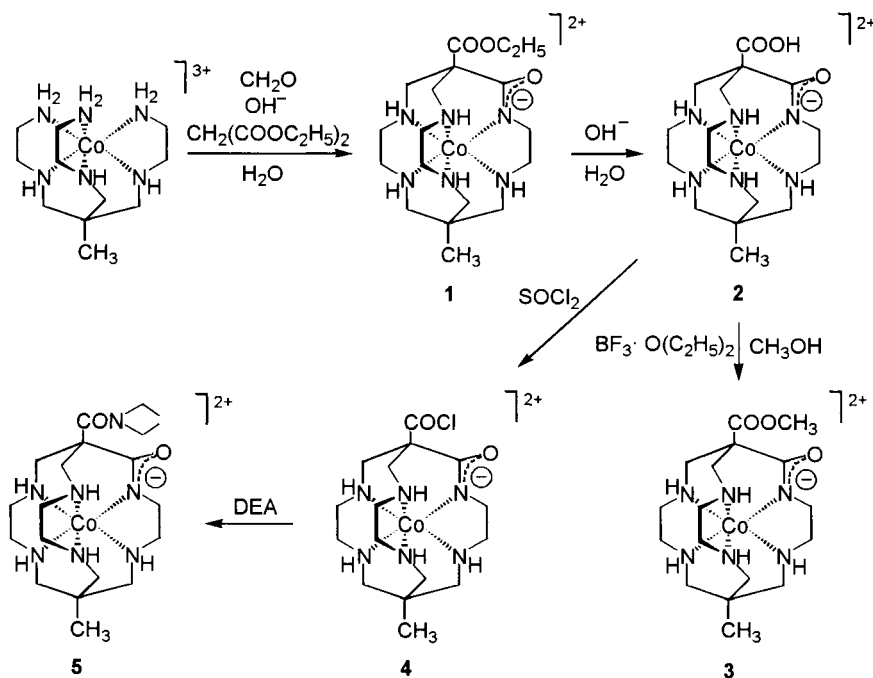
Scheme 54

When ethyl cyanoacetate was used instead of diethylmalonate, the macrocyclization reaction yielded mostly [Co(CNMEoxosar–H)]$^{2+}$ oxosarcophaginate with an apical nitrile group.

$$
\left[\text{H}_2\text{N–N–N–NH}_2 \text{ Co complex, CH}_3 \right]^{3+} \xrightarrow[\text{H}_2\text{O}]{\substack{\text{CH}_2\text{O} \\ \text{NCCH}_2\text{COOC}_2\text{H}_5, \text{ OH}^-}} \left[\text{CN ... Co oxosarcophaginate, CH}_3 \right]^{2+} \tag{39}
$$
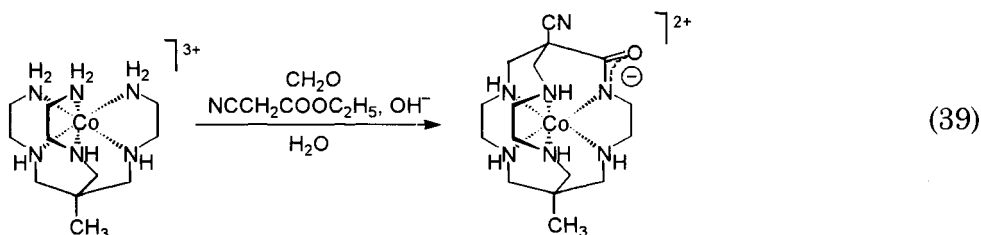
The [Co(azasen)]Cl$_3$ semisepulchrate underwent an analogous reaction with diethylmalonate [133]:

$$
\left[\text{H}_2\text{N–N–N–NH}_2 \text{ Co complex} \right]^{3+} \xrightarrow{\substack{\text{CH}_2\text{O, OH}^- \\ \text{CH}_2(\text{COOC}_2\text{H}_5)_2}} \left[\text{COOC}_2\text{H}_5 ... \text{Co complex} \right]^{2+} \tag{40}
$$
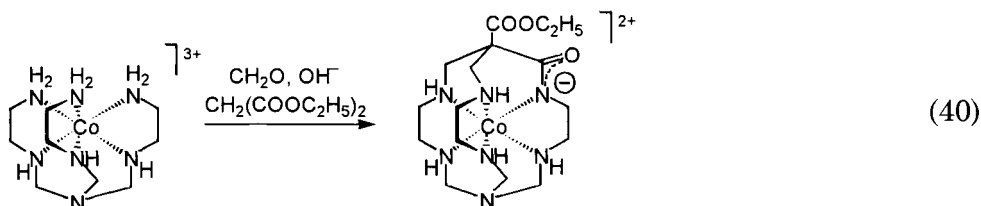
The *exo*-imine formed at the first stage *via* the addition of formaldehyde to the [Co(sen)]$^{3+}$ semisarcophaginate coordinated amino group condenses with an ethyl cyanoacetate anion through a deprotonated methylene unit. A second coordinated amino group follows the same condensation pathway, and then the remaining amino group condenses mainly with an ether group to give an amide fragment (Scheme 55). An attempt to isolate a free sarcophagine by demetallation of the cobalt(III) complex proved to be unsuccessful [134].

The amidine-functionalized cobalt(III) sarcophaginates with apical carboxylic acid and the complex resulting from its decarboxylation, as well as the [Co(MEazasar)]$^{3+}$ azasarcophaginate (formed by capping with ammonia resulting from the hydrolysis of the ethyl cyanoacetate nitrile groups), are minor clathrochelate products of this reaction [134].

The [Co(EFoxosen–H)]Cl$_2$ semisarcophaginate, preliminarily synthesized by reaction of [Co(en)$_3$]Cl$_3$ tris-ethylenediaminate with diethylmalonate and formaldehyde, was capped with nitromethane in the presence of formaldehyde. The resultant nitrosarcophaginate underwent reactions involving both the apical groups (Scheme 56) [133].

The protons of alkyl groups in the α- and γ-positions relative to the pyridine nitrogen atom are, to a great extent, apt to be detached because of delocalization of a negative charge of the carbanion in the heterocycle. In the case of NH^+ salts and N-oxides, this tendency evidently increases.
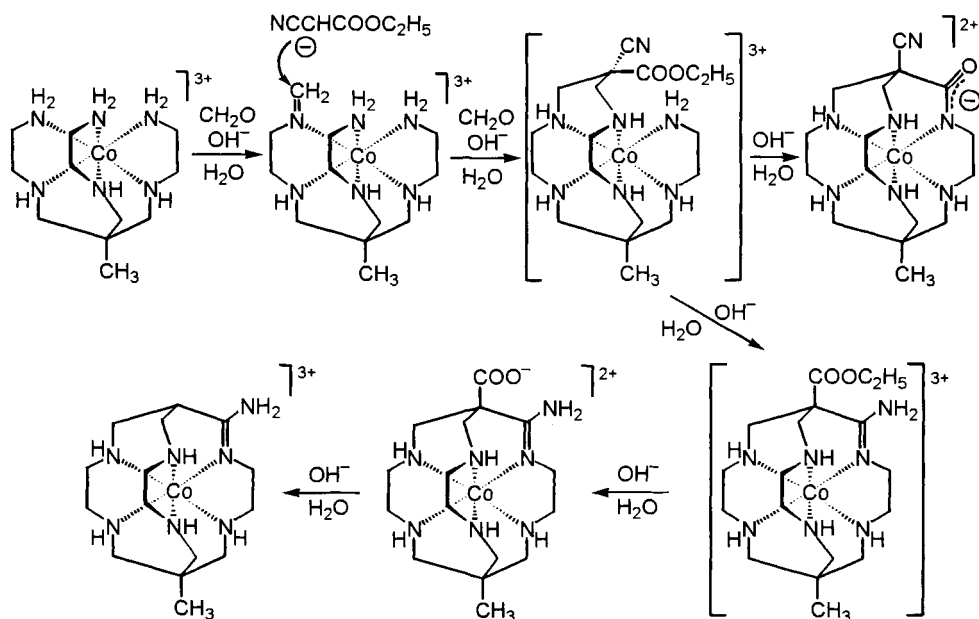
Scheme 55
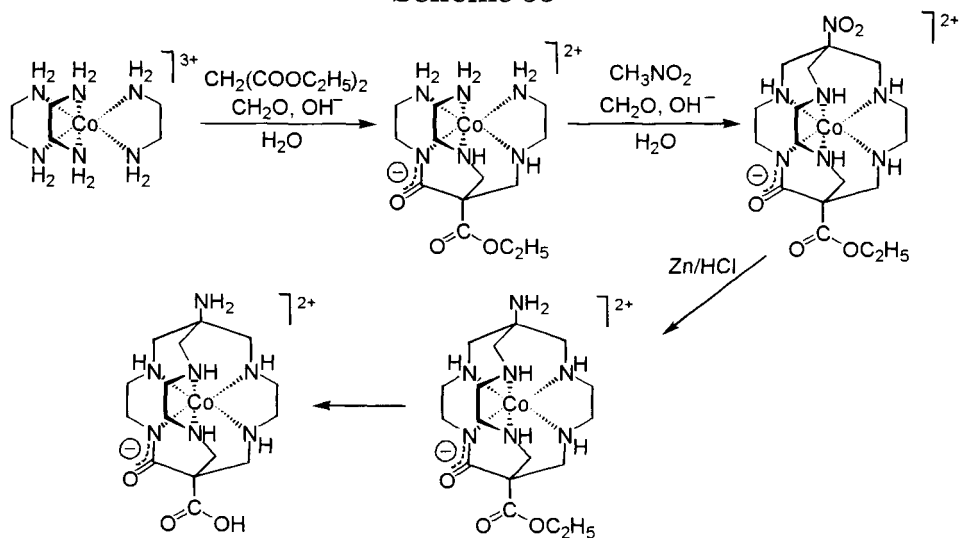
Scheme 56

An attempt to utilize the reactivity of the methyl group protons of N-alkylated γ-picoline and γ-quinoline in the reaction of the semiclathrochelate $[Co(sen)]^{3+}$ cation with paraformaldehyde proved to be successful (Scheme 57).

The subsequent dealkylation of a heterocyclic nitrogen atom led to the formation of $[Co(MEPYsar)]Cl_4 \cdot 4H_2O$ and $[Co(MEQNsar)]Cl_4 \cdot \cdot 3H_2O$ sarcophaginates [135].

The facile reactions of the preliminarily synthesized semisarcophaginate with aromatic ketones and diketones and paraformaldehyde in acetonitrile allowed one to obtain polyfunctional aromatic substituted cobalt(III) sarcophaginates in high yields by Scheme 58.

Only one diimine cage complex was isolated with dibenzoylmethane (both carbonyl groups and one formaldehyde molecule are involved in its formation) while acetophenone formed two clathrochelates (imine and carbonyl-containing complexes) in a relatively high yield. Such imine sarcophaginates are readily reduced by $NaBH_4$, and the mixture of isomers induced by the chirality of a benzyl carbon atom has been formed in the case of a dibenzoylmethane derivative [136].

It was assumed that a methaneimine complex accepting a β-diketone carbanion is formed at the first stage of the dibenzoylmethane derivative synthesis. Two ketone groups would then undergo condensation with the remaining deprotonated primary
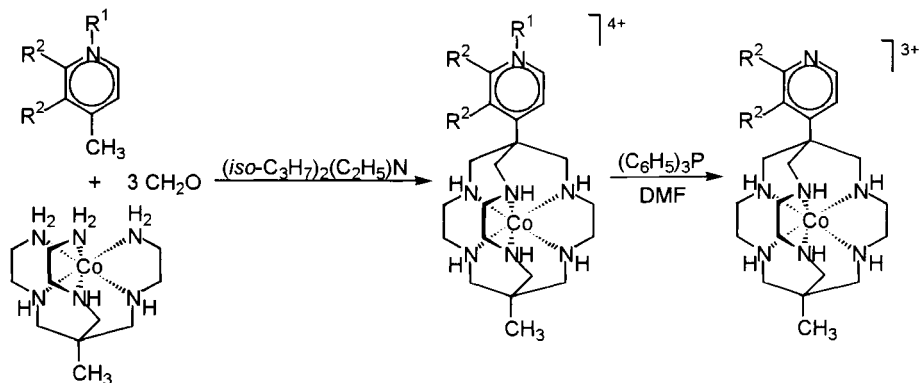
2; $R^1=CH_3$, $R^2=H$ [Co(ME(N–mePY)sar)]$^{4+}$ 5; $R^1=CH_2C_6H_5$, $2R^2=[CH]_4$ [Co(ME(N-bnQN)sar]$^{4+}$
3; $R^1=CH_2C_6H_5$, $R^2=H$ [Co(ME(N–bnPY)sar)]$^{4+}$ 6; $R^2=H$ [Co(MEPYsar)]$^{3+}$
4; $R^1=CH_3$, $2R^2=[CH]_4$ [Co(ME(N-meQN)sar)]$^{4+}$ 7; $2R^2=[CH]_4$ [Co(MEQNsar)]$^{3+}$

Scheme 57
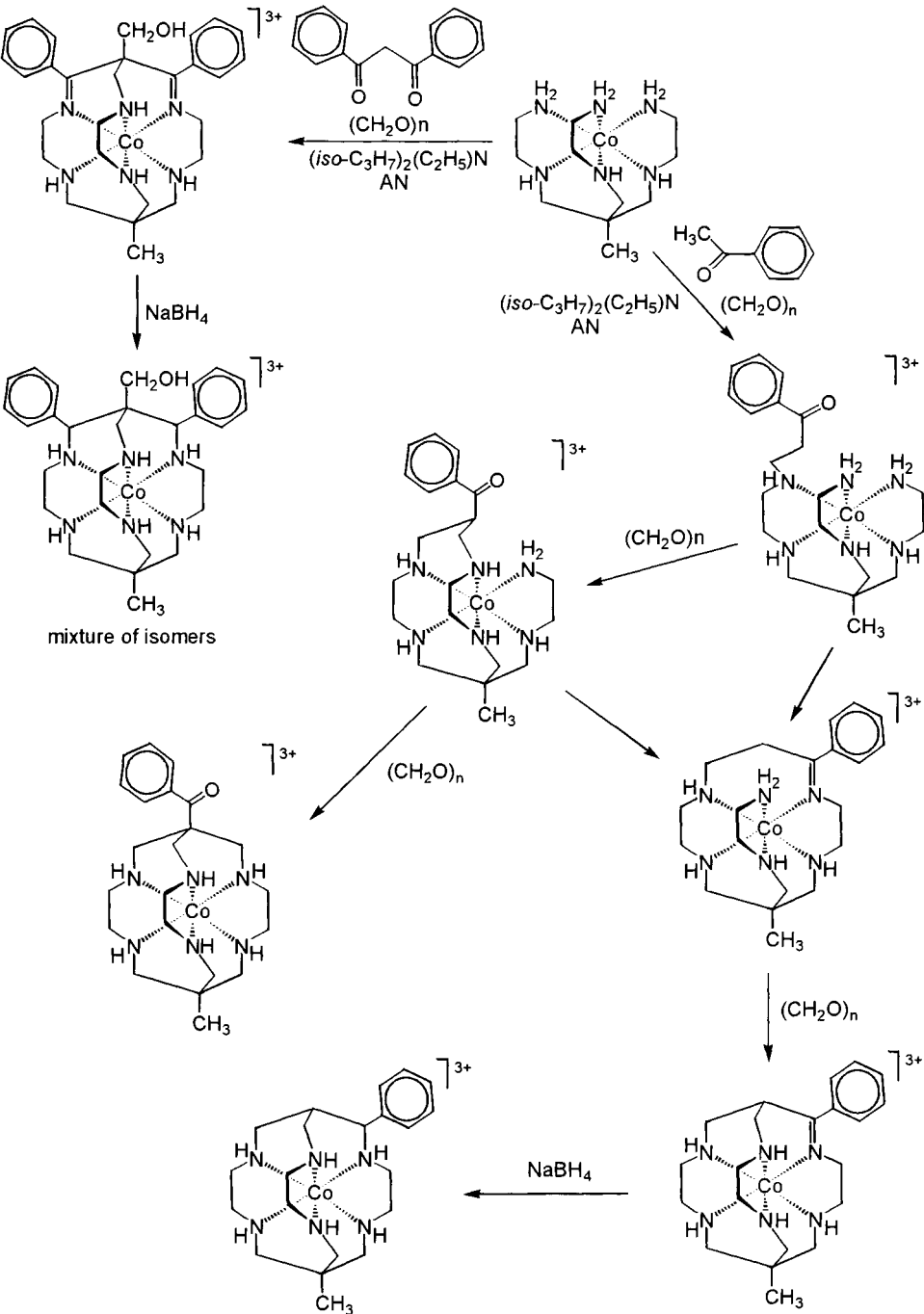
Scheme 58

amino groups of the semiclathrochelate. The tertiary capped carbon atom activated by two imine groups reacts with a formaldehyde molecule to give the apical methoxyl substituent.

In the case of an acetophenone derivative, the reaction also involves the formation of a methaneimine complex that has undergone intermolecular reaction with the carbanion. Two processes may then take place: an intramolecular condensation with the two remaining methaneimine fragments of the same molecule to yield a C_3-symmetric apical functionalized sarcophaginate and a reaction of the ketone group with the remaining deprotonated primary amino groups to give meridional-substituted imine sarcophaginate [136].

A more detailed synthesis of 4-nitrophenyl-, 2-naphthyl-, 2-phenanthryl-, 9-anthryl-, and 2-anthraquinonyl-substituted cobalt(III) sarcophaginates starting from the corresponding methylarylketones was reported in Ref. 137.

In all cases, except for 9-acetylanthracene, both C_3-symmetric amine clathrochelates with apical aromatic substituents and C_3-nonsymmetric imine sarcophaginates with substituents in the methylene units have been formed (Scheme 59). The reaction of 9-acetylanthracene under the same conditions led only to the aroyl-type sarcophaginate, since in this case a bulky substituent inhibits the condensation of a keto group with an amino group to give imine.

Both types of compounds obtained were reduced with $NaBH_4$ in aqueous solution (except the anthraquinone imine complex, which under given conditions an aryl substituent has been reduced). The resultant 4-nitrophenylsarcophaginate with substitution in the methylene unit was further reduced to a 2-aminophenyl-substituted clathrochelate with metallic tin in aqueous HCl.

Since the hydrogen atoms in phosphorus(III) and antimony(III) hydrides are also active, these compounds have been used as capping agents for cobalt(III) semiclathrochelates. The reaction of the $[Co(sen)](CF_3SO_3)_3$ complex with an excess of paraformaldehyde, phosphine, and triethylamine in acetonitrile at room temperature resulted in a phosphorus-containing $[Co(MEphosphasar)]^{3+}$ sarcophaginate, which was readily oxidized to $[Co(MEOphosphasar)]^{3+}$ cation with air oxygen or hydrogen peroxide in aqueous solution [138]:

$$(41)$$
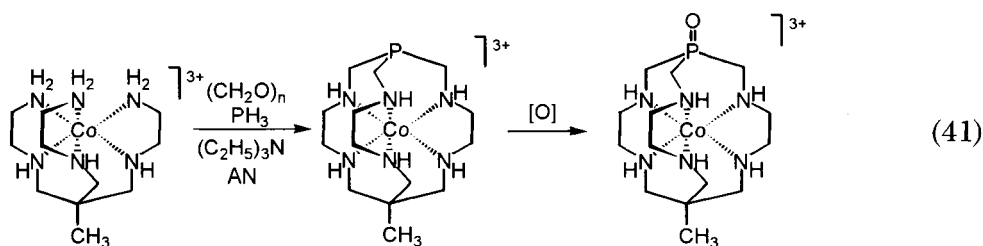
Arsine is a less reactive capping agent, and tris-imine complex was preliminarily obtained by reaction of the [Co(sen)]Cl₃ semisarcophaginate with an excess of paraformaldehyde in
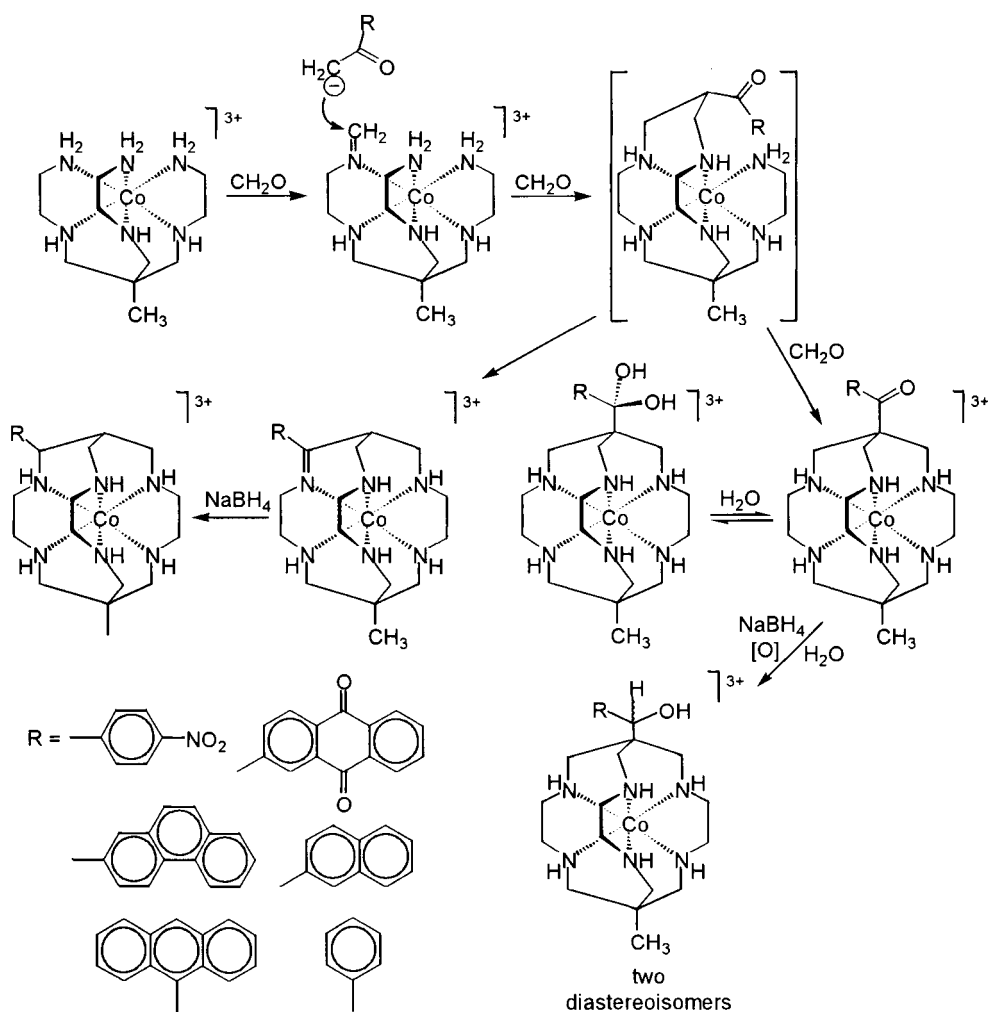
Scheme 59

acetonitrile, catalyzed by triethylamine. After treatment of the reaction mixture with aqueous hydrochloric acid, the yield of the imine [Co(sim)]Cl$_3$ complex was 95%. The trifluoromethane-sulphonic salt of a [Co(sim)]$^{3+}$ cation was reacted with arsine in the presence of triethylamine to form an arsine-capped sarcophaginate in good yield:

$$(42)$$
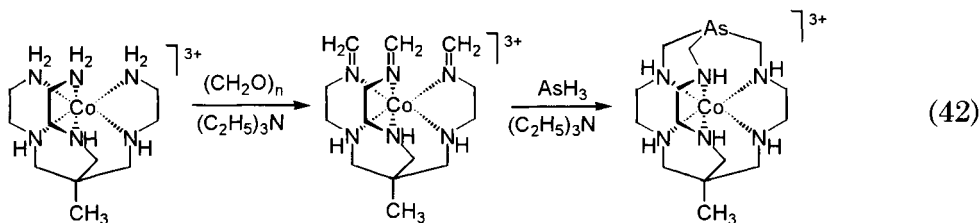
This complex was isolated from the reaction mixture by IEC after treatment with hydrochloric acid [139].

A novel strategy for the synthesis of sarcophaginates is based on the interaction of the [Co(sim)]$^{3+}$ complex with other primary aldehydes, in particular, acetaldehyde [140]. The reaction carried out in acetonitrile in the presence of triethylamine yielded the two main products, aldehyde sarcophaginate **1** and imine complex **2**, Scheme 60. The latter resulted from the removal of formaldehyde in the presence of water to give a diimine complex that reacted with aldehyde. The reduction of imine clathrochelate **2** with NaBH$_4$ yielded saturated sarcophaginate **3**. A template condensation of [Co(sen)]$^{3+}$ semisarcophaginate with two equivalents of formaldehyde and one equivalent of acetaldehyde also produced imine complex **2** in a good yield. A novel strategy for sarcophaginate synthesis was also extended for the preparation of complexes with other substituents at the apical carbon atom [140].

The reactivity of aldehyde groups was also used for the synthesis of the long-chain cobalt (III) sarcophaginates, which display anthelmintic properties [110, 141].

Semiclathrochelate complexes containing macrocyclic fragments have been employed in the synthesis of sarcophaginates with apical macrocyclic rings. Such macrotricyclic cobalt(III) compounds were obtained starting from the macrocyclic hexamine *taetacn* precursor [142]. This precursor was preliminarily synthesized by reductive alkylation of 1,4,7-triazacyclononane *(tacn)* with phthalimidoace-taldehyde in the presence of NaNCBH$_3$. The desired product was

Scheme 60

R=H, CH₃, C₆H₅
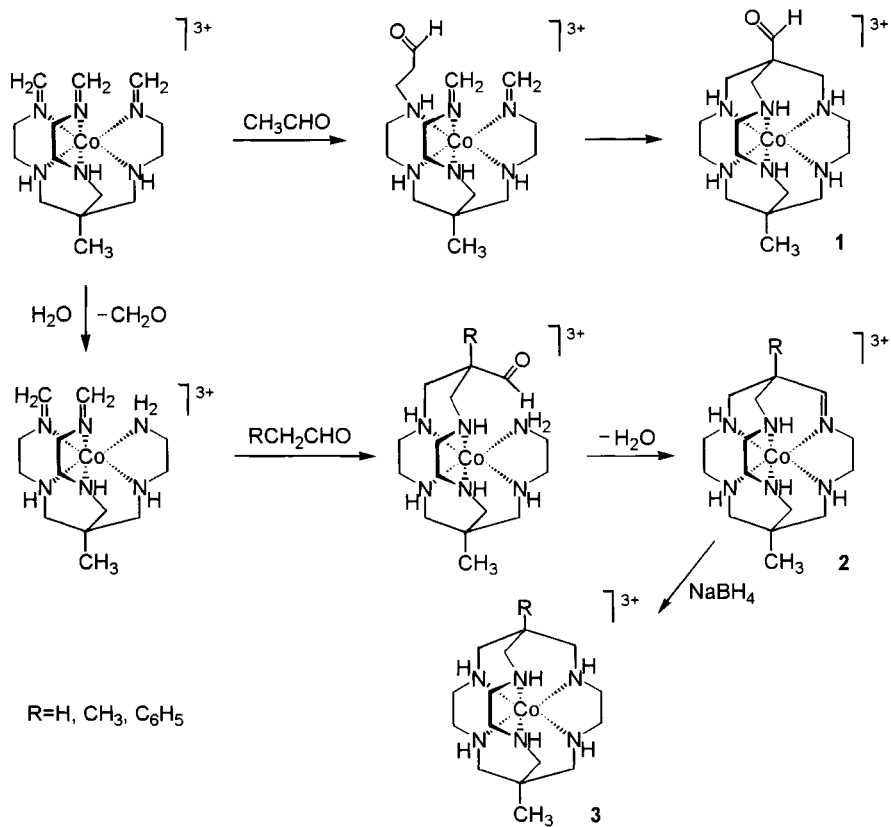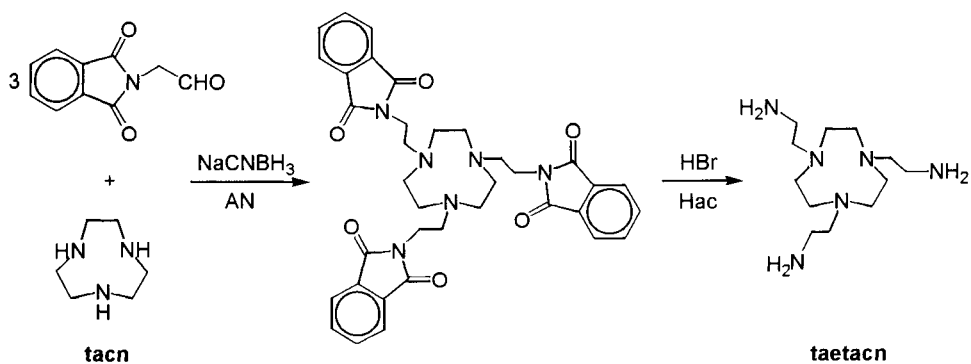
Scheme 61

obtained by acidic hydrolysis of the protecting phthaloyl groups (Scheme 61).

A mixture of a crude *taetacn*·6HBr, $CoCl_2$·6H_2O, NaOH and activated carbon in water was air-bubbled followed by treatment with an excess of $NaClO_4$ to give a mixture of semiclathrochelate Λ- and Δ-[Co(taetacn)](ClO_4)$_3$ isomers. This mixture was separated by eluation with aqueous sodium (+)-tartrate on an ion-exchange column. The free ligand was readily obtained upon demetallation of the purified complex with H_2S [142]. The capping of [Co(taetacn)]$^{3+}$ cation with nitromethane and formaldehyde in aqueous solution in the presence of Na_2CO_3 followed by separation on an ion-exchange column yielded a racemic [Co(NOsartacn)]Cl_3·2H_2O sarcophaginate.

$$(43)$$
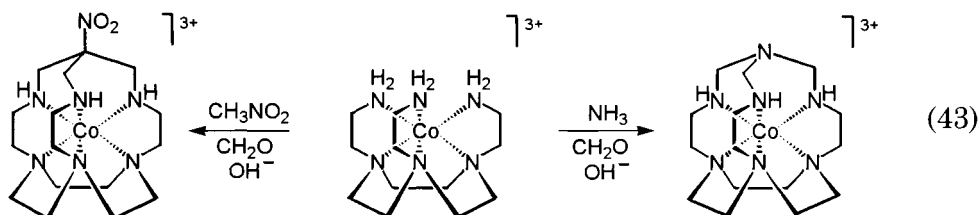
The dithionate salt of the (+) and (−)-[(Co(NOsartacn)]$^{3+}$ trication was resolved using aqueous sodium-antimony (+)-tartrate as an eluents. The reduction of [Co(NOsartacn)]Cl_3·2H_2O complex with zinc dust in aqueous hydrochloric acid followed by treatment with hydrogen peroxide led to the formation of the [Co(AMHsartacn)]$^{4+}$ aminosarcophaginate. This complex was separated into optically active forms by the same procedure [142].

The racemic [Co(azasartacn)]Cl_3·1/2CH_3OH·C_2H_5OH complex resulted from capping of [Co(taetacn)]$^{3+}$ cation with ammonia and formaldehyde in aqueous solution in the presence of lithium carbonate. Only partial separation was achieved when attempts were made to resolve azasarcophaginate [Co(azasartacn)]$^{3+}$ cation into Λ- and Δ-forms by IEC. Therefore, the pre-resolved Λ- and Δ-[Co(taetacn)](ClO_4)$_3$ semiclathrochelates were used as initial compounds. As result, the Λ- and Δ-[Co(azasartacn)]$^{3+}$ sarcophaginates were isolated as PF_6^- salts and were additionally purified by fractional crystallization from aqueous solution [142].

Semiclathrochelate N_3S_3- and N_6-complexes with one of the tetrapodal units as apical substituent were prepared by the interaction of cobalt(III) ion with potentially octadentate tetrapodal N_4S_4- and N_8-ligands (Scheme 62). Cyclization of these complexes
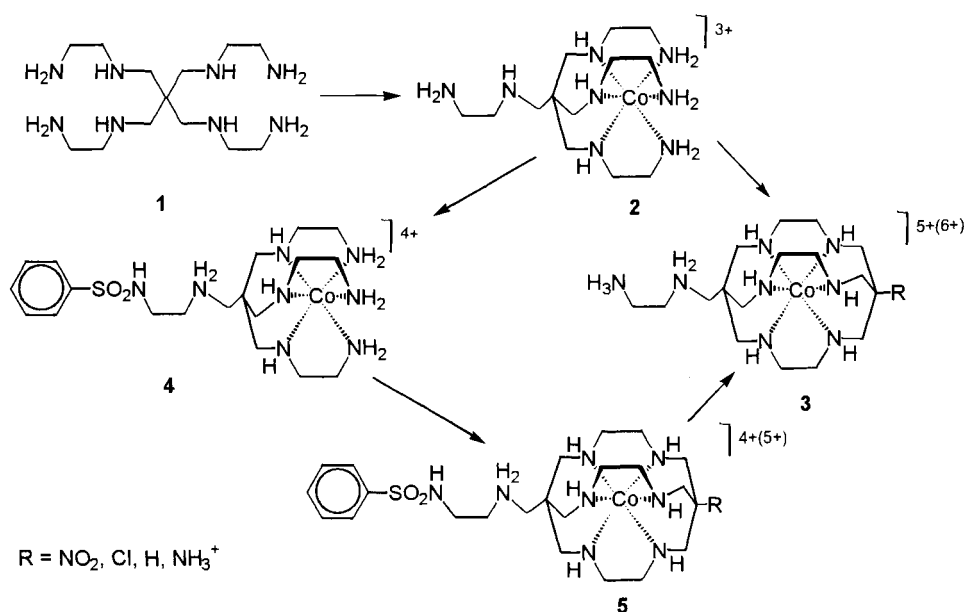
Scheme 62

with nitromethane yielded so-called reinforced sarcophaginates apt to undergo reaction with participation of the nitro group and a reinforcing substituent. For instance, as a result of the above reactions, the tetrapodal 5,5'-bis-(4-amino-2-azabutyl)-3,7-diaza-nonane-1,9-diamine **1**, preformed *via* reaction of ethylenediamine with pentaerythritotosylate, gave sarcophaginate **3** containing apical ethylenediamine fragments [143].

The N_3S_3-containing analog of sarcophaginate **3** was obtained from 5,5'-bis-(4-amino-2-thiabutyl)-3,7-dithianonane-1,9-diamine by Scheme 63 [144]. After reduction with zinc dust the resultant N_3S_3-sarcophaginate underwent demetallation with NaCN. Thus, the ligand obtained may be employed for the synthesis of other metal ion complexes.

The synthesis of S_6-sepulchrate was primarily performed by Lehn and coworkers [145] *via* condensation of dithiadiamine and chloroanhydride of dithiadicarboxylic acid under high-dilution conditions to produce macrocyclic diamide **2** which after reduction to corresponding diamine **3** was built up to macrobicyclic ligand **4** (Scheme 64).
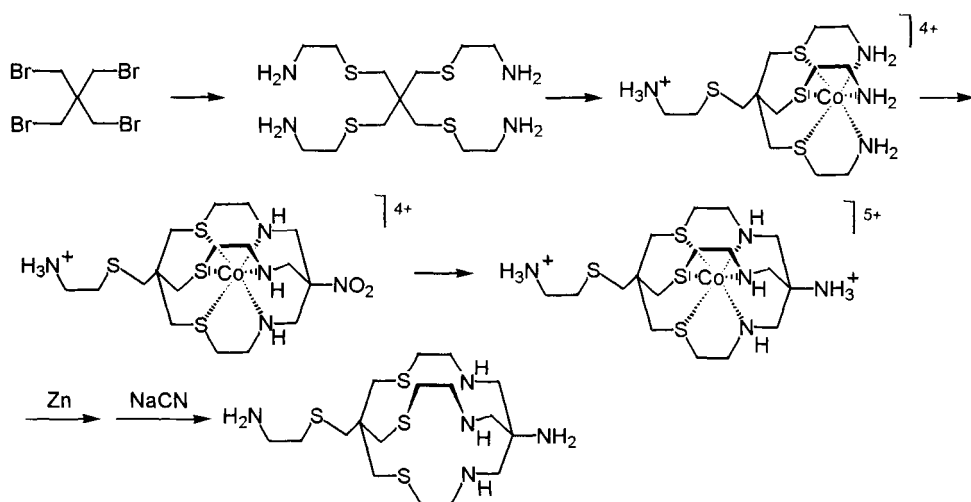
Scheme 63
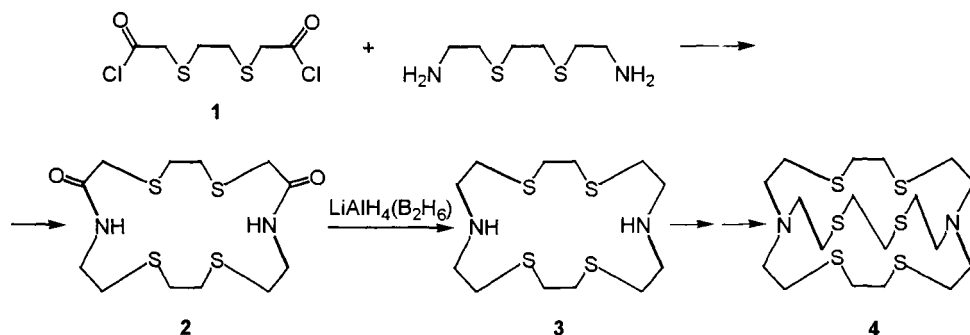
Scheme 64

The first cobalt(II) and cobalt(III) S$_6$-sarcophaginates were obtained by Sargeson and coworkers [146] from the preliminarily synthesized free *diMEsar-S$_6$* ligand (Scheme 65).

A caesium ion was used as the template in this synthesis. The resultant ligand easily formed a cobalt(II) complex in methanol-methylene dichloride mixture. The isolated [Co(diMEsar-S$_6$)] (CF$_3$SO$_3$)$_2$ clathrochelate was readily oxidized by AgCF$_3$SO$_3$ in aqueous solution to the cobalt (III) [Co(diMEsar-S$_6$)](CF$_3$SO$_3$)$_3$ S$_6$-sarcophaginate [146].

The expanded S$_6$-sarcophaginate *diMEl,3pnsar-S$_6$* ligand displaying high conformational lability and, therefore, apt to be readily demetallate, was synthesized by Scheme 66 [147].
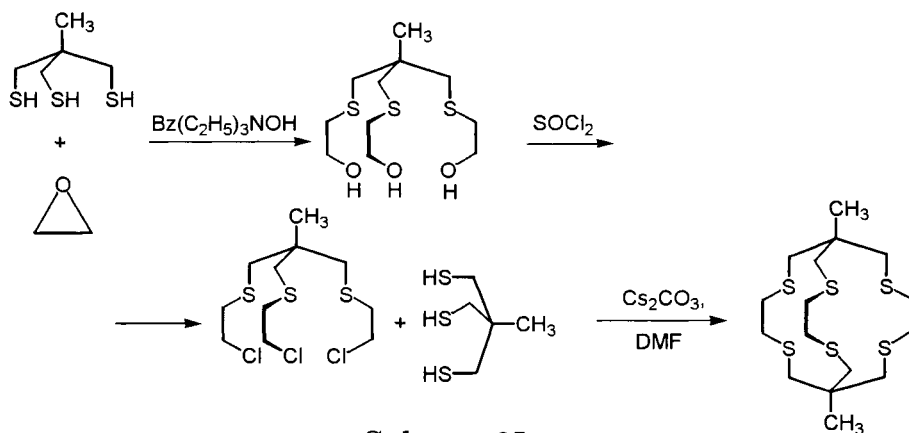
Scheme 65
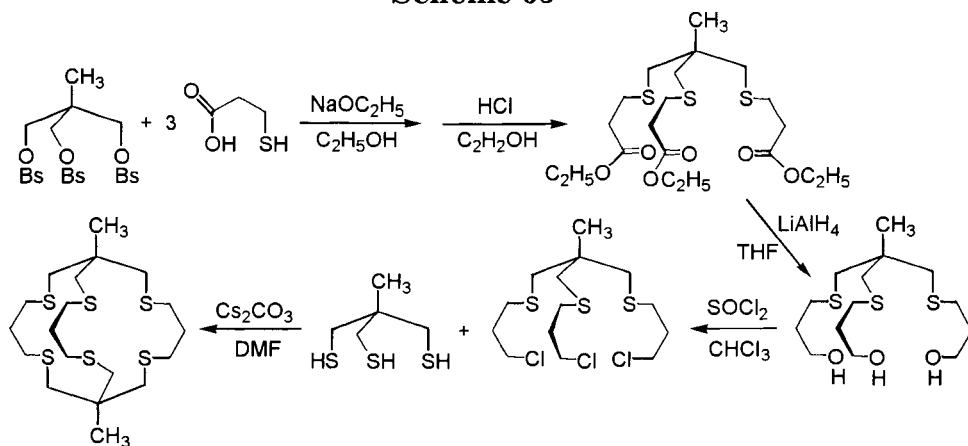
Scheme 66

The interaction of the free ligand with cobalt(II) perchlorate in the presence of AgClO$_4$ as a precipitant in the nitromethane-methanol mixture made it possible to isolate the [Co(diME 1,3pnsar-S$_6$)](ClO$_4$)$_3$ clathrochelate. The reduction of this clathrochelate with sodium dithionate led to the formation of a cobalt (II) complex that readily produced a free sarcophagine [147].

Sarcophaginates can also be prepared by template condensation of bis-triamine metal complexes with formaldehyde and nitromethane or ammonia. Macrotricyclic and macrotetracyclic complexes of different structures have simultaneously been formed [148, 149].

Treatment of [Co(tame)$_2$]$^{3+}$ cation (where *tame* is 1,1,1-tris-(aminomethyl)ethane) in aqueous solution at pH 10.5 with formaldehyde and nitromethane gave mainly a macrotricyclic [Co(NOtrisartame)]$^{3+}$ cation **1** in high yield (*ca* 50%), isolated as a

Scheme 67

1   2   3   4
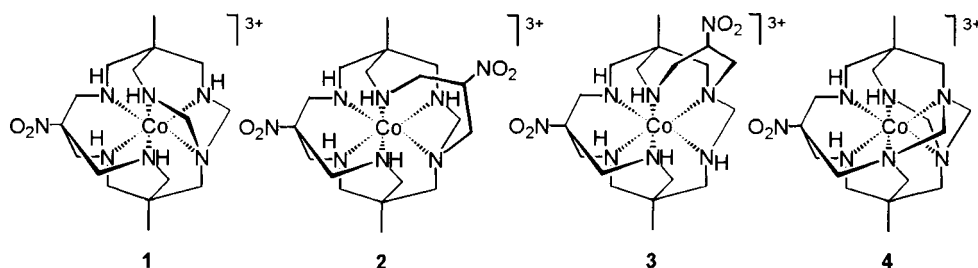
[Co(NOtrisartame)](ZnCl$_4$)Cl·0.5H$_2$O complex. Two other macrocyclic complexes **2** and **3** with different rings (Scheme 67) were isolated in much lower yield (*ca* 10%) [149].

The reduction of sarcophaginate **1** with zinc dust under acidic conditions converted the apical nitro group into an amino substituent with cleavage of the four-membered rings and extrusion of the Co^{2+} ion.

The use of ammonia instead of nitromethane in the template condensation with [Co(tame)$_2$]$^{3+}$ cation gave the macrotricyclic [Co(azatrisartame)]$^{3+}$ heptazasarcophaginate (yield *ca* 30%). Like its nitromethane analog, this complex is remarkably stable in aqueous hydrochloric acid. Furthermore, treatment of [Co(azatrisartame)]$^{3+}$ cation with trifluoromethanesulphonic acid for several days resulted in a triimine complex (*ca* 80%) with a ruptured *aza*-cap, but the methylene units and the four-membered rings remained unaffected [149].

One more product of the condensation of [Co(tame)$_2$]$^{3+}$ with nitromethane and formaldehyde with a yield of *ca* 10% was identified in Ref. 148 as macrotetracyclic [Co(NOtetrasartame)]Cl$_3$·3H$_2$O sarcophaginate **4**. Its reduction with zinc dust in aqueous hydrochloric acid resulted in the corresponding cobalt(II) [Co(AMtetrasartame)]$^{2+}$ aminosarcophaginate, which can either oxidize to a cobalt(III) complex or demetallate with hydrochloric acid to cleave four-membered chelate fragments. Both macrotetracyclic cobalt(III) complexes are remarkably stable to hydrolysis in acidic (6 molar hydrochloric acid at 60°C) and mildly basic (pH < 9 at 25°C) conditions, although they decompose at pH >9.

A bis-triamine [Co(tame)]$^{3+}$ complex also reacted with formaldehyde and aldehydes of carboxylic acids RCHO (where R is CH$_3$, C$_2$H$_5$, or (CH$_3$)$_2$CH)) to form cobalt (III) triiminosarcophaginates

with an expanded cavity, which after their reduction with $NaBH_4$, were demetallated with hydrochloric acid:

$$
\begin{array}{ccc}
\text{[structure]} & \xrightarrow[\substack{(CH_3)_2CHCHO \\ (C_2H_5)_3N}]{(CH_2O)_3} & \text{[structure]} \xrightarrow[HCl]{NaBH_4} \text{[structure]}
\end{array}
\tag{44}
$$
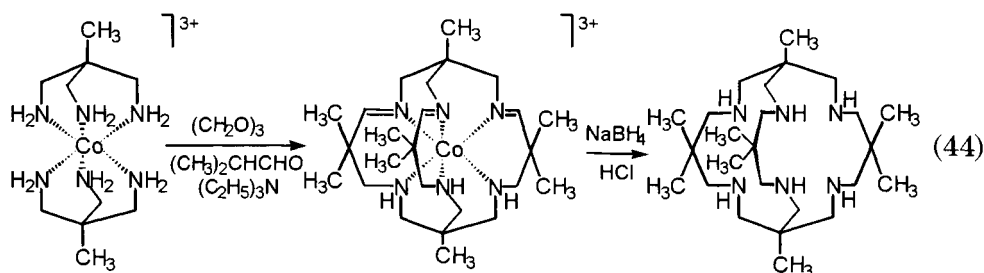
The isolation of the free *Me₈tricosasar* ligand enabled a variety of transition metal complexes to be synthesized and studied [150].

The reduction of triimine sarcophaginate [Co(Me₈tricosatriene-sar)]³⁺ and [Co(Me₅tricosatrienesar)]³⁺ cations with $NaBH_4$ in aqueous solution at pH 10 led to the formation of saturated cobalt(II) and cobalt(III) sarcophaginates [151]:

$$
\text{[structure]} \xrightarrow[H_2O]{NaBH_4} \text{[structure]} \qquad R = CH_3, H
\tag{45}
$$
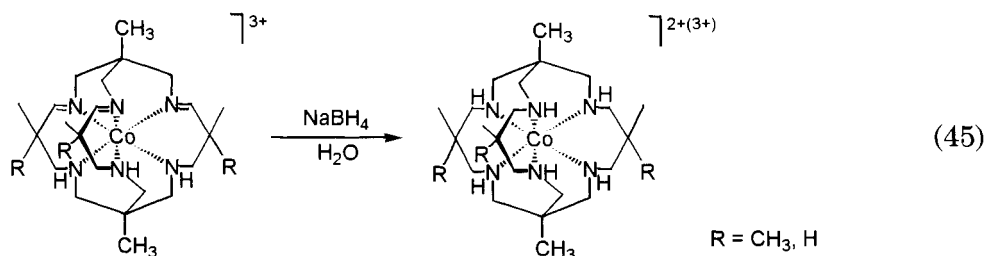
Condensation of [Co(tame)₂]³⁺ cation with propanal is described in more detail in Ref. 152. The resultant [Co(*fac*-Me₅tricosanesar)]³⁺ sarcophaginate was demetallated, and the free ligand was employed for the synthesis of a chromium(III) sarcophaginate with unusual spectral characteristics (Scheme 68) [153].

The [Co(tame)₂]³⁺ and [Pt(tame)₂]⁴⁺ bis-triaminates underwent a template condensation with propanal under basic conditions to give with remarkable regio- and stereo-selectivities rigid sarcophaginates with an expanded cavity [154].

$$
\text{[structure]} \xrightarrow[AN]{\substack{C_2H_5CHO \\ OH^-}} \text{[structure]} \qquad M=Co(III), Pt(IV)
\tag{46}
$$
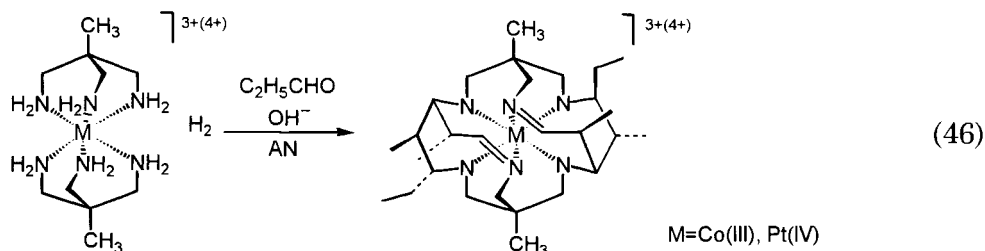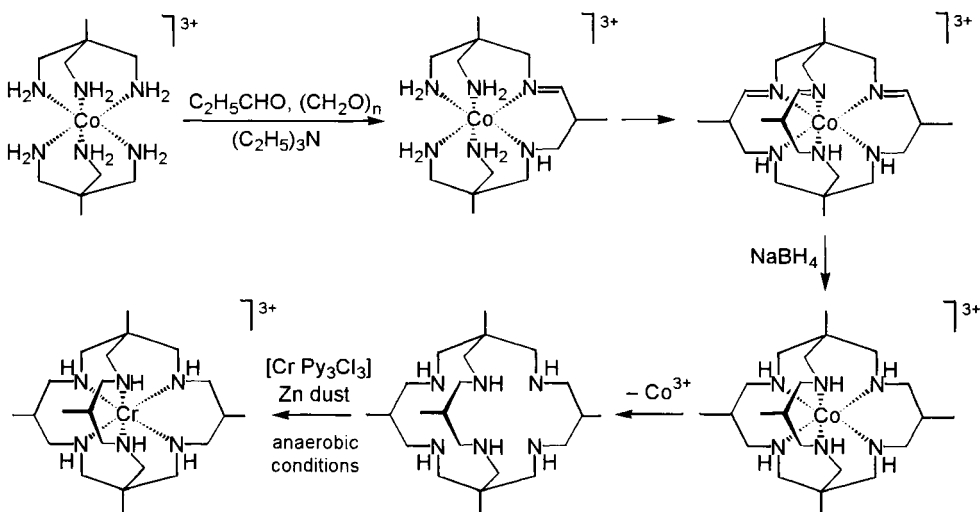
Scheme 68

The two pairs of protonated units condense with amino groups to form six-membered chelate cycles (the so-called "straps") cross-linking two *tame* fragments to produce two tetradentate moieties. The two remaining primary amine groups, being in the *trans* position, then condense with propanal to form bridges ("cross straps") between straps.

As a result, a rigid cage structure involving fourteen chiral sites (ten carbon atoms and four secondary nitrogen atoms of the framework) was obtained [154].

Condensation of $[Co(tacn)_2]^{3+}$ bis-triaminate with formaldehyde and nitromethane led to an unusual clathrochelate complex with a stable carbanion. A tripodal cap from three formaldehyde and one nitromethane species formed on one octahedral face as expected by the conventional route. However, on another octahedral face, the capping process proceeded in an unusual way to stabilize a carbanion chelate and to methylate the remaining coordinated amino group:

$$(47)$$
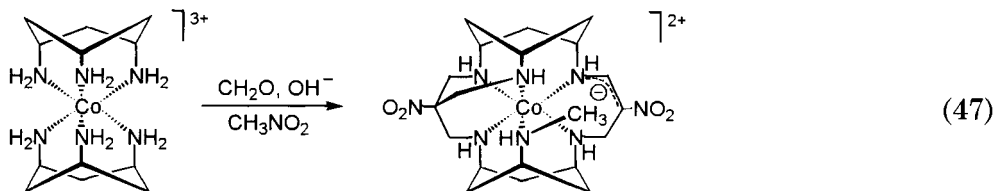
An intermediate carbanion cycle is stable because of coordination to cobalt(III) ion and charge delocalization in the six-membered

nitro group-containing chelate cycle. The further condensation to yield a tripodal capping fragment does not take place. Methylation of a coordinated amino group of the *tacn* moiety accomplished this process [155].

The platinum(IV), rhodium(III), and iridium(III) sepulchrates, dinitrosarcophaginates, and diaminosarcophaginates have been synthesized in high yields (45–65% for Pt(IV), 40% for Ir(III), and 90–100% for Rh(III)) starting from their tris-ethylenediaminates [94, 156, 157]. The rhodium(III) and iridium(III) complexes were prepared in a similar manner to that for cobalt (III) complexes, except of the elevated temperatures (Rh, 60°C; Ir, 90°C) required for the quoted yields. Moreover, if chiral [Rh(en)$_3$]$^{3+}$ cation was used initially, clathrochelate complexes were obtained in *ca* 100% chemical and chiral yields, despite the seven centres of chirality [157].

Recrystallization of the [Pt(diNOsar–H)]Cl$_3$·3H$_2$O complex from a 1:1 diluted hydrochloric acid gave the [Pt(diNOsar)]Cl$_4$·3H$_2$O·HCl sarcophaginate. It was initially suggested [156] that reduction of this complex with SnCl$_2$ solution in 1:1 diluted hydrochloric acid yields a [Pt(diAMsar)]Cl$_4$·2H$_2$O clathrochelate. However, the X-ray diffraction data indicate that the complex obtained is actually a dihydroxylamine [Pt(diNHOHsar)]Cl$_4$·2H$_2$O sarcophaginate. Its recrystallization from hot trifluoromethanesulphonic acid resulted in the [Pt(diNHOHsar)](CF$_3$SO$_3$)$_4$·4H$_2$O compound.

Attempts of Sargeson and coworkers [158] to cross-link the chromium(III) tris-ethylenediaminate have not been successful because of rapid dissociation of intermediate imine species. However, Endicott and coworkers [159] have managed to synthesize chromium(III) sepulchrate, not isolating its tris-ethylenediaminate, upon heating of anhydrous chromium sulphate with concentrated aqueous ethylenediamine for several hours followed by the addition of formaldehyde and ammonia with constant heating. The [Cr(sep)](ClO$_4$)$_3$ sepulchrate was isolated from the reaction mixture in 10% yield by IEC.

The template synthesis of the nickel sepulchrate proved to be rather complicated because of macrocyclic and acyclic amines (Scheme 69), competitive formation reactions occurred upon refluxing ethylenediamine, formaldehyde, and ammonia in the presence of Ni^{2+} ion.
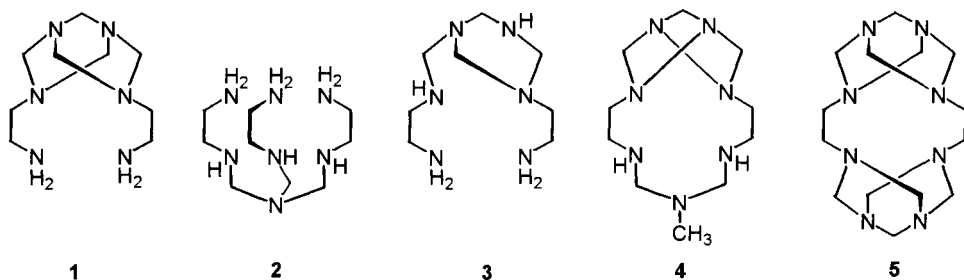
Scheme 69

Nevertheless, after precipitation of the major reaction products (the nickel(II) complex with ligand **1**, yield *ca* 90%, and a complex with *azasen* ligand **2** as perchlorate salts). [Ni(sep)](ClO$_4$)$_2$ sepulchrate was isolated from the solution by fractional recrystallization (yield *ca* 1%) [160]. Attempts to obtain the nickel(II) sepulchrate from the preformed [Ni(azasen)](ClO$_4$)$_2$ semisepulchrate have not been successful. However, the free *azasen* ligand isolated is essential for the synthesis of clathrochelate complexes of other metal ions.

The use of 1,2-diaminopropane instead of ethylenediamine in the condensation on the nickel(II) ion matrix also leads to the formation of the nickel(II) complex with the corresponding semiclathrochelate ligand [161].

Condensation of [Cu(en)$_2$]$^{2+}$ cation with nitromethane and formaldehyde yielded copper(II) complexes with macrocyclic and polydentate nitrogen-containing ligands, though a copper(II) sarcophaginate was not isolated [162, 163].

When 1,3-propanediamine semiclathrochelates have been used instead of ethylenediamine derivatives, the encapsulation of large metal ions in low oxidation states predominated. For instance, the rhodium(III) sarcophaginate was obtained by template condensation of the corresponding semiclathrochelate with formaldehyde and nitromethane in a high yield [5]:

(48)

Scheme 70

1   2
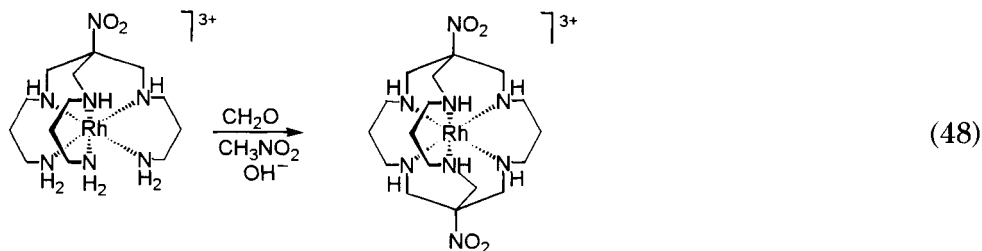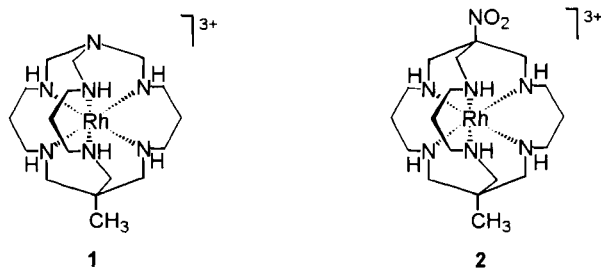
The synthesized complex was easily reduced to the rhodium(II) sarcophaginate. The rhodium sarcophaginates **1** and **2** with other apical substituents were also prepared (Scheme 70).

The synthetic procedure for these complexes in acetonitrile with paraformaldehyde as a cross-linking agent is described in more detail in Ref. 164.

A standard procedure was also employed to isolate the [Rh(MEAMHsar)](CF$_3$SO$_3$)$_4$ aminosarcophaginate.

$$
\text{(49)}
$$
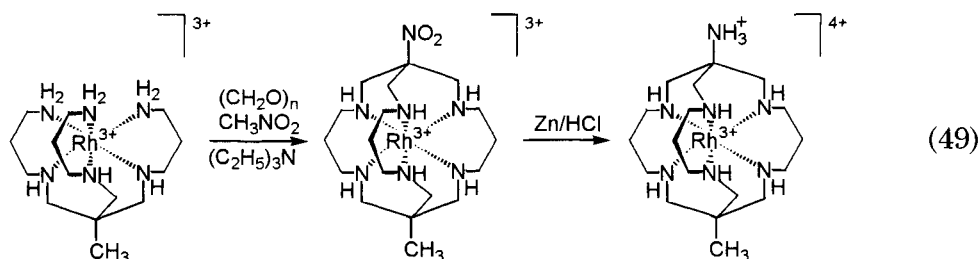
Attempts to synthesize the clathrochelate complexes of lanthanide ions *via* template condensation of the tripodal amine *tren* with formaldehyde bis-(dimethylamino)methane derivative on the rare-earth metal ion were successful only for ytterbium. The [Yb(metr)](CF$_3$SO$_3$)$_3$·AN clathrochelate was obtained in 3–5% yield [165]. With ytterbium cation, as well as with cerium, praseodymium, europium, yttrium, and lanthanum ions, the major reaction products proved to be mono- and dibridged semiclathrochelate complexes with ligands **1** and **2** (Scheme 71).

As mentioned above, a template synthesis is a very efficient approach to the preparation of sarcophaginates and sepulchrates of certain metals. For all other metal ions, this synthetic pathway is inapplicable or gives the desired products in low yields. For instance, the yields of nickel(II) and chromium(III) sepulchrates resulting from template condensation are only *ca* 1 and 10%, respectively. This problem can largely be overcome if the synthesis of a variety of metal

sarcophaginates performs from free ligands obtained by demetallation of the corresponding cobalt(II) complexes with concentrated HBr and HCl at 130–150°C. This synthetic pathway has been employed for the isolation of free *sar* and *diAMsar* ligands.

The clathrochelate [Cr(diAMsar)]Cl$_3$·3H$_2$O complex was synthesized by reaction of free *diAMsar* ligand with CrCl$_3$ in dry DMF in the presence of zinc powder. The use of free *sar* ligand instead of *diAMsar* ligand and treatment of the reaction mixture with aqueous NaCF$_3$SO$_3$ resulted in a [Cr(sar)](CF$_3$SO$_3$)$_3$ sarcophaginate. The encapsulation of the inert chromium(III) ion by the macrobicyclic ligand has accomplished *via* trace amounts of the labile Cr^{2+} ion generated by metallic zinc, followed by rapid oxidation to chromium(III) clathrochelate. Chromium(II) compounds have not been isolated because of their low stability [158]. The chromium(III) [Cr(AMHMEsar-N$_5$S)]Br$_4$·3H$_2$O N$_5$S-sarcophaginate was synthesized by an analogous route [166].

The reaction of vanadium(III) V(acac)$_3$ acetylacetonate with free *diAMsar* ligand in aqueous ethanol at 40°C for three days led to the formation of a vanadium(IV) [V(diAMHsar–2H)](S$_2$O$_6$)$_2$·2H$_2$O sarcophaginate. The central ion presumably was oxidized by air oxygen. The isolated complex is stable over a wide pH range (1–10) but decomposes in the presence of oxidants [167].

Like vanadium(IV) and chromium(III) sarcophaginates, ruthenium(II) complexes have readily been obtained from free ligands. The initial [Ru(DMF)$_6$](CF$_3$SO$_3$)$_2$ solvato-complex was prepared by treating [Ru(H$_2$O)$_6$](CF$_3$SO$_3$)$_2$ salt with pure DMF under argon followed by dehydratation with triethyl orthoformate, concentration of the solution, and crystallization at –20°C. Prolonged reflux (2 days) of this solvato-complex and free *sar* ligand in dry ethanol in a strictly oxygen-free atmosphere resulted in a *ca* 60% yield of the [Ru(sar)](CF$_3$SO$_3$)$_2$ sarcophaginate, extremely sensitive to
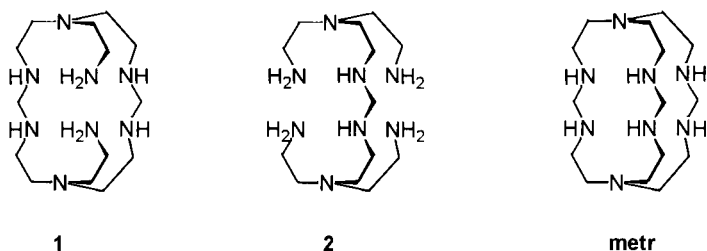
Scheme 71

oxidants [168]. Demetallation of the [Co(capten)]$^{3+}$ cation also made it possible to synthesize a [Ru(capten)]$^{2+}$ N_3S_3-sarcophaginate by interaction of a free ligand with [Ru(DMF)$_6$]$^{2+}$ solvato-complex.

The corresponding clathrochelate ruthenium(III) complexes have not been isolated because of spontaneous oxidation of the ligand with the central metal ion, whereby ruthenium(II) sarcophaginate and its monoimine analogue were obtained [5, 169].

(50)
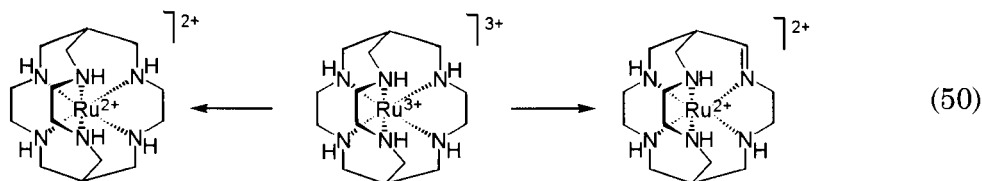
The complexes of nickel(II) and copper(II) ions with sar-N_4S_2 and AMHsar-N_4S_2 ligands, respectively, have been produced from the free ligands and corresponding perchlorate salts in methanol [170, 171].

An analogous scheme has also been used for the synthesis of the nickel, copper, mercury, and zinc(II) diaminosarcophaginates [172-175], their N-methylated analogs [173], and simplest [Hg(sar)](ClO$_4$)$_2$ and [Ni(sar)](ClO$_4$)$_2$ sarcophaginates [174, 176].

One should take notice of an unusual Co^{3+} ion extrusion procedure from the [Co(diAMHsar)]$^{5+}$ cage using an 8-hydroxyquinoline that was described in Ref. 177. The resulting ligand readily encapsulated nickel and copper(II) ions to produce octahedral complexes.

The copper(II) diaminosarcophaginate underwent condensation with 4-nitrobenzaldehyde to give nitrobenzylimine and bis-nitrobenzylimine sarcophaginates, which were reduced with a cyanoborohydride ion to corresponding saturated copper(II) clathrochelates. The copper(II) nitrobenzyldiaminosarcophaginate isolated underwent a reductive demetallation with NaBH$_4$ in the presence of palladium on activated charcoal under basic conditions. The resulting free aminobenzyldiaminosarcophagine sarAr ligand readily formed complexes with copper, nickel, and cobalt(II) ions (Scheme 72) [175].

Numerous magnesium(II), manganese(II), iron(II, III), silver(II), gallium(III), vanadium(III), and indium(III) sarcophaginates and diaminosarcophaginates are synthesized and structurally characterized [4, 178].

Manganese(II) Mn(sar)](ClO$_2$)$_4$, and [Mn(diAMHsar)](NO$_3$)$_4\cdot$H$_2$O sarcophaginates arose from the manganese(II) acetate and the
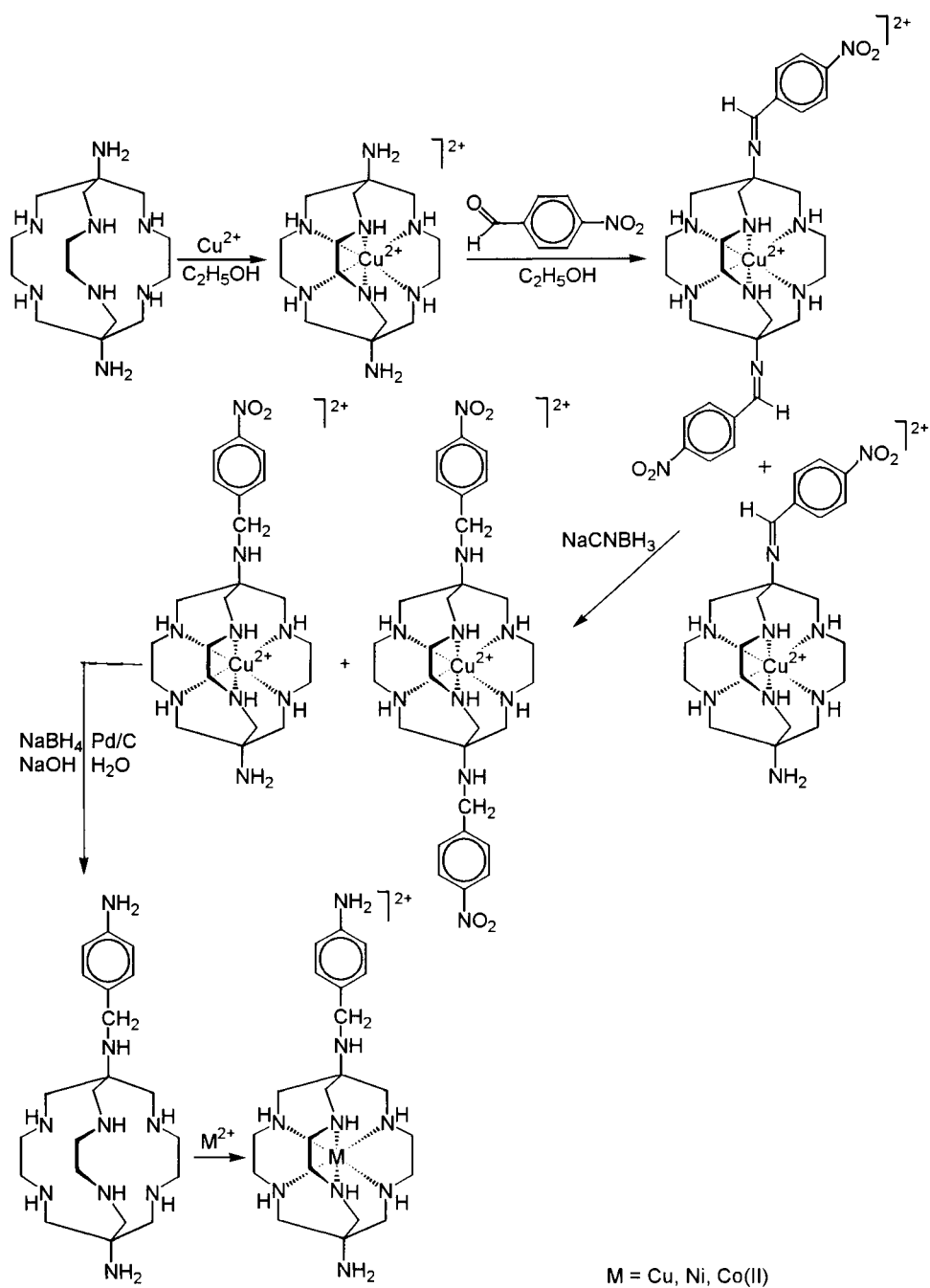
Scheme 72
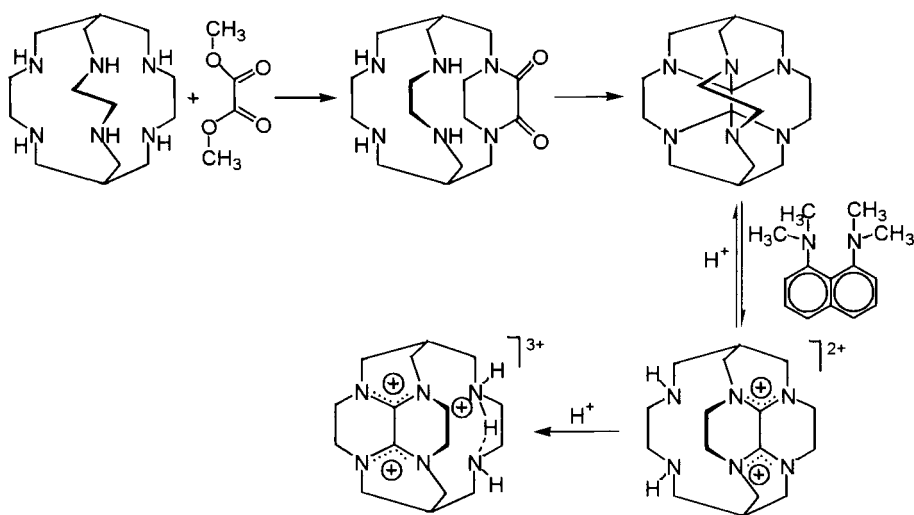
Scheme 73

corresponding free ligands in the absence of oxidant. The electrochemical and chemical oxidation of these complexes resulted in manganese(III) [Mn(sar)](CF$_3$SO$_3$)$_3$, [Mn(sar)](NO$_3$)$_3$·0.5H$_2$O, and [Mn(diAMHsar)](NO$_3$)$_5$·2H$_2$O clathrochelates [179, 180].

The first step on the way to the synthesis of the so-called "superclathrochelates" containing a second shell, which reinforces the clathrochelate framework and completely excludes any possibility of metal ion extrusion without clathrochelate ligand destruction, is described in Ref. 181. The interaction of the simplest free sarcophagine with dimethyoxalate in methanol at room temperature resulted in the formation of the ethanosarcophagine. The protonation of ethanosarcophagine involving the splitting of two C–N bonds first led reversibly to the formation of an oxamidinium salt with nonprotonated amino groups and then irreversibly to the formation of a sarcophagine trication (Scheme 73) [181].

Hexadentate trioximetriamine compounds proved to possess properties intermediate between those of macrobicyclic tris-dioximates and sarcophaginates. The hexadentate *tamox* ligand arises from the reaction of the corresponding polyamine with 2-chlor-2-methyl-3-nitrosobutane [182]:

$$Co^{2+} + 1/4O_2 + H^+ + tamox \left(\begin{array}{c} \end{array} \right) \longrightarrow [Co(tamox)]^{3+} \qquad (51)$$
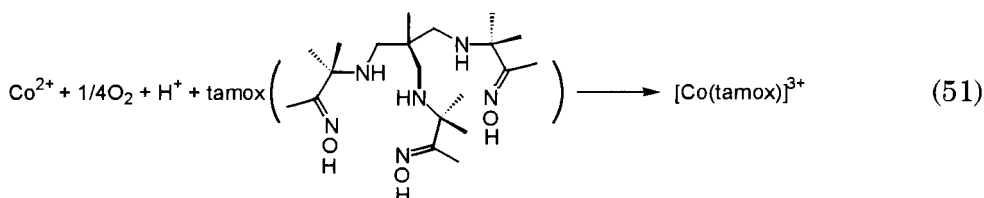
The interaction of *tamox* ligand with Co^{2+} ions in the presence of air oxygen led to the formation of $[Co(tamox)]Cl(ClO_4)_2 \cdot H_2O$ and $[Co(tamox-H)]Cl_2 \cdot 3H_2O$ complexes. These compounds appear to be promising for the synthesis of the corresponding clathrochelate complexes.

Methods for the synthesis of sarcophaginates and sepulchrates based on redox and photochemical reactions are discussed in Chapter 5.

2.4 SYNTHESIS OF POLYENE AND OTHER TYPES OF CLATHROCHELATE COMPLEXES

The methods for the preparation of the clathrochelate complexes discussed in this section are, in most cases, similar to those for the macrocyclic compounds described in detail in Refs. 7, 11, 14, 15 and 17. In contrast to clathrochelates of other types, they are prepared largely *via* interaction between a preformed clathrochelate ligand and the appropriate metal salt. In other cases, the synthesis of these clathrochelates occurs *via* either template encapsulation or rearrangement from square-planar complexes (Scheme 74).

The condensation of butanedione-2,3-dihydrazone with formaldehyde on a metal ion (Fe^{2+}, Co^{2+} and Ni^{2+}) matrix (Scheme 74), performed by Goedken and Peng, led to the formation of clathrochelate $[M(thz)](BF_4)_2$ complexes. Direct reaction between the three components proved to be efficient only with iron(II) ion [183]. Therefore, nickel, cobalt, and iron(II) tris-dihydrazonates were preliminarily synthesized. It was noted that even when the reaction was carried out under nitrogen and cobalt(II) tris-dihydrazonate was used as the starting material, only cobalt(III) clathrochelate could be isolated from the reaction mixture. Its reduction with anhydrous hydrazine yielded cobalt(II) clathrochelate [95, 183].

In the case of cyclohexanedione-1.2-dihydrazone, the macrobicyclic dihydrazonate formation proceeded on the template Fe^{2+} ion more

Scheme 74

Scheme 75

efficiently compared with the formation of butanedione-2,3-dihydrazone clathrochelate (Scheme 75) [184].

Goedken and Peng's idea to employ the reaction between the amino groups, bound to the metal ion, and formaldehyde for the synthesis of clathrochelates proved to be beneficial. It has served as a basis for later studies of Sargeson and coworkers on the synthesis of sepulchrates and sarcophaginates.

When α-oximehydrazones were used as the chelating agents, researches succeeded in the synthesis of mono- and bis-clathrochelate iron and cobalt(II) oximehydrazonates [185-187]. At the first stage, mono- and bis-semiclathrochelate iron and cobalt(II) complexes were isolated by a cross-linking with phenylboronic or ferrocenylboronic acids, and with benzene-1,4-diboronic or 1,1'-ferrocenyldiboronic acids,

respectively. A subsequent cyclization of these semiclathrochelates with an excess of formaldehyde in the presence of catalytic amounts of HBF_4 or HPF_6 led to the formation of clathrochelates. The interaction of the equimolar quantities of formaldehyde and semiclathrochelate complexes resulted in partially cross-linked compounds with two methylene units (Scheme 76).

With the *n*-butylboronic acid, a semiclathrochelate intermediate product was not pre-isolated and the clathrochelate complex was produced from a template reaction [185].

$R = C_6H_5, \; n\text{-}C_4H_9, \; Fc$
$R^1 = CH_3, \; C_6H_5, \; H$
$M^{n+} = Fe^{2+}, \; Co^{2+}, \; Co^{3+}$ (in the presence [O])
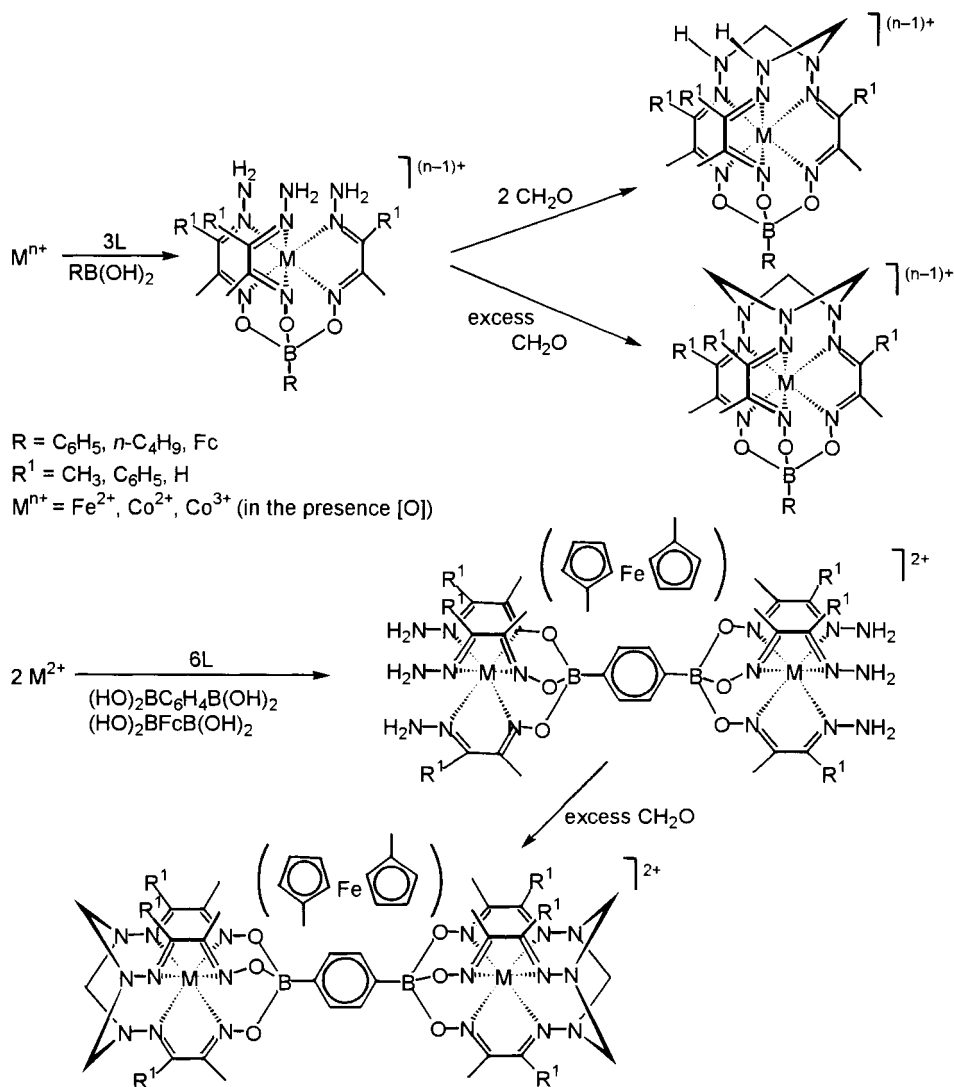
Scheme 76

The above-mentioned semiclathrochelate oximehydrazonates are visualized as highly intriguing compounds for capping since their geometry may be varied over a wide range from trigonal prism to trigonal antiprism by changing the first capping fragment, in particular, in passing from a boron- to a tin-containing capping group. In this manner one specifies the geometry of the resulting clathrochelates and the orientation of substituents in the second capping fragment [188].

Syntheses of the overwhelming majority of clathrochelate complexes have proceeded *via* an intermediate nonmacrocyclic compound containing spatially oriented oxime, amine, or hydrazonate nitrogen atoms in the triangular bases of the coordination polyhedron. The trifunctional reagents are evidently thought to be the most natural capping agents. To form a tripod apical fragment in the syntheses of the most thoroughly studied complexes, such as sarcophaginates, methyl groups with C–H acidic properties (e.g., in nitromethane or cobalt pyruvate) or active hydrogen atoms of Group 5 hydride compounds (ammonia, phosphine, or arsine) interacting with intermediate amine complexes in the presence of aldehyde (mainly formaldehyde forms methylene bridging units between the apical and the coordinated nitrogen atoms) have been used (see Section 2.3). Condensation reactions of tripod amines or imines with activated and oriented carbonyl groups have been used in the syntheses of mono- and binuclear azomethine clathrochelates (see below). Finally, the template condensation of *d*-metal tris-dioximates with Lewis acids produced a tripod capping fragment formed by the capping atom and three oxygen atoms (see Section 2.1).

As mentioned above, with bifunctional reagents such as formaldehyde, the oriented hydrazonate amino groups react in the plane of the triangular base to produce 1,3,5-triazacyclohexane ring. It is clear that the formation of the macrobicyclic structure requires bi- and trifunctional agents exhibiting high activity toward reactive groups, e.g., trichloroacetaldehyde (TAA) or triethyl orthoformate (TOF).

Iron and cobalt (III) tris-dioximates and tris-ethylenediaminates have not been capped by TOF and TAA. The reaction of iron(II) tris-diacetyldihydrazonate with TOF has yielded no tripod capping fragment. However, the condensation of three apical hydrazonate amino groups and three TOF molecules gave a 1,3,5-triazacyclohexane fragment with statistical orientation of substituents (hydrogen atoms and ethoxy groups) relative to the ring. The use of
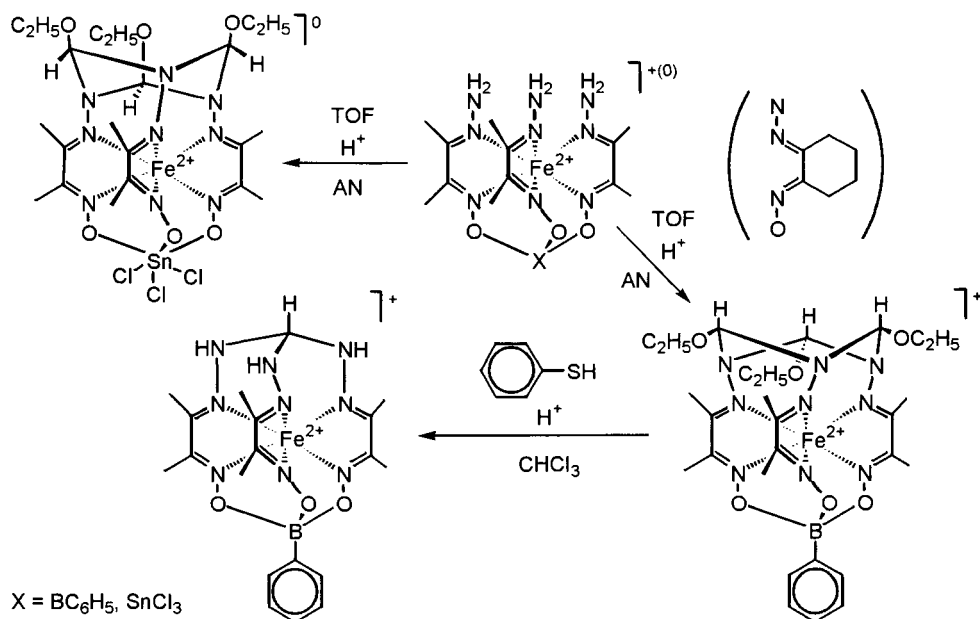
Scheme 77

TOF in equimolar amounts also failed to produce the tripod capping fragment [188].

Attempts to employ tris-oximehydrazonate complexes with *HDXO* and *HCXO* ligands proved to be successful. The H$^+$-catalyzed interaction of preliminarily obtained boron- and tin-capped semiclathrochelates **1** and **2** with excess TOF resulted in only one isomer (Scheme 77) with *cis* or *trans* orientation of the ethoxy groups and the semiclathrochelate fragment relative to the 1,3,5-triazacyclohexane ring [188].

Clathrochelate complexes resulting from reaction with TOF involving ethoxy groups are thought to be highly promising compounds for functionalization and for the synthesis of novel clathrochelates with improved properties. One of the most interesting types of modification reactions of the sarcophaginates proved to be intramolecular rearrangement, e.g., a partial rearrangement of the regular sarcophagine framework to yield a macrobicyclic ligand with a contracted cavity during nitrosation of cobalt(III) aminosarcophaginates (see Section 2.3). The H$^+$-catalyzed intramolecular condensation of boron-capped complexes was also observed. This reaction requires prolonged refluxing and occurs in the presence of
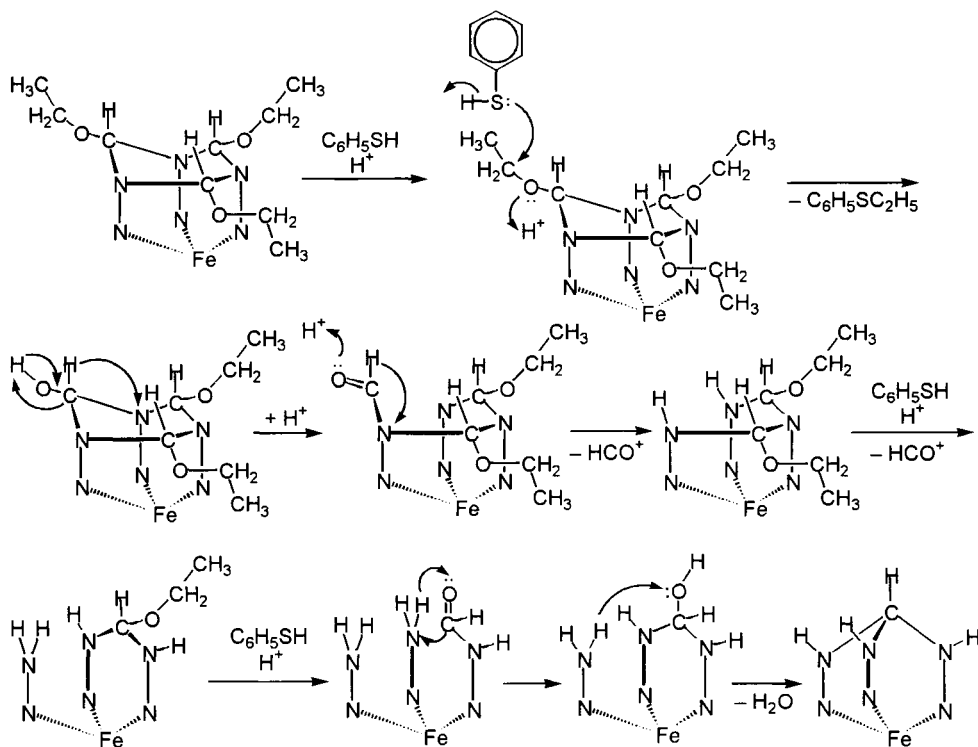
Scheme 78

thiophenol, which binds the ethoxy-containing fragments that are detached in the course of the reaction.

The mechanism of this intramolecular condensation resulting in a tripodal capping fragment is represented in Scheme 78. The alkyl ethers can be smoothly cleaved by a thiophenol derivative in the presence of a strong acid. The reaction "push-pull" mechanism involves the cooperative H^+ ion addition to the ether oxygen atom and the nucleophilic attack of sulphur on the ethyl group. As a result, the transformation of two amino fragments into amide fragments occurs. The amide fragments detach of formyl groups, and the intramolecular condensation with the third amide fragment results in a tripodal cap.

The apical functionalized oximehydrazonate clathrochelates were also obtained stepwise from initial semiclathrochelate precursors followed by H^+-catalyzed condensation with an excess of formaldehyde or TOF (Scheme 79) [67].

The first antimony-capped oximehydrazonate semiclathrochelate was obtained by condensation of FeCl$_2$·4H$_2$O and diacetylmonooxime
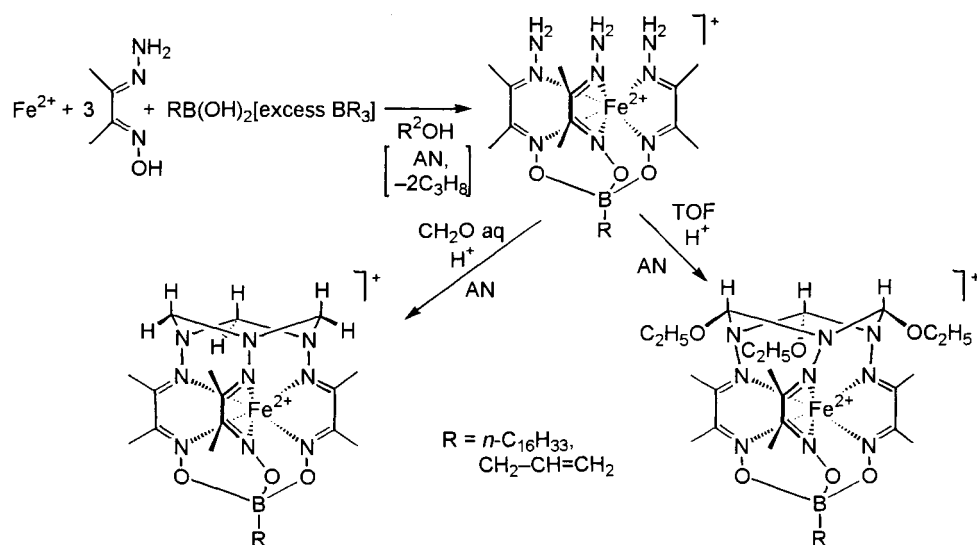
Scheme 79
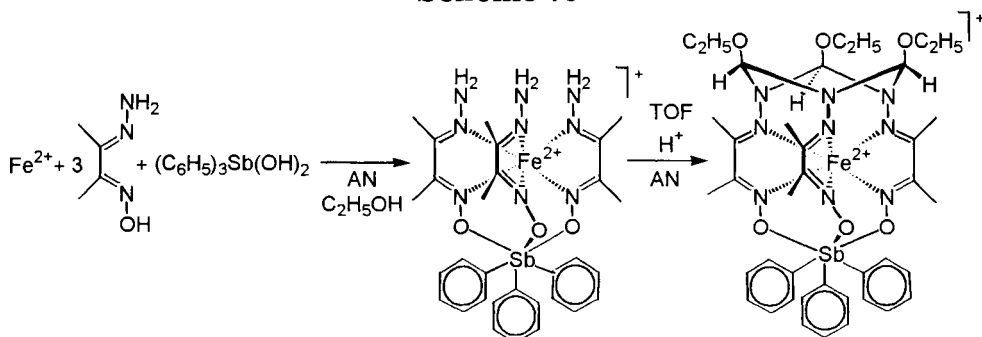
Scheme 80

hydrazone with $(C_6H_5)_3Sb(OH)_2$ in acetonitrile / ethanol mixture (Scheme 80). H^+-ion-catalysed reaction of semiclathrochelate in acetonitrile with fivefold excess of TOF resulted in the desired antimony-capped clathrochelate [74].

The condensation of three *HDXO* molecules with $IGe(CF_3)_3$ on the iron(II) ion as template gave of $FeDXO_3(Ge(CF_3)_3)$ semiclathrochelate in high yield, even in the absence of base neutralizing the H^+ ions. In this case the *HDXO* ligand itself proved to be a base. The semiclathrochelate formed underwent H^+-ion-catalysed condensation with formaldehyde and TOF, resulting to the first clathrochelate germanium-capped oximehydrazonates with a capping 1,3,5-triazacyclohexane group (Scheme 81) [73].
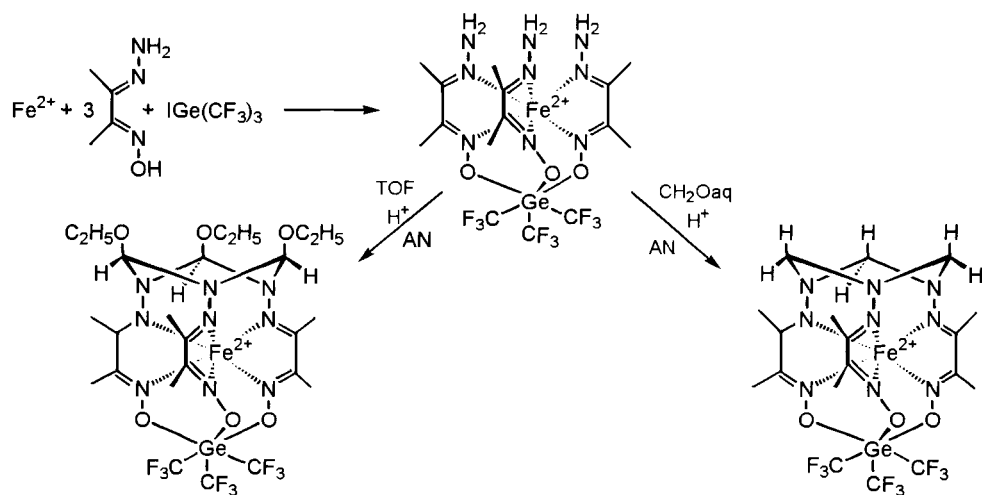
Scheme 81
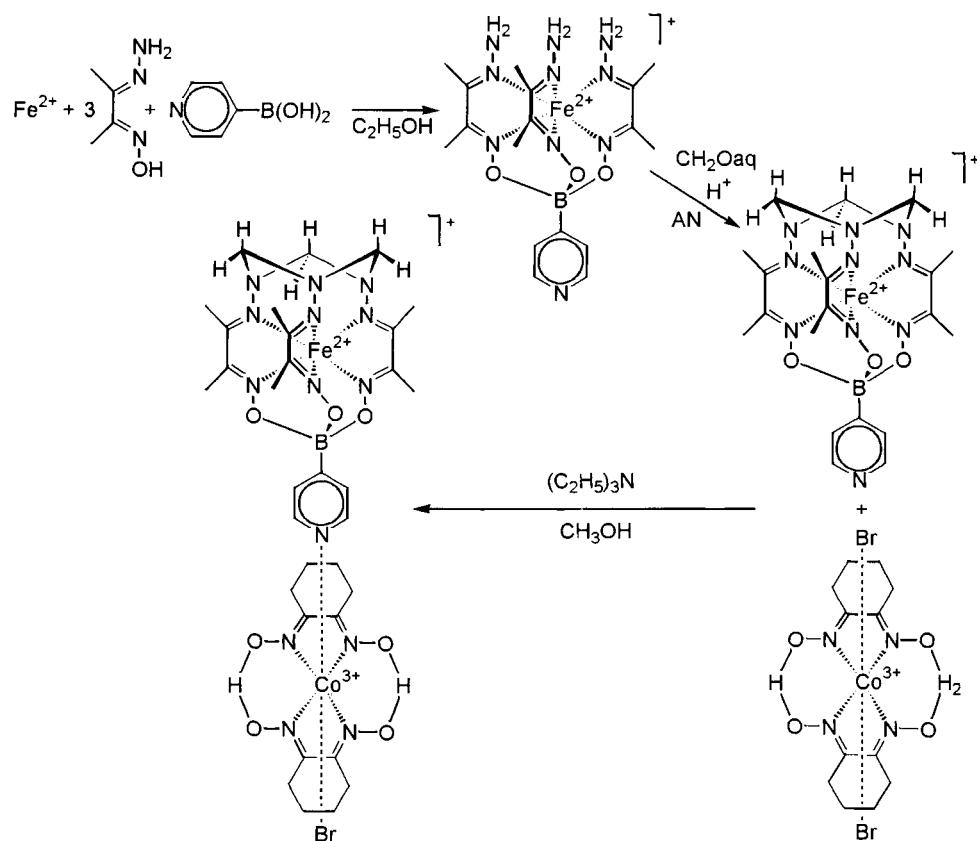
Scheme 82

Apically functionalized clathrochelate iron(II) oximehydrazonate with an appended pyridyl and its complex with [Co(H$_2$Nx)(HNx)]Br$_2$ cobaloxime were prepared by Scheme 82 [189].

An alternative pathway for the synthesis of bis-clathrochelates that was proposed in Ref. 75, can be realized with bis-capping agents, which are apt to accept an additional two electron pairs, and if the electron-donor groups of C_2-nonsymmetric ligands, participating in the capping, demonstrate essentially different chemical properties. Scheme 83 shows a pathway for the synthesis of an oximehydrazonate iron(II) bis-clathrochelate starting from HDXO ligand, the oxime and hydrazonate groups of which displayed appreciably different chemical properties. With bis-capping germanium(IV) tetraethoxide, oximehydrazonate iron(II) bis-semiclathrochelate was presumably formed at the first stage. A further H$^+$-catalyzed macrocyclization through the hydrazonate groups was implemented with triethyl orthoformate as described above [75].

For an efficient synthesis of clathrochelates, the orientation of active carbonyl-containing (e.g., acylchloride) groups in their reactions with amines has been used alongside that of coordinated amino groups in their reactions with carbonyl-containing cross-linking agents. A macrobicyclic ruthenium(II) tris-diiminate was prepared [190] via template cross-linking of nonmacrocyclic precursor with tripodal amine (Scheme 84).

The analogous iron(II) complex was isolated [191] by interaction of an iron(II) salt with the tabpy ligand preliminarily obtained by Scheme 85.

A clathrochelate binucleating trom ligand was synthesized via two-step condensation of the tripodal tren amine with 2-oxy-5-methylisophthalaldehyde (Scheme 86) [192].

Homobinuclear macrobicyclic copper, cobalt, and iron(II) complexes and a heteronuclear iron(II)/cobalt(II) clathrochelate of the [M$_1$M$_2$(trom)]$^+$ type arise from interaction of a sodium complex of trom ligand with the corresponding metal salts.

Polynuclear iron(II) and cobalt(III) oximehydrazonates have arisen from the template macrocyclization of the initial nonmacrocyclic tris-complexes with polydentate ligands resulting from the condensation of the corresponding diketones and their monooximes with hydrazine [193]. The tris-complexes formed have
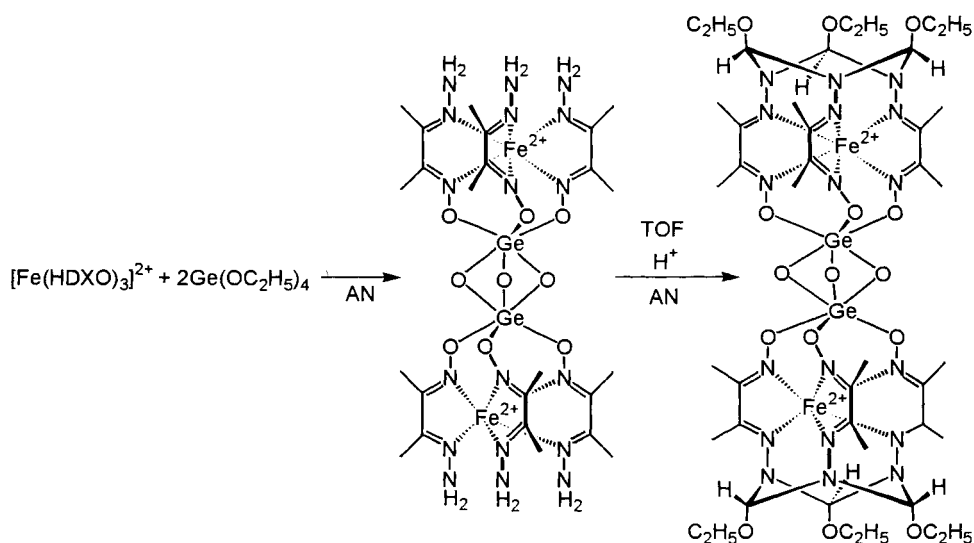
Scheme 83

Scheme 84

Scheme 85

Scheme 86

Scheme 87

interacted with Lewis acids *via* oxime-containing fragments to give clathrochelate complexes.

The initial oximehydrazonate ligands were prepared by the methods represented in Scheme 87. Different strategies employed in the synthesis of these compounds permit one to prepare ligands of a tailor-made structure by varying the diketones, their monooximes, the molar ratios of reactants, and the reaction sequence. In addition,

oximehydrazonate ligands can be prepared from fragments by a template reaction on a metal ion, for instance, by building up mononuclear tris-complexes to binuclear ones [193].

Binuclear clathrochelate iron(II) oximehydrazonates may be synthesized by the main methods used for the synthesis of macrobicycles of this type proposed for clathrochelate tris-dioximates: by a direct template reaction on a metal ion; the cross-linking of initial nonmacrocyclic complexes; a cross-linking group exchange reaction; and a ligand modification reaction. The template condensation of a mononuclear complex to a binuclear one followed by the encapsulation of another metal ion and capping reaction may be also used for the preparation of these compounds. The main methods for the synthesis of these complexes are shown in Scheme 88 [193].

With tetradentate ligands, the direct template reaction is accompanied by a large number of side reactions, which substantially decreases the interest in this commonly employed method of synthesis. Therefore, cross-linking of tris-complexes and condensation reactions of lacunar compounds have been mainly used to prepare the complexes. In the case of C_2-nonsymmetric ligands, the latter method allows one of the steric isomers (*fac* or *mer*) instead of their mixture to be obtained, provided that presynthesized ligands are utilized. The fact that the second metal ion can be encapsulated by a clathrochelate with a vacant cavity is due to the reversibility of a capping reaction with Lewis acids. In appropriate conditions a cross-linking fragment reversibly dissociates to yield a semiclathrochelate product with a vacant cavity. The latter can encapsulate a second metal ion with the subsequent reversible addition of the capping fragment. It is obvious that with a proper metal ion, the stability of the resultant binuclear complex is substantially higher than that of the initial mononuclear complex, which leads to the equilibrium shift toward the binuclear clathrochelate.

When Fe^{2+} ions interact with oximehydrazonates in solution, a mixture of complexes is formed by a stepwise complexation. In the case of the *H₂DAO* and *H₂TMAO* ligands (L), the $[Fe_2L_3](BF_4)_4$ and $[FeL_3](BF_4)_2$ complexes were isolated. The mononuclear compound disproportionates quickly to form a binuclear complex and the parent ligand. The Fe^{2+} ions interact with the *H₂IAO* ligand to form an insoluble polymeric complex, which, however, reacts with efficient cross-linking agents [193].

Scheme 88

Y=BC$_6$H$_5$, BF, SnCl$_3$, SnBr$_3$

IAO: R^1=R^4=H

R^2=R^3=CH$_3$

DAO: R^1=R^2=R^3=R^4=CH$_3$

TMAO: R^1=R^2=R^3=CH$_3$

R^4=H
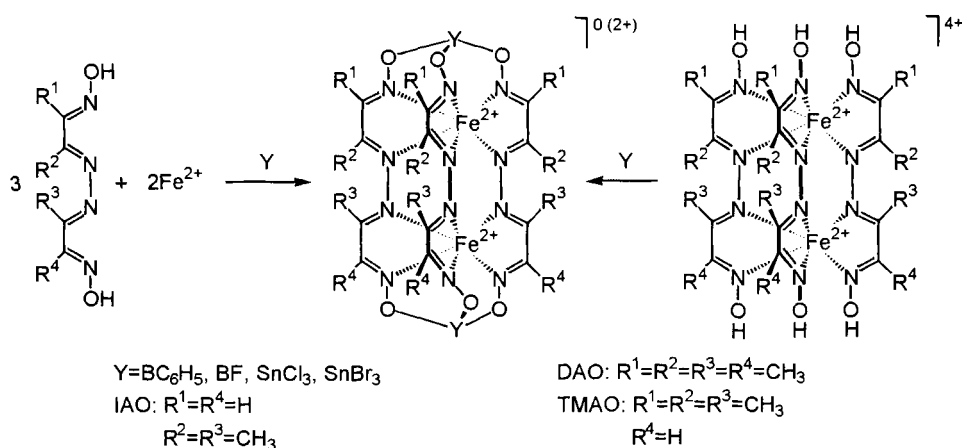
Scheme 89

Macrobicyclic binuclear iron(II) oximehydrazonates were synthesized by encapsulation of initial nonmacrocyclic tris-complexes with boron- and tin-containing Lewis acids and by direct template reactions on the Fe^{2+} ion (Scheme 89).

The [Fe(DAOBz)$_3$(BC$_6$H$_5$)](BF$_4$), [Fe$_2$(DAOBz)$_3$(BC$_6$H$_5$)](BF$_4$)$_3$, [Fe(HDAOBz)$_3$](ClO$_4$)$_2$ and [Fe$_2$(HDAOBz)$_3$](ClO$_4$)$_4$ complexes of the monobenzylated *HDAOBz* ligand were also isolated. This ligand allows one the stepwise preparation of clathrochelates with cross-linking groups of various types [193].

The binuclear germanium-capped clathrochelate [Fe$_2$DAO$_3$(Ge(CF$_3$)$_3$)$_2$] oximehydrazonate was obtained by a template condensation of the tetradentate *H$_2$DAO* ligand with IGe(CF$_3$)$_3$ in an aqueous solution in the presence of CaCO$_3$ (Reaction 52). The resulting intramolecular macrobicyclic compound precipitated from the reaction mixture, and the equilibrium shift due to the formation of the solid allowed one to isolate this complex in a relatively high yield [73].

(52)
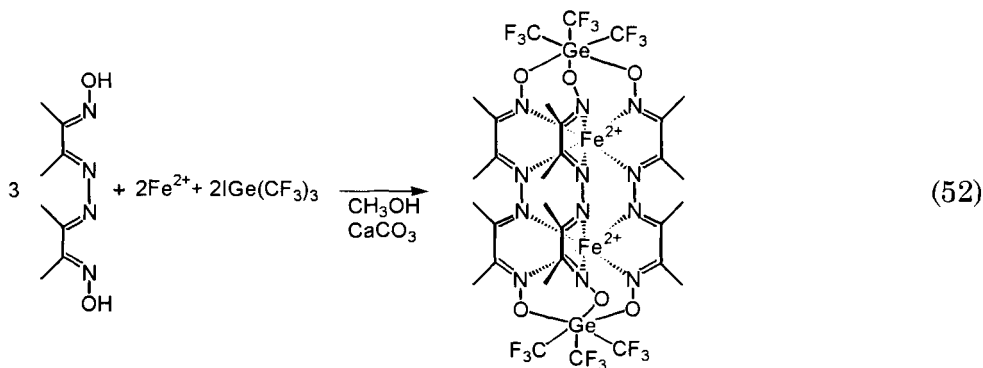
Potentially hexadentate tetraazinedioximate ligands were described in Ref. 194. The condensation of diacetyl monooxime with diacetyl dihydrazone in water (Scheme 90) initially proposed in literature for the synthesis of H_2TAO azineoxime has failed to give this compound: according to the ^{1}H and ^{13}C NMR data, the oximehydrazone resulting from 1:1 condensation is predominant in the reaction product mixture. A synthetic route for potentially hexadentate H_2TAO, H_2EAO, and H_2GAO azineoximes based on the condensation of diacetyl monooxime hydrazone with the corresponding active α-dicarbonyl compound (diacetyl, 3,4-butandione and glyoxal, respectively) in methanol was more successful (Scheme 90) [194].

The reaction of the resultant azineoximes with Fe^{2+} ions in the presence of cross-linking agents (Lewis acids, in particular $SnCl_4$) proceeded by an unexpected pathway. In all cases, even in aprotic
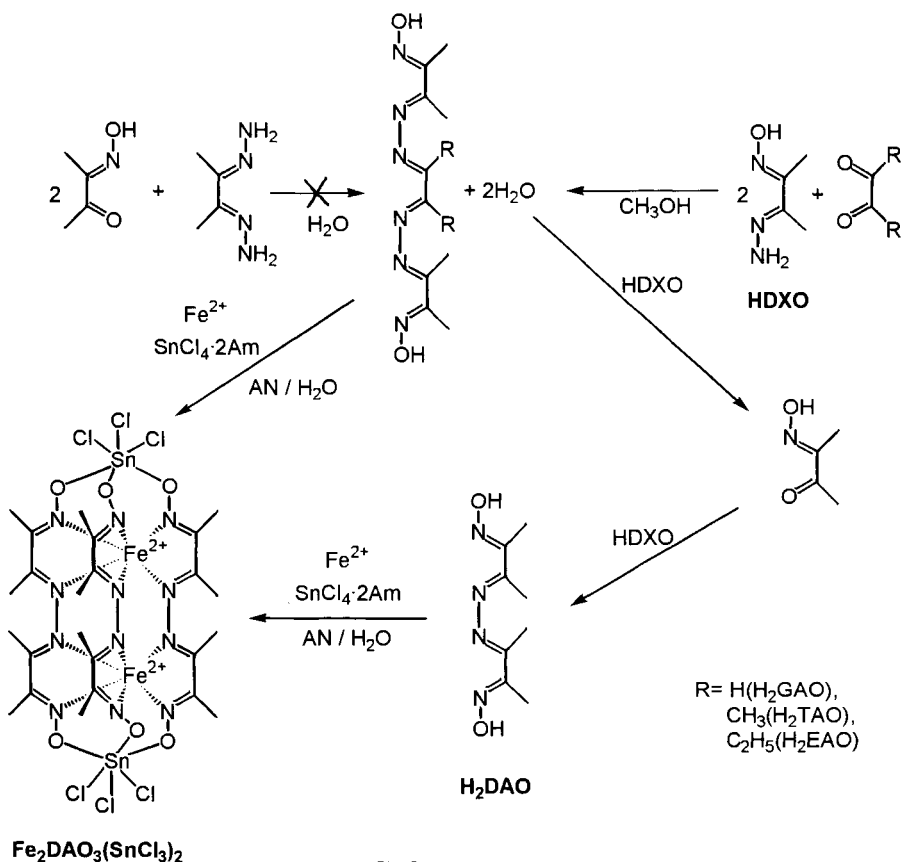
Scheme 90

media (e.g., in dry acetonitrile), instead of the expected trinuclear [Fe$_3$L$_3$(SnCl$_3$)$_2$]$^{2+}$ clathrochelates (where L is TAO^{2-}, EAO^{2-}, GAO^{2-} dianions), only one clathrochelate Fe$_2$DAO$_3$(SnCl$_3$)$_2$ complex in an essential yield (*ca* 20%) was obtained (Scheme 90). The initial azineoximes apparently disproportionated in the course of the reaction, "kicking out" the central fragment to form a highly stable and poorly soluble binuclear clathrochelate that precipitated from the reaction mixture [194].

The one-stage condensation of *tren* with 5,5'-diformyl-2,2'-bipyridine made it possible to also obtain the macrobicyclic Schiff base, whose hydrogenation on the palladium catalyst yielded the clathrochelate tris-bipyridine *tranbpy* ligand **1** (Scheme 91) [195].
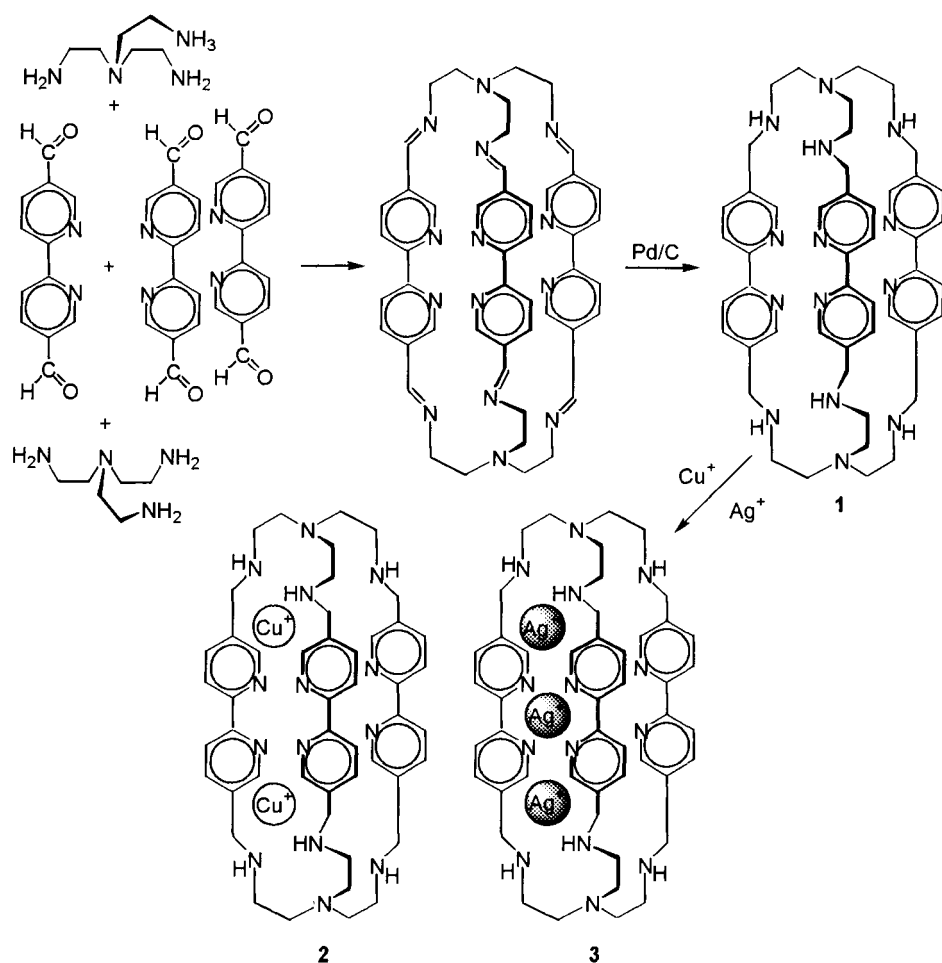
Scheme 91

The interaction of *tranbpy* ligand with an excess of [CuAN₄](BF₄) and AgBF₄ led to the formation of a binuclear [Cu₂(tranbpy)](BF₄)₂ (**2**) and a trinuclear clathrochelate [Ag₃(tranbpy)](BF₄)₃ (**3**) compounds, as well as allowed one to isolate the heteroronuclear Cu^I–Ag^I–Cu^I complex.

A new type of octaazamacrobicyclic Schiff bases was synthesized in high yields *via* a template condensation on Group 2 metal ions in ethanol at 40–50°C (Scheme 92) [196]. The resultant kinetically labile complexes readily transmetallize when reacted with transition metal (cobalt, nickel, iron, copper(II)) salts to form the corresponding mononuclear [M(imBT)]X₂ complexes (where X is BF_4^- and ClO_4^-).

With an excess of [CuAN₄](ClO₄)₂, the first binuclear compound with a possibly delocalized bond of Cu(I)/Cu(II) was also prepared [197]. A detailed template synthesis of the binuclear copper(II) complexes of macrobicyclic *imBT* ligand with a regular cavity and an *imbistrpn* ligand with an expanded cavity (Scheme 93) is described in Ref. 198.

The isolated compounds of transition metals are kinetically inert. The interaction between [Co(imBT)]²⁺ cation and an aqueous solution of NaCN leaves no Co(CN)₂ precipitate within several weeks. Irrespective [196], the clathrochelate *imBT* ligand was obtained *via* a

M₁ = Group **2** metal ion
M₂ = Co, Ni, Fe, Pb, Cd, Hg, Mg, Cu(II), Gd, Ln(III)
M₃ = Mn, Fe, Co, Cu, Ni, Zn(II)
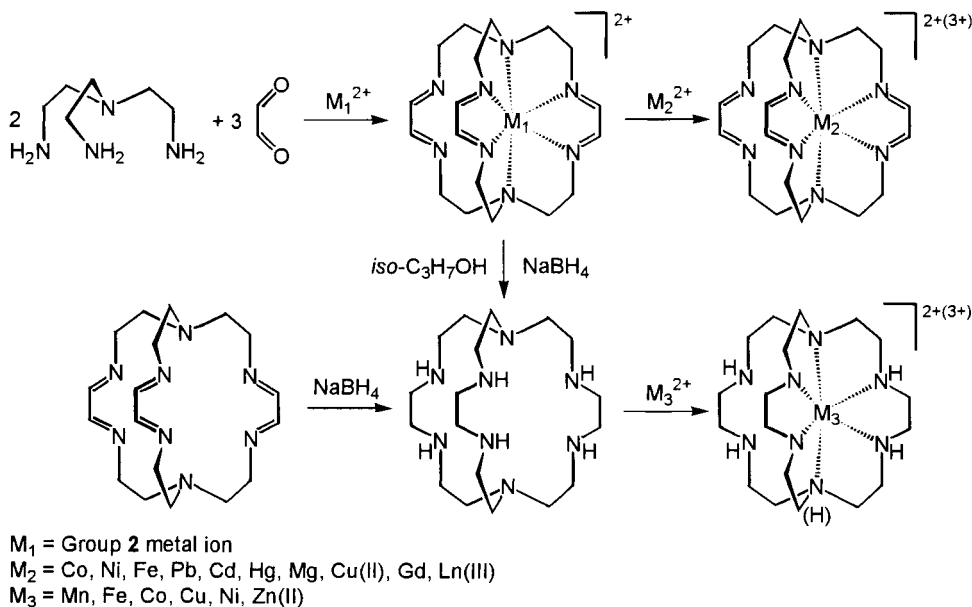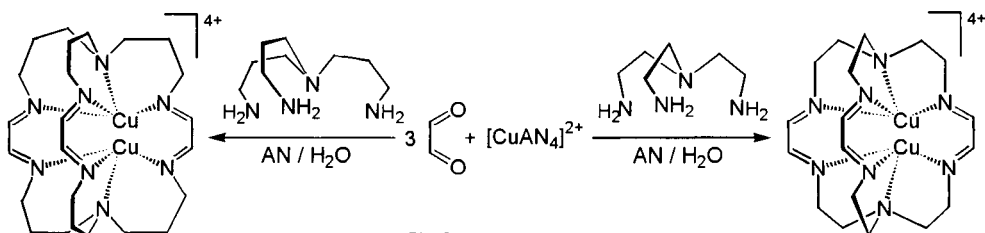
Scheme 92

Scheme 93

template reaction in the presence of Rb^+ and Cs^+ ions in methanol at 50°C (yield *ca* 60%) [199].

A detailed procedure for the synthesis of a free *imBT* ligand by the slow addition of aqueous glyoxal to *tren* solution in *iso*-propanol is described in Ref. 200. The free ligand obtained readily reacted with lanthanum and gadolinium(III) ions in an acetonitrile-chloroform mixture [201] and with lead, cadmium, and mercury(II) salts in acetonitrile-ethanol medium [202].

The reduction of *imBT* ligand with $NaBH_4$ in methanol led to the formation of a saturated octaazamacrocyclic *amBT* ligand that forms binuclear complexes with zinc(II) and copper(II) [199] and mononuclear clathrochelates with manganese, iron, cobalt, nickel, and zinc(II) [203] by treatment of the free ligand with the corresponding metal ion salts.

The cobalt(II) ion has been encapsulated with both neutral and protonated *amBT* ligand forms. In the case of nickel and zinc(II) ions, complexes with the sole protonated ligand form were obtained [203].

With pentaazamacrobicyclic clathrochelates, not only the nitrogen atoms of the side units but also capping apical nitrogen atoms take part in the coordination. Synthesis of such complexes was performed by interaction of the presynthesized macrobicyclic ligand (Scheme 94) with copper, zinc, cobalt, and nickel(II) perchlorates in boiling methanol [204].

The anthracene-functionalized N_5-cages have been obtained by two different procedures [205]: first, starting from the initial pentaazaclathrochelate precursor by condensation with mono- or dichloride anthracene derivatives to yield mono- and bis-clathrochelates, respectively (by Scheme 95 in the case of ethylene chains in the capping groups); and second, starting from the tetraazamacrocycle, containing two secondary amino groups in the *trans* position, by condensation with a protected diol derivative by the

TsO

$N-Ts$

TsO

$\xrightarrow[Na_2CO_3]{AN}$

CH_3

$\xrightarrow[\text{NaOH}]{H_2SO_4}$

HBr

$\cdot\,3HBr\cdot H_2O$

$\xrightarrow[\text{NaOH}]{CH_2Cl_2}$

$\cdot\,HBr\cdot H_2O$

penar

Scheme 94

$\xleftarrow[\text{AN, reflux}]{Na_2CO_3}$

$\xrightarrow[\text{AN, reflux}]{Na_2CO_3}$
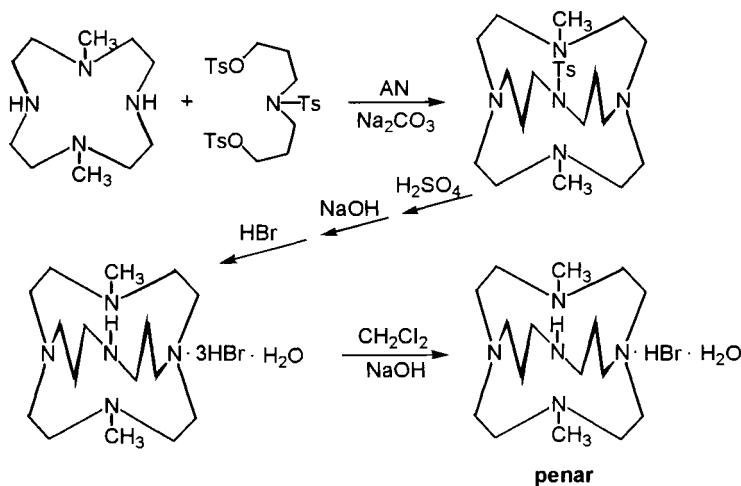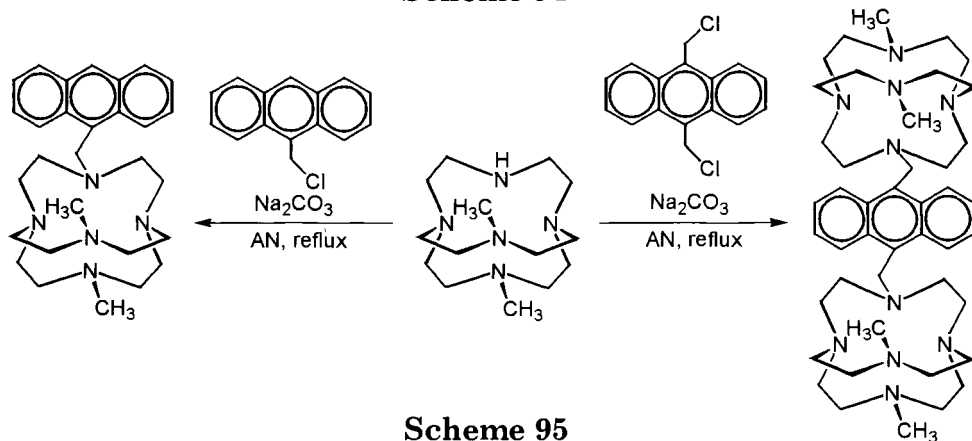
Scheme 95

well-known synthetic procedure from crown ether chemistry (Scheme 96, in the case of propylene chains in the capping groups).

The anthracene-functionalized N_5-cage ligands readily reacted with an excess of LiOH in methanol to form complexes with an encapsulated Li^+ ion that are very soluble in organic solvents [205].

The use of 3,3'-thiodipropionicacylchloride instead of bis-(3-tosyloxy-propyl)tosylamine in the first step led to the formation of a macrobicyclic N_4S-pentadentate ligand (Scheme 97).

This ligand readily reacted with $Cu(ClO_4)_2$ in methanol to form a clathrochelate complex [206]. The macrobicyclic *mepenar* ligand with *N*-methylated ribbed fragments was obtained starting from bis-(3-tosyloxypropyl)methylamine. This ligand formed complexes with Li^+ ions (upon refluxing with 20-fold excess LiOH in ethanol),

Scheme 96

MsCl = methylsulphonyl chloride

Scheme 97

thiapenar

X= NCH$_3$, Y= NR,
where R= CH$_3$, C$_6$H$_5$CH$_2$, H

X= O, Y= NCH$_3$
X=Y=O
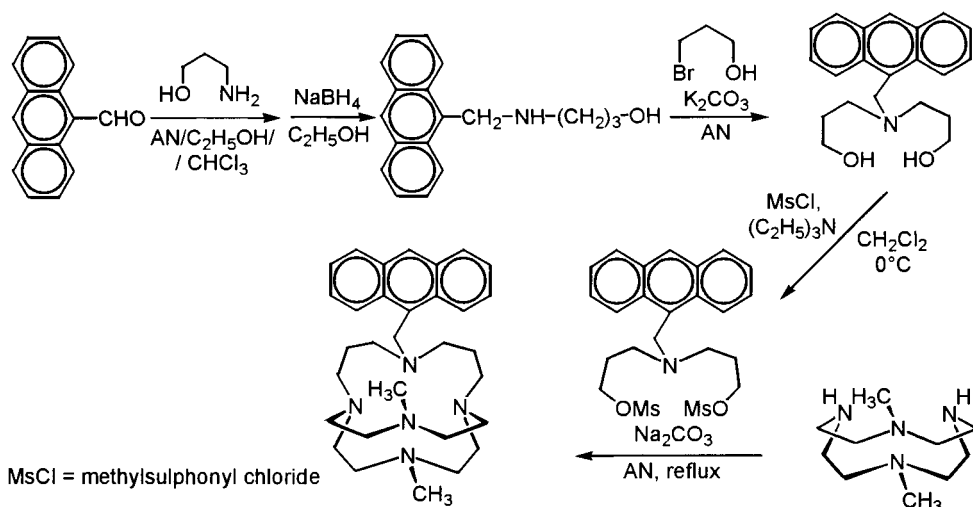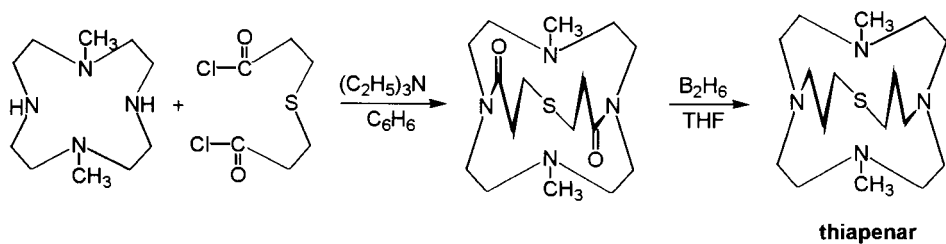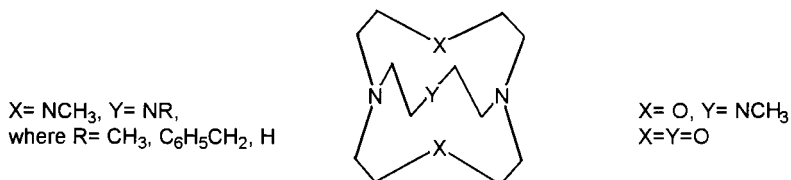
Scheme 98

Cu^{2+} ions *(via* interaction with Cu(ClO$_4$)$_2 \cdot$6H$_2$O at a molar ratio of 1:1), and Zn^{2+} ions (upon refluxing with ZnBr$_2$ in acetonitrile at a molar ratio of 1:1). No reactions between the free N$_5$- and N$_4$S-macrobicyclic ligands and Na$^+$, K$^+$, Al^{3+}, Be^{2+}, or Ni^{2+} ions have been revealed [207-209].

The synthesis of N$_5$-, N$_3$O$_2$- and N$_2$O$_3$-pentadentate macrobicyclic ligands (Scheme 98) with unusually high basicity of the nitrogen-

[Na(bpy.bpy.bpy)]$^+$
1

(phen. phen.phen)
2

(bpz.bpz.bpz)
3
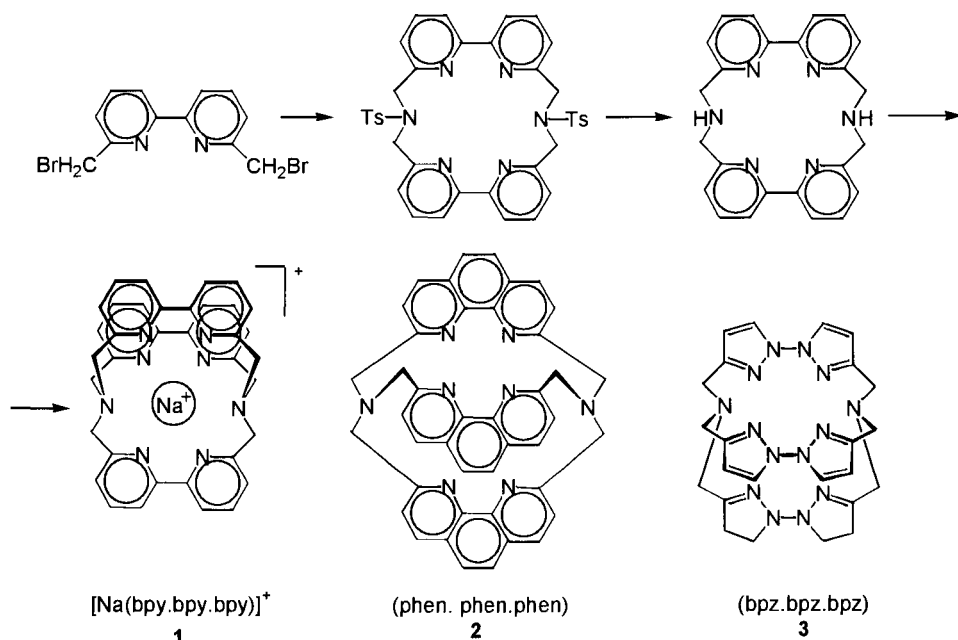
Scheme 99

containing fragment of the clathrochelate framework was realized in Ref. 210.

Macrobicyclic tris-bipyridinate **1** and tris-phenanthrolinate **2** as well as mixed *bpy.bpy.phen* ligand have also been prepared by a stepwise procedures (Scheme 99) involving the synthesis of a macrocyclic intermediate followed by its reaction with a capping agent on Na$^+$ ion [211]. The clathrochelate tris-bipyridinates and tris-phenanthrolinates of rare-earth elements have been produced by an exchange reaction between the corresponding sodium complexes and rare-earth metal nitrate or chloride upon prolonged heating in acetonitrile [212]. Interaction of the macrobicyclic tris-bipyridine ligand **1** (performed by a procedure slightly different from that proposed in [211]) with RuDMSO$_4$Cl$_2$ solvato-complex in aqueous ethanol resulted in the [Ru(bpy.bpy.bpy)]Cl$_2$ clathrochelate [213].

A more rigid tris-bipyrazole clathrochelate ligand **3** (Scheme 99) was synthesized by the scheme proposed for its bipyridine and phenanthroline analogs [214]. In contrast, the product isolated at the final stage was not a sodium clathrochelate, which makes it impossible to establish whether a template condensation on the Na$^+$ ion occurs.

Hexaene clathrochelate iron(II) complexes have been prepared by rearrangement of the preformed square-planar complexes in the presence of base upon refluxing in methanol [215]:

$$X = -(CH_2)_2-$$
$$-(CH_2)_3-$$
$$-(CH_2)_4-$$
$$-(H_2C)_3 \quad (CH_2)_3-$$

(53)
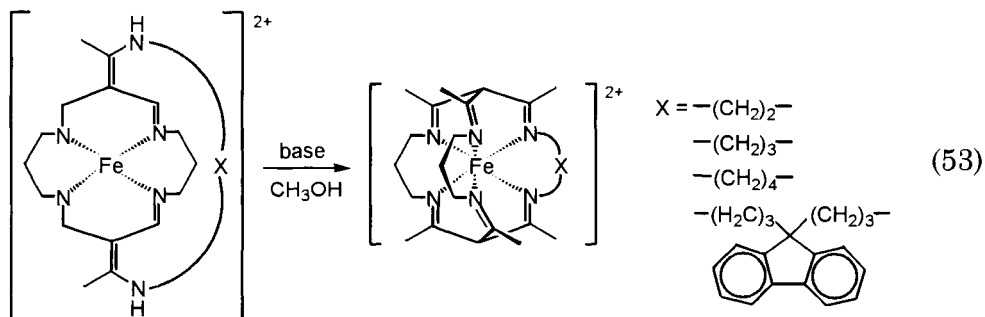
The same reaction route has been employed to isolate penta- and hexadentate semiclathrochelate iron(II) and cobalt(III) complexes [216, 217].

Chapter 3

Spatial and electronic structure of clathrochelates

To gain information on the spatial and electronic structure of clathrochelates, researchers employ first, a direct method, X-ray crystallography, permitting them to obtain unambiguous data on the crystal and molecular structure of complexes, and second, indirect methods, such as IR, multynuclear NMR, UV-vis, and Mössbauer spectroscopies.

Since sarcophaginates and sepulchrates are relatively easy to crystallize, a great number of these compounds are studied by X-ray crystallography, which together with molecular geometry calculations makes it possible to establish their three-dimensional structures both in crystal and in solution. The optical activity of such clathrochelates enables one routinely to utilize circular dichroism measurements to investigate their structure. The spatial and electronic structures of sarcophaginates and sepulchrates are much more seldomly determined by alternative spectral techniques compared with clathrochelates of other types.

Phosphorus-containing tris-diimine d-metal complexes are isolated as ionic associates with a bulky inorganic BF_4^- anion and readily crystallize. Therefore, monocrystals of these compounds, suitable for X-ray analysis, were obtained, and X-ray crystallography – the major method for determining their geometry – was applied to all complexes of this type. The subtle features of the electronic structure of macrobicyclic phosphorus-containing d-metal tris-diiminates have been examined by a variety of spectral methods and quantum-chemical calculations.

For macrobicyclic d-metal tris-dioximates, the X-ray crystallography analysis is performed least often. This is because the charge of the central metal atom in the majority of such compounds is balanced by that of the clathrochelate ligand, and crystals of the resulting intramolecular complexes are purely molecular. Alongside the structural peculiarities in the structure of such complexes, this

hinders the formation of a stable crystal lattice, and single crystals are neither formed nor decomposed within a short time. Therefore, to establish the structure of macrobicyclic d-metal tris-dioximates, different physical and physicochemical methods have been used, which – with allowance for the X-ray crystallographic data for their macrocyclic, nonmacrocyclic, and clathrochelate analogs – enable one to determine the composition and geometry of the central ion and capping fragment polyhedra. These methods combined with some available X-ray and EXAFS data confirm the clathrochelate nature of the compounds obtained, and permit one to establish the spatial structure of some peripherical fragments and especially the electronic structure of the macrobicyclic d-metal tris-dioximates studied. ^{57}Fe Mössbauer spectroscopy is very informative about the structure of tris-diimine iron(II) complexes. ^{1}H, ^{13}C, ^{11}B, ^{119}Sn, and ^{59}Co NMR spectroscopies were also often used in the case of diamagnetic macrobicyclic iron(II) and cobalt (III) tris-dioximates.

The coordination polyhedron of the majority of clathrochelate complexes, formed by six donor atoms, has a geometry intermediate between a trigonal prism (TP) and a trigonal antiprism (TAP) (Scheme 100).

The main parameters describing such a coordination polyhedron are the distortion angle φ (0° and 60° correspond to the TP and TAP, respectively), bite angle α (half the chelate angle), distance h between the coordination polyhedron bases, and the metal-donor atom distance a.
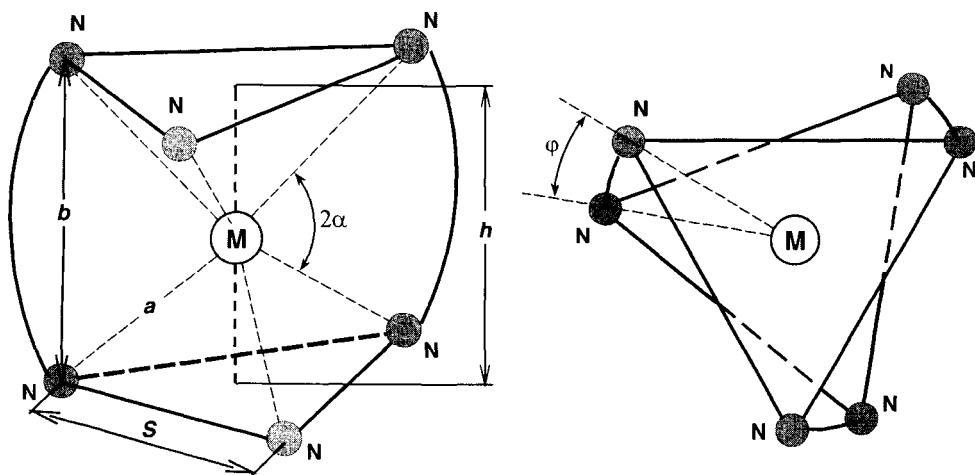
Scheme 100

3.1 SARCOPHAGINATES AND SEPULCHRATES

As mentioned above, the three-dimensional structure of a considerable number of these compounds has been established mainly by X-ray crystallography. The main structural characteristics for sepulchrate and sarcophaginate complexes as well as for free ligands are listed in Tables 2 and 3.

Owing to the relative flexibility of these structures and the presence of numerous chiral centres in sepulchrate and sarcophaginate molecules, a variety of their geometric and optic isomers is expected to exist, unlike the clathrochelates described in Sections 3.2 and 3.3.

Therefore, circular dichroism and rotationary dispersion as well as energy minimization analysis play a key role in structural investigations of sarcophaginates and sepulchrates in solution. Thus, two main interrelated approaches to studying the steric structure of these complexes can be distinguished: establishing the dependence of the coordination polyhedron geometry on the nature of both the clathrochelate ligand and the encapsulated metal ion, and determining the conformation of the ligand or complex in the solid state and in solution. The flexibility of sarcophaginate and sepulchrate ligands and their relatively big cavities have made it possible to examine systematically the effect of the metal ion electronic configuration on the structural parameters of the complex formed by this ion [178]. First, it should be noted that the majority of structural parameters (b, s, and α) have the same values for all the complexes represented in Table 3. The metal-ligand distance a essentially changes and becomes higher with an increasing metal ion radius. The distortion angles φ – for such complexes depending mainly on the metal ion electronic configuration – also change (Fig. 1). It is interesting that the nature of substituents in sarcophaginate capping groups has practically no effect on the coordination polyhedron geometry and especially on the φ angle magnitude [178]. The analogous phenomenon is also observed for macrobicyclic d-metal dioximates (see Section 3.3).

For metal ions with d^0, d^1, d^2 (low-spin), d^5, d^6 (high-spin), and d^{10} electronic configuration, the ligand-field force is small. The structure of their complexes resembles that of the free sarcophagine ($\varphi = 28°$) and may be regarded as trigonal-prismatic. The φ angles for all other configurations are appreciably higher and increase with
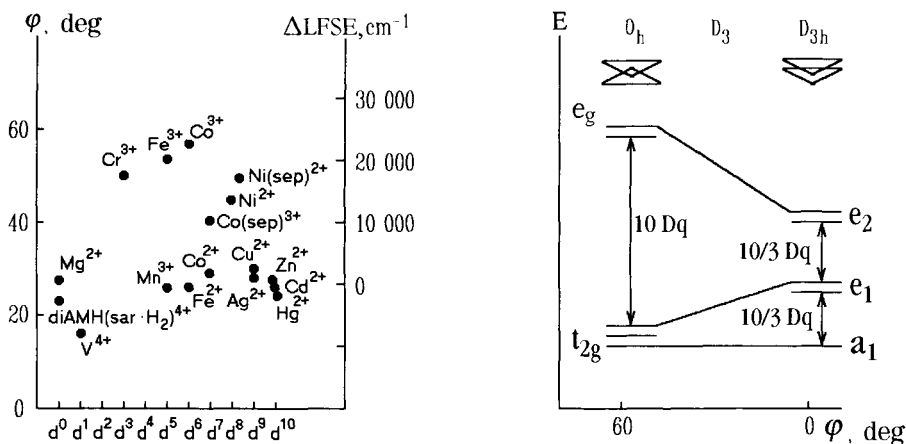
Figure 1. Plot of distortion angles φ *versus* the d-electron occupancy of the metal centers [178].

Figure 2. Energy level scheme for TAP and TP geometries of a coordination polyhedron [178].

increasing differences in ligand-field stabilization energies (Δ LFSE) in TAP and TP. The energy level scheme shown in Fig. 2 was used for calculations as the first approximation [178].

The preference of TAP geometry is insufficient for the d^9 configuration and reaches a maximum for the low-spin d^6 configuration. This simple qualitative ligand-field model, and the spectral data obtained, permit the φ angles to be evaluated with high accuracy [178].

Thus, for theoretical calculations of the sarcophaginate and sepulchrate structures, one should take into account inter- and intramolecular nonbonded interactions and electronic effects. The calculations based on geometric and/or repulsion models are obviously justified only for complexes with insufficient or no preference for TAP or TP structure (ΔLFSE = 0). In this case, the ligand determines the complex geometry. In all other cases, the contribution of the metal ion electronic configuration cannot be neglected [178].

The experimentally observed φ angle (*ca* 18°) decrease from the expected one (*ca* 28°) for the [V(diAMHsar–2H)]$^{4+}$ cation was attributed to two main factors. First, the deprotonated and coordinated amino groups become practically planar, which leads to a decrease in the distortion angle. Second, with allowance for π-donation, for the d^1 configuration, TP geometry is preferable to TAP geometry, since the ligand π-orbitals with e_1 symmetry interact with

Table 2.

The metal–donor atom distance and conformation for cobalt(II,III) and platinum(IV) sepulchrates and sarcophaginates.

Compound	Conformation	a (obtained), Å	a (estimated), Å	Reference
Δ-[Co(taetacn)](ClO$_4$)$_3$		(1)-1.963	1.974	[218]
		(2)-2.009	1.994	
Λ-[Co(NOsartacn)](S$_2$O$_6$)$_{1.5}$ · 4H$_2$O		(1)-1.999		[218]
		(2)-1.962		
[Co(azacapten)](ClO$_4$)$_3$	C_3lel_3	2.226(Co–S)	2.240	[219]
		2.009(Co–N)	1.982	
[Co(azacapten)](ClO$_4$)$_2$	C_3lel_3	2.313(Co–S)	2.307	[219]
		2.076(Co–N)	2.164	
[Co(azacapten)](S$_2$O$_6$)$_{1.5}$ · 4H$_2$O	C_3lel_3	2.22 (Co–S)		[121]
		1.96 (Co–N)		
(+)-[Co(azacapten)](ZnCl$_4$)Cl	C_3lel_3	2.226(Co–S)		[121]
		2.009(Co–N)		
[Co(diMEsar-S$_6$)](CF$_3$SO$_3$)$_2$	D_3lel_3	2.299		[146]
Λ-[Co(sep)]Cl$_3$ · H$_2$O	D_3lel_3	1.990		[3, 220]
Δ-[Co(MEazasar)](ClO$_4$)$_3$ · 3H$_2$O	D_3lel_3	1.977		[221]
[Co(diNOsar · 2NHOH)](CF$_3$SO$_3$)$_2$Cl		1.978		[108]
[Co((ZnCl$_3$)sar)]Cl · 2H$_2$O		1.981		[120]
Λ-[Co(diNOsar–H)]Cl$_2$ · 4H$_2$O	D_3ob_3	2.016(Co–N)		[101]
		1.980(Co–NH)		
[Co(NOPENsar)]I$_4$ · 3H$_2$O	D_3lel_3	1.969		[143, 222]
[Co(NOtetrasartame)]Cl$_3$ · 3H$_2$O		1.940		[148]
[Co(diNOdisartame)]Cl$_3$ · 2H$_2$O		1.97÷2.07		[149]
[Co(NOtrisartame)](ZnCl$_4$)Cl · 0.5H$_2$O		1.95		[149]
[Co(diNOdisartacn)]ZnCl$_4$ · H$_2$O		2.033		[155]
[Co(diNOsar)](S$_2$CN(CH$_2$)$_4$)$_3$	C_3lel_3	1.975		[223]
[Co(MECAoxosar–H)](ClO$_4$)$_2$ · 7H$_2$O	lel_3	1.973		[133]
[Co(tamox)]Cl(ClO$_4$)$_2$ · H$_2$O		1.97(NH)		[182]
		1.91(NO)		
[Co(tamox–H)]Cl$_2$ · 3H$_2$O		1.98(NH)		[182]
		1.90(NO)		
[Co(MENOsar-N$_3$Se$_3$)]Cl$_3$ · 5H$_2$O	lel_2ob	2.340(Co–Se)		[125]
		2.001(Co–N)		
[Co(Me$_8$tricosatrienesar)]$_2$(ZnCl$_4$)$_3$		2.011		[151]
[Co(Me$_8$tricosatrienesar)](ZnCl$_4$)	Λ (S_6)	2.223		[151]
	Λ (S_4R_2)	2.232		
[Co(MEH$_2$NCO-7-amino-6-enesar-N$_3$S$_3$)](ClO$_4$)$_3$ · H$_2$O	lel_2ob	1.915		[126]
[Co(MEPhreCOsar)]Cl$_3$ · 3.35H$_2$O	lel_3	1.967		[137]
[Co(CNMEoxosar–H)](ClO$_4$)$_{3/2}$Cl$_{1/2}$ · H$_2$O	lel_2ob	1.963		[134]
[Pt(sep)](S$_2$O$_6$)$_2$·2.5H$_2$0	D_3lel_3	2.071		[224]
[Pt(diNHOHsar)] (CF$_3$SO$_3$)$_4$ · H$_2$O		2.06		[225]

Table 3.

The main structural parameters for *d*-metal sepulchrates and sarcophaginates.

Compound	Confor-mation	r_i, Å	a, Å	b, Å	s, Å	s/h	α, deg	φ, deg	Reference
[diAMHsar·2H](NO$_3$)$_4$				2.873	3.043	1.092		23.9	[178]
[Mg^{II}(diAMHsar)](NO$_3$)$_4$ · H$_2$O	D_3lel_3	0.86	2.188	2.822	2.984	1.106	40.2	27.8	[178]
[Mg((AMH)AMsar)](NO$_3$)$_3$ · 1/2H$_2$O	D_3lel_3		2.188				43.0	27.8	[115]
[V^{IV}(diAMHsar–2H)] (S$_2$O$_6$)$_2$ · 2H$_2$O		0.72	2.085	2.644	2.828	1.090	39.4	17.7	[178]
[Cr^{III}(diAMsar)]Cl$_3$ · H$_2$O	D_3lel_3	0.76	2.073	2.777	2.929	1.222	42.1	49.0	[178]
[Cr(AMHMEsar-N$_5$S)]Br$_3$ · 3H$_2$O	lel_2ob		2.067(Cr–N) 2.399(Cr–S)				42.1		[166]
[Mn^{II}(diAMHsar)] (NO$_3$)$_4$ · H$_2$O	$D_3lel'_3$	0.97 (*hs*)	2.238	2.884	3.053	1.107	40.1	27.6	[178]
rac-[Mn(sar)](NO$_3$)$_3$ · H$_2$O	D_3lel_3	0.79(*hs*)	2.13				42.0	28.0	[179]
[Mn(diAMHsar)] (NO$_3$)$_5$ · H$_2$O	D_3lel_3		2.122				40.7	28.0	[180]
[Fe^{III}(sar)](NO$_3$)$_3$	D_3lel_3	0.69(*ls*)	2.007	2.719	2.857	1.247	42.6	52.8	[178]
[Fe^{II}(diAMHsar)](NO$_3$)$_4$ · H$_2$O	$D_3lel'_3$	0.92(*hs*)	2.202	2.864	2.979	1.090	40.6	28.6	[178]
[Co^{III}(sep)](NO$_3$)$_3$	D_3lel_3	0.69(*ls*)	1.974	2.717	2.818	1.260	43.5	56.7	[178]
[Co^{III}(diNHOHsar)]Cl$_3$ · 4H$_2$O	D_3ob_3		1.974	2.730	2.827	1.273	43.8	58.3	[103]
[Co^{II}(sep)] (S$_2$O$_6$) · H$_2$O	D_3lel_3	0.89(*hs*)	2.164	2.831	3.036	1.200	41.0	42.4	[96]
[Co^{II}(diAMHsar)](NO$_3$)$_4$ · H$_2$O	$D_3lel'_3$		2.170	2.830	2.944	1.091	40.7	29.0	[178]
[Co(AMHAMsar)](ClHCl)$_3$ · 5H$_2$O	D_3lel_3		2.175					28.0	[105]
[Co(*fac*-Me$_5$tricosanesar)]$^{3+}$	D_3lel_3		2.022				47.6	67.0	[152]
Δ,Λ-[Co(NOazasar)]Cl$_3$ · 3H$_2$O	D_3lel_3		1.977				42.9	54.4	[119]
Δ,Λ-[Co(diNOsar)]Cl$_3$ · 3H$_2$O	D_3lel_3		1.982				43.2	54.4	[119]
[Co(diAMHsar)]Cl$_5$ · 3H$_2$O	D_3lel_3		1.974					55.0	[105]
Δ,Λ-[Co(CL(ClME)absar)](NO$_3$)$_3$	C_2lel_2ob		1.96				43.4	52.0	[119]
[Co(MEOHabsar)]Cl$_3$ · H$_2$O	lel_2ob		1.97				43.3	52.0	[114]
[Co(AMHsar-N$_5$S)]Br$_4$ · 2H$_2$O	lel_3		1.984(Co–N) 2.219(Co–S)				43.3		[127]

Compound	Config								Ref
$[Co(diMe_3AMHsar)](NO_3)_5 \cdot 3H_2O$	C_3ob_3		1.961				43.6	57.8	[116]
$[Co(MEsar-N_4S_2)](ClO_4)_2$	lel_3		2.102(Co–N) 2.361(Co–S)				39.9		[226]
$[Co(NOMEsar-N_4S_2)](ZnCl_4)Cl \cdot H_2O$	lel_3		2.008(Co–N) 2.219(Co–S)				42.9		[128]
$[Ni^{II}(diAMHsar)]Cl_4 \cdot H_2O$	C_2lel_2ob	0.83 (hs)	2.111	2.819	2.963	1.202	41.9	45.7	[172,178]
$[Ni^{II}(diAMHsar)](NO_3)_4 \cdot H_2O$	D_3lel_3		2.110	2.816	2.971	1.207	41.9	47.1	[178,227]
$[Ni^{II}(sep)](ClO_4)_2$			2.111	2.790	3.000	1.247	41.4	48.0	[160]
$[Ni(AMMEsar-N_4S_2)](ClO_4)_2$	lel_2ob		2.103(Ni–N) 2.398(Ni–S)				42.8	49.0	[170]
$[Ni(fac\text{-}Me_5tricosanesar)](ClO_4)_2 \cdot 0.53\ H_2O$			2.140					62.4	[228]
$[Cu^{II}(diAMHsar)](NO_3)_4 \cdot H_2O$	$D_3lel'_3$	0.87	2.169	2.820	2.965	1.110	40.6	29.8	[178]
$[Cu(diMe_3AMHsar)](ClO_4)_4$	$D_3lel'_3$		2.165				42.4	29.7	[173]
$[Cu(AMHMEsar-N_4S_2)](ClO_4)_3 \cdot 3H_2O$	lel_3		2.436(Cu–S) 2.04(Cu–N$_{av}$) 2.600(Cu–S') 2.447(Cu–N)				41.2		[171]
$[Ag^{II}(diAMHsar)](NO_3)_4 \cdot H_2O$	$D_3lel'_3$	1.08	2.286	2.953	3.120	1.111	40.2	28.8	[178]
$[Zn^{II}(diAMHsar)](NO_3)_4 \cdot H_2O$	$D_3lel'_3$	0.88	2.190	2.833	2.933	1.085	40.3	28.6	[173,178]
$[Zn(diMe_3AMHsar)](ClO_4)_4$	$D_3lel'_3$		2.19				42.3	28.9	[173]
$[Zn(sar)]Cl_2 \cdot 4H_2O$	D_3lel_3		2.169				43.6	29.8	[115]
$[Zn(fac\text{-}Me_5tricosanesar)](ClO_4)_2 \cdot 0.608\ H_2O$			2.196				43.6	60.7	[228]
$[Cd^{II}(diAMHsar)](NO_3)_4 \cdot H_2O$	D_3lel_3	1.09	2.30	2.966	3.132	1.103	40.2	27.4	[178]
$[Hg^{II}(diAMHsar)](NO_3)_4 \cdot H_2O$	$D_3lel'_3$	1.16	2.35	3.006	3.213	1.112	39.8	25.8	[178]
$[Rh(MENOsar)](ZnCl_4)Cl$	D_3lel_3	0.81	2.069				42.5	52.0	[164]
$[Rh(MENO1,3pnsar)](ZnCl_4)Cl$	D_3lel_3		2.114				47.7	66.0	[164]
$[Ru(MEsar)]^{2+}$	D_3lel_3	(0.88)	2.105				41.8	49.7	[229]
$[Ru(capten)](CF_3SO_3)_2$	C_3lel_3		2.136(Ru–N) 2.284(Ru–S)				43.2	55.5	[229]

vanadium(IV) d_{z^2} orbitals (in the plane of chelate ethylenediamine fragments, perpendicular to the threefold axis).

It should be noted that the models proposed for analysis of sarcophaginate and sepulchrate structures cannot be used for the rigid clathrochelates with a smaller cavity, since the metal central ion size and the ligand strain energy change may predominante. For example, in α-dioximate $CoDm_3(BF)_2$ and $[CoDm_3(BF)_2](BF_4)$ clathrochelates, the φ angles are 8.6 and 31.2°, respectively, whereas in $[Co(sep)](S_2O_6)\cdot 6H_2O$ and $[Co(sep)](NO_3)_3$ complexes, one is 42.4 and the other 56.7°, respectively.

The majority of the structural data available for sarcophaginates and sepulchrates were obtained for cobalt(III) complexes. Despite the diversity of the clathrochelate frameworks and substituents in them, the Co(III)–N distance remains practically the same and is from 1.94 to 2.01Å (for N_6-cages it is from 1.94 to 1.98Å). This bond length is minimal for rigid macrotricyclic $[Co(NOtrisartame)](ZnCl_5)\cdot 0.5H_2O$ and macrotetracyclic $[Co(NOtetrasartame)]Cl_3\cdot 3H_2O$ complexes and maximal for thia- and selen-containing compounds. An unusually high Co(III)–N distances observed in the carbanion $[Co(diNOdisartacn)](ZnCl_4)\cdot H_2O$ complex is caused by strong steric hindrances and deformations in the ligand [155]. The Co(III)–S bond length in *azacapten* ligand complexes occupies the lower part of the known Co(III)–thioester ligand bond length range. The effect of macrobicyclic ligand deprotonation of the metal-nitrogen bond length may be illustrated by data for the $[Co(diNOsar–H)]Cl_2\cdot 4H_2O$ complex (Table 2). The cobalt–N(deprotonated) (6) bond length is markedly (by 0.042Å) shorter and the *trans*-cobalt–N(1) bond is markedly (by 0.028Å) longer than the mean of the four other distances. This is largely due to a planar deprotonated amino group structure that affects the molecular structure along the N(1)–N(6) axis [101].

In mixed oximesarcophaginate $[Co(tamox)]Cl(ClO_4)_2\cdot H_2O$ and $[Co(tamox–H)]Cl_2\cdot 3H_2O$ semiclathrochelates whose symmetry resembles a TAP ($\varphi \sim 52°$), the Co–N(oxime) and Co–N(amine) distances are substantially different (*ca* 1.90–1.91 and *ca* 1.97–1.98Å, respectively). The observed N–O distance (*ca* 1.90Å) in these compounds is appreciably greater than that of clathrochelate cobalt(III) tris-dioximates (*ca* 1.83Å). This may account for unsuccessful attempts to prepare the corresponding clathrochelate complexes *via* cross-linking with boric and phenylboronic acids [182].

Table 4.
Structural parameters of the strain energy-minimized structures of the
$[Co(sar)]^{3+}$ conformers [230].

Conformer	Distortion angle φ, deg	α, deg	Torsion angle (en), deg	Torsion angle (cap), deg
D_3lel_3	53.4	43.35	172.8	119.8
			172.8	119.8
	53.4	43.35	172.8	119.8
			172.8	119.8
	53.4	43.35	172.8	119.8
			172.8	119.8
C_3lel_3	48.2	42.35	162.0	150.5
			162.0	150.5
	48.2	42.35	162.0	150.5
			178.2	108.3
	48.2	42.35	178.2	108.3
			178.2	108.3
C_2lel_2ob	59.0	42.45	88.4	159.7
			165.1	144.7
	42.1	42.2	175.8	137.2
			84.4	159.7
	42.1	42.2	175.8	137.2
			165.1	144.7
C_2ob_2lel	57.2	42.65	95.5	161.4
			87.8	160.3
	57.2	42.65	167.3	143.0
			87.8	160.3
	42.9	42.15	95.5	161.4
			167.3	143.0
D_3ob_3	57.4	43.05	94.6	159.8
			94.6	159.8
	57.4	43.05	94.6	159.8
			94.6	159.8
	57.4	43.05	94.6	159.8
			94.6	159.8

For cobalt(III) compounds, P. Comba calculated five of the six
conformations possible for sarcophaginate complexes (Fig. 3), using
strain energy minimization [230]. The sixth D_3lel_3' conformation does
not exist in cobalt(III) cages. Some structural parameters of the
strain energy-minimized structures of the cobalt (III) complex
conformers are presented in Table 4.

It is evident that the total strain of various conformers of the
$[Co(sar)]^{3+}$ cation is quite similar. Thus, the conformation in the
solid state and in solution results from fine structural effects in the
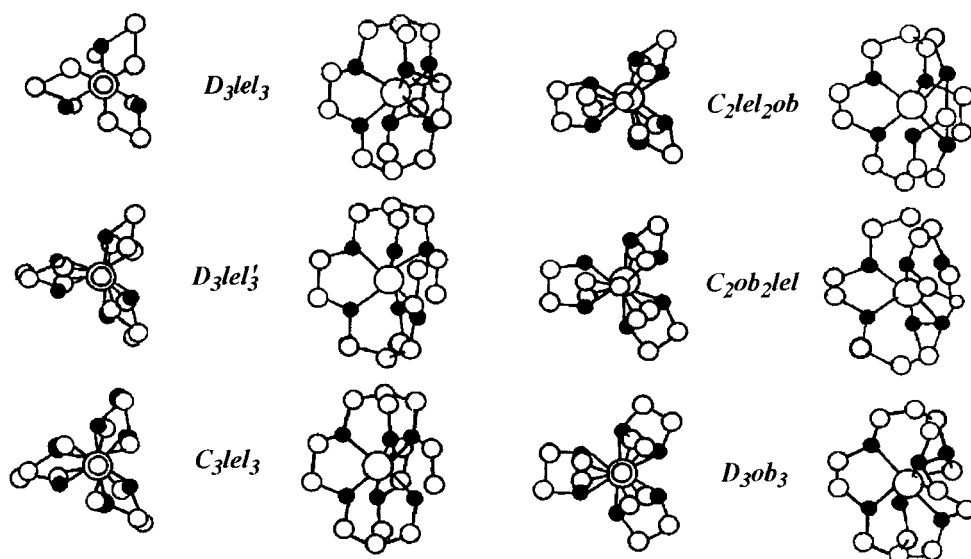
Figure 3. Conformations of [M(sar)]$^{n+}$ cation. The structures are energy minimized with distance M–N approximately 2.06Å [230].

sarcophaginate and sepulchrate framework and by environmental factors.

$D_3 lel_3$ conformation has been observed in the cobalt(II) and cobalt(III) sepulchrates, whereas cobalt(III) hydroxylaminosarcophaginates and the monodeprotonated dinitrosarcophaginate adopt a $D_3 ob_3$ configuration (see Tables 2 and 3). Still more striking proved to be the fact that for [Ni(diAMHsar)]$^{4+}$ cation, the replacement of the anion brings about changes in the conformation from $D_3 lel_3$ to $C_2 lel_2 ob$ (Table 3), although the possibility of the coexistence of lel and ob orientations in the chelate cycle was not considered in the first paper that reported the conformation of such complexes [220].

All the above considerations impose substantial restrictions on the use of the data obtained by molecular mechanics to compare different types of hexamine complexes. Moreover, the comparison may be reasonable only for isomers with a similar number and mode of interaction exhibiting identical electronic effects [230].

A comparison of the data reported in Ref. 231 for conformers of cobalt(III) sepulchrates with data for sarcophaginates indicates that the free energies calculated at 289K (ΔG_{rel}) equal to 3.8, 5.0, 0.0, 1.1, and 10.3, in the first case and 6.9, 4.0, 0.0, 0.7, and 7.0 kJ·mol^{-1} in the second one for $D_3 lel_3$, $C_3 lel_3$, $C_3 lel_2 ob$, $C_3 ob_2 lel$, and $D_3 ob_3$

conformations, respectively, are of the same order of magnitude. An appreciable decrease of ΔG_{rel} for the D_3ob_3 conformation in the case of cobalt(III) sarcophaginate compared with the cobalt(III) sepulchrate, is because the apical fragment of the latter is more planar, and along with a cavity that is too small for cobalt(III) ion in this conformation, the causes considerable steric hindrances. The same factors are responsible for stability inversion for two conformers with lel_3 geometry (the cavity in the C_3lel_3 conformer is slightly contracted compared with that in the D_3lel_3 conformer) [230].

The minimized deformation energies U_{gen} of the $[M(sar)]^{n+}$ complexes were also calculated [230] as a function of the M–N distance over the 1.90–2.36Å range for each of the six possible conformers with allowance for the fact that all coordinating nitrogen atoms assume either R- or S-configuration. Other configurations (e.g., RRR, SSS, and others) were not taken into account in the calculations, since they have not been detected experimentally. The D_3lel_3' and D_3lel_3 conformations are preferred by most of the $[M(sar)]^{n+}$ compounds (Tables 2 and 3), which confirms the assumption that the M–N bond length is fixed. A plot of U_{gen} *versus* the M–N bond length is shown in Fig. 4. Only five isomers exist up to M–N distances approximately 2.05 Å, and the stability of these isomers is equal up to 1.98 Å. Above approximately 2.0, 2.1, and 2.2Å, the D_3ob_3, C_2ob_2lel, and C_2lel_2ob conformers, respectively, become unstable. Only one D_3lel_3' conformer is stable above approximately 2.2Å.

The dependence of the distortion angle φ on conformation of sarcophaginates is shown in Fig. 5. The preference for an octahedral structure decreases with increases in the number of chelate fragment with lel conformation and in the lel conformer series, from D_3lel_3 to C_3lel_3 and then to D_3lel_3'. Alongside the increase of the cavity size with decreasing φ angle, this is the reason why neither the D_3lel_3' nor the D_3ob_3' conformation has been detected for short M–N bonds [230].

Thus, the application of the ligand field model [178] in combination with the strain energy minimization model [230] makes it possible to calculate with high accuracy the geometrical parameters of sepulchrate and sarcophaginate frameworks.

In the case of amidine- and amide-functionalized cobalt(II) N_6- and N_3S_3-sarcophaginates, two of the three five-membered chelate cycles display the lel conformation, while the third one, which is on the same strand as the amide or amidine group, has the ob conformation
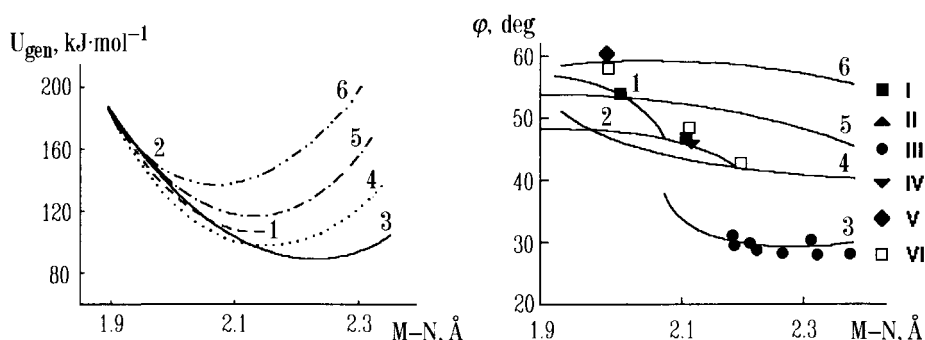
Figure 4. Plot of U_{gen} *versus* M–N bond length for [M(sar)]$^{n+}$ complexes:
1 – D_3lel_3; **2** – C_3lel_3; **3** – D_3lel_3'; **4** – C_2lel_2ob; **5** – C_2ob_2lel; **6** – D_3ob_3 [230].

Figure 5. Plot of calculated and experimental φ values for [M(sar)]$^{n+}$ cations *versus* M–N bond length: D_3lel_3 (**1, I**); C_3lel_3 (**2, II**); D_3lel_3' (**3, III**); C_2lel_2ob (**4, IV**); C_2ob_2lel (**5, V**); D_3ob_3 (**6, VI**) [230].

[126, 134]. An unusual feature of their sarcophaginate frameworks is the structure of the cap: the amidine and amide fragments are cross-linked with a methylene unit to form a near-planar diazine heterocycle fused to the cap as a subsidiary feature [126].

The expanded cobalt(II) [Co(Me$_8$tricosanesar)]$^{2+}$ and cobalt(III) [Co(Me$_8$tricosatrienesar)]$^{3+}$ sarcophaginates have demonstrated usual sterically induced structural and spectral characteristics [151]. The Co–N distances in [Co(Me$_8$tricosatrienesar)]$^{3+}$ cation are remarkably long (*ca* 2.01 Å) compared with those found in relatively unstrained systems (*ca* 1.90 Å). As result, the first spin-allowed ligand field bands in its UV-vis spectrum are remarkably (up to 2000 cm^{-1}) red shifted compared with corresponding bands of the pentamethyl homologue. More striking CoN$_6$ coordination polyhedron spectral and structural behavior has resulted when triimine cobalt(III) sarcophaginate was reduced to the more sterically crowded saturated amine [Co(Me$_8$tricosanesar)]$^{2+}$ cation. This cation has crystallized with different anions (NO$_3^-$ and ZnCl$_4^{2-}$) from different-coloured Λ(S$_6$)-isomer with virtual D_3 symmetry and Λ(S$_4$R$_2$)-isomer with C_2 symmetry, respectively. Mean Co(II)–N distances are very similar for both these structures, but the latter has two short and two very long bonds. These two conformations of the free expanded amine ligand prefer a larger ion than Co^{2+}, and the implication is that strong steric influences in this system stabilize larger cavity conformations, which markedly expand both Co(II)N$_6$ and Co(III)N$_6$ coordination polyhedra.

As a result, the $^4T_{1g}$(F)$\rightarrow$ $^4T_{2g}$, $^4T_{1g}$(P) transitions in the UV-NIR spectrum of the [Co(Me$_8$tricosanesar)]$^{2+}$ cation are remarkably (>1500 cm^{-1}) red shifted from those of analogous sarcophaginates with relatively optimal chromophore dimensions [151].

A comparative analysis of the structure and spectra of the regular and contracted cobalt(III) N$_3$S$_3$-sarcophaginates was performed in Ref. 124. In the regular sarcophaginate [Co(diMEcapten)]$^{3+}$ cation, the Co–S bond length (*av* 2.235 Å) is typical for homoleptic thioether and mixed amino-thioether cobalt(III) sarcophaginates. To the contrary, the Co–N bonds are substantially longer (*av* 2.022 Å) compared with the ones typical for cobalt(III) N$_6$-sarcophaginates (from 1.96 to 1.98 Å). For the contracted sarcophagine [Co(diMEabcapten)]$^{3+}$ cation, there is no significant difference between the Co–S bond lengths (*av* 2.21 Å) and those in the analogous regular sarcophaginate nor between the Co–N bond lengths (*av* 2.00 Å) in the "regular" arms. However, the Co–N distance in the "contracted" arm of the [Co(diMEabcapten)]$^{3+}$ cation is significantly lower (*ca* 1.93 Å), in contrast to the cobalt(III) *absar*-N$_6$ complexes, in which the Co–N distances in the "regular" and "contracted" arms are the same (*ca* 1.97 Å).

The molecules of all the apically and ribbed-carboxymethylated cobalt(III) sarcophaginates (N-protonated, neutral, and carboxy-deprotonated, and the nitrozation product) as well as their hexacoordinate 1,8-bis- and 1,3,8-tris-carboxymethylated analogs adopt the *lel*$_3$ configuration [117, 232]. The chirality of the coordination polymeric cobalt(III) 1,8-bis(carboxymethylamino)sarco-phaginate / Mn^{2+}, Mn$_2$$^{2+}$, Co^{2+}, and Zn^{2+} systems was studied by X-ray crystallography [233].

The X-ray crystallography of the sepulchrate-calyx[6]arene [Co(sep)]$_2$A ion pair showed that the unit cell consists of four cobalt(III) sepulchrate and two calixarene units with several water molecules but no counter ions [234].

As seen from X-ray data for pentanuclear Co$_2$Ag$_3$ aminoethanethiol bis-N$_3$S$_3$-azasarcophaginate [131], two approximately octahedral cobalt(III)-encapsulating units are spanned by three silver(I) atoms; each one is linearly coordinated by two sulphur atoms from two semiclathrochelate fragments. These three S–Ag–S linkages form a triple helical structure. The two cobalt(III)-encapsulating units have the same chiral configuration ($\Delta\Delta$ isomer with S configuration of all six bridging sulphur atoms and $\Lambda\Lambda$ isomer

with R configuration of the bridging sulphur atoms; the isomers coexist in the crystal form not as a racemic compound but as a solid solution). The helical structure due to the three S–Ag–S linkages is left-handed for the $\Delta\Delta$ isomer and right-handed for the $\Lambda\Lambda$ one. All the five-membered chelate cycles in this sarcophaginate possess the *lel* conformation. All six nitrogen donor atoms are also asymmetric, and their configurations are R for the $\Delta\Delta$ isomer and S for the $\Lambda\Lambda$ isomer. Thus, the overall symmetry of pentanuclear Co_2Ag_3-clathrochelate with three kinds of chiral centres besides the helical and conformational chiralities is very close to D_3 [131].

The octanuclear Co_4Zn_4 complex cation consists of four zinc(II) ions and a central μ_4-oxygen atom, which form a capping Zn_4O group, and four aza-capped cobalt(III)-encapsulating units. The latter units have the same chiral configuration to form the $\Delta\Delta\Delta\Delta$ isomer (all twelve bridging sulfur atoms are fixed in the S configuration, and twelve nitrogen atoms are all R) and its enantio $\Lambda\Lambda\Lambda\Lambda$ isomer (all twelve bridging sulphur atoms are fixed in the R configuration, and twelve nitrogen atoms are all S). Thus, only a pair of enantiomers with a T symmetry, $(\Delta)_4(S_S)(R_N)_{12}$ and $(\Lambda)_4(R_S)(S_N)_{12}$, are formed for this octanuclear tetraclathrochelate, which contains a total of 28 chiral centers. All twelve chelate rings adopt the *lel* conformation. The main M–N(S) distances and angles for both above-described polyclathrochelates are similar to that of the initial bis-semiclathrochelate $[Ag_3(Co(aet)_3)_2]^{2+}$ complex [131].

The essential information on the spatial and electronic structure of diamagnetic sarcophaginates and sepulchrates in solution has been obtained from their ^1H and ^{13}C NMR spectra. ^{13}C NMR is a more precise and more reliable instrument for investigations of such complexes due to a wide chemical shift range. The carbon atoms of the macrobicyclic framework are numbered as shown in Scheme 101.
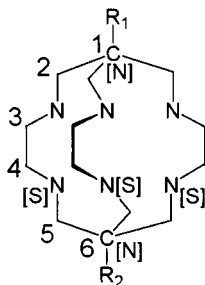
Scheme 101

First, ^{1}H and ^{13}C{^{1}H} NMR data confirmed the composition of the compounds isolated and a high symmetry (in most cases, C_3 or D_3) of clathrochelate molecules in solution. Such symmetry has not been observed for compounds that do not have this type of symmetry *a priori* (in particular, for complexes with *sar · 2NOH* or *absar* ligands). The ^{1}H NMR spectra of the latter, for example, exhibits three signals assigned to amino group protons [101].

The signals of the methylene units of capping groups in sarcophaginates and sepulchrates are easily identified in the ^{1}H NMR spectra of symmetric macrobicyclic compounds as an AB-type doublet (J_{A-B} *ca* 10–15 Hz) from 3.5 to 4.5 ppm. For systems without formal symmetry plane l, passes through the middle of the chelate C–C bonds (i.e., when the donor atoms and/or capping groups are nonequivalent), this signal is doubled (four lines).

In most cases, the signals of the ethylenediamine chelate fragment protons from 2.5 to 3.5 ppm are AA'BB'-type multiplets, and their superimposition on those of the substituents in the capping fragments is usually more complicated and less informative [96, 121, 156, 157].

According to the ^{1}H and ^{13}C{^{1}H} NMR data, practically all the cobalt(III) sepulchrates and sarcophaginates have the *lel* configuration of the chelate fragments in solution. However, attempts to determine the general molecular symmetry (D_3 or C_3) were not successful due to the dynamic $C_3 \leftrightarrows D_3$ transition that readily occurs on the NMR time scale. In such cases, the molecular symmetry is determined by the symmetry of a capping group. For complexes with C_3 symmetry, the cap has a "skewed-bath" conformation, and the cap's protons are moved relative to the secondary amino group. For complexes with D_3 symmetry, these protons are practically "frozen."

However, individual D_3 and C_3 forms were not detected either for [Co(sep)]$^{3+}$ ion in solution cooled down to 178 K or for dynamically more stable complexes with the *char* ligand. In both cases, the signal of the capping fragment methylene units was observed as an AB doublet [107].

The ^{1}H and ^{13}C NMR spectra have also been used for identification of some capping reaction intermediates and by-products. For instance, the synthesis of complexes with the *char* ligand yields in the first stage monoimine compounds whose ^{1}H NMR spectrum exhibits a characteristic set of signals in the 8÷9 ppm range [107]. In the same range, the imine group proton signal was observed in the spectrum of a macrocyclic carbanion, stabilized by coordination to the cobalt(III)

Table 5.
Parameters of the $^{13}C\{^1H\}$ NMR spectra (ppm) for some cobalt, rhodium, iridium(III), and platinum(IV) sepulchrates and sarcophaginates (relative to TMS).

Compound	Carbon atom numbering						Reference
	1	2	3	4	5	6	
[Co(en)₃]³⁺			44.8	44.8			[156]
[Co(sep)]³⁺		70.0	53.4	53.4	70.0		[156]
[Co(diNOsar)]³⁺	88.0	51.5	55.3	55.3	52.5	88.0	[156]
[Co(diAMsar)]³⁺	56.3	55.0	55.0	55.0	55.0	56.3	[156]
[Co(MEazasar)]³⁺		67.1	53.9	52.6	55.4	42.4	[96]
[Co((ZnCl₃)sar)]Cl · 2H₂O	37.1					35.7	[120]
[Co(ten)]Cl₂(ClO₄) · H₂O			44.5	41.9	39.5	42.0	[121]
[Co(azacapten)](ClO₄)₃ · 2H₂O		67.5	53.5	41.0	39.2	42.1	[121]
[Co(NOcapten)]Cl₂(ClO₄) · 1.5H₂O	87.4	55.3	52.3	40.4	38.7	42.3	[121]
[Co(AMcapten)]Cl₃ · 2.5H₂O	55.7	54.9	52.9	40.9	38.3	42.6	[121]
[Co(diMEl,3pnsar-S₆)]Cl₃	40.88	42.25	31.92	8.44	42.25	40.88	[147]
[Co(diMEsar-S₆)]³⁺	42.7	41.9	41.1	41.1	41.9	42.7	[146]
[Co(MEPYsar)]⁴⁺	43.8	54.5	56.2	56.4	56.7	50.3	[135]
[Pt(en)₃]⁴⁺			48.5	48.5			[156]
[Pt(sep)]⁴⁺		69.3	57.4	57.4	69.3		[156]
[Pt(diNOsar–H)]³⁺	96.2	54.8	59.5	59.5	54.8	96.2	[156]
[Pt(diAMsar)]⁴⁺	72.7	54.2	58.8	58.8	54.2	72.7	[156]
[Rh(sep)]Cl₃ · H₂O		68.6	54.3	54.3	68.6		[157]
[Rh(diNOsar)]Cl₃ · H₂O	91.2	57.5	56.5	56.5	57.5	91.2	[157]
[Rh(diAMHsar)]Cl₅ · 3.5H₂O	59.9	53.6	56.5	56.5	53.6	59.9	[157]
[Rh(diAMsar)]³⁺	60.2	57.4	56.4	56.4	57.4	60.2	[157]
[Ir(sep)]Cl₃ · 2H₂O		70.2	56.6	56.6	70.2		[157]
[Ir(diNOsar)]Cl₃ · 2H₂O	96.6	55.8	58.9	58.9	55.8	96.6	[157]
[Ir(diAMHsar)]Cl₅	62.5	55.4	58.9	58.9	55.4	62.5	[157]
[Ir(diAMsar)]³⁺	62.5	59.5	58.8	58.8	55.4	62.5	[157]

cation [155]. A characteristic feature in the ^1H NMR spectrum of macrotetracyclic cobalt (III) complexes is the presence of signals in an unusually low field, which correspond to the four-membered chelate rings [148].

The parameters of the $^{13}C(^1H)$ NMR spectra of some cobalt, rhodium, iridium(III), and platinum(IV) sepulchrates and sarcophaginates, as well as of some initial nonmacrocyclic complexes, are listed in Table 5.

^{13}C NMR spectra, like ^1H NMR data, confirmed the existence of a threefold symmetry axis in symmetric sarcophaginate and sepulchrate molecules, as well as the existence of only one diastereomer in solution. It has been pointed out [121] that three diastereomers are

possible for the N_3S_3-sarcophaginates. However, as seen from ^{1}H and ^{13}C{^{1}H} NMR spectra, only one form exists; therefore, amine and thioester centres exhibit their own type of configuration (the same for each of the atoms) (e.g., Co-Λ,S (thioester) – R,R,R; (N(amine) – S,S,S). Moreover, ^{13}C NMR spectra allowed all the main carbon-containing ligand moieties to be identified. The deshielding of chelate ring atoms takes place in passing from nonmacrocyclic tris-ethylenediaminates and semiclathrochelates to clathrochelate complexes whose signals are shifted downfield by 7–12 ppm (Table 5). A slight upfield shift of the signals of chelate ring carbon atoms that are directly bonded to sulphur atoms has been observed only for N_3S_3-sarcophaginates. There is also an essential influence of the apical substituent electron donation on the chemical shift of the quaternary carbon capping atom signal [121, 156]. When the substituent passes from a methyl to an amino group, this carbon atom signal shifts by ca 15 ppm, and when it passes from an amino group to a nitro group, the downfield shift is ca 30 ppm, which reflects the decrease in the substituent inductive effect and, as a consequence, the decrease of the electron density on the quaternary carbon. Passing from the quaternary carbon cap to aza cap hardly affects the chemical shift of the chelate fragments carbon signals but considerably changes the electron density on the methylene units of the capping groups (downfield shift is ca 20 ppm). Deshielding of the methylene units of both chelate rings and caps has been observed when coordinated amine centres oxidize to hydroxylamine groups and also on passing to macrotricyclic ligands, when carbon atoms bound to tertiary amine centres [108, 149, 155]. The ^{13}C NMR spectra were also used for identification of the amine and imine sarcophaginates, resulting from condensation of [Co(sen)]$^{3+}$ semisarcophaginate with acetaldehyde [140].

The ^{13}C NMR spectra of platinum(IV) and rhodium(III) sarcophaginates distinctly show ^{195}Pt–^{13}C and ^{103}Rh–^{13}C spin-spin interaction. The spin-spin interaction constants are maximal (40–50 and 3–4 Hz, respectively) for the quaternary capping carbon atoms [156, 157]. Analysis of these constants is described in Ref. 235. The discrepancies in the spin-spin interaction constants of the metal ion with the capping carbons are accounted for by the different gyromagnetic ratios for ^{195}Pt and ^{103}Rh: the relative interaction constants are practically the same. For cobalt and iridium(III) complexes, $J_{M-^{13}C}$ constants were not detected due to quadrupole broadening. The spin-spin interaction constants of the encapsulated

metal ion with carbon atoms of other types are much lower (*ca* 7–8 Hz with a ^{195}Pt nucleus, and *ca* 0.3 Hz with a ^{103}Rh nucleus for the capping fragment methylene units, and 2–3 Hz with a ^{195}Pt nucleus, and *ca* 0.3 Hz with ^{103}Rh nucleus for the ethylenediamine chelate fragments). The increase in the $J_{M\ 13C}$ value in the series CH_2(en) < CH_2 (capping) < C (quaternary) fits the Karplus relationship for heteroatom $-^{13}$C interaction constants [235].

IR spectroscopy has occasionally been used to identify and study the electronic structure of sepulchrates and sarcophaginates. Characteristic stretching vibrations at 1350 and 1560 cm^{-1} for the apical nitro groups in cobalt(III) nitrosarcophaginates and at 3050 cm^{-1} for apical protonated amino groups in cobalt(III) diaminosarcophaginate [101], as well as deformation and stretching vibrations for the coordinated amino group N–H bonds in nickel(II) sepulchrate, were also detected [160].

For cobalt(III) sepulchrate, IR and Raman spectra were examined in detail, and the basic frequencies were assigned [97]. The N–H and C–H bond stretching vibrations, observed for nonmacrocyclic $[Co(en)_3]^{3+}$ tris-ethylenediaminate at 3220, 3150, and 3095 cm^{-1} manifest themselves as a broad band at 3080 cm^{-1}, when the clathrochelate structure is formed, and a new band of the capping fragment methylene units appears at 2850 cm^{-1}. These bands may be used for identification and purity determination of the cobalt (III) sepulchrate. The Raman spectrum of the cobalt(III) sepulchrate contains a well-resolved band at 520 cm^{-1}, comparable to a vibration at 526 cm^{-1} for the $[Co(en)_3]^{3+}$ cation. The calculation performed in a normal coordinate approximation allows one to assign *ca* 84% of this band to the Co–N bond stretching vibration and *ca* 15% to the N–Co–N deformation vibration observed in this region [97]. The bands belonging to the ν(Co–N e_g) and ν(ligand e_g) vibrations are at 415 and 499 cm^{-1}, respectively. For cobalt(II) sepulchrate, only two bands at 356 and 368 cm^{-1} and no band at 520 cm^{-1} were observed, which agrees with the lower force constants for cobalt(II) cation compared with cobalt(III) cation. The force constants determined together with the other IR and Raman spectral characteristics for cobalt sepulchrates were used for molecular mechanical calculations of their conformations [97].

The UV-vis spectra of the cobalt(III) sarcophaginates and sepulchrates contain two bands of *d–d* transitions from the $^1A_{1g}$ term to the $^1T_{1g}$ and $^1T_{2g}$ terms in the UV and visible regions, which are

characteristic for low-spin octahedral cobalt (III) complexes with the electronic configuration d^6 [236]. In some cases, the spectra of the cobalt(III) sarcophaginates contain, along with d–d transition bands, a very intense band ($\varepsilon \sim 2 \times 10^4$ mol^{-1}l·cm^{-1}) in the UV region, assigned to metal→ligand CTB. As seen from Fig. 6 and Table 6, passing from the nonmacrocyclic [Co(en)$_3$]$^{3+}$ cation to its clathrochelate analogs gives rise to a sharp increase in the d–d transition band intensity, although in most cases only a slight longwave shift of these bands has been detected. A similar phenomenon was also observed when compound pass from the semiclathrochelate [Co(ten)]$^{3+}$ cation to the completely capped products [121]. A considerable (by ca 700 cm^{-1}) UV shift occurs when compound pass from complexes with the regular sar framework to ones with a contracted $absar$ ligand, which essentially increases the ligand field strength [4, 101]. This conclusion is also confirmed by the d-d transition band UV shift (by ca 1400 cm^{-1}) of these bands, when the sarcophaginate ligand changes conformation from lel_3 to ob_3 with a much smaller cavity size [5]. For macrotetracyclic complexes and macrocyclic carbanion, a considerable increase in the d–d transition band intensity is accounted for both by drastic deviation from octahedral symmetry and by the decrease in the Co–N distance [4, 148, 155].

Stepwise methylation of the apical primary amino groups of cobalt(III) diaminosarcophaginate had a marked effect on the UV-spectra in solution. A substantial UV-shift of both d–d transition bands was observed on methylation of [Co(diAMHsar)]$^{5+}$ cation to form [Co(diMe$_2$AMHsar)]$^{5+}$ cation and then [Co(diMe$_3$AMHsar)]$^{5+}$
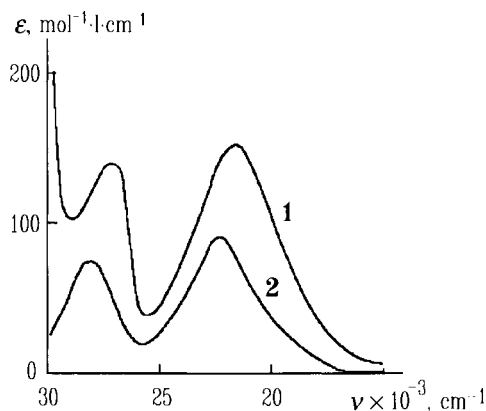
Figure 6. UV-vis spectra of the [Co(diNOsar)]Br$_3$ (**1**) and [Co(en)$_3$]Br$_3$ (**2**) complexes in aqueous solution [101].

Table 6.

Maxima ($\times 10^{-3}$, cm^{-1}) in UV-vis spectra, intensity (ε, mol^{-1}l·cm^{-1}), and spectroscopic parameters (cm^{-1}) for cobalt(III) sarcophaginates and sepulchrates in aqueous solution.

Cation	$^1A_{1g} \rightarrow {}^1T_{1g}$ (ε)	$^1A_{1g} \rightarrow {}^1T_{2g}$ (ε)	CTB ($\varepsilon \times 10^{-3}$)	Dq	B	Reference
[Co(en)$_3$]$^{3+}$	21.46(75)	29.56(68)		2349	508	[102]
[Co(diNOsar)]$^{3+}$	20.66(197)	28.74(172)	40.65(17.50)	2268	505	[108]
[Co(diNOsar · 2NOH)]$^{3+}$ (A)	20.49(212)	28.49(255)	40.00(16.80)	2249	500	[108]
[Co(diNOsar · 3NOH)]$^{3+}$(B)	20.24(254)	28.49(292)	38.91(18.89)	2230	515	[108]
[Co(diNOsar · 3NOH)]$^{3+}$(C)	20.24(285)	27.93(450)	38.91(19.50)	2216	480	[108]
[Co(diCLsar · NOH)]$^{3+}$	20.92(164)	28.88(155)	40.32(16.70)	2291	497	[108]
Λ-lel_3-[Co(diNOchar)]$^{3+}$	20.83(122)	28.65(111)	40.16(20.64)	2279	489	[107]
Λ-lel_3-[Co(NOsemichar)]$^{3+}$	21.10(110)	29.15(116)	43.47(24.24)	2311	503	[107]
Λ-lel_3-[Co(diAMchar)]$^{3+}$	20.66(144)	28.57(156)	40.82(20.36)	2264	494	[107]
[Co(ten)]$^{3+}$	20.66(574)	27.25(676)		2231	412	[121]
[Co(azacapten)]$^{3+}$	20.45(831)	26.81(965)		2204	397	[121]
[Co(NOcapten)]$^{3+}$	20.45(735)	27.17(789)		2213	420	[121]
[Co(AMcapten)]$^{3+}$	20.45(774)	27.10(848)		2211	416	[121]
[Co(diNOsar)]$^{3+}$	21.12(146)	29.12(124)		2312	500	[101]
[Co(CLNOsar)]$^{3+}$	21.10(148)	29.08(123)		2310	499	[101]
[Co(HONOsar)]$^{3+}$	21.10(148)	29.08(127)		2310	499	[101]
[Co(diCLsar)]$^{3+}$	21.12(143)	29.08(121)		2311	498	[101]
[Co(CLHOsar)]$^{3+}$	21.10(148)	29.08(127)		2310	499	[101]
[Co(diHOsar)]$^{3+}$	21.10(146)	29.07(129)		2309	498	[101]
[Co((ClME)NOabsar)]$^{3+}$	21.79(189)	29.85(179)		2381	504	[101]
[Co((ClME)HOabsar)]$^{3+}$	21.79(191)	29.81(179)		2380	501	[101]
[Co(CLsar)]$^{3+}$	21.19(137)	28.99(121)		2314	488	[101]
[Co(sar)]$^{3+}$	21.23(135)	29.15(108)		2321	495	[101]
[Co(MENOsar)]$^{3+}$	21.19(135)	29.07(117)		2316	493	[101]
[Co(AMMEsar)]$^{3+}$	21.19(139)	28.99(123)		2314	488	[101]
[Co(CLMEsar)]$^{3+}$	21.19(143)	29.07(122)		2316	493	[101]
[Co(HOMEsar)]$^{3+}$	21.19(124)	29.07(124)		2316	493	[101]
[Co((ClME)MEabsar)]$^{3+}$	21.83(164)	29.94(170)		2386	507	[101]
					599	[124]
[Co(diNOsar)]$^{3+}$	21.10(158)	28.99(131)		2307	493	[103]
[Co(sep)]$^{3+}$	21.19(109)	29.41(116)		2325	514	[96]
[Co(MEazasar)]$^{3+}$	21:28(125)	29.24(114)		2327	498	[96]
[Co(NOtetrasartame)]$^{3+}$	21.28(337)	29.24(423)		2327	498	[148]
[Co(AMsar-N$_5$S)]$^{3+}$	20.66(322)	28.33(319)		2193	562	[127]
[Co(NOsar-N$_5$S)]$^{3+}$	20.66(317)	28.25(318)		2194	555	[127]
[Co(azasar-N$_5$S)]$^{3+}$	20.45	27.50		2177	509	[127]
[Co(AMHsar-N$_5$S)]$^{4+}$	20.45	27.70		2175	526	[127]
					566	[124]

Table 6 (continued).

Cation	$^1A_{1g} \rightarrow {}^1T_{1g}$ (ε)	$^1A_{1g} \rightarrow {}^1T_{2g}$ (ε)	CTB $(\varepsilon \times 10^{-3})$	Dq	B	Reference
$[Co(NOsar-N_5S)]^{3+}$	20.45	27.70		2175	526	[127]
$[Co(CLsar-N_5S)]^{3+}$	20.45	27.70		2175	526	[127]
$[Co(sar-N_5S)]^{3+}$	20.49	27.55		2180	510	[127]
$[Co(fac\text{-}Me_5tricosansar-S_6)]^{3+}$	20.24	26.31		2158	426	[146]
$[Co(MENOsar-N_3Se_3)]^{3+}$	19.53(746)	25.77(909)	47.62(9.68) 42.74(9.40) 32.26(10.84)			[125]
$[Co(diAMsar)]^{3+}$	21.05(150)	29.15(130)	45.05, 41.67			[116]
$[Co(diAMHsar)]^{5+}$	21.05(150)	29.03(150)	43.10			[116]
$[Co(diMe_2AMsar)]^{3+}$	21.93(113)					[116]
$[Co(diMe_2AMHsar)]^{5+}$	22.03(104)		42.92(19.5)			[116]
$[Co(diMe_3AMsar)]^{5+}$	22.47(94.4)	30.40(110)	43.29(10.8)			[116]
$[Co(AMHMEsar)]^{4+}$	21.19(139)	28.99(123)			575	[116]
$[Co(Me_2AMMEsar)]^{3+}$	21.14(164)					[116]
$[Co(Me_2AMHMEsar)]^{4+}$	21.28(151)	29.41(134)	41.67(18.3)			[116]
$fac\text{-}lel_3\text{-}[Co(diAM1,2pnsar)]^{3+}$	21.10(148)	29.41 sh (178)				[116]
$fac\text{-}ob_3\text{-}[Co(diAM1,2pnsar)]^{3+}$	22.22(83)	30.30 sh (107)				[116]
$fac\text{-}lel_3\text{-}[Co(diAMH1,2pnsar)]^{5+}$	20.83(152) (calc.20.62)	28.90(135) (calc.28.98)	40.65(19.5)			[116] [237]
$fac\text{-}ob_3\text{-}[Co(diAMH1,2pnsar)]^{5+}$	22.22(81.4) (calc.21.79)	30.21(93.8) (calc.30.21)	43.29(19.3)			[116] [237]
$[Co(Me_3tricosatrienesar)]^{3+}$	19.31(150)	27.25(150)				[151]
$[Co(Me_5tricosatrienesar)]^{3+}$	21.37(107)	29.15(135)				[152]
$[Co(MEH_2NCO-7-amino-6-enesar-N_3S_3]^{3+}$	20.16(720)	27.55(815)	34.72(14) 47.62(20)			[126]
$[Co(CNMe-2-oxosar–H)]^{3+}$	20.33(233)	29.24(216)				[134]
$[Co(MECOOH-2-amino-2-enesar)]^{3+}$	20.49(233)	29.24(277)				[134]
$[Co(ME-2-amino-2-enesar)]^{3+}$	20.49(228)	29.24(208)				[134]
$[Co(diMEsar)]^{3+}$	21.05	29.10			598	[124]
$[Co(AMHMEsar-N_4S_2)]^{4+}$	20.45	27.70			530	[128]
$[Co(Mesar-N_4S_2)]^{3+}$	20.49	27.55			514	[128]
$[Co(AMHMEcapten)]^{4+}$	20.49	27.10			475	[123]
	20.46	26.96			465	[238]
$[Co(diMEcapten)]^{3+}$	20.53	27.10			471	[124]
$[Co(diMEabcapten)]^{3+}$	21.55	28.49			499	[124]
$[Co(diMEsar-S_6)]^{3+}$	20.24	26.31			432	[146]

sarcophaginate. The intensity of the lower energy d–d maximum in the latter sarcophaginate is reduced to ca 60% of the intensity of this band in the former sarcophaginate. The stepwise methylation has also resulted in inversion of the visible CD maxima of both derivatives relative to the [Co(diAMHsar)]$^{5+}$ cation of the same absolute configuration. This is caused by the conformational difference in these sarcophaginates: the N-methylated one exists mainly as the ob_3 isomer in aqueous solution and in crystal, and the initial sarcophaginates are in the lel_3 or lel_2ob conformation in solution and in the lel_3 conformation in crystal. The ob_3 cage exhibits a higher ligand field, whereas the lel_3 cage displays d–d band maxima more typical of hexamine cobalt(III) complexes. The structure of the N-methylated sarcophaginate did reveal that the symmetry of its CoN$_6$ coordination polyhedron is very close to TAP (φ ca 58°), whereas the structures of analogous lel_3 sarcophaginates show greater distortion from TAP geometry (φ ca 54°) [116].

An analysis of the ligand field strength change in passing from N$_6$- to S$_6$-sarcophaginates was performed in Ref. 170. The Dq value in passing from N$_6$- to N$_5$S-complexes becomes smaller by 40 cm^{-1}. A further passing over to S$_6$-compounds leads to a decrease in the Dq magnitude by only 30 cm^{-1}. It is evident that the properties of a thioester coordinating fragment resemble those of a saturated amine fragment. The Racah B parameter practically linearly depends on the sulphur atom number: the introduction of one sulfur atom in clathrochelate framework lowers B by 30 cm^{-1} [170].

The d–d transition bands in UV-vis spectra of the contracted cobalt(III) N$_3$S$_3$-sarcophaginate are substantially UV-shifted with respect to the regular ones; this is a consequence of a higher ligand field imposed by the former sarcophaginate. The ligand field parameters for numerous cobalt(III) N$_x$S$_{6-x}$-sarcophaginates were calculated in Ref. 124. The Δ_{O_h} value decreases by a mean 200 cm^{-1} when each amine donor group is replaced by a thioether one. This indicates a weaker ligand field of the thioether donor compared with a secondary amino group. The contraction of the N$_3$S$_3$-cage cavity also has a dramatic effect on the Δ_{O_h} value, whereas the B value is practically unaffected. The bands in the spectrum of the contracted cobalt(II) N$_3$S$_3$-sarcophaginate are also UV-shifted with respect to that of the regular one [124].

The d–d transition bands in the UV-vis spectrum of the heterocyclic amidine cobalt(III) N$_3$S$_3$-sarcophaginate are intermediate

in energy and intensity between those of amide-functionalized and triamine N_3S_3-cages. Two intense bands in the UV-region were attributed to $L\pi(S) \rightarrow Md(Co)$ CTBs [126].

The UV-vis spectra of the trinuclear aza- and nitro-capped aminoethanethiol cobalt sarcophaginates are very similar to those for the initial $[Co(Co(aet)_3)_2]^{3+}$ cation and intermediate hexaimine complex. The absorption band at $18\ 180\ cm^{-1}$ is due to the $^1A_{1g} \rightarrow {}^1T_{1g}$ d–d transition for a cobalt(III) ion in octahedral symmetry, and another one at $23\ 260\ cm^{-1}$ was observed. These broad asymmetric bands have more than one contributing component, consistent with a deviation from octahedral symmetry and with an overlap of both terminal CoN_3S_3 and central CoS_6 chromophore transitions. The UV bands for these complexes are much more intense than the visible ones and were attributed to CT from ligand (sulphur atoms) to terminal and central cobalt(III) ions. The band at $28\ 570\ cm^{-1}$ was assigned to the CT transition from the bridged sulphur to cobalt ion, because this one is not observed in the spectrum of the mononuclear complex [129].

The UV-vis spectrum of pentanuclear Co_2Ag_3 aminoethanethiol bis-N_3S_3-azasarcophaginate, like its previously described trinuclear cobalt(III) analog, is quite similar to that of initial semiclathrochelate $[Ag_3(Co(aet)_3)_2]^{3+}$ cation and contains two spin-allowed d–d transition bands in the visible region and two intense ligand (sulphur atoms) $\rightarrow$ cobalt(III) ion CT ones in UV region. Optically resolved (+)-and (–)-enantiomers of the pentanuclear bis-sarcophaginate trication mentioned were assigned to the $\Lambda\Lambda$ isomer and the $\Delta\Delta$ one, respectively, from their CD spectra. This assigment is supported by the fact that only (–)-isomer was formed when the $\Delta\Delta$-isomer of the initial bis-semiclathrochelate was used in the capping reaction. The $\Delta\Delta$-isomer has left-handed triple-helical chirality due to three S–Ag–S bridging moieties besides the three kinds of chiralities (two cobalt(III) chiral centres with the Δ-configuration, six asymmetric sulphur donor atoms with the S configuration, and six nonsymmetric nitrogen atoms with the R-configuration). The amount of the triple-helical chirality is predominate in the CD spectrum of the pentanuclear Co_2Ag_3-sarcophaginate over the whole region [131].

The UV-vis spectrum of the octanuclear aminoethanethiol Co_4Zn_4-sarcophaginate also shows two spin-allowed d–d bands in the visible region and two intense sulphur-to-cobalt CT bands in UV region. The (+)- and (–)-isomers of this complex were assigned to the $\Lambda\Lambda\Lambda\Lambda$– and

ΔΔΔΔ–configurations, respectively, from the CD spectra. The ΔΔΔΔ-isomer possesses three kinds of chiralities: four cobalt(III) chiral centres with the Δ-configuration, twelve nonsymmetric sulphur atoms with the S configuration, and twelve nonsymmetric nitrogen atoms with the R configuration. The first two kinds of chiralities were detected in the CD spectrum; the third one is relatively small. When the ΔΔ-isomer of the pentanuclear sarcophaginate was used as the initial complex, only the ΔΔΔΔ-isomer of the octanuclear sarcophaginate was formed. Thus, the former complex is converted to the latter one with retention of the chiral configuration of macrobicyclic cobalt-encapsulating units [131].

The UV-vis spectrum of nickel(II) [Ni(sep)] $(PF_6)_2$ sepulchrate in acetonitrile solution exhibits low-intensity bands at 19 600 cm^{-1} ($\varepsilon = 8.0$ mol^{-1}·l·cm^{-1}) and at 31 600 cm^{-1} ($\varepsilon = 11.2$ mol^{-1}·l·cm^{-1}), which were assigned to $^3A_{2g} \rightarrow {}^3T_{1g}(F)$ and $^3A_{2g} \rightarrow {}^3T_{1g}(P)$ type d–d transitions, respectively. These bands are UV-shifted compared with the bands at 18 500 and 30 000 cm^{-1} for the [Ni(en)$_3$]$^{2+}$ cation, which is attributed to a ligand-field strength increase due to clathrochelate structure formation [160]. The reflectance UV-vis spectrum of nickel(II) [Ni(sep)](ClO$_4$)$_2$ sepulchrate was recorded in Ref. 176. The calculated $10Dq$ value for this clathrochelate is 8400 cm^{-1}. The AOM was employed for the detailed analysis of the UV-vis spectrum of the [Ni(AMsar-N$_4$S$_2$)](ClO$_4$)$_2$·1/2H$_2$O complex [170].

A systematic study of spin-orbit mixing and nephelauxetic effects in UV-vis spectra of the series nickel(II) N$_x$S$_{6-x}$-sarcophaginates was reported in Ref. 239. The nitrogen and sulphur donor atoms exerting similar ligand-field strengths but substantially different nephelauxetic effects on these spectra and the nitrogen / sulphur donor ratio was systematically altered without substantial changes in the clathrochelate framework geometry (Table 7). The anomalous spin-allowed $^3A_{2g} \rightarrow {}^3T_{2g}$ transition band shapes were attributed to the spin-orbit induced between the E spin-orbit components of the ^2E_g and $^3T_{2g}$ states. The spin-forbidden $^3A_{2g} \rightarrow {}^1E_{1g}, {}^1A_{1g}$ transitions shifted dramatically to the longwave region with an increase in the sulphur donor atom number, which indicates a significant differential nephelauxetic effect arising from the covalence differences between the t_{2g} and e_g orbitals. These differences were successfully calculated from a differential covalence ligand field model with allowance for spin-orbit coupling effects; only three independent variables corresponding to the cubic field-splitting parameter $10Dq$ and two

Table 7.
Band assignments and ligand-field parameters (cm^{-1}) for nickel(II) sarcophaginates [239].

Compound	d–d transitions					CTB			ligand-field parameters			
	$^3A_{2g}{\rightarrow}^3T_{2g}$	$^3A_{2g}{\rightarrow}^3T_{1g}(F)$	$^3A_{2g}{\rightarrow}^3T_{1g}(P)$	$^3A_{2g}{\rightarrow}^1E_g$	$^3A_{2g}{\rightarrow}^1A_{1g}$	S→Ni	(S,N)→Ni	N→Ni	B	C	C/B	$10Dq$
[Ni(diAMsar)]$^{2+}$	12725	20360	31100	12505	not obs				826	3101	3.8	12940
[Ni(AMsar-N$_5$S)]$^{2+}$	12440	19995	30525	10890	not obs		39650	44600	816	2933	3.6	12680
[Ni(AMsar-N$_4$S$_2$)]$^{2+}$	12730	19900	30660	10485	17515		36580	45175	795	2206	2.8	12830
							38420					
[Ni(AMcapten)]$^{2+}$	12425	19180	30135	9980	16515		35555		762	2074	2.7	12640
							37380					
[Ni(diMEsar-S$_6$)]$^{2+}$	13675	19885		8365		30695			653	1660	2.5	13670

covalence parameters associated with t_{2g} and e_g orbitals were used. The relatively small reduction in one of these covalence parameters from unity was attributed to central-field covalence effects, whereas the dramatic drop in the second parameter with an increase in the sulphur donor number is a direct consequence of the increased nickel-ligand covalence associated with a thioether donor. The mentioned covalence differences also resulted in larger $10Dq$ values than those obtained from the energy of the spin-allowed $^3A_{2g}{\to}^3T_{2g}$ transition [239].

The Jahn-Teller effect for both N-methylated and initial copper(II) diaminosarcophaginates (the electronic configuration d^9 of the encapsulated metal ion, ground state ^2E_g, excited state $^2T_{2g}$) manifested itself in their vis-NIR, CD, MCD, and EPR spectra as well as in X-ray diffraction structures [173]. The results obtained were compared with data for the analogous zinc(II) complexes (electronic configuration d^{10}; the Jahn-Teller coupling is absent). Combined trigonal and tetragonal distortions of the CuN_6 coordination polyhedra arise from steric effects of encapsulating ligands and Jahn-Teller coupling, respectively. As a result, despite the symmetry of the initial N-methylated ligand, the six Cu–N bonds are not equivalent: one pair of *trans* Cu–N bonds is significantly longer than the remaining four. The molecule has lost the C_3 symmetry axis as a result of tetragonal distortion and an additional pseudotrigonal distortion ($\varphi \sim 30°$) is superimposed.

The peculiarities of the vis-NIR spectra of these copper(II) sarcophaginates are caused by strong tetragonal elongation in the CuN_6 chromophores. The near-IR bands correspond to the $^2B{\to}^2A$ transition state (splitting of the ^2E_g level, results in trigonal distortion only) of a tetragonally elongated and trigonally twisted CuN_6 chromophore in C_2 symmetry ($d_{x^2-y^2} \to d_{z^2}$ orbital jump). The visible band corresponds to transitions into three components of a exited $^2T_{2g}$ state split by the superimposed effects of tetragonal and trigonal distortions and spin-orbital coupling. Two components separated by 700–1000 cm^{-1} were identified by CD and polarized electronic spectra and confirmed by MCD spectra [173].

The UV-vis spectra of the high-spin chromium(III) sarcophaginates with the electronic configuration d^3 of the encapsulated metal ion exhibit the quartet $^4A_{2g}{\to}^2T_{1g},^2E_g$ and $^4A_{2g}{\to}^4T_{2g}$ transitions, which are different from those in the spectrum of [Cr(en)$_3$]$^{3+}$ tris-ethylenediaminate: the spin-allowed quartet-quartet

transition in the shortwave region is much more intense, and the splitting (*ca* 400 cm^{-1}) of this low-energy transition, as well as an increase in the $^4A_{2g} \rightarrow ^2E_{2g}$ doublet absorption band width, was observed for macrobicyclic complexes. The ligand field parameters for [Cr(diAMsar)]$^{3+}$ and [Cr(sar)]$^{3+}$ cations ($Dq = 2200$ and 2200 cm^{-1}, $B = 640$ and 630 cm^{-1}, $C = 3300$ and 3300 cm^{-1}, respectively) were calculated from the spectral data. The transition energies into the $^2T_{2g}$ and $^2T_{1g}$ states, calculated for sarcophaginates, are *ca* 15 000 and 23 000 cm^{-1}, respectively. The appearance of transition splitting in the longwave region may be attributed to trigonal distortion of the ligand field or to a partial superimposition of the $^4A_{2g} \rightarrow ^4T_{2g}$, $^2T_{2g}$ bands [158].

The reasons for an extremely long ^2E state lifetime (235 μs at 293 K) of expanded sarcophaginate [Cr(*fac*-Me$_5$tricosanesar)]$^{3+}$ cation are discussed in Ref. 153. The regular chromium(III) N$_6$-sarcophaginates demonstrate unusual short ^2E lifetimes (<10 ns at 298 K) in comparison with that of the [Cr(NH$_3$)$_6$]$^{3+}$ hexaammiacate (2.2 μs at 293 K). Cooling to 77 K doubles the ^2E lifetime to 440 μs, and deuteration of the secondary amino group increases it to 1.5 ms. In contrast, the ^2E state lifetime for the [Cr(sar)]$^{3+}$ cation increases by ≥10^4-fold (to 60 μs) on cooling to the same temperature [153].

The *0–0* transition for the ^2E state is accompanied by relatively intense vibrational sidelines in the expanded chromium(II) sarcophaginate spectrum, characteristic of a magnetic dipole-allowed transition. For regular [Cr(sar)]$^{3+}$ cation, this transition dominates the emission spectrum and the vibrational fine structure is poorly resolved due to more pronounced inhomogeneous broadening. This broadening is caused by the existence of [Cr(sar)]$^{3+}$ cation in different conformations from the *ob$_3$*-conformer (C_3 symmetry) through the *ob$_2$lel* and *oblel$_2$* ones to *lel$_3$*-conformer (D_3). This conformational lability is anticipated in the ^2E state, since its electronic configuration and geometry are similar to that of the ground state, and the conformational changes result in promoting of thermally activating mode [153]. In the case of expanded [Cr(*fac*-Me$_5$tricosanesar)]$^{3+}$ sarcophaginate, the conformer interconversion is more difficult: the topological constraints require that cap twisting convert the six-membered chelate cycles from the stable "chair" to the less stable "skew-boat" conformations, and the equatorial methyl substituents occupy more axial and less stable positions. The excited state complex also has the same conformation, and conformational interconversion

would not act as a promoting mode. As result, this rigidity may account for the long-lived ^2E state for expanded chromium(III) sarcophaginate [153].

The UV-vis spectra of sarcophaginates and sepulchrates of the platinum subgroup metal ions are much less informative. In most cases, the d–d transition bands have been observed as a shoulder at ca 4000 cm^{-1} to more intensive CTB. Only spectra of rhodium(III) complexes with electronic configuration d^6 of the encapsulated metal ion show the $^1A_{1g}{\rightarrow}^1T_{1g}$ and $^1A_{1g}{\rightarrow}^1T_{2g}$ d–d transition bands at 33 000 and 40 000 cm^{-1}, respectively [157].

The UV-vis spectra of the [Ru(capten)]$^{2+}$ complex contain two d–d bands at ca 34 500 (shoulder) and at 29 590 cm^{-1} ($\varepsilon = 650$ mol^{-1}l·cm^{-1}), caused by $^1A_{1g}{\rightarrow}^1T_{1g}$ and $^1A_{1g}{\rightarrow}^1T_{2g}$ ligand field transitions. The intensive ($\varepsilon = 3880$ mol^{-1}l·cm^{-1}) band at 40 000 cm^{-1} corresponds to the transition from the lone electron pair on sulphur to the d^* orbitals of the ruthenium ion (LMCT) (since the lowest unoccupied ligand $3d$ orbitals on the sulphur are very high in energy). The energies obtained for the ligand field transition and the Racah approximation $C = 4B$ were used in Ref. 229 to calculate the ligand field parameters ($Dq = 3110$ and $B = 300$ cm^{-1}). The Dq value is somewhat lower and the Δ/B ratio is higher than those of the N$_6$-systems ($Dq = 2500$ cm^{-1}, $B \approx 430$ cm^{-1}) [229].

The combination of the AOM and molecular mechanics was used in Ref. 240 for prediction and interpretation of UV-vis spectra of the transition metal sarcophaginates (Table 8).

The spectrum calculated for the C_2lel_2ob conformer of [Cr(sar)]$^{3+}$ cation is in good accordance with that experimentally found in solution, and this conformation also possessed the lowest strain-minimized energy. The C_3lel_3, C_3lel_3, and C_2lel_2ob conformers of [Ni(sar)]$^{2+}$ cation all possessed similar strain-minimized energies, and all spectra calculated corresponded with those found in solution. The range of minimized strain energies for the five stable conformations of [Co(sar)]$^{3+}$ sarcophaginate is less than 3 kJ·mol^{-1}; however, for the three most stable C_3lel_3, C_2lel_2ob and C_2ob_2lel conformers, calculated spectra are similar to the experimental ones [240].

The spin-allowed $^1A_{1g}{\rightarrow}^1T_{1g}$ transition was also found in the UV-vis spectrum of the [Ru(sar)]$^{2+}$ cation as a weak shoulder ($\varepsilon \sim 35$ mol^{-1}l·cm^{-1}) at 25 840 cm^{-1}. The d–d transition in the UV region is masked by an intense ($\varepsilon \sim 2000$ mol^{-1}l·cm^{-1}) CTB at 35 460 cm^{-1} [168].

Table 8.
Calculated and experimental transition bands (cm⁻¹) and minimized strain
energies (kJ·mol⁻¹) for [M(sar)]³⁺ complexes (underscore: degenerate state) [240]

	Cr(III)		Co(III)		Ni(II)		
D_3lel_3	23570	30950	21730	30130	12250	18830	30450
	23740	31310	21780	30180	12410	19530	30640
Strain Energy	90.61		128.17		122.48		
D_3ob_3	25440	32720	22560	30810	14050	21110	32860
	25520	33660	22690	31560	14090	22110	33790
Strain Energy	101.76		128.84		141.60		
C_3lel_3	23030	30290	21020	29200	12480	19270	30900
	23310	30910	21240	29700	12630	19740	
Strain Energy	87.13		126.81		120.73		
	21940	29190	20200	28830	12140	18540	29990
C_2lel_2ob	22420	29540	20260	29450	12200	19100	30270
	22850	30850	20670	30430	12450	19920	30830
Strain Energy	85.68		126.89		121.10		
	23790	30790	21090	29800	13020	19700	31300
C_2ob_2lel	23870	31580	21140	30600	13110	20440	31880
	24060	31920	21320	30920	13290	20740	32410
Strain Energy	91.53		126.18		129.57		
	21860				12390	19760	
Experimental		28820	21230	29150			30300
	22250				12820	20410	

The ligand field parameters for sarcophaginates allows one to realize a spin crossover by changing the temperature. These ligand field spin crossovers are easily detected by magnetic susceptibility measurements and UV-vis spectroscopy. Sargeson and coworkers studied the temperature dependence of magnetic susceptibility from 4 to 300K for d-metal complexes with the *sar, diAMHsar, diAMsar*, and *diAMHsar·2H* ligands [241, 242].

Iron, cobalt, and nickel(III) complexes are low-spin over the whole temperature range, whereas the manganese(III) complex is high-spin. All the compounds with encapsulated M²⁺ ions were characterized as high-spin ones, except the iron(II) diaminosarcophaginate, which is diamagnetic. The magnetic moments $\mu_{eff} = 4.72$BM for [Co(sep)](ZnCl₄) and 4.56BM for [Co(MEazasar)](ZnCl₄) [96] complexes; $\mu_{eff} = 3.78$BM for [Cr(sar)]³⁺, 3.74BM for [Cr(diAMsar)]³⁺ and 3.80BM for [Cr(diAMHsar)]⁵⁺ cations [158]; $\mu_{eff} = 1.8$BM for [V(diAMHsar–2H)]⁴⁺ ion [167] at room temperature practically

coincide with the magnetic moments of metal aqua ions and tris-ethylenediaminates, which characterize these clathrochelates as high-spin complexes.

The temperature-dependent spin $t_{2g}^6 \leftrightarrow t_{2g}^4 e_g^2$ equilibrium for iron(II) sarcophaginates in solution was studied by magnetic susceptibility, UV-vis, NMR, and EPR spectra. This equilibrium is strongly dependent on temperature for the [Fe(sar)]$^{2+}$, [Fe(diAMsar)]$^{2+}$, and [Fe(MEsar)]$^{2+}$ dications (Fig. 7). The μ_{eff} magnitude for the [Fe(diAMHsar)]$^{4+}$ tetracation is practically independent of temperature. The equilibrium constants were calculated from the equation:

$$K_{eq} = \frac{[t_{2g}^6]}{[t_{2g}^4 e_g^2]} = \frac{\mu_{eff}^2}{24 - \mu_{eff}^2} \tag{34}$$

In this case, the pure spin value $\mu_{eff} = 24$ for $t_{2g}^4 e_g^2$ configuration was taken into account (without allowance for the spin-orbital interaction).

Temperature dependences of lnK_{eq} (Fig. 8) for the K_{SO} constant (calculated for the $t_{2g}^4 e_g^2$ configuration without allowance for the spin-orbital interaction) and for the K_{LS} constant (calculated with
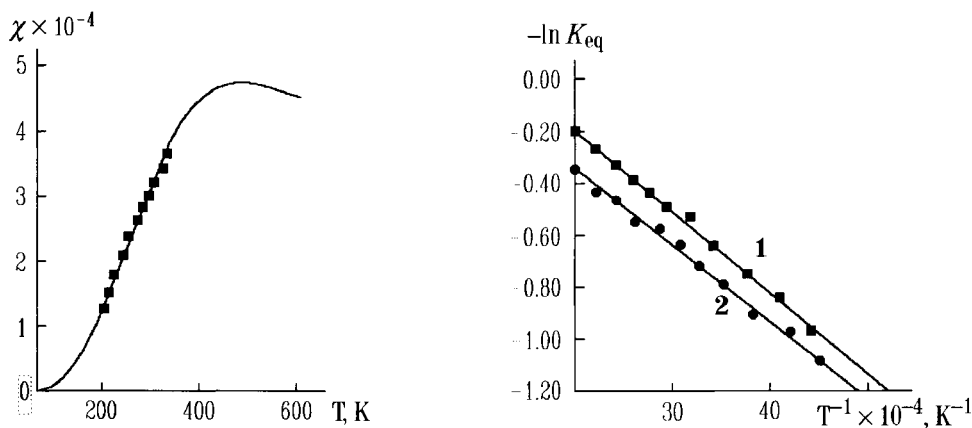
Figure 7. Calculated and experimental temperature-dependent magnetic susceptibilities for [Fe(sar)]$^{2+}$ cation in acetonitrile [243].

Figure 8. Plots of spin equilibrium *versus* temperature for [Fe(sar)](CF$_3$SO$_3$)$_2$ sarcophaginate solution in acetonitrile obtained without (1) and with (2) allowance for the spin-orbital interaction [243].

allowance for the spin-orbital interaction) enable one to obtain practically equal enthalpy ΔH values. The structural data available indicate that in solution, a high-spin complex form (the Fe–N distance ca 2.2Å and geometry intermediate between a TP and a TAP) coexists with a low-spin form (the Fe–N distance ca 2.0Å and the geometry close to a TAP). In both cases, the symmetry is lower than O_h and approaches D_3. Thus, in such a system the spin equilibrium can be regarded as a reversible transition from the ground singlet $^1A_1$ state to the ground quintet $^5A_1$ state [241-243].

On the energy scale, the high-spin $^5A_1$ state for the [Fe(sar)]$^{2+}$, [Fe(diAMsar)]$^{2+}$, and [Fe(MEsar)]$^{2+}$ sarcophaginates is higher by ca 1000 cm^{-1} than the diamagnetic $^1A_1$ one. Since for the [Fe(diAMHsar)]$^{4+}$ cation these states have very close energy characteristics (ΔH is approximately 100 cm^{-1}), the equilibrium constant is practically temperature-independent. The choice of a pure spin or a spin-orbital model affects the equilibrium constant estimation but not ΔH. The μ_{eff} value is well described by both models (Fig. 8) except the one for [Fe(diAMHsar)]$^{4+}$ tetracation, in which case the first model gives much better agreement with the experimental data [241-243].

Magnetic data for the spin $^1A_1 \leftrightarrows {}^5A_1$ equilibrium was also confirmed by UV-vis spectra. A broad low-intensity band at 11 000 cm^{-1} was found in the spectrum of the [Fe(diAMHsar)]$^{4+}$ tetracation at pH 4.5. This band describes high-spin quintet $^5T_{2g} \rightarrow {}^5E_g$ transition that splits according to the dynamic Jahn-Teller effect. Along with this band, the spectrum contains bands at 17 000 and 25 000 cm^{-1}, which are due to the $^1A_1 \rightarrow E_1, A_2$ and $^1A_1 \rightarrow E_1, A_1$ transitions in its low-spin isomer. The pH increase up to 8.5 causes deprotonation of the NH$_3^+$ groups and an increase in the low-spin form concentration [241-243].

The clathrochelate [V(diAMHsar–2H)]$^{4+}$ cation was investigated by EPR spectroscopy to obtain more detailed information on its structure in different media (such as solutions, glasses, polymeric matrix, and powder) in a wide temperature range [244]. The vanadium(IV) sarcophaginate (electronic configuration d^1 of the encapsulated metal ion) was chosen for investigation mainly because deviations of the complex symmetry may change their ground $^2A_1$ and $^2B_2$ states for a TP geometry and a TAP one, respectively. As mentioned above, the geometry of this complex approaches to a TP

(the φ angle is 18°). Studies performed in different media allow one to elucidate the factors determining this specific feature of the [V(diAMHsar–2H)]$^{4+}$ cation.

The isotropic EPR spectrum in aqueous (X-band) and methanol (Q-band) solutions contains eight superfine lines (^{51}V; $I = 7/2$; 99.76%). The anisotropic spectrum at X-band frequency is actually independent of the medium (diluted powder, methanol or aqueous frozen solutions, and polyvinyl alcohol films) and temperature (77 and 4K). The spectrum consists of two almost unresolved sets of overlapping signals. They cannot be regarded as axially symmetric tensor A_{II} and A_{I} components, but they were well described as the A_x and A_y components of the A_{I} splitting in the rhombic-symmetry field. The Hamiltonian spin parameters are consistent with the parameters obtained from the single-crystal EPR study (1% [V(diAMHsar–2H)]Cl$_4$·6H$_2$O in [Zn(AMHsar)]Cl$_4$·6H$_2$O [244] and [V(diAMH(sar–2H))](S$_2$O$_6$)$_2$·2H$_2$O [167]). Thus, EPR spectra demonstrate a great similarity of structures in the solid state and in solution, and in both cases indicate a rhombic distortion of the complex.

The Hamiltonian spin parameters ($g_x = g_y = g_z = 2.0$, $A_x > A_y > A_z$) indicate that the unpaired electron locates on the metal ion d_{z^2} orbital (the ground $^2A_1$ state in D_3 symmetry). This is the ground state for the d^1 system with a TP geometry.

The X-ray crystallography and EPR data, as well as pK$_a$ measurements, allow one to propose a structure in which the apical amino groups are protonated and the two coordinated amine sites are deprotonated [244]. The observed rhombic distortion results from structural disorder due to the presence of deprotonated groups in the framework.

The formation of platinum(III) [Pt(diAMsar)]$^{3+}$ sarcophaginate by the γ-radiolysis of [Pt(diAMsar)]X$_4$ samples (where X = Cl$^-$ or CF$_3$SO$_3^-$) was detected by EPR spectroscopy [156]. The strong split signals in the EPR spectra were observed at 4 and 77K and did not disappear even after storage of the samples at room temperature for several days. Since ^{195}Pt isotope with nuclear spin $I = 1/2$ is a dominant, the EPR spectrum must contain a triplet with the relative peak intensities equal to 1:4:1. Nearly the same spectrum ($g = 2.01$, the hyperfine interaction constant $A \sim 50$G) was observed for [Pt(diAMsar)](CF$_3$SO)$_3$ sarcophaginate. For a chloride complex, the spectrum ($g = 2.01$, $A \sim 60$G) is more diffuse, which may be due to the

outer-sphere interaction of the macrobicyclic framework with the anion [156].

The short-lived $[Pt(diAMsar)]^{3+}$ complex was detected in solution (acetone at $-80°C$ and acetonitrile at $-40°C$) during the electrochemical reduction of the corresponding platinum(IV) complex. The EPR spectrum of the complex obtained contains a weak signal with $g = 2.1$, which quickly disappears even at low temperatures. A similar experiment with sepulchrate $[Pt(sep)]^{4+}$ cation revealed the formation of a long-lived platinum(III) complex with $g = 2.22$. The lack of EPR signal anisotropy at $g \sim 2$ indicates that the platinum(III) ion arrangement approaches an octahedral one. Hyperfine coupling constants for clathrochelate platinum(III) complexes are unusually low. The value of $A \sim 800G$ is characteristic of axially and rhombic distorted platinum(III) compounds. For $[Pt(en)_3]^{3+}$ tris-ethylenediaminate, a spectrum with $g = 2.3$ and $A \sim 200G$ was obtained in the frozen aqueous solution after γ-radiolysis. The low hyperfine coupling for $[Pt(diAMsar)]^{3+}$ sarcophaginate is due to certain electron delocalization on macrobicyclic ligand donor nitrogen atoms.

The static and dynamic Janh-Teller effects in copper(II) $[Cu(diAMHsar)](NO_3)_4 \cdot H_2O$ sarcophaginate and the dynamic one in analogous iron(II) complex were detected by variable temperature EPR, optical, and magnetic studies, and by ^{57}Fe Mössbauer spectroscopy, respectively [245, 246], and calculated using a density functional approach [247].

3.2 MACROBICYCLIC PHOSPHORUS-CONTAINING
d-METAL TRIS-DIIMINATES

X-ray diffraction studies were performed for all the complexes of this type [248-251] to gain unambiguous information on the structure of phosphorus-containing d-metal clathrochelates. A detailed analysis of the geometry of macrobicyclic phosphorus-containing d-metal tris-diiminates and a number of d-metal complexes with nonmacrocyclic hexadentate ligands, shown in Fig. 9, was reported in Ref. 93. Some structural parameters of these complexes with geometry intermediate between a TP and a TAP are listed in Table 9.

In the complexes with a certain metal ion, the tendency of the ligand to acquire a TP geometry decreases in the order

$$Pcc(BF) > (Py)_3tach > (Py)_3tame > (Py)_3tren$$

[MPcc(BF)]⁺   [M(XPy)₃tacn]²⁺   [M(XPy)₃tame]²⁺   [M(XPy)₃tren]²⁺

[M(P(Mepox)₃)]²⁺   [M(P(bpy)₃)]²⁺   [M(P(Py)₃)₂]²⁺
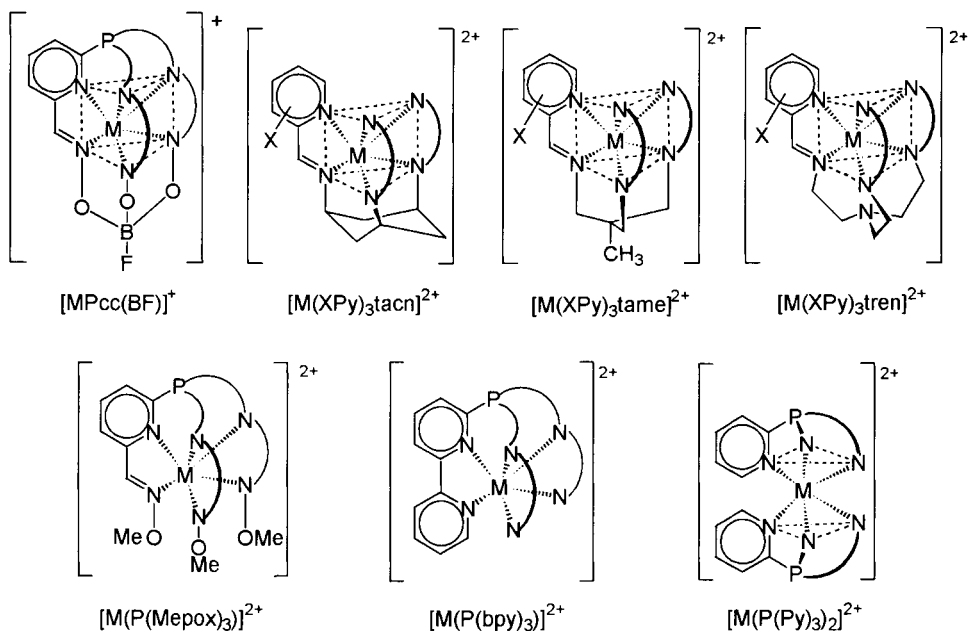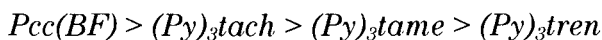
Figure 9. Schematic structures of some N_6-complexes with geometry intermediate between a TP and a TAP (M = Fe, Co, Ni and Zn(II)) [93].

Table 9.
Distortion angle φ of the coordination polyhedra in d-metal tris-diiminates [93].

Compound	Distortion angle φ, deg	Reference
[FePcc(BF)](BF₄)	21; 22; 22	[248]
[CoPcc(BF)](BF₄)	0.4; 1.0; 3.2	[249]
[NiPcc(BF)](BF₄)	1.1; 1.8; 1.8	[250]
[ZnPcc(BF)](BF₄)	1.1; 2.3; 2.3	[251]
[Ni(Py)₃tacn](ClO₄)₂	30; 33; 34	[252]
[Zn(Py)₃tacn](ClO₄)₂	2.0; 5.0; 6.6	[253]
[Fe(Py)₃tame](ClO₄)₂	39; 45; 45	[254]
[Zn(Py)₃tame](ClO₄)₂	28	[255]
[Fe(Py)₃tren](BF₄)₂	54	[256]
[Co(Py)₃tren]²⁺	49	[93]
[Ni(Py)₃tren](PF₆)₂	51	[93]
[Zn(Py)₃tren]²⁺	46	[93]

In the series of metal ions with the same ligand, this relationship is as follows:

$$Zn(II) > Co(II) > Ni(II) > Fe(II)$$
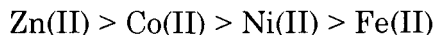
It is evident that clathrochelate *Pcc(BF)* ligand compounds and their nonmacrocyclic analogues differ markedly in structure. Zinc, cobalt, and nickel(II) complexes have a TP geometry with a small distortion angle ($\varphi < 2$) owing to their rigid macrobicyclic structure. Only for iron(II) complex the φ angle value is relatively high ($\varphi = 22°$). Potentially stable configurations for sterically unhindered chelate complexes ensuring the most favorable *d*-electron energy were investigated by AOM [93]. This model enables *d*-orbital energies to be calculated as a function of bite α and distortion φ angles. Plots of one-electron *d*-orbital energies *versus* the φ angle at a constant bite angle $\alpha = 38.5°$ that is typical of complexes **1-4** are shown in Fig. 10.

The energy levels have the order $a_1 < e_1 < e_2$ for TP geometry and $e_1 < a_1 < e_2$ for TAP complexes. These orders remain unchanged with allowance for the insignificant contribution of π-bonding, which can exert a stabilizing or destabilizing effect [93]. The optimal geometry for a given metal *d*-orbital can be determined from a plot of the sum of one-electron *d*-orbital energies *versus* φ at a constant α value. These plots for low-spin d^6 and d^8 configurations are shown in Fig. 11. The φ values from 48 to 56° are optimal at $\alpha = 45°$, which is
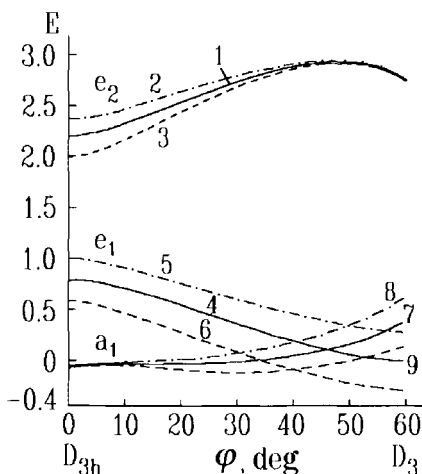
Figure 10. Plots of the one-electron *d*-orbital energies *versus* distortion angle φ values with allowance for π-bonding at $e_\pi = 0$ (**1**, **4**, and **7**), $e_\pi = +0.1$ (**2**, **3**, and **8**), $e_\pi = -0.1$ (**3**, **6**, and **9**) at $\alpha = 38.5°$ [93].
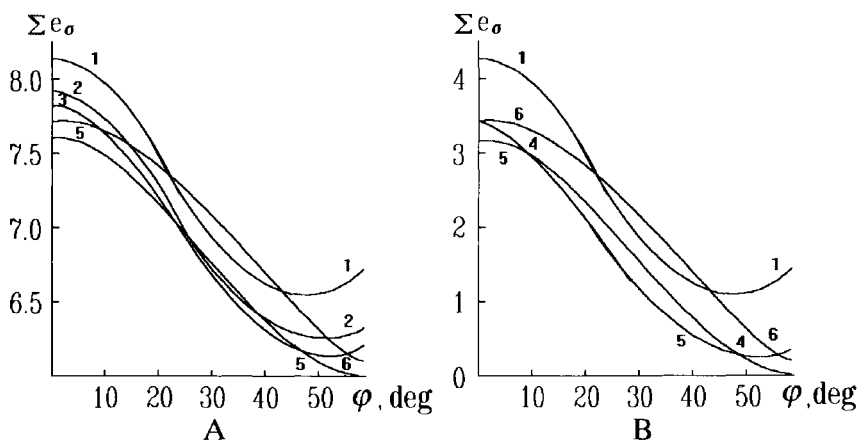
Figure 11. Sums of one-electron d-orbital energies for d^8(A) and low-spin d^6(B) complexes with various bite angles α depending on the distortion angles φ: (1) 35°, (2) 38.5°, (3) 40°, (4) 41.5°, (5) 45°, and (6) 48.5° [93].

characteristic of the complexes shown in Fig. 9. Such values were observed for most of the nonmacrocyclic complexes listed in Table 8.

The deviations of the experimental φ angles from calculated ones in the remaining (mostly clathrochelate) complexes are partly accounted for by the difference in destabilization energies for complexes with a TP geometry and a TAP one. A plot of this difference *versus* the electronic configuration is shown in Fig. 12. It is maximal for high-spin complexes with the d^3 and d^8 configurations and for low-spin complexes with the d^6 configuration, which agrees with the experimental data: the maximal structure distortion toward TAP compared with other metal ion complexes with the same ligand is observed for low-spin iron (II) complexes with electronic configuration d^6 [93].

Moreover, the geometry of the complexes is greatly affected by the physical (Shannon) ionic radius of the encapsulated metal ion: in a series of compounds with the same ligand, a decrease in the ionic radius leads to an increase in the φ angle. Thus, the superimposition of both main factors affecting the geometry of clathrochelates of this type (stabilization of the d-electronic configuration and the metal ion size) leads to a practically undistorted TP geometry for cobalt, nickel, and zinc(II) complexes and to an essentially TAP distorted one for macrobicyclic phosphorus-containing iron(II) tris-diiminate [93].
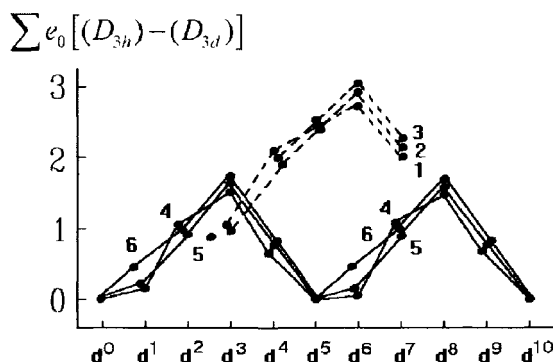
Figure 12. Differences in destabilization energies for the low- (1-3) and high-spin (4-6) tris-complexes with TP and TAP geometries at $\alpha = 35°$ [1 and 4], 38.5° [2 and 5], 45° [3 and 6] as a function of the d-electron number. The π-bonding effect is not taken into account [93].

An octahedral or TAP geometry cannot be distinguished from a TP one in low-spin iron(II) complexes by UV-vis and NMR spectra as well as by magnetic susceptibility, and a ^{57}Fe Mössbauer spectroscopic study was performed [257] for macrobicyclic phosphorus-containing iron tris-diiminate (the decrease of the φ angle value from 60° [TAP] to 0° [TP] causes an increase in the quadrupole splitting, which characterizes the electric field gradient on the iron atom nucleus, from ca 0 to 1 mm·s⁻¹). The QS sign was also determined for some complexes with extremal φ angle values using transverse magnetic fields: for the [Fe(phen)$_3$](C$_2$O$_4$) and [FePcc(BF)]⁺ complexes (φ is 56 and 22°, respectively), the QS value is −0.29 and +0.95 mm·s⁻¹, respectively.

In the case of coordination compounds, the EFG may be represented as the sum of three amounts:

$$q = q_{latt} + q_{MO} + q_{lig} \qquad (35)$$

where the first amount q_{latt}, responsible for the crystal lattice charge contribution, may be neglected because of the large size of the macrobicyclic ion (this contribution to EFG is inversely proportional to the cube of the distance). The q_{MO} amount is associated with unequal electron occupancy of different MO of the same level. For low-spin iron(II) ion in their tris-complexes, all such MO are either vacant or occupied, i.e., $q_{MO} = 0$. It follows that the main contribution to the EFG is made by the ligand amount q_{lig} due to the symmetry of occupation of iron atom orbitals, responsible for their different

interaction with ligands *via* σ- and π-bonds. In the case of the close-to-TAP geometry of the iron(II) coordination polyhedron, the valence contribution to the QS value is equal to zero for the spin-paired t_{2g}-configuration. To the contrary, with TP geometry, the valence contribution is substantially different from zero and the splitting has a positive sign.

The nonzero splitting observed for the TAP compound is usually small and is due to covalence anisotropy. In the case of tris-diiminates, the elongation or contraction along the threefold axis results in the different covalent bonding at the t_{2g} orbitals. The negative QSs for [Fe(phen)₃]²⁺ (–0.29), [Fe(bipy)₃]²⁺ (–0.39) and [Fe(Py)₃tren]²⁺ (–0.38 mm·s⁻¹) cations are caused by higher electron density on the t_{2g}^0 orbital than on the $t_{2g}^{\pm}$ ones. The QS value is determined by superimposition of the positive valence and negative covalence contributions [257].

Magnetochemical measurements for the solid phosphorus-containing zinc, iron, nickel, and cobalt tris-diiminates showed that the first two are diamagnetic and low-spin complexes. The cobalt and nickel(II) complexes proved to be high-spin clathrochelates with magnetic moments of 4.91BM ($S = 3/2$) and 3.11BM ($S = 1$), respectively [92, 93].

The IR spectra of macrobicyclic cobalt, nickel, and zinc(II) complexes of this type are practically identical. Besides the bands characteristics of B–F bond stretching vibrations (519 and *ca* 960 cm⁻¹), they contain bands that were assigned to B–O (820 and 1180 cm⁻¹) and N–O (1110 and 1230 cm⁻¹) stretching vibrations. However, the C=N bond stretching vibrations at 1600 cm⁻¹ were not identified like those in the initial semiclathrochelate complexes. The spectra also showed distinct stretching and deformation vibrations of the pyridine ring. It is presumably these vibrations that mask C=N stretching vibrations since they are observed in the same spectral region. The IR spectrum of the [FePcc(BF)](BF₄) complex is substantially different from those of the other *d*-metal clathrochelates in the ranges 1400–1600 and 400–800 cm⁻¹, which confirmed that its structure does not resemble those of other complexes [92].

The UV-vis spectra of phosphorus-containing cobalt(II) and nickel(II) diiminates were obtained both in solution and in the solid state (the [CoPcc(BF)](BF₄) and [NiPcc(BF)](BF₄) complexes were diluted in the monocrystal of zinc clathrochelate). Pure crystals of

these three complexes are isomorphous and contain four clathrochelate cations in the monoclinic unit, which are oriented such that their threefold C_3 pseudoaxes are parallel. The axial and perpendicular spectra obtained indicate that absorption at 8000–12 000 cm^{-1} for the nickel(II) complex is polarized perpendicular to the threefold pseudoaxis. The other bands in the UV-vis spectrum of the nickel clathrochelate and a band at 8100 cm^{-1} in the spectrum for its cobalt analogue are not polarized. Energy level diagrams [93] for complexes with D_{3h} symmetry (electronic configurations d^7 and d^8 if the metal ion), shown in Fig. 13, enabled the assignment of some CTBs in the UV-vis spectra.

The bands at 9380 and 11 000 cm^{-1} in the spectrum of a [NiPcc(BF)](BF$_4$) single crystal are polarized perpendicular to the C_3 pseudoaxis, which corresponds to the $^3A_2' \rightarrow {}^3E'; {}^1E'$ transitions. The resolution of these bands indicates that the spin-forbidden transition is of greater energy than the spin-allowed one. The spin-allowed transition is responsible for an increase in the intensity of the spin-forbidden transition. The nonpolarized shoulder at ca 20 500 cm^{-1} was assigned to the forbidden $^3A_2' \rightarrow {}^3E''$ and/or $^3A_2'$ transitions. The bands of the transitions to the $^3A_1''$, $^3A_2''$, and $^3E''$ states occur below 4000 cm^{-1} and therefore were not localized [93].

The UV-vis spectrum of the [CoPcc(BF)](BF$_4$) complex in the near-IR and visible regions contained four bands. Two of them, observed at
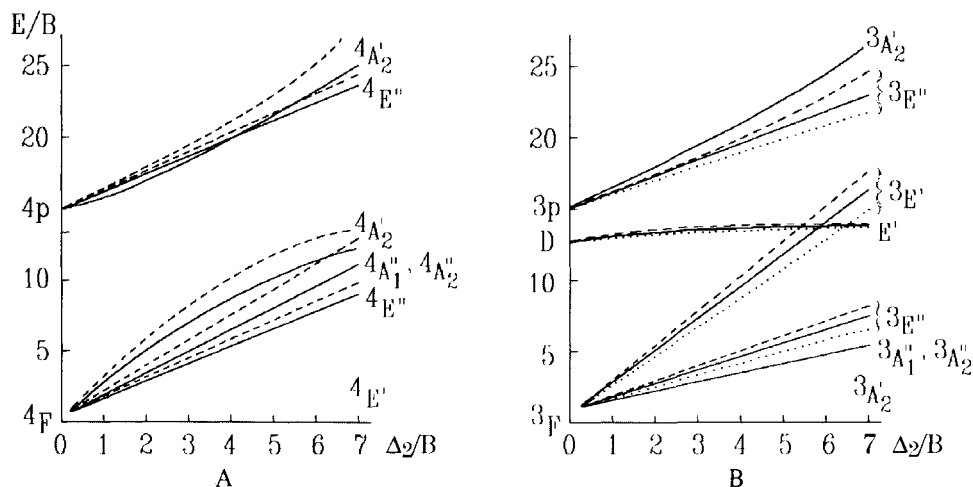
Figure 13. Energy level diagrams for d^7 (high-spin) (A) and d^8 (B) electronic configurations in D_{3h} symmetry for C/B = 4.0 and Δ_1/Δ_2 = 0.4 (dotted line), Δ_1/Δ_2 = 0.6 (solid line); 0.8 (dashed line) [93].

11 800 and 14 250 cm^{-1}, corresponded to the clathrochelate cobalt(I) complex in trace amounts, and this was confirmed by electrochemical reduction. The bands at 8130 and 22 000 cm^{-1} are caused by transitions in two quartet states (Fig. 13).

The ^{19}F NMR spectra of [MPcc(BF)](BF$_4$) complexes in solution exhibited two signals with 1:4 intensity ratio corresponding to the capping BO$_3$F fragment and the BF$_4^-$ counter-ion. It is interesting to note that the spin-spin ^{11}B–^{19}F interaction constants in the capping fragment are 12 and 13 Hz in the case of diamagnetic zinc and iron(II) complexes [92]. These constants coincide with those obtained for fluoroboron-capped macrobicyclic iron(II) dioximates (see Section 3.3) and suggest a high symmetry of the tetrahedral BO$_3$F fragment.

The ^{1}H NMR spectra of the diamagnetic [FePcc(BF)](BF$_4$) and [ZnPcc(BF)](BF$_4$) complexes along with multiplet signals from the aromatic ring from 8 to 8.85 ppm contain singlet signals at 9.33 and 8.31 ppm, respectively, of the H–C=N moiety methine protons, which confirmed the equivalence of the macrobicyclic ligand diimine fragments [93].

3.3 MACROBICYCLIC d-METAL TRIS-DIOXIMATES

3.3.1 Cobalt complexes

Measurements of the magnetic moments of macrobicyclic cobalt(III) and cobalt(II) tris-dioximates showed that cobalt(III) compounds are diamagnetic and the magnetic moments for the CoDm$_3$(BF)$_2$ and [CoDm$_3$(SiO)$_2$]·HPF$_6$ compounds are 2.12 and 2.28BM, respectively [39]. This is indicative of their low-spin nature: the bonding t_{2g} level is completely occupied in the high field of the macrobicyclic tris-dioxime ligands. For cobalt(III) with electronic configuration d^6, this leads to the fully occupation of three bonding t_{2g} orbitals (the resultant spin S = 0), whereas for cobalt(II) ion with electronic configuration d^7, it leads to one unpaired electron on the e_g orbitals (the resultant spin S = 1/2). The clathrochelate tris-dioxime ligands have a higher field strength than their phosphorus-containing tris-diimine analogs (see Section 3.2).

An X-ray diffraction study for the [CoDm$_3$(BF)$_2$](BF$_4$) and CoDm$_3$(BF)$_2$ clathrochelates was performed by Lingafelter and coworkers [258]. The φ angle values for these complexes are 31.2 and 8.6°, respectively. Both clathrochelates have D_3 symmetry and the

Co–N distance that is characteristic of low-spin cobalt(II) and cobalt(III) complexes. But the difference in Co–N distance (0.08 Å) for these clathrochelates is twice as large as normal for a cobalt(II)/(III) pair with a given nonmacrocyclic ligand.

The change in the clathrochelate ligand geometry in passing from a cobalt(III) complex to a cobalt(II) one can be understood in terms of matching the ligand cavity and metal ion size. A larger cobalt(II) ion increases the clathrochelate ligand cavity by rotation about the symmetry C_3 pseudoaxis toward a pure TP structure in combination with the translational motion of N_3-bases.

X-ray diffraction data were also obtained for a series of clathrochelate tin-capped cobalt(III) complexes (Table 10).

As seen from Table 10, even the $[CoDm_3(BF)_2](BF_4)$ complex that was the least distorted from TP has an appreciably higher degree of distortion than boron-capped iron(II) analogs (see below). The distortion angle φ values in tin-capped cobalt(III) tris-dioximates (ca 40÷42°) are greater than those observed for boron-capped cobalt(III) complexes and the clathrochelate $[FeNx_3(SnCl_3)_2]^{2-}$ anion ($\varphi = 37.5°$). These differences are caused by the change in the physical ionic (Shannon) radius in passing from a low-spin Fe^{2+} ion (0.75 Å) to a low-spin Co^{3+} ion (0.69 Å) and an increase in the size of a capping group in passing from a boron- to a tin-capped complexes. In these cases, the metal-nitrogen bond lengths remain practically unchanged (ca 1.91 Å), but the distances between the coordination polyhedron bases substantially decrease (Table 10). Thus, the structures that resembles TAP (octahedron), optimal for d^6 configuration, are realized in tin-capped cobalt(III) tris-dioximates.

The IR spectra of macrobicyclic cobalt tris-dioximes confirmed their clathrochelate nature and contained characteristic bands of

Table 10.
The main structural characteristics of the macrobicyclic cobalt(III) tris-dioximates.

Compound	a, Å	h, Å	a, deg	φ, deg	Reference
$[CoDm_3(BF)_2](BF_4)$	1.89	2.29	40.0	31.2	[258]
$CoDm_3(BF)_2$	1.97	2.43	38.3	8.6	[258]
$CoNx_3(Bn-C_4H_9)_2$	1.94	2.36	37.5	5.7	[259]
$H[CoDm_3(SnCl_3)_2] \cdot 2C_6H_6$	1.90	2.18	40.2	42.3	[45]
$((n-C_4H_9)_4N) [CoNx_3(SnCl_3)_2]$	1.91	2.24	40.5	41.0	[260]
$((n-C_4H_9)_4N) [CoNx_3(SnBr_3)_2]$	1.89	2.20	40.7	39.9	[44]
$((n-C_4H_9)_4N)[CoDm_3(SnBr_3)_2]$	1.89	2.18	41.0	45.1	[260]

dioxime fragments (N–O bond stretching vibrations at 1100 and 1250 cm^{-1}, and C=N bond stretching vibrations at 1600 cm^{-1}) and capping groups. With boron-capped compounds, characteristic vibrations of tetrahedral capping fragments (B–F and B–O bond stretching vibrations at 1000 and 1200 cm^{-1}, respectively, and O–B–O deformation vibrations near 800 cm^{-1}) were observed.

The singlet nature of most bands in the IR spectra of cobalt complexes confirmed the C_3 symmetry of their molecules. The C=N stretching vibration bands were appreciably shifted and intensified compared with those of the initial dioximes. Only one band of this type was observed for cobalt(III) complexes, and its position and intensity were more affected than those of cobalt(II) clathrochelates.

With acyclic dioximes, N–O stretching vibrations undergo still greater changes (*ca* 100 cm^{-1}) presumably due to a conformational change in the dioximate fragment, exhibiting a *trans* conformation in the free dioxime and a *cis* one in the complex. The frequencies of the corresponding vibrations in the spectrum of nioxime, which exists only in a *cis* form, were only slightly (5÷10 cm^{-1}) affected by complexation [42].

The UV-vis spectra of the CoNx$_3$(BR)$_2$ and CoDm$_3$(BR)$_2$ complexes contain two high-intensity bands ($\varepsilon \sim 5 \times 10^3$ mol^{-1}·l·cm^{-1}) assigned to CTB. In the CoBd$_3$(BF)$_2$ complex, only a longwave band is resolved; the shortwave band was observed as a shoulder. The position of the CTBs of cobalt(II) and cobalt(III) complexes correlated with that of the π–π^* transition bands in the initial dioxime and with that of the CTBs in analogous iron(II) clathrochelates [42].

An analysis of a second-order derivatives of the UV-vis spectra for cobalt(III) complexes allowed the resolution of the bands assigned to the *d–d* transitions $^1A_{1g} \rightarrow {}^1T_{1g}$ and $^1A_{1g} \rightarrow {}^1T_{2g}$. The calculated ligand field parameters (for [CoNx$_3$(BF)$_2$](BF$_4$) clathrochelate: $Dq = 2240$ cm^{-1}; $B = 600$ cm^{-1}; for [CoDm$_3$(BF)$_2$](BF$_4$) clathrochelate: $Dq = 2250$ cm^{-1}, $B = 420$ cm^{-1}) are characteristic of low-spin cobalt(III) complexes with macrocyclic polyamines [10].

The spectra of clathrochelate cobalt(III) tris-dioximates obtained by cross-linking with chromium, nickel, and zinc(II) complexes, alongside the bands assigned to the π–π^* transitions in dioximate fragments, contained the *d–d* transition bands from the capping metal ions that masks the corresponding transitions for the central Co^{3+} ion [46].

The NMR spectra were recorded only for diamagnetic cobalt(III) complexes (Table 11). Integral intensities of the signals from cross-linking BO_3F group and those from the BF_4^- counter-ion in the ^{19}F NMR spectra for boron-capped complexes are in a 1:2 ratio, thus confirming the formula proposed [2].

The ^1H NMR spectra of macrobicyclic cobalt(III) dimethylgly-oximates and nioximates indicate that the increases in chemical shifts of protons on complexation is essentially greater (0.3÷0.5 ppm) than those for the corresponding iron dioximates (0.2÷0.4 ppm). A similar effect was also detected in ^{11}B NMR spectra: in iron complexes the degree of shielding of the capping boron atom nucleus was higher than that in analogous cobalt complexes. Neither the substituent displacement in dioxime nor the complexation process affected the position of a signal from the BF_4^- counter-ion in the ^{11}B NMR spectra [42].

Multinuclear NMR spectroscopy makes it possible to obtain data on electron density distribution in clathrochelate molecules and their structure. The resonance on the ^{59}Co nucleus provides information on the spatial and electronic structure of the coordination polyhedron of an encapsulated cobalt(III) ions. A dominant contribution to the chemical shift $\delta_{59_{Co}}$ is made by the paramagnetic component B_0, which is linearly determined by d–d transition energy: $B_0 = -32\beta^2/\Delta \cdot r^{-3}$, where $\Delta = E(^1A_1) - E(^1T_1)$ is the difference between the energies of the ground and excited Co^{3+} ion states, respectively. Thus, for complexes of the same type, the chemical shift value reflects the ligand field strength. As seen from Table 12, the $\delta_{59_{Co}}$ values are minimal for trichlorotin-capped clathrochelate complexes, somewhat higher for boron-capped compounds, and are shifted downfield for nonmacrocyclic complexes. This indicates that ligand field strength increases from nonmacrocyclic to boron-capped and further to tin-capped ligands ("macrocyclic" effect), leading to an increase in electron density on the ^{59}Co nucleus. A decrease Δ in the case of tribromotin-capped complexes must lead to an increase in $\delta_{59_{Co}}$, and this effect was observed experimentally: in comparison with $[CoD_3(SnCl_3)_2]^-$ anions, the signals in the ^{59}Co NMR spectra of tribromotin-capped clathrochelates are downfield shifted by about 2700 ppm (Table 12).

In the case of nonsymmetric methylglyoxime, the spectrum exhibits two lines of different intensity that correspond to the *mer-*

Table 11.

The main parameters of IR , UV-vis (ν_{max}, cm^{-1}; ε, mol^{-1}·l·cm^{-1}), and NMR (ppm) spectra of the boron-capped cobalt tris-dioximates [42].

Compound	Infrared			UV-vis		NMR				
						^{1}H	^{13}C		^{11}B	
						relative to TMS			relative to NaB(C$_6$H$_5$)$_4$	
	ν(C=N)	ν(N–O)	ν(B–O)	$\nu_{max}\times10^{-3}$	$\varepsilon\times10^{-3}$	R	R	C=N	B–F	BF$_4^-$
[CoDm$_3$(BF)$_2$](BF$_4$)	1624	1107	819	34.0	10.1	2.51	15.71	167.25	11.08	5.30
		1256	1210	^{a} 30.2	0.5					
				^{a} 19.8	0.5					
CoDm$_3$(BF)$_2$	1600	1099	818	28.5	5.92					
	1632	1230	1197	21.6	5.25					
[CoBd$_3$(BF)$_2$](BF$_4$)	1592	1080	840	30.0	25.5	7.35			10.72	5.34
		1231	1195	^{a} 27.3	0.5	7.42				
				21.7	0.5	7.54				
CoBd$_3$(BF)$_2$	1585	1062	840	25.7	5.0					
	1600	1228	1205	20.3	4.91					
[CoNx$_3$(BF)$_2$](BF$_4$)	1632	1035	815	33.5	10.1	1.83	21.49	166.65	11.04	5.32
		1245	1210	29.6	0.5	3.03	29.40			
				19.8	0.5					
CoNx$_3$(BF)$_2$	1595	1080	810	28.0	6.15					
	1630	1250	1190	21.4	5.78					

^{a} This band manifests itself in the spectrum of a second derivative.

and *fac*-isomers of (HDEA)[CoMm₃(SnHal₃)₂] clathrochelate. The most intense line corresponds to the *mer*-isomer, the probability of whose formation is much higher (without allowance for thermodynamic factors). The presence of these isomers manifests itself in the NMR spectra on other nuclei too (see below).

The signal in the ^{119}Sn NMR spectra of the tribromotin-capped complexes is upfield shifted by 350 ppm. This indicates an increase in the ligand field strength about the tin atom: replacement of one chlorine atom by a bromine atom usually results in an upfield shift about 120 ppm [44]. It is evident that replacement of three chlorine atoms by three bromine atoms should cause a 360-ppm upfield shift, and this is in good agreement with the result observed. The capping tin atoms in cobalt(III) complexes are much more deshielded than those in the iron(II) complexes, leading to a downfield shift of the signals by 30 ppm. The chemical shift on the ^{119}Sn nucleus, which is also determined mainly by paramagnetic contributions, does not, however, reflect the *s*-electron density on a tin atom nucleus, which is much higher for [CoD₃(SnBr₃)₂]⁻ anions than that for their trichlorotin-capped analogs. This leads to a significant increase in IS value in ^{119}Sn Mössbauer spectra (Table 12). The increase in the capping tin atom charge leads to the ligand field strength decrease.

The UV-vis spectra of these complexes contain three intense absorption bands. The most intense ($\varepsilon \sim 5{\times}10^4$ mol⁻¹·l·cm⁻¹) one is from intramolecular $\pi{-}\pi^*$ transitions in the range 40 000–42 000 cm⁻¹, and the two less intensive ones are from M*d*→Lπ^* CTBs (the first band with an intensity approximately $1{\times}10^4$ mol⁻¹·l·cm⁻¹ in the range 36 000–38 000 cm⁻¹ and the second one with an intensity approximately $4{\times}10^4$ mol⁻¹·l·cm⁻¹ in the range 28 500–29 500 cm⁻¹). These bands mask the low-intensity *d–d* transitions, and they are found in the second-order derivatives of the spectra (Table 13). The ligand field parameters were calculated using equations for cobalt (III) compounds with pseudooctahedral coordination [10]:

$$v_1 = E(^1A_{1g} - {}^1T_{1g}) = 10Dq - C \qquad (36)$$
$$v_2 = E(^1A_{1g} - {}^1T_{2g}) = 10Dq - C + 16B \qquad (37)$$

In such cases it is usually assumed that C = 4B, and the ligand field parameters can be calculated as follows:

$$Dq = (3v_1 + v_2)/40 \qquad (38)$$
$$B = (v_2 - v_1)/16 \qquad (39)$$

Table 12.
Parameters of NMR (ppm) and ^{119}Sn Mössbauer (mm·s^{-1}) spectra of the tin-capped cobalt(III) clathrochelates and their analogs [44, 45].

Compound	^{1}H relative to TMS		^{13}C relative to TMS			^{119}Sn relative to Sn(CH$_3$)$_4$	^{59}Co relative to K$_3$[Co(CN)$_6$] ($v_{1/2}$, Hz)	^{119}Sn Mossbauer IS
	H–C=NO	R	H–C=NO	R–C=NO	R			
(HDEA) [CoGm$_3$(SnCl$_3$)$_2$]	7.86		149.06			−595.7	4603 (519)	0.48
(HDEA)[CoMm$_3$(SnCl$_3$)$_2$]	7.88m	2.45,	151.21,	160.26,	13.35	−594.3,	4662 (100)	0.44
		2.47,	151.30,	160.45,	13.40	−599.0,	4687 (700)	
		2.59	151.78,	161.06,	13.65	−601.5		
			152.01	161.16				
H[CoDm$_3$(SnCl$_3$)$_2$]		2.45		161.81	13.05	−608.4	4684 (370)	0.46
(HDEA)[CoDm$_3$(SnCl$_3$)$_2$]		2.44		161.90	13.25	−609.2		0.48
H[CoNx$_3$(SnCl$_3$)$_2$]		1.72		161.72	20.14	−607.8	4741 (946)	0.44
		3.02			26.50			
(HDEA)[CoBd$_3$(SnCl$_3$)$_2$]		7.32		161.19	127.33	−538.4		0.40
					128.46			
					129.16			
					130.50			
(HDEA)[CoGm$_3$(SnBr$_3$)$_2$]	7.83		148.63			−969	7209 (950)	0.62
(HDEA)[CoMm$_3$(SnBr$_3$)$_2$]	7.87,	2.51,	151.08,	159.91,	13.78,	−996,	7243 (1530),	0.68
·(CH$_3$)$_2$CO	8.02	2.53,	151.27,	160.09,	13.91,	−984,	7299 (1190)	
		2.71	151.83	160.95	13.29	−975,		
			152.04	161.10		−965		

(HDEA) [CoDm$_3$(SnBr$_3$)$_2$]	2.42		161.68	13.79	−995	7313 (550)	
H[CoNx$_3$(SnBr$_3$)$_2$]	1.77m, 3.09m		161.33	20.22, 26.71	−1011	7365 (1380)	0.62
(HDEA) [CoNx$_3$(SnBr$_3$)$_2$]	1.74m, 3.13m		161.33	20.23, 26.72	−998	7361 (1400)	
H[CoBd$_3$(SnBr$_3$)$_2$]	7.32, 7.34, 7.46		161.12	121.61m, 128.98, 129.48, 129.83	−1013	7232 (610)	
(HDEA)[CoBd$_3$(SnBr$_3$)$_2$]	7.32, 7.58m		161.23	127.27, 127.44, 128.45, 129.49, 129.66, 130.12	−1013		0.65
[CoDm$_3$(BF)$_2$](BF$_4$)						5002 (12000)	
[CoNx$_3$(BF)$_2$](BF$_4$)						5067 (28000)	
[CoBd$_3$(BF)$_2$](BF$_4$)						5167 (880)	
[Co(diNOsar)]Cl$_3$						6887 (1100)	
[Co(diAMHsar)]Cl$_5$						7324 (3000)	
[Co(en)$_3$]Cl$_3$						7121	
K$_3$CoDm$_3$						5160	

Table 13.
Characteristics of IR (cm^{-1}) and UV-vis (ν_{max}; Dq; B, cm^{-1}; ε, $mol^{-1}\cdot l\cdot cm^{-1}$) spectra of the tin-capped cobalt (III) tris-dioximates [44, 45]

Compound	ν (C=N)	ν (N–O)	ν (Sn–Cl)	$\nu_{max}\times10^{-3}$ ($\varepsilon\times10^{-4}$)	$\nu_{max}\times10^{-3}$ (ε)	Dq	B
(HDEA)[CoGm₃(SnCl₃)₂]	1564	872,1044, 1128,1176	338	30.2 (0.88) 37.4 (2.19) 41.06 (5.27)	21.4 (150) 25.8 (150)	2250	275
(HDEA)[CoMm₃(SnCl₃)₂]	1584	924,1036, 1166,1242	298, 328	29.5 (0.64) 37.7 (2.89) 41.68 (4.31)	21.6 (150) 25.6 (150)	2260	250
H[CoDm₃(SnCl₃)₂]	1592	988,1094, 1218	322	30.2 (0.72) 37.8 (2.55) 42.48 (4.75)	21.8 (200) 26.3 (200)	2290	280
(HDEA)[CoDm₃(SnCl₃)₂]	1592	988,1094, 1218	320	29.8 (0.81) 37.9 (3.36) 42.48 (6.05)	22.2 (200) 26.2 (200)	2320	250
H[CoNx₃(SnCl₃)₂]	1590	970,1066,	330	29.7 (1.04) 37.7 (3.30) 41.54 (5.41)	22.3 (200) 26.5 (200)	2330	245
H[CoBd₃(SnCl₃)₂]	1578	896,1077 1126	330				
(HDEA)[CoBd₃(SnCl₃)₂]	1580	894,1072 1140 1225,1250	324				
(HDEA)[CoGm₃(SnBr₃)₂]	1564	872,1044, 1128,1176		29.4 (0.28) 35.9 (1.45) 40.3 (6.00)	20.9 (100) 25.8 (100)	2213	310
(HDEA)[CoMm₃(SnBr₃)₂]	1584	924,1036, 1166,1242		29.5 (0.30) 36.9 (0.96) 40.80 (4.82)	20.9 (100) 25.3 (100)	2200	275
(HDEA)[CoDm₃(SnBr₃)₂]	1592	985,1092, 1216		29.9 (0.50) 37.9 (0.92) 41.53 (5.42)	21.1 (100) 25.7 (100)	2220	290
H[CoNx₃(SnBr₃)₂]	1590	970,1064, 1206		29.5 (0.50) 37.6 (0.92) 40.68 (5.42)	20.9 (100) 25.2 (100)	2198	270
(HDEA)[CoNx₃(SnBr₃)₂]	1588	970,1064 1208		29.5 (0.28) 37.4 (0.78) 40.80 (5.6)	20.9 (100) 25.7 (100)	2210	300
H[CoBd₃(SnBr₃)₂]	1580	896,1070 1124,1266		29.0 (0.27) 36.5 (1.55) 40.54 (6.65)	20.8 (150) 24.8 (150)	2180	250
(HDEA)[CoBd₃(SnBr₃)₂]	1580	892,1074, 1124,1268		28.9 (0.37) 36.7 (1.49) 40.65 (6.46)	21.2 (150) 25.7 (150)	2233	280

The calculated ligand field parameters are close to the values obtained for low-spin macrocyclic polyamines and clathrochelate boron-capped cobalt(III) tris-dioximates (see above). The ligand field strength in trichlorotin-capped cobalt(III) tris-dioximates is substantially higher than that in nonmacrocyclic and tribromotin-capped complexes and slightly exceeds that in their boron-capped analogs [44].

The substantial difference in electron density distribution among the macrobicyclic trichlorotin- and tribromotin-capped anions seems to be primarily due to steric hindrance. This hindrance gives rise to compounds with a geometry that is not optimal in terms of the low-spin electronic configuration d^6 of the cobalt(III) ion. A decrease in the electron-donor properties in passing from chlorine- to bromine-containing capping fragments should also be taken into account. As a result, the mentioned substantial decrease in the ligand field strength was observed [44].

The ^{1}H and ^{13}C$\{^1$H$\}$NMR spectra of tin-capped cobalt(III) dioximates confirmed their composition and allowed one to obtain information about the electron density distribution in the molecules. The shielding increases (and, hence, the chemical shift in the ^{1}H NMR spectra decreases) in the order

$$[CoD_3(BF)_2]^+ > FeD_3(BF)_2 \sim [CoD_3(SnHal_3)_2]^- > [FeD_3(SnHal_3)_2]^{2-}$$

The shielding of azomethine carbon atoms in ^{13}C$\{^1$H$\}$ NMR spectra varies with a similar order

$$[CoD_3(BF)_2]^+ > [CoD_3(SnHal_3)_2]^- > [FeD_3(SnHal_3)_2]^{2-} \sim FeD_3(BF)_2$$
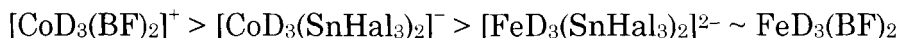
The shielding of protons and carbon atoms of the dioxime fragments is determined by the superimposition of the central ion and macrobicyclic ligand contributions. Both these types of atoms are maximally deshielded in the fluoroboron-capped cobalt (III) tris-dioximates [44].

The ^{1}H and ^{13}C$\{^1$H$\}$NMR spectra permitted one also to detect the isomers of nonsymmetric (HDEA)[CoMm$_3$(SnHal$_3$)$_2$] clathrochelate, which is especially pronounced in the case of azomethine carbon atom signals. Either type of these atoms (methine or methyl-substituted type) manifests itself as four lines. Three of them correspond to the *mer*-isomer, whose dioximate fragments are magnetically nonequivalent. In the *fac*-isomer, all of these three fragments are equivalent and demonstrate one line for each type of carbon atom in the spectra.

The IR spectra of the trichlorotin-capped cobalt(III) complexes contain intense bands in the range 298–338 cm^{-1}, which corresponds to Sn–Cl bond stretching vibrations. These characteristic bands have a singlet character for all compounds except nonsymmetric methylglyoximate. The positions of the intense bands of the C=N bond stretching vibration from 1578 to 1592 cm^{-1} are actually the same for all tin-capped clathrochelate cobalt(III) complexes. An exception is, as with other clathrochelate compounds, the glyoximate complexes, whose spectra demonstrates this band at a lower frequency (*ca* 1560 cm^{-1}). The $\nu_{C=N}$ frequencies, which were observed for tin-capped cobalt complexes, are substantially lower than those of the corresponding boron-capped cobalt clathrochelates (1592–1632cm^{-1}); the maximal C=N bond stretching vibrations (*ca* 1630 cm^{-1}) correspond to boron-capped cobalt(III) tris-dioximates. Due to the larger size of the cross-linking groups, tin-capped cobalt(III) complexes have a less rigid structure and a somewhat lower $\nu_{C=N}$ value, which is approximately equal to those observed for boron-capped iron(II) dioximates. A further $\nu_{C=N}$ decrease takes place in passing to tin-capped iron(II) dioximates.

3.3.2 Iron and ruthenium complexes

Boron-capped iron and ruthenium dioximates

The composition of most FeD$_3$(BR)$_2$ complexes was confirmed by their electron impact (EI), plasma desorption (PD), and fast atom bombardment (FAB) mass spectra. The molecular ion peaks were the most intense and corresponded to the theoretically calculated isotope peak series.

The ^{57}Fe Mössbauer parameters for macrobicyclic iron(II) tris-dioximates and their analogs, listed in Table 14, characterize the *s*-electron density (IS) and electric field gradient (QS) on the iron atom nucleus. The FeD$_3$(BR)$_2$ complexes are diamagnetic like other iron(II) dioximates. The IS values in the series of complexes with the same ligand and different capping fragments are only slightly dependent on the nature of a substituent at the boron atom and can be regarded as typical of a given dioxime [56, 263].

For the evaluation of the main contributions of various factors affecting IS values on the basis of the partial IS (PIS) additivity principle in pseudo- and octahedral low-spin iron(II) complexes, the expected ISs of nioximates and phenanthrolinates were calculated.

Table 14.

^{57}Fe Mössbauer parameters (mm·s^{-1}) for iron(II) dioximates.

Compound	^{a}IS	IS (calcd)	QS	Distortion angle φ obtained (predicted), deg	Reference
FeGm$_3$(BF)$_2$	0.31		0.56	(21–23)	[56]
FeMm$_3$(BF)$_2$	0.32		0.70	(20–22)	[56]
FeDm$_3$(BF)$_2$	0.31		0.90	^{b} 21.2	[56]
FePhm$_3$(BF)$_2$	0.29		0.44	(22–26)	[56]
FeFd$_3$(BF)$_2$	0.35		0.14	(26–30)	[56]
FeBd$_3$(BF)$_2$	0.32		0.25	^{b} 29.3	[56]
Fe(4MNx)$_3$(BF)$_2$	0.32		0.69	(18–22)	[56]
Fe(4MNx)$_3$(BOH)$_2$	0.32		0.63	(18–22)	[56]
Fe(4MNx)$_3$(BOn-C$_4$H$_9$)$_2$	0.34		0.61	(18–22)	[56]
Fe(4MNx)$_3$(BOCH$_3$)$_2$	0.34		0.60	(18–22)	[56]
FeGx$_3$(BF)$_2$	0.29		0.58	(18–22)	[56]
FeGx$_3$(BOH)$_2$ · 3H$_2$O	0.32		0.47	^{b} 23.4	[56]
FeGx$_3$(BOCH$_3$)$_2$	0.33		0.49	(22–26)	[56]
FeGx$_3$(BOn-C$_4$H$_9$)$_2$	0.34		0.46	(22–26)	[56]
FeGx$_3$(BCH$_3$)$_2$	0.35		0.34	(20–24)	[56]
FeNx$_3$(BCH$_3$),	0.33	0.40	0.66	(18–20)	[56]
FeNx$_3$(BF)$_2$	0.33	0.40	0.68	(18–22)	[56]
FeNx$_3$(BOH)$_2$	0.33	0.40	0.67	(18–22)	[56]
FeOx$_3$(BF)$_2$	0.32		0.59	(18–22)	[61]
FeOx$_3$(BOH)$_2$	0.31		0.47	(22–26)	[61]
FeOx$_3$(BOn-C$_4$H$_9$)$_2$	0.32		0.49	(22–26)	[61]
FeOx$_3$(BCH$_3$)$_2$	0.34		0.48	(22–26)	[61]
FeOx$_3$(BC$_6$H$_5$)$_2$	0.29		0.36	(20–24)	[61]
FeOx$_3$(Bn-C$_4$H$_9$)$_2$	0.29		0.33	(22–24)	[61]
Fe(HNx)$_2$Py$_2$	0.45	0.46	1.76		[261]
[Fe(H$_2$Nx)$_3$]Cl$_2$	0.52	0.52	0.28		[262]
Fe(HNx)$_2$(H$_2$Nx)	0.44	0.44	0.61		[262]

^{a} Relative to sodium nitroprusside. ^{b} X-ray crystallography data

The PIS ligand values were used with allowance for the fact that the PIS of the molecular H_2Nx form is greater than that of the HNx^- anion by 0.02 mm·s^{-1}. Comparison of the calculated and experimental IS values shows good agreement in the case of nonmacrocyclic tris-complexes. To the contrary, for macrobicyclic ligands the experimental IS values are much lower than the calculated ones [56].

The IS values for iron(II) complexes decrease in the order $phen >$ $bpy > NO_2^- > H_2Nx > CN^- > NO$ and correlate with an increase in the ligand field force. This suggests that the ligand field strength

increases due to the presence of intraligand cross-linking boron-containing fragments, i.e., a "macrocyclic" effect manifests itself accompanied by an increase in the s-electron density on the iron atom nucleus and, as a consequence, by a decrease in the IS value [56, 263].

Thus, the significant decrease in the magnitude of the IS in the [57]Fe Mössbauer spectra was observed when semiclathrochelate and nonmacrocyclic tris-dioximates passed to clathrochelates. This correlates with the corresponding increase in the ligand field strength during cage structure formation.

The QS in the [57]Fe Mössbauer spectra is determined by the geometry of the iron(II) coordination polyhedron and has been utilized to gain information on the structure of the complexes from the "spectral parameter *vs* structure" correlation. Conversely, the data available on the structure of clathrochelates employed for working out a modern version of the partial quadrupole splitting (PQS) concept permits one to obtain absolute PQS values and to analyse the results for macrobicyclic complexes [264, 265].

In low-spin iron(II) complexes, the three lowest d-orbitals are fully occupied (for octahedral complexes these are t_{2g}-orbitals). In the case of trigonal distortion, the t_{2g}-level splits into a_1 and e_1. The value of such splitting, with allowance for the insignificant contribution of π-bonding, has been calculated for macrobicyclic tris-diiminates [93]. At $\varphi = 60°$, these complexes have D_3 symmetry instead of O_h, which results in the nonzero value of splitting. With a decrease in φ, the splitting goes down to zero ($\varphi = 40–50°$), after which an inversion of the levels takes place, and the splitting increases again (Fig. 14). The splitting of the t_{2g}-levels and the absolute value of QS are parallel [264]. The sign of QS (obtained from [57]Fe Mössbauer experiments in a magnetic field [257]) is negative for the iron(II) tris-phenanthrolinate ($\varphi = 56°$) and positive for [FePcc(BF)]$^+$ clathrochelate ($\varphi = 22°$) (see Section 3.2). When the geometry of the coordination polyhedron is close to TP, QS is large and positive (ca 1 mm·s^{-1}). In complexes with TAP geometry QS is small and negative. The structures of the [FePcc(BF)]$^+$ and FeD$_3$(BR)$_2$ complexes and their positive QS values are similar and the measured QS values correspond to distortion angles 18–24° for aliphatic dioximates and 26–32° for α-benzyl- and α-furyldioximates [56, 263]. The quadrupole splitting in boron-capped complexes with aromatic dioximes is appreciable smaller, and this is accounted for by an increase in the distortion angle φ of the
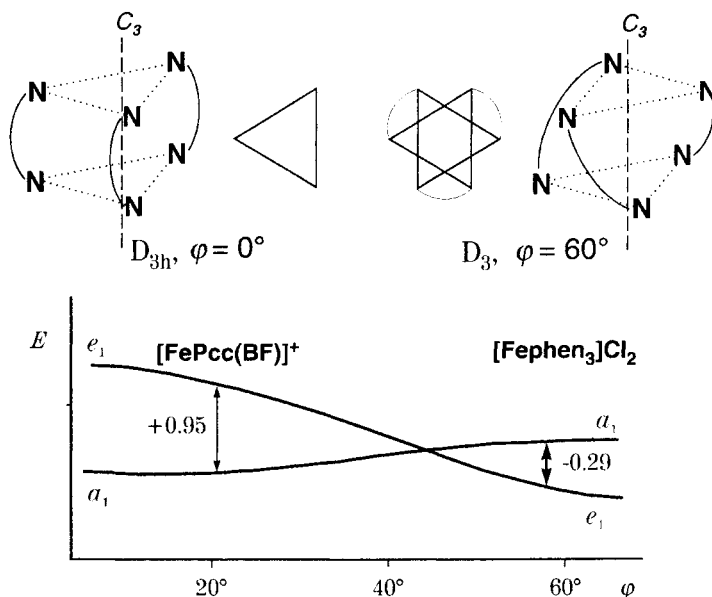
Figure 14. Plot of t_{2g}-level splitting *versus* coordination polyhedron distortion angle φ [56].

coordination polyhedron due to steric hindrances and the fact that oxime oxygen atoms are cut of the chelate ring plane. This allows to cross-link three dioximate fragments at high distortion angles as was evidenced from the X-ray data of several clathrochelate complexes (Table 15). The distortion angle φ increases from 10.9° for the glyoximate clathrochelate, 10–20° for boron-capped tris-nioximates, and 20–23° for macrobicyclic heptoximates and dimethylglyoximates to 26–30° for the α-furyldioximate and α-benzyldioximate clathrochelates.

The structural peculiarities of the hexachloride precursors and triribbed-functionalized iron(II) dioximates were analyzed in Ref. 65. The fact that the geometry of the coordination polyhedron of the precursors changed depending on the nature of a substituent on the boron atom attracted attention first. In the phenylboronic complex, the distortion angle φ is the smallest of all those known for macrobicyclic iron(II) tris-dioximates (Table 16), whereas for the *n*-butylboronic and fluoroboronic precursors, the magnitude of φ is close to that most common for boron-capped clathrochelates. Functionalized complexes have exhibited a geometry with still greater octahedral distortion, but the Fe–N distances and the bite angle α have remained practically unchanged. However, a rather

Table 15.

The Fe–N bond lengths a, base spacings h (Å), bite α and distortion φ angles (deg), QS and PQS (mm·s^{-1}), and f values (calculated from Eq. (45)) for macrobicyclic iron complexes.

Compound	a	h	α	φ	QS	f	$f \times$ PQS	QS $- f \times$ PQS	Ref.
FePhm$_3$(BC$_6$H$_5$)$_2$ · BF$_3$	1.91	2.34	39.2	21.8	(+)0.48	0.79	0.40	+0.1	[266]
FeBd$_3$(BF)$_2$ · 5CHCl$_3$	1.91	2.29	39.3	29.3	(+)0.28	0.49	0.25	+0.0	[267]
FeBd$_3$(BF)(Bn-C$_4$H$_9$)$_2$ · 1/2 iso-C$_8$H$_{10}$	1.89	2.31	39.5	17.9	(+)0.28	1.02	0.51	−0.2	[64]
FeFd$_3$(BC$_6$H$_5$)$_2$ · 1/4CHCl$_3$	1.91	2.31	39.2	26.4	0.0	0.60	0.30	−0.3	[268]
FeGx$_3$(BOH)$_2$ · 3H$_2$O	1.91	2.33	39.1	23.4	(+)0.50	0.70	0.35	+0.15	[63]
FeGx$_3$(BC$_6$H$_5$)$_2$ · 2CHCl$_3$	1.915	2.35	38.9	20.2	(+)0.50	0.75	0.38	+0.1	[269]
FeDm$_3$(BF)$_2$ · C$_6$H$_6$	1.91	2.40	39.0	21.2	(+)0.67	0.71	0.36	+0.3	[270]
FeGm$_3$(Bn-C$_4$H$_9$)$_2$	1.92	2.39	38.6	10.9	(+)0.84	0.90	0.45	+0.4	[268]
[FePcc(BF)]$^+$	1.91		39.5	21.8	+0.95	0.90	0.45	+0.4	[248]
FeNx$_3$(BFc)$_2$ · 2CCl$_4$	1.90	2.38	39.3	9.5	(+)0.72(Fe^{2+}) (+)2.36(Fc)	1.16	0.58	+0.15	[66]
FeNx$_3$(Bn-C$_4$H$_9$)$_2$	1.91	2.34	39.1	20.3	(+)0.58	0.81	0.41	+0.2	[259]
FeGx$_3$(Bn-C$_3$H$_7$)$_2$	1.90	2.31	38.8	21.8	(+)0.37	0.66	0.33	0	[271]
FeOx$_3$(Bn-C$_4$H$_9$)$_2$ · CCl$_4$	1.90	2.34	39.2	25.2	(+)0.33	0.65	0.33	0	[271]
[FeCXO$_3$(BC$_6$H$_5$)(HCOC$_2$H$_5$)$_3$](BF$_4$) · 1/2C$_6$H$_6$	1.90 1.91	2.37	38.7	10.8	(+)0.38	0.94	0.47	−0.1	[188]
[FeDXO$_3$(BC$_6$H$_5$)(HCOC$_2$H$_5$)$_3$](BF$_4$)	1.90 1.93	2.34	38.8	18.2	(+)0.34	0.79	0.40	−0.1	[188]

FeNx₃(BAllyl)₂		1.90	2.36	38.9	13.8	(+)0.74	0.94	0.47	+0.3	[67]
					17.0		0.85	0.43	+0.3	
FeNx₃(BHd)₂ (at 298K)		1.91	2.37	38.9	10	(+)0.68	1.01	0.51	+0.2	[67]
			2.35		18		0.83	0.42	+0.3	
FeDm₃(BAllyl)₂		1.90	2.35	38.4	8.1	(+)0.69	0.89	0.45	+0.25	[67]
FeNx₃(BC₆H₃(OCH₃)₂)₂ · CHCl₃		1.90	2.35	39.1	17.8	(+)0.84	0.89	0.45	+0.4	[272]
FeNx₃(BC≡C–C₆H₅)₂ · C₆H₅CH₃	(type A)	1.90	2.36	38.7	11.5	(+)0.67	0.93	0.47	+0.2	[272]
	(type B)	1.91	2.35	39.1	20.0		0.82	0.41	+0.3	
Fe(Cl2Gm)₃(BC₆H₅)₂		1.90	2.39	39.0	5.4	(+)0.68	1.11	0.55	+0.1	[273]
Fe(Cl2Gm)₃(Bn-C₄H₉)₂		1.90	2.38	39.1	16.1	(+)0.62	0.94	0.47	+0.15	[65]
Fe(Cl2Gm)₃(BF)₂·2THF		1.91	2.36	39.0	17.1	(+)0.64	0.88	0.44	+0.2	[65]
Fe((C₆H₅O)2Gm)₃(Bn-C₄H₉)₂		1.91	2.36	39.8	25.2	(+)0.52	0.84	0.42	+0.1	[65]
Fe((CH₃S)2Gm)₃(BC₆H₅)₂·THF		1.91	2.32	39.3	25.3	(+)0.29	0.68	0.34	+0.05	[65]
Fe((C₆H₅S)2Gm)₃(BC₆H₅)₂		1.91	2.33	39.5	25.6	(+)0.25	0.73	0.37	+0.1	[273]
Fe((n-C₄H₉NH)2Gm)₂(Cl2Gm)(BC₆H₅)₂ (type A)		1.92	2.33	39.5	27.3	(+)0.69	0.65	0.33	+0.4	[65]
(type B)		1.91	2.30	39.0	29.2	(+)0.69	0.55	0.28	+0.4	
FeBd₂(Cl2Gm)(BF)₂·2C₆H₆		1.91	2.33	39.3	24.8	(+)0.62	0.70	0.35	+0.3	[68]
FeBd₂(((C₂H₅)₂N)ClGm)(BF)₂ · C₆H₆		1.91	2.31	39.3	26.6	(+)0.31	0.62	0.31	0.0	[68]
FeBd₂((CH₃S)2Gm)(BF)₂		1.90	2.31	39.3	25.8	(+)0.36	0.66	0.33	0.0	[68]
FeNx₃(Sb(C₂H₅)₃)₂		1.91	2.26	39.8	35.7	(–)0.27	0.27	0.14	–0.4	[75]
[FeNx₃(SnCl₃)₂]²⁻		1.92	2.23	39.5	37.5	(–)0.19	0.04	0.02	–0.2	[274]

Table 16.

Parameters of ^{57}Fe Mössbauer spectra (mm·s^{-1}) and the main X-ray data for chloride clathrochelate C_3-non- and symmetric iron(II) and ruthenium(II) precursors and their functionalized derivatives [65, 78, 259, 273].

Compound	IS	QS	φ, deg	[a] a, Å	[b] h, Å	[c] α, deg	[a] C–C, Å	[a] C=N, Å	[d] N–O, Å	[e] Δ, Å	[f] N=C–C=N, deg
Fe(Cl2Gm)₃(BC₆H₅)₂	0.39	0.68	5.4	1.90	2.39	39.0	1.418	1.274	1.363	0.009	0.9
Fe(Cl2Gm)₃(Bn-C₄H₉)₂	0.37	0.62	16.1	1.90	2.38	39.1	1.422	1.285	1.376	0.089	8.6
Fe(Cl2Gm)₃(BF)₂·2THF	0.37	0.64	17.1	1.91	2.36	39.0	1.429	1.276	1.370	0.083	8.1
Fe((C₆H₅O)2Gm)₃(Bn-C₄H₉)₂	0.41	0.52	25.2	1.91	2.36	39.8	1.440	1.296	1.372	0.096	9.2
Fe((CH₃S)2Gm)₃(BC₆H₅)₂·THF	0.36	0.29	25.3	1.91	2.32	39.3	1.461	1.298	1.377	0.115	10.9
Fe((C₆H₅)2Gm)₃(BC₆H₅)₂	0.34	0.25	25.6	1.91	2.33	39.5	1.452	1.302	1.364	0.128	11.3
Fe((n-C₄H₉NH)2Gm)₂ (Cl2Gm)(BC₆H₅)₂ (type A)	0.38	0.69	27.3	1.92	2.33	39.5	1.427	1.306	1.362	0.102	9.8
				1.89		40.3	(Cl₂Gm)	(Cl₂Gm)	(Cl₂Gm)	(Cl₂Gm)	(Cl₂Gm)
				(Cl₂Gm)		(Cl₂Gm)	1.458	1.305	1.396	0.282	26.8
				1.96		39.0	(N₂Gm)	(N₂Gm)	(N₂Gm)	0.206	19.4
				(N₂Gm)		(N₂Gm)				(N₂Gm)	(N₂Gm)
Fe((n-C₄H₉NH)2Gm)₂ (Cl2Gm)(BC₆H₅)₂ (type B)	0.38	0.69	29.2	1.91	2.30	39.5	1.435	1.304	1.367	0.105	10.0
				1.89		40.4	(Cl₂Gm)	(Cl₂Gm)	(Cl₂Gm)	(Cl₂Gm)	(Cl₂Gm)
				(Cl₂Gm)		(Cl₂Gm)	1.476	1.291	1.400	0.203	19.2
				1.93		39.0	(N₂Gm)	(N₂Gm)	(N₂Gm)	0.206	19.6
				(N₂Gm)		(N₂Gm)				(N₂Gm)	(N₂Gm)
Fe(CwGm)₂(Cl2Gm)(Bn-C₄H₉)₂	0.36	0.64									
Fe(CwGm)₃(Bn-C₄H₉)₂	0.39	0.63									
Fe((12anS₄)Gm)₃(BC₆H₅)₂	0.32	0.39									
FeBd2(Cl2Gm)(BF)₂·2C₆H₆	0.35	0.62	24.8	1.91	2.33	39.3	1.435	1.301	1.370	0.08	7.7
				1.91			(Cl₂Gm)	(Cl₂Gm)		0.08	7.6
				(Cl₂Gm)			1.456	1.312		(Cl₂Gm)	(Cl₂Gm)
				1.91			(Ph₂Gm)	(Ph₂Gm)		0.08	7.8
				(Ph₂Gm)						(Ph₂Gm)	(Ph₂Gm)

	[a]		[b]		[c]		[d]			[e]	[f]
FeBd$_2$(((C$_2$H$_5$)$_2$N)ClGm)(BF)$_2$ · C$_6$H$_6$	0.34	0.31	26.6	1.91 1.92 (ClGm) 1.92 (NGm) 1.90 (Ph$_2$Gm)	2.31	39.3	1.447 (ClNGm) 1.464 (Ph$_2$Gm)	1.323 (NGm) 1.281 (ClGm) 1.309 (Ph$_2$Gm)	1.374	0.09 (ClGm) 0.10 (NGm) 0.12 (Ph$_2$Gm)	9.2 (ClNGm) 10.6 (Ph$_2$Gm)
FeBd$_2$((CH$_3$S)2Gm)(BF)$_2$	0.32	0.36	25.8	1.90 1.90 (Ph$_2$Gm) 1.91 (S$_2$Gm)	2.31	39.3	1.42 (Ph$_2$Gm) 1.46 (S$_2$Gm)	1.321 (Ph$_2$Gm) 1.283 (S$_2$Gm)	1.373	0.05 (Ph$_2$Gm) 0.07 (S$_2$Gm)	3.9 (Ph$_2$Gm) 6.7 (S$_2$Gm)
FeBd$_2$((n-C$_4$H$_9$NH)2Gm)(BF)$_2$	0.35	0.76	(24÷29)								
FeBd$_2$((aza18-C-6)ClGm)(BF)$_2$	0.34	0.45	(24÷29)								
FeBd$_2$(((C$_2$H$_5$)$_2$N)(NH(CH$_2$)$_5$NH$_2$)Gm)(BF)$_2$	0.34	0.53	(24÷29)								
(FeBd$_2$(((C$_2$H$_5$)$_2$N)Gm)(BF)$_2$)$_2$(NH(CH$_2$)$_5$)NH)	0.34	0.47	(24÷29)								
FeBd$_2$(CwGm)(BF)$_2$	0.36	0.50	(24÷29)								
FeBd$_2$((OctS)2Gm)(BF)$_2$	0.32	0.34	(26÷31)								
Ru(Cl2Gm)$_3$(Bn-C$_4$H$_9$)$_2$			2.6	1.98	2.47	38.8	1.419	1.301	1.355	0.08	0.8
Ru((CH$_3$S)2Gm)$_3$(BF)$_2$			20.2	1.99	2.42	38.6	1.451	1.313	1.372	0.11	10.5
Ru((C$_6$H$_5$O)2Gm)$_3$(Bn-C$_4$H$_9$)$_2$			19.5	1.99	2.45	39.0	1.442	1.304	1.373	0.10	9.8
Ru((CH$_2$)4Gm)$_3$(Bn-C$_4$H$_9$)$_2$			12.0	1.97		38.6	1.425	1.314	1.370		

[a] The average of the main structural parameters of chelate cycles.   [b] Distance between the coordination polyhedron bases.
[c] Bite angle (half the chelate angle).   [d] The average of the main structural parameters of capping fragments.
[e] Mean deviation of the coordinated nitrogen atoms from C–Fe–C plane.   [f] Dihedral angle values for the chelating fragments.

significant decrease (0.06–0.09 Å) in the distance h between the coordination polyhedron bases was noted: the change in h is a consequence of the constancy of Fe–N bond lengths as φ increases. Thus, the change in the coordination polyhedron on passing from a TP geometry to a TAP one is described as a rotary-translation contraction along the C_3 symmetry axis that passes through the boron atoms and the iron atom. It was also noted that a reduction of h takes place despite the increase in the C–C bond lengths in chelate rings by 0.03–0.04 Å on passing from hexachloride precursors to functionalized clathrochelates (Table 16). The most obvious difference in such bond lengths manifested itself for both types of molecules of nonsymmetric tetraamine clathrochelate [65]. The TAP distortion also led to an increase in a torsion angle in the N=C–C=N chelate fragment (and, therefore, to an increase in the displacement Δ of coordinating nitrogen atoms from the C–Fe–C fragment plane), and the symbatic growth in the distortion angle φ. In addition, the rotary-translation contraction of a coordination polyhedron on passing from phenylboronic precursor to its derivatives essentially affected the geometry of tetracoordinated boron atoms in the capping groups. The bond angles at these atoms in the precursor indicate a significant trigonal-pyramidal distortion of an ideal tetrahedron (the coordination polyhedron of boron atoms is elongated along the C_3 axis). At the same time, the trigonal-pyramidal distortion in functionalized clathrochelates is induced by contraction of the coordination polyhedra of boron atoms along the same axis. The same distortion has also been observed in O_3BF fragments of both fluoroboronic cobalt dimethylglyoximates [39, 258] and fluoroboronic iron(II) precursor. The bond angles at the capping boron atoms in n-butylboronic precursor and its derivative, and also in thiophenol complex, displayed ideal tetrahedron values [65].

The structures of two other amine clathrochelates were also determined by X-ray crystallography [69]. For tetracyclohexylamine $Fe((C_6H_{11}NH)2Gm)_2(Cl2Gm)(BC_6H_5)_2$ clathrochelate, the average Fe–N distance (1.897 Å) and the bite angle α (39.4°) are typical for those in boron-capped iron(II) clathrochelates. However, an essential difference between the Fe–N distances in a dichloroglyoximate fragment (1.882 Å) and in diaminoglyoximate moieties (1.914 and 1.915 Å) was emphasized. The φ value in the tetracyclohexylamine clathrochelate is 28.7°, approaching an intermediate between a TP and a TAP ($\varphi = 30°$) and a maximal φ value known for boron-capped

tris-dioximates ($\varphi = 29.3°$). Because the Fe–N distance in this case remained typical of that for clathrochelate iron(II) tris-dioximates, the distance between the coordination polyhedron bases ($h = 2.298$ Å) reached a minimum. The essential distinctions between the parameters of diamine and dichloride chelate fragments were also noted in the Fe(($C_6H_{11}NH$)2Gm)$_2$(Cl2Gm)(BC$_6$H$_5$)$_2$ molecule: the coordinated nitrogen atoms of amine-containing moieties deviate from the plane of chelate cycles by 0.21 Å and in the dichloroglyoxime fragment by only 0.08 Å. This correlates with the magnitudes of dihedral angles in N=C–C=N moieties (19.8 and 8°, respectively).

The main bond lengths and angles for the monoamine Fe((n-C$_4$H$_9$NH)Cl)(Cl2Gm)$_2$(BC$_6$H$_5$)$_2$ molecule are also typical for macrobicyclic iron(II) tris-dioximates: the distortion angle φ is equal to 17°; the distance between polyhedron bases h is 2.35 Å, and the average Fe–N distance is 1.91 Å [69].

For C_3-nonsymmetric clathrochelate monoribbed-functionalized iron(II) α-dioximates, it was noted that the distortion angle φ value (25÷27°) of the iron(II) coordination polyhedron for the (FeBd$_2$(Cl2Gm)(BF)$_2$·2C$_6$H$_6$, (FeBd$_2$(((C$_2$H$_5$)$_2$N)ClGm)(BF)$_2$·C$_6$H$_6$, and (FeBd$_2$((CH$_3$S)2Gm)(BF)$_2$ complexes is close to that of the symmetric clathrochelate FeBd$_3$(BF)$_2$ α-benzyldioximate ($\varphi = 29.3°$). This distortion is roughly halfway between a TP and a TAP. Meanwhile, the Fe–N distances (ca 1.91 Å) and bite angle α (ca 39°) in these clathrochelates are typical for boron-capped iron(II) tris-dioximates. As a result, the increasing coordination polyhedron distortion angle causes a squeeze along the B–Fe–B axes, and the distance h between the polyhedron bases is minimal in FeBd$_3$(BF)$_2$, Fe((n-C$_4$H$_9$NH)2Gm)$_2$(Cl2Gm)(BC$_6$H$_5$)$_2$, FeBd$_2$(((C$_2$H$_5$)$_2$N)ClGm)(BF)$_2$, and FeBd$_2$((CH$_3$S)2Gm)(BF)$_2$ molecules along with the maximal distortion angle (Table 15).

Among specific features of the molecular structures for chloride-containing (FeBd$_2$(Cl2Gm)(BF)$_2$·2C$_6$H$_6$ and (FeBd$_2$(((C$_2$H$_5$)$_2$N)ClGm)(BF)$_2$·C$_6$H$_6$ complexes, one could highlight a tendency for the C–C=N angles in the chlorine-containing chelate fragments to have larger values compared with those in phenyl-containing moieties (Table 16). In diethylamine complex, the dihedral angle between the plane of the diethylamine group and that of the chelate fragment is 37.7°. In monoribbed-functionalized clathrochelates, phenyl substituents have a similar mutual orientation: dihedral angles between phenyl substituents and corresponding chelate fragments were observed in the range 44.2–60.4° [68].

Attempts to obtain crystals of other clathrochelate iron(II) tris-dioximates suitable for X-ray analysis were not successful. Therefore, to obtain information about their geometry, one utilized the results of indirect methods, and, initially, QSs in ^{57}Fe Mössbauer spectra.

The QS values for meridional (C_3) nonsymmetric iron(II) tris-dioximates are intermediate between those for the corresponding symmetric complexes of known structure (Table 17).

The introduction of some "new" dioximate fragments into the clathrochelate cage, as a rule, exerts much more influence on the QS and φ values than when the second such fragment is introduced. The above statements were clearly shown for α-benzydioxime:

	FeDm$_3$(BF)$_2$	FeDm$_2$Bd(BF)$_2$	FeDmBd$_2$(BF)$_2$	FeBd$_3$(BF)$_2$
QS, mm·s^{-1}	0.90	0.47	0.37	0.25
ΔQS, mm·s^{-1}	0.22 (increment Dm→Bd)	0.43	0.10	0.12
φ, deg	13.3	20–25	22–27	29.3

A similar phenomenon was observed on introduction of a glyoximate or nioximate fragment into the clathrochelate framework instead of α-benzyldioximate and dimethylglyoximate fragments.

For axial (C_2) nonsymmetric complexes, just like for symmetric boron-capped iron (II) tris-dioximates, distinct dependences of QS and φ values on the nature of a substituent at the boron atom were observed (Table 17). The QS value in a mixed boron-tin-capped clathrochelate is equal to zero, which is also in agreement with the above statement: the QS for the corresponding trigonal-prismatic boron-capped FeNx$_3$(BC$_6$H$_5$)$_2$ complex has a positive sign, while the corresponding trigonal-antiprismatic tin-capped clathrochelate [FeNx$_3$(SnCl$_3$)]$^{2-}$ dianion is characterized by a negative QS value (see below). A superimposition of these two contributions results in distortion angle φ close to 30°, and, hence, the QS value is equal to zero [64].

Thus, QS in boron-capped macrobicyclic iron(II) dioximates has a positive sign that follows from large values of QS, and in some cases the sign of QS was confirmed by direct measurements [272].

The QS values in the ^{57}Fe Mössbauer spectra for tin-, antimony-, and germanium-capped clathrochelate iron(II) complexes [70-75] are small; they change in the dioxime series in an order that differs

Table 17.

^{57}Fe Mossbauer (mm·s^{-1}) and ^{1}H, ^{13}C{^{1}H}, ^{11}B, and ^{119}Sn NMR (ppm) data for nonsymmetric macrobicyclic iron(II) tris-dioximates [64].

Compound	IS	QS	φ obtained (predicted), deg	^{1}H relative to TMS		^{13}C relative to TMS			^{11}B rel. NaB(C$_6$H$_5$)$_4$ (^{119}Sn rel. Sn(CH$_3$)$_4$)
				^{a}R^1	^{a}R^2	^{a}R^1	^{a}R^2	C=N	
FeNx$_3$(BC$_6$H$_5$)(BF)	0.32	0.78	(12–17)	1.79m	2.92m	21.5	26.1	151.7	7.9 (BF,
						21.6	26.2	151.8	$J_{^{11}B-^{19}F}$=14Hz)
									9.2(BC$_6$H$_5$)
FeDm$_3$(BC$_6$H$_5$)(BF)	0.32	0.54	(17–22)	2.45	2.46	13.35	13.50	151.9	8.2 (BF,
								152.7	$J_{^{11}B-^{19}F}$=14Hz)
									9.7(BC$_6$H$_5$)
FeBd$_3$(BF)(Bn-C$_4$H$_9$)	0.32	0.28	^{b} 17.9	7.27m		127.6	127.8	154.9	7.6 (BF,
				7.42m		129.4	129.7	156.4	$J_{^{11}B-^{19}F}$=15Hz)
						130.7	130.9		9.8(Bn-C$_4$H$_9$)
((n-C$_4$H$_9$)$_4$N)[FeNx$_3$(BC$_6$H$_5$)(SnCl$_3$)]	0.33	0.0	(27–32)	1.70m	3.01m	21.2	25.7	154.1	15.9(BC$_6$H$_5$)
						21.3	25.9	155.1	–660(SnCl$_3$)
FeDm$_2$Bd(BF)$_2$	0.34	0.47	(20–25)	2.46	7.26m	13.6	127.8	153.7	8.5 (BF,
							129.6	153.8	$J_{^{11}B-^{19}F}$=13.5Hz)
							130.6		
FeBd$_2$Dm(BF)$_2$	0.31	0.37	(22–27)	2.52	7.28m	13.8	127.8	154.8	
					7.35m		129.8	155.7	
					7.38m		130.8		
FeBd$_2$Nx(BF)$_2$	0.33	0.58	(17–22)	1.87m	7.28m	21.2	127.8	155.2	7.9
				3.02m	7.31m	26.5	129.8	155.4	($J_{^{11}B-^{19}F}$=15.3Hz)
					7.38m		130.8		
FeDm$_2$Gm(BF)$_2$	0.33	0.67	(14–19)	2.45	7.75	13.6		140.2	
								153.5	
FeBd$_2$Gm(BF)$_2$	0.32	0.44	(20–25)	8.00	7.27m	127.9		142.2	
					7.31m	130.2		156.2	
					7.38m	130.7			
[FeNx$_3$(BC$_6$H$_5$)(AlOH)]	0.37	0.36	(17–22)						

^{a} R^1, R^2 are different type of substituents or different fragments of these substituents in the dioximate moieties. ^{b} X-ray crystallographic data

greatly from that observed for boron-capped compounds. The temperature dependences of QS for the $[FeNx_3(SnCl_3)_2]^{2-}$ and $[Fe(Cl2Gm)_3(SnCl_3)_2]^{2+}$ dianions, macrobicyclic $[FeNx_3(Ge_2O_3)]_n$ and $FeNx_3(Sb(C_2H_5)_3)_2$ tris-nioximates show an increase in splitting as the temperature decreases. This trend is the same as in the nonmacrocyclic $[Fe(H_2Nx)_3]SO_4$ complex [56] (TAP geometry) and opposite to that of boron-capped iron(II) dioximates (TP geometry).

This allows one to suggest a negative sign of QS and TAP geometry with distortion angles φ 40–55° in the case of the clathrochelate tin-, germanium-, and antimony-capped tris-dioximates. The minimal distortion angle value (*ca* 40°) was predicted in Ref. 71 for the nioxime complexes with the lowest QS value. Two years later, the structure of clathrochelate $[FeNx_3(SnCl_3)_2]^{2-}$ dianion was determined by X-ray crystallography [274]. The encapsulated iron(II) ion of this dianion has a coordination polyhedron intermediate between a TAP and a TP with $\varphi = 37.5°$. This distortion angle is somewhat lower than the value predicted from the QS value.

The data obtained have made it possible to propose a new approach to the PQS concept, which, in turn, may by used for interpretation of the results obtained and for prediction of the new low-spin iron(II) complex structures.

A very simple concept of partial quadrupole splitting (PQS) was developed in order to explain the peculiarities of QS in various compounds [275-277]. For example, the substitution of one or two ligands B in an octahedral low-spin iron complex FeB_6 (QS=0) results in the following QS values:

$$QS = 2(PQS_A - PQS_B) \qquad FeAB_5 \qquad (40)$$
$$QS = 4(PQS_A - PQS_B) \qquad trans\text{-}FeA_2B_4 \qquad (41)$$
$$QS = -2(PQS_A - PQS_B) \qquad cis\text{-}FeA_2B_4 \qquad (42)$$

In these cases, QS is a function of the difference between PQS_A and PQS_B. Therefore, the absolute value of PQS cannot be calculated from the experimental QS value using these equations, and the relative PQS values depend on the choice of the reference value.

Unlike the situation with octahedral geometry, the TP environment of some iron(II) complexes provides a unique opportunity to obtain the QS of a complex with all donor groups being exactly the same. Therefore, the resulting PQSs are "absolute." An attempt to find the PQS absolute values from X-ray and Mössbauer

data for distorted TP low-spin iron(II) complexes is reported in Refs. 264 and 265.

The QS for ^{57}Fe can be expressed as

$$QS = \frac{1}{2} e^2 qQ(1 + \eta^2 / 3)^{1/2} \tag{43}$$

where $q = V_{zz}/e$, $\eta = (V_{xx} - V_{yy})/V_{zz}$, and V are the components of the electric field gradient tensor. Two of Bancroft's assumptions from Ref. 276 were used:

(1) QS can be regarded as a sum of independent contributions, one from each ligand
(2) PQSs are constants for a given electronic state.

Two other assumptions were modified [264, 265]:

(3) The structure of a distorted TP complex is determined by the bite α and the distortion φ angles (Scheme 100)
(4) The z axis corresponds to the C_3 symmetry axis

For symmetry reasons, it is clear that $V_{xx} = V_{yy}$ and $\eta = 0$. Applying the same approximation as in the octahedral case, QS can be expressed as

$$QS = 6(3\cos^2\theta - 1)\, PQS, \text{ or } QS = f \times PQS \tag{44}$$

where f is a function of iron atom arrangement geometry and θ is the angle between the z axis and the Fe–N bond. For a given bidentate ligand, the θ value is a function of both bite angle α and distortion angle φ. Simple calculations give the following expression:

$$f = 12 - 18 \cos^2\alpha/\cos^2(\varphi/2) \tag{45}$$

For example, for an octahedron $\alpha = 45°$, $\varphi = 60°$, and $QS = f \times PQS = 0$. Using the available structural data for iron complexes and experimental QS values from the Mössbauer spectra, one can calculate the corresponding PQS values for each ligand (Table 17). For all angles α, the coefficient f has a negative sign in the case of pseudo-octahedral iron atom arrangement ($\varphi = 50 \div 60°$). For a TP iron atom, the f values are comparatively high and positive. The effect of capping groups on QS is much lower due to the significantly larger distance from the iron atom. Nevertheless, it can be described using the PQS treatment. The capping groups are located directly on the z axis of the complex; the contribution of each of these groups is $\Delta V_{zz} = (3 \cos^2\theta - 1)z/r^3 = 2z/r^3$, where z is the charge on the capping atom. The overall QS value increases with q. For iron tris-dioximates,

the range of α usually observed is narrow (38–40°), and the QS value is a function of only the φ angle and the effect of capping groups.

It is useful to compare the PQS values calculated by Bancroft and from a modern version (Table 18). The modified PQS scale can be obtained from the Bancroft scale by adding 1.3 mm·s^{-1}. This difference was obtained by comparing the PQS values for nioxime, phenanthroline, and bipyridine complexes in both scales. All PQS values obtained are positive, in contrast to Bancroft's scale with negative PQS for all ligands except NO. It is clear that the nature of PQS is rather different from the pure electrostatic effect of the charge of ligand atoms. The reason for a positive PQS value is a decrease in

Table 18.
PQS values for some ligands and quadrupole splittings (mm·s^{-1}) for iron(II) complexes used for PQS calculations [264, 265].

Compound	Δ (calc.)	Δ (exp.)	Bancroft scale	[a] PQS	[b] Σ
phen			−0.95	0.35	0.35
bipy			−0.85	0.45	0.45
HDm$^-$, HNx$^-$			−0.92	0.38	0.38
Fe(HNx)$_2$Py$_2$	1.76	1.79			
Fe(HDm)$_2$Py$_2$	1.76	1.74			
HBd$^-$			−0.97		0.33
Fe(HBd)$_2$Py$_2$	1.96	1.97			
Fe(HNx)$_2$(C$_6$H$_{11}$CN)$_2$	0.92	0.94			
Macrocyclic			−0.86		0.44
TAAB			−0.62		0.68
[Fe(TAAB)AN$_2$](BF$_4$)$_2$	0.76	0.82			
NH$_3$			−0.52		0.78
Fe(HNx)$_2$(NH$_3$)$_2$	1.60	1.72			
Py, n–C$_4$H$_9$NH$_2$			−0.48		0.82
Fe(HNx)$_2$(n–C$_4$H$_9$NH$_2$)$_2$	1.76	1.83			
Iz			−0.53		0.77
Fe(HNx)$_2$Iz$_2$	1.56	1.38			
CN$^-$			−0.84		0.46
Fe(HNx)$_2$(CN)(Iz)	0.94	0.93			
Pc			−0.98		0.32
FePc(n-C$_4$H$_9$NH$_2$)$_2$	2.0	1.94			
K$_2$FePcIz$_2$	1.80	1.75			
FePc(CN)$_2$	0.56	0.56			
FePcPy$_2$	2.0	1.97			
NO			+0.04		1.34

[a] Calculated from Eqs. (44) and (45).
[b] Σ is calculated from Bancroft PQS by addition of 1.3 mm·s^{-1}.

electron density around the iron atom ($r < 0.5$ Å), which was observed by direct electron density measurements in sodium nitroprusside, [Co(CN)$_6$]$^{3-}$ and [Co(NH$_3$)$_6$]$^{3+}$ cations [278, 279]. The highest electron density decrease has been observed along the Fe–NO and Co–NH$_3$ bonds, and the lowest one is along the Fe–CN and Co–CN bonds. These data correlate with the magnitude of PQS for NO, NH$_3$, and CN (Table 18).

In most cases, slightly negative-charged boron-capped capping groups increase the QS value. The total effect for the slightly positively charged SnCl$_3^+$ cross-linking group proved to be a superimposition of four atomic charges (a positive one due to the tin atom and three negative ones due to chlorine atoms, which are at a distance of 6 Å from the iron atom). As result, the QS values for trihalogenotin-capped compounds are *ca* 0.2 mm·s^{-1} lower than those estimated from PQS.

A plot of QS *versus* φ for each type of cross-linking groups retaining a certain common shape represented in Fig. 15 slightly shifts along the QS axis. The magnitude of this shift can by found using the above-proposed equations.
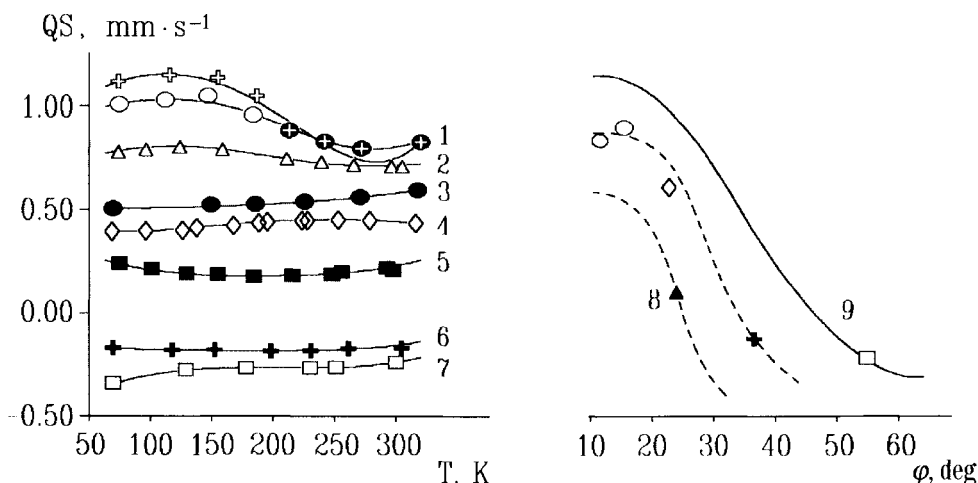
Figure 15. Plot of quadrupole splitting in the ^{57}Fe Mössbauer spectra of FeDm$_3$(BF)$_2$ (1), FeGm$_3$(Bn-C$_4$H$_9$)$_2$ (2), FeNx$_3$(BOH)$_2$ (3), FeGx$_3$(BOH)$_2$·3H$_2$O (4), FeBd$_3$(BF)$_2$·5CHCl$_3$ (5), (HDEA)$_2$[FeNx$_3$(SnCl$_3$)$_2$] (6), [Fe(H$_2$Nx)$_3$](SO$_4$) (7), FeFd$_3$(BC$_6$H$_5$)$_2$·1/4CHCl$_3$ (8) complexes *versus* temperature and corresponding φ values. The theoretical dependence QS *versus* φ (9) is also shown [274].

The modern PQS values have a real physical meaning and reflect the electron density distribution (EDD) in the molecule, allowing one to explain QS for a great number of iron coordination compounds with different geometry. These values make it possible to predict the structure of new compounds from the "structure-vs-quadrupole splitting" type of correlation dependence. Taking into account the peculiarities of ligands (e.g., capping groups, substituents, protonation-deprotonation processes) may noticeably change the QS.

This modern version of PQS has been applied successfully to the prediction of the geometry of the hexadecyl- and allylboron-capped tris-dioximates, ferrocenylboronic clathrochelates, and macrobicyclic tris-oximehydrazonates. A good agreement between QS_{exp} and QS_{calcd} was observed even in the case of nonsymmetric $FeBd_2((N(C_2H_5)_2)ClGm)(BF)_2$ and $FeBd_2((CH_3S)2Gm)(BF)_2$ complexes (Table 15).

The applicability of the major concepts of the PQS model to iron(II) complexes is associated with an axial symmetry of the EDD about the iron atom. Such symmetry is important to establish the correlation between QS and the geometry of the coordination environment. In the case of octahedral complexes, this assumption was confirmed by the results of calculations and by the experimental measurements of the EDD. For example, the deformation electron density (DED) map for sodium nitroprusside (FeB_5A geometry) demonstrated a nearly axial charge distribution around the iron atom in the equatorial plane [278].

However, an example of deviation from DED axial symmetry was observed even in the case of the formally C_3-symmetric complex. A single crystal of $FeDm_3(BF)_2 \cdot C_6H_6$ complex was studied by X-ray diffraction at 138, 208, and 291 K and by ^{57}Fe Mössbauer spectroscopy in the temperature range from 135 to 290 K [270]. The molecular geometry of the $FeDm_3(BF)_2$ clathrochelate (Fig. 16) does not substantially change in the temperature range under study. The complex has pseudo-C_3 symmetry, and φ is equal to 21.2°. The iron atom is displaced from the center of the N_6 coordination polyhedron along the threefold pseudoaxis by 0.034, 0.026, and 0.023 Å at 138, 208, and 291 K, respectively.

The presence of the local C_3 symmetry in the $FeDm_3(BF)_2$ molecule implies that the EDD is meridional (C_3) symmetric. The DED for the $FeDm_3(BF)_2$ molecule was examined by X-ray diffraction. The maxima of the DED in the vicinity of the metal ion correspond to
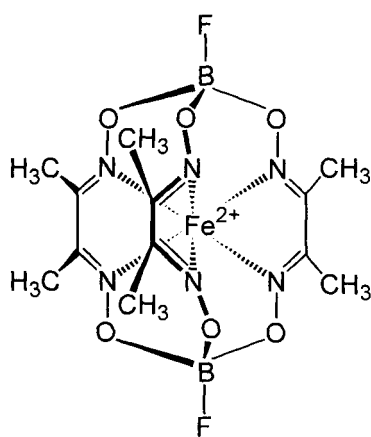
FeDm₃(BF)₂
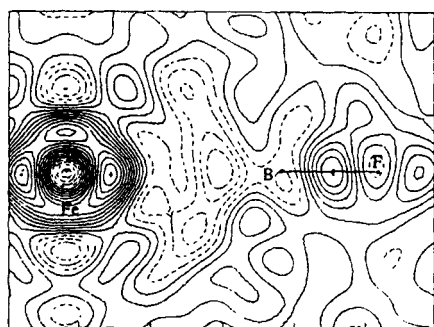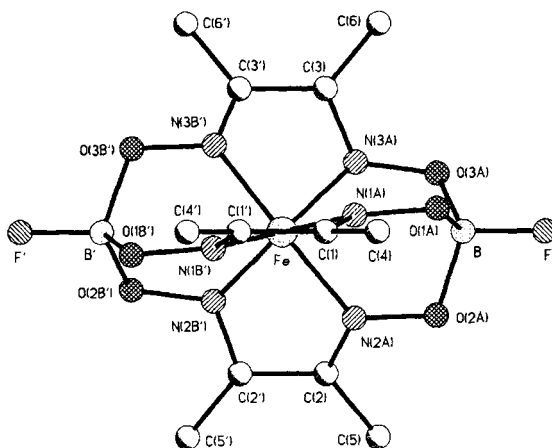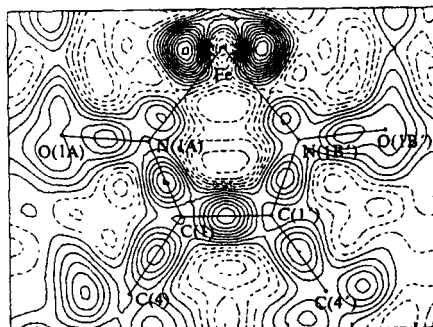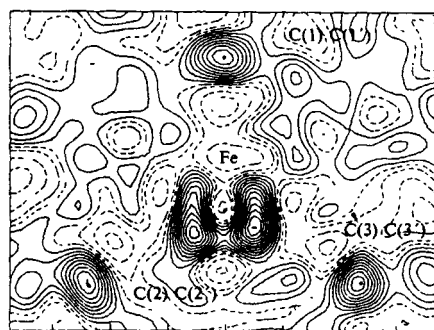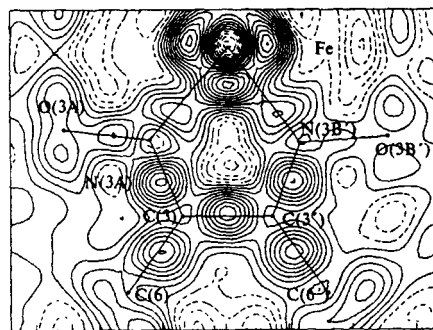
Figure 16. General view of FeDm₃(BF)₂ molecule and the deformation electron density maps passing through the iron, boron, and fluoride atoms (*a*), through the midpoints of the C(1)—C(1'), C(2)—C(2'), and C(3)—C(3') bonds (*b*), and in the mean planes of the chelate rings (*c* and *d*) [270].

the partial or complete localization of the complex on the metal ion. Actually, the maxima of the DED were found in the vicinity of the iron ion in the DED sections (Fig. 16) passing through the iron, boron, and fluoride atoms (section A) and in the equatorial plane (section B). The accumulation of the DED along the threefold axis and in the equatorial plane corresponds to the a_1-MO and the e_1-MO, respectively. However, unlike the expected C_3 symmetry of the DED distribution, it is characterized (see section B) only by the symmetry plane passing through the C(1), C(1'), and iron atoms (the local symmetry C_s). Therefore, in spite of the equivalence of the α-dioximate fragments, the interaction of the iron(II) ion with the macrobicyclic ligand (according to the DED map) is anisotropic. As a result, the experimental QS value (ca 0.7 mm·s^{-1}) for FeDm$_3$(BF)$_2$·C$_6$H$_6$ complex is higher than the value calculated from the PQS model (0.38 mm·s^{-1}). In this case, one of the major assumptions of the PQS concept, regarding the equivalence of the PQS values for donor atoms, is inapplicable. Thus, the displacement of the iron ion from the center of the coordination polyhedron along the threefold axis and the C_3-nonsymmetry of EDD about the iron(II) ion leads to a significant increase in the electric field gradient on the iron nucleus [270].

Thus, in spite of a significant change in the distortion angle φ of the coordination polyhedron in the TP÷TAP range, the Fe–N distance in all X-ray crystallographically studied macrobicyclic p-element-capped iron(II) tris-dioximates is within very narrow limits, namely, 1.91÷1.92 Å. Simultaneously, the distance h between the coordination polyhedron bases markedly changes; it is maximal (2.39 Å) for the least distorted dichloroglyoxime and glyoxime complexes (φ is 5.4 and 10.9°, respectively) and minimal (2.23 Å) for the most distorted trichlorotin-capped compounds. The remaining compounds represented in Table 14 also obey this correlation. Thus, the change in the coordination polyhedron geometry observed for these compounds can be described as a rotational-translational contraction of the trigonal prism bases along the threefold symmetry axis of the molecule.

The CuN$_6$ coordination polyhedra of the ttn-ended copper(II) tris-dioximates bridge two terminal capping ions with a separation Cr^{III}(distorted octahedral)...Cu 3.583 Å (Cr...Cr separation is 7.16 Å), Fe^{III}...Cu 3.58 Å and Mn^{IV}...Cu 3.54 Å (Mn...Mn separation is 7.06 Å). The trinuclear M–Cu–M units are not perfectly linear: the

copper(II) ion is displaced from the center of the coordination polyhedra and closer to two of the dioximate fragments; the distance to the third one is remarkable long. The geometry of the encapsulated copper(II) ions was envisaged as pseudosquare pyramidal with an η^2-dioximate ligand at the apical position [79, 83, 85].

The trinuclear $Mn^{IV}...Zn^{II}...Mn^{IV}$ and $Cr^{III}...Zn^{II}...Cr^{III}$ moieties in clathrochelate $[ZnNx_3(ttnMn)_2]^{4+}$ and $[ZnDm_3(ttnCr)_2]^{2+}$ cations are linear (179.9 and 179.7°, respectively); and intramolecular separation of 6.97 and 7.14 Å of the distorted octahedral capping manganese(IV) atoms was found [83, 86].

As seen from X-ray data (Table 19), the distorted octahedral chromium(III) centres in free $[H_2Dm_3(ttnCr)_2](ClO_4)_2$ ligand are coplanar with the nitrogen atoms of dimethylglyoximate fragments with a Cr...Cr separation of 7.265 Å. Two significant electron densities of residues at a distance of ca 1 Å from the nitrogen atoms were assigned to two statistically disordered protons [84].

The linear trinuclear $[NiDm_3(ttnFe)_2](PF_6)_2 \cdot 0.5H_2O$ complex contains two high-spin capping iron(III) ions with d^5 configuration 7.37 Å apart. The Ni–N bond distance in the coordination polyhedron (2.035 Å) is much higher than those in the square-planar $Ni(HDm)_2$ bis-dimethylglioximate (1.85 Å), and clathrochelate iron(III) and cobalt (III) dioximates (M–N ca 1.9 Å) [80].

The geometry of the macrobicyclic ttn-ended tris-dioximes is governed by several factors significantly different from those for their p-element-capped analogs. The cavity size of the ttn-ended d-metal tris-dioximes essentially exceeds that of the p-element-capped clathrochelates. The cavity of p-element-capped complexes is optimal for Fe^{2+} and Co^{3+} ions and makes it impossible to encapsulate ions with higher physical ionic (Shannon) radius than a low-spin cobalt and ruthenium ions. In particular, the p-element-capped complexes with encapsulated nickel, copper, and zinc(II) ions have not been synthesized so far. It is obvious that in the macrobicyclic ttn-ended tris-dioximes obtained, the size of the clathrochelate ligand cavity is not a limiting factor, and their geometry (as in the case of d-metal sarcophaginates and sepulchrates) depends mainly on the superimposition of ΔLFSE and the strain energy of the conformationally labile ligand. As mentioned above, ΔLFSE between a TAP and a TP geometries is negligible for zinc(II) (d^9) and copper(II) (d^{10}) ions. As a result, the geometry of their complexes approaches that of a free ligand and is practically trigonal-prismatic.

Table 19.
The main X-ray data for 1,4,7-trimethyl-1,4,7-triazacyclononane-ended macrobicyclic tris-dioximates

Compound	[a] Electronic configuration (spin)	[b] r_i, Å	a, Å	φ, deg	α, deg	h, Å	Reference
$[H_2Dm_3(ttnCr)_2](ClO_4)_2 \cdot CH_3OH$				5.7		2.67	[84]
$[ZnDm_3(ttnMn)_2](ClO_4)_2$	d^{10} (S = 0)	0.88	2.163	8.4	36.8	2.58	[81]
$[ZnNx_3(ttnMn)_2](ClO_4)_4 \cdot AN$			2.091	5.1	37.7	2.52	[83]
$[ZnDm_3(ttnCr)_2](ClO_4)_2 \cdot CH_3OH$			2.149	7.0	37.0		[86]
$[FeDm_3(ttnCr)_2](ClO_4)_2 \cdot H_2O$	d^6 (S = 0)	0.75	1.936	34.7	39.3	2.27	[85]
$[CuNx_3(ttnMn)_2](ClO_4)_4 \cdot AN$	d^9 (S = 1/2)	0.87	2.09 $\begin{pmatrix} 2.30 \\ 2.00 \\ 1.96 \end{pmatrix}$	7.6 $\begin{pmatrix} 5.9 \\ 8.4 \\ 8.4 \end{pmatrix}$			[83]
$[CuDm_3(ttnFe)_2](ClO_4)_2 \cdot 0.5CH_3OH$			2.16 $\begin{pmatrix} 2.42 \\ 2.04 \\ 2.00 \end{pmatrix}$	11.5	40.4	2.53	[79]
$[CuDm_3(ttnCr)_2](ClO_4)_2 \cdot CH_3OH$			2.125	8.3	37.3	2.55	[85]
$[NiDm_3(ttnCr)_2](ClO_4)_2$	d^8 (S = 1)	0.83	2.066	23.8	38.1	2.46	[85]
$[NiDm_3(ttnFe)_2](PF_6)_2 \cdot 0.5CH_3OH$			2.035	27.5	37.9	2.37	[80]

[a] Electronic configuration (spin state) of an encapsulated metal ion.
[b] r_i is physical ionic (Shannon) radius of an encapsulated metal ion [280]

The ΔLFSE for iron(II) (low-spin d^6) and nickel(II) (d^8) ions is maximal among d-metal ions and this implies that the geometry of their ttn-ended clathrochelates is much closer to an octahedron compared with that of a free ligand. A negligible (7–10°) decrease in the distortion angle φ for nickel(II) complexes compared with analogous iron(II) clathrochelates may caused by a greater ΔLFSE value in the case of a low-spin d^6 configuration compared with that for a d^8 configuration or as an essentially higher Shannon radius of a nickel(II) ion (in the case of TP geometry the size of the clathrochelate ligand cavity is appreciably larger than that in the case of TAP geometry).

The tris-dioximatometalate(II) anions are capable of functioning as bridging ligands to give linear homo- and heterotrinuclear complexes and can mediate a wide range of antiferromagnetic (AF) and ferromagnetic (F) interactions. The summary coupling constants are expressed by the equation

$$J = J_{AF} + J_F \tag{46}$$

where J_{AF} is negative and J_F is a positive term.

Because of their quasi-isostructural nature, trinuclear clathrochelates are unique for the study of intramolecular exchange interaction between three paramagnetic transition metal ions as a function of their d^n electronic configuration by magnetic susceptibility measurements and EPR spectra.

There are two different coupling constants determined from magnetic susceptibility data: $J_{12} = J_{23} = J$, operating between adjacent metal centres ($M_1 \ldots M_2$ distance is approximately 3.5 Å) and J_{13}, between the terminal ones, separated by a large distance of approximately 7 Å. An analysis of the interacting magnetic orbitals in trinuclear macrobicyclic tris-dioximates was performed in Refs. 79-86. Magnetic coupling constants and g-factors for dinuclear and trinuclear complexes are listed in Table 20.

As seen from these data, the π-conjugated system of the α-dioximate fragments, delocalized over all of the bridging groups and perpendicular to the plane of these fragments, appears to provide the dominant antiferromagnetic exchange between the terminal paramagnetic ions separated by as large as approximately 7 Å. The diamagnetic encapsulated metal units can act as "spacers" for the paramagnetic centers and thus change the distances between the interacting units.

Two reversible phase transitions at $T_{c1} = 290$ K and $T_{c2} = 190$ K in the single crystal of the $FeNx_3(BHd)_2$ complex (Fig. 17), indicated by differential scanning calorimetry, ^{57}Fe Mössbauer spectroscopy and X-ray crystallography, were observed [67, 281]. The X-ray diffraction studies were performed for all phases I, II, and III at 303, 243, and 153 K, respectively.

The phases I, II, and III of the $FeNx_3(BHd)_2$ complex are triclinic, space group $P1$, and each unit cell contains four symmetrically independent molecules. The phases II and III have similar

Table 20.
Magnetic susceptibility data for the binuclear and trinuclear complexes [79-86].

Compound	$J,$ $(J_{12} = J_{23})$ cm^{-1}	$J_{13},$ cm^{-1}	g
$[H_2Dm_3(ttnCr)_2]Br_2$		−5.1	1.91
$[H_2Dm_3(ttnCr)_2](ClO_4)_2$		−4.7	2.04
$[H_4Dm_3(ttnCr)_2]^{4+}$		−3.1	2.04
$[LiDm_3(ttnCr)_2]^+$		−5.8	2.07
$[CuDm_3(ttnCr)_2]^{2+}$	18.5	−7.0	1.96
$[NiDm_3(ttnCr)_2]^{2+}$	−0.7	−1.8	$g_{Cr} = 2.0,$ $g_{Ni} = 2.15$
$[Co(ls)Dm_3(ttnCr)_2]^{3+}$		−0.3	1.99
$[Fe(ls)Dm_3(ttnCr)_2]^{2+}$		0	1.98
$[Fe(ls)Dm_3(ttnCr)_2]^{3+}$	−15.7	−3.0	1.99
$[MnDm_3(ttnCr)_2]^{2+}$	4.5	−11.5	2.06
$[ZnDm_3(ttnCr)_2]^{2+}$		−4.4	2.00
$[ZnDm_3(ttnFe)_2]^{2+}$		−3.4	1.98
$[CuDm_3(ttnFe)_2]^{2+}$	−42	−3.4	2.00
$[Fe(ls)Dm_3(ttnCr)_2]^{2+}$		−4.4	1.98
$[MnDm_3(ttnMn)_2]^{2+}$	4.7	−3.0	1.95
$[NiDm_3(ttnMn)_2]^{2+}$	−5.3	2.7	1.98
$[CuDm_3(ttnMn)_2]^{2+}$	−63.1	−2.8	1.97
$[ZnDm_3(ttnMn)_2]^{2+}$		−0.4	2.13
$[MnDm_3(ttnMn)_2]^{4+}$	19.6	−19.2	1.99
$[NiDm_3(ttnMn)_2]^{4+}$	19.2	−10.1	2.10
$[CuDm_3(ttnMn)_2]^{4+}$	72.7	−25.0	2.02
$[ZnDm_3(ttnMn)_2]^{4+}$		−19.2	2.10
$[ZnNx_3(ttnMn)_2]^{2+}$		−2.4	1.94
$[CuNx_3(ttnMn)_2]^{2+}$	−70	−3.9	1.98
$[MnNx_3(ttnMn)_2]^{2+}$	4.7	−3.4	1.99
$[ZnNx_3(ttnMn)_2]^{4+}$		−20.6	2.02
$[CuNx_3(ttnMn)_2]^{4+}$	50.1	−17.7	1.94
$[MnNx_3(ttnMn)_2]^{4+}$	25.2	−25.7	2 (fixed)
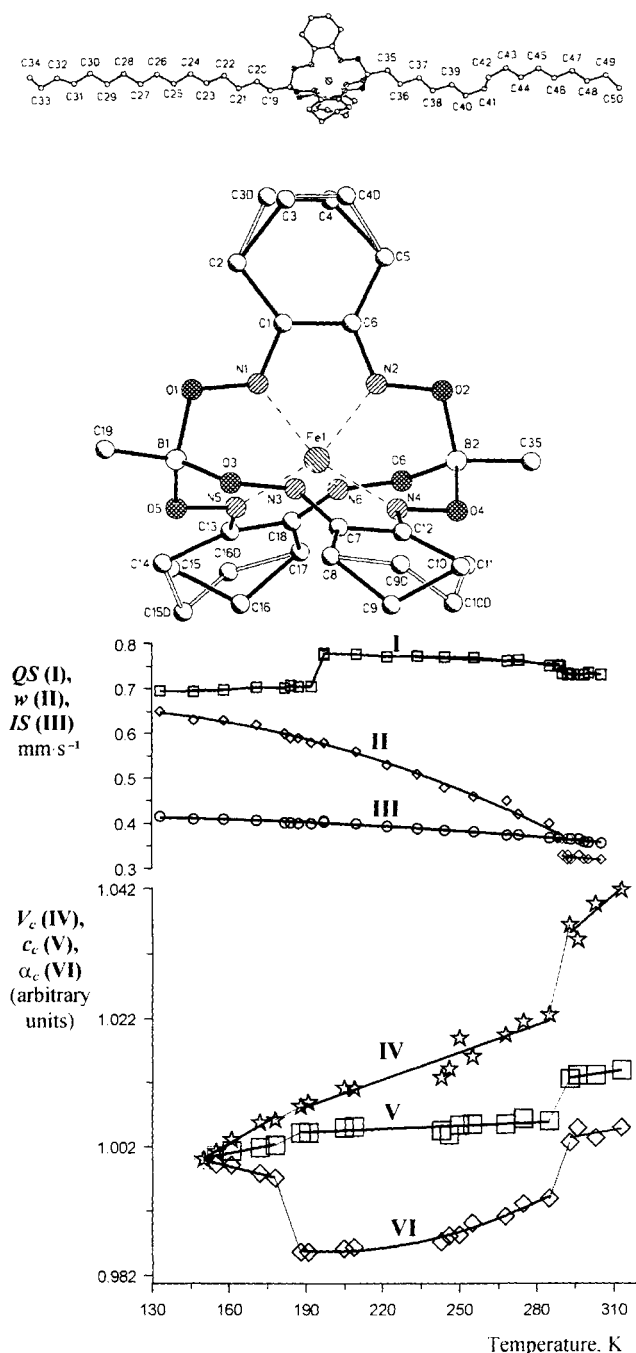
Figure 17. The molecular structure and temperature dependence of the ^{57}Fe Mössbauer parameters (IS and QS) and half-width of the absorption line (w) and some parameters of the nonprimitive unit cell of the FeNx$_3$(BHd)$_2$ crystal [67].

crystallographic settings, whereas in phases **II** and **I** only three parameters are approximately equal. For a better comparison of the two unit cells of phases **I** and **II** (for **III** as for phase **II**), their initial parameters were transformed to similar crystal settings. Thus, the triclinic phase **I** was transformed into a new C-centred triclinic phase, and phase **II** (and **III**) was transformed to the *I*-centered triclinic phase – both with doubled unit cell volume [67, 281].

All parameters in these non-standard crystallographic settings have commensurate values; such a cell is "common" for all three phases. The type of the common cell in phases **I** and **II** (**III**) is different: *C*-centered in **I** and *I*-centered in **II**.

The phase transition **I** ↔ **II** is accompanied by abrupt changes in all unit cell parameters and volume, whereas near T_{c2} (phase transition **II** ↔ **III**) only the discontinuities in angle parameters were observed (Fig. 17). The interesting feature of phase **II** is the existence of the negative thermal expansion of the crystal [67, 281].

In all phases **I**, **II**, and **III**, the molecular packing has a smectic-like ordering. The molecules form layers parallel to the crystallographic plane *bc*; their long axes (directors) are parallel to each other and form an angle approximately 15° with the plane *bc*. Moreover, the structures of the *bc* molecular layers in all three phases are the same. The difference between phases **I** and **II** is related to a different mutual arrangement of these layers. The non-primitive unit cells during the phase transition **I** ↔ **II** change from *C*-centered to *I*-centered and *vice versa*. The temperature dependence of intensities of symmetry-sensitive reflections in the temperature range 250÷313 K confirmed the change of translation type from *I*-symmetric to *I*-symmetric during the phase transition **I** ↔ **II**. Such a transformation would occur as a *c*/2 shift of every second *bc* layer (Fig. 18).

The routes of these phase transitions in FeNx$_3$(BHd)$_2$ crystal were proposed in Refs. 67 and 281. The structure of phase **I** has a pseudotranslation, which is broken by a different mutual orientation of the B...B axis of the clathrochelate fragment (Fig. 18). In phase **II**, such molecules become a translationally equivalent that could be a result of conformational change of every second *bc* layer connected with a rotation on 20° of the B...B axis around the molecular centre of mass. This conformational transition has a collective character and concerns all molecules in the *bc* layer at the change of *C*-type on the common cell to *I*-type. After this transformation, the molecular
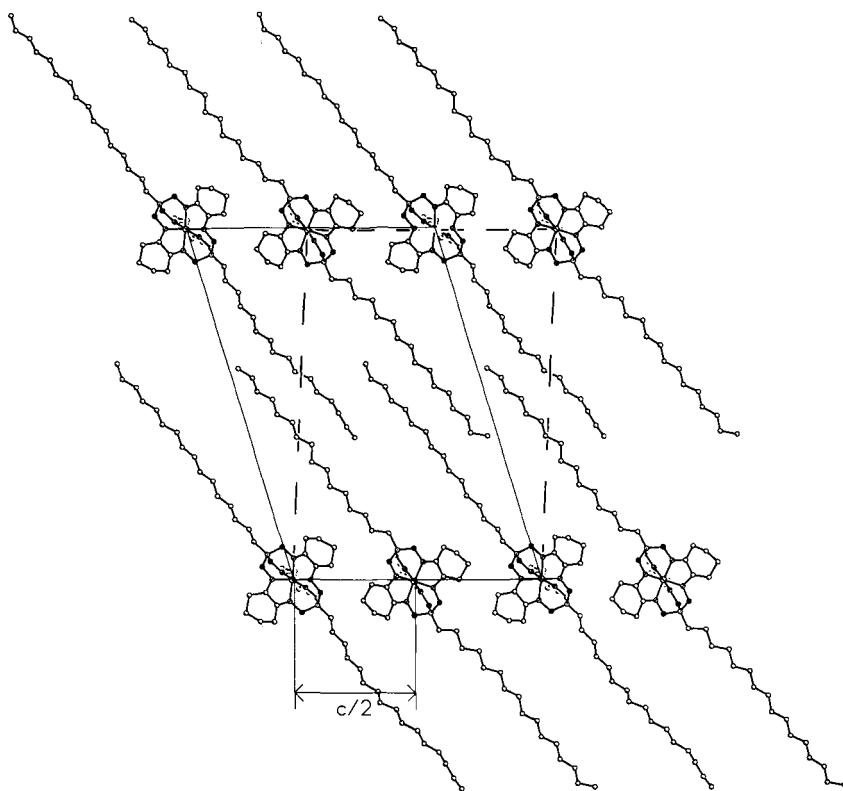
Figure 18. Fragment of the molecular packing of $FeNx_3(BHd)_2$ molecules at 243 K (phase **II**). The rows of molecules belong to the neighboring bc molecular layers. The two-dimensional primitive unit cells of phases **I** and **II** are shown by dashed and solid lines, respectively [67, 281].

centres of mass and hexadecyl substituents are kept almost in the same positions. Moreover, the appearance of the bc layer remains the same, but it seems to be $c/2$ translated.

The phase transition **II** $\leftrightarrow$ **III** is accompanied only by minor alternations in the molecular packing and is not connected with the change in translational symmetry. At the same time, the intermolecular distortion of the hexadecyl substituents from that of the "classical" plane – zigzag aliphatic chains seems more remarkable. Unlike in phases **I** and **II**, in phase **III** all four molecules have a hexadecyl substituent including a double fragment with *gauche*

conformation. Such distortion decreases the effective length of the aliphatic chain to approximately 1 Å. By this shortening, the molecules from the neighbouring layers bc probably remove the mechanical obstacles during thermal compression of the crystal. On the other hand, the lengthening of this effective longitudinal dimension during the temperature increase can trigger the phase transition **III ↔ II**.

Thus, the transitions **I ↔ II** and **II ↔ III** are examples of two different types of phase transition without the multiplication of the unit cell volume – the so-called *ferrodistortion phase transitions*, one of which (**I ↔ II**) is connected with the unusual change of translational symmetry, but another (**II ↔ III**) only with an abrupt distortion of the crystal lattice parameters.

The phase transitions **I ↔ II** and **II ↔ III** are also accompanied by a change in distortion angle φ of the iron(II) coordination polyhedron. Distortion angles φ are equal to 17 and 10°, 19 and 14° for two pairs of the four symmetrically independent molecules in phases **I** and **II**, respectively, and 20° for all molecules in phase **III**.

The temperature dependence of the ^{57}Fe Mössbauer parameters over the temperature range investigated is presented in Fig. 17. The IS values increase slightly and practically linearly with a temperature decrease: the phase transitions in the crystal insignificantly affect the s-electron density on the central iron atom nucleus. In contrast, the QS values are sensitive to such variations (see above) and undergo two sudden changes at both phase transitions: a smaller one (about 0.02 mm·s^{-1}, 10σ) at approximately 290 K and a greater one (about 0.07 mm·s^{-1}, 35σ) at approximately 190 K. Despite the presence in phases **I** and **II** of two types of iron(II) ions in essentially different arrangement, the ^{57}Fe Mössbauer spectra contain only one doublet signal. This was explained both by dynamic transformations in the crystal and by a rather large half-width of the ^{57}Fe Mössbauer absorption bands [67].

The temperature-dependent disorder of molecules in two or more positions is of interest with a view to the realization of structural phase transitions of the "order–disorder" type in crystals. C_3-symmetric clathrochelate complexes display a variety of specific features that favour the occurrence of temperature-dependent disorder. As an example, these specific features were examined in crystals of clathrochelate $Fe(Cl2Gm)_3(Bn\text{-}C_4H_9)_2$ precursor [282]. The phase transition accompanied by the mechanical destruction of the

sample was observed for these crystals from 155 to 163 K, and eleven X-ray diffraction experiments were carried out from 165 to 330 K. A detailed X-ray diffraction study of a high-temperature phase of the $Fe(Cl2Gm)_3(Bn\text{-}C_4H_9)_2$ crystals revealed a number of striking peculiarities in the geometry and packing of the molecules that are associated with the occurrence of phase transition and, presumably, induce it. The clathrochelate molecule can change conformation from one that is clockwise twisted about the C_3 axis (a left-handed conformer) to one that is counter clockwise twisted (a right-handed conformer). In this case, a distortion angle φ is changed by more than 40°, while the spatial position of the substituents in dioximate fragments, the interaction between which determines the packing of the molecules in crystal, actually remains intact. Owing to the high lability of the Fe–N coordination bond, the molecules in the crystal fairly readily change one of the two possible conformations to the other one with temperature.

This also favours the occurrence of temperature-dependent disorder. Computer simulation of structural variations and comparison of both theoretical and experimental behaviour of the integral intensities of structure-sensitive diffraction reflections allow one to prove the presence of the temperature-dependent disorder of the $Fe(Cl2Gm)_3(Bn\text{-}C_4H_9)_2$ molecules in crystals. The thermal expansion anomalies and the relative shift of the molecules preced the phase transition and, presumably, promot its realization in this crystal [282].

The IR spectra of boron-capped iron(II) tris-dioximates confirmed the macrobicyclic nature of these complexes since they show no broad characteristic ν_{O-H} bands in the range 2600–3200 cm^{-1} [56] belonging to the vibrations of free oxime groups, and several intense bands characteristic of tetrahedral boron-containing caps (B–O bond stretching vibrations in the range 1100–1200 cm^{-1}) appear. The C=N bond stretching vibrations near 1600 cm^{-1} were shifted and intensified in the spectra of these complexes compared with the initial dioxime. The shift value was small for alicyclic dioximes and appreciable for acyclic dioximates, which is indicative of variations in the ligand structure on complexation. The C=N bond stretching vibrations observed at ca 1580 cm^{-1} for all dioximates, except that of the dichloro- and glyoximate clathrochelates, is evidence of the resemblance of the coordination polyhedron structure of all macrobicyclic boron-capped iron (II) dioximates.

The C–H bond stretching vibrations at ca 3000 cm^{-1} in alicyclic, acyclic and aromatic dioximes are not affected by complexation: only for clathrochelate glyoximates does the narrow C–H absorption band shift by 90 cm^{-1} [50]. With alicyclic dioximates, the deformation vibrations of the cycloalkane methylene units proved to be the most sensitive to coordination. Their absorption bands are shifted by 15–40 cm^{-1} to the longwave region [59, 60]. The spectra of the FeNx$_3$(BH)$_2$ and FeDm$_3$(BH)$_2$ complexes contain intense bands at 2490 and 2495 cm^{-1}, respectively, assigned to B–H bond stretching vibrations [52, 58].

The IR spectra of the apically functionalized compounds, together with characteristic C=N, N–O, and B–O stretching vibrations, have been found to contain some additional intense bands of functionalizing substituents (for the hexadecyl fragment at ca 2850÷2950 (ν_{C-H}) and at 1440–1470 cm^{-1} (δ_{C-H})); for the allyl fragment at ca 1630 ($\nu_{C=C}$) and at 1400–1480 cm^{-1} (δ_{C-H})).

The absence of the symmetry elements in the meridional (C_3) and axial (C_2) nonsymmetric clathrochelate molecules manifests itself in their IR spectra. The C=N and N–O stretching vibrations in the dioximate fragments of C_3-nonsymmetric clathrochelates and in the mixed boron-tin-capped C_2-nonsymmetric complex proved to be the most sensitive ones. These vibrations were assigned to the corresponding dioximate groups or their fragments bound to a certain type of capping group. In particular, the C=N stretching vibrations in the spectrum of the FeDm$_2$Gm(BF)$_2$ complex are a superimposition of two signals: one at 1560 cm^{-1}, which was assigned to a glyoximate complex (for the FeGm$_3$(BF)$_2$ clathrochelate, it was detected at 1559 cm^{-1}) and another at 1583 cm^{-1}, which was assigned to dimethylglyoximate fragment (for the FeDm$_3$(BF)$_2$ clathrochelate, it was detected at 1585 cm^{-1}). The same vibration in the IR spectrum of the mixed boron-tin-capped compound appears in the form of a band at 1565 cm^{-1} (for the (HDEA)$_2$[FeNx$_3$(SnCl$_3$)$_2$] complex, $\nu_{C=N}$ is at 1568 cm^{-1}) and a band at 1573 cm^{-1} (for the FeNx$_3$(BC$_6$H$_5$)$_2$, $\nu_{C=N}$ is at 1580 cm^{-1}); these were attributed to the oxime fragments bound to tin- and boron-containing capping fragments, respectively. The IR spectrum of the mixed clathrochelate also clearly showed intense characteristic stretching vibration bands for both capping fragments (ν_{B-O} at ca 1200 and ν_{Sn-Cl} at ca 320 cm^{-1}). It was noted that for clathrochelate FeBd$_3$(BF)$_2$ tris-α-benzyldioximate the ν_{B-O} bands were observed at a higher frequency (1212 cm^{-1}) than for its

C_3-nonsymmetric derivatives (for $FeBd_2Dm(BF)_2$ and $FeDm_2Bd(BF)_2$ complexes ν_{B-O} is at 1197 and at 1196 cm^{-1}, respectively). For $FeDm_3(BF)_2$ tris-dimethylglyoximate, this band was detected at 1194cm^{-1} [64].

The $\nu_{C=N}$ values in IR spectra of the di- and hexachloride clathrochelate precursors are the lowest of all those known so far for clathrochelate iron(II) tris-dioximates. The $\nu_{C=N}$ bands of both types of dioximate fragments distinctly appeared in the case of partially substituted C_3-nonsymmetric complexes. Alongside the ν_{N-O} and ν_{B-O} bands of the macrobicyclic framework, the IR spectra of ribbed-functionalized clathrochelates also contained characteristic lines of the substituents in dioximate fragments [65, 68].

The UV-vis spectra of clathrochelate boron-capped iron(II) complexes contain characteristic absorption bands with maxima at 19 000–23 000 cm^{-1} in the visible and near-UV regions that are essentially nonsymmetric. The same bands have been observed in the reflection spectra of the solid samples. A more intense band ($\varepsilon \sim (2-3) \times 10^4$ mol^{-1}l cm^{-1}) and a less intense one ($\varepsilon \sim 3 \times 10^3$ mol^{-1}l cm^{-1}) have been resolved as Gaussian components. The longwave band is interpreted as a metal-ligand $Md{\rightarrow}L\pi^*$ CTB. The UV intraligand $\pi-\pi^*$ transitions in the spectra for clathrochelate iron(II) tris-dioximates are shifted relative to the UV-vis spectra for the initial dioxime. For macrobicyclic boron-capped iron (II) dioximates, these spectra contain no bands assigned to $d-d$ transitions. These weak bands seem to be masked by extremely intense CTBs observed in the same spectral region.

The position of CTBs in the visible region for the clathrochelate complex correlates with that of the initial dioxime in the UV region (Fig. 19). This correlation confirms the assumption about metal-ligand charge transfer: the position of the highest occupied iron(II) orbital is, in the first approximation, independent of the nature of the substituent in the dioximate fragment. Meanwhile, the decrease in the electron transfer energy in the dioxime molecule reduces the difference in the energies of the iron ion's highest occupied orbital and the ligand's lowest unoccupied orbital and leads to a CTB red shift [50].

The CTB molar absorption coefficient values for macrobicyclic complexes are much (1.5–2 time) higher than that of their nonmacrocyclic analogs. To the contrary, the band half-widths for the latter are markedly higher (Fig. 20) (i.e., when macrobicyclic
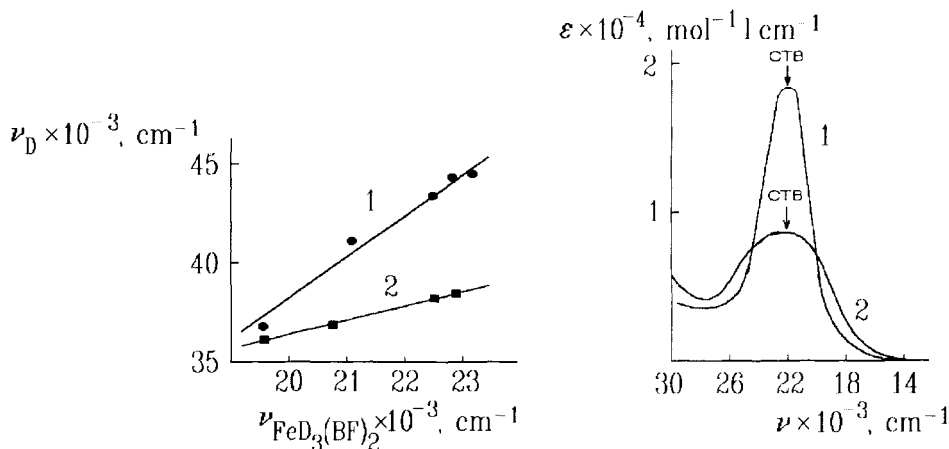
Figure 19. Correlation of CTB v_{max} for $FeD_3(BF)_2$ complexes with an intraligand π,π^* transition band v_{max} for the H_2D molecule (1) and for the HD^- anion (2).

Figure 20. Fragments of UV-vis spectra for $FeNx_3(BOH)_2$ (1) and $[Fe(H_2Nx)_3]SO_4$ (2) complexes in aqueous solution at equal concentrations [56].

complexes are formed, the band integral intensity is retained). A decrease in the CTB half-width in macrobicyclic complexes is accounted for by the increase in the dynamic rigidity of the metal-ligand bonds on encapsulation.

To verify this assumption, the temperature dependence of the Mössbauer parameters (Figs. 21 and 22) were measured for the clathrochelate $FeNx_3(BOH)_2$, $Fe(4MNx)_3(BOH)_2$, and $FeGx_3(BOH)_2$ complexes and their nonmacrocyclic $[Fe(H_2Nx)_3](SO_4)$ analog [56].

The temperature shift ΔV in the Mössbauer lines is described by the equation

$$\Delta V = \Delta V_0 - \frac{3E_\gamma}{4Mc^2}k\Theta_D ctg\left(\frac{\Theta_D}{2T}\right) \tag{47}$$

where Θ_D is the Debye temperature. The Θ_D value was determined for each of the complexes from plots shown in Fig. 21. The Debye temperatures are 600±30K for clathrochelate complexes and 470±30 K for the nonmacrocyclic $[Fe(H_2Nx)_3](SO_4)$ tris-dioximate [56].

In the harmonic approximation of the interatomic forces, the probability of absorption without energy loss (probability of the Mössbauer effect) in crystal can be expressed as

$$f' = \exp\left(-\langle x^2 \rangle 4\pi^2/\lambda\right) \tag{48}$$

where λ is the γ-quantum wavelength and $\langle x^2 \rangle$ is the mean square of the amplitudes of the nuclear vibrations [283].

Moreover, an equation for f', as a function of absorptive crystal temperature, was obtained from the Debye's model for solids:

$$f' = \exp\left\{ -\frac{6R}{K\Theta_D}\left(\frac{T}{\Theta_D} + \frac{\Theta_D}{36T} \right) \right\} \tag{49}$$

where R is the Mössbauer nucleus recoil energy. Taking into account the Θ_D and T values, the $\Theta_D/36T$ ratio may be neglected compared with the T/Θ_D ratio, and the equation assumes the form

$$f' = \exp\left\{ -\frac{6RT}{K\Theta_D^2} \right\} \tag{50}$$

Comparing these two expressions for the Mössbauer effect probability, one obtains the following equation:

$$\langle x^2 \rangle = \frac{6RT\lambda}{4\pi^2 \Theta_D^2} \tag{51}$$

which relates the mean square of the amplitudes of the nuclear vibrations and the square of the Debye temperature. Thus, the higher Debye temperature observed in macrobicyclic complexes
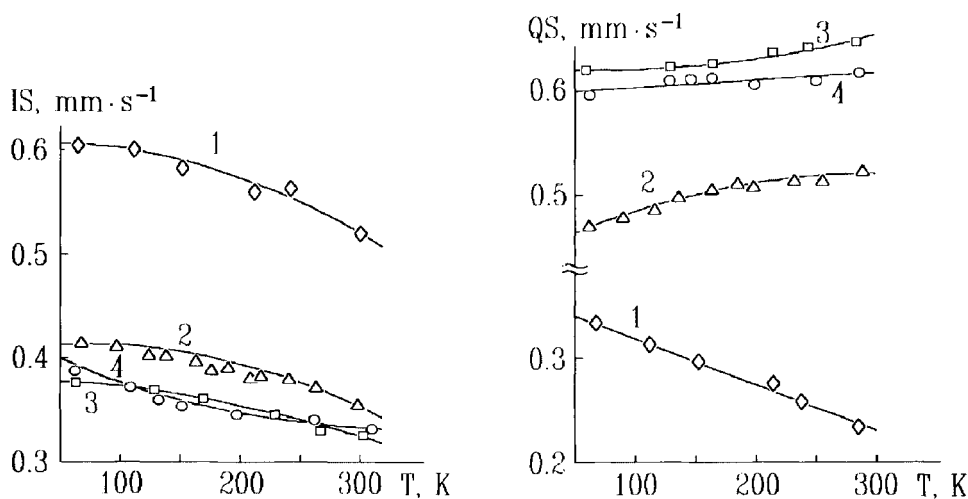
Figure 21. Plots of IS in the ^{57}Fe Mössbauer spectra of [Fe(H$_2$Nx)$_3$](SO$_4$) (1), FeGx$_3$(BOH)$_2$ (2), Fe(4MNx)$_3$(BOH)$_2$ (3), and FeNx$_3$(BOH)$_2$ (4) complexes *versus* temperature [56].

Figure 22. Plots of QS in the ^{57}Fe Mössbauer spectra of [Fe(H$_2$Nx)$_3$](SO$_4$) (1), FeGx$_3$(BOH)$_2$ (2), Fe(4MNx)$_3$(BOH)$_2$ (3), and FeNx$_3$(BOH)$_2$ (4) complexes *versus* temperature [56].

compared with their nonmacrocyclic analogs unambiguously indicates a lowering of the dynamic flexibility of the clathrochelate molecules [56].

Since the main bands in the UV-vis spectra of the macrobicyclic tris-dioximates are stipulated by intraligand $\pi-\pi^*$ transitions in the dioximate fragments (UV range) and the $Md{\to}L\pi^*$ charge transfer (visible range), the UV-vis spectra of the apically functionalized compounds are practically identical to those of clathrochelates with fluoroboronic, hydroxyboronic, and phenylboronic fragments.

The UV-vis spectra of the C_3-nonsymmetric compounds indicate a more complex chromophore system than that of symmetric clathrochelates, while the spectra for boron-capped axial (C_2) nonsymmetric compounds closely resemble those of the corresponding symmetric ones. The UV-vis spectra of the latter with the same dioximate fragments and different boron-containing caps are practically identical. The spectrum of the mixed boron-tin-capped $((n\text{-}C_4H_9)_4N)[FeNx_3(BC_6H_5)(SnCl_3)]$ clathrochelate alone essentially differs from that of the $FeNx_3(BC_6H_5)_2$ complex: apart from a singlet band at $21\,740$ cm^{-1} characteristic of boron-capped compounds, a more intense one appears at $20\,000$ cm^{-1} detectable in the UV-vis spectrum of the trichlorotin-capped tris-nioximate $[FeNx_3(SnCl_3)_2]^{2-}$ dianion. The intensities of these bands are redistributed. An analogous phenomenon was also observed in the spectra of $FeDm_2Bd(BF)_2$, $FeBd_2Dm(BF)_2$, and $FeBd_2Nx(BF)_2$ C_3-nonsymmetric clathrochelates. The intense $Md{\to}L\pi^*$ CTB in the UV-vis spectra of these compounds proved to be a superimposition of two bands with maxima slightly shifted to the longwave region compared with the corresponding symmetric $FeDm_3(BF)_2$, $FeBd_3(BF)_2$, and $FeNx_3(BF)_2$ complexes, but an unusual and unexpected ratio of the intensities of these bands has been observed [64].

The UV-vis spectrum of the $FeBd_2Gm(BF)_2$ complex also proved to be quite unexpected since it contains only one band with an intermediate ν_{max} value ca $21\,550$ cm^{-1}, rather than two bands at $22\,730$ and $20\,880$ cm^{-1}. With this complex, maximal tension in π-systems of different dioximate fragments has presumably been observed. Since UV-vis spectral characteristics of the $FeDm_3(BF)_2$ and $FeGm_3(BF)_2$ complexes are identical in the visible region, the CTB in the spectrum of the nonsymmetric $FeDm_2Gm(BF)_2$ clathrochelate is nearly the same as that of the first two complexes. To the contrary,

the position of intraligand π–π^* transition bands differs from that of symmetric compounds [64].

The UV-vis spectra of hexachloride clathrochelate iron(II) precursors and their functionalized derivatives with C_3-symmetric molecules, like those of all symmetric macrobicyclic boron-capped iron(II) tris-dioximates with trigonal-prismatic structure, contain an intense CTB in the visible and near-UV region that has two Gaussian components: the main band at 18 180–22 220 cm^{-1} ($\varepsilon \sim$ 1–2×10^4 mol^{-1}l·cm^{-1}) and an additional one at 23 260–25 640 cm^{-1} with essentially less intensity ($\varepsilon \sim$ 3–7×10^3 mol^{-1}l·cm^{-1}). In the case of hexachloride precursors, phenoxyl and symmetric oxocrown ether compounds, the main band has an appreciable (up to 2000 cm^{-1}) UV shift compared with that of sulphur-containing complexes. The bands of intraligand π–π^* transitions for sulphur-containing dioximate fragments in the UV region have a longwave shift (and, therefore, are lower in energy) compared with chlorine- and phenoxy-containing dioximate fragments. As mentioned above, for the first approximation, the energy level of the highest occupied iron(II) d-orbitals is independent of the nature of the substituent in the dioximate fragment, and the position of the CTB is a function of levels of π^* orbitals of this fragment. The decrease in the π–π^* transition energy in the dioximate fragment leads to decreasing CT energy in the iron(II) complex and to a longwave shift of the corresponding band. The main band in the UV-vis spectra of the meridional (C_3) nonsymmetric n-butylamine complex and partially substituted oxocrown ether clathrochelate split into two bands of approximately equal intensity. An analogous phenomenon was mentioned above for the spectra of other C_3-nonsymmetric iron(II) dioximates [65].

A single intense CTB Md→Lπ^* with v_{max} intermediate between those found in the corresponding C_3-symmetric clathrochelate tris-dioximates was evident in the visible region of the UV-vis spectra of C_3-nonsymmetric monoribbed-functionalized iron(II) clathrochelates. The position of the CTB in the UV-vis spectra depends somewhat on the nature of the capping group, and therefore the resemblance of the v_{max} for the monoribbed-functionalized clathrochelates and those for the FeBd$_3$(BF)$_2$ complex is obvious, unlike the v_{max} for triribbed-functionalized clathrochelates. This indicates that the influence of two diphenylglyoximate fragments on the electronic system of a highly conjugated macrobicyclic ligand predominates over that of the functionalized fragment [68].

Among the amine-functionalized clathrochelates, the shape of the UV-vis spectra, typical for symmetric boron-capped tris-dioximates, has been observed only in the case of the amine derivatives of a dichloride $FeBd_2(Cl2Gm)(BF)_2$ precursor. Their spectra indicate that the contributions of two diphenylglyoximate fragments distinctly dominate over the contribution of the amine one [69]. The UV-vis spectra of the amine derivatives of hexachloride iron(II) precursors significantly differ from the spectra mentioned: three lines of similar intensity ($\varepsilon \sim 4$–8×10^3 $mol^{-1}l \cdot cm^{-1}$) have been detected in the visible region. Therefore, the π-systems of nonequivalent dioximate fragments in these clathrochelates are relatively independent, and their contributions to the CTB are the same [69].

The UV-vis spectrum of the clathrochelate nickel(II) $[NiDm_3(ttnFe)_2]^{2+}$ tris-dioximate in solution contains an intense ($\varepsilon = 6.9 \times 10^3$ $mol^{-1} \cdot cm^{-1}$) CTB $Md \rightarrow L\pi^*$ at 22 520 cm^{-1} and a band of the d–d transition at 11 760 cm^{-1} ($\varepsilon = 448$ $mol^{-1}l \cdot cm^{-1}$). A relatively high value of ε in the latter case compared with that of the octahedral nickel(II) complexes is accounted for by a distortion in the coordination polyhedron symmetry to a TP [80].

In the ^1H NMR spectra of the $FeD_3(BR)_2$ complexes (Table 21), the chemical shift of the aliphatic group protons increases by 0.1÷0.5 ppm compared with that of the initial dioxime, which is indicative of the overall electron density redistribution in the ligand bond system due to charge transfer from the ligand to the metal ion and the change in ligand conformation. The signals of the methine protons in acyclic dioximates and the signals of the α-methylene protons in alicyclic dioximates are the most sensitive to complexation, which correlates with IR data. The somewhat broadened singlet lines of alicyclic group protons have been observed in the spectra of macrobicyclic nioximes, heptoximes, and octoximes. Such line shapes in most sterically unhindered cycloalkanes with large rings suggest their dynamic character: no spin-spin interactions between nonequivalent methylene units have been observed because the cycloalkane ring conformation changes readily at room temperature. Introduction of a methyl substituent into the cyclohexane ring hampers conformational transitions. The ^1H NMR spectra of 4-methylnioxime and its complexes distinctly show a spin-spin interaction. The spectra for complexes with alkyl-, aryl-, and alkoxyboron-containing capping fragments also contain the signals from the substituents at the capping boron atom [49, 59-61].

Table 21.
Parameters of ^{1}H, ^{13}C{^{1}H}, and ^{11}B NMR spectra (ppm) for fluoroboron-capped clathrochelate iron(II) tris-dioximates and the initial dioximes [56, 263].

Compound	^{13}C relative to TMS			^{1}H relative to TMS		^{11}B relative to NaB(C$_6$H$_5$)$_4$ ($J_{11_B-19_F}$, Hz)
	H–C=N	R–C=N	R	H–C=N	R	
FeGm$_3$(BF)$_2$	143.10			8.27		10.30 (15.7)
H$_2$Gm	145.31			7.77		
FeMm$_3$(BF)$_2$	145.41	152.29	13.41	7.18	2.36	10.33 (14.7)
						10.38 (14.7)
H$_2$Mm	147.29	151.73	9.11	7.65	1.92	
FeDm$_3$(BF)$_2$		153.15	13.12		2.26	10.38 (14.2)
H$_2$Dm		152.98	9.22		1.97	
FeBd$_3$(BF)$_2$		156.62	127.81		1.37	10.24 (11.7)
			129.17			
			129.98			
			130.87			
H$_2$Bd		155.19	127.48		7.37	
			127.81			
			128.88			
			132.81			
FePhm$_3$(BF)$_2$	147.07	151.55	128.47	8.86	7.39	10.49 (15.3)
			129.58		7.56	
			130.79			
H$_2$Phm		150.82	127.63	8.53	7.33	
			128.44		7.54	
FeNx$_3$(BF)$_2$		152.47	20.65		1.74	10.35 (13.7)
			25.76		2.81	
H$_2$Nx		151.81	21.86		1.56	
			24.66		2.51	
FeGx$_3$(BF)$_2$		154.38	25.00		1.67	10.35 (14.1)
			26.46		2.76	
			29.55			
H$_2$Gx		156.33	23.22		1.53	
			26.06		2.41	
			28.57			
FeOx$_3$(BF)$_2$		158.64	26.40		1.37	10.10 (14.1)
			26.67		1.59	
			28.57		2.99	
H$_2$Ox		156.31	24.18		1.45	
			26.09		2.50	
			26.50			

If ^{1}H NMR spectra showed an essential deshielding of cycloalkane ring protons on complexation, the ^{13}C NMR chemical shifts changed substantially less and were even different in sign for α- and β-methylene unit carbons in the case of alicyclic dioximates. The relative shift for carbon atoms in the substituted and unsubstituted oxime groups of the acyclic dioximes on complexation was also different in sign. For acyclic dioximates, the chemical shift for the substituent lines is substantially varied on complexation. This was attributed to the change in the dioxime conformation: initial acyclic *trans*-dioximes assume a *cis*-configuration, and corresponding lines in the ^{13}C NMR spectra essentially shift (up to 4 ppm) [56].

The ^{11}B NMR spectra for fluoroboron-capped complexes exhibited a doublet, which appears due to the spin-spin [11]B–[19]F interaction in the cross-linking BO_3F fragments. The chemical shift value ($\delta_{NaB(C_6H_5)_4}$ = 10–12 ppm) suggests a tetrahedral coordination of the capping boron atoms, and small $J_{^{11}B-^{19}F}$ values (*ca* 10–15 Hz) indicate a high symmetry of this coordination polyhedron. The ^{11}B NMR spectra for the $FeD_3(BR)_2$ complexes, where R ≠ F, H, contained a singlet with the same chemical shift broadened due to an interaction between boron atoms and substituent protons [56]. The line half-widths for $FeNx_3(BR)_2$ complexes change greatly depending on the nature of the substituent at the boron atom (from 0.013 to 2.7 ppm for $FeNx_3(BF)_2$ and $FeNx_3(Bn-C_4H_9)_2$ clathrochelates, respectively). This also confirmed a high symmetry of the fluoroboron capping groups. Meanwhile, attempts to correlate the ^{11}B NMR chemical shift with substituent electronegativity (according to the Pauling and Milliken-Jaffe principle) led no results (first, for hydridoboron-capped clathrochelate) [52].

The multinuclear NMR data confirmed the composition and structure proposed for the nonsymmetric clathrochelate iron(II) tris-dioximates, first, using the integral intensity ratios of the signals in the ^{1}H NMR spectra of the protons in the dioximate fragments, substituents at the boron atom, and the tetra-*n*-butylammonium cation (for the mixed boron-tin-capped complex). The ^{1}H NMR spectrum of the C_2-nonsymmetric $FeDm_3(BC_6H_5)(BF)$ dimethylglyoximate also reveals the nonequivalence of methyl substituents. The nonequivalence of dioximate fragments in C_2-nonsymmetric clathrochelates is still more pronounced in the ^{13}C{^{1}H} NMR spectra (Table 17). The ^{11}B NMR spectra for these complexes (except for the mixed boron-tin-capped complex) reveal signals for both the caps: a

broadened singlet of alkyl- or arylboronate fragments and a doublet of fluoroboron capping tetrahedral fragments (judging from the δ_{11_B} value). The values of $J_{11_B-19_F}$ spin-spin coupling constant (*ca* 15 Hz) indicate a high symmetry of the BO_3F fragments. The same symmetry of fluoroboron capping fragments has been detected in C_3-nonsymmetric clathrochelates (Table 17). In the ^{119}Sn NMR spectra of the mixed boron-tin-capped compound, an octahedral SnO_3Cl_3 fragment manifests itself as a singlet ($\delta_{119_{Sn}} = -660$ ppm), which is slightly different from the chemical shift value in the case of a symmetric $[FeNx_3(SnCl_3)_2]^{2-}$ dianion ($\delta_{119_{Sn}} = -640$ ppm).

The nonadditivity effect of the introduction of α-benzyldioximate fragments instead of dimethylglyoximate ones in the ^1H NMR spectra of the C_3-nonsymmetric mixed α-benzyldioximate–dimethylglyoximate complexes was clearly observed: the introduction of the first fragment increases chemical shifts of the methyl protons by approximately 0.2 ppm, while the appearance of the second diphenyl chelate ring increases the shifts by only 0.06 ppm (Table 17) [64].

The ^1H and ^{13}C {^1H} NMR spectra of apically functionalized boron-capped iron(II) clathrochelates are enriched by the signals assigned to functionalizing substituents: the hexadecyl fragment at 0.5–1.3 ppm (^1H), 14–33 ppm ($^{13}C\{^1H\}$) and the allyl one at 1.6 (CH_2), 5.0 (CH_2=); 6.0 (–CH=) ppm (^1H), 24 (CH_2); 112 (CH_2=); and 138 (–CH=) ppm ($^{13}C\{^1H\}$) [67].

The ^1H and ^{13}C NMR spectra of the di- and hexachloride clathrochelate precursors and the ribbed-functionalized complexes also confirmed their composition and the symmetry of the molecule (the presence or absence of the C_3 symmetry axis passing through boron capping atoms and the iron ion). The integral intensity ratio of the signals of the substituents at capping atoms and in dioximate fragments in ^1H NMR spectra for these clathrochelates was in agreement with the supposed composition [65, 68].

In the case of ^{13}C NMR spectra, despite the electron-accepting character of the chlorine substituent, the chemical shift of the carbon atoms in the azomethine groups of dichloroglyoxime, hexachloride precursors, and chloro- and dichloroglyoximate fragments of clathrochelates was unusually low ($\approx$125 ppm). For aromatic, acyclic, and alicyclic dioximes and their complexes, as well as in the case of the ribbed-functionalized clathrochelates, the δ_{13_C}(C=N) signals were observed in the range 150÷160 ppm with the exception of glyoxime

and its derivatives, for which $\delta_{13_C}(C=N) \approx 140-150$ ppm. An extraordinarily low value of $\delta_{13_C}(C=N)$ for chloroglyoximates once more confirmed the predominance of a paramagnetic contribution over a diamagnetic one in the chemical shift value on the ^{13}C nucleus and correlated with a decrease in the frequency of the C=N bond stretching vibrations in the IR spectra (see above) [65, 68].

The high selectivity of macrobicyclic boron-capped iron(II) dioximate formation and the stability of these compounds may be attributed to a favourable action of the main factors that govern the metal ion capability to form macrobicyclic clathrochelate compounds:

(a) In the high ligand field with symmetry D_3 generated by six nitrogen donor atoms of three dioximate fragments, the t_{2g} binding level is fully occupied, ensuring a high stability of electronic configuration d^6 of the encapsulating iron(II) ion.

(b) According to Pearson's HSAB principle [284], the nitrogen donor atoms possess the best affinity for an iron(II) ion, which leads to an essential gain in energy on formation of N_6-complexes.

(c) The fact that the size of the macrobicyclic ligand cavity fits that of the low-spin iron(II) ion can be interpreted in terms of physical ionic (Shannon) radii, depending on the coordination number and ion spin state. X-ray diffraction data indicate that the M–N distance in such macrobicyclic complexes is ca 1.9 Å, which (with allowance for the nitrogen physical radius) provides the optimal metal ion physical radii of 0.6÷0.7 Å. Similar values are observed for low-spin iron(II) and cobalt(III) complexes (0.75 and 0.69 Å, respectively). Hexacoordinate nickel and copper(II) ions have a higher physical radius and cannot be encapsulated in this macrobicyclic ligand cavity. The presence of conjugated π-bonds in dioximate fragments and the rigidity of a boron-containing capping fragment are responsible for the rigidity of these clathrochelate ligands. Thus, the number of metal ions for which boron-capped tris-dioximates can be formed is sharply restricted [56].

The crystallographic data for $CoNx_3(Bn-C_4H_9)_2$, $FeNx_3(Bn-C_4H_9)_2$, and $RuNx_3(Bn-C_4H_9)_2$ clathrochelates displayed an unexpected trend in distortion angle φ values (Co < Ru < Fe) that is different from predicted by LFSE factors (Co < Fe < Ru) [259]. Surprisingly, the φ value for ruthenium(II) clathrochelate is approximately one half of the φ for iron(II) clathrochelate. Another striking feature of this ruthenium(II) complex is the unusually short Ru–N bond length (ca

1.97 Å) compared with the one estimated from the magnitude of the physical ionic radius (r_i for ruthenium(II) ion is *ca* 0.88 Å; the Co–N distance is *ca* 1.94 Å at r_i = 0.79 Å, and the Fe–N distance is *ca* 1.92 Å at r_i = 0.75 Å). This value of the Ru–N distance was explained by the presence of substantial π-backbonding between the low-spin ruthenium(II) ion with electronic configuration d^6 and the α-dioximate chelating fragments. Thus, the typical considerations of LFSE, ligand features, and metal ion size as well as pure π-backbonding effect cannot rationalize the φ values for the clathrochelates mentioned. LFSE considerations in combination with π-backbonding effects were used to interpret the experimental results [259].

The structures of one clathrochelate precursor and two macrobicyclic ribbed-functionalized ruthenium(II) tris-dioximates were determined by X-ray analysis (Table 16). The Ru–N distances (1.98÷1.99 Å) are longer than the Fe–N ones (1.90 – 1.91 Å), but the increase (0.07 ÷0.08 Å) is not significant. A similar variation in the metal-nitrogen distance has also been observed in the series of nioximate clathrochelates (see above): judging from the magnitude of the physical ionic (Shannon) radius of a low-spin Ru^{2+} ion in an octahedral environment, one might have expected a more significant increase in the M–N distance. However, such an increase is impeded by strong π-backbonding effects in the ruthenium(II) complexes. The increase in the metal-nitrogen distance in ruthenium complexes led to a decrease in the magnitude of the distortion angle φ of the coordination polyhedron. The variation in geometry of a coordination polyhedra in passing from iron complexes to their ruthenium analogs may be described as a rotary-translational expansion that gave rise to a considerable (0.06–0.09 Å) increase in the h distance and, consequently, to an increase in the size of a macrobicyclic ligand cavity. In the series of both iron and ruthenium compounds, the maximal distance between the coordination polyhedron bases and minimal distortion angle φ (and, consequently, a maximal cavity size) were observed for hexachloride precursors. Their functionalized derivatives have greater distortion angles φ and smaller h values (Table 16) [78].

The UV–vis spectra of the ribbed-functionalized ruthenium(II) complexes exhibited bands of high intensity in the visible region, characteristic of clathrochelates. A shortwave shift of such asymmetric Rud→Lπ^* CTBs proved to be 800÷1500 cm^{-1} compared

with the position of CTBs in analogous iron complexes. The CTBs in C_3-symmetric ruthenium complexes were decomposed into three Gaussian components: two of less intensity at the edges and one of higher intensity in the centre. The CTBs in the UV–vis spectra of the sulphur-containing ruthenium(II) clathrochelates are substantially (by ca 3000 cm^{-1}) shifted compared with their hexachloride precursors. At the same time, the oxygen-containing substituents in dioximate fragments had practically no effect on the position of the CTB. In passing from iron(II) to ruthenium(II) complexes, the position of bands of high intensity in the UV region, stipulated by the π–π* transitions in dioximate fragments, changed negligibly as well [78].

The spectral characteristics of the boron-capped ruthenium(II) RuNx$_3$(BC$_6$H$_5$)$_2$ dioximate nearly coincide with those of the analogous iron(II) complex. Only a shift of the characteristic CTB in the UV-vis spectrum of the RuNx$_3$(BC$_6$H$_5$)$_2$ complex in the UV region was observed (ν_{max} = 25 100 cm^{-1}, ε = 1.8×10^4 mol^{-1}·cm^{-1}) compared with that of the FeNx$_3$(BC$_6$H$_5$)$_2$ complex (ν_{max} = 22 300 cm^{-1}, ε = 1.7×10^4 mol^{-1}·cm^{-1}) [76].

The composition of the ribbed-functionalized ruthenium(II) clathrochelates was first confirmed by ^{1}H and ^{13}C NMR spectroscopy (the integral intensities of functionalizing and apical substituent protons in the ^{1}H NMR spectra, the number of the signals in the ^{13}C NMR spectra was in accordance with the proposed composition and symmetry of the molecule). A small (from 1 to 2 ppm) systematic decrease in the chemical shift of the signals assigned to azomethine fragments in the ^{13}C NMR spectra of ruthenium complexes compared with their iron-containing analogs was noted in Ref. 78. A substantial (from 30 to 40 cm^{-1}) systematic short-frequency shift in the stretching vibrations $\nu_{C=N}$ of such fragments was also observed in the IR spectra of the ruthenium(II) complexes compared with iron(II) compounds. The magnitudes of chemical shifts and spin-spin interaction constants ($J_{^{11}B-^{19}F}$ ≈ 15 Hz) in the ^{11}B NMR spectra of a fluoroboronic Ru(Cl2Gm)$_3$(BF)$_2$ precursor and its ribbed-functionalized derivatives confirmed a tetrahedral character of the apical boron atom coordination polyhedron and a high symmetry of the O$_3$BF moiety [78].

Tin-, antimony- and germanium-capped iron dioximates

The spectral characteristics for tin-, germanium-, and antimony-capped macrobicyclic iron(II) dioximates differ greatly from those of the corresponding boron-capped complexes discussed above.

This refers especially to the parameters of the UV-vis and Mössbauer spectra, which are determined by the coordination polyhedron geometry and electron density distribution on the metal ion and nitrogen donor atoms.

The ^{57}Fe Mössbauer parameters for the tin-, germanium-, and antimony-capped clathrochelate compounds (Tables 22-24) are typical low-spin iron(II) complexes. The increase in the ligand field strength (a "macrocyclic" effect), causes the increase in s-electron density on the iron nucleus, is less pronounced for these compounds than for their boron-capped analogs: experimental ISs are only slightly lower than those calculated from a PIS concept.

The coordination polyhedron geometry of tin-, antimony- and germanium-capped iron(II) dioximates was analyzed in the previous section. As mentioned above, the boron-capped clathrochelates have a distorted TP structure and positive QS values, whereas tin-, antimony- and germanium-capped clathrochelates have distorted TAP geometry, preferably for complexes with electronic configuration d^6, and a negative QS sign.

The solution UV-vis spectra of the monomeric clathrochelate tin-, germanium-, and antimony-capped complexes (Tables 23 and 25) and the UV-vis reflection spectra of the germanium-capped polymeric clathrochelates (Table 22) are appreciably different from those for the FeD$_3$(BR)$_2$ complexes and resemble the spectra for iron(II) tris-phenanthrolinates and tris-bipyridinates [236]. In the visible region, two metal-ligand CTBs at 17 560–18 480 and 20 560–21 320 cm^{-1}

Table 22.

Parameters of IR, UV- vis (cm^{-1}), and ^{57}Fe Mössbauer spectra (mm·s^{-1}) for polymeric germanium-capped iron(II) dioximates [72].

Compound	ν (C=N)	ν (N–O)	$\nu_{max} \times 10^{-3}$	IS	QS
[H$_2$FeGm$_3$(Ge$_2$O$_3$) · iso-C$_3$H$_7$OH]$_n$	1548	882, 116	19.44, 21.24	0.34	0.10
[H$_2$FeMm$_3$(Ge$_2$O$_3$) · 5H$_2$O]$_n$	1572	920, 1122	20.00, 21.72	0.31	0.24
[H$_2$FeDm$_3$(Ge$_2$O$_3$) · DMF]$_n$	1572	964, 1070	19.50, 21.40	0.31	0.22
[H$_2$FeNx$_3$(Ge$_2$O$_3$) · DMSO]$_n$	1572	968, 1040	19.20, 21.20	0.32	0.35
[H$_2$FeBd$_3$(Ge$_2$O$_3$) · DMF]$_n$	1578	942, 1064	20.60	0.33	0.24

Table 23.

Characteristics of ^{57}Fe Mössbauer (mm·s^{-1}), UV-vis (ν_{max}, cm^{-1}; ε, mol^{-1}l·cm^{-1}), ^{1}H, ^{19}F and ^{13}C{^{1}H} NMR (ppm), and IR (cm^{-1}) spectra of antimony- and germanium-capped iron(II) clathrochelates [73, 74].

Compound	ν(C=N)	ν(N–O)	$\nu_{max}\times10^{-3}$ ($\varepsilon\times10^{-3}$)	^{1}H relative to TMS			^{13}C relative to TMS				IS	QS
				$^{a}R^{1}$	$^{a}R^{2}$	^{b}R	$^{a}R^{1}$	$^{a}R^{2}$	C=N	^{b}R ($J_{^{13}C-^{19}F}$, Hz)		
[FeDXO$_3$(Sb(C$_6$H$_5$)$_3$)](BF$_4$)	1583 1630	1084m	41.15(9.2), 34.48(13) 30.96(2.3), 21.46(3.6) 19.01(3.0)	2.00	2.27	7.37m 7.65m	13.2	13.7	153.0 159.0	128.1 129.2 134.8 147.4	0.42	0.36
[FeDXO$_3$(Sb(C$_6$H$_5$)$_3$)(HCOC$_2$H$_5$)$_3$](BF$_4$)	1578 1617	1083m	38.76(13), 33.67(18) 27.47(3.4), 21.19(2.9) 18.42(3.3)	2.03	2.27	1.30m 4.21m 7.36m 7.67m	14.0	14.2	159.8 165.4	16.7 64.0 128.5 129.5 134.8 146.2 156.2	0.41	0.49
FeNx$_3$(Sb(C$_6$H$_5$)$_3$)$_2$	1560	908 1054	40.49(18), 33.22(16) 30.96(4.9), 21.10(6.4) 18.35(2.8), 17.09(2.9)	1.50m	2.76m	7.25m 7.66m	21.5	26.4	154.1	127.9 128.8 135.0 149.0	0.33	0.22
FeNx$_3$(Sb(CH=CH$_2$)$_3$)$_2$	1572	910 1049	34.25(11), 31.45(3.0) 21.14(5.6), 18.55(2.1) 17.27(3.0)	1.64m	2.83m	6.08m 6.62m	21.3	26.3	156.0	130.7 146.9	0.33	0.17

FeNx₃(Sb(C₂H₅)₃)₂	1570	912	33.11(17), 20.96(7.2)	1.56m	2.83m	1.21m	21.9	25.8	152.2	10.4		0.36	0.27
		1053	18.32(3.6), 17.01(5.1)			2.51m				24.0			
((n-C₄H₉)₄N)₂[FeNx₃(Ge(CF₃)₃)₂]	1566	992	48.54(42), 40.98(23),	1.49m			22.7		151.2	137.3(363)		0.32	0.19
		1074m	34.25(7.6), 29.85(2.9),	2.68m			26.1		$\delta_{^{19}F} = -54.5$				
			21.32(6.7), 19.08(3.9)										
			17.95(3.0)										
[FeDXO₃(Ge(CF₃)₃)]·O(C₂H₅)₂	1587	992	46.51(27), 34.97(14),	2.26			13.6		154.0	136.6(360)		0.41	0.23
	1615	1025	31.15(35), 21.93(5.8),	2.34			14.3		157.2	$\delta_{^{19}F} = -55.0$			
		1080	19.80(7.4)	6.34									
				(NH₂)									
[FeDXO₃(Ge(CF₃)₃)(CH₂)₃]	1563	996	46.54(20), 37.31(10),	2.31	3.65d		13.1	76.4	154.2	136.3(368)		0.38	0.58
	1617	1032	25.71(1.7), 20.04(5.1),	2.33	5.37d		13.3		167.6	$\delta_{^{19}F} = -54.5$			
		1076	17.86(2.7)										
[FeDXO₃(Ge(CF₃)₃)(HCOC₂H₅)₃]	1560	994	46.54(32), 34.84(13),	2.27	1.35t		13.6	16.3	158.2	136.1(356)		0.40	0.47
	1620	1034	26.38(1.6), 20.79(3.5),	2.30	4.31q		14.4	64.0	165.1	$\delta_{^{19}F} = -54.5$			
		1080	18.87(5.1)		7.28			156.6					
[Fe₂DAO₃(Ge(CF₃)₃)₂]	1565	989	46.30(45), 40.82(21),	2.28			13.2		157.4	135.5(336)		0.35	0.49
		1044	34.13(27), 28.90(10),	2.35			17.3		171.2	$\delta_{^{19}F} = -53.8$			
		1082	24.15(4.3), 19.31(14)										

[a] Different substituents in dioximate and oximehydrazonate fragments.   [b] Substituents in the capping groups.

Table 24.

Parameters of ^{1}H, ^{13}C(^{1}H), ^{119}Sn, and ^{19}F NMR (ppm) and ^{57}Fe, and ^{119}Sn Mössbauer (mm·s^{-1}) spectra of tin-capped iron(II) tris-dioximates [70, 71].

Compound	^{1}H relative to TMS		^{13}C relative to TMS			^{119}Sn relative to Sn(CH$_3$)$_4$	^{19}F relative to C$_6$F$_6$ ($J_{^{119}Sn-^{19}F}$, Hz)	^{57}Fe		^{119}Sn
	H–C=N	R	H–C=N	R–C=N	R			IS	QS	IS
(HPy)$_2$[FeGm$_3$(SnBr$_3$)$_2$]	7.78		143.78			−970		0.37	0.32	0.57
(HDEA)$_2$[FeMm$_3$(SnBr$_3$)$_2$]	7.80m	2.22m	145.35, 145.60, 145.86	153.34, 153.67, 154.00	12.90m	−980m		0.33	0.33	0.58
(HDEA)$_2$[FeMm$_3$(SnF$_3$)$_2$]	7.85m	2.40m	146.84m	153.95m	12.31m	−758m	9.8 (2030), 11.2 (2030)	0.35	0.27	
(HPy)$_2$ [FeDm$_3$(SnBr$_3$)$_2$]		2.45		155.50	12.5	−996		0.33	0.38	0.60
(HDEA)$_2$[FeDm$_3$(SnF$_3$)$_2$]		2.46		154.67	12.71	−759	12.9 (2060)			
(HPy)$_2$[^{57}FeDm$_3$(SnF$_3$)$_2$]		2.44		155.34	13.13	−758	13.7 (2030)	0.36	0.25	
(HDEA)$_2$[FeNx$_3$(SnBr$_3$)$_2$]		1.44, 1.72, 2.68, 2.92		155.20	20.42, 25.3	−998		0.36	0.00	0.63
(HDEA)$_2$[FeNx$_3$(SnF$_3$)$_2$]		1.43, 1.62, 2.47, 2.67		154.82	20.43, 25.13	−763	13.7 (2030)	0.38	0.18	−0.01
(HDEA)$_2$[FeGm$_3$(SnCl$_3$)$_2$]	7.74		144.72			−625		0.35	0.25	0.44
(HDEA)$_2$[FeMm$_3$(SnCl$_3$)$_2$]	7.74m	2.25m	146.59m	154.84m	12.98m	−631m		0.36	0.28	0.42

(HDEA)$_2$ [FeDm$_3$(SnCl$_3$)$_2$]	2.29	156.06	12.68	−637	0.34	0.31	0.38
(HDEA)$_2$[FeBd$_3$(SnCl$_3$)$_2$]	7.23m, 7.42m	157.62	127.21, 128.35, 130.57, 131.60	−634	0.34	0.31	0.41
(HDEA)$_2$[FeNx$_3$(SnCl$_3$)$_2$]	1.52m, 1.78m, 2.47m, 2.92m	156.14	21.31, 26.09	−637	0.37	0.20	0.43
(HPy)$_2$[FeNx$_3$(SnCl$_3$)$_2$]	1.45m, 1.70m, 2.66m, 2.87m	154.96	21.09, 25.79	−640	0.38	0.18	0.43
(HDEA)$_2$[Fe(4MNx)$_3$(SnCl$_3$)$_2$]	1.02, 1.77m, 2.08, 2.20m, 2.54m, 3.13m	155.40 155.69	19.81, 20.22, 24.41, 25.14, 27.47, 27.86, 33.16, 33.59	−637	0.36	0.24	0.46
(HDEA)$_2$[FeOx$_3$(SnCl$_3$)$_2$]	1.22, 2.15÷2.30m	161.48	22.23, 25.66, 30.38	−634	0.37	0.36	0.42

with a similar intensity ($\varepsilon \sim 5$–10×10^3 mol^{-1}l·cm^{-1}) have been detected for the mentioned clathrochelates compared with one intense ($\varepsilon \sim 2$–3×10^4 mol^{-1}l·cm^{-1}) asymmetric CTB in the range 19 000–23 000 cm^{-1} for boron-capped complexes. Correlation of these band positions with π–π^* transition in the initial dioximes is clearly observed. The UV bands in the spectra of the tin-, germanium-, and antimony-capped clathrochelate complexes were assigned to either intraligand π–π^* transitions or a charge transfer from the iron(II) d-orbitals to the second accepting π^* level of the ligand [70-74, 236].

Thus, some specific features of the UV-vis spectra for the tin-, germanium-, and antimony-capped complexes suggest that their coordination polyhedra have a TAP geometry (close to an octahedral one) approaching the geometry of the iron(II) tris-phenanthrolinates and tris-bipyridinates. The main specific feature in the UV-vis spectra of the low-spin iron(II) tris-dioximates proves to be a highly intense Md→Lπ^* CTB observed in the visible region. This masks the low-intensity bands of d–d transitions for a Fe^{2+} ion [236]. For TAP complexes in the visible region, this proves a superimposition of two or more CTBs of similar intensity ($\varepsilon \sim 3$–5×10^3 mol^{-1}l·cm^{-1}) has been observed, whereas the TP compounds are characterized by the presence of one asymmetric band with a higher intensity ($\varepsilon \sim 2$–3×10^1 mol^{-1}l·cm^{-1}).

The ^{119}Sn Mössbauer spectra of tin-capped complexes contain a singlet with nearly the same QS as that for the corresponding K$_2$SnHal$_6$ salts. This suggests that the capping tin atoms have an octahedral environment. The IS values increase in the cross-linking group order:

$$SnO_3F_3 < SnO_3Cl_3 < SnO_3Br_3,$$

This is due to a decrease in the electron-accepting properties of halogenide substitutents and, hence, leads to an increase in the s-electron density on the tin atom nucleus (a similar effect was observed for tin(IV) tetrahalides). The ^{119}Sn NMR chemical shift values increase in the halogen series Br < F < Cl (Table 24), which is different from the previous order. Similar results were discussed above for cobalt(III) compounds and were explained by a predominance of the paramagnetic component in the ^{119}Sn NMR chemical shift.

For complexes with nonsymmetric methylglyoxime, the nonequivalence of capping tin atoms was detected. The ^{119}Sn NMR spectra of the nonsymmetric (HDEA)$_2$[FeMm$_3$(SnHal$_3$)$_2$] methylgly-

Table 25.
Characteristics of IR (cm^{-1}) and UV-vis (ν_{max}, cm^{-1}; ε, mol^{-1}l·cm^{-1}) spectra of the macrobicyclic tin-capped iron(II) dioximates [70, 71].

Compound	ν(C=N)	ν(N–O)	ν(Sn–Cl)	$\nu_{max} \times 10^{-3}$ ($\varepsilon \times 10^{-3}$)
(HDEA)$_2$[FeNx$_3$(SnCl$_3$)$_2$]	1568	968, 1046	310	17.92 (6.16), 20.88 (7.16) 33.56 (17.3)
(HPy)$_2$[FeNx$_3$(SnCl$_3$)$_2$]	1572	958, 1052	312	18.00 (5.85), 20.88 (6.92) 33.56 (16.7)
(HDEA)$_2$[FeGm$_3$(SnCl$_3$)$_2$]	1544	996, 1122	318	18.48 (4.53), 21.24 (4.88) 32.84 (16.8)
(HDEA)$_2$[FeMm$_3$(SnCl$_3$)$_2$]	1570	918,1126	316	18.36 (5.15), 21.24 (5.71) 33.40 (17.5)
(HDEA)$_2$[FeDm$_3$(SnCl$_3$)$_2$]	1580	966, 1074	314	18.16 (4.95), 21.32 (5.66) 34.08 (15.4)
(HDEA)$_2$[FeBd$_3$(SnCl$_3$)$_2$]	1578	892, 1094	318	17.56 (9.41), 20.56 (11.4) 35.00÷36.00sh (26.0)
(HDEA)$_2$[Fe(4MNx)$_3$(SnCl$_3$)$_2$]	1572	936, 1006 1080	306	17.92 (5.64), 20.88 (6.49) 33.52 (15.5)
(HDEA)$_2$[FeOx$_3$(SnCl$_3$)$_2$]	1568	954, 1028	312	18.04 (5.85), 21.00 (6.78) 33.80 (15.6)
(HPy)$_2$[FeGm$_3$(SnBr$_3$)$_2$]	1534	840, 1120, 1164		17.84 (3.89), 21.12 (4.31) 32.32 (20.0)
(HDEA)$_2$[FeMm$_3$(SnBr$_3$)$_2$]	1562	916, 1044, 1124, 1224		17.76 (3.81), 21.12 (4.43) 32.80 (18.6)
(HDEA)$_2$[FeMm$_3$(SnF$_3$)$_2$]	1562	920, 1046, 1139, 1230		18.48 (3.76), 21.36 (4.31) 35.30 (20.5)
(HPy)$_2$[FeDm$_3$(SnBr$_3$)$_2$]	1570	964, 1070, 1192		17.44 (4.05), 21.20 (4.62) 33.36 (18.4)
(HPy)$_2$[FeDm$_3$(SnF$_3$)$_2$]	1572	972, 1082, 1196		19.40 (5.70), 21.60 (6.78) 35.44 (20.6)
(HDEA)$_2$[FeDm$_3$(SnF$_3$)$_2$]	1578	968, 1976, 1196		19.04 (5.36), 21.28 (5.72) 35.12 (20.0)
(HDEA)$_2$[FeNx$_3$(SnBr$_3$)$_2$]	1570	968, 1044		18.48 (5.60), 20.96 (6.70) 33.84 (13.8)
(HDEA)$_2$[FeNx$_3$(SnF$_3$)$_2$]	1572	968, 1048		18.96 (7.98), 21.04 (9.16) 34.80 (21.1)

oxime exhibit distinct signals from their *fac-* and *mer*-isomers with the intensity ratios close to statistical ones (1:3): two middle signals of higher intensity correspond to two nonequivalent tin atoms of the *mer*-isomer capping groups, and two lower intensive side signals correspond to *fac*-isomer tin atoms, which differ still more greatly in

arrangement. The chemical shift values for all tin atom types are intermediate between the values for tin-capped iron(II) tris-glyoximates and those for tris-dimethylglyoximates.

Like the cobalt(III) analogs (see above), the δ_{119Sn} for tin-capped iron(II) clathrochelates exhibits additivity of the halogenide substituent amounts. Replacement of one chlorine atom by a bromine atom decreases δ_{119Sn} by 120 ppm, which is clearly shown in Fig. 23. As a result, the ^{119}Sn NMR signals for tribromotin-capped complexes are shifted upfield by 360 ppm relative to signals for their trichlorotin-capped analogs.

The δ_{119Sn} values for trifluorotin-capped complexes are intermediate between $\delta_{119SnO_3Cl_3}$ and $\delta_{119SnO_3Br_3}$. Replacement of one chlorine atom by a fluorine atom increases δ_{119Sn} by 45 ppm. The ^{119}Sn NMR spectra for $(HAm)_2[FeD_3(SnF_3)_2]$ clathrochelates clearly exhibit a spin-spin interaction of the ^{119}Sn nucleus (nuclear spin $I = 1/2$) with three ^{119}F nuclei ($I = 1/2$). As a result, the ^{119}Sn NMR signal has a quartet character with a line intensity 1:2:2:1 and a very high $J_{119Sn-19F}$ constant (2000 Hz) [70].

The ^1H and $^{13}C\{^1H\}$ NMR spectra of the monomeric germanium-, antimony-, and tin-capped iron(II) tris-dioximates (Tables 22 and 23) are also greatly different from the spectra of boron-capped ones. The signals from organic cations appear in the spectra of the clathrochelate germanium-, antimony-, and tin-capped ionic associates. Their integral intensities correspond to the compositions proposed. The ^1H NMR spectra of tin-capped iron(II) tris-dioximates reveal a singlet character of dioximate fragment protons only for
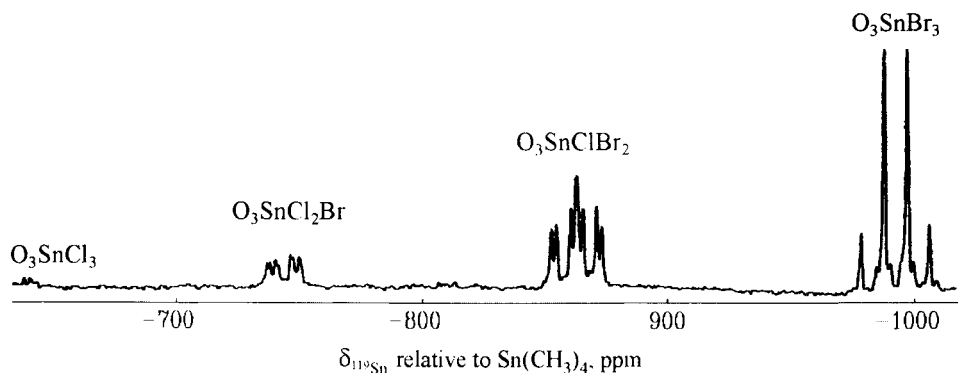

Figure 23. The ^{119}Sn NMR spectrum for macrobicyclic compounds from a $FeCl_2$-$SnBr_4$-H_2Nx-DEA reaction mixture [70].

glyoximates and dimethylglyoximates. The chemical shift of methyl group protons is much lower than that for their boron-capped dimethylglyoximate analogs and practically coincides with the value obtained for the initial dioxime. For the other complexes, the signals from the dioximate fragment protons are multiplets. With the nioximates and α-benzyldioximates, ^{1}H NMR spectra distinctly show that these signals are doubled. In the case of tin-capped complexes, the appearance of such magnetic nonequivalence was explained by the considerable change in the symmetry of their molecules in solution compared with their boron-capped analogs [70, 71].

In addition to the bands assigned to the vibrations in the dioximate fragments, the IR spectra of the $(HAm)_2[FeD_3(SnCl_3)_2]$ complexes contain the characteristic bands of the Sn–Cl bond stretching vibrations in the cross-linking fragment at 306–318 cm^{-1} (Table 25) and a set of stretching and deformation vibrations in the organic cation.

The Sn–F bond stretching vibrations appear in the IR spectra for trifluoroboron-capped clathrochelates from 300 to 500 cm^{-1}. The Sn–Br bond stretching vibrations are usually observed at much lower frequencies and, therefore, were not found in the range studied. Numerous intense bands from 2800 to 3200 cm^{-1} for these complexes are essentially intensified and shifted toward low frequencies. The C=N bond stretching vibrations appear at 1568–1580 cm^{-1} for all tin-capped clathrochelates except for glyoximates (their IR spectra contain $v_{C=N}$ bands at 1534–1544 cm^{-1}, Table 25) [71].

Thus, the structure of tin-, germanium-, and antimony-capped iron(II) tris-dioximates is essentially different from the structure of the corresponding boron-capped ones. This is mainly associated with changes in the geometric and electronic parameters of the capping groups, permitting dioximate fragments to be cross-linked at high distortion angles, optimal for electronic configuration d^6 of the encapsulated iron(II) ion: the physical ionic (Shannon) radius of the hexacoordinate Ge^{4+} cation (0.67 Å) is much higher than that of the tetracoordinate B^{3+} cation (0.25 Å) and is close to the radius of hexacoordinate Sn^{4+} and Sb^{5+} cations (0.84 and 0.74 Å, respectively).

As a result, the geometry of the coordination polyhedron approaches a TAP. Besides, the tin-, germanium-, and antimony-containing cross-linking agents used are weaker Lewis acids than their boron-containing analogs. The former capping agents cause much smaller discrepancies in electron density distribution in the

clathrochelate complexes compared with those observed in nonmacro-cyclic iron(II) tris-dioximates [72].

3.4 POLYENE AND OTHER TYPES OF CLATHROCHELATE COMPLEXES

There are only scarce data available on the spatial and electronic structure of these types of clathrochelates, except for the papers describing the complexes with the binucleating *trom* and azineoximate ligands and the iron(II) and cobalt(III) complexes with hexaene and oximehydrazonate clathrochelate ligands. In all other publications, the data obtained by physical methods have been used mainly to confirm the composition of compounds.

Analysis of the crystal and molecular structure of a copper(II) complex with a pentadentate clathrochelate *penar* ligand showed that the metal ion is completely encapsulated by the ligand and the copper(II) coordination polyhedron has a distorted square-pyramidal geometry with a secondary nitrogen atom in the apical position. This geometry is caused by an internal strain in the macrobicyclic ligand with five- and six-membered chelate rings. The Cu–N distance (2.067 Å) is typical of fivecoordinate amine copper(II) complexes. Despite the possible existence of four diastereomers, the resultant [Cu(penar)](ClO$_4$)$_2$·H$_2$O complex has crystallized in only one diastereomer [204].

An X-ray diffraction study was also performed for one of the iron(II) complexes with hexaene clathrochelate ligands obtained by Reaction 99. The coordination polyhedron in the complex with a hexadentate ligand (X = –(CH$_2$)$_3$–) differs insignificantly (by 5°) from octahedron geometry. This geometry, optimal for a low-spin iron(II) ion with the electronic configuration d^6, was observed in the case of hexaene complexes with saturated and unstrained six-membered chelate cycles, which relatively easily change the conformation. Therefore, these clathrochelate ligands are essentially different from the macrobicyclic boron-capped tris-dioximates with conjugated five-membered chelate cycles, discussed above, whose geometry is mainly determined by the ligand geometry and approaches D_{3h}. The Fe–N distance in this hexaene complex (1.96 Å) is somewhat higher than those in the corresponding macrobicyclic tris-dioximates, which is indicative of a larger ligand cavity size. All chelate rings have "skew" conformations with the

absolute configuration $\Lambda\Lambda\Lambda(\Delta\Delta\Delta)$. A striking feature of this structure proved also to be the unambiguous identification of a *cis*-geometry for rearranged imine donor centres [215].

The *endo-endo* conformations for the tripodal capping amino groups in the free *tranbpy* ligand and its [Ag$_3$(tranbpy)](BF$_4$)$_3$ complex were established [195]. The distances between the apical nitrogen atoms are 14.70 and 14.66 Å, respectively. The free ligand has C_3 symmetry with *anti*-conformation of the bipyridine units, which minimaze lone-pair repulsion. The complex has D_3 symmetry, and all the nitrogen atoms are directed inside *via* coordination to silver(I) ions. The bipyridinate N–N distance decreases from 4.43–4.52 Å in the free ligand to 3.82–3.94 Å in the complex. The Ag–N and Ag...Ag distances are from 2.44 to 2.51 and *ca* 4.90 Å, respectively. The coordination polyhedron of the central silver ion is close to a TAP geometry, whereas two terminal silver(I) polyhedra possess a TP one [195].

The crystal and molecular structure of the macrobicyclic heteronuclear [FeCo(trom)](BF$_4$) complex with the encapsulated high-spin Fe^{2+} and Co^{2+} ions in the strongly distorted coordination polyhedra, intermediate between a TP and a TAP, was described in Ref. 192. The X-ray powder diffraction patterns obtained for other hetero- and homobinuclear complexes of the binucleating *trom* ligand confirmed that they are isomorphic to heterobinuclear [FeCo(trom)](BF$_4$) clathrochelate (except the homobinuclear [Cu$_2$(trom)](BF$_4$)·H$_2$O complex). However, the X-ray data re-refinement, described in Ref. 285, showed that in the study described in Ref. 192, the space group and unit cell were determined incorrectly. This novel refinement allowed one to establish that the encapsulated metal ions, lying on the C_3 axis, are equivalent. All six M–N distances in the complex are 2.17 Å, and the M–O distances are 2.11 Å. It was suggested [285] that the monocrystal chosen for the X-ray diffraction study described in Ref. 192 was an admixture phase and had the [Fe$_2$(trom)](BF$_4$)·H$_2$O composition. A chaotic distribution of iron and cobalt ions between two equivalent coordination centres cannot be excluded either [285].

The temperature-dependent magnetic susceptibility study of the homobinuclear [M$_2$(trom)](BF$_4$) complexes indicated that the magnetic moment decreases substantially with decrease in the temperature. The intramolecular antiferromagnetic exchange between the metal centres was also observed. This interaction occurs

though bridging oxygen atoms rather than by a direct metal-metal interaction, because the metal-metal distance is *ca* 3 Å [192].

The ^{57}Fe Mössbauer parameters for the clathrochelate [FeMn(trom)](BF$_4$) and [Fe$_2$(trom)](BF$_4$) complexes are characteristic of high-spin iron complexes. The spectrum of the [FeMn(trom)](BF$_4$) clathrochelate exhibits one doublet line, which indicates the sole type of coordination centre. The QS value increases regularly with a temperature decrease. A major contribution to the QS value is made by the valence component (the lattice component is small and practically independent of temperature). For [FeMn(trom)](BF$_4$) clathrochelate, all three spin-quintet states are presumably within kT, and the QS value depends on temperature [192].

The Mössbauer spectrum of the [Fe$_2$(trom)]BF$_4$ complex exhibited an unusually low QS value *(ca* 0.20 mm·s^{-1}) at room temperature and one doublet was observed at temperatures up to *ca* 80K. At 73K, the splitting sharply increases and the lines double. The low QS value at room temperature seems to be because the coordination centres of both iron atoms are practically identical. When the temperature decreases, a structural phase transition takes place, resulting in two different types of complexes, each being more distorted than its high-temperature form [192].

As seen from X-ray diffraction data, the N$_6$-coordination arrangement of an encapsulated iron(II) ion in macrobicyclic tris-cyclohexanedione-1,2-dihydrazonate [Fe(cxcage)]$^{2+}$ cation is intermediate between a TAP and a TP (φ = 22.1°) and results from superimposition of the ligand field effects and steric constraints imposed by the ligand. The average of the bite angle α (*ca* 40°) and the Fe–N distance (*ca* 1.91 Å) are typical for tris-diimine iron(II) clathrochelate, but variations of the Fe–N distance from 1.896 to 1.930 Å were noted [184].

The X-ray diffraction data for both free unsaturated and saturated *imBT* and *amBT* ligands exhibit pseudo- and crystallographic D_3 symmetry of their molecules, respectively. The two tertiary amines of these free ligands are respectively 6.84 and 6.37 Å apart and have their lone pairs directed toward the centre of the cavity. The hydrogens of the secondary amino groups in *amBT* ligand are also directed toward the centre of the cavity, and the lone pairs participate in an extended network of hydrogen bonds with crystallizing water molecules. The conformation of the α-diimine fragments in *imBT*

ligand molecule is *s-trans*, and the imine lone pairs are directed tangential to the ellipsoid-shaped cavity [200].

The structure of the [Co(imBT)](ClO$_4$)$_2$ complex was determined by X-ray crystallography. The central cobalt ion and the two apical nitrogen atoms lie on a crystallographic threefold axis. The metal ion coordinates all six imino donors (only two of which are crystallographical independent) and its coordination polyhedron has D_3 symmetry. The Co–N (imine) distances are similar to those in the [Co(sep)]$^{2+}$ cation and the distortion angle is *ca* 55°. The uncoordinated apical nitrogen atoms lie ~3 Å from the metal ion within a near-planar arrangement of adjacent methylene carbons.

The *amBT* ligand in its unprotonated manganese(II) complex has an overall *lel* conformation. The manganese(II) cation is symmetric placed within a slightly elliptical cavity, but a relatively wide range of Mn–N distances (the shortest and longest bonds are *trans* to each other) no doubt because of steric strain in the complex has been observed [203]. An X-ray diffraction study of the gadolinium(III) [Gd(imBT)(H$_2$O)$_2$](NO$_3$)$_3$·2H$_2$O clathrochelate demonstrated an unusual coordination of the two solvent water molecules to the encapsulated metal ion. As result, the Gd(eight-coordinate)–N(imino) distances are somewhat longer (2.60 *vs.* 2.57 Å) on the strands adjacent to these water molecules [201]. The structure of its hexacoordinate mercury(II) [Hg(imBT)](ClO$_4$)$_2$ analog is closer to TAP than TP geometry ($\varphi = 38.5°$) [202].

The molecular structures of clathrochelate boron-capped [FeDXO$_3$(BC$_6$H$_5$)(HCOC$_2$H$_5$)$_3$](BF$_4$) and [FeCXO$_3$(BC$_6$H$_5$)(HCOC$_2$H$_5$)$_3$](BF$_4$)·1/2C$_6$H$_6$ oximehydrazonates were determined by X-ray crystallography [188]. The iron(II) ion has a distorted TP coordination (distortion angle $\varphi = 18.2°$ and 10.8°, respectively) with Fe–N distances (average 1.90 Å) and bite angles α (38.8° and 38.7°, respectively) typical of clathrochelate tris-dioximates. All the ethoxy groups and the semiclathrochelate fragment are located on the same side of the 1,3,5-triazacyclohexane ring, which has a "chair" conformation. Thus, the boron-capped oximehydrazonate complexes have a *cis* configuration [188]. The ^{1}H and ^{13}C NMR spectra of orthoformate iron(II) oximehydrazonates indicate that the boron- and tin-capped ones represent different isomers: the δ_{13C} values for methyne carbon atoms differ by approximately 60 ppm and the δ_{1H} values for methyne hydrogens differ by approximately 1.5 ppm. Tin-capped compounds are expected to have a *trans* configuration.

Different configurations of boron- and tin-capped complexes are accounted for by essential differences in their structures: the geometry of the former approaches a TP, whereas that of the latter is close to a TAP. The distortion angle φ values for macrobicyclic iron(II) oximehydrazonates were predicted from QS values in their ^{57}Fe Mössbauer spectra [188]. The predicted φ values for X-ray studied boron-capped oximehydrazonates (21.3° and 15.9°, respectively) are similar to the experimental ones without making allowance for an effect of the capping fragments. The predicted φ values for tin-capped oximehydrazonates (*ca* 50°) are essentially higher, like those that have been observed for other tin-capped clathrochelates.

The ethoxy groups in boron-capped complexes with TP geometry are located between "petals" formed by three planar oximehydrazonate chelate fragments. In addition, the C–C bonds in chelate cycles are oriented parallel to the C_3 symmetry axis of the clathrochelate molecule (i.e., *lel*-conformation), and the substituents at these atoms induce no steric hindrances in the space between "petals."

With tin-capped complexes having TAP geometry, the C–C bonds in the chelate rings are cross-oriented toward the C_3 symmetry axis (i.e., *ob*-conformation), and the substituents in oximehydrazonate fragments cause steric hindrances in the space between the "petals" of the clathrochelate ligands. Therefore, in the case of tin-capped complexes, only *trans* isomers are formed. The same approach has been used in interpreting unsuccessful attempts to obtain analogous clathrochelates *via* cross-linking with hexafluoroacetone and trichloroacetaldehyde in the case of boron-capped oximehydrazonates: CF_3 and CCl_3 substituents are more bulky than ethoxy ones, and cause steric hindrances in cavities between the "petals" of clathrochelate ligands.

The direct X-ray diffraction study is undoubtedly the most optimal and informative structural method for all compounds. Unfortunately, no one has obtained crystals of the binuclear iron(II) azineoximates, which are suitable for X-ray crystallography [193]. The structure of these complexes was deduced from EXAFS data, which allow one to obtain the function of the radial atom distribution (RAD) and hence to determine coordination numbers and the distances from the encapsulated iron ions to the clathrochelate framework atoms, and from ^{57}Fe Mössbauer spectra, which make it possible to predict the distortion angle φ (see above). Macrobicyclic iron(II) tris-dioximates

with known structure (determined by X-ray crystallography) were used as model compounds for EXAFS. The results of the EXAFS investigations of the $FeFd_3(BC_6H_5)_2$, $FeGm_3(Bn\text{-}C_4H_9)_2$, $FeBd_3(BF)_2$, and $FeGx_3(BOH)_2$ complexes were in good agreement with the X-ray data. The presence of a second heavy atom of the capping group must manifest itself by an appearance of an intense structural peak in the range from 3.4 to 3.8 Å. For the polymeric germanium-capped $[H_2FeNx_3(Ge_2O_3)]_n$ complex, an obvious intense peak at 3.4 Å is observed and is accounted for by scattering on the capping germanium atoms (Fe...Ge distance is 3.5±0.1 Å).

The high-intensity shoulder at 3.8 Å in the RAD curves for $[Fe_2DAO_3(BF)_2](BF_4)_2$ and $[Fe_2TMAO_3(BF)_2](BF_4)_2$ complexes, which is absent in the spectra of mononuclear compounds, was assigned to the Fe...Fe intramolecular distance 3.90 ± 0.05 Å. It is obvious that there is no chemical bond between these iron ions. In the case of the $Fe_2DAO_3(SnCl_3)_2$ complex, the RAD curve for the $[Fe_2DAO_3(BF)_2](BF_4)_2$ complex is fully retained, and the intense peak at 3.6 Å substantially increases, which allows one to assign it to the Fe...Sn distance 3.8 ± 0.1 Å. This value is somewhat higher than that in the clathrochelate $[FeNx_3(SnCl_3)_2]^{2-}$ dianion (ca 3.6 Å). An identical shape of the RAD curves was observed for the $Fe_2TMAO_3(SnCl_3)_2$ and $Fe_2IAO_3(SnCl_3)_2$ complexes. The presence of intense peaks at 1.9 and 2.8 Å also confirmed the structural similarity of the coordination polyhedra for the binuclear azineoximate clathrochelates and the macrobicyclic tris-dioximates. The parameters of ^{57}Fe Mössbauer spectra of these clathrochelate types are also very similar and characteristic of low-spin iron(II) complexes. The binucleating ligand field strength is somewhat lower than that of their tris-dioximate analogs, which leads to an IS increase (Table 26).

The main problem that arises in this case is determination of the QS sign. For boron-capped binuclear complexes, the QS sign and the φ values are not very obvious. The measured QS values may correspond to 22–27° (sign "+") and 37–42° (sign "–"). A comparison of UV-vis spectra of the boron- and tin-capped compounds allows one to make a choice in favour of a TP geometry in the case of the boron-capped azineoximes and a TAP geometry in tin-capped ones [193].

The UV-vis spectra of most complexes discussed in this section contain intense metal-ligand CTBs in the visible region. In the spectra of iron(II) complexes with macrobicyclic hexaene ligands these bands appear at ca 22 200 cm^{-1} ($\varepsilon \sim (6{\div}8){\times}10^3$ mol^{-1}l·cm^{-1}) along

Table 26.

Parameters of ^{57}Fe and ^{119}Sn Mössbauer (mm·s^{-1}), UV-vis (ν_{max}, cm^{-1}), ^{1}H and ^{13}C{^{1}H} NMR (ppm), and IR (cm^{-1}) spectra for iron(II) azineoximates [193].

Compound	v(C=N)	v(N–O)	v(B–O) [v(Sn–Cl)]	$\nu_{max}\times10^{-3}$	^{1}H relative to TMS H–C=N	R	^{13}C relative to TMS C=NO	C=N–N=	R	^{119}Sn rel. to Sn(CH$_3$)$_4$; ^{11}B rel. to NaB(C$_6$H$_5$)$_4$ ($J_{^{11}B, ^{19}F}$, Hz)	^{57}Fe IS	QS	^{119}Sn IS
[Fe$_2$(H$_2$DAO)$_3$]Cl$_4$											0.38	0.51	
[Fe$_2$(H$_2$IAO)$_3$]Cl$_4$											0.37	0.49	
[Fe$_2$DAO$_3$(BF)$_2$](BF$_4$)$_2$	1590	986 1106	1190	42.02, 37.31, 20.79		2.29 2.67	160.4	173.6	13.6 17.4	5.9 11.6 (13)	0.37	0.49	
[Fe$_2$DAO$_3$(SnCl$_3$)$_2$]	1562	988 1108	[310]	45.45, 35.71, 32.26, 28.17, 19.31		2.10 2.48	157.8	170.9	12.5 16.2	– 620	0.35	0.40	0.42
[Fe$_2$TMAO$_3$(BF)$_2$](BF$_4$),	1580	1060sh	1190	43.48, 35.09, 31.75, 20.41	8.39m	2.10m 2.37m	152.0 [3 lines] 16.03 [3 lines]	173.2 [6 lines]	13.2 [3 lines] 17.1 [6 lines]	6.7 12.4 [4 doublets] [12]	0.47	0.36	
[Fe$_2$TMAO$_3$[SnCl$_3$]$_2$]	1578	988 1085 1110	[330]	44.44, 35.21, 32.26, 28.09, 19.23	8.20	2.15m 2.34m	148.1 [3 lines] 156.6 [3 lines]	169.4 [6 lines]	11.2 [3 lines] 15.2 [6 lines]	– 618 [4 lines]	0.45	0.44	0.48

Compound											
[Fe₂IAO₃[SnCl₃]₂]	1565	988 1130	[335]	45.45, 42.37, 32.05, 27.78, 19.38	8.30	2.21	158.1 155.6	179.6 163.7	24.2		0.45 0.43 0.45
[Fe₂DAO₃[SnBr₃]₂]	1585	990 1103	1195	45.45, 40.16, 35.71, 32.15, 19.46			155.6	163.7	15.0 17.8	−998	0.36 0.54 0.38
[FeDAO₃[BC₆H₅]₂]						2.13 2.26 2.34 2.42 7.34 7.67 7.73	149.8 154.5	159.6 164.7	13.3 13.5 15.5 15.6	18.0	0.32 0.62
[Fe₂DAO₃[BC₆H₅]₂][BF₄]₂	1600	995 1110	1128	41.67, 37.17, 32.68, 28.01, 20.28		2.27 2.49 7.41 7.77	159.6	173.2	13.8 17.6 127.3 128.1 131.2	6.7 18.3	0.33 0.68

with a shoulder near 24 600 cm^{-1}. An intense ($\varepsilon \sim 4{\times}10^3$ mol^{-1}·l·cm^{-1}) band of the intraligand π–π^* transition was observed at 32 600 cm^{-1}. Thus, the parameters of the UV-vis spectra of the hexaene clathrochelate iron(II) complexes resemble those of boron-capped iron(II) tris-dioximates. The spectrum of [Fe(thz)](BF$_4$)$_2$ complex also contains the M$d{\rightarrow}$Lπ^* CTB in the visible region (ν_{max} = 19 100 cm^{-1}, ε = $1.16{\times}10^4$ mol^{-1}·l·cm^{-1}) along with a π–π^* transition in the UV region (ν_{max} = 32 300 cm^{-1}, ε = $8.4{\times}10^3$ mol^{-1}·l·cm^{-1}), and this spectrum is close to the spectra of the iron(II) tris-bipyridinates and tris-phenanthrolinates [236]. It was noted in Ref. 191 that a CTB in the spectrum of the clathrochelate [Fe(tabpy)]$^{2+}$ cation is more intense and detected at higher frequency (ν_{max} = 19 000 cm^{-1}) than that of its nonmacrocyclic analog (ν_{max} = 18 300 cm^{-1}). A similar phenomenon was observed for ruthenium(II) complex with the same ligand: a CTB in the spectrum of [Ru(tabpy)]$^{2+}$ cation manifested itself at 22 000 cm^{-1} (ε = $1.03{\times}10^4$ mol^{-1}·l·cm^{-1}), whereas in the initial nonmacrocyclic tris-complex it has a maximum at 20 000 cm^{-1} (ε = $1.0{\times}10^4$ mol^{-1}·l·cm^{-1}) [190].

The CTB in the UV-vis spectra of nonmacrocyclic iron(II) oximehydrazonates and their semi- and clathrochelate derivatives ($\nu_{max} \sim$ 19 600–20 600 cm^{-1}) occupies an intermediate position between those of macrobicyclic iron(II) tris-dimethylglyoximates and those of clathrochelate complexes with dihydrazone *thz* ligand. A CTB maxima in the spectra of clathrochelate complexes are substantially red shifted compared with that in the spectra of the initial semi-clathrochelates [185-187].

Considerable discrepancies in the geometry of macrobicyclic boron- and tin-capped oximehydrazonates were observed in their UV-vis spectra: the intense M$d{\rightarrow}$Lπ^* CTBs in the spectra of the boron-capped clathrochelates are UV-shifted compared with the spectra of the tin-capped ones. The shape of the spectra is also somewhat changed: an asymmetric singlet band is characteristic of the boron-capped compounds, whereas the spectra of the tin-capped ones in the visible region consist of two overlapping bands of nearly the same intensity. Similar differences have also been detected for clathrochelate iron(II) tris-dioximates (see Section 3.3) [188].

The UV-vis spectra of the monomeric germanium- and antimony-capped iron(II) oximehydrazonates and azineoximates (Table 23) are similar to the spectra of their tin-capped analogs. Two or three bands of similar intensity in the range 17 540–22 220 cm^{-1}, assigned to the

$Md{\rightarrow}L\pi^{*}$ CTB characteristic of clathrochelates, were detected in the visible region. The exception was the spectrum of the binuclear clathrochelate $[Fe_2DAO_3(Ge(CF_3)_3)_2]$ azineoximate: only one intense ($\varepsilon = 1.4{\times}10^4$ $mol^{-1}1{\cdot}cm^{-1}$) singlet band at 19 230 cm^{-1} and a much less intense ($\varepsilon = 4{\times}10^3$ $mol^{-1}1{\cdot}cm^{-1}$) one at 25 000 cm^{-1} were observed. Such a shape of the UV-vis spectrum is characteristic of TP boron-capped clathrochelates, but in this case two CTBs overlap due to the peculiarities of $\pi{-}\pi$ conjugation in the binuclear clathrochelate ligand [73].

The UV-vis spectra of the macrobicyclic cobalt(II) oximehydrazonates contain two CTBs in the visible region (at 18 000–19 000 and at 24 000–25 000 cm^{-1}). In the spectra of cobalt(III) complexes, a shoulder at 18 000–20 000 cm^{-1} and a peak at 24 000–30 000 cm^{-1} were observed. All the absorption bands for the tris-dioxime complexes occur at slightly higher energy than the corresponding lines in spectra of the oximehydrazonate compounds [186].

The UV-vis spectra of the clathrochelate $[Co(imBT)](B(C_6H_5)_4)_2$, $[Co(imBT)](ClO_4)_2$, and $[Ni(imBT)](B(C_6H_5)_4)_2$ Schiff bases contain the ligand-metal CTB in the range 11 000–12 500 cm^{-1} and indicate that the symmetry of the Co^{2+} and Ni^{2+} ions arrangement is close to O_h [196].

The NMR spectra indicated that the clathrochelate oximehydrazonates in solution have a high symmetry. The most striking feature of the ^1H NMR spectra of the clathrochelate iron(II) complexes with *HDXO* ligand proved to the occurrence of two intense sets of AB-type signals from 1,3,5-triazacyclohexane methylene units at 3.5 and 5.2 ppm ($J = 13$ Hz). The same spectrum was observed for the iron(II) complex with clathrochelate *thz* ligand [183]. The ^1H NMR spectrum of partially cross-linked $[FeDXO_3(BC_6H_5)(CH_2)_2](PF_6)$ complex also contained a signal from amine protons at 6.3 ppm ($J = 6.4$ Hz), which is a doublet due to interaction with the methylene unit proton. As a consequence, the signal from the latter at 3.84 ppm also doubles and becomes a doublet of a doublet ($J = 6.4$ and 13 Hz).

The ^{13}C NMR chemical shifts of the methyl groups in boron-capped iron(II) diacetylmonooxime hydrazonates (14.0 and 17.7 ppm) are lower than that in the $[Fe(thz)](BF_4)_2$ complex (18.6 ppm). A second signal was assigned to the methyl substituent in a hydrazonate fragment. A signal from the azomethine carbon atoms at 168 ppm is also attributed to this fragment, whereas a line at 154 ppm corresponds to an oxime fragment. The ^{13}C NMR

spectrum of a nonsymmetric [FeDXO₃(BC₆H₅)(CH₂)₂](PF₆) semi-clathrochelate exhibited a greater number of lines, in particular, four lines at 14.1–18.0 and 156.8–170 ppm from methyl and azomethine groups [185].

The ^{1}H and ^{13}C NMR spectra of iron(II) oximehydrazonate clathrochelates, obtained by cross-linking with TOF, were discussed above. It was also noted in Ref. 188, that the spectra of the intramolecular condensation product [FeDXO₃(BC₆H₅)(CH)](BF₄) contain no ethoxy group signals, and the signals characteristic of methyne cap have been detected.

The ^{119}Sn NMR spectra of the oximehydrazonate tin-capped complexes consist of a signals from the octahedral SnO₃Hal₃ capping groups with δ_{119Sn} from –654 to –662 ppm for the trichlorotin-capped clathrochelates and from –995 to –1030 ppm for the tribromotin-capped ones. This confirms the additivity of the halogen replacement influence on δ_{119Sn} values for tin halogenides (about ~120 ppm for replacement of one chlorine atom by a bromine atom and ~360 ppm for replacement of three chlorine atoms by three bromine atoms).

In the ^{11}B NMR spectra of the boron-capped iron(II) oximehydrazonates, both a BF₄⁻ counter-ion narrow signal and a tetrahedral capping fragment broadened singlet have been observed [188].

The ^{1}H and ^{13}C NMR spectra of the antimony-capped oximehydrazonates consist of not only the signals of oximehydrazonate fragments, but also the lines of substituents in the capping groups at the expected integral intensity ratio (Table 23). The ^{13}C NMR spectra of the clathrochelates that resulted from cross-linking with TOF are similar to those of the tin-capped ones and indicate a *trans* orientation of the ethoxy substituents and the semiclathrochelate fragment relative to the 1,3,5-triazacyclohexane ring, unlike boron-capped analogs, which are *cis* isomers [74].

The NMR spectra of the monomeric germanium-capped iron(II) oximehydrazonates (Table 23) confirmed their composition (in particular, the integral intensity ratio of the proton signals of oximehydrazonate fragments and capping groups in the ^{1}H NMR spectra; the appearance of CF₃ group signals in the ^{13}C and ^{19}F NMR spectra) and allowed some conclusions about the structure of the molecules in solution to be drawn. C_3 symmetry axis is obviously present in such molecules, as well as a *trans* orientation of all three ethoxy groups and semiclathrochelate fragment in the orthoformate complex. As seen from Table 23, the parameters of the ^{1}H and ^{13}C

NMR spectra of the germanium-capped orthoformate complex are close to those of the above-described TAP antimony- and tin-capped clathrochelates, which have a *trans* configuration, and are markedly different from the data for TP boron-capped complexes, which have a *cis* configuration (all ethoxy groups and the semiclathrochelate fragment are equally oriented with respect to the 1,3,5-triazacyclohexane ring). In the ^{13}C NMR spectra of all the complexes, a quartet of the CF_3 groups has been observed in the range 135–138 ppm stipulated by a spin-spin interaction of one ^{13}C nucleus with three ^{19}F nuclei and a singlet (due to the insignificant natural abundance of ^{13}C atoms) signal of the fluorine atoms in these groups with $\delta_{^{19}F} = -55$ ppm.

The IR spectra of all these complexes also consist of two characteristic very intense and narrow bands of the C–F bond stretching vibrations at 1150–1185 cm^{-1}. Apart from the $\nu_{C=N}$ of oxime groups at 1560–1590 cm^{-1}, characteristic of clathrochelate α-dioximates, for germanium-capped oximehydrazonate clathrochelates, the $\nu_{C=N}$ of hydrazonate fragments have been observed at 1620 cm^{-1} [73].

The UV-vis reflection and absorption spectra of the clathrochelate [Cu(thiopenar)](ClO$_4$)$_2$ complex made it possible to establish that the copper(II) polyhedron both in solution and in the solid state has a distorted square-pyramidal structure [206].

The ^1H and $^{13}C\{^1H\}$ NMR spectra have primarily been used to establish the fact of complexation [204, 205, 212], which gives rise to a significant change in the chemical shift of the signals assigned to the ligand fragments and a change in the line shape.

The coordination of the alkaline metal ions by three anthracene-appended N$_5$-sarcophaginates was studied by ^1H, ^{13}C, and ^7Li NMR spectroscopies in alcohol media [205]. No evidence was found for complex formation with sodium and potassium ions. In contrast, all these ligands readily bound the smaller Li$^+$ ion. The ^7Li NMR spectra of preliminarily synthesized clathrochelate lithium complexes contained a sharp peak, shifted downfield with respect to the free ion. Li$^+$ ion coordination was clearly detected by ^{13}C and ^7Li NMR spectra in the alkaline methanol solution of the ligands: on the addition of an excess of Li$^+$ ion, the ^7Li NMR spectrum showed two sharp peaks, one due to the free ion and another peak downfield-shifted up to 3.3 ppm due to the encapsulated one. The simultaneous presence of these peaks denotes a slow exchange of encapsulated lithium ion on the NMR

time scale. On this scale, as seen from ^{13}C NMR spectra, the complexation of the Li$^+$ ion produces a decrease in molecular symmetry for all these ligands [205].

In addition, the ^{1}H NMR spectra made it possible to determine the molecular D_3 symmetry for the [Ru(tabpy)]$^{2+}$ cation in solution [190] and the C_3 symmetry for the corresponding semiclathrochelate complex as well as to reveal dynamic effects in macrobicyclic tris-phenanthrolinates and tris-bipyridinates [211].

Chapter 4

Kinetics and mechanism of synthesis and decomposition of clathrochelates

The kinetics and mechanism of synthesis and decomposition of macrocyclic compounds are regarded as one of the most important aspects in the chemistry of these compounds. The majority of papers concern metal ions complexing with preliminarily synthesized macrocyclic ligands and metal ion substitutions by other metal ions in the preliminarily prepared complexes. Template synthesis, the most promising approach to the directed preparation of macrocyclic compounds with desired structures [17], plays a still more decisive role in the chemistry of macrobicyclic complexes with encapsulated metal ion. However, the literature contains only scarce data on the kinetics and the mechanism of the template synthesis of macrocyclic compounds because of the difficulties encountered in experimental determinations of kinetic and thermodynamic parameters, such as low product yields, nonaqueous media, high temperatures, and side reactions.

At the same time, the term "template synthesis" implies that the formation of a complex occurs *via* a reaction step at which the metal ion activates, arranges, and orients the reacting species. As a result, the selective directivity and yield of the process increase, and in many cases, template synthesis has led to the formation of desired complexes that cannot be obtained by other methods.

Some believe that there are two main template effects: kinetic and thermodynamic [8]. The latter is responsible for an increase in the yield of the complex with ligands formed *in situ* in the presence of metal ions. which bind products that result from ordinary reactions and to withdraw them from the reaction medium. These procedures are not true template reactions since they do not satisfy the above-mentioned conditions, and the metal ion causes equilibrium shift only. It is impossible to distinguish between kinetic and thermodynamic contributions to the template effect, since the coordination to the metal ion simultaneously causes both steric

changes, facilitating the occurrence of reactions, and electron density redistribution, affecting the energetics of such interactions. Therefore, it is expedient to discuss the template effect as a whole, as a superposition of these two contributions.

Sufficient physicochemical parameters of clathrochelates have also been gained from the data on kinetics and the mechanism of their decomposition both in solution and in the gas phase. Moreover, such results provide additional information about the complexation mechanism.

4.1 EXPERIMENTAL APPROACHES

The kinetics and mechanism of synthesis and decomposition of macrobicyclic boron-capped iron(II) tris-dioximates with six-(nioxime and 4-methylnioxime), seven-(heptoxime) and eight-(octoxime) membered alicyclic dioximes of the general formula $FeD_3(BR)_2$ (where R is OH, C_6H_5, and n-C_4H_9) have been studied. These complexes were obtained in quantitative yields in dilute solutions at room temperature. The alicyclic dioximes exist only in a *cis*-configuration (unlike acyclic ones, which are mostly in the *trans*-form in solution and in crystals, see Section 3.3), facilitating the occurrence of synthesis reactions and making the resultant compounds more stable. The presence of intense CTB in the spectra of these complexes made it possible to elucidate the kinetics of template synthesis and decomposition using photometry [59, 62, 271, 286-290].

At low concentrations of Fe^{2+} ions, the effective synthesis rate constant and the decomposition rate constant are determined as pseudo-first-order rate constants since the change in the concentrations of other reactants is negligible [291]. The dependence of optical density on time is described by a first-order equation respectively in the concentration of iron(II) ions (Fig. 24)

$$\ln \frac{\varepsilon[Fe]l}{\varepsilon[Fe]l - A} = k_{obs}t \tag{52}$$

or in the concentration of the complex

$$\ln A = k'_{obs}t \tag{53}$$

At high concentrations of iron(II) ions, the initial rate has been measured and k_{obs} has been determined as a pseudo-zero-order rate constant $dc/dt = k_{obs}$ or, in terms of optical density, $A = k_{obs} \, \varepsilon \, l \, t$.
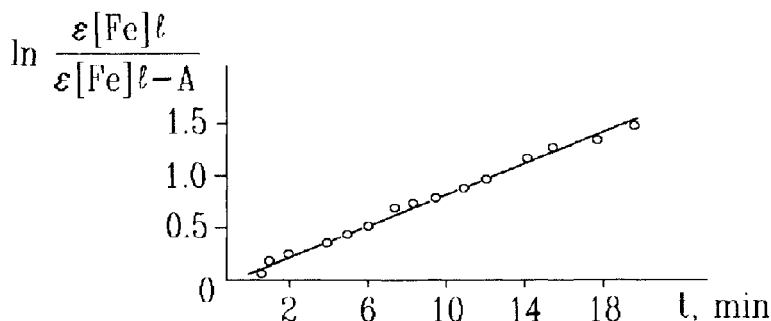
Figure 24. Example of the determination of the synthesis reaction first-order rate constant, k_{obs}, for the $FeNx_3(BOH)_2$ complex.

When the reaction order of a certain component is determined for complexes with six- or seven-membered dioximes, the concentration of this component is changed, whereas those of the other components are kept constant. In this case, k_{obs} may be expressed as $k_{obs} = k^* c^n_{comp}$ or, if $k_{obs}/k^* = k_{conv}$, $\text{Log } k_{conv} = n \text{ Log } c_{comp}$. The reaction order of the given component is equal to the slope of the straight line plotted with the $\text{Log } k_{conv}$ vs $\text{Log } c_{comp}$ coordinates. Introduction of the k_{conv} constant, which is independent of the concentrations of all other components, allows one to compare the data obtained at different concentrations. For the $FeOx_3(BOH)_2$ complex with eight-membered dioximates fragments, attempts to extend a similar approach to the determination of the reaction order in boric acid and H^+ ions failed (Figs. 25 and 26).
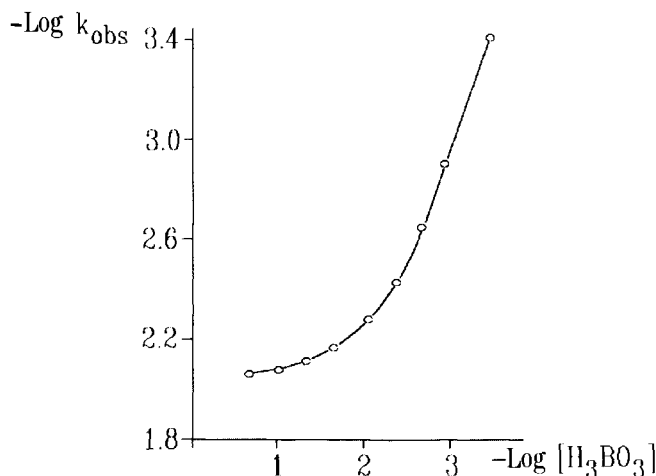
Figure 25. Plot of synthesis reaction rate constant, k_{obs}, versus boric acid concentration for the $FeOx_3(BOH)_2$ complex [289].
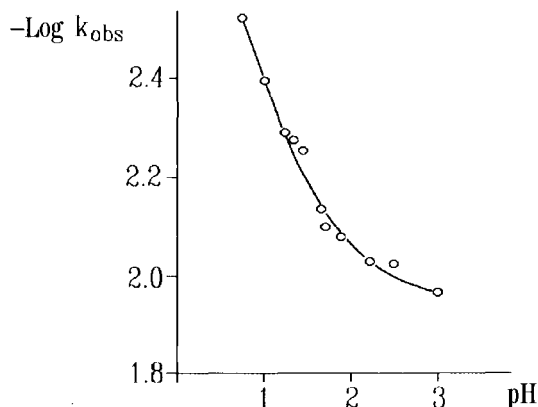
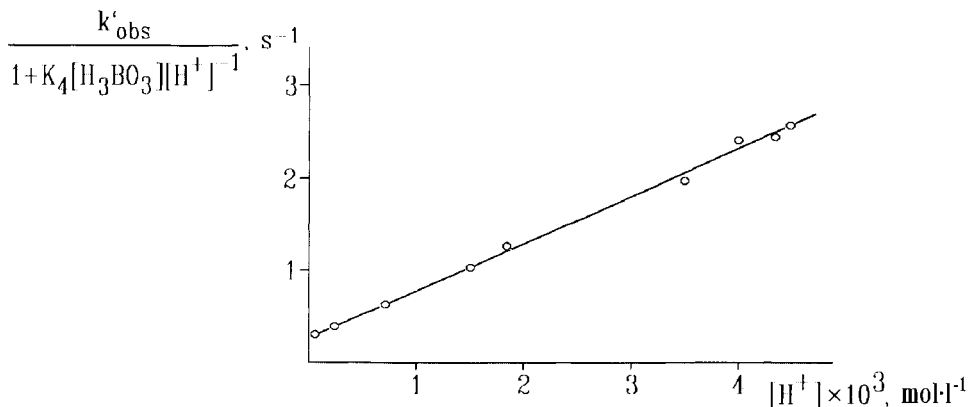Figure 26. Plot of synthesis reaction rate constant, k_{obs}, *versus* pH for the FeOx$_3$(BOH)$_2$ complex [289].

Figure 27. Determination of the k_5 and k_6 constants for the FeNx$_3$(BOH)$_2$ complex [286].

The plot of Log k_{obs} *vs* Log c_{comp} has its usual reaction order appearance only for the octoxime concentration.

Decomposition of such complexes has also been described by fairly simple rate equations. In the absence of boric acid, FeD$_3$(BOH)$_2$ complexes irreversibly decompose in acidic media, and the rate of this process depends linearly on the concentration of H$^+$ ions (Fig. 27). Decomposition of FeD$_3$(BC$_6$H$_5$)$_2$ and FeD$_3$(Bn-C$_4$H$_9$)$_2$ complexes is detectable only in strongly acidic media. The dependence of decomposition rates of these compounds on the activity of the H$^+$ ion is shown in Fig. 28. It is evident that complexes have been protonated with subsequent irreversible decomposition [288].
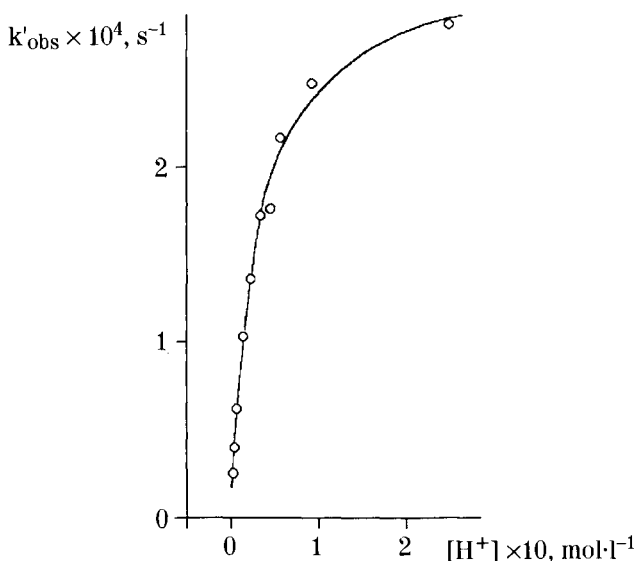
Figure 28. k_{obs} as a function of H$^+$ ion concentration in the absence of
n-butylboronic acid for the FeNx$_3$(Bn-C$_4$H$_9$)$_2$ complex [288].

In the presence of the corresponding boronic acid, decomposition of
the compounds decreases and, depending on the nature of the
substituent at the boron atom, is described by various equations.

The activation energies for several synthesis and decomposition
rate constants, as well as equilibrium enthalpy at certain stages,
have been determined from the temperature dependences, plotted
with the Arrehenius coordinates (Fig. 29).
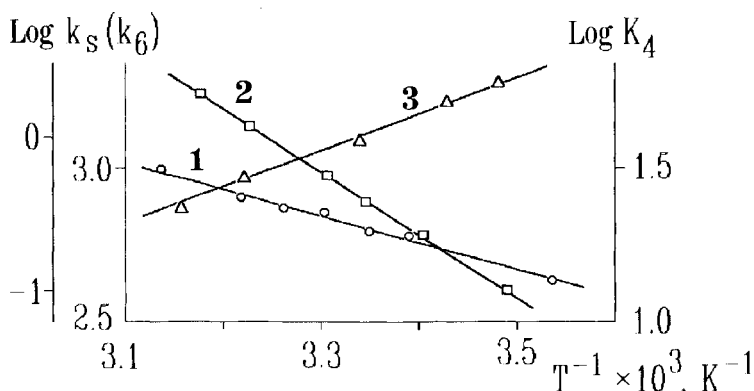
Figure 29. Plot of k_s (1), k_6 (2) and K_4 (3) values *versus* temperature for the
Fe(4MNx)$_3$(BOH)$_2$ complex [59]

Similar approaches have been employed by Sargeson and coworkers to investigate the kinetics of metal ion extrusion from presynthesized *d*-metal (in particular, copper(II)) sarcophaginates in acidic media [4, 5, 174].

Demetallation of zinc, cadmium, and mercury(II) sarcophaginates has rather efficiently been examined by ^{1}H NMR spectroscopy. The data on proton exchange obtained by this method indicate that $[Zn(diAMHsar)]^{4+}$ cation is stable towards 2M deuterated perchloric acid, and only partial proton exchange has been observed. In deuterated hydrochloric acid at an equal concentration, the same complex decomposes, and proton exchange in this case proceeds more rapidly than that in perchloric acid at an equal concentration, and the extrusion of the Zn^{2+} ion occurs. For $[Cd(diAMsar)]^{2+}$ dication in DCl, the proton exchange and the extrusion of the Cd^{2+} ion occur simultaneously.

The rate of the mercury ion extrusion from the cavity of sarcophaginate ligands depends not only on the concentration of H^+ ions, but also on the concentration of Cl^- anions (Fig. 30).

In all cases mentioned, the spectral and X-ray diffraction data on reaction intermediates and by-products have widely been used in considering kinetic and thermodynamic relationships. The identification of intermediates and by-products is still more important in determination of the mechanisms of sarcophaginate and sepulchrate synthesis because in this case kinetic approaches cannot be used.

Fast atom bombardment (FAB) mass spectroscopy has been employed to get information about the routes of the fragmentation of macrobicyclic $FeNx_3(BOH)_2$, $Fe(4MNx)_3(BOH)_2$, $FeGx_3(BOH)_2$, and $FeOx_3(BOH)_2$ tris-dioximates in the gas phase, and the FAB data have been compared with the stability data for macrobicyclic complexes in solutions [292].

The scheme of Mn^{2+} ion extrusion from corresponding sarcophaginate has been deduced using UV-vis spectrophotometry, EPR and cyclic voltammetry [179]. The extrusion of the copper ion after its reduction to copper(I) ion is too fast to be examined by cyclic voltammetry, and the kinetics of the reduction of $[Cu(sar)]^{2+}$ cation to copper(II) $[Cu(sar)]^+$ complex has been followed by pulse radiolysis over a shorter time using the hydrated electron to probe for extrusion of the metal ion. This reduction process has been registered spectrophotometrically to yield a second-order rate constant. The
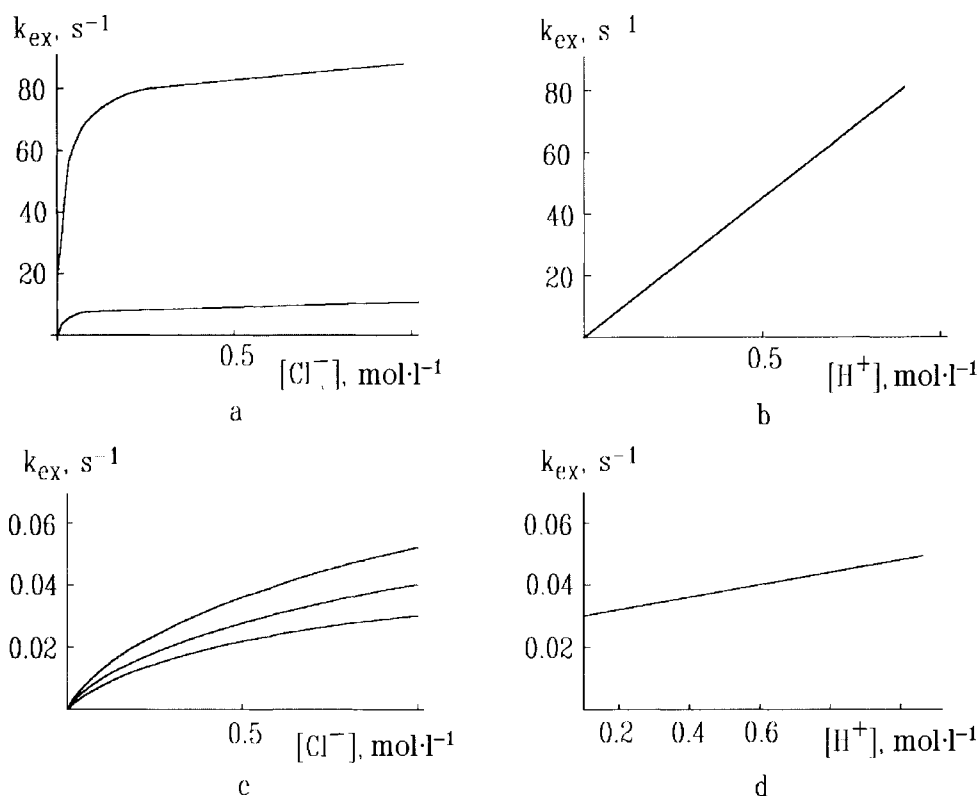
Figure 30. Kinetic dependencies of the Hg^{2+} ion extrusion reaction from [Hg(sar)]$^{2+}$ and [Hg(AMHsar)]$^{4+}$ sarcophaginates [5, 174].

subsequent reactions of copper(I) complexes cannot be observed by this technique. The conductivity detection system proved to be rather successful for measuring the reaction rate. Over the time scale 10^{-7}–10^{-2} s the two observable conductivity changes at pH 3–5 are first order in H^+ ion concentration and consume one proton each with second-order rate constants of 2×10^{10} and 2×10^7 mol^{-1}l·s^{-1}, respectively [293].

The use of kinetic and thermodynamic approaches along with physicochemical and X-ray diffraction data, as well as their comparison with earlier results for complexes with synthetic macrocyclic ligands, have allowed one to make sufficiently well-grounded conclusions about the mechanisms of synthesis and decomposition of clathrochelates.

4.2 REACTIONS OF BORON-CAPPED IRON(II) DIOXIMATES

The kinetic relationships for the formation of clathrochelate $FeD_3(BR)_2$ complexes with six- and seven-membered alicyclic dioximes over a wide range of concentrations of reagents are represented by a rather simple Scheme 102 with one rate-determining stage (3) and an equilibrium that rapidly occurs at the previous (1 and 2) and subsequent (4) stages.

A small amount of $[Fe(H_2D)_3]^{2+}$ cation with three closely situated oxime OH groups is primarily formed. The distortion angle φ for pseudo-octahedral $[Fe(H_2D)_3]^{2+}$ complex is equal to 50–60°. When the tris-dioxime interacts with the corresponding boronic acid, the proton detaches from the oxime group, and boron atom becomes bound to them. The trigonal geometry of the boron atom coordination polyhedron changes to a tetrahedral one. The two water molecules detach and the inner sphere undergoes rearrangement. The φ angle decreases to 20–25° for partially cross-linked complex with TP geometry (see Section 3.3). This is the rate-determining stage, which is consistent with corresponding data for several transition metal complexes with synthetic macrocyclic ligands [10]. Condensation of the second molecule of the corresponding boronic acid, accompanied by proton detachment, requires no rearrangement in the coordination sphere and therefore proceeds much faster (Fig. 31). The reaction rate is described by the equation

$$dc / dt = k_3[Fe(H_2D)_2(HD) \cdot RB(OH)_2^+] =$$
$$= k_3 K_2 \beta_3 [Fe^{2+}][H_2D]^3[RB(OH)_2][H^+]^{-1}, \quad k_S = k_3 K_2 \beta \tag{54}$$

which corresponds to experimental data [59, 62, 271, 286-288, 290].
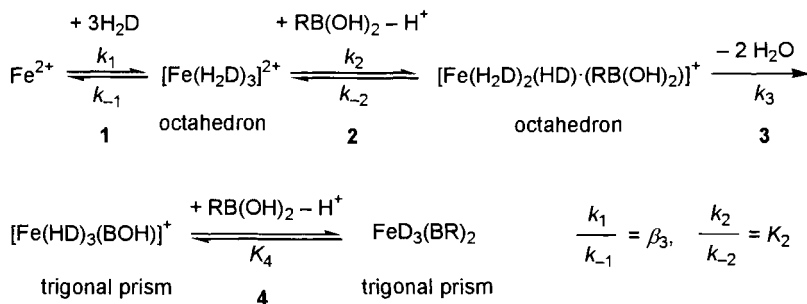
Scheme 102
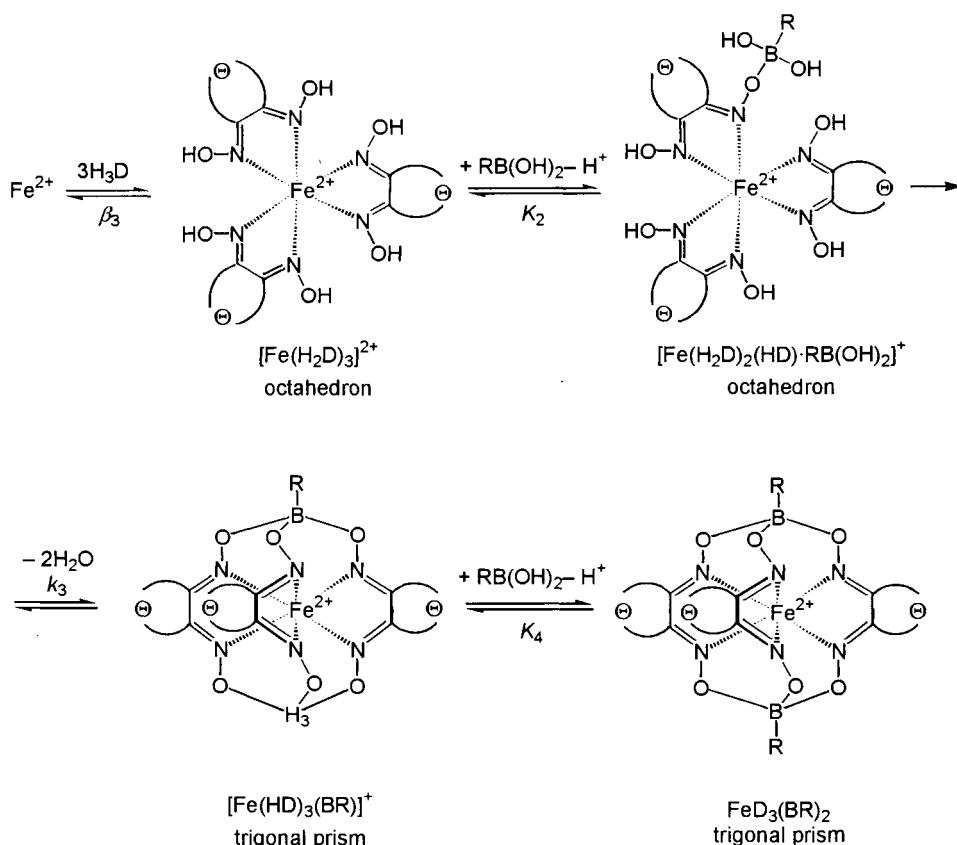
R = OH, C_6H_5, n-C_3H_7, n-C_4H_9
$\ominus$ = $(CH_2)_4$, $CH_2CH_2CH(CH_3)CH_2$, $(CH_2)_5$, $(CH_2)_6$

Figure 31. Scheme of macrobicyclic $FeD_3(BR)_2$ complex formation [271].

The k_S values obtained for several compounds with six- and seven-membered dioximes together with the independently determined stability constants β_3 for nonmacrocyclic $[Fe(H_2D)_3]^{2+}$ tris-complexes are listed in Table 27.

A similar approach cannot be extended to octoxime because the rate of the two first stages becomes comparable with that of the rate-determining one. In this case one can write the equations describing three consecutive reactions, the first two of which are reversible [289].

It is assumed that the rates of these individual reactions are equal, i.e., the concentrations of intermediate forms are constant:

$$\mathrm{d}c/\mathrm{d}t = k_1[\mathrm{Fe}^{2+}][\mathrm{H_2Ox}]^3 - k_{-1}[\mathrm{Fe(H_2Ox)}_3^2] \tag{55}$$

$$\mathrm{d}c/\mathrm{d}t = k_2[\mathrm{Fe(H_2Ox)}_3^{2+}][\mathrm{H_3BO_3}] - $$
$$-k_{-2}[\mathrm{Fe(H_2Ox)_2(HOx)}\cdot\mathrm{B(OH)}_3^+][\mathrm{H}^+] \tag{56}$$

$$\mathrm{d}c/\mathrm{d}t = k_3[\mathrm{Fe(H_2Ox)_2(HOx)}\cdot\mathrm{B(OH)}_3^+] \tag{57}$$

Solving these equations relative to the reaction rate, one obtains Eq. (58) corresponding to the experimental data:

$$\mathrm{d}c/\mathrm{d}t = \frac{k_3k_1k_2[\mathrm{Fe}^{2+}][\mathrm{H_2Ox}]^3[\mathrm{H_3BO_3}]}{k_{-1}k_3 + k_3k_2[\mathrm{H_3BO_3}] + k_{-1}k_{-2}[\mathrm{H}^+]} \tag{58}$$

The calculated ratios of the reaction rate constants made it possible to determine the magnitudes of some of them or their ratios with allowance for the independently obtained stability constant for the $[\mathrm{Fe(H_2D)_3}]^{2+}$ complexes.

The $\mathrm{FeD_3(BR)_2}$ compounds chosen to elucidate the alicyclic dioxime structure effect on the kinetic and thermodynamic parameters of synthesis reactions of such complexes [271].

The methyl β-substituent in cyclohexane ring affects insignificantly on the kinetic parameters of the synthesis and decomposition reactions. More significant changes in the majority of these parameters are caused by the increase in the alicyclic ring size.

Table 27.
Kinetic and thermodynamic parameters of the synthesis and decomposition reactions of macrobicyclic iron(II) tris-dioximates [271].

Complex	Log β_3	k_S, $\mathrm{s^{-1}l^3mol^{-3}}$	k_{-3}, $\mathrm{s^{-1}l^2mol^{-2}}$	K_4	K_7	$k_8\times10^5$, $\mathrm{s^{-1}l^2mol^{-2}}$	k_{-8}, $\mathrm{s^{-1}l^2mol^{-2}}$
FeNx$_3$(BOH)$_2$	4.94	3.2×10^2	0.54	62			
Fe(4MNx)$_3$(BOH)$_2$	5.22	2.9×10^2	0.32	40			
FeGx$_3$(BOH)$_2$	2.37	7.1×10^{-1}	0.09	80			
FeOx$_3$(BOH)$_2$	[a]5.37	[b]	0.12	129			
FeNx$_3$(BC$_6$H$_5$)$_2$	4.94	3.1×10^3	3.9	107	846	7.9	7.2
FeNx$_3$(Bn-C$_4$H$_9$)$_2$	4.94	3.9×10^3	14.9	325	140	27.8	12.5
Fe(4MNx)$_3$(BC$_6$H$_5$)$_2$	5.22	2.1×10^3	1.51	402	522	6.0	12.6
Fe(4MNx)$_3$(Bn-C$_4$H$_9$)$_2$	5.22	4.1×10^3	0.32	8.7	471	13.7	0.56
FeGx$_3$(BC$_6$H$_5$)$_2$	2.37	10.6	4.0	5.4×10^3	69	7.2	28.6
FeGx$_3$(Bn-C$_4$H$_9$)$_2$	2.37	15.6	28.5	3.0×10^3	220	7.3	48.1
FeGx$_3$(Bn-C$_3$H$_7$)$_2$	2.37	11.4	2.75	454	180	16.9	13.9
FeOx$_3$(BC$_6$H$_5$)$_2$	[a]5.37	1.2×10^4	0.09	292	240	5.0	3.5
FeOx$_3$(Bn-C$_4$H$_9$)$_2$	[a]5.37	2.1×10^4	0.11	147	129	31.1	5.9

[a]$k_1 = 4.45\times10^4$; $k_{-1} = 0.19$ [b]$k_1 = 22$; $k_{-2}/k_3 = 424.4$ [c]$K_4 = K_7^{-1}K_8^{-1}$

A considerable (approximately 300–500-fold) decrease in the synthesis rate constant for the $FeGx_3(BR)_2$ complexes was observed compared with those for nioximates and 4-methylnioximates. It correlates with the corresponding decrease in β_3 stability constant for the $[Fe(H_2Gx)_3]^{2+}$ dication (Table 27) and indirectly confirms the fact that the synthesis of clathrochelate occur *via* formation of the protonated $[Fe(H_2D)_3]^{2+}$ tris-complex.

To elucidate this phenomenon, an X-ray diffraction study of the three alicyclic dioximes, such as nioxime, heptoxime, and octoxime, was performed [294]. The torsion angle between oxime groups (47.2°) is much higher for heptoxime than for nioxime and octoxime (26.2 and 26.6°, respectively). These differences remain in solution: the increase in the torsion angle between oxime groups causes a decrease in the conjugation in dioximate fragment and hence leads to the UV shift of the intramolecular π–π^* transition band. As a result, the UV-vis spectrum of heptoxime is essentially UV-shifted compared with the spectra of nioxime and octoxime (Fig. 32).

The structural subtleties revealed account for essential differences in the coordination-chemical behaviours in alicyclic dioxime series that give rise to appreciable changes in kinetic and thermodynamic complexation parameters.

For $FeD_3(BOH)_2$ complexes with six- and seven-membered dioximes, the first two formation stages are equilibrium, and the
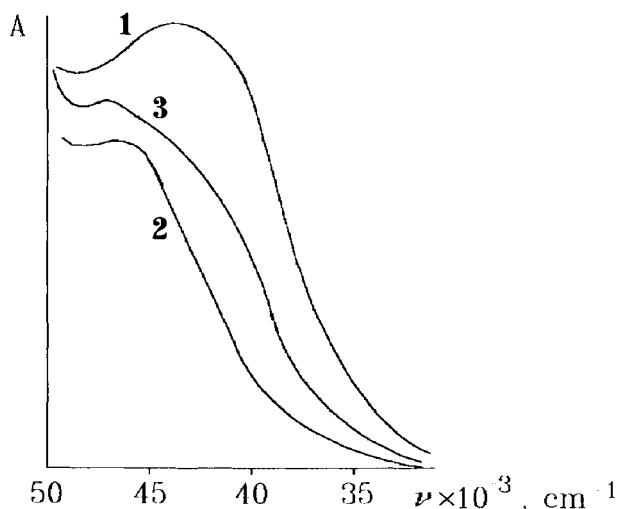

Figure 32. Fragments of UV-vis spectra of nioxime (1), heptoxime (2), and octoxime (3) [294].

third stage is the rate-determining one. In the case of octoxime, the reaction rates in the first two stages are comparable with that in the third stage, when the coordination polyhedron changes from a pseudo octahedral to a TP one. Thus, in passing to the eight-membered dioxime, either the intramolecular condensation rate with detachment of two water molecules increases or both the nonmacrocyclic $[Fe(H_2Ox)_3]^{2+}$ dication formation and boric acid addition rates decrease, or these changes occur simultaneously. The ^{57}Fe Mössbauer and multinuclear NMR spectroscopies indicate that the structure of $FeOx_3(BOH)_2$ complex resembles those of their analogs with smaller cycloalkane ring [61]. As mentioned above, peculiarities of the chelating fragment geometry are not responsible for the observed changes either. It is more probable that the conformational changes in the bulky cyclooctane fragment during the formation of the protonated $[Fe(H_2Ox)_3]^{2+}$ tris-complex and shielding of oxime groups by this fragment decrease both the rate of first product formation and the rate of boric acid addition to this product.
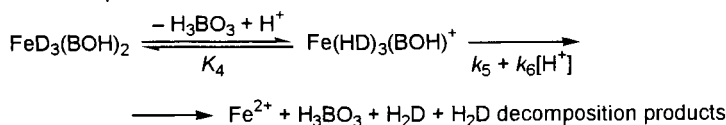
The synthesis rate constant of this type of clathrochelates is also appreciably affected by the nature of the substituent at the boron atom. The synthesis rate constants for $FeNx_3(BC_6H_5)_2$ and $FeNx_3(Bn\text{-}C_4H_9)_2$ complexes are ten times higher than k_s for $FeNx_3(BOH)_2$ complex. As seen from Scheme 102, k_s may be expressed as $k_s = k_3K_2\beta_3$. The β_3 value for all nioximate complexes is the same. Since alkyl- and arylboronic acids are weaker Lewis acids than boric acid, one might expect a lower K_2 value than that for $FeNx_3(BOH)_2$ complex. Thus, the increase in k_s for both $FeNx_3(BC_6H_5)_2$ and $FeNx_3(Bn\text{-}C_4H_9)_2$ clathrochelates is attributed to the rise in k_3.

The iron(II) clathrochelate formation schemes are also confirmed by investigations on the kinetics of their decomposition in solution. In aqueous solution of $FeD_3(BOH)_2$ complexes, it is equilibrium

$$FeD_3(BOH)_2 + H^+ + 2H_2O \underset{K_4}{\rightleftharpoons} Fe(HD)_3(BOH)^+ + H_3BO_3 \qquad (59)$$
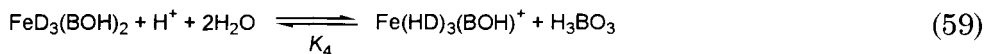
This equilibrium in the absence of boric acid is shifted towards formation of the $Fe(HD)_3(BOH)^+$ cation. In acidic media, hydrolysis of this compound, promoted by H^+ ion, occurs with the loss of a H_3BO_3 molecule and is described by the equation

$$-d[complex]/dt = (k_5 + k_6[H^+])[Fe(HD)_3(BOH)^+] \qquad (60)$$

$$FeD_3(BOH)_2 \xrightleftharpoons[K_4]{-H_3BO_3 + H^+} Fe(HD)_3(BOH)^+ \xrightarrow{k_5 + k_6[H^+]}$$

$$\xrightarrow{\quad} Fe^{2+} + H_3BO_3 + H_2D + H_2D \text{ decomposition products}$$

Scheme 103

Decomposition of $FeD_3(BOH)_2$ complexes in the presence of boric acid is represented by the Scheme 103.

Light absorption is stipulated by the presence of two complexes:

$$[complex] = [FeD_3(BOH)_2] + [Fe(HD)_3(BOH)^+] \tag{61}$$

$$K_4 = \frac{[FeD_3(BOH)_2][H^+]}{[Fe(HD)_3(BOH)^+][H_3BO_3]} \tag{62}$$

It follows from these equations that

$$[Fe(HD)_3(BOH)^+] = \frac{[complex]}{1 + K_4[H_3BO_3][H^+]^{-1}} \tag{63}$$

and, taking into account Eq. (60), one obtains the equation

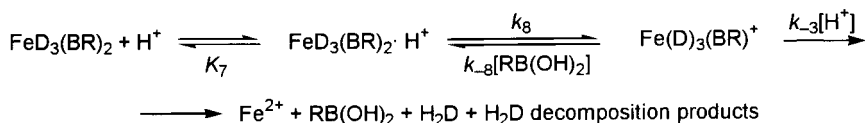$$-d[complex]/dt = \frac{k_5 + k_6[H^+]}{1 + K_4[H_3BO_3][H^+]^{-1}}[complex] \tag{64}$$

which is in accordance with the experimental results and data on decomposition of the $[Fe(H_2D)_3]^{2+}$ complexes; the $k_6[H^+]$ term in Eq. (64) describes an irreversible decomposition of the complex.

The activation energy for the second stage (k_6) and enthalpy for the first equilibrium (K_4) have been determined from the temperature-dependent decomposition rate constants obtained in the presence and absence of boric acid.

Decomposition of $FeD_3(BR)_2$ clathrochelates requires protonation. For the $FeD_3(BOH)_2$ compounds, the complex decomposition is likely to start with protonation of the hydroxyl group in the boron-containing capping group followed by detachment of this group. In the case of $FeNx_3(BC_6H_5)_2$ and $FeNx_3(Bn-C_4H_9)_2$ clathrochelates, the substituent cannot be protonated, and the proton adds to the ester oxygen atoms of the B–O–N moieties only in strongly acidic media.

Subsequent detachment of capping groups and protonation of the reaction products led to the irreversible decomposition of the compounds. Introduction of a great amount of the corresponding boronic acid substantially enhances the reverse (cross-linking)

$$\text{FeD}_3(\text{BR})_2 + \text{H}^+ \underset{K_7}{\rightleftharpoons} \text{FeD}_3(\text{BR})_2 \cdot \text{H}^+ \underset{k_{-8}[\text{RB(OH)}_2]}{\overset{k_8}{\rightleftharpoons}} \text{Fe(D)}_3(\text{BR})^+ \xrightarrow{k_{-3}[\text{H}^+]}$$

$$\xrightarrow{} \text{Fe}^{2+} + \text{RB(OH)}_2 + \text{H}_2\text{D} + \text{H}_2\text{D decomposition products}$$

Scheme 104

reaction rate at the second stage, which causes a decrease in the decomposition rate.

Thus, the Scheme 104 for decomposition of n-butylboron- and phenylboron-capped complexes has been proposed [271, 290].

When the rates of the individual stages are ensured to be equal (the concentrations of intermediates are constant), this scheme may be represented by equations

$$-\mathrm{d}[complex]/\mathrm{d}t = k_{-3}[\text{Fe(HD)}_3(\text{BR})^+][\text{H}^+] \tag{65}$$

$$-\mathrm{d}[complex]/\mathrm{d}t = k_8[\text{FeD}_3(\text{BR})_2 \cdot \text{H}^+] - $$
$$- k_{-8}[\text{Fe(HD)}_3(\text{BR})^+][\text{RB(OH)}_2] \tag{66}$$

$$K_7 = \frac{[\text{FeD}_3(\text{BR})_2 \cdot \text{H}^+]}{[\text{FeD}_3(\text{BR})_2][\text{H}^+]} \tag{67}$$

Since the photometry detects the disappearance of all colored complexes, in solving these equations one should take into account that

$$[complex] = [\text{Fe(HD)}_3(\text{BR})_2] + [\text{Fe(HD)}_3(\text{BR})_2 \cdot \text{H}^+] + [\text{Fe(HD)}_3(\text{BR})^+] \tag{68}$$

and the decomposition effective rate constant is described by the following equation

$$k'_{obs} = \frac{k_{-3}k_8K_7[H^+]^2}{k_{-3}[H^+] + k_{-8}[RB(OH)_2] + k_{-3}K_7[H^+]^2 + k_{-8}K_7[H^+][RB(OH)_2] + k_8K_7[H^+]} \tag{69}$$

This enables one to determine the magnitudes of the constants. In the absence of the corresponding boronic acid in strongly acidic media, the terms k_{-8} [RB(OH)$_2$] and K_7k_{-8} [H$^+$][RB(OH)$_2$] become negligible compared with the other ones and k'_{obs} may be expressed as

$$k'_{obs} = \frac{k_{-3}k_8K_7[H^+]^2}{k_{-3} + k_8K_7 + k_{-3}K_7[H^+]} \tag{70}$$

The temperature-dependent decomposition rate constants of the clathrochelate complexes can be measured providing that the proton

Table 28.
The most abundant ionic species arising from unimolecular decomposition of $FeD_3(BOH)_2$ clathrochelates.

Ionic species	$FeNx_3(BOH)_2$	$Fe(4MNx)_3(BOH)_2$	$FeGx_3(BOH)_2$	$FeOx_3(BOH)_2$
$[MH]^+$	533(100)	574(100)	575(100)	617(100)
$[MH - H_2O]^+$	515(33)	557(40)	557(49)	599(52)
$[MH - BO(OH)]^+$			531(10)	573(10)
$[MH - BO_2(OH)]^+$			515(16)	557(16)
$[MH - BO_3(OH)]^+$	457(13)		499(16)	541(10)
$[MH - (D - O)]^+$	409(18)	437(42)	437(27)	465(21)
$[MH - H_2D]^+$	392(8)	420(42)	420(33)	448(33)
$[MH - 2(D - O)]^+$	285(12)	299(100)	299(72)	313(29)
$[MH - (D - O) - D]^+$		283(46)	283(30)	297(12)
$[MH - H_2O - D]^+$	375(15)	403(66)	403(60)	431(19)
$[MH - B(OH)(D - O)D]^+$	241(5)		255(26)	269(10)
$[MH - B(OH)D_2]^+$		239(48)	239(73)	253(31)
$[D_2(BOH)]^+$		336(28)		

activity is high. Under these conditions, with allowance for the k_{-3}, $k_{-3}k_8[H^+]$, and k_8k_7 relationships, one can write $k'_{obs} \sim k_{-3}[H^+]$. Thus, a plot of the decomposition rate constant k'_{obs} in the absence of phenylboronic and n-butylboronic acids *versus* temperature in the $Log(k'_{obs}/[H^+]) - T^{-1}$ coordinates permits one to obtain the activation energy for the irreversible decomposition stage (Table 27).

Fragmentation of the molecules of macrobicyclic boron-capped iron(II) tris-dioximates in the gas phase occurs mainly by an alternative scheme compared with the reactions in solution [292]. Excited molecules of the complexes that gained from a cascade of reactions sufficient energy for rupture of bonds with fragmentation occurred by similar routes for all complexes considered (Table 28).

Fig. 33 shows the pathways for fragmentation of the $FeOx_3(BOH)_2$ molecule.

The most bulky fragmental ions resulted from heterolytic bond rupture and withdrawal of the apical substituent (OH-group) from a boron-containing capping fragment after addition of the proton:

$$[FeD_3(BOH)_2 + H]^{+,*} \rightarrow [FeD_3B(BOH)]^+ + H_2O \qquad (71)$$
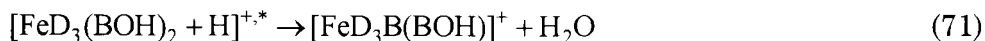
According to the data on the dissociation of $FeD_3(BOH)_2$ complexes in aqueous solutions, this process proceeds *via* two stages: detachment of capping groups and subsequent decomposition of the protonated $[Fe(H_2D)_3]^{2+}$ tris-dioximate. More complete fragmentation of the complexes excited in the gas phase
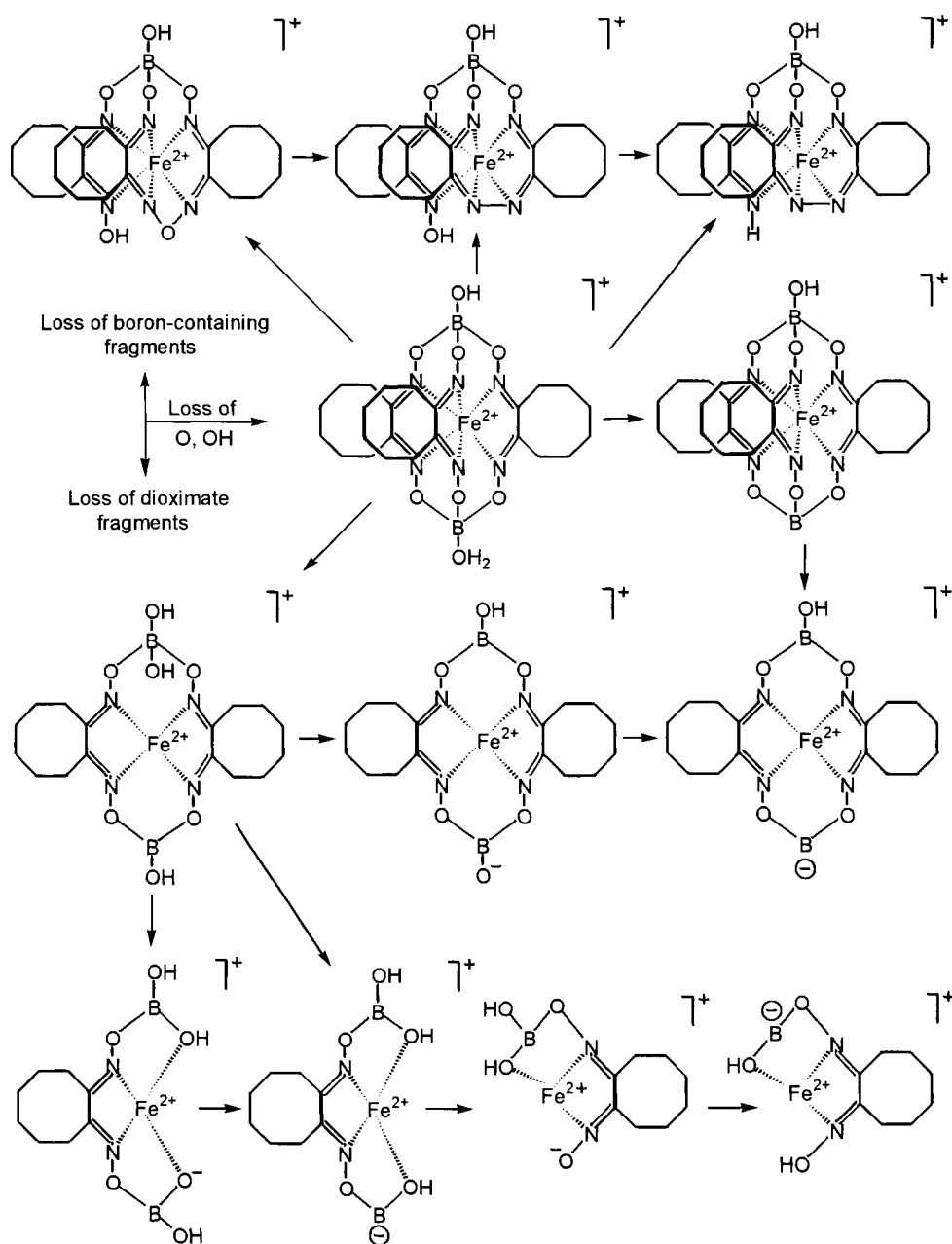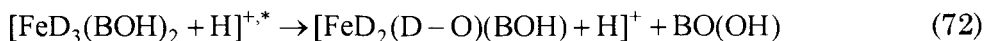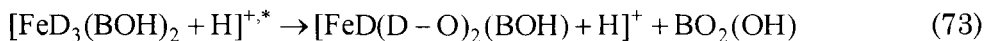
Figure 33. Scheme of FeOx$_3$(BOH)$_2$ complex fragmentation in the gas phase [292].

might be achieved *via* the same route. However, the intensities of peaks of fragmental ions formed by the reaction
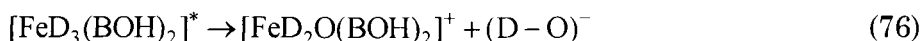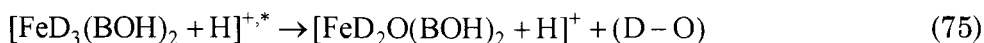
$$[FeD_3(BOH)_2 + H]^{+,*} \rightarrow [FeD_2(D-O)(BOH) + H]^+ + BO(OH) \tag{72}$$

are negligible in the mass spectra for $FeGx_3(BOH)_2$ and $FeOx_3(BOH)_2$ complexes. In the spectra for compounds with six-membered dioximes, these ions were not observed [292].
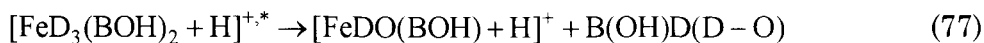
The peaks corresponding to the products of Reactions 73 and 74 were detected in the mass spectra for $FeGx_3(BOH)_2$ and $FeOx_3(BOH)_2$ complexes. However, these products cannot result from hydrolysis. They are formed only in the gas phase *via* a homolytic N–O bond rupture:

$$[FeD_3(BOH)_2 + H]^{+,*} \rightarrow [FeD(D-O)_2(BOH) + H]^+ + BO_2(OH) \tag{73}$$

$$[FeD_3(BOH)_2 + H]^{+,*} \rightarrow [Fe(D-O)_3(BOH) + H]^+ + BO_3(OH) \tag{74}$$

Nearly all fragments in the mass spectra for the complexes investigated showed sets of isotopic peaks, which indicate the presence of boron-containing fragments in these species. As seen from the composition of the ionic fragments, their formation in the gas phase largely occurs with detachment of dioximate fragments from the "parent" molecule or ion:

$$[FeD_3(BOH)_2 + H]^{+,*} \rightarrow [FeD_2O(BOH)_2 + H]^+ + (D-O) \tag{75}$$

$$[FeD_3(BOH)_2]^* \rightarrow [FeD_2O(BOH)_2]^+ + (D-O)^- \tag{76}$$

The total intensity of the fragmental ions resulting from the detachment of dioximate moieties not affecting borate capping groups (Reactions 75 and 76) is higher than the total intensity of the ions that have "lost" fragments of the both types (Reactions 77 and 78).

$$[FeD_3(BOH)_2 + H]^{+,*} \rightarrow [FeDO(BOH) + H]^+ + B(OH)D(D-O) \tag{77}$$

$$[FeD_3(BOH)_2 + H]^{+,*} \rightarrow [FeD(BOH) + H]^+ + B(OH)D_2 \tag{78}$$

This suggests that the detachment of the borate capping groups takes place after the detachment of dioximate fragments. Thus, greater excitation energy of the complex species is required for the borate fragment detachment.

The results of FAB-MS study of the macrobicyclic boron-capped iron(II) dioximates indicated that in the gas phase the energetics of bond rupture in their molecular complexes changes compared with

that in aqueous solution. In the gas phase, a fragment with three conjugated energetically favourable five-membered chelate cycles is the most stable one:
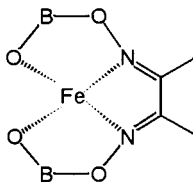
(79)

The formation of these cycles ensures a considerable energy gain when two dioximate fragments are detached. Actually, in Ref. 39 it was noted that the $[CoDm_3(BF)_2](BF_4)$ and $CoDm_3(BF)_2$ complexes are volatile and thermally stable during sublimation, and they were studied by electron impact mass spectrometry. The parent mass peaks in the spectral region 400–500 a.m.u. were the most intense, and their magnitude depends on temperature. The cobalt(III) complex, despite being ionic associate, sublimates at a lower temperature than an analogous cobalt(II) intracomplex. The main feature characterizing the fragmentation of clathrochelate cobalt dioximates was a loss of one or two dioximate fragments without previous detachment of capping groups [39].

The preferential detachment of the boron-containing cross-linking fragment during dissociation in solution was presumably associated with the high solvation energy of this fragment.

In the alicyclic dioxime series, one can trace the effects of substituents and ring size on the fragmentation of the corresponding clathrochelate complexes. The intensity of the peak, which corresponds to detachment of the apical hydroxyl group from the framework, slightly increases with the increase in the ring size. Detachment of boron-containing capping groups is mainly characteristic of seven- and eight-membered dioximes. Fragmentation with detachment of dioximate moieties is quite insignificant for nioximate and the most essential for 4-methylnioximate; it decreases further with increases in the ring size. Consequently, the introduction of a substituent into the cyclohexane ring and the increase of the ring size to seven result in a noticeable destabilization of the clathrochelate framework. The subsequent transition to an eight-membered dioxime, less strained than the seven-membered one, reduces the strain in the clathrochelate framework and stabilizes it [292].

In contrast to FAB mass spectra for macrobicyclic tris-dioximates, electrospray ionization (ESI) spectra for the complexes of divalent (manganese, copper, zinc, cadmium, mercury, nickel, cobalt, magnesium) and trivalent (cobalt) metal ions with regular and expanded sarcophaginate ligands were considerably simpler and showed ions corresponding to the intact complexes and ion pairs. The fragmentation of these ions is negligible, and the reduction of encapsulated metal ion was observed in some cobalt(III) sarcophaginates only [295].

4.3 REACTIONS OF SARCOPHAGINATES AND SEPULCHRATES

Sarcophaginates and sepulchrates arise from the condensation of aldehydes with coordinated amines followed by the condensation of imine products with nucleophilic agents, e.g., ammonia or a nitro-methane carbanion. The resultant amine or nitroethyl fragment undergoes condensation with adjacent imine groups without metal ion–ligand bond rupture to produce the first capping fragments. Activation of the coordinated imine towards nucleophilic agents occurs with the action of the metal ion, which facilitates nucleophilic attack. In their reactivity, coordinated imines occupy an intermediate position between the imine base and iminium ion. This activation nucleophilic attack prevents protonation that leads to imine rupture [96].

As an example of such a reaction, we consider the preparation of cobalt(III) sepulchrate by template condensation of tris-ethylene-diaminate with formaldehyde and ammonia. At the first stage the condensation of the coordinated and deprotonated amino group with formaldehyde yields carbinolamine, which easily detaches (the imine was isolated and characterized) [4, 96]. The imine is further attacked by ammonia to give *heme*-diamine, which undergoes intermolecular condensation with first one and then a second adjacent imino group, resulting from condensation of amino groups with formaldehyde, producing a capping fragment. Then the process replicates on another face, whereby the metal ion is encapsulated by sepulchrate ligand (Scheme 105).

The fact that the synthesis of sarcophaginates and sepulchrates proceeds *via* the formation of an imine complex was also confirmed by isolation of the semiclathrochelate [Co(sen)]$^{3+}$ complex (as a by-

product of capping) and the methylated $[Co(N\text{-mesen})]^{3+}$ compound [96]. The methylated product results from the Cannizzaro reaction:

$$+ \text{ HCOO}^- \tag{80}$$
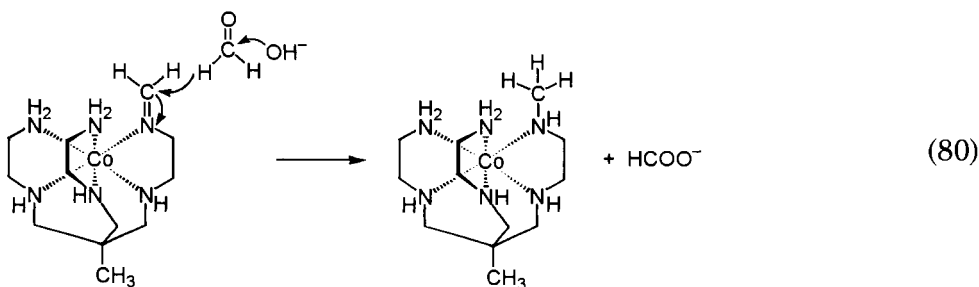
The mechanism proposed for the formation of the sepulchrates accounts for the fact that, despite seven chiral centres and six nitrogen-metal bonds, the synthesis of $[Co(sep)]^{3+}$ cation yields only one isomer. After the formation of the first heminal diamine and second imine centre, the chiral nitrogen centre must be oriented so that the methylene unit of the amine fragment and the proton are apical and equatorial, respectively, before intramolecular cyclization. In this case, six-membered ring closure takes place. The same apical orientation of the six-membered chelate cycle must be retained to complete the formation of a capping group. After the completed encapsulation, the methylene unit and the proton cannot
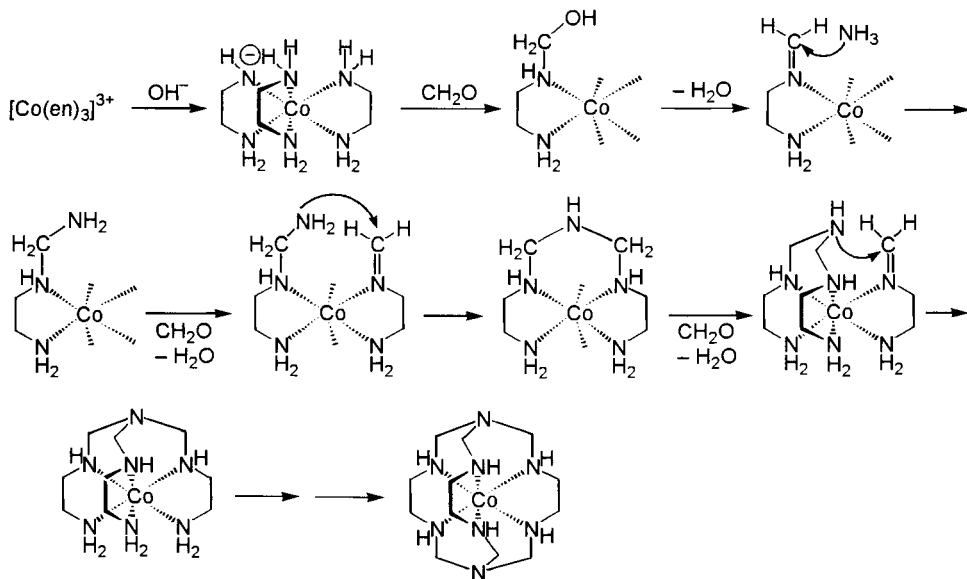
Scheme 105
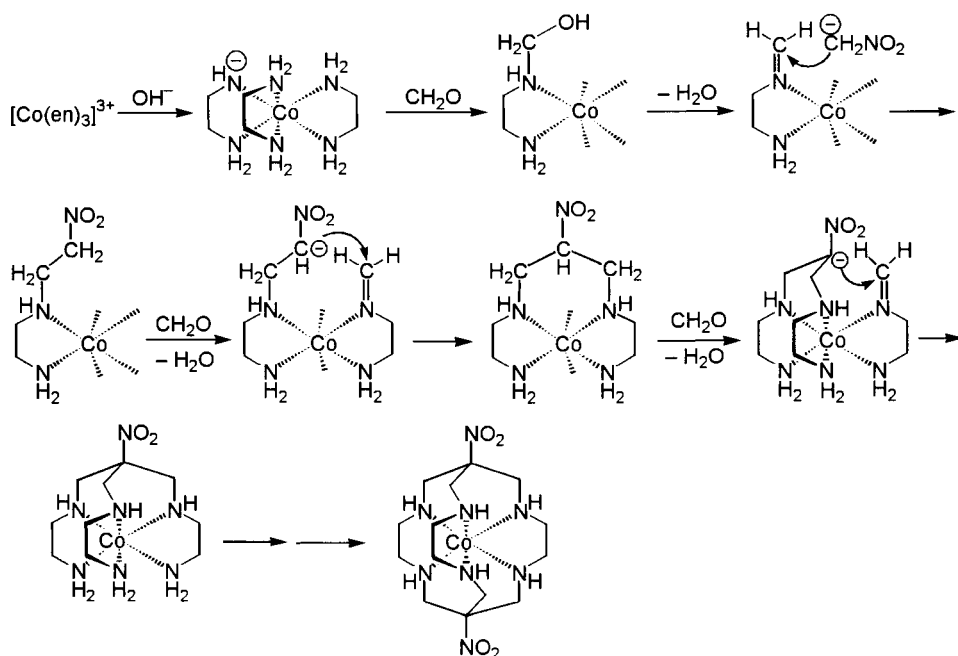
Scheme 106

be inverted, and such a configuration retained for all six chiral nitrogen centres [96].

When nitromethane is used as the capping agent instead of ammonia, either the interaction of the nitromethane anion with coordinated ethyleneimine or the addition of nitroethylene to deprotonated coordinated amine yields an intermediate nitroethyl complex. Nitroethylene is formed by a base-catalyzed condensation of nitromethane and formaldehyde. The experimental data suggest that the mechanism of formation of the nitroethyl complex *via* coordinated imine by Scheme 106 is favoured [101].

The fact that one of the capping groups is formed faster than another was confirmed by isolation of an intermediate [Co(NOsen)]Cl₃ complex and the [Co(N-meNOsen)]Cl₃ product of its methylation that arises from the Cannizzaro reaction between an imine [Co(NOsen)]Cl₃ derivative and formaldehyde. At the same time an attempt to obtain the [Co(en)₂(N-meen)]³⁺ complex in appreciable amounts met with failure.

A mechanism similar to that of Scheme 106 was also proposed for macrobicyclic cobalt(III) tris-cyclohexanediaminates [107].

One should expect that rhodium(III), iridium(III) and platinum(IV) sarcophaginates and sepulchrates form in the same way. Attempts to synthesize chromium(III) clathrochelates from $[Cr(en)_3]^{3+}$ tris-ethylenediaminate proved to be less successful. In this case a rapid Cr–N bond rupture reaction competes with the capping process and markedly reduces the yield of the clathrochelate complex [4, 158]. Similar problems arise with the capping of labile copper(II) and nickel(II) ethylenediaminates, as well as of ruthenium(III) and osmium(III) ones. In the last two cases, the formation of macrobicyclic complexes has been complicated by spontaneous disproportionation of the resultant imines under basic conditions to compounds whose central ion oxidation states are (2+) and (4+) [4].

The macrocyclization reaction proceeds by an analogous route when bifunctional methylene compounds, e.g., diethylmalonate, were used as cross-linking agents [133]. In this case as with nitromethane, the attacking imine carbanion is also formed under basic conditions. The diethoxycarbonylethylamine resulting from the addition of the carbanion to the coordinated imine undergoes two intramolecular condensations to a produce macrobicyclic structure (Scheme 107).

Condensation of the bis-triamine $[Co(tame)_2]^{3+}$ complex **1** with nitromethane and formaldehyde proceeds *via* an unusual route
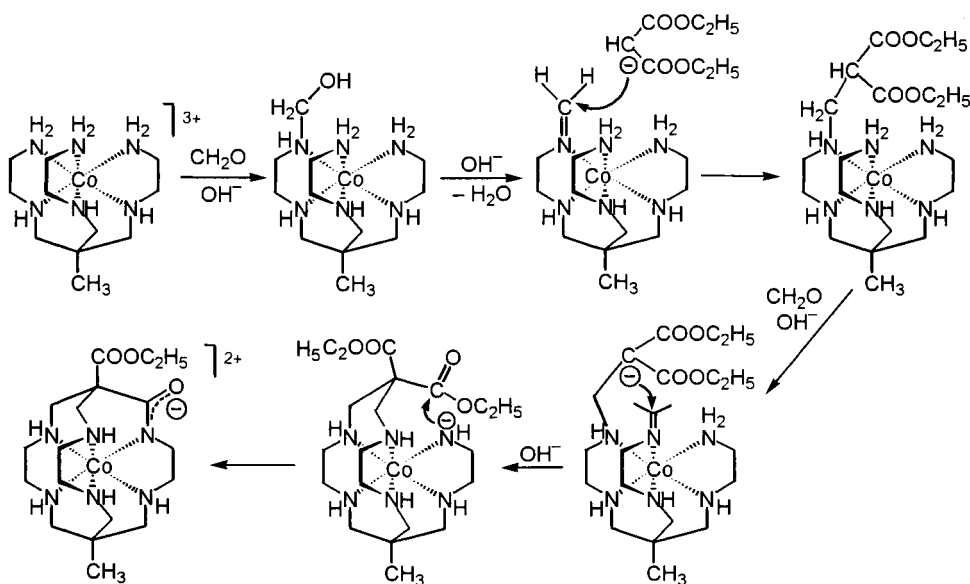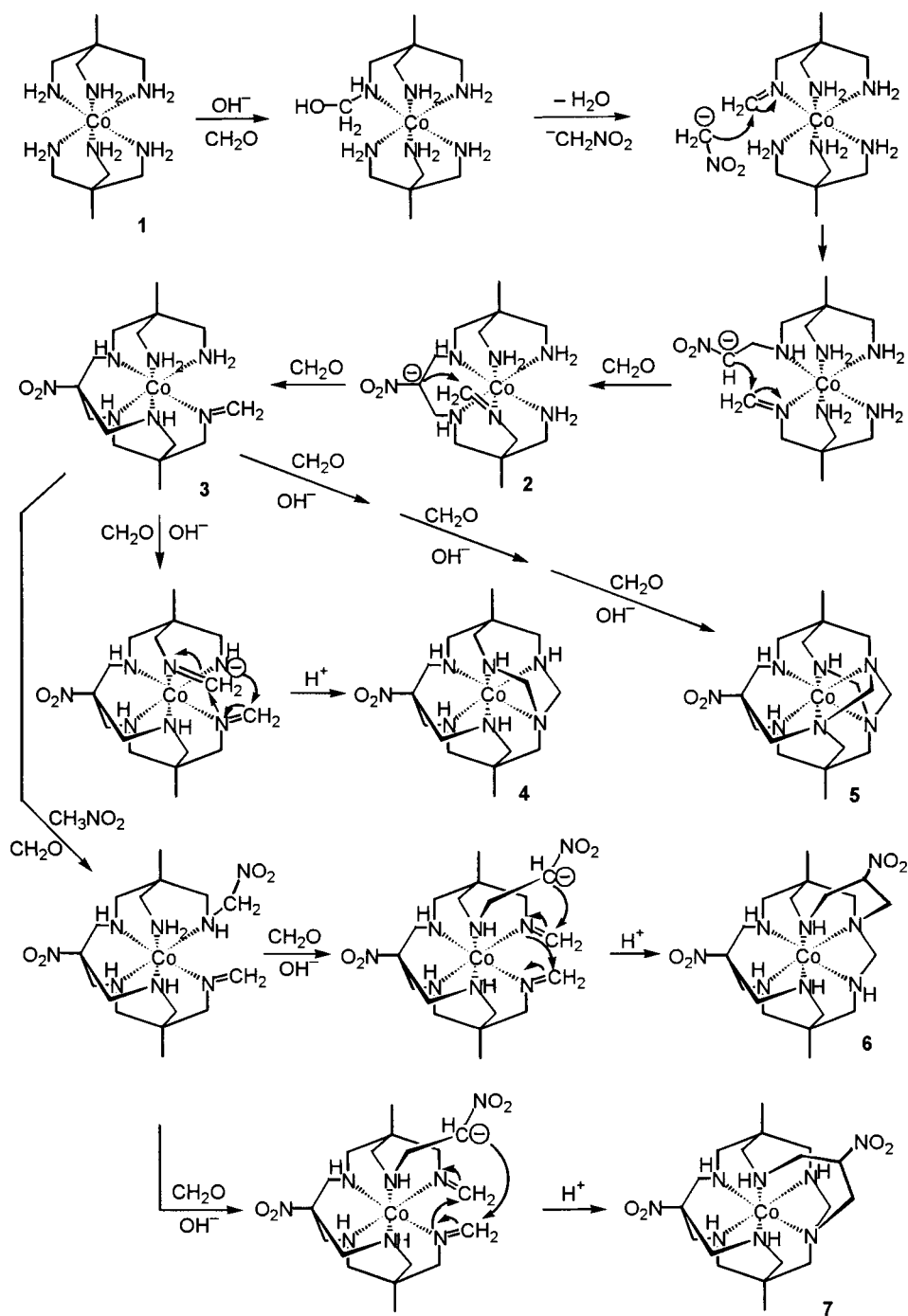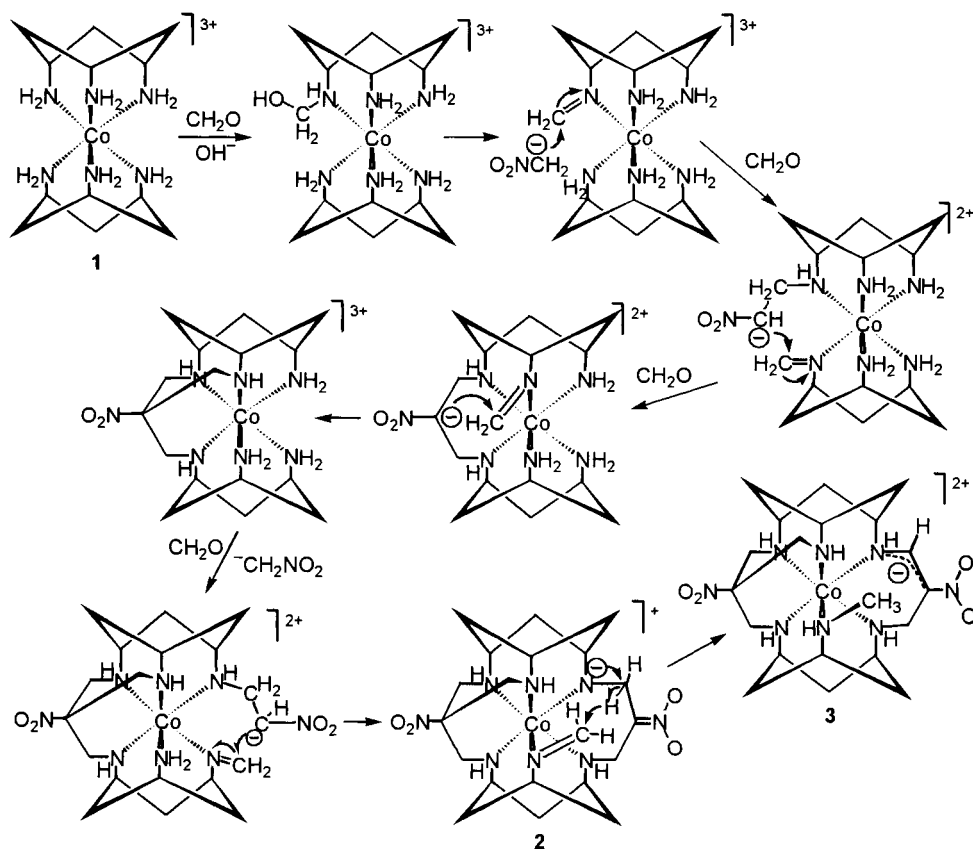

Scheme 107

(Scheme 108). At the beginning, as is the case with tris-diaminates, a capping fragment with an apical nitro group is formed. The semiclathrochelate complex **2** undergoes condensation with formaldehyde to yield imine **3**, which interacts mainly with coordinated amine or imine nitrogen rather than with the nitromethane nucleophilic carbanion. As a result, macrotricyclic complex **4** with two four-membered chelate cycles is obtained. By an analogous route, a macrotricyclic heptaazasarcophaginate is formed in the condensation of $[Co(tame)_2]^{3+}$ ion with formaldehyde and ammonia [149].

A further condensation of the macrobicyclic nitromethyl-containing complex with formaldehyde, which gives one more four-membered chelate cycle, is far less efficient, and a macrotetracyclic cobalt(III) complex **5** with very rigid structure was isolated [148]. Imine complex **3** undergoes a nucleophilic attack of nitromethane carbanion to a lesser extent; however a capping fragment analogous to the first one is not formed. Complexes **6** and **7** contain, along with four-membered rings, six-membered chelate rings that result from the condensation of one nitromethane molecule and two formaldehyde molecules. The formation of six-membered rings is likely to precede condensation that leads to the formation of four-membered rings. This is confirmed by the fact that during the capping process of bis-triamine $[Co(tacn)_3]^{3+}$ cation **1** (Scheme 109), similar to $[Co(tame)_2]^{3+}$ cation, an unusual product, carbanion **2** with a nitro group, containing a six-membered chelate cycle stabilized by coordination to cobalt(III) ion, is formed. The subsequent intramolecular hydride transfer from the methylene unit bound to the nitro group to the adjacent imine fragment (Scheme 109), lead to stabilization of the carbanion chelate with delocalization, affecting the nitro group, and to methylation of the coordinated amino group (complex **3**) [155].

Macrobicyclic cobalt (III) sarcophaginates undergo an unusual rearrangement to *absar* type clathrochelates with a contracted cavity [4, 101]. This rearrangement is largely due to the discrepancies in the size of Co^{3+} ion and the macrobicyclic ligand cavity. In organic chemical reactions, e.g., for adamantyl derivatives, such a reaction takes place in the reverse direction [4]. Moreover, this rearrangement in the case of nitrosation of the aminosarcophaginates decreases repulsion between the Co^{3+} ion and the positive charge, localized on the capping group (Scheme 110).

272

Scheme 108

Scheme 109
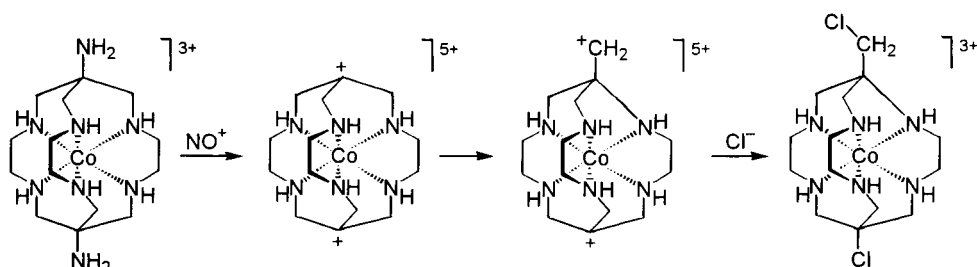
Scheme 110

A similar rearrangement has been observed when the base attacks nitrosarcophaginates, in particular [Co(MENOsar)]³⁺ cation. At the first stage, a reaction of the retro-aldol type occurs to decompose the capping fragment. Then the base favours the detachment of an imine species, and the primary amine moiety is formed. The latter reacts

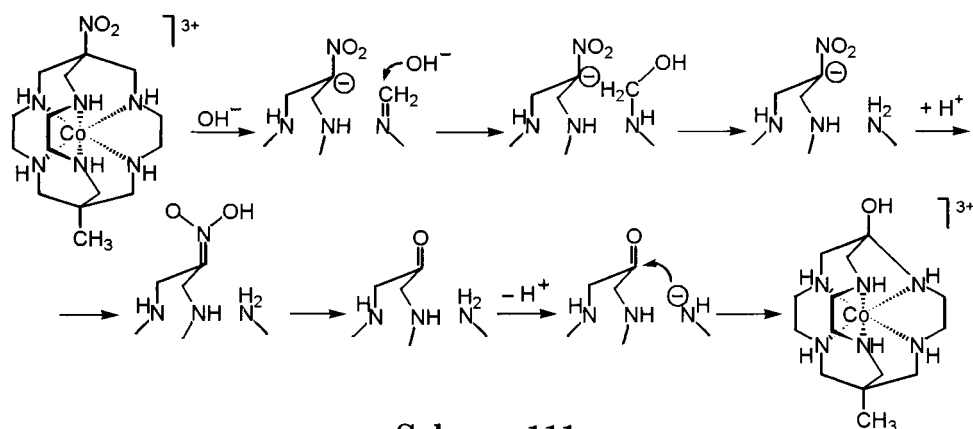**Scheme 109**

Scheme 110

A similar rearrangement has been observed when the base attacks nitrosarcophaginates, in particular $[Co(MENOsar)]^{3+}$ cation. At the first stage, a reaction of the retro-aldol type occurs to decompose the capping fragment. Then the base favours the detachment of an imine species, and the primary amine moiety is formed. The latter reacts

Scheme 111

with ketone formed from the nitromethane fragment in slightly acidic medium by the Nef reaction (Scheme 111).

As result a hydroxy-containing clathrochelate complex with a contracted ligand cavity is formed [4].

The kinetics and mechanism of the rearrangement of a regular cobalt(III) nitrosarcophaginate into a contracted one under basic conditions have been examined more thoroughly by ^{1}H and ^{13}C NMR spectroscopy, UV-vis spectrophotometry, and X-ray analysis [106]. The addition of one base equivalent to an aqueous solution of the [Co(MENOsar)]$^{3+}$ cation results in the deprotonation of a coordinated secondary amino group. The further addition of a base causes a first-order destruction of one capping fragment with a loss of a methylene unit. This retro-Mannich type reaction involves the formation of imine after the protonation of a secondary amino group by elimination of a carbanion from a negatively charged species. The resulting imine is then hydrolysed more slowly under basic conditions with a loss of a methylene unit. The next methylene units are eliminated still more slowly, and therefore the rearrangement semiproduct **1** was isolated, as well as its isomer **2** formed during the chromatographic procedure (Scheme 112).

Both semiproducts with a pendant arm macrocyclic structure undergo macrocyclization in neutral solution *via* a Nef reaction intermediate step with detachment of a NO species, followed by condensation of the resulting carbonyl group with a deprotonated and coordinated primary amino group [106].

In the case of a cobalt(III) N$_3$S$_3$-nitrosarcophaginate, the rearrangement of the deprotonated complex with the loss of a

methylene unit under basic conditions proceeds far more slowly and leads to a product of a different type, an oxidized deprotonated carbanion with partial charge delocalization (Scheme 113).

The mechanism of this process was studied in Ref. 296 by the same methods as those employed to examine a N_6-nitrosarcophaginate. The macrocyclic cobalt(III) complex with a pendant arm, formed at the first stage by a retro-Mannich reaction with loss of a methylene unit, is in equilibrium with a nitronate species. The
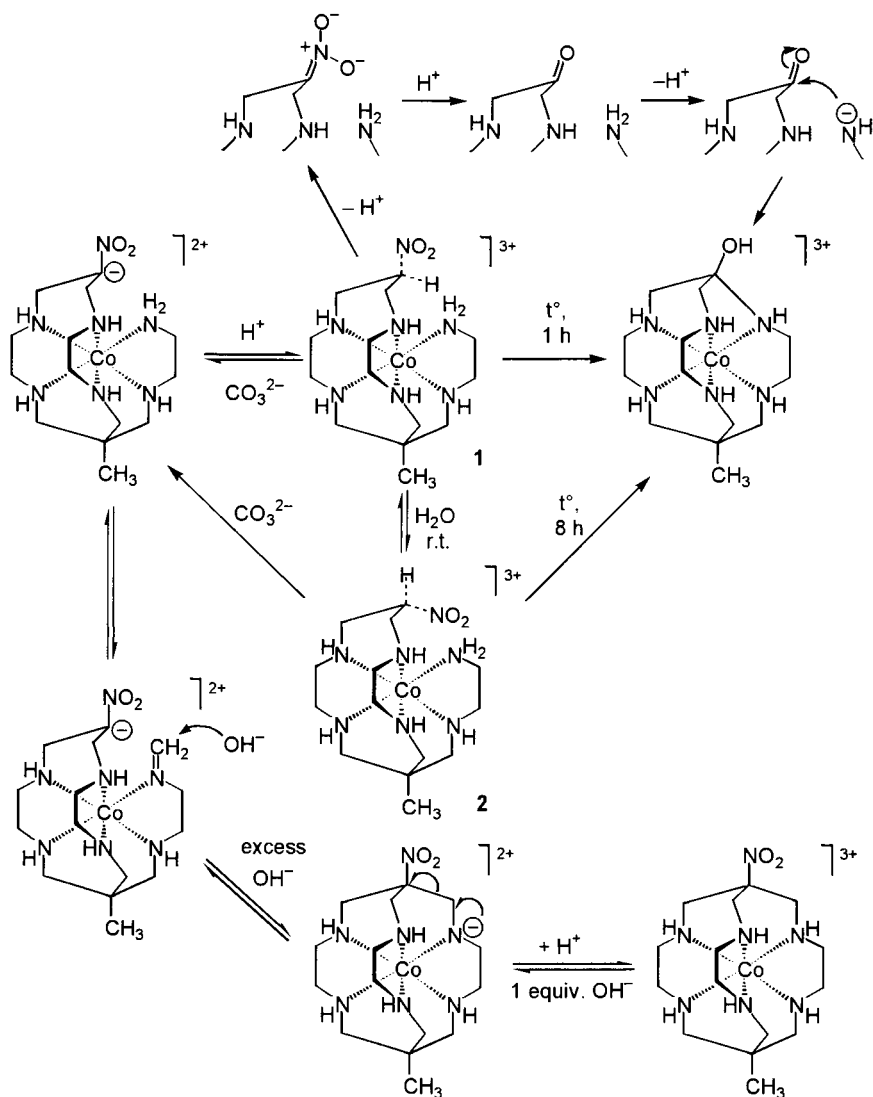
Scheme 112
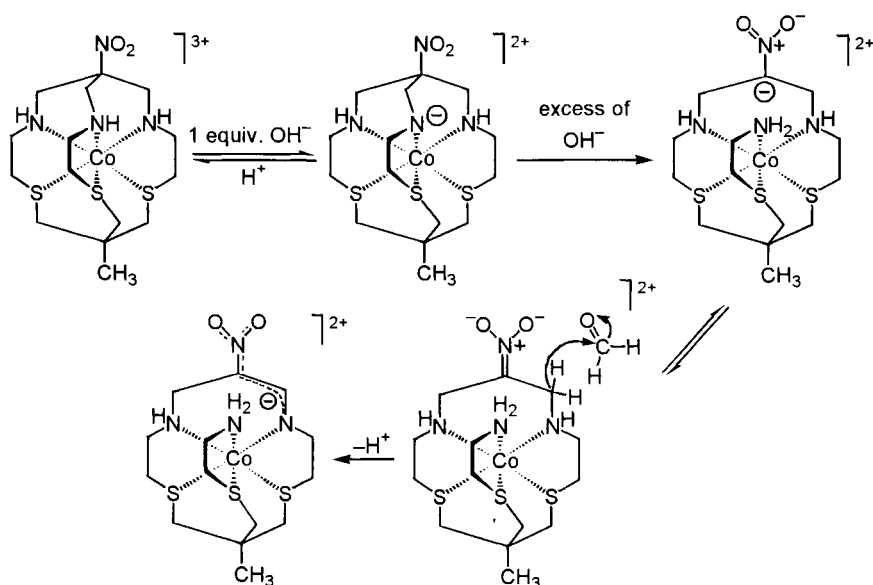
Scheme 113

hydride transfer onto either a formaldehyde molecule or to another cobalt(III) ion results in the formation of a stable carbanion with charge delocalization. Since the cobalt(III) N_3S_3-sarcophaginates are reduced more readily than their N_6-analogs, it is possible that intermolecular hydride transfer involving reduction of mentioned cobalt(III) centre takes place. The stability of this carbanion increases by deprotonation and it is not reprotonated even under the action of strong acids [296].

The fact that free ligands can be obtained by demetallation of the preliminarily synthesized complexes is a striking feature observed in the chemistry of sarcophaginates and sepulchrates. Studies on the mechanism of the demetallation (extrusion) occurring in acidic media are of great importance.

Analysis of kinetic and structural data permitted Sargeson and coworkers to establish a mechanism of Cu^{2+} ion extrusion from a sarcophaginate cavity [4, 5]. A spontaneous Cu–N bond rupture *via* a dissociative mechanism takes place at the first stage. It accounts for the fact that the rate of transition of a clathrochelate complex to a square-planar one is independent of the concentration of H^+ ion. Then noncoordinated amino group protonates and a second amino group of the same ethylenediamine moiety coordinates in the apical position

against the square-planar macrocyclic CuN_4 fragment formed. The dissociation and transition to a square-planar complex seem to occur subsequently and concurrently with the rupture of the two Cu–N bonds of one chelate cycle. In this case, the configuration of the four macrocyclic nitrogen atoms is the same as in the initial sarcophaginate. Inversion of two nitrogen atoms to the reverse configurations occurs after dissociation of two more Cu–N bonds. Free amino groups protonate, followed by inversion, deprotonation, and recoordination.

X-ray diffraction data for the stable purple complex indicate that four coordinated amino groups have R, S, R, S-configurations. It is obvious that two of the three groups undergo inversion. Two non-coordinated amino groups in the cis-position are protonated (Scheme 114). When the process proceeds in strongly acidic media after the rupture of two more Cu–N bonds amino groups are protonated without recoordination. The complete rupture of these bonds to give a protonated ligand and CuX_4^{2-} anion was observed.

When the sarcophaginate is synthesized from free ligand, such a process can proceed through the same steps in the reverse direction [4].

A similar extrusion mechanism was also observed for zinc and cadmium(II) sarcophaginates using deuterium exchange [5]. Demetallation of mercury(II) sarcophaginates in the presence of chloride ions exhibits essential peculiarities [5, 174]. It is evident that in such acidic medium a hydroxyl ion cannot act as a reagent that deprotonates amino groups, and metal–nitrogen bond rupture takes place at the first step. Then a free secondary amino group deuterates. Detachment of H^+ ion from the resultant NHD^+ groups and subsequent recoordination of the nitrogen atom leads to the deuterated complex. The metal ion extrusion is either faster or equal to proton exchange (Scheme 115).
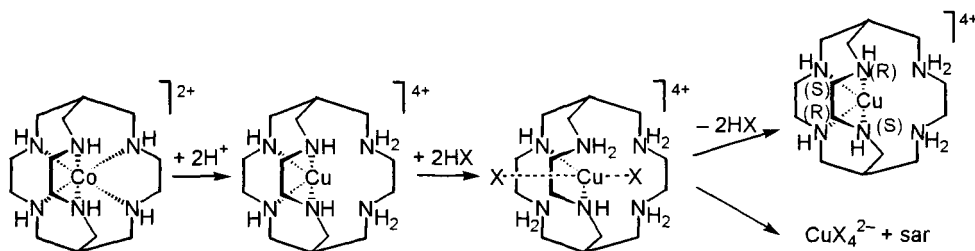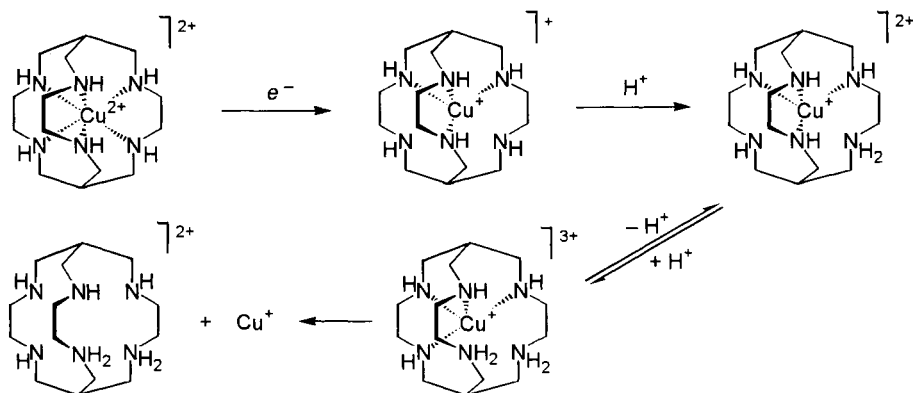

Scheme 114
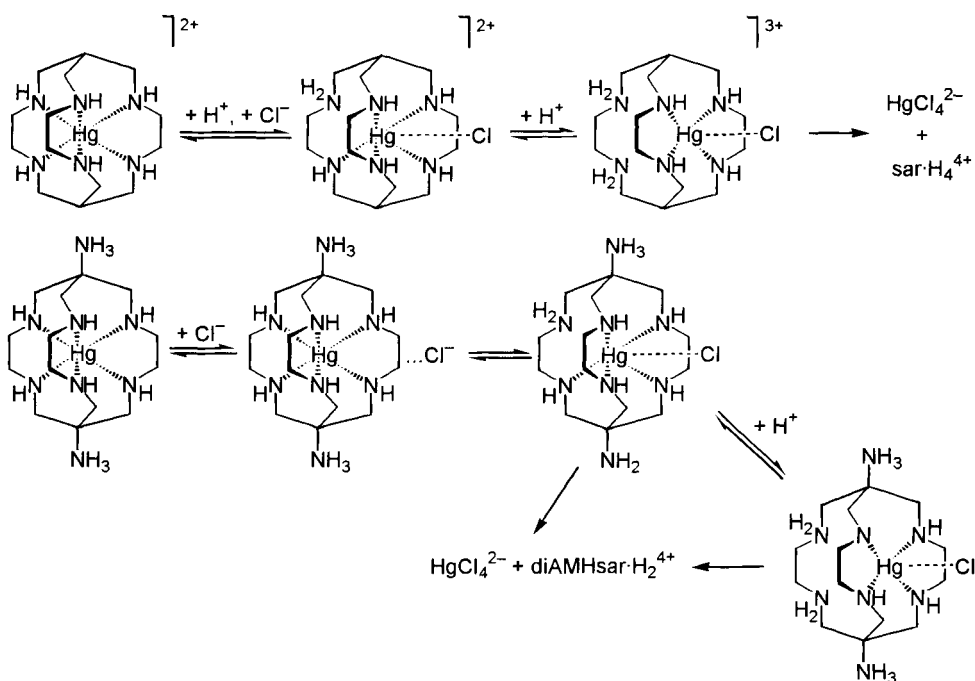
Scheme 115

At the first stage, association with Cl⁻ anion occurs after protonation of the two amino groups resulting from Hg–N bond rupture (Scheme 115). The ion pairing has been observed for the [Cd(diAMsar)]²⁺...Cl⁻ system by ¹H NMR spectroscopy (a chemical shift in the signals without loss of the sarcophaginate cation D_3 symmetry). Clearly, Cl⁻ anion has not coordinately bound the metal centre. The same experiments are not feasible with mercury(II) systems since the extrusion reaction occurs too rapidly. A high H⁺ ion concentration is required to observe association since protonation of amino groups and association of Cl⁻ anion to the coordinately unsaturated metal ion are interrelated processes [5, 174]. Once a protonated ionic associate has been formed, protonation of a second amino group of the same ethylenediaminate moiety occurs by removal of mercury(II) ion in the form of $HgCl_4^{2-}$ anion. The rates of [Hg(sar)]²⁺ and [Hg(diAMHsar)]⁴⁺ sarcophaginate decomposition differ due to the positive charge of the apical protonated amino groups in the latter, which hampers protonation of coordinated species [5, 174].

Scheme 116

An analogous scheme of manganese(II) ion extrusion from a sarcophaginate cavity was proposed in Ref. 179.

To elucidate the mechanism of extrusion of the copper ion from the cage after reduction to copper(I), the basicity of the free sarcophaginate is taken into consideration: despite the six basic sites available, only four are protonated observably. Two adjacent nitrogen atoms in the crystal structure do not share a proton between them either. The existence of uncoordinated nitrogen donor atoms for certain metal oxidation states can be gauged from pK_a values for a series of transition metals. An analysis of the above-mentioned results has enabled one to propose the copper(II) ion extrusion mechanism that is represented in Scheme 116. The copper ion coordination number diminishes from six to four, and then the protonation of one of the free amino groups takes place. The next slow process depends on the concentration of H^+ ions and occurs in two consequent stages: unfavourable pre-equilibrium and further protonation, presumably followed by the rate – determination stage of copper(I) ion elimination from the cage cavity [293].

Chapter 5

Properties of clathrochelates

5.1 ION ASSOCIATION OF CLATHROCHELATES IN SOLUTION

Ion association or ion-pairing reactions are most commonly studied for clathrochelate complexes exhibiting unique inertness. These reactions attract particular interest due to their marked effect on the kinetics and direction of the redox and photochemical reactions and on the characteristics of electrochemical processes. In certain cases, ion association reactions govern the catalytic activity of compounds. The ion-pairing ability of clathrochelates is utilized to resolve racemates into optical isomers (enantiomers) and to separate optically active anions using clathrochelates as chiral eluents.

Most studies deal with cobalt clathrochelates. In several cases, nonmacrocyclic tris-diamine complexes have also been investigated to elucidate the specificity of interactions brought about by the formation of cage structures.

The results of polarographic and spectrophotometric investigation of the reduction and deprotonation of $[Co(sep)]^{3+}$ cation in the presence of different electrolytes were described in Ref. 297, and remarkably specific anion effects were observed. The half-wave potential $E_{1/2}$ becomes more negative by increasing the ionic strength in the series $ClO_4^- < NH_2SO_3^- < Cl^-$, $Br^- < F^- < OH^-$. Data for different electrolytes extrapolate to the same value at $\mu = 0$ mol·l^{-1} with the exception of NaOH, which gives value much more negative than the values of all the other electrolytes with μ from 0 to 0.8 mol·l^{-1}. This was thought to be caused by the formation of the ion pairs in the anion series from ClO_4^- to F^- and by deprotonation of the $[Co(sep)]^{3+}$ cation in the presence of NaOH. The last assumption was confirmed by spectrophotometric study.

At present, the formation of ion pairs between cobalt clathrochelates and inorganic (ClO_4^-, F^-, Cl^-, Br^-, I^-, NO_3^- [118, 297-302], SO_4^{2-}, $S_2O_3^{2-}$ [118, 303, 304]), organic (oxalate, malonate,

tartrate, and anthracene carboxylate) [118, 305-307], complex anions [308-315], and metalloproteins [316-321] has been reported.

Ion pairing of $[Co(sep)]^{3+}$ cation with Br^- and I^- anions was confirmed by the occurrence of CTBs in UV-vis spectra at 33 898 and 37 037 cm^{-1} in the presence of NaBr and NaI, respectively [299, 300]. The association constants of $[Co(sep)]^{3+}$ cation and halogenide anions ($K_{Cl^-} = 5.5$, $K_{Br^-} = 2.3$ and $K_{I^-} = 1.7$ at $\mu = 0.5$ $mol \cdot l^{-1}$) were determined by a kinetic method when the reduction of $[Co(sep)]^{3+}$ cation with chromium(II) ion in the presence of these anions has been studied. The halogenide anions were found to affect the rate and activation parameters of electron transfer [301], and a model of anion transfer catalysis involving ion pairing was proposed. The CD data for $[Co(en)_3]^{3+}...X^-$ ion pairs demonstrated the presence of strong hydrogen bonds in the associates.

Hydrogen bonding between coordinated amino groups and ClO_4^- anions in the crystal of nickel(II) sarcophaginate was determined by X-ray crystallography (Fig. 34) [176].

It was established that there is a correlation between the association constants for the $[Co(sep)]^{3+}...Hal^-$ ion pairs and the basicity of halogenide anions (Fig. 35), which indirectly confirmed the coordination *via* hydrogen bonds in solution [301]. Association constants for the $[Co(sep)]^{3+}...F^-$, Cl^-, I^-, ClO_4^-, and $C_2O_4^{2-}$ ion pairs were calculated from
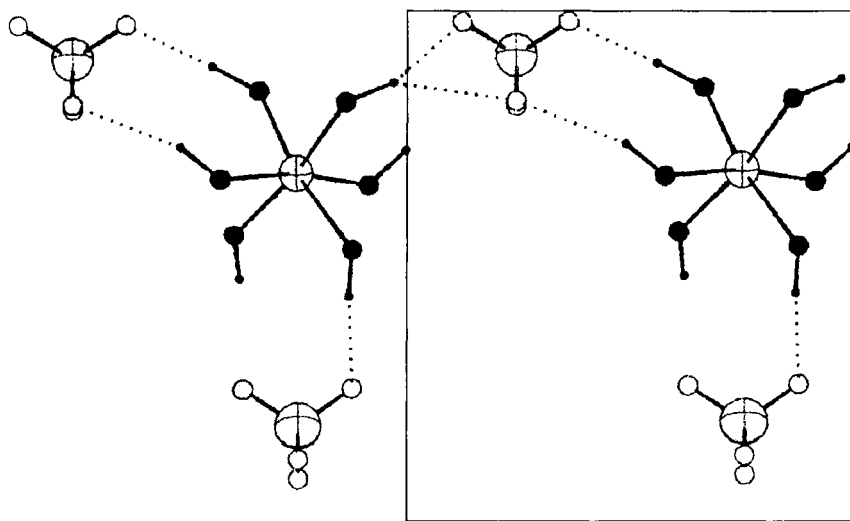

Fig. 34. Hydrogen bonding network between $[Ni(sar)]^{2+}$ and ClO_4^- ions [176].

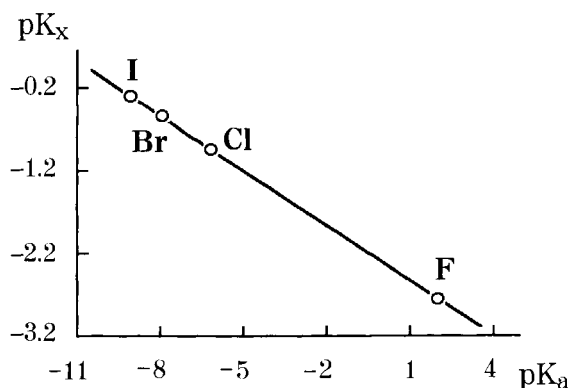Fig. 35. Correlation between the association constants (pK_x) for the
[Co(sep)]$^{3+}$...Hal$^-$ ion pairs and the basicity of halogenide anions (pK_a).

the ^{59}Co NMR chemical shifts ($K_{F^-} = 35 \pm 1$, $K_{Cl^-} = 23 \pm 1$, $K_{I^-} = 31 \pm 1$,
$K_{ClO_4^-} = 41 \pm 2$, $K_{C_2O_4^{2-}} = 277 \pm 68$ at $\mu = 0$ mol·l^{-1}) [302].

A detailed study of ionic associates of the [Co(sep)]$^{3+}$ cation with
$S_2O_3^{2-}$ and SO_4^{2-} anions was reported in Ref. 304. The formation of
the associates with one and two anionic species was detected by
UV-vis spectrophotometry, optical CD, and solubility measurements.
For the ion pair with $S_2O_3^{2-}$ ion, the first- and second-stage
association constants were found to be $\beta_1 = 2.5 \times 10^2$ and
$\beta_2 = 2.0 \times 10^4$, respectively. The concentrations of the associates and
cationic forms in both the systems were calculated depending on the
concentrations of sulphate and thiosulphate anions. The degree of
formation of the associates at equal concentrations of these anions
was approximately the same [304].

The association of four clathrochelates (Table 29) with
perchlorate, sulphate, and malonate ions was detected from their CD
spectra [118]. The Δ-[Co(diNOsar)]$^{3+}$ and Δ-[Co(NOMEsar)]$^{3+}$ cations
formed 1:1 associates with perchlorate cations in water. The
association constant of the former cation with perchlorate ion was
determined to be 0.54. The association constant for the perchlorate
salt of the latter cation was not obtained, but it is expected to be
lower than that for the Δ-[Co(diNOsar)]$^{3+}$ cation. The 1:1 association
constants for clathrochelate cobalt(III) cations with sulfate and
malonate anions were determined from the CD spectra using a
wavelength at which the CD intensity was not affected by the
perchlorate anion concentration. The constants obtained are listed in

Table 29.

Association constants of cobalt(III) sarcophaginates and sepulchrate with SO_4^{2-} and mal^{2-} anions ($T = 298$ K, $\mu = 0.1$ mol·l^{-1} (NaClO$_4$)) [118].

Cation		SO_4^{2-}		mal^{2-}		pK_1	pK_2
		$\nu_{max} \times 10^{-3}$, cm^{-1}	K, mol^{-1}l	$\nu_{max} \times 10^{-3}$, cm^{-1}	K, mol^{-1}l		
Δ-[Co(diNOsar)]$^{3+}$	(I)	27.4	269	28.2	232	10.0	11.5
		27.8	289	27.8	247		
Δ-[Co(NOMEsar)]$^{3+}$	(II)	27.4	209	27.4	131	10.9	13.5
					135		
Δ-[Co(sep)]$^{3+}$	(III)	19.6	94	23.2	85	12.6	a
				20.0	80		
Δ-[Co(MEazasar)]$^{3+}$	(IV)	23.0	57	23.6	62	13.2	a
				20.0	59		

[a] An attempts to obtaine the pK_2 values for complexes III and IV met with failure.

Table 29. In most cases, the association constants for malonate anions are less than those for sulphate anions and are markedly affected by substituents at the clathrochelate framework. When the association occurs *via* hydrogen bonds, one might expect a correlation between the basicity of the NH-groups (Table 29) and the association constants. The pK_1 values of clathrochelate trications are lower than those for [Co(en)$_3$]$^{3+}$ cation ($pK_1 = 15.9$), and their association constants with sulphate and malonate anions are substantially higher (Fig. 36). This effect was attributed to a combined action of the inductive effect of the capping groups and the change of donor centres from primary to secondary amino groups.

The CD and DCD spectra also provide information on the mode of coordination. Ion association with the optically active metal complex changed the rotational strength (R) of the transitions polarized along the anion–cation direction. The first ligand-field band for trigonal CoN$_6$ complexes contains A_2 and E_a transitions and is polarized along the C_3 and C_2 axes, respectively. The longwave CD peak was assigned to an E_a transition, whereas the shortwave peak was assigned to an A_2 transition.

Except for Δ-[Co(diNOsar)]$^{3+}$ cation, all the changes in CD spectra due to ion pairing are in such a direction that they enhance the E_a rotational strength. This type of CD changes is characteristic of complexes with D_3 symmetry and indicates the association of an anion in the equatorial plane. This inference coincides exactly with the deduction from the structural features of macrobicyclic
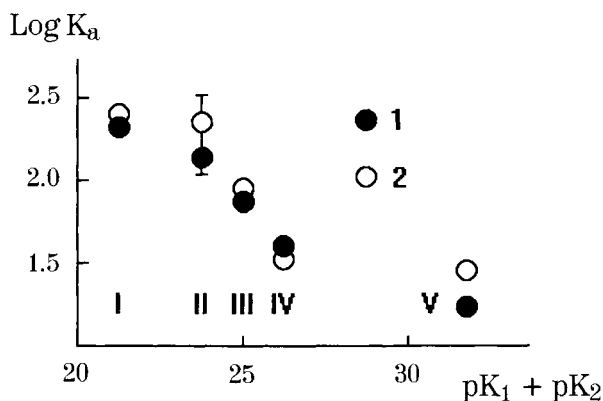
Fig. 36. Correlation between Log K_a and (Σ pK_n) of NH groups for associates of the Δ-[Co(diNOsar)]$^{3+}$ (I); Δ-[Co(NOMEsar)]$^{3+}$ (II); Δ-[Co(sep)]$^{3+}$ (III); Δ-[Co(MEazasar)]$^{3+}$ (IV), [Co(en)$_3$]$^{3+}$ (V) cations with mal^{2-} (1) and SO$_4$$^{2-}$ (2) anions [118].

complexes. Owing to the presence of capping groups, the hydrogens of the donor amino groups are directed only in the D_3 equatorial plane and can form bonds with two oxygen atoms of both sulphate and malonate anions in this plane. This mode of association is shown in Fig. 37. In fact, such a type of bonding was found in [Co(sep)](S$_2$O$_6$)·H$_2$O crystal [96].

The factors that may affect the value of the outer-sphere association constants for aqueous solution are discussed in Ref. 118. It can be inferred that both electrostatic forces and hydrogen bonding contribute significantly to trication complexes. With mono- and

Fig. 37. Proposed mode of sarcophaginate [Co(XYsar)]$^{3+}$ trication association with a sulphate anion [118].

dicationic complexes, the size of interacting ions becomes dominant. The association constants increase for ions with a big size.

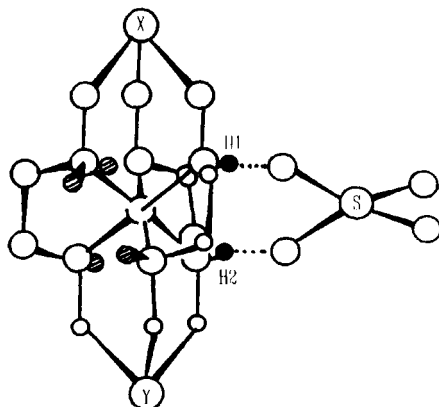In aqueous solution, the $[Co(sep)]^{3+}$ cation formed an ion pair with oxalate ions that exhibited a CTB in the near UV region. The addition of $(NH_4)_2C_2O_4$ at pH 3.0 and pH 5.5 gave rise to an intense CTB ($\nu_{max} = 36\ 364$ cm^{-1}) assigned to $[Co(sep)]^{3+}...(HC_2O_4)^-$ (pH = 3.0) and $[Co(sep)]^{3+}...(C_2O_4)^{2-}$ (pH = 5.5) ion pairs [306].

A calyx[6]arene hexasulphonate $[A^{6-}]$ formed a stable 1:1 complex with $[Co(sep)]^{3+}$ cation in aqueous solution, while at 2:1 $[Co(sep)]^{3+}/A^{6-}$ stoichiometry, the neutral $[Co(sep)]_2A$ complex is precipitated [234]. The stability of the 1:1 complex in aqueous 0.2 M NaCl was determined by ^1H NMR spectra (the association constant $K = 1770$ mol^{-1}) and calorimetry ($\Delta H = -1.0$ kcal·mol^{-1}, $T\Delta S° = 3.4$ kcal·mol^{-1} at 298 K, $\Delta G° = -4.4$ kcal·mol^{-1}, $K = 1770$ mol^{-1}).

The cobalt(III) $[Co(sep)]^{3+}...(B(C_6H_5)_4)_3^{3-}$ and cobalt(II) $[Co(sep)]^{2+}...(B(C_6H_5)_4)_2^{2-}$ ion pairs are formed in aprotic media (THF, AN, and DMF). Solutions of cobalt(III) complexes show "tailing off" of the ligand-metal CTB, the position of which is affected by the solvent used. In THF, this band was observed in the visible region. The formation of associates with $B(C_6H_5)_4^-$ anion was also established from a broadening and a shift of the ^1H NMR signals [309].

A great number of papers deal with the stereospecificity of the interaction of optically active $[CoN_6]^{3+}$ complex cations with optically active anions and the stereospecificity depending on the structures of these cations and anions. A variety of tris-diamine cobalt(III) complexes with different structures, clathrochelates with diverse capping groups, and the semiclathrochelate $[Co(sen)]^{3+}$ cation have been investigated. Many investigators have employed d- and l-tart^{2-}, $[Sb_2(d-,l-tart)_2]^{2-}$, and $[As_2(d-,l-tart)_2]^{2-}$ dianions as optically active reagents [307, 310-312].

The interaction of Δ-forms of $[Co(en)_3]^{3+}$, $[Co(sen)]^{3+}$, $[Co(sep)]^{3+}$, lel_3-$[Co(l-chxn)_3]^{3+}$, and fac-lel_3- and mer-lel_3-$[Co(l-1,2pn)_3]^{3+}$ cations with d- and l-tartrate and $[Sb_2(d-,l-tart)_2]^{2-}$ anions has been studied in [307, 310].

In all the systems, changes in the intensity of the CD band at a given wavelength depend on the molar anion/cation ratios indicate the formation of 1:1 associates. The 1:2 associate was detected for the Δ-$[Co(sen)]^{3+}...Sb_2(l-tart)_2^{2-}$ system. The association constants of Δ-complexes with l-(K_l) and d-(K_d) chiral anions have been estimated (Table 30).

Table 30.
First-step association K_l and K_d constants for Δ-CoN$_6$ trications ($T = 298K$, $\mu = 0.1$ mol·l^{-1} (NaClO$_4$)) [307, 310].

Cation		tart^{2-}				[Sb$_2$(tart$_2$)]$^{2-}$			
		$\nu_{max} \times 10^{-3}$, cm^{-1}	K_l, mol·l^{-1}	K_d, mol·l^{-1}	$^a D$	$\nu_{max} \times 10^{-3}$, cm^{-1}	K_l, mol·l^{-1}	K_d, mol·l^{-1}	$^a D$
Δ-[Co(en)$_3$]$^{3+}$	(I)	22.2	13.3	11.7	7	22.2	47.3	26.0	29
Δ-[Co(sen)]$^{3+}$	(II)	22.2	71.7	49.0	18	20.6	73.0	4.1	89
Δ-[Co(sep)]$^{3+}$	(III)	20.4	38.9	38.1	0	20.8	52.4	39.0	15
Δ-mer-[Co(l-1,2pn$_3$)]$^{3+}$	(IV)	22.2	27.3	20.6	11	21.7	27.9	19.5	18
Δ-fac-[Co(l-1,2pn$_3$)]$^{3+}$	(V)	22.2	30.3	22.5	15	21.7	25.8	16.8	21
Δ-[Co(l-chxn)$_3$]$^{3+}$	(VI)	21.0	21.4	15.4	16	21.3	21.3	14.0	21

^{a} $D = 100(K_l - K_d)/(K_l + K_d)$ and characterizes the chiral recognition
^{b} The second-step association constant with [Sb$_2$(tart)$_2$]$^{2-}$ dianion is 15.0 ± 3.0

For all the complexes, except for the Δ-[Co(sep)]$^{3+}$...tart^{2-} system, the K_l value substantially is higher than the K_d value, which indicates that these Δ-forms favour the association with the l-chiral anion. For the Δ-[Co(sep)]$^{3+}$...tart^{2-} system, the K_d and K_l values are nearly the same.

Both the K_l and K_d values for the systems with tart^{2-} anions (Table 30) decrease in the order II-III-V-IV-VI-I. For the systems with [Sb(tart)$_2$]$^{2-}$ anion, this order is different: II-III-I-IV-V-VI (K_l) and III-I-IV-V-VI-II (K_d). Dissimilar K_l and K_d changes affect the order of chiral discrimination: II-VI-V-IV-I-III for tartrate anions and II-I-VI-V-IV-III for the [Sb$_2$(tart)$_2$]$^{2-}$ anion. Changes in the order of stereospecificity suggest different modes of coordination in various systems, which are governed by the geometry of cations and anions.

Information on coordination modes has been obtained from the changes in the CD spectra combined with the data on the complex structures and the stability of associates. The DCD spectra, except those for the Δ-[Co(sen)]$^{3+}$...[Sb$_2$(d-tart)$_2$]$^{2-}$ (d-tart) systems, contained single peaks. For nonmacrocyclic diamine complexes, deviations were positive; for Δ-[Co(sep)]$^{3+}$ cation, they were negative. For the systems with Δ-[Co(sen)]$^{3+}$ cation, DCD deviations were positive and negative. Positive DCDs indicate a positive change in $R(A_2)$, which agrees with a dominant association along the C_3 axis. There may also be two types of association (along the C_2 and C_3 axes) with dominant interaction along the C_3 axis. A negative change in $R(A_2)$ is caused by anion interaction along the C_2 axis. According to this criterion, ion pairing exerts axial
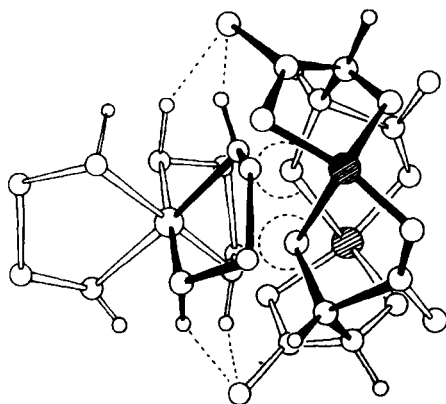
Fig. 38. Structure model of the Δ-[Co(en)$_3$]$^{3+}$...[Sb$_2$(l-tart)$_2$]$^{2-}$ ion associate [310].

perturbations in tris-diamine cobalt (III) complexes. In this case, the two triangular N$_3$-bases can be used for coordination. X-ray diffraction data for the Δ-[Co(en)$_3$]$^{3+}$...[Sb$_2$(l-tart)$_2$]$^{2-}$ system with allowance for association along the C_3 axis, and this made it possible to envisage the mode of ion pairing (Fig. 38). The anion interacts with the cation along the C_2 axis. The two blades of the right-handed propeller of the chelate cycle and the two oxygen atoms of the [Sb(l-tart)$_2$]$^{2-}$ anion hydroxyl groups (encircled in Fig. 38) fit nicely. The axial hydrogen atoms of the donor amino groups take part simultaneously in hydrogen bonding with carbonyl oxygen atoms of the anion, and these hydrogen bonds anchor the complex cation. Such double anchoring may be also expected for the favourable Λ-[Co(en)$_3$]$^{3+}$...[Sb$_2$(d-tart)$_2$]$^{2-}$ pair. However, this is not the case with Δ-[Co(en)$_3$]$^{3+}$ and [Sb$_2$(d-tart)$_2$]$^{2-}$ ions, whereby a decrease in the association constants is accounted for.

As seen from the DCD spectra, the tartrate ion interacts with tris-diamine complexes along the C_3 axis. In this case, however, steric hindrances for a Δ-[Co(en)$_3$]$^{3+}$...tart^{2-} associate are drastically enhanced and K_d and K_l decrease compared with the values for associates with [Sb$_2$(tart)$_2$]$^{2-}$ dianions and other tartrate dianions.

The lel-amine cations (IV-VI) and the tartrate anion were suggested to be better disposed stereochemically [307]. The association constants for these complexes are of the same order of magnitude (l-tartrate dianion) or ever higher (d-tartrate dianion) than with the [Sb$_2$(d-tart)$_2$]$^{2-}$ anion. Such changes in the association constant values for systems with two chiral anions may be caused by different factors

weakening the cation-anion bond, i.e., steric hindrances in the case of a more bulky ligand (for the system with $[Sb_2(tart)_2]^{2-}$ dianion) and stereochemical incompatibility with a small anion (the systems with $tart^{2-}$ dianion). In the latter case, the influence of steric effects decreases the effect of factors that alter the stereospecificity order in systems containing $tart^{2-}$ and $[Sb_2(tart)_2]^{2-}$ anions with respect to *mer*- and *fac*-isomers. The steric incompatibility increases for $[Co(en)_3]^{3+}...tart^{2-}$ associates, which possess a TAP configuration with shorter distances between axial protons of donor amino groups. The association of the tartrate anion with *lel*-amines may occur in the same manner as it does in the case of $[Co(en)_3]^{3+}$ trication with sulphate anion, i.e., *via* triangular bases [118].

The negative DCD peak for the $[Co(sep)]^{3+}...d$-, l-$tart^{2-}$, and $[Sb_2(tart)_2]^{2-}$ associates is indicative of the anion association along the C_2 axis. The change in the association mode, compared with nonmacrocyclic cobalt(III) tris-diaminates, is stipulated by the presence of the capping groups in the clathrochelate $[Co(sep)]^{3+}$ cation that screen trigonal N_3-bases of the CoN_6 coordination polyhedron.

The mechanism of chiral recognition of the enantiomers in series of clathrochelates was studied in research reported in Ref. 311, in which $[Sb_2(d\text{-}tart)_2]^{2-}$ anion was employed as a chiral eluent. It was established that in the majority of cases, Λ-enantiomer is eluted first, and that bulky alkyl capping groups increase the degree of resolution.

Structural models proposed for Λ-$[Co(sep)]^{3+}...[Sb_2(d\text{-}tart)_2]^{2-}$ and Δ-$[Co(sep)]^{3+}...[Sb_2(d\text{-}tart)_2]^{2-}$ systems are given in Fig. 39.

A   B
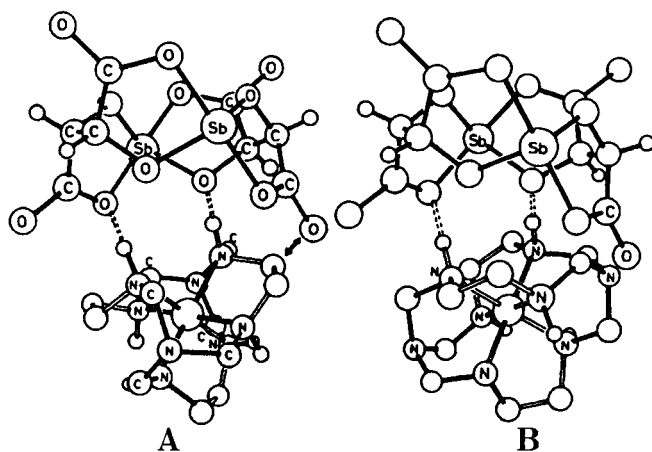
Fig. 39. Structural models of Λ-$[Co(sep)]^{3+}...[Sb_2(d\text{-}tart)_2]^{2-}$ (A) and Δ-$[Co(sep)]^{3+}...[Sb_2(d\text{-}tart)_2]^{2-}$ (B) ion associates [311].

These models show that the two oxygen atoms (hydroxyl and carboxyl groups, coordinated to the same antimony atom of the $[Sb_2(d\text{-tart})_2]^{2-}$ anion) form a hydrogen bonds with two protons of two coordinated amino groups located along the C_2 axis of the clathrochelate molecule. If the complex has Λ-conformation, a steric hindrance arises between the distal carboxyl group of $[Sb_2(d\text{-tart})_2]^{2-}$ anion and the ethylenediamine ring of the clathrochelate. This mode of coordination implies that alkyl caps are so far disposed from the chiral anion that they exert no steric influence on it. In the case of Δ-conformation, on coordination the distal carboxyl groups are located between two ethylenediamine rings, and no steric repulsion hindrance is observed with these ethylenediamine rings. However, there is a capping fragment adjacent to the distal carboxyl group whose size may affect the stability of associate.

It was shown [311] that $[Sb_2(d\text{-tart})_2]^{2-}$ dianion first eluted $\Delta\text{-}[Co(sep)]^{3+}$ cation. In this case, structure **B** (Fig. 39) is more favourable than structure **A**, and this is attributed to a small capping nitrogen atom and weaker steric hindrance. In the case of more bulky capping groups, the steric hindrance in **B** begins to play a key role: the relative stability of the Δ-enantiomer with $[Sb_2(d\text{-tart})_2]^{2-}$ dianion is reduced, Λ-enantiomer is eluted first, and the degree of resolution of enantiomers is enhanced. Comparison of association constants K_1 and K_d of the $\Delta\text{-}[Co(sep)]^{3+}$ trication with l- and d-tartrate ions demonstrated the same mode of association. These constants in tartrate systems are lower than those for systems with $[Sb_2(tart)_2]^{2-}$ anion, which may be accounted for by the increased steric hindrance between the ethylenediamine ring and the tartrate anion due to association along the C_2 axis (Fig. 39, A). The stability of heterochiral and homochiral (d-and l-) tartrate and $[Sb_2(d\text{-tart})_2]^{2-}$ associates is leveled: the K_d and K_1 for associates with the tartrate dianion and K_d for associates with $[Sb_2(tart)_2]^{2-}$ dianion are about the same.

It should be noted that the $\Delta\text{-}[Co(sen)]^{3+}$ trication gives the most stable associates with $l\text{-tart}^{2-}$ and $[Sb_2(l\text{-tart})_2]^{2-}$ dianions (their K_1 values are approximately equal), the less stable associate with d-tartrate dianion, and the least stable associate with $[Sb_2(d\text{-tart})_2]^{2-}$ dianion (Table 30). One of the triangular N_3-bases in the $[Co(sen)]^{3+}$ cation is screened, which can hamper the association along the C_3 axis. The CD and DCD spectra for associates of this cation with d- and l-tartrate and $[Sb_2(tart)_2]^{2-}$ anions [307, 310], as well as for two enantiomers with $[Sb_2(d\text{-tart})_2]^{2-}$ anion [311], shows that the

A   **B**
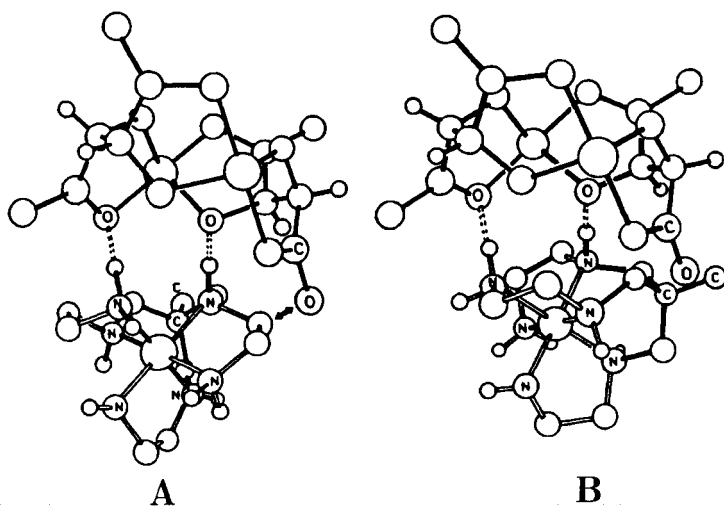
Fig. 40. Schematic structure of Λ-[Co(sen)]$^{3+}$...[Sb$_2$(d-tart)$_2$]$^{2-}$ (**A**) and Δ-[Co(sen)]$^{3+}$...[Sb$_2$(d-tart)$_2$]$^{2-}$ (**B**) ion associates [311].

interaction of the Δ-enantiomer with [Sb$_2$(l-tart)$_2$]$^{2-}$ dianion and the Λ-enantiomer with [Sb$_2$(d-tart)$_2$]$^{2-}$ dianion increases the A_2 component, whereas the interaction of Δ-enantiomer with [Sb$_2$(d-tart)$_2$]$^{2-}$ dianion increases the E_a component. Hence, the [Sb$_2$(d-tart)$_2$]$^{2-}$ dianion with Λ- and Δ-[Co(sen)]$^{3+}$ cations is associated along the C_3 and C_2 axes, respectively. One may assume that the Λ-[Co(sen)]$^{3+}$...[Sb$_2$(d-tart)$_2$]$^{2-}$ associate is formed predominantly, and an ion pair like the [Co(en)$_3$]$^{3+}$...[Sb$_2$(d-tart)$_2$]$^{2-}$ system retains the Λ-[Co(sen)]$^{3+}$ cation due to the association of axial and equatorial hydrogen atoms (Fig. 40, **A**).

No smooth association of type C_2 is possible between the Δ-[Co(sen)]$^{3+}$ and [Sb$_2$(d-tart)$_2$]$^{2-}$ ions (Fig. 40, **B**) when the hydroxyl and the carboxyl oxygen atoms of the chiral anion are hydrogen bonded to the secondary and primary amine protons, respectively. These protons are directed along the pseudo-C_2 axis of the complex, since the apical methyl substituent lies in the vicinity of the distal carboxyl group and imposes steric hindrances [311]. When the second [Sb$_2$(l-tart)$_2$]$^{2-}$ anion is coordinated to the Δ-[Co(sen)]$^{3+}$ cation, the DCD spectral changes were positive for the A_2 component and negative for the E_a component, which demonstrated association along both the C_2 and C_3 axes. The reorientation of the first anionic species is likely to occur [310].

As seen from the DCD spectra of the Δ-[Co(sen)]$^{3+}$...d- and l-tart^{2-} systems, the C_3 association is dominant. The small negative peak observed in the Δ-[Co(sen)]$^{3+}$...d-tart^{2-} system is caused by a weak association along the C_2 axis. It is possible that the O–O distances in tartrate ion and the H–H distances in Δ-[Co(sen)]$^{3+}$ cation fit best in the C_3 association with l- and d-tartrates.

The interaction of optically active CoN$_6$ trications with two chiral anions was investigated under different conditions of chromatographic resolution of enantiomers. Comparison of [Sb$_2$(d-tart)$_2$]$^{2-}$ and [As$_2$(d-tart)$_2$]$^{2-}$ dianions as potential chiral eluents indicated that the latter is the more efficient one [312]. The efficiency of [Sb$_2$(d-tart)$_2$]$^{2-}$ dianion increases when it is employed in the form of a salts with hydrophobic cations in reversed-phase ion-pair chromatography (RPIPC).

The clathrochelate [Ni(sar)]$^{2+}$ cation was resolved into enantiomeres by fractional crystallization of its salt with [Sb$_2$(d-tart)$_2$]$^{2-}$ dianion. On slow evaporation, the less soluble l-diastereomer precipitated exclusively until the volume was quite small, whereupon the more soluble d-isomer started to deposit [227].

Some optically active cationic and racemic anionic complexes were examined to elucidate the mechanism of chiral recognition of cations and anions capable of forming hydrogen bonds [313]. The chromatographic study showed that enantiomers of some anionic complexes form favourable ion pairs with cationic Δ-complexes (Table 31).

Table 31.
Enantiomers of anionic complexes, which form favourable ion pairs with Δ-cationic species [313].

Cation	C_2^-		C_3^-	$C_2^- + C_3^-$	
	[Co(ox)$_2$(en)]$^-$	C_2-cis(N)-[Co(ox)(gly)$_2$]$^-$	C_1-cis(N)-[Co(ox)(gly)$_2$]$^-$	[Co(ox)$_2$(gly)]$^{2-}$	[Co(ox)$_2$(acac)]$^{2-}$
C_2^+					
Δ-[Co(sep)]$^{3+}$	Λ	Λ	Λ	Λ	Λ
Δ-[Co(acac)(en)$_2$]$^{2+}$	Λ	Λ	Λ	Λ	Λ
Δ-cis-[Co(NO$_2$)$_2$(en)$_2$]$^+$	Λ	Λ	Λ	Λ	Λ
C_3^+					
Δ-[Co(l-chxn)$_3$)]$^{3+}$	Δ	Δ	Δ	Δ	Δ
Δ-[Co(l-1,2pn)$_3$)]$^{3+}$	Λ	Λ	Δ	Δ	Δ
$C_2^+ + C_3^+$					
Δ-[Co(en)$_3$]$^{3+}$	Δ	Δ	Λ	Λ	Λ
Δ-[Co(gly)(en)$_2$]$^{2+}$	Δ	Λ	Λ	Λ	Λ
Δ-[Co(sen)]$^{3+}$	Λ	Λ	Λ	Λ	Λ

The association models that explain the data obtained were proposed with following assumption:

(a) The $[Co(sep)]^{3+}$ cation may form hydrogen bonds with the anion only along cation C_2 axis (C_2^+ group). $[Co(acac)(en)_2]^{2+}$ and cis-$[Co(NO_2)_2(en)_2]^+$ cations are also classified in the C_2^+ group, since they are expected to approach the anion along cation C_2 axis from the side of the ethylenediamine fragments so as to avoid the electrostatic repulsion between the negatively charged acac or NO_2 ligands and the negative charge on the associating anion.

(b) The tris-lel-diamine complexes belong to the C_3^+ group.

(c) It is strongly expected that both C_2 and C_3 accesses are possible for $[Co(en)_3]^{3+}$, $[Co(gly)(en)_2]^{2+}$, and $[Co(sen)]^{3+}$ cations, which thus belong to the $(C_2^+ + C_3^+)$ group.

The anions are also classified into three groups when the charge localization on chelate rings is taken into account (Table 31).

A typical C_2^+ Δ-$[Co(sep)]^{3+}$ cation always forms favourable pairs with the Λ-anion, whereas a typical C_3^+ Δ-$[Co(l\text{-}chxn)_3]^{3+}$ cation always favours the Δ-anionic complexes. Thus, homochiral (Δ–Δ and Λ–Λ) and heterochiral (Λ–Δ or Δ–Λ) combinations are favoured when the cationic complex "uses" the C_3 and C_2 axes, respectively.

With the $(C_2^+ + C_3^+)$ group cations, a heterochiral combination is certainly favoured in the interaction with C_3^- group and $(C_2^- + C_3^-)$ group anions. When Δ-$[Co(en)_3]^{3+}$ and Δ-$[Co(gly)(en)_2]^{2+}$ cations are employed as chiral selectors, the degree of resolution is very low for the C_2^- group anions. This implies that the $(C_2^+ + C_3^+)$ group cations "use" both C_2 and C_3 axes in association with anions, which results in the formation of approximately equal ion pairs with Δ- and Λ-enantiomers. Semiclathrochelate $[Co(sen)]^{3+}$ trication generally forms more stable heterochiral associates. The cations "using" either the C_2 axis or the C_3 one in association with anions are the most efficient chiral selectors.

An analogous study on chiral resolution of racemic $[Cr(ox)_2(acac)]^{2-}$ and $[Cr(ox)_2(gly)]^{2-}$ anions in aqueous 1,4-dioxane was performed with Λ-$[Co(sep)]^{3+}$ cation as a chiral selector [314]. The Δ-enantiomers of both anionic complexes were identified by CD spectra. When Λ-$[Co(en)_3]^{3+}$ trication served as a chiral selector, Λ-enantiomers were also eluted; the Λ-$[Co(d\text{-}1,2pn)_3]^{3+}$ and Λ–$[Co(d\text{-}pm)_3]^{3+}$ cations eluted Λ-enantiomers [314]. These results are consistent with those obtained in aqueous solutions [313].

The effect of stereoselectivity on the oxidation of $[Co(en)_3]^{2+}$, $[Co(sen)]^{2+}$, $[Co(sep)]^{2+}$, $[Co(d,l\text{-}bn)_3]^{2+}$, and $[Co(d,l\text{-}chxn)_3]^{2+}$ cations with $[Co(ox)_3]^{3-}$, $[Co(EDTA)]^-$, and $[Co(mal)_3]^{3-}$ anions is discussed in Ref. 308.

The ability of clathrochelates to form ion pairs and covalently attached complexes is utilized in biochemistry [315-321]. The stereoselectivity of the redox reactions of plastocyanine and horse heart cytochrome C with several cage complexes was reported in Ref. 319. Studies on stereoselective electron transfer in different systems provide information on the importance of close ion pair association of a cage complex with protein in chiral discrimination.
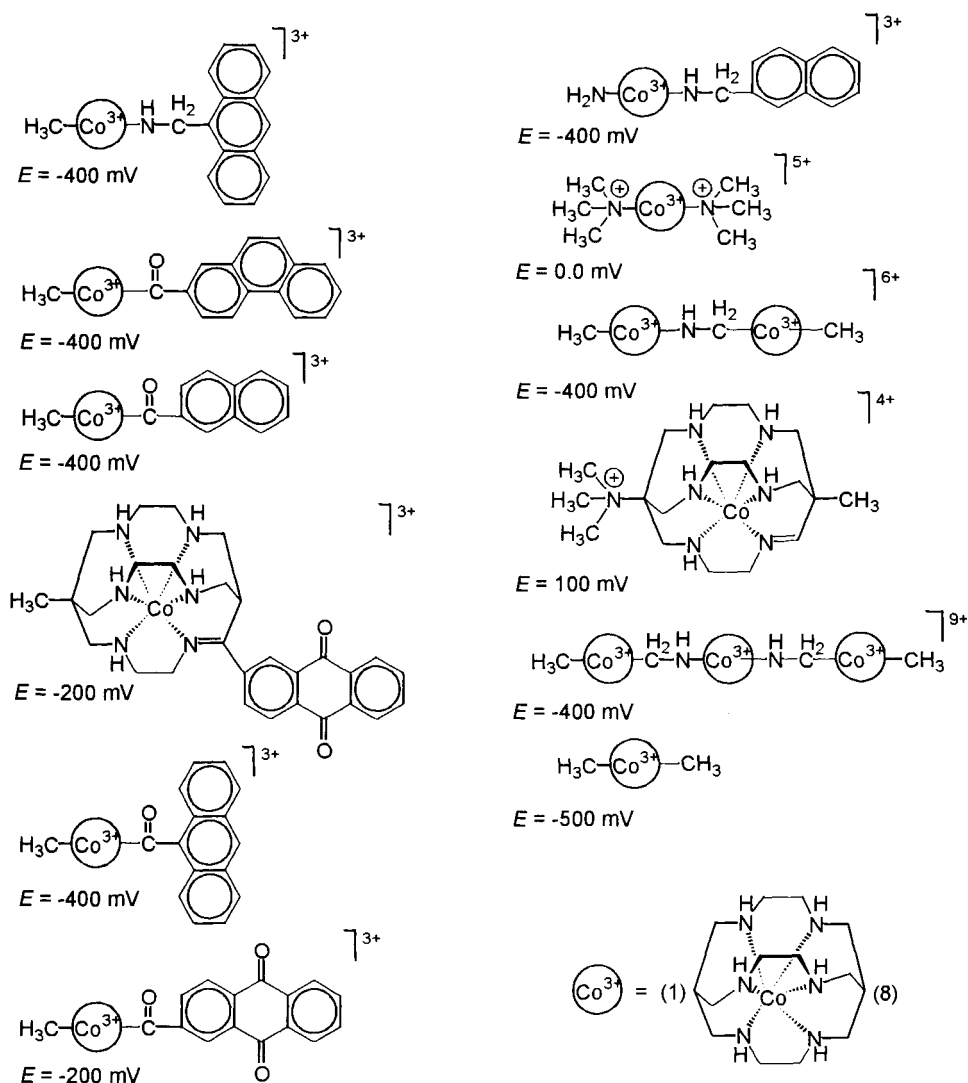
Reduction of horse cytochrome C with $[Co(sep)]^{2+}$, $[Co(diAMsar)]^{2+}$, and $[Co(NOcapten)]^{2+}$ cations was reported in Refs. 316-320. The intrinsic reactivity of these complexes with proteins make it possible the use of clathrochelates as potential protein redox titrants, electrochemical mediators, and electrode modifiers.

Seven horse heart cytochrome C derivatives, each with a single sarcophaginate $[Co(diAMsar)]^{3+}$ cation covalently attached to a specific surface carboxylate side chain, were synthesized. The experimental intramolecular electron transfer rate constants is nearly independent of the $[Co(diAMsar)]^{3+}$ cation attachment site [320].

Outer-sphere complexes of lasalocid A (LAS) anion with $[Co(NH_3)_6]^{3+}$, $[Co(en)_3]^{3+}$, and $[Co(sep)]^{3+}$ cations were isolated as reported in Ref. 321. The X-ray data for these complexes demonstrated that three lasalocid anions (in cyclic conformation) surround the cobalt complexes so that the overall shape is approximately spherical. In consequence of its hydrophobic outer surface, the adduct is soluble in nonpolar solvents such as chloroform. Lasalocid anion was showed to act as an ionophore for selective enantiomeric transport of the $[Co(sep)]^{3+}$ cation through a chloroform membrane.

The intercalation of polycyclic aromatic-substituted cobalt(III) sarcophaginates (Scheme 117) with DNA is discussed in Ref. 315. The hydrophobic polycyclic aromatic groups bound to the hydrophilic cobalt(III) cages are effectively solubilized in water. The complexes, being cationic, should associate with the negatively charged phosphodiester backbone of DNA.

The influence of solvent reorganization on optical and thermal electron-transfer processes in clathrochelate complexes is theoretically calculated in Ref. 322.

H₃C—(Co³⁺)—N—C ...]³⁺
E = -400 mV

H₃C—(Co³⁺)—C ...]³⁺
E = -400 mV

H₃C—(Co³⁺)—C ...]³⁺
E = -400 mV

]³⁺
E = -200 mV

H₃C—(Co³⁺)—C ...]³⁺
E = -400 mV

]³⁺
E = -200 mV

H₂N—(Co³⁺)—N—C ...]³⁺
E = -400 mV

H₃C,⊕ ... H₃C—N—(Co³⁺)—N—CH₃ ...]⁵⁺
E = 0.0 mV

H₃C—(Co³⁺)—N—C—(Co³⁺)—CH₃]⁶⁺
E = -400 mV

]⁴⁺
E = 100 mV

H₃C—(Co³⁺)—C—N—(Co³⁺)—N—C—(Co³⁺)—CH₃]⁹⁺
E = -400 mV

H₃C—(Co³⁺)—CH₃
E = -500 mV

(Co³⁺) = (1) ... (8)

Scheme 117

The solvation of clathrochelate iron(II) cyclohexanedione-1,2-dihydrazonate in methanol-water mixtures was studied in research reported in Ref. 184. The comparison of transfer chemical potentials (Fig. 41) illustrates the greater preference of the larger and more hydrophobic [Fe(cxcage)]²⁺ cation for methanol in a series of cage complexes. However, these complexes appear to exhibit somewhat less hydrophobic behaviour than their nonmacrocyclic analogs.
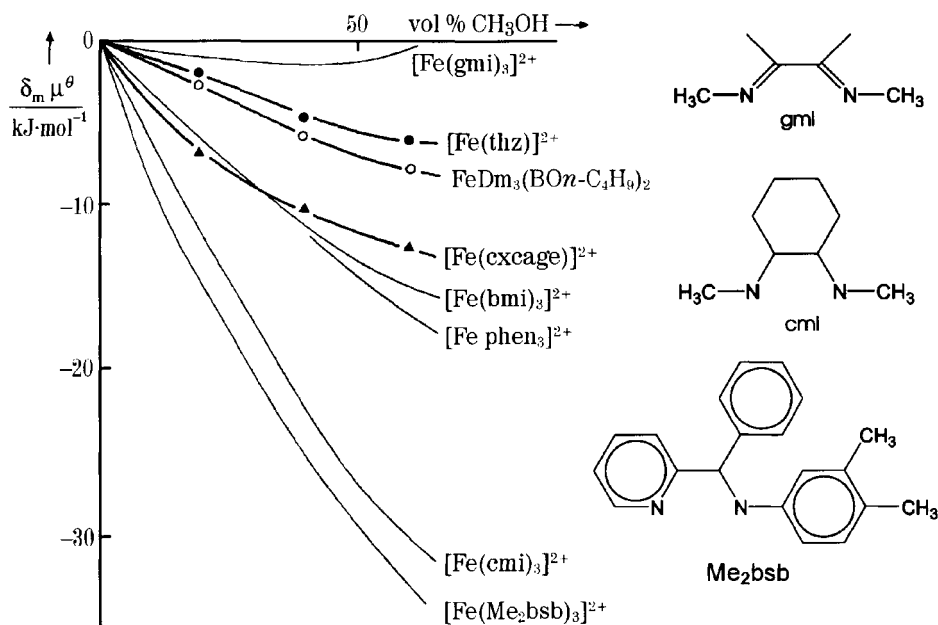
Fig. 41. Transfer chemical potentials for iron(II) complexes [184].

5.2 ELECTRON-TRANSFER PROCESSES IN MACROBICYCLIC COMPLEXES

Macrobicyclic transition metal complexes are unique objects for studies of electron transfer processes because these complexes display high stability, which practically excludes dissociation side reactions in both oxidized and reduced forms. Since all coordination sites are occupied by macrobicyclic ligand donor atoms, the reaction mechanism involving intrasphere-coordinated bridging groups cannot be realized. A great variety of the known macrobicyclic ligands allows scientists to alter the coordination centre geometry and redox potential values.

Relatively simple syntheses for the majority of macrobicyclic complexes, compared with conventional techniques for the preparation of macrocyclic compounds, have made such complexes attractive not only for research, but also for practical application as electron carriers, catalysts for electro- and photochemical processes, and some other purposes (e.g., protein redox titrants, biological electrochemical mediators, and ionophore and electrode modifiers).

There have been numerous publications concerning electron transfer processes with the participation of macrobicyclic complexes. Moreover, cobalt(II) and cobalt(III) complexes have received the most attention, presumably due to their availability. Several papers deal with electrochemistry of chromium, ruthenium, rhodium, manganese, nickel, iron, and copper complexes.

5.2.1 Redox properties of d-metal sarcophaginates and related compounds

The redox potentials of macrobicyclic complexes vary over a wide range. They are much lower than those of metal aqua ions and are dependent on the central ion and on the nature of the cage. In this section, the dependence of the redox properties on the central ion is discussed. The redox potentials for several d-metal aqua ions and sarcophaginates are summarized in Table 32 and Fig. 42. Fig. 42 also shows ionization potentials $\Sigma^3_{n=1} I_n$ and LFSEs [323].

The redox potentials of aqua ions in the $3d$-metal series are affected by changes both in the overall ionization potential (M^{3+} ion formation) and the metal ion hydration energy. The plot of $E_{1/2}$ *versus* the number of d-electrons for aqua ions resembles that of ionization potentials. The ligand field effect of water molecules surrounding the metal ion only slightly changes the character of this dependence (mainly for Ni^{2+} and Cu^{2+} ions). A minimum on this plot is observed for the electronic configuration d^5 (Fig. 42). For sarcophaginates, the shapes of the curve at the beginning and at the end of the $3d$-metal series are about the same as for aqua ions. The general decrease in the redox potentials due to stabilization of the higher oxidation state

Table 32.

Redox potentials (mV) of d-metal aqua ions and sarcophaginates (relative to NHE) [4, 158, 179, 180, 227, 323, 325, 326].

Metal	$E_{1/2}$			
	$M_{aq}^{3+/2+}$	$[M(sar)]^{3+/2+}$	[a]$[M(sar)]^{3+/2+}$	$[M(diAMHsar)]^{5+/4+}$
Cr	−410	[b] −1100		−790
Mn	1490	519	490	950
Ru		290		
Fe	770	93	−50	
Co	1800	−400	−485	−20
Ni	1800	855	820	
Cu	2300	1200		

[a] In the Nafion films, *vs* SCE   [b] The same values are for $[Cr(sep)]^{3+/2+}$ and $[Cr(diAMsar)]^{3+/2+}$ couples.
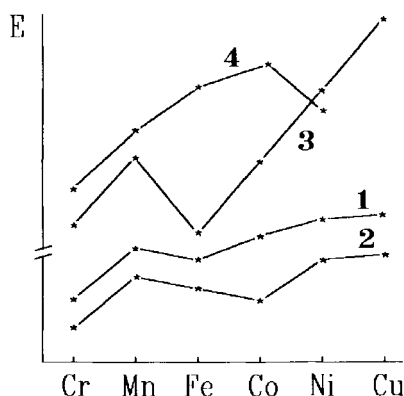
Fig. 42. Variation in the redox potentials of aqua ions (1), sarcophaginates (2), total ionization potentials (3), and LFSEs (4) for a series of $3d$-metals.

in the sarcophaginates is about the same for chromium, manganese, nickel, and copper (700–1100 mV). In the middle of this series (Fe > Co > Ni), the redox potentials change in the opposite direction with regard to the LFSE [93]. The maximal stabilization of the cobalt(III) complex inducing the most drastic lowering in $E_{1/2}$ compared with that of the aqua ion (2200 mV) is attributed to the occurrence of the low-spin d^6 electronic configuration.

The redox potentials of iron and ruthenium sarcophaginates are higher than those of cobalt complexes and increase from the iron to the ruthenium complexes ($3d$- and $4d$-metals with the same electronic configurations). The same dependence of the redox potentials was observed for the series of $3d$-metal sarcophaginates incorporated in high concentrations in thin Nafion films covering graphite electrodes [326] and for the diaminosarcophaginate $[M(diAMHsar)]^{5+/4+}$ couples (Table 32).

A correlation between $E_{1/2}$ values and M–N distances in manganese, iron, ruthenium, and cobalt(III) sarcophaginates (Table 3, Section 3.1) is observed.

In the case of sarcophaginates and sepulchrates, the M–N distances exceed the sum of the nitrogen radius and the corresponding metal ionic radius in the appropriate oxidation state. Thus, a redox process is not limited by the cavity size, which in bonding can either decrease or increase with the change in the radius of the central ion owing to structural rearrangement. The increase in the cavity size in a reduction process occurs on translational rotation
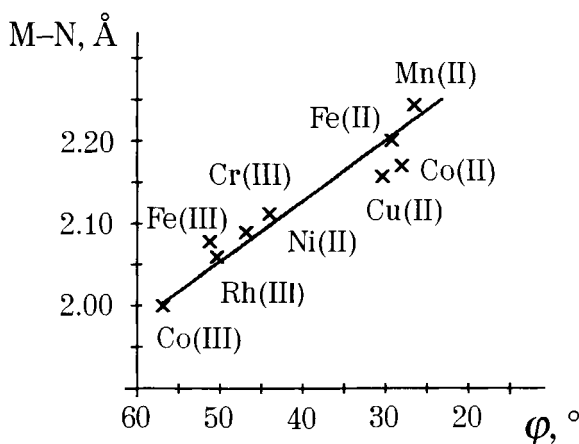
Fig. 43. Correlation between distortion angle φ and M–N distances in M(III) and M(II) sarcophaginates.

of the N_3-bases of a coordination polyhedron reducing the distortion angle φ as the structure approaches TP geometry. To the contrary, in an oxidation process, the cavity size decreases and the φ angle increases. The redox process in its structural aspect may be regarded as a clathrochelate framework pulsation: a contraction in oxidation and an expansion in reduction. Such processes in d-metal sarcophaginates are confirmed by a correlation between the φ values and M–N distances in most M(III) and M(II) sarcophaginates (Fig. 43).

The redox properties of ruthenium(II) sarcophaginates are discussed in Refs. 324 and 327. The [Ru(sar)]$^{2+}$ cation oxidized readily to the corresponding ruthenium(III) complex, which spontaneously disproportionated to the initial cation and a monodeprotonated intermediate ruthenium(IV) complex. This complex quickly produced the imine ruthenium(II) clathrochelate by both base- and acid-catalyzed pathways (Scheme 118). Intermediate di- and triimine species were also observed. The kinetic and thermodynamic data for the disproportionation process demonstrated that the secondary amino group in [Ru(sar)]$^{3+}$ cation is quite acidic (pK_a = 5÷6) and that the ruthenium(IV) state is stabilized at more than 2000 mV.

The redox potential of the [Ru(capten)]$^{3+/2+}$ couple is by approximately 900 mV higher than that of the [Ru(sar)]$^{3+/2+}$ couple (1260 mV in AN). Oxidation of the encapsulated Ru^{2+} ion to Ru^{3+} ion in AN leads to dehydrogenation of the clathrochelate framework to
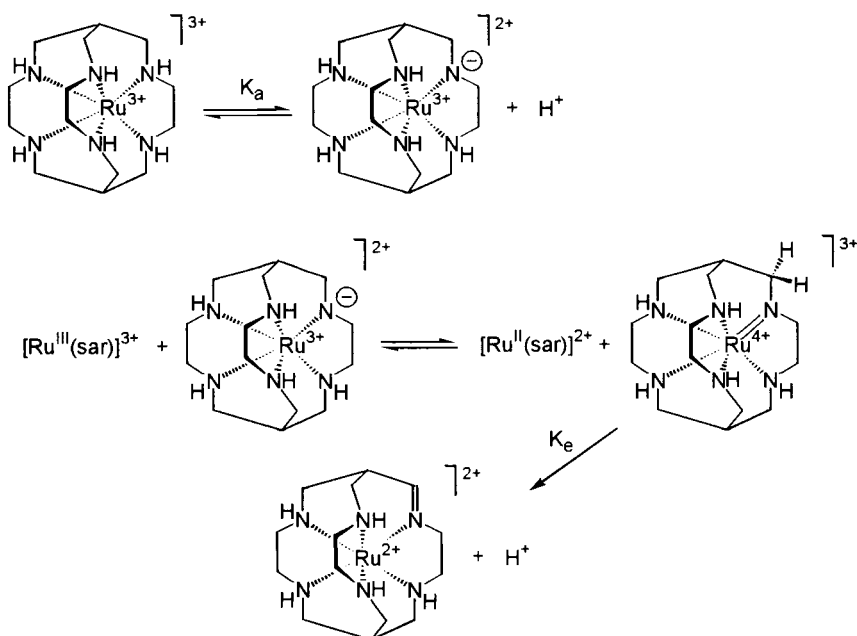
Scheme 118

form mono-, di-, and triimine species. These oxidation reactions are also inferred to proceed through ruthenium(IV) intermediates that produce the imine complexes by an intramolecular two-electron process [229].

The reduction potentials for [Rh(sep)]$^{3+/2+}$, [Rh(AMHMEsar)]$^{4+/3+}$, and [Rh(AMME1,3pnsar)]$^{4+/3+}$ couples in acetone are −1800, −1720, and −1340 mV vs SCE, respectively [157, 164].

The macrobicyclic $3d$-metal aza-capped 1,3pn-sarcophaginates were studied by voltammetry. In contrast to sepulchrates and sarcophaginates, these complexes should favour to some degree the adoption of low oxidation states (+2 and +1). The oxidation M$^{2+/3+}$ waves are observed in DMF at 1380, 820, 227, 1180, and 1220 mV vs SCE, respectively, for manganese, iron, cobalt, nickel, and copper complexes. The dependence of redox potentials on the number of d-electrons is the same as for [M(sar)]$^{3+/2+}$ couple redox potentials.

A series of d-metal complexes with clathrochelate $imBT$ ligand showed enhanced stability of their oxidation state (+2) compared with the corresponding sepulchrates: the oxidation $E_{1/2}$ potentials 50 and 1000 mV were obtained for [Fe(imBT)]$^{2+}$ and [Mn(imBT)]$^{2+}$ cations, respectively [203].

The electrochemical irreversible reduction of $[Cu(sar)]^{2+}$ cation in aqueous solution was studied by cyclic voltammetry [293]. This cation is kinetically and thermodynamically stable except toward reduction of encapsulated copper(II) ion to copper(I) ion ($E = -800$ mV vs SCE). After reduction, the coordination number of this copper ion diminishes from six (copper(II)) to four (copper(I)).

The same method was used for N-methylated nickel and copper(II) sarcophaginates [113]. The $E_{1/2}$ values for $[Ni(Me_5sar)]^{2+/1+}$, $[Ni(Me_6sar)]^{2+/1+}$, and $[Ni(Me_7sar)]^{2+/1+}$ couples are -1260, -1050 and -910 mV vs SCE. For corresponding copper complexes, the $E_{1/2}$ values are -780, -650, -530 mV vs SCE. The X-ray crystallography for N-methylated complexes demonstrated four-coordinate nickel and copper ions (see Section 3.1). The stabilization of monocationic complexes is caused by an increase in the macrobicyclic cavity size. This is consistent with decreasing $E_{1/2}$ values and M–N distances in copper complexes compared with the corresponding nickel complexes. The increase in the M–N distance results in a ligand-field strength decrease for dicationic clathrochelates and an increase in this field strength for monocationic complexes.

The rate constants of the electron self-exchange in the series of d-metal sarcophaginates are listed in Table 33.

First, it should be emphasized that the rate of electron self-exchange in the macrobicyclic complexes essentially increases compared with those of the initial nonmacrocyclic $[M(en)_3]^{3+}$ cation. It is generally attributed to the fact that the macrobicyclic ligands are more rigid than noncapped ones, which practically minimizes structural differences between complexes in the oxidation states +2 and +3 and, as consequence, leads to smaller Frank-Condon barriers. The second important parameter is electronic configurations in both the higher and the lower oxidation states.

Table 33.
Electron self-exchange rates for the $[M(sar)]^{3+/2+}$ couples [4, 324].

Complex	Electron Configuration	Δr, Å	Log k_{11}
Ru(sar)	$(t_{2g})^5 \leftrightarrow (t_{2g})^6$	0.008	5.08
Mn(sar)	$(t_{2g})^3(e_g) \leftrightarrow (t_{2g})^3(e_g)^2$	0.110	1.2
Fe(sar)	$(t_{2g})^5 \leftrightarrow (t_{2g})^6 \leftrightarrow (t_{2g})^1(e_g)^2$	0.195	3.8
Co(sar)	$(t_{2g})^6 \leftrightarrow (t_{2g})^5(e_g)^2$	0.196	0.3
Ni(sar)	$(t_{2g})^6(e_g)^1 \leftrightarrow (t_{2g})^6(e_g)^2$	0.080	3.2

For [Ru(sar)]$^{3+/2+}$ pair, in which on a change in their oxidation states the Ru–N distances (Δr) vary only 0.008Å on average and electronic transition is not forbidden, the maximal value of Log k_{11} was observed. The changes in M–N distance increase in the order Ru < Ni < Mn < Fe < Co. Log k_{11} values decrease with an increasing the Δr values (Fig. 44). The variation of rate constants for electron exchange in these sarcophaginates is expressed by the equation

$$\text{Log}\, k_{11}(M) - \text{Log}\, k_{11}(Ru) = const \cdot \Delta r^2 \tag{81}$$

which reflects a dependence on Frank-Condon parameters.

For cobalt, iron, and ruthenium sarcophaginates, the Log k_{11} values increase with an increase in the redox potentials. This is the case when the main factor affecting a variation in both values in the same direction is the electronic configuration. The increase in E values in a series of clathrochelates from cobalt to ruthenium is attributed to differences in spin states: $ls > hs$ for cobalt, $ls > hs$, ls for iron, $ls > ls$ for ruthenium complexes. The increase in Log k_{11} values correlates with ΔLFSE for +3 and +2 oxidation states.

5.2.2 Redox properties of macrobicyclic d-metal tris-dioximates and related compounds

The electrochemical behaviour of the macrobicyclic boron-, germanium-, antimony-, and tin-capped iron, cobalt, and ruthenium dioximates has been studied by cyclic voltammetry, polarography, and electrolytic experiments [41, 52, 64, 65, 68, 73, 74, 77, 78, 328-330]. For every metal ion, the dependence of the redox potentials on the electronic characteristics of the substituents in the dioximate
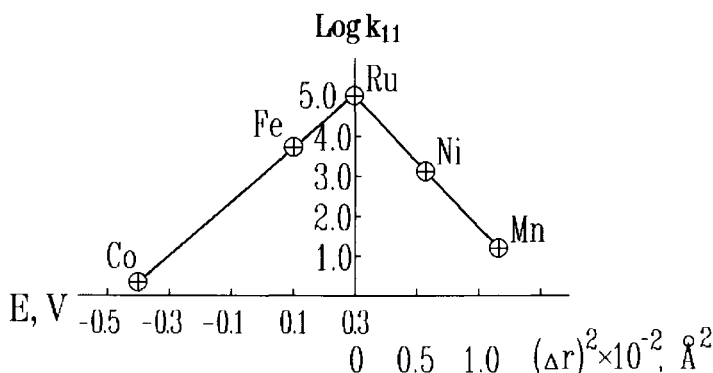

Fig. 44. Plot of Log k_{11} *versus* the difference in the M^{II}–N and M^{III}–N distances (Δr) and E values for [M(sar)]$^{3+/2+}$ couples [4, 324].

fragments and at the capping atom has been examined. The redox characteristics ($E_{1/2}$) of the macrobicyclic boron-capped iron, cobalt, and ruthenium dioximates are listed in Table 34.

Polarograms of the alkoxyboron-capped iron(II) tris-dioximates [328] exhibited well-defined reduction waves with the $E_{1/2}$ from −1 330 to −1 390 mV. The reduction is accompanied by one-electron $Fe^{2+/1+}$ process. The apical alkoxy groups do not significantly affect the reduction potentials of the various complexes in the same series. Two series of complexes derived from structurally different systems (dimethylglyoximates and acetylacetonedioximates) have almost similar $E_{1/2}$ values [328].

The oxidation of iron(II) clathrochelates to iron(III) complexes is a quasi-reversible process with $E_{1/2}$ from 775 to 580 mV for clathrochelate dimethylglyoximates, from 850 to 570 mV for nioxime compounds, from 1 250 to 1 040 mV for glyoximates, and from 940 to 760 mV for α-benzyldioxime complexes. In the dioxime series Nx > Dm > Bd > Gm, the $E_{1/2}$ values becomes higher.

On passing from clathrochelate iron(II) nioximates to dimethylglyoximates with the same capped groups, the $E_{1/2}$ values slightly increase (only by 10÷30 mV), whereas on passing to α-benzyldioximates and glyoximates, the $E_{1/2}$ magnitude becomes higher by 200÷500 mV.

It has been pointed out [52] that there is a correlation between the Hammet's σ_{para} constants of the apical substituents and the redox potentials of the corresponding iron clathrochelates. Meanwhile, such a correlation is observed only inside the two groups of complexes with (a) OH, OCH_3, F, Cl, and Br and (b) CH_3, C_6H_5, and n-C_4H_9 substituents. No reasons are given for the existence of two groups of complexes. In spite of the fact that the cyclic voltammetry evidence indicates that the $Fe^{2+/3+}$ couple is quasi-reversible, the electrolytic oxidation has failed to isolate stable iron(III) complexes [52].

The redox processes in macrobicyclic cobalt dioximates are reversible; their redox potentials are higher than those of the $[Co(sar)]^{3+/2+}$ couple, and this can be attributed to relative stabilization of the cobalt(II) oxidation state. As consequence, the cobalt dioximates have been isolated in both +2 and +3 oxidation states. The data on redox potentials of macrobicyclic cobalt dioximates are not sufficient to establish dependence on electronic characteristics of the apical substituents. Yet in this case, a distinct growth in the $E_{1/2}$ values was observed on increasing the σ_I value of

Table 34.

Redox characteristics (mV) of macrobicyclic boron-capped $MD_3(BR)_2$ tris-dioximates in nonaqueous solutions.

| Apical substituent | $^aFe^{2+/3+}$ | | | | $^aCo^{3+/2+}$ | | | $^bRu^{3+/2+}$ | | | σ_{para} | σ_I |
	Dm [52,64]	Nx [52,64]	Gm [65]	Bd [52,64]	Dm [41]	Nx [41]	Bd [41]	Dm [77,329]	Nx [77,329]	Bd [77,329]		
F	775	745	1250	940	−28	−13			1330		0.062	0.52
Cl		825									0.227	0.47
Br		850									0.232	0.45
OH	620	610									−0.370	0.25
OCH₃	655	640		775				1230	1210	1430	−0	0.26
OC₂H₅	650								1200		−0.240	
On-C₃H₇									1200			
On-C₄H₉									1200			
H	650	640									0	0
CH₃	580	575							1140		−0.170	−0.05
n-C₄H₉		570	1040	760	−370	−282		1150	1170	1340	−0.190	−0.06
C₆H₅		635	1090		−212	−200	−99				−0.010	0.10

[a] vs Fc/Fc$^+$ couple in AN, the potential of this couple vs SCE is 310 mV.   [b] vs SCE in CH_2Cl_2

substituents in the series n-C_4H_9 < C_6H_5 < F (Table 34). In accordance with this order, the passing from aliphatic dioximates to α-benzyldioximates also leads to a substantial $E_{1/2}$ value increase.

The oxidation of encapsulated ruthenium(II) ion to ruthenium(III) ion is a quasi-reversible process with $E_{1/2}$ from 1 430 to 1 140 mV. As on additional parameter, the cathodic and anodic current ratio (I_{pc}/I_{pa}) obtained from voltammetric data was used to determine the relative stability of the resulting ruthenium(III) complexes. It was shown that the stability of these complexes increases with lengthening of the linear chain of alkoxy-groups and decreases with an increase in their volumes [77, 329].

The electrochemical characteristics of macrobicyclic ferrocenyl-boron-capped iron(II) tris-dioximates are listed in Table 35 .

The results obtained in both acetonitrile and dichloromethane solutions are similar. Normally, the voltammograms included two reversible or quasi-reversible waves with a Tomeš criterion $\Delta E = E_{3/4} - E_{1/4}$, characterizing the reversibility of electrochemical processes [335], of ca 60 mV and a distance between them of 855 ± 20 mV. The first and more intensive wave was attributed to the oxidation of two independent ferrocenylboron caps. A substantial ($100 \div 200$ mV) cathodic shift of this wave $versus$ the Fc^+/Fc potential is caused by the donor effect of the macrobicyclic substituent in cyclopentadienyl rings.

The second wave, which appears at higher potentials, was attributed to the oxidation of encapsulated iron(II) ion. The $E_{1/2}$

Table 35.
Electrochemical characteristics (mV, vs Fc^+/Fc) of ferrocenylboron-capped trinuclear iron(II) clathrochelates [66].

Compound	Acetonitrile				Dichloromethane			
	$E_{1/2}$	ΔE	$E'_{1/2}$	$\Delta E'$	$E_{1/2}$	ΔE	$E'_{1/2}$	$\Delta E'$
FeGx$_3$(BFc)$_2$	−125	60	742	60	−210	65	665	65
FeNx$_3$(BFc)$_2$	−125	60	742	60	−162	65	713	65
Fe(4MNx)$_3$(BFc)$_2$	−125	60	742	60	−185	65	720	65
FeMm$_3$(BFc)$_2$	−105	60	a	a	−185	65	950	a
FeDm$_3$(BFc)$_2$	−130	60	770	60	−170	65	710	65
FeFd$_3$(BFc)$_2$	−050	87	656	132	−120	65	585	200
FeBd$_3$(BFc)$_2$	−146	64	549	110	−215	70	565	110

a The second wave appears as a peak at scan rates of at least 10 mV·s⁻¹. This process passivates the electrode and the reaction becomes irreversible.

values for this ion are quite comparable with potentials observed for clathrochelate iron(II) tris-dimethylglyoximates and tris-nioximates (Table 34). Both the potentials of these two waves and the distance between them are practically independent of the solvent. This can be accounted for by a weak interaction of all three iron centres in complexes with solvent molecules. Obviously, the interaction between these centres within a complex molecule is negligible as well. However, in complexes with bulky substituents, e.g., furyl or phenyl, in dioximates fragments both waves become quasi-reversible, and the distance between them decreases.

The electrochemical properties of the clathrochelate C_3-nonsymmetric $FeD_nD'_{3-n}(BX)_2$ and C_2-nonsymmetric $FeD_3(BX)(BY)$ tris-dioximates and their dependence on electronic characteristics of the substituents in the dioxime fragments and ones at capping atoms are discussed in Refs. 64 and 68. Table 36 lists the $E_{1/2}$ and the Tomeš criterion values for these complexes. As seen from this table, the oxidation process for most of the boron-capped iron(II) clathrochelates is reversible or quasi-reversible.

In the case of C_3-nonsymmetric complexes, the $Fe^{2+/3+}$ couple oxidation potentials increase in passing from dimethylglyoxime clathrochelates to α-benzyldioxime ones: $Dm_3 < Dm_2Bd < DmBd_2 < Bd_3$. For C_2-nonsymmetric clathrochelate iron(II) tris-nioximates and tris-α-benzyldioximates, $E_{1/2}$ values decrease in the series of capping groups $(BF)_2 > BF(BC_6H_5) > (BC_6H_5)_2$ and $(BF)_2 > (BF)(Bn$-$C_4H_9) > (Bn$-$C_4H_9)_2$, respectively.

Table 36.
Electrochemical characteristics (mV, vs SCE) of C_3- and C_2-nonsymmetric iron clathrochelates.

Compound	[a] $E_{1/2}$	ΔE	Compound	[b] $E_{1/2}$	ΔE
$FeDm_3(BF)_2$	785	60	$FeBd_2Gm(BF)_2$	1041	65
$FeDm_2Bd(BF)_2$	850	70	$FeBd_2Nx(BF)_2$	890	56
$FeDmBd_2(BF)_2$	900	70	$FeBd_3(BF)_2$	925	100
$FeBd_3(BF)_2$	940	70	$FeBd_2Dm(BF)_2$	875	60
$FeNx_3(BC_6H_5)_2$	635	65			
$FeNx_3(BF)(BC_6H_5)$	710	85			
$FeNx_3(BF)_2$	745	80			
$FeBd_3(BF)(Bn$-$C_4H_9)$	880	70			
$FeBd_3(Bn$-$C_4H_9)_2$	760	60			

[a] Solvent: AN   [b] Solvent: CH_2Cl_2

The electrochemical behaviour of the ribbed-functionalized iron(II) [65, 68] and ruthenium(II) [78] clathrochelates with alkylamine, thioaryl, thioalkyl, phenoxyl and crown ether substituents in α-dioximate fragments was characterized by $E_{1/2}$ values for $Fe^{3+/2+}$ and $Ru^{3+/2+}$ couples (Table 37). The Tomeš criterion values of most complexes exhibited reversible or quasi-reversible anodic processes. Moreover, the quasi-reversible oxidation processes are accompanied by the formation of insoluble products followed by passivation of the working electrode. The $E_{1/2}$ values depend on the electron-donating properties of the substituents in the ribbed fragments. The correlations of $E_{1/2}$ values for $Ru^{3+/2+}$ and $Fe^{3+/2+}$ couples with these substituents Hammet's σ_{para} constants were observed in Refs. 65, 68, and 78. These correlations are rather qualitative, but they enable one to conclude that ruthenium complexes are less sensitive to the change of substituents in dioximate fragments. There was no correlation between the $E_{1/2}$ values and the inductive Taft's (σ_i) constants for substituents in dioximate fragments.

The peculiarity of the electrochemical behaviour of ruthenium clathrochelates, which distinguishes them from analogous iron(II) complexes, is their lower sensitivity to the replacement of substituents in the capping groups (Table 37). Moreover, if the dioximate fragments contain electron-accepting substituents, the ruthenium complexes, oxidation potential becomes practically independent of apical substituent features. At the same time, for the macrobicyclic ruthenium(II) tris-nioximates, the replacement of fluoroboronic capping groups onto n-butylboronic groups resulted in the cathodic shift of $E_{1/2}$ value by ca 200 mV (Table 37).

The cyclic voltammograms of the $[FeDAO_3(BC_6H_5)_2]$ and $[Fe_2DAO_3(BC_6H_5)_2](BF_4)_2$ azineoximates with binucleating clathrochelate ligand are discussed in Ref. 188. A quasi-reversible wave was observed for a mononuclear complex with a vacant cavity from 700 to 800 mV. The oxidation of binuclear dication occurs in two steps at more positive potentials (1 200 and 1 540 mV, Table 38). These waves were attributed to stepwise oxidation of encapsulated iron(II) ions to form mixed valence iron(II)/iron(III) complex as an intermediate product [188].

The electrochemical properties of an extended series of the clathrochelate mononuclear and binuclear iron and cobalt oximehydrazonates have been reported in Refs. 186, 187, and 189 and the cyclic voltammetric data are presented in Table 39. Most of the

Table 37.

Electrochemical characteristics for ribbed-functionalized macrobicyclic iron and ruthenium(II) tris-dioximates, their precursors and analogs [65, 68, 78].

Compound	$\sigma_i{}^a$	$\sigma_{para}{}^a$	$E_{1/2}$	ΔE
Ru(Cl2Gm)₃(BC₆H₅)₂	0.47 [0.10]	0.227 [−0.01]	1360	60
Fe(Cl2Gm)₃(BC₆H₅)₂			1360	80
Ru(Cl2Gm)₃(Bn-C₄H₉)₂	0.47 [−0.08]	0.227 [−0.19]	1330	60
Fe(Cl2Gm)₃(Bn-C₄H₉)₂			1320	90
Ru(Cl2Gm)₃(BF)₂	0.47 [0.52]	0.227 [0.062]	1340	80
Fe(Cl2Gm)₃(BF)₂			1415	60
Ru((C₆H₅S)2Gm)₃(BF)₂	0.27 [0.52]	0.15 [0.062]	1120	60
Fe((C₆H₅S)2Gm)₃(BC₆H₅)₂	0.27 [0.10]	0.15 [−0.01]	895	80
Ru((CH₃S)2Gm)₃(BF)₂	0.19 [0.52]	0.00 [0.062]	830	65
Fe((CH₃S)2Gm)₃(BC₆H₅)₂	0.19 [0.10]	0.00 [−0.01]	670	60
Ru((C₆H₅O)2Gm)₃(Bn-C₄H₉)₂	0.38 [−0.08]	−0.32 [−0.19]	840	85
Fe((C₆H₅O)2Gm)₃(Bn-C₄H₉)₂			800	100
Ru(CwGm)₃(Bn-C₄H₉)₂	0.38 [−0.08]	−0.32 [−0.19]	690	90
Fe(CwGm)₃(Bn-C₄H₉)₂			460	60
Ru(CwGm)₂(Cl2Gm)(Bn-C₄H₉)₂	0.38(OPh) ⎱ 0.41	−0.32(OPh) ⎱ −0.14	780	60
Fe(CwGm)₂(Cl2Gm)(Bn-C₄H₉)₂	0.47(Cl) ⎰	0.227(Cl) ⎰	670	65
	[−0.08]	[−0.19]		
Ru((n-C₄H₉NH)2Gm)₂(Cl2Gm)(BC₆H₅)₂	0.47(Cl) ⎱ 0.22	0.227(Cl) ⎱ −0.14	560	95
Fe((n-C₄H₉NH)2Gm)₂(Cl2Gm)(BC₆H₅)₂	0.10(n-BuNH) ⎰	−0.63(n-BuNH) ⎰	200	170
	[−0.10]	[−0.01]		
Ru((CH₂)4Gm)₃(BF)₂	−0.05 [0.52]	−0.15 [0.062]	850	70
Fe((CH₂)4Gm)₃(BF)₂			745	80
Ru((CH₂)4Gm)₃(Bn-C₄H₉)₂	−0.05 [−0.08]	−0.15 [−0.19]	645	60
Fe((CH₂)4Gm)₃(Bn-C₄H₉)₂			570	70
Fe((C₆H₅)2Gm)₃(BF)₂	0.10 [0.52]	−0.01 [0.062]	940	70
Fe((CH₃)2Gm)(BF)₂	−0.05 [0.52]	−0.17 [0.062]	785	60
FeGm₃(BF)₂	0.00 [0.52]	0.00 [0.062]	1250	65
Fe((C₆H₅)2Gm)₂(Cl2Gm)(BF)₂	0.10(Ph) ⎱ 0.223	−0.01(Ph) ⎱ 0.069	1100	70
	0.47(Cl) ⎰	0.227(Cl) ⎰		
	[0.52]	[0.062]		
Fe((C₆H₅)2Gm)₂(CwGm)(BF)₂	0.10(Ph) ⎱ 0.193	−0.01(Ph) ⎱ −0.113	800	90
	0.38(OPh) ⎰	−0.32(OPh) ⎰		
	[0.52]	[0.062]		
Fe((C₆H₅)2Gm)₂ ((n-C₄H₉NH)2Gm)(BF)₂	0.10(Ph) ⎱ 0.10	−0.01(Ph) ⎱ −0.217	400	75
	0.10(n-BuNH) ⎰	−0.63(n-BuNH) ⎰		
	[0.52]	[0.062]		
Fe((C₆H₅)2Gm)₃((CH₃S)2Gm)(BF)₂	0.10(Ph) ⎱ 0.13	−0.01(Ph) ⎱ −0.007	880	70
	0.19(CH₃S) ⎰	−0.00(CH₃S) ⎰		
	[0.52]	[0.062]		

[a] Taft's (σ_i) and Hammet's (σ_{para}) constants for substituents in α-dioximate fragments [capping groups]. $\sigma_\Sigma = \dfrac{n}{m+n}\sigma_1 + \dfrac{m}{m+n}\sigma_2$, $\sigma_{n+1} = \sigma_n/2.5$ [336, 337].

Table 38.

Cyclic voltammetric data (mV) for macrobicyclic boron-, tin-, antimony- and germanium-capped iron(II) oximehydrazonates and α-dioximates [73, 74, 188].

Compound	$E_{1/2}$	ΔE	Compound	$E_{1/2}$	ΔE
FeNx$_3$(BC$_6$H$_5$)$_2$	635	60	FeDXO$_3$(Ge(CF$_3$)$_3$)(CH$_2$)$_3$	400	130
FeNx$_3$(Sb(C$_6$H$_5$)$_3$)(BC$_6$H$_5$)	415	110	FeDXO$_3$(Ge(CF$_3$)$_3$)(HCOC$_2$H$_5$)$_3$	460	95
FeNx$_3$(Sb(C$_6$H$_5$)$_3$)$_2$	370	120	Fe$_2$DAO$_3$(Ge(CF$_3$)$_3$)$_2$	810	55
FeNx$_3$(Sb(C$_2$H$_5$)$_3$)$_2$	−65	60	Fe$_2$DAO$_3$(SnCl$_3$)$_2$	880	65
[FeNx$_3$(Sb(C$_2$H$_5$)$_3$)]$_2$(BC$_6$H$_4$B)	290	65		1170	60
FeNx$_3$(Bn-C$_4$H$_9$)$_2$	570	60	[Fe$_2$DAO$_3$(BC$_6$H$_5$)$_2$](BF$_4$)$_2$	1200	55
FeNx$_3$(Sb(C$_2$H$_5$)$_3$)(Bn-C$_4$H$_9$)	230	60		~1550	a
FeNx$_3$(Sb(CH=CH$_2$)$_3$)$_2$	460	80	FeDAO$_3$(BC$_6$H$_5$)$_2$	790	110
[FeNx$_3$(Ge(CF$_3$)$_3$)$_2$]$^{2-}$	−30	85	Fe$_2$IAO$_3$(SnCl$_3$)$_2$	1120	85
FeDXO$_3$(Ge(CF$_3$)$_3$)	360	55		1360	80

Table 39.

Cyclic voltammetric data (mV, vs SCE in AN) for macrobicyclic iron and cobalt oximehydrazonates [186, 187, 189].

Compound	Oxidation			Reduction		
	$^aE_{1/2}$	ΔE	^{b}Current ratio	$^aE_{1/2}$	ΔE	^{b}Current ratio
[FeDXO$_3$(CH$_2$)$_3$(BC$_6$H$_5$)](PF$_6$)	1140	75	0.83	−1020	90	0.79
[FePXO$_3$(CH$_2$)$_3$(BC$_6$H$_5$)](PF$_6$)	1290	75	0.90	−890	75	0.90
[FeMXO$_3$(CH$_2$)$_3$(BC$_6$H$_5$)](PF$_6$)	1450	irr		−840		
[{FeDXO$_3$(CH$_2$)$_3$}$_2$(BC$_6$H$_4$B)](PF$_6$)$_2$	1140	70	0.88	−1040	90	0.89
[{FePXO$_3$(CH$_2$)$_3$}$_2$(BC$_6$H$_4$B)](PF$_6$)$_2$	1250	50	1.3	−890	80	0.83
[FeDXO$_3$(CH$_2$)$_3$(BPy)](PF$_6$)$_2$	1230	66		−960	66	
				−580	irr	
[FeDXO$_3$(CH$_2$)$_3$(BPy)](PF$_6$)	1340	65		−960	irr	
[CoDXO$_3$(CH$_2$)$_3$(BC$_6$H$_5$)](BF$_4$)	260	65	0.99	−670	65	0.87
[CoPXO$_3$(CH$_2$)$_3$(BC$_6$Hs)](BF$_4$)	340	65	1.0	−500	65	0.96
[{CoPXO$_3$(CH$_2$)$_3$}$_2$(BC$_6$H$_4$B)](BF$_4$)$_2$	310	55	1.3	−500	80	0.90
[FeDXO$_3$(CH$_2$)$_3$(BFc)](PF$_6$)	1150	80	0.73	−1050	70	0.91
	320	65	1.0			
[FeDXO$_3$(CH$_2$)$_3$(BFc)$_2$](PF$_6$)	1380	irr	1.0	−900	70	0.7
	330	65				
[FeMXO$_3$(CH$_2$)$_3$(BFc)](PF$_6$)	1160	irr	1.0	−880	75	0.70
	330	65				
[{FeDXO$_3$(CH$_2$)$_3$}$_2$(BFcB)](PF$_6$)$_2$	1160	90	0.76	−1080	95	0.91
	230	70	1.0			

^{a} $E_{1/2} = (E_{Pa} - E_{Pc})/2$ ^{b} I_{Pc}/I_{Pa} for oxidation and I_{Pa}/I_{Pc} for reduction

iron(II) clathrochelates undergo a quasi-reversible oxidation to corresponding iron(III) complexes and quasi-reversible reduction to iron(I) complexes. The oxidation potentials of the iron(II) complexes become more anodic as the substituents in oximehydrazonate fragments are varied from methyl to phenyl. Although the iron(III) complexes appear to be stable on the cyclic voltammetric time scale, attempts to isolate these clathrochelates *via* exhaustive electrolysis have not proved to be successful. This lack of stability for the iron(III) complexes is comparable to that observed for the clathrochelate iron tris-dioximates.

The clathrochelate pyridine-appended iron(II) complexes show different potentials depending on whether they are core protonated or not (Table 39). In addition to typical redox $Fe^{3+/2+}$ and $Fe^{2+/1+}$ couples, the second irreversible reduction at cathode peak potential of −580 mV was observed in a protonated form and attributed to the reduction of H^+ ion that is protonating the pyridine nitrogen [189].

The mononuclear cobalt complexes are stable and are able to be isolated in both 2+ and 3+ oxidation states. Cyclic voltammetric studies reveal reversible waves for both $Co^{3+/2+}$ and $Co^{2+/1+}$ reduction couples. These redox couples are shifted anodically as the ligand substituents are changed from methyl to phenyl. Electrolytic and cyclic voltammetric studies before and after electrolysis support the idea that the integrity of the complexes is maintained during electrolytic cycles of the 2+/3+ oxidation states. The I_{Pc}/I_{Pa} values of the $Co^{3+/2+}$ couple for the binuclear cobalt complexes are identical to those observed for the oxidation of the analogous iron complex. Attempts to produce the binuclear cobalt(III) species by exhaustive electrolysis have been limited by adsorption of the cobalt(III) complexes on the electrode surface [186, 187].

Cyclic voltammetry of the ferrocenylboron-capped oximehydrazonate iron(II) complexes with the same ribbed substituents (Table 39) reveal a reversible one-electron oxidation of the ferrocenyl iron at 320÷340 mV *vs* SCE. Electrolytic oxidation of the ferrocenyl iron at a potential of 750 mV in solution produces a stable mixed-valence complex. Cyclic voltammograms at this potential the solution before and after electrolysis indicate that the integrity of the complexes is maintained as the ferrocenyl is cycled between the +2 and +3 oxidation states. The redox potentials associated with the encapsulated iron ion are not affected by the oxidation state of the ferrocenyl iron, i.e., there is no apparent interaction between the two

iron centres in the molecule. The other redox potentials observed for these dinuclear complexes are quite comparable to the potentials observed for other clathrochelate iron(II) oximehydrazonates (Table 39). Attempts to electrolytically produce a fully oxidized species have lead to reverse results with decomposition of the complex. Cyclic voltammetry of the trinuclear complexes produced results that are very similar to those observed for the dinuclear species [186, 187].

The electrochemistry of macrobicyclic tin-capped iron and cobalt tris-dioximates has also been studied by cyclic voltammetry [330]. The one-electron oxidation potentials of the clathrochelate $[FeD_3(SnHal_3)_2]^{2-/1-}$ anions are determined by the nature of the chelating dioximate fragments, but they are independent of the halogenide substituents in the capping $SnHal_3$ fragments (Table 40). This indicates that the contribution of the μ_3-$SnHal_3$ capping group orbitals to the HOMO of the complex is negligible, i.e., oxidation processes are associated with the $Fe^{2+/3+}$ couple. The capping group orbitals make the main contribution to the LUMO of the complexes,

Table 40.
Voltammetric data (mV, *vs* SCE) for clathrochelate $[MD_3(SnHal_3)_2]^{2-/1-}$ anions in THF (0.05 mol·l^{-1} ((n-C$_4$H$_9$)$_4$N)PF$_6$) and AN (0.1 mol·l^{-1} ((n-C$_4$H$_9$)$_4$N)ClO$_4$) [330].

| Initial complex | M = Fe(II) | | | | | M = Co(III) |
| | Oxidation, $E_{1/2}$ | | Reduction, $E_{1/2}$ | | $^aI_{Pa}/I_{Pc}$ | Reduction, $E_{1/2}$ |
	THF	AN	THF	AN		
((n-C$_4$H$_9$)$_4$N)$_2$[MGm$_3$(SnCl$_3$)$_2$]	760	960				−610
(HDEA)$_2$[MGm$_3$(SnCl$_3$)$_2$]		960				
((n-C$_4$H$_9$)$_4$N)$_2$[MMm$_3$(SnCl$_3$)$_2$]	540	730	−240	0.0	1.54	−770
(HDEA)$_2$[MMm$_3$(SnCl$_3$)$_2$]	530	730				
((n-C$_4$H$_9$)$_4$N)$_2$[MDm$_3$(SnCl$_3$)$_2$]	340	560	−250	20	0.74	−990
(HDEA)[MDm$_3$(SnCl$_3$)$_2$]		560				
((n-C$_4$H$_9$)$_4$N)$_2$[MNx$_3$(SnCl$_3$)$_2$]	340	570	−240	20	1.28	−960
(HDEA)[MNx$_3$(SnCl$_3$)$_2$]		550				
((n-C$_4$H$_9$)$_4$N)$_2$[MBd$_3$(SnCl$_3$)$_2$]	560	810	−260	10	1.04	
(HDEA) [MBd$_3$(SnCl$_3$)$_2$]	800					
((n-C$_4$H$_9$)$_4$N)$_2$[MGm$_3$(SnBr$_3$)$_2$]		950				−610
((n-C$_4$H$_9$)$_4$N)$_2$[MMm$_3$(SnBr$_3$)$_2$]		540	−60		0.29	−810
((n-C$_4$H$_9$)$_4$N)$_2$[MDm$_3$(SnBr$_3$)$_2$]		340	−40		0.13	−990
((n-C$_4$H$_9$)$_4$N)$_2$[MNx$_3$(SnBr$_3$)$_2$]		340	−40		0.27	−950
(HDEA) [MNx$_3$(SnBr$_3$)$_2$]		570				
(HPy)$_2$[MNx$_3$(SnBr$_3$)$_2$]		570				
((n-C$_4$H$_9$)$_4$N)$_2$[MBd$_3$(SnBr$_3$)$_2$]						−760

^{a} ratio of reduction (A) and oxidation (B) current peaks in AN

i.e., in the case of reduction, an electron is transferred to the capping group. In a series of solvents, the oxidation potential of the complexes increases, and the reduction potential decreases with solvent acceptor properties. The one-electron reduction potentials of the tin-capped cobalt complexes depend on the nature of the substituents in the dioximate fragments and are independent of the halogenide substituents in the capping groups (Table 40). The reduction of clathrochelate cobalt(III) $[CoD_3(SnHal_3)_2]^-$ anions via encapsulated metal ion produced cobalt (II) $[CoD_3(SnHal_3)_2]^{2-}$ dianions. The main contribution to the LUMO of cobalt complexes is made by the metal ion AO. A linear correlation between the redox potentials of $[FeD_3(SnHal_3)_2]^{2-/1-}$ and $[CoD_3(SnHal_3)_2]^{1-/2-}$ couples was observed (Fig. 46). Passage from encapsulated iron ion to cobalt ion in a series of isoelectronic and isostructural low-spin clathrochelate complexes is accompanied by frontier orbital inversion: the orbital localized on the encapsulated metal ion is a HOMO for iron complexes and a LUMO for cobalt complexes. The contribution of the dioximate fragment orbitals to complex orbitals is approximately equal in both cases [330].

The redox properties of macrobicyclic iron(II) mono- and binuclear oximehydrazonates and α-dioximates formed by capping with antimony(V) and germanium(IV) triorganyles were studied by cyclic voltammetry [73, 74]. The electrochemical behaviour of these compounds is similar to that of analogous boron- and tin-capped clathrochelates. Oxidation of all mononuclear complexes involves a one-electron process, assigned to the oxidation of encapsulated iron(II) ion to iron(III) ion. This process is electrochemically
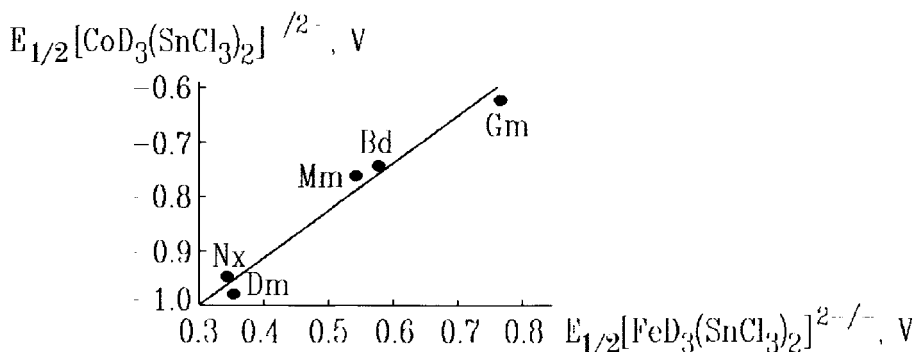
Fig. 45. Correlation of oxidation $Fe^{2+/3+}$ potentials versus $Co^{3+/2+}$ reduction ones [330].

reversible or quasi-reversible; the position and shapes of voltam-metric curves depend on the nature of capping groups. The $E_{1/2}$ and ΔE values for antimony- and germanium-capped complexes are listed in Table 38.

The ability of encapsulated iron(II) ion to be oxidized to iron(III) ion drops in the series of capping atoms $Ge > Sn > Sb > B$. In C_2-nonsymmetric clathrochelate complexes, the oxidation potentials are near average between the values for symmetric complexes with corresponding capping groups (Table 38).

For binuclear germanium-capped iron(II) complexes two waves of oxidation of encapsulated iron(II) ion to iron(III) ion were observed. The iron(III) complexes seem to be stable only in the cyclic voltammetric scale. Attempts to prepare fully oxidized species led to irreversible decomposition of this complex.

The electrochemical behaviour of trinuclear clathrochelate $[M^ID_3(ttnM)_2]^{2+/4+}$ and $[CoDm_3(dienM)_2]^{3+}$ cations has been investigated by cyclic voltammetry, polarography, and coulometry. The data obtained are summarized in Table 41.

Two consecutive reversible steps of oxidation for all studied manganese-capped tris-dimethylglyoximates and tris-nioximes with $E_{1/2}$ from 650 to 740 and $430 \div 470$ mV were attributed to the following electrochemical processes:

$$Mn^{III}M^{II}Mn^{III} \xleftrightarrow{ox_1} Mn^{IV}M^{II}Mn^{III} \xleftrightarrow{ox_2} Mn^{IV}Mn^{II}Mn^{IV} \qquad (82)$$
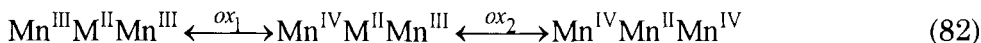
The reversible character of $E_{1/2}{}^{ox_1}$ and $E_{1/2}{}^{ox_2}$ precludes any significant structural rearrangement during the redox process.

Two additional quasi-reversible reduction steps with $E_{1/2}{}^{red_1} = -210 - (-310)$ mV and $E_{1/2}{}^{red_2} = -630 - (-590)$ mV were attributed to the following processes:

$$Mn^{III}M^{II}Mn^{III} \xleftrightarrow{red_1} Mn^{II}M^{II}Mn^{III} \xleftrightarrow{red_2} Mn^{II}M^{II}Mn^{II} \qquad (83)$$
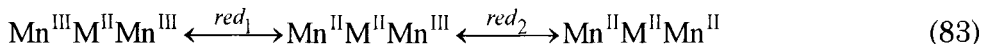
The encapsulated divalent metal ions in these complexes are redox inactive.

The reduction potentials for the clathrochelate $[CoDm_3(dienCo)_2]^{3+}$ complex fall in the range observed for a number of $Co^{3+/2+}$ couple redox potentials. For the chromium-capped $[CoDm_3(dienCr)_2]^{3+}$ complex, they are much more negative and also fall in the range for $Cr^{3+/2+}$ reduction. These results show that the reduction in both Co^{III}–Co^{III}–Co^{III} and Cr^{III}–Co^{III}–Cr^{III} complexes is caused by redox activity of the capping metal ions rather than that of the
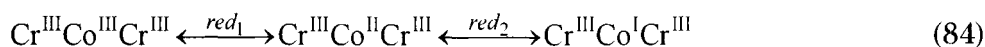
Table 41.
Cyclic voltammetric data for trinuclear macrobicyclic tris-dioximates.

Cation	Oxidations (reversibility)		Reductions (reversibility)		Reference
$E_{1/2}$ vs SCE in acetonitrile					
$[CoDm_3(dienCo)_2]^{3+}$			−150(r)	−460(r)	[46]
$[CoDm_3(dienCr)_2]^{3+}$			−980(r)	−1580(r)	[46]
$[CoDm_3(dienNi)_2]^{+}$	460(qr)	850(qr)			[46]
$[CoDm_3(Ni(H_2O)_6)_2]^{2+}$	700(ir)	1160(ir)			[46]
$E_{1/2}$ vs NHE in acetonitrile [a]					
$[CoDm_3(ttnCr)_2]^{3+}$			−350(r)	−1140(r)	[85]
$[ZnDm_3(ttnCr)_2]^{2+}$	1690(ir)	1100(ir)			[85]
$[H_2Dm_3(ttnCr)_2]^{2+}$	1690(ir)	1100(ir)		−1610(ir)	[85]
$[CuDm_3(ttnCr)_2]^{2+}$	1430(qr)	1020(qr)	−850(qr)		[85]
$[NiDm_3(ttnCr)_2]^{2+}$	1320(r)	890(r)		−1650(qr)	[85]
$[FeDm_3(ttnCr)_2]^{2+}$		530(r)		−1860(qr)	[85]
$[MnDm_3(ttnCr)_2]^{2+}$	1300(qr)	570(qr)		−1630(ir)	[85]
$[NiDm_3(ttnFe)_2]^{2+}$	1310(qr)	840(qr)	−670(r)	−1020(r)	[80]
$[MnDm_3(ttnMn)_2]^{2+/4+}$	730(r)	440(r)	−230(qr)	−60(qr)	[82]
$[NiDm_3(ttnMn)_2]^{2+/4+}$	710(r)	470(r)	−250(qr)	−52(qr)	[82]
$[CuDm_3(ttnMn)_2]^{2+/4+}$	730(r)	430(r)	−330(qr)	−610(qr)	[82]
$[ZnDm_3(ttnMn)_2]^{2+/4+}$	670(r)	430(r)	−310(qr)	−590(qr)	[82]
$[ZnNx_3(ttnMn)_2]^{2+/4+}$	650(r)	430(r)	−310(qr)	−620(qr)	[83]
$[CuNx_3(ttnMn)_2]^{2+/4+}$	720(r)	430(r)	−340(qr)	−630(ir)	[83]
$[MnNx_3(ttnMn)_2]^{2+/4+}$	740(r)	430(r)	−210(qr)	−560(qr)	[83]

[a] NHE vs SCE potential is −244 mV

encapsulated cobalt(III) ion. The data on the zinc- and nickel-capped cobalt(III) complexes confirmed this conclusion. No reductions and oxidations of the zinc-capped complexes were observed over the potential range from +2 400 to −2 100 mV. Two irreversible oxidation waves (nickel(II) to nickel(III)) were observed for the nickel-capped clathrochelates (Table 41). The apparent inert behaviour of the encapsulated cobalt(III) ion in trinuclear complexes toward reduction was assigned to an unusually high stability of the cobalt(III) state in these clathrochelates. It attributed to increasing the strain in the ligand system and to increasing the LFSE [46].

The one-electron transfer waves at $E_{1/2}{}^{red_1} = -350$ mV and $E_{1/2}{}^{red_2} = -1\,440$ mV for $[CoDm_3(ttnCr)_2]^{3-}$ cation were assigned in Ref. 85 to the following processes:

$$Cr^{III}Co^{III}Cr^{III} \xleftrightarrow{\ red_1\ } Cr^{III}Co^{II}Cr^{III} \xleftrightarrow{\ red_2\ } Cr^{III}Co^{I}Cr^{III} \qquad (84)$$
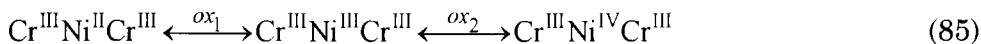
However, the chromium(III)-capped cobalt(II) complex was not obtained. In contrast, both the corresponding boron-capped cobalt(II) and cobalt(III) dimethylglyoximates were isolated (see Section 2.1).

Two irreversible electron-transfer waves were detected in the potential range from 1900 to 0.0 mV at $E_{1/2}^{ox_1} = 1100$ and $E_{1/2}^{ox_2} = 1700$ mV for clathrochelate $[ZnDm_3(ttnCr)_2]^{2+}$ cation and free $[H_2Dm_3(ttnCr)_2]^{2+}$ ligand (Table 41). The first oxidation process corresponded to the redox $Cr^{4+/3+}$ couple, followed by decomposition of the oxidized form. The second oxidation process and irreversible reduction of free ligand at −1610 mV were assigned to the dimethylglyoxime fragments.

The encapsulated copper(II) ion in clathrochelate $[CuDm_3(ttnCr)_2]^{2+}$ cation is quasi-reversibly oxidized to copper(III) ion at 1020 mV and to copper(IV) clathrochelate at 1430 mV. The negative potential range showed a quasi-reversible one-electron reduction at −850 mV, which was assigned to the redox $Cu^{2+/1+}$ couple.

Two consecutive reversible steps of oxidation at $E_{1/2}^{ox_1} = 890$ mV and $E_{1/2}^{ox_2} = 1320$ mV were detected for $[NiDm_3(ttnCr)_2]^{2+}$ cation, and the following scheme involving the oxidation of encapsulated nickel(II) ion was proposed:

$$Cr^{III}Ni^{II}Cr^{III} \xleftarrow{\;ox_1\;} Cr^{III}Ni^{III}Cr^{III} \xleftarrow{\;ox_2\;} Cr^{III}Ni^{IV}Cr^{III} \tag{85}$$

A quasi-reversible reduction at −1 650 mV, observed for this cation, was attributed to a reduction of the ligand dimethylglyoxime moieties.

The clathrochelate $[FeDm_3(ttnCr)_2]^{2+}$ cation shows two one-electron transfer waves: one reversible oxidation at 530 mV and one reversible reduction at −1860 mV. The former wave was attributed to the redox $Fe^{3+/2+}$ couple. There are several reports of the electrochemical oxidation of encapsulated iron(II) ions to iron(III) ions, but none of the macrobicyclic iron(III) tris-dioximates could be isolated because of their instability. But in this case, the $[FeDm_3(ttnCr)_2]^{3+}$ cation was isolated in the solid state. The reduction wave for the initial trinuclear clathrochelate was attributed to the $Fe^{2+/1+}$ couple.

The cyclic voltammograms of clathrochelate $[MnDm_3(ttnCr)_2]^{2+}$ cation showed two quasi-reversible one-electron oxidations at 570 and 1 300 mV attributed to the redox $Mn^{3+/2+}$ and $Mn^{4+/3+}$ couples, respectively. An irreversible reduction at −1 600 mV was attributed to the reduction of the dioxime fragments.

The cyclic voltammetry of $[NiDm_3(ttnFe)_2]^{2+}$ cation in AN detected two consecutive reversible steps of reduction in a range of potentials from 0.0 to −1 600 mV at $E_{1/2}^{red_1} = -640$ and $E_{1/2}^{red_2} = -1020$ mV [80]. These two reversible transfers of one electron per centre are evident from differences in peak potential values $\Delta E = 65$ mV and the ratio $I_{Pa}/I_{Pc} \sim 1.0$. The following redox scheme containing a reversible formation of a mixed-valent Fe^{III}–Ni^{II}–Fe^{III} species was ascribed to the electrochemical reduction processes:

$$Fe^{III}-Ni^{II}-Fe^{III} \xleftrightarrow{red_1} Fe^{III}-Ni^{II}-Fe^{II} \xleftrightarrow{red_2} Fe^{II}-Ni^{II}-Fe^{II} \qquad (86)$$
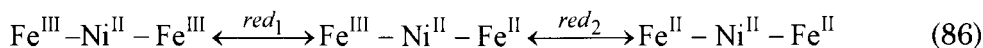
Electrochemically reversible one-electron-transfer steps preclude any significant structural rearrangement during the redox processes. No reduction current from encapsulating nickel(II) ion to nickel(I) ion is observed in the potential range from 0.0 to 2 000 mV.

Analysis of the cyclic voltammograms in the positive potential range from 0.0 to 1 500 mV indicates a simple one-electron mechanism for the quasi-reversible oxidation processes at 840 mV and 1310 mV. These oxidation processes were attributed to the equilibrium:

$$Fe^{III}-Ni^{II}-Fe^{III} \xleftrightarrow{ox_1} Fe^{III}-Ni^{III}-Fe^{III} \xleftrightarrow{ox_2} Fe^{III}-Ni^{IV}-Fe^{III} \qquad (87)$$
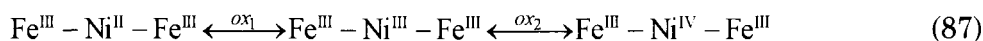
The quasi-reversible character of these redox reactions indicates that some geometrical changes are taking place without changing the clathrochelate framework. As in the case of trinuclear cobalt complexes, macrobicyclic nickel dioximates are characterized by a high oxidation state stabilization in comparison with other nickel complexes. For example, for $Ni(HDm)_2$ bis-dioximate, two processes (oxidation and reduction) were observed for nickel(II) ion [80].

Thus, the cyclic voltammograms of these complexes demonstrated both oxidation and reduction waves and indicated the formation of uncommon species such as copper(III), nickel(III), nickel(IV), and low-spin iron(III) complexes. The data for manganese(III)- and manganese(IV)-capped complexes showed that it is possible to stabilize the tris-dioximatometalate(II) tetraanions with the different $ttnMn^{III}$ or $ttnMn^{IV}$ caps.

5.2.3 Redox properties of cobalt sarcophaginates and related compounds

Kinetically inert low-spin cobalt (III) clathrochelates are reversibly reduced by accepting one electron to yield kinetically labile cobalt(II) complexes. In the case of the usual amines (for instance, ammonia), the reduction is, as a rule, accompanied by irreversible decay of the amine cobalt complex. This reaction is slower for chelating amines; macrocyclic and especially macrobicyclic amines produce complexes with cobalt(II) ion that are stable over a long time. This fact facilitates the study of the reduction of cobalt(III) complexes to cobalt(II) ones. In most cases, the reactions of macrobicyclic ligands do not interfere with this process.

The redox potentials E for the $Co^{3+/2+}$ couple in these compounds have been measured by several methods in aqueous solutions [4, 106, 338-340] and also in organic solvents, such as acetonitrile and acetone [338-339].

The E values obtained by various methods are slightly different. For instance, the redox potentials for $[Co(sep)]^{3+}$ cation in 0.1–0.2 mol·l^{-1} NaClO$_4$ and 0.2 mol·l^{-1} NaCl were found to be $-260 – (-280)$ and -320 mV by polarography, $-300 – (-290)$ and $-330 – (-320)$ mV by cyclic voltammetry, and $-280 – (-310)$ mV by potentiometry. There are some more E values available in the literature: -260 [325, 338], -270 [342], -300 [4] and -320 mV [341]. Nearly the same spread in E values has been observed for $[Co(sar)]^{3+}$ and $[Co(en)_3]^{3+}$ cations and some other complexes studied by several authors. Thus even for the most thoroughly examined systems, a reliable range amounts to approximately $\pm(10 – 20)$ mV. The systematic decrease of the potentials in the passing from perchlorate to chloride systems may be attributed to the greater stability of $CoL^{3+}...Cl^-$ ion pairs to compared with $CoL^{3+}...ClO_4^-$ ones. The E values obtained for aqueous and nonaqueous solutions are listed in Tables 42 and 43, respectively. Table 42 also contains the data for structurally similar nonmacrocyclic cobalt complexes.

The E values for macrobicyclic cobalt complexes in aqueous solutions differ by 1400 V (from -550 to $+840$ mV). For nonmacrocyclic cobalt complexes with diamines and triamines, the E values change from -630 to $+280$ mV. The potentials for $[Co(NH_3)_6]^{3+}$ and $[Co(en)_3]^{3+}$ ions occupy an intermediate position in this range [4, 344].

The macrocycle formation effect on the reduction potential was calculated in Ref. 345. The following model was proposed: the

Table 42.
Redox potentials ($E_{1/2}$, mV) of macrobicyclic cobalt complexes (relative to NHE).

Ligand	Calculated from Eq. (90)	Experimental	Reference
$(NH_3)_6$		100	[338]
en_3		−259	[338]
diNOsar	60	60(40)	[4,338]
diAMHsar	20	40(−10; 50; 32)	[4,338,341,342]
AM(AMH)sar	−150	−150	[341]
AMMEsar	−350	−330(−360)	[4,340]
diAMsar	−320	−320(−350; −245)	[4,341,342]
AMHMEsar	−200	−190	[341]
sar	−400	−400(−420)	[5,97,340]
diCLsar	−140	−130	[4]
diOHsar	−200	−200	[4]
sep	−300	−300(−420; −320; −270)	[4,340,342,343]
MEazasar	−340	−340	[338,341]
(sartacn)	(−130)		
NOsartacn	+100	60	[142]
AMsartacn	−90	−80	[142]
AMHsartacn	80	70	[142]
azasartacn	−80	−60	[142]
ten		48	[123]
capten[a]	−130	−81	[123]
azacapten[a]	−80	−14	[123,339,340]
NOcapten[a]	100	100 (−70)	[123,125,339]
AMHcapten[a]	70	60	[123,339]
AMcapten[a]		−51	[123]
AMcapten–H		−120	[123]
CLcapten		25	[123]
HOcapten		−16	[123]
(ClME)abcapten		−100	[123]
(HOME)abcapten		−144	[123]
EFoxocapten–H		−200	[123]
CAAoxocapten–H		−333	[123]
CAoxocapten–H		−202	[123]
diMEsar-S_6		245(3+/2+)	[146,147]
		−686(2+/1+)	
diME1,3pnsar-S_6		400(3+/2+)	[147]
		−500(2+/1+)	
MENOsar-N_4S_2		253	[226]
AMHMEsar-N_4S_2		253	[226]
MECLsar-N_4S_2		194	[226]
MEsar-N_4S_2		75	[226]
MEazasar-N_4S_2		147	[226]
EFMEoxosar–H		−550	[133]
EFMEoxosar		−420	[133]

Table 42. (continued)

Ligand	Calculated from Eq. (90)	Experimental	Reference
diAMH1,2pnsar			
fac-(Δ+Λ)-*lel*		8	[5]
mer-(Δ+Λ)-*lel*		17	[5]
fac-(Δ+Λ)-*ob*		−32	[5]
mer-(Δ+Λ)-*ob*		−31	[5]
diMe₃AMsar		50	[338]
diMe₃AMHsar	40	50	[338]
diBzAMHsar		50	[338]
diNH2OHsar	80	60	[338]
(NH2OH)AMHsar	40	60	[338]
(NH2OH)NOsar	70	50	[338]
AMHOsar	40	50	[338]
CLNOsar	−40	−50	[338]
HONOsar	−70	−70	[338]
AMNOsar	−130	−120	[338]
NHOHNOsar	−100	−120	[338]
NOazasar	−120	−120	[338]
MENOsar	−160	−190	[338]
AMHCLsar	−060	−30	[338]
HOCLsar	−170	−160	[338]
AMCLsar	−230	−230	[338]
CLsar	−270	−260(−290)	[338,340]
CLMEsar	−260	−260	[338]
MEN-MePYsar		−310	[135]
MEN-BnPYsar		−320	[135]
MEN-MeQNsar		−290	[135]
MEN-BnQNsar		−300	[135]
MEsar	−290	−300	[106,338]
NHOHAMsar	−290	−280	[338]
diNHOHsar	−260	−260	[338]
NHOHMEsar	−320	−330	[338]
diMe₂AMsar	−300	−290	[338]
Me₂AMMEsar	−340	−340	[338]
diAAsar	−240	−240	[338]
AAMEsar	−300	−340	[338]
MEsar	−290	−400	[338]
AMH(ClME)absar	−290	−280	[338]
NO(ClME)absar	−270	−280	[338]
CL(ClME)absar	−370	−360	[338]
HO(ClME)absar	−400	−420	[338]
AM(ClME)absar	−460	−440	[338]
ME(ClME)absar	−490	−510	[338]
(absar)	−630		[338]
MEOHabsar		−550	[106]

[a] $Co^{2+/1+}$ reduction wave is close to the solvent reduction wave and is quasi-reversible

Table 43.
Redox potentials (mV) of macrobicyclic cobalt complexes in acetonitrile.

Ligand	$E_{1/2}$ experimental	$E_{1/2}$ calculated from Eq. (90)	Reference
Ag(AgCl)LiCl (sat)			
diAMsar	140	210	[338]
diNOsar	256	250	[338]
CLNOsar	159	150	[338]
NOazasar	057	70	[338]
MENOsar	−4	20	[338]
MEAMsar	−7	10	[338]
diCLsar	60	60	[338]
HOCLsar	−4	20	[338]
CLsar	−100	−70	[338]
diHOsar	−6	−10	[338]
sep	−222	−100	[338]
MEazasar	−189	−140	[338]
sar	−208	−210	[338]
NOcapten	170		[125]
MENOsar–N_3Se_3	−130		[125]
Ag(AgCl)LiCl (0.1 mol·l⁻¹)			
azacapten	90	90	[339]
AMHcapten	300	250	[339]
NOcapten	210	270	[339]
(capten)		(40)	
NOsartacn	220	230	[142]
AMHsartacn	240	210	[142]
azasartacn	70	50	[142]
(sartacn)		(0)	
$Dm_3(BF)_2$	−28		[41]
$Dm_3(BC_6H_5)_2$	−212		[41]
$Dm_3(Bn\text{-}C_4H_9)_2$	−374		[41]
$Nx_3(BF)_2$	−13		[41]
$Nx_3(BC_6H_5)_2$	−200		[41]
$Nx_3(Bn\text{-}C_4H_9)$,	−282		[41]
$Bd_3(BC_6H_5)_2$	−99		[41]

variation in the E value, in passing from a regular chelate complex
(for instance, $[Co(en)_3]^{3+}$ cation) to a macrobicyclic complex (such as
$[Co(sep)]^{3+}$ cation), is equal to the difference in their energies in the
oxidation 3+ state (E_{III}) minus the same difference in the oxidation 2+
state (E_{II}):

$$\Delta E = \Delta E_{III} - \Delta E_{II} \qquad (88)$$

The difference ΔE_a (a = II, III) is expressed as

$$E_a = (n/2)f_a(x_a - x_{am})$$ (89)

where n is the number of donor atoms, f_a is the force constant, and x_a and x_{am} are interatomic distances for chelate and macrobicyclic complexes, respectively. The calculation described in Ref. 345 made it possible to evaluate ΔE = 30 mV for a [Co(sep)]/[Co(en)$_3$] couple, while the experimental magnitudes are 70–150 mV depending on the conditions.

A quantitative evaluation of the steric effect contribution to the redox potentials of the hexamine cobalt complexes was undertaken using a molecular mechanics calculations [237, 344]. The overall strain energy was expressed as the sum of the bond length deformations, valent and torsion angles, and the energy of nonvalent effects. The model proposed was useful to predict Co–N bond lengths in 20 cobalt(II) and cobalt(III) complexes including the sepulchrate and simplest sarcophaginate. Deviations of the calculated values from the observed ones did not exceed 0.01 Å.

The sign of the potential variation in passing from [Co(sar)]$^{3+}$ cation to [Co(sep)]$^{3+}$ cation was predicted correctly. Nevertheless, the absolute value of this variation (4.4 kJ·mol^{-1} or 45 mV) is half as large as the experimental difference (Table 42). Meanwhile, in the passing from the nonmacrocyclic chelate [Co(en)$_3$]$^{3+}$ cation to the macrobicyclic [Co(sep)]$^{3+}$ cation, this model predicts the difference in the potentials as high as –200 mV instead of the observed 150 mV value.

For amine cobalt complexes, the E values correlate with the calculated differences in strain energy for cobalt(III)/cobalt(II) complex pair. The structures of all the cobalt(III) complexes are more strained than those of the corresponding cobalt(II) complexes. The correlation does not hold when the number of protons in the coordinated amino groups is changed (for example, [Co(NH$_3$)$_6$]$^{3+}$, [Co(en)$_3$]$^{3+}$, [Co(sep)]$^{3+}$, and [Co(sar)]$^{3+}$ cations). For a series of N$_6$-sarcophaginates with different apical substituents, no calculation of differences in strain energy changes has been done [344].

The simple but rather useful molecular mechanics calculations were applied to both electron transfer kinetics and reduction potentials for a wide range of hexamine cobalt(III/II) complexes with primary, secondary, tertiary, and macrobicyclic amine ligands [237]. The redox potentials of the Co$^{3+/2+}$ couples varied from
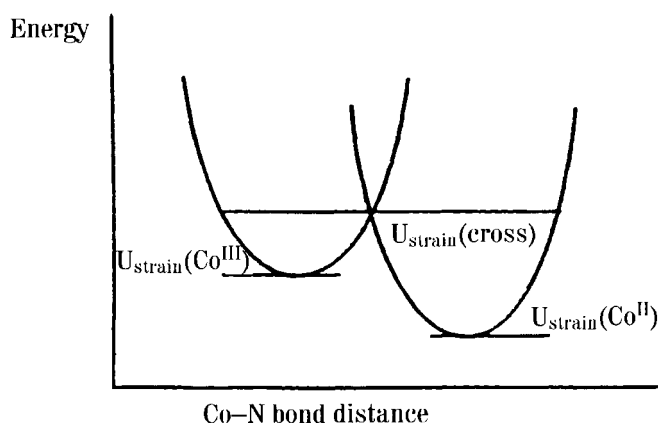
Fig. 46. Plot of strain energy *versus* Co–N distance [237].

–600 mV to +800 mV *vs* SHE, the Co(III)–N distances from 1.94 to 2.05 Å, and the ligand field $^1A_1 \rightarrow ^1T_1$ transitions for cobalt(III) ion from 16 700 to 22 200 cm^{-1}. The basic principles behind this simplistic approach toward modelling of redox properties are assembled in Fig.46; the important features are differences in the minima of the potential energy curves $\Delta G° \sim \Delta U_{strain}$ (cobalt(III)/cobalt(II)).

Plots of the experimentally determined redox potentials *versus* differences in strain energies for two cobalt(III) and cobalt(II) complexes with the same ligand and the correlation between these potentials and the calculated ones are shown in Figs. 47 and 48, respectively.

The linear regression (Fig. 47) has a slope of 61 kJ·mol^{-1}V^{-1} and a correlation coefficient of $r^2 = 0.78$. The deviation of the slope from the theoretical value of 96 kJ·mol^{-1}V^{-1} is caused by influence of different factors (entropy contributions, electronic effects and the force field parametrization etc.). The calculated value of the slope is *ca* 65% of the theoretically expected one. This indicates that strain relaxation is a major component, and from the linear variation it follows that the neglected factors vary roughly linearly with strain energy effects. The mean error of calculated reduction potentials is ±100 mV (Fig. 48).

The dependence of redox potentials on the substituent in the apical position was reported in Ref. 346. The detailed analysis of the experimental data, given in Tables 41 and 42, indicated the approximate additivity of the contributions of various substituents to the redox potential of the corresponding complexes. The magnitude of E
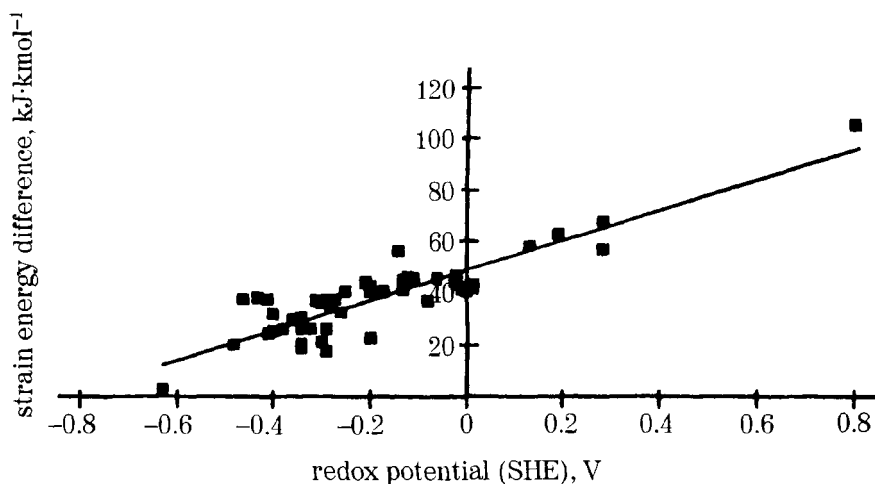
Fig. 47. Plot of the strain energy differences *versus* the observed redox potential for hexamine $Co^{3+/2+}$ couples [237].
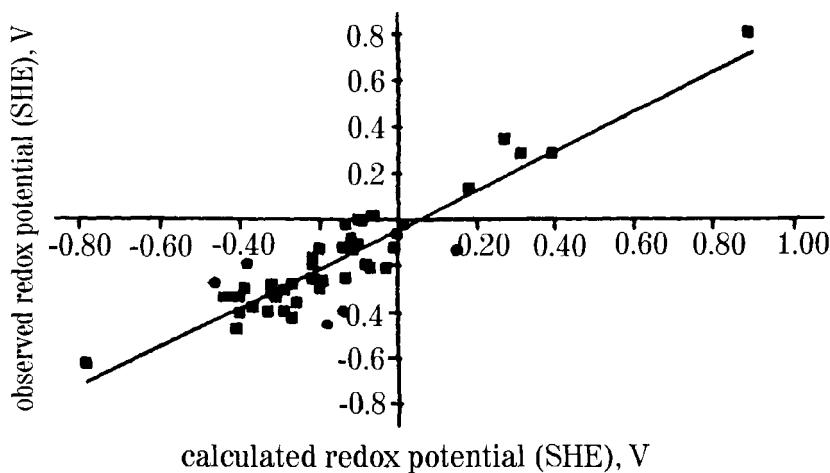
Fig. 48. Correlation between observed and calculated redox potentials for hexamine $Co^{3+/2+}$ couples [237].

for a number of complexes of the same type can be obtained by the equation

$$E = E_H + \sum_i E_i \tag{90}$$

where E_H corresponds to an unsubstituted macrobicyclic $[Co(sar)]^{3+}$ cation and E_i stands for the contributions from the substituents. The amounts of these substituents, listed in Table 44, were obtained by

Table 44.
Parameters of the substituents used in the calculation of redox potentials (mV) from Eq. (90) [346].

Substituent	E_i	σ_i	Substituent	E_i	σ_i
aza	50	(0.20)	HO	100	0.25
AM	40	0.10	CL	130	0.47
Me2AM	50	0.10	ME	10	−0.05
NHOH	70	(0.20)	AMH	210	0.60
NO	230	0.63	AA	90	0.28

minimization of the discrepancies between the theoretical and experimental values and best describe the experimental data represented in Table 42 [346].

The E values calculated from Eq. (90) for 46 clathrochelate complexes differ from the observed values by no more than 20 mV, and only for $[Co(AMMEsar)]^{3+}$, $[Co(MENOsar)]^{3+}$, and $[Co(HOClsar)]^{3+}$ cations does the discrepancy approach 30 mV. For the acetonitrile solutions, the estimated E values are consistent within 20 mV for 11 of the 13 calculations (Table 43).

The E_i parameters correlate with the Taft's inductive σ_i constants of the substituents (Table 44) [347]. As a consequence, one can observe a correlation between the redox potential E values and the sum of the inductive constants for all the substituents (Figs. 44-51).

This correlation was established for complexes of the *sar, absar, sartacn,* and *capten* ligands, not only for aqueous solutions (Fig. 49), but also for acetonitrile and acetone solutions (Fig. 50). Aza-capped
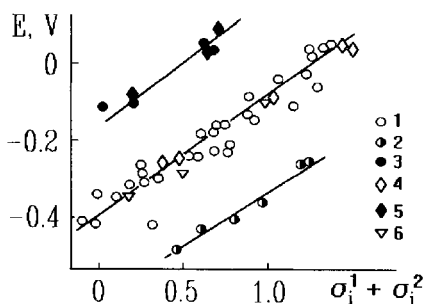
Fig. 49. Plots of the E values *versus* the sum of inductive σ_i constants in aqueous solutions. Ligands: (1) sar, (2) absar, (3) sartacn, (4) NHOHsar, (5) capten, (6) azasar.
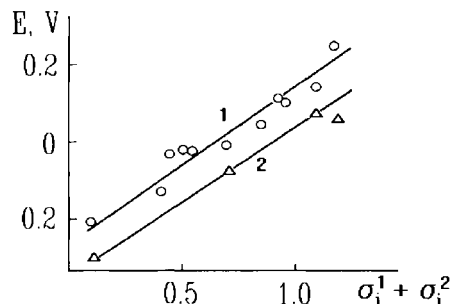
Fig. 50. Plots of the E values for cobalt sarcophaginates *versus* the sum of the inductive σ_i constants in AN (1) and acetone (2) solutions.
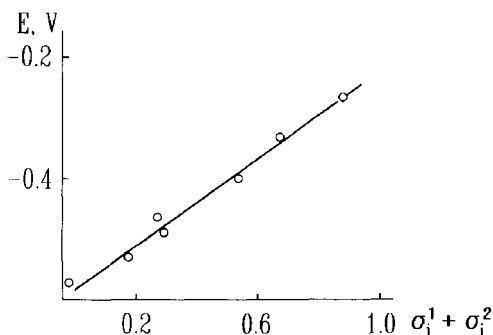
Fig. 51. A plot of the E values *versus* the sum of the inductive σ_i constants for cobalt complexes of oxo- and sarcophaginate ligands in aqueous solutions.

complexes were also included in this correlation, providing the same method of evaluation of the capping group inductive constant as that used for pyridine. The equation $\sigma_i = (3\sigma_{meta} - \sigma_{para})/2$ was used to approximate the inductive constant (0.2–0.3) for *aza* caps [348]. The estimated inductive constant of the hydroxylamine group was calculated taking into account the additivity of inductive constants: the overall effect of this group is assumed to be the sum of the effects of the amino group and the hydroxyl groups. In this case, the fact that the removal of the substituent at a one-atom distance decreases its effect by approximately a factor of 2–2.5 was taken into consideration [349]. Therefore $\sigma_{NHOH} = \sigma_{NH_2} + \sigma_{OH}/2.5 = 0.20$, and the hydroxylamine derivatives were also included into the correlation using this σ_i value (Fig. 49).

A similar calculation of the difference in the redox potentials was undertaken for complexes with *sar* and *oxosar–H* ligands, which contain a negatively charged oxygen atom incorporated into one methylene unit of the capping group instead of two hydrogen atoms. With allowance for the inductive constant (for the $-O^-$ group $\sigma_i = 0.5$ [348]) and the effect of a double increase because a cobalt-substituent distance shortens by one atom, the difference in E values *ca* 340 mV was calculated for cobalt complexes with *sar* and *oxosar–H* ligands. The observed difference is smaller, which was attributed to the resonance of the structures

$$\text{\Large$>$}\!\!-\!O^- \longleftrightarrow \text{\Large$>$}\!\!=\!O \tag{91}$$

in the *oxosar–H* framework.

Taft's inductive constants for substituents are rather obvious forms of the correlation constants for macrobicyclic systems, since they are determined for structurally similar organic compounds, namely, bicyclic esters of the type

$$X-\boxed{}-COOC_2H_5 \tag{92}$$

where X is the substituent. It should be noted that the correlation between the redox potentials of the transition metal complexes and the Hammet's σ_{para} constants of substituents was reported early [350, 351]. Such a correlation does not allow one to distinguish between the inductive and the resonance effects of a substituent [351].

The correlation obtained permits one to affirm that variations in the redox potentials in the series of clathrochelates are stipulated by the effect of the substituents. In the case of the (–)I-substituent, the electron density on the cobalt atom decreases and, as a consequence, the reduced form (i.e., cobalt(II) complex) stabilizes and the redox potential of the $Co^{3+/2+}$ couple increases. A small positive effect ($0 \div 10$ mV) of the methyl substituent (this substituent is generally regarded as the (+)I-one) is consistent with examples available [349] in which this group acts as an electron-accepting group.

Nevertheless, the inductive effect of a substituent is independent of the solvent used. Therefore, the slope of the linear correlations for water, acetone, and acetonitrile is the same (Figs. 49 and 50). The E values increase in the organic solvents (acetone and AN). This fact may be attributed to a greater stabilization of the oxidation +2 state of the clathrochelates in these solvents.

The E values depend on the electron density on the encapsulated metal ion and on donor atoms, and as a result, correlate a sum of the inductive constants of apical substituents. The slope of three linear correlation regressions for N_6-sarcophaginates (including a sepulchrate) and for *sartacn* and *capten* (higher potentials) and *absar* (lower potentials) ligand complexes is the same; hence, in each group the E values are governed by an inductive effect.

The difference in redox potentials between these three groups of clathrochelates is attributed to additional parameters associated with the cavity size and strain energy for cobalt(III) and cobalt(II) clathrochelates [237, 344, 345]. When the size of the cavity exceeds that of the central ion, the Co(III)–N distances increase and the stability of the cobalt(III) clathrochelate decreases. In the case of the

small cavity size with ions in the lower oxidation state, the macrobicyclic framework gets strained. As a result, large cavities stabilize the lower oxidation state (potentials increase) and small cavities stabilize the higher oxidation state (potentials decrease).

Due to a larger cavity size, the redox potentials of the compounds with *capten* ligand are higher than those of N_6-sarcophaginates. The X-ray data for [Co^{III}(azacapten)]$^{3+}$ and [Co^{II}(azacapten)]$^{2+}$ cations (see Section 3.1) reveal two factors that govern the E value. These are strain enhancement and lowering of the stability of the cobalt(III) clathrochelate and increases in the stability of the cobalt(II) clathrochelate. The latter is stipulated by the formation of the low-spin cobalt(II) complex.

The redox potentials increase with increase in the cavity size from *capten* ligand complexes ($E = -100$ mV) to [Co(diMEsar-S_6)]$^{3+}$ ($E = 245$ mV), [Co(diME1,3pnsar-S_6)]$^{3+}$ ($E = 400$ mV), and [Co(Me$_8$tricosanesar)]$^{3+}$ cations ($E_{red} = 300$ mV, $E_{ox} = 800$ mV).

Thioetheric macrobicyclic cobalt complexes were also reduced *via* a second stage to form a cobalt (I) complex. The stabilization of the cobalt(I) oxidation state was attributed to the increased ligand cavity owing to enlargement of a carbon-donor atom distance along with partial transfer of the electron density from the cobalt ion onto the sulphur atoms [339].

Complexes of the *sartacn* ligand lie in the linear correlation regression obtained for *capten* clathrochelates. In [Co(NOsartacn)]$^{3+}$ cation, the Co–N distances are smaller than those in the [Co(diNOsar)]$^{3+}$ cation, and the increase in the redox potentials for *sartacn* ligand complexes is due to distortion of their coordination polyhedra and the flexibility of the clathrochelate framework, which facilitates its conformational changes. The flexibility is an additional parameter affecting the E magnitude: the redox potential increases if the structural rearrangement requires less energy.

The magnitudes of the E values for contracted *absar* ligand complexes are smaller than those of the corresponding regular sarcophaginates. Some difficulties encountered in structural rearrangement are attributed to the contracted ligand cavity and the enhancement of the strain in the cobalt(III) clathrochelate structure.

The correlation obtained enables one to make certain conclusions about the conformation of the macrobicyclic complexes in solution. Two types of conformers (*lel*$_3$ and *ob*$_3$) with different E values (+100 and −330 mV) were isolated for 1,2-propanediamine [Co(diAMHl,

2pnsar)]$^{5+}$ sarcophaginate [5]. According to the linear correlation regression, for cobalt(III) sarcophaginate with two protonated apical amino groups and with three methyl substituents in the ribbed chelate fragments, the redox potential is from 0.0 to 30 mV, which is like the E value for lel_3-conformer and markedly differs from that calculated for the ob_3 conformer. Thus, this complex possesses the lel_3-conformation in solution.

In Ref. 352, the effect of substituents on $E_{1/2}$ variations was defined in terms

$$\mathrm{Log}\, K = \sigma p \tag{93}$$

where σ is Taft's, Charton's, or Grob's inductive constant, $p = 1$ for the standard reaction

$$[\mathrm{Co}^{\mathrm{III}}(\mathrm{xy\text{-}sar})]^{3+} + [\mathrm{Co}^{\mathrm{II}}(\mathrm{sar})]^{2+} \rightleftharpoons [\mathrm{Co}^{\mathrm{II}}(\mathrm{xy\text{-}sar})]^{2+} + [\mathrm{Co}^{\mathrm{III}}(\mathrm{sar})]^{3+} \tag{94}$$
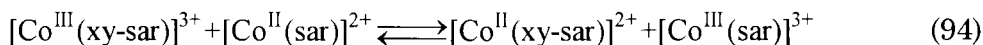
Substituting Eq. (93) into thermodynamic relationships and equating these expressions yield

$$\sigma_{\mathrm{E}} = nF \Delta E_{1/2}/2.3RT \tag{95}$$

where $\Delta E_{1/2}$ is the difference in the $E_{1/2}$ values of the substituted and the parent clathrochelates. At 20°C, Eq. (95) reduces to the form

$$\sigma_{\mathrm{E}} = 17.2 \Delta E_{1/2} \tag{96}$$

which was applied for calculations of substituent effects. A composite substituent effect was performed by the equation

$$\sum \sigma_{\mathrm{E}} = \sigma_{\mathrm{E}}(X) + \sigma_{\mathrm{E}}(Y) + \sigma_{\mathrm{E}}(cap_1) + \sigma_{\mathrm{E}}(cap_2) + 3\sigma_{\mathrm{E}}(en) \tag{97}$$

where X and Y are the apical substituents, en is the ethylenediamine chelate unit, and cap_1 and cap_2 are two caps of the cage ligand. This composite parameter was used to calculate $E_{1/2}$ for every cage complex relative to $[\mathrm{Co(NH_3)_6}]^{3+}$ cation ($E_{1/2} = -260$ mV, $\Sigma\sigma_{\mathrm{E}} = 0$, aqueous solution) and $[\mathrm{Co(sar)}]^{3+}$ one ($E_{1/2} = -640$ mV, $\Sigma\sigma_{\mathrm{E}} = -6.52$, aqueous solution). Similar calculations were performed for selected complexes in the aprotic solvents (AN and acetone). Shifts in $E_{1/2}$ for substituents ($\Delta E_{1/2}$) relative to the $\mathrm{Co}^{3+/2+}$ couple and the corresponding parameters σ_{E} are presented in Table 45. Data determined for different solvents (Table 45) indicate that the substituent effects are dependent on the nature of the solvent, being largest for apical amino and nitro groups. In addition to the apical group parameters σ_{E}, it proved possible to assign analogous

Table 45.
Constants ($\Delta E_{1/2}$, mV) for the inductive substituent effect [352].

Substituent	$\Delta E_{1/2}^{aq}$	$\sigma_{1/2}^{aq}$	$\Delta E_{1/2}^{AN}$	$\sigma_{1/2}^{AN}$	σ_i(Grob)	σ_i(Charton)	σ_i(Taft)
N(CH₃)₃⁺	225	3.87			4.15	0.73	0.92
NH(CH₃)₂⁺	227	3.89				0.70	
NH₂Bz	225	3.87					
NH₂OH⁺	230	3.91					
NH₃⁺	229	3.94	174	2.99		0.60	0.60
NO₂	220	3.78	232	3.99	3.54	0.76	0.65
CN	145	2.49			3.04	0.58	0.56
Cl	134	2.30	134	2.30	2.51	0.47	0.46
COOH	108	1.85				0.39	
COOC₂H₅	093	1.59			1.70	0.34	0.30
COCl			125	2.15			
COOAc			111	1.91			
OH	99	1.69	75	1.29	1.76	0.25	0.25
NHAc	83	1.43			1.66	0.28	0.26
NPhth	70	1.20					
NHOH	66	0.14					
N(CH₃)₂	53	0.91			1.12		0.12
NHBz	61	1.05				0.27	
NH₂	50	0.86			1.08		0.10
N=CHPh	55	0.95					
NHTs	20	0.34				0.32	
COO⁻	30	0.51			0.72	−0.17	−0.35
H	0	0.0	0	0.0	0.0	0.0	0.0
CH₃	−11	−0.18	−28	−0.48	0.11	−0.05	−0.04

parameters to fragments of the clathrochelate framework, such as chelate cycles and capping groups. The apparent E group parameters from Ref. 352 are listed in Table 46.

The transportability of these parameters determined from a limited number of compounds is illustrated by the excellent linear relationship between the calculated $\Sigma \sigma_E$ for any clathrochelate and the experimental $E_{1/2}$ values for this compound (Fig. 52). Data for *oxosar, azasar*, and *absar* ligand complexes, where $\Sigma \sigma_E$ parameters for N₆-sarcophaginates were used, are included in this correlation (Table 46).

There is a correlation between $E_{1/2}$ (Table 45) and three (Taft's, Charton's and Grob's) inductive substituent constants. The best correlation was observed with Grob's parameters for the quinuclidium salts employed as probes in aqueous solutions (Fig. 53).

Table 46.
Apparent group substituent effects [352].

Fragment	$\Delta E_{1/2}$, mV	$\sigma_E{}^{aq}$	Fragment	$\Delta E_{1/2}$, mV	$\sigma_E{}^{aq}$
(structure: N–CH₂CH₂–N)	[a] −36	−0.62	(structure: HO–C(=N)– with N, N)	[b,c] −59	−1.01
(structure: H–C with N, N, N)	[b] −136	−2.33	(structure: N with N, N, N ring)	[b] −64	−1.10
(structure: O⁻–C(=O)⁻ with H, N, N, N)	[b] −312	−5.38	$Cl-CH_2$– (structure with N, N, N)	[b] −233	−4.01

[a] Shift relative to that of $[Co(NH_3)_6]^{3+}$ cation.   [b] Shift relative to that of $[Co(en)_3]^{3+}$ cation.   [c] in 6 mol·l⁻¹ CF_3SO_3H.

The mechanisms for the transmission of substituent effects through a saturated framework to an encapsulated ion are discussed in Ref. 352. Inductive (or polar) substituent effects in clathrochelates were considered to be a combination of induction *via* σ bond and through-space field effects. For transition metal complexes, σ induction should be reflected in both the ligand field parameters of
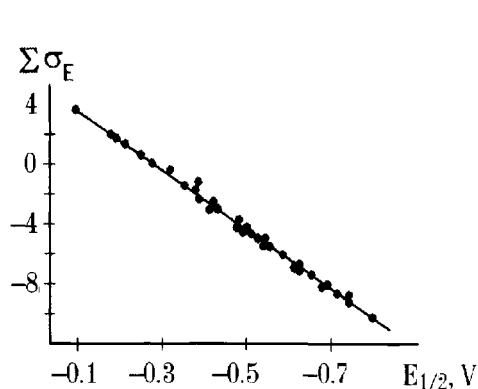
Fig. 52. Relationship of the calculated $\Sigma \sigma_E$ and experimental $E_{1/2}$ values (*vs* SCE) for the cobalt sarcophaginates [352].
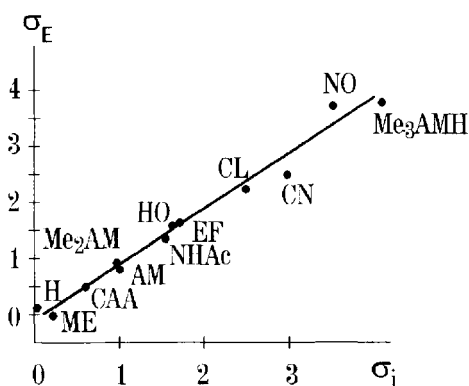
Fig. 53. Correlation of σ_E for apical substituents of the macrobicyclic cobalt (III) complexes with Grob's σ_i values [352].

both oxidation states and the electrochemical potential of the $Co^{3+/2+}$ couple, since it implies a change in electron density on the coordinated amino groups. Conversely, these effects should be mainly influence on the electrochemical potentials with minor contributions to ligand field parameters.

The redox potentials are determined by the differences in energy between two cobalt(III) and cobalt(II) states as a function of the apical substituents. Therefore, the electrochemical characteristics of the substituents should also correlate with other physical properties of the individual oxidation states provided these physical properties are affected by the substituents *via* the same mechanism [352].

UV-vis and ^{1}H, ^{13}C, and ^{59}Co NMR spectra of the cobalt(III) sarcophaginates were discussed in Section 3.1. With the exception of the apical N-methylated cobalt(III) complexes, the maxima of the *d–d* absorption bands in their UV-vis spectra were remarkable invariant (21 186 ± 130 and 29 240 ± 200 cm^{-1}), and no correlations with redox $Co^{3+/2+}$ potentials were observed. Maxima for [Co(diMe$_3$AMHsar)]$^{5+}$ and [Co(diMe$_2$AMHsar)]$^{5+}$ cations are markedly different and approximate those observed for clathrochelate with an *ob$_3$*-configuration [352]. The ^{1}H NMR chemical shifts of the coordinated amino group protons of regular cobalt(III) sarcophaginates show a good linear correlation with $E_{1/2}$ values for these complexes (Fig. 54), except N-methylated ones. A general linear relationship between δ_{59Co} for cobalt(III) clathrochelates and redox potentials for their $Co^{3+/2+}$ couples was also observed. The ^{13}C NMR
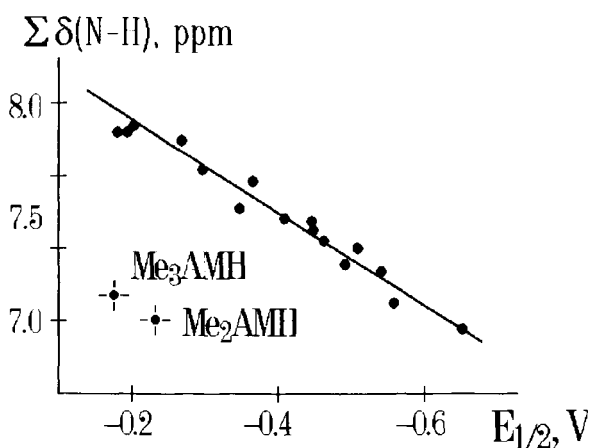
Fig. 54. Relationship of δ(N–H) in ^{1}H NMR spectra for cobalt(III) sarcophaginates and $E_{1/2}$ for their Co$^{3+/2+}$ couple [352].

chemical shifts of the apical carbon atoms correlate with shifts of adjacent methylene carbons of substituted sarcophaginates and of the bicyclic organic equivalents. The lack of correlation between the ligand field parameters and σ_E can be an indirect evidence that the dominant contributions to inductive effects are through-space field contributions [352]. The reason for the marked variation in properties of the apical N-methylated clathrochelates can be a conformational change from a lel_3-conformer to an ob_3-conformer induced by the substituents. This conclusion is supported by X-ray data for $[Co(diMe_3AMHsar)](NO_3)_5 \cdot 3H_2O$ complex and spectral (^{13}C NMR, CD, and UV-vis) studies of the $[Co(diMe_3AMHsar)]^{5+}$ and $[Co(diMe_2AMHsar)]^{5+}$ cations in solution.

The dependence of $E_{1/2}$ values for the cobalt(III) sarcophaginates with apical neutral and protonated amino substituents on their structures is discussed in Ref. 116. The redox potentials for these complexes are listed in Table 47.

There are two dependences in changing $E_{1/2}$ values for protonated cage complexes: (a) a positive shift about 200–300 mV per substituent in $[CoMe_xAMHsar]$ complexes relative to the $[Co(sar)]^{3+/2+}$ couple and (b) a positive shift about 160 mV per substituent on protonation or permethylation of the neutral amine. This is not surprising due to a difference in the charge and inductive effect of the positively charged substituent. Both effects make the

Table 47.
Redox potentials (mV) of the cobalt(III) sarcophaginates with apical amino substituents [116].

Couple	Medium		
	[a]pH 1.0	0.1 mol·l⁻¹ NaClO₄	[b]pH 7.5
$[Co(sar)]^{3+/2+}$	−400		
fac-ob_3-$[Co(diAM1,2pnsar)]^{3+/2+}$	−320		−640
fac-lel_3-$[Co(diAM1,2pnsar)]^{3+/2+}$	20		−320
$[Co(diAMsar)]^{3+/2+}$	20		−350
	[c]59		[d]−299
lel_3-$[Co(diAMchar)]^{3+/2+}$	0		−350
ob_3-$[Co((Me_2AMH)(MeAMH)sar)]^{5+/4+}$	[c]54		
$[Co(diMe_2AMsar)]^{3+/2+}$	[c]55		[d]−293
ob_3-$[Co(diME_3AMHsar)]^{5+/4+}$		51	
$[Co(AMMEsar)]^{3+/2+}$	[c]−186		[d]−347
$[Co(Me_2AMMEsar)]^{3+/2+}$	[c]−189		[d]−341

[a]All primary amino groups are protonated [b]No primary amino groups are protonated [c]in 0.05 mol·l⁻¹ HClO₄/NaClO₁ [d]in 0.1 mol·l⁻¹ NaClO₄

cobalt (III) complexes more susceptible to reduction. The decrease in the cavity size of the lel_3 conformer to that of an ob_3 conformer for [Co(diAM1,2pnsar)]$^{3+}$ and [Co(diAMH1,2pnsar)]$^{5+}$ cations leads to the lowering of the redox potential (Table 47).

The apparently surprising results are that the redox potential of the ob_3-[Co(Me$_3$AMHsar)]$^{5+}$ cation is much more positive than that of the ob_3-[Co(diAM1,2pnsar)]$^{3+}$ cation when superficially they are expected from cavity reason to be in the opposite order. This result may be attributed to a transition from lel_3 to ob_3 conformation in the oxidation process, governed by Me$_3$AMH-substituent [116, 352]. A very small increase in the E values was observed in passing from lel_3-[Co(diAMchar)]$^{3+}$ cation to lel_3-[Co(diAM1,2pnsar)]$^{3+}$ and lel_3-[Co(diAMsar)]$^{3+}$ cations either in protonated or nonprotonated forms.

The redox potentials of oxo-, amide-, and amidine-functionalized cobalt(III) sarcophaginates with deprotonated coordinated amino groups are shifted to negative potentials relative to regular cobalt(III) sarcophaginates (Table 48) [123, 133, 134]. The electronic effects of these substituents at a sarcophagine framework stabilize the cobalt(III) oxidation state. Cobalt(III) complexes with these ligands were less easy to reduce to their cobalt(II) forms, but the cobalt(IV) state was still not accessible under these more favorable conditions [123, 133, 134].

The electrochemical data for cobalt(III) sarcophaginates with apical aromatic substituents are listed in Table 49 [137]. The nature of the aromatic substituents for the most part did not greatly affect the Co$^{3+/2+}$ reduction potentials. The anthraquinone imine complex, however, showed a two-electron wave due to reduction of the anthraquinone substituent at ca 230 mV and a one-electron wave of

Table 48.
Reduction potentials (mV, vs SCE) of the amide- and amidine-functionalized cobalt(III) sarcophaginates [134].

Compound	$E_{1/2}$		
	pH = 1.68	pH = 6	pH = 12.04
[Co(CNMEoxosar–H)]$^{2+}$	–710 (ir)		–760 (r)
[Co(MECAamino-2-sar-2-ene)]$^{3+}$	–680		
[Co(MEamino-2-sar-2-ene)]$^{3+}$	–720 (ir)		–740 (r)
[Co(MECAAsar)]$^{2+}$		–600	
[Co(MECAsar)]$^{3+}$		–550	

Table 49.

Cyclic voltammetric data (mV, *vs* SHE) for some cobalt(III) sarcophaginates with apical aromatic substituents [137].

Cation	$E_{1/2}$	ΔE	Cation	$E_{1/2}$	ΔE
[Co(PhCOMEsar)]$^{3+}$	−380	118	[Co(2-PhreMEsar-2-ene)]$^{3+}$	−450	84
[Co(NpCOMEsar)]$^{3+}$	−390	101	[Co(2-AqMEsar-2-ene)]$^{3+}$	−500	74
[Co(AntCOMEsar)]$^{3+}$	−370	63		−230	68
[Co(2-NpMEsar-2-ene)]$^{3+}$	−450	71	[Co(2-NOPhMEsar-2-ene)]$^{3+}$	−490	68

Table 50.

Cyclic voltammetric data (mV) for the trinuclear cobalt N_6S_6-complexes in AN (0.1 mol·l^{-1} ((*n*-$C_4H_9)_4$N)BF$_4$) [129].

Cation	E_{pc}	E_{pa}	$E_{1/2}$	ΔE
meso-[Co(Co(aet)$_3)_2$]$^{3+}$	−460 −940	−400	−430	60
rac-[Co(Co(aet)$_3)_2$]$^{3+}$	−500 −950	−450	−475	50
meso-[Co(Co(SCH$_2$CH$_2$N=CH$_2)_3)_2$]$^{3+}$	−390 −840	−300	−340	90
rac-[Co(Co(SCH$_2$CH$_2$N=CH$_2)_3)_2$]$^{3+}$	−430 −840	−340	−385	90
meso-[Co(Coaza(SCH$_2$CH$_2$N)$_3)_2$]$^{3+}$	−460 −990	−360	−410	100
rac-[Co(Coaza(SCH$_2$CH$_2$N)$_3)_2$]$^{3+}$	−480 −1200	−340	−410	100
meso-[Co(CoNO(SCH$_2$CH$_2$N)$_3)_2$]$^{3+}$	−460 −950	−330	−390	130
rac-[Co(CoNO(SCH$_2$CH$_2$N)$_3)_2$]$^{3+}$	−470 −1010	−340	−405	120

$Co^{3+/2+}$ couple at −300 mV. Reduction of the protonated ligand takes place at a more positive potential $E = 120$ mV.

The reduction potential of the anthraquinone moiety is more positive than that of any of the $Co^{3+/2+}$ couples in the sarcophaginates with apical aromatic substituents. Hence the opportunity now exists to place an electron donor (for example, anthracene in its excited state linked to the cage by a longer spacer group) and an electron acceptor (anthraquinone) at opposite ends of a cobalt(III) cage. After photolysis, charge separation could be achieved in a cascade, mediated by the encapsulated metal ion [137].

Cyclic voltammograms for clathrochelate and semiclathrochelate trinuclear cobalt N_6S_6-complexes demonstrated one quasi-reversible

couple with $E_{1/2}$ from -340 to 475 mV and an irreversible reduction with E_{pc} from -840 to $-1\,200$ mV (Table 50). The first redox process was attributed to the redox $Co^{3+/2+}$ couple of the capping cobalt ion:

$$[Co^{III}\, Co^{III}\, Co^{III}]^{3+} + e^- \leftrightarrows [Co^{III}\, Co^{II}\, Co^{III}]^{2+} \tag{98}$$

The second reduction wave was attributed to the reaction

$$[Co^{III}\, Co^{II}\, Co^{III}]^{2+} + 2e^- \rightarrow [Co^{II}\, Co^{II}\, Co^{II}]^0 \rightarrow decomposition\,products \tag{99}$$
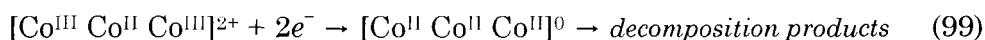
The $E_{1/2}$ values for the clathrochelate complexes are more positive (by 70 mV) than those for the semiclathrochelate precursor, indicative of a stabilization of the cobalt(II) oxidation state relative to the cobalt(III) state on capping [129].

Some data on the redox reactions of the substituents at the macrobicyclic framework are represented in Table 51. A comparison of the data from Tables 42 and 51 indicates that the encapsulated cobalt(III) ion and the substituents reduce at substantially different potential values. The nitro group reduction depends slightly on the

Table 51.

Redox potentials (mV, recalculated to NHE) of cobalt(II) sarcophaginates covered by intraligand processes [338].

Complex	Reaction	Electron number	$E_{1/2}$
[Co(HANOsar)]$^{2+}$	NO$_2$ → NHOH	4	-180
[Co(AMNOsar)]$^{2+}$	NO$_2$ → NHOH	4	-180
[Co(diNOsar)]$^{2+}$	NO$_2$ → NHOH	4	-450
[Co(CLNOsar)]$^{2+}$	NO$_2$ → NHOH	4	-470
	Cl → H	2	-1050
[Co(HONOsar)]$^{2+}$	NO$_2$ → NHOH	4	-400
[Co(NOazasar)]$^{2+}$	NO$_2$ → NHOH	4	-470
[Co(MENOsar)]$^{2+}$	NO$_2$ → NHOH	4	-490 (pH 6)
	NO$_2$ → NO$_2$ $^\bullet$	1	-460 (pH 6.7)
			-400 (pH 7.3)
[Co(AMCLsar)]$^{2+}$	Cl → H	2	-990
[Co(diCLsar)]$^{2+}$	Cl → H	4	-980
[Co(HOCLsar)]$^{2+}$	Cl → H	2	-1000
[Co(CLsar)]$^{2+}$	Cl → H	2	-800
[Co(ClMEsar)]$^{2+}$	Cl → H	2	-990
[Co((ClME)AMHabsar)]$^{3+}$	Cl → H	2	-1080
[Co((ClME)HOabsar)]$^{2+}$	Cl → H	2	-1250
[Co((ClME)CLabsar)]$^{2+}$	Cl → H	2	-1100
[Co((ClME)NOabsar)]$^{2+}$	NO$_2$ → NHOH	4	-450
[Co(CAANOoxosar–H)]	NO$_2$ → NHOH	4	-440

macrobicyclic framework nature except its appreciable variation for [Co(HANOsar)]$^{3+}$ and [Co(AMNOsar)]$^{3+}$ cations. The reduction of Cl-substituted complexes to H-substituted ones within the experimental error occurs at the same potential value [338].

5.2.4 Reactions of electron self-exchange in macrobicyclic cobalt complexes

Electron self-exchange reactions in macrobicyclic cobalt complexes have intensively been investigated. The rate constant of such reactions obtained for a variety of complexes, listed in Table 52, differ by several orders of magnitude (from 0.011 and 0.02 for the [Co(diMe$_3$AMHsar)]$^{5+}$ and [Co(diAMHsar)]$^{5+}$ cations to 2.8×10^4 for the hexathioether macrobicyclic [Co(diMEsar-S$_6$)]$^{3+}$ cation). The available data allow one to determine certain rules for the variation in the rate of electron self-exchange in macrobicyclic cobalt complexes.

As mentioned above, the electron self-exchange constants increase sharply in passing from nonmacrocyclic [Co(NH$_3$)$_6$]$^{3+}$ and [Co(en)$_3$]$^{3+}$ cations to macrobicyclic cobalt(III) N$_6$-sarcophaginates with a more rigid ligand framework. It should be noted that for the same reason, the rate of electron self-exchange in cobalt tris-phenanthrolinates and tris-bipyridinates is slightly higher (k_{11} = 42 and 17.5 respectively) than that in cobalt N$_6$-sarcophaginates.

As seen from Table 52, the lowest k_{11} values are observed for the [Co(diMe$_3$AMHsar)]$^{5+/4+}$ and [Co(diAMHsar)]$^{5+/4+}$ couples. A very small increase in the rate of exchange is observed in passing from ethylene to 1,2-propane and cyclohexane bridging moieties in chelate cycles. The increase by a factor of 3.5 was observed for the [Co(*ob$_3$*-1,2pnsar)]$^{3+/2+}$ couple compared with the *lel$_3$* conformer. The reaction rate increases for the diaminosarcophaginate [Co(diAMsar)]$^{3+/2+}$ couple compared with its protonated analogs due to a decrease in the charge of the species, with changing caps from *sar* ligand complexes, to *sep* complexes and with passing from regular *sar* to contracted *absar* and alicyclic *char* complexes. These variations are interpreted in terms of the concept that the electron self-exchange rate increases with ligand rigidity: the conformational flexibility of the macrobicyclic ligand is decreased more significantly by the cyclohexane ring than by the bulky methyl substituents.

Table 52.
Electron self- exchange rate constants for macrobicyclic cobalt complexes.

Ligand	k_{11} mol^{-1}l·s^{-1}	Log k_{11} experimental	Log k_{11} from Eq. (100)	Reference
sep	5.1 (5.0;11.5)	0.71	0.72	[4]
sar	2.1	0.32	0.32	[4]
diAMsar	0.50	−0.30	−0.28	[4]
AMHAMsar	0.1	−1	−1	[341]
diAMHsar	0.02 (0.024)	−1.7	−1.68	[4,341]
diMe$_3$AMHsar	0.011	−1.96		[116]
diCLsar	3.0	0.48	0.50	[4]
CLMEsar	2.4	0.38	0.36	[4]
CL(ClME)absar	7.3	0.86		[4]
diazachar	23	1.36	1.02	[4]
diAMchar	1.0	0.0	0.0	[4]
diAMHchar	0.04	−1.4	−1.4	[4]
AMsartacn	0.04	−1.40	−1.7	[4]
diNOsar	0.25	−0.6		[353]
MEazasar	2.9	0.47	0.47	[4,341]
AMHMEsar	0.1	−1	−0.73	[341]
diAMH1,2pnsar				
fac-(Δ+Λ)-*lel*	0.031	−1.5	−1.68	[5]
mer-(Δ+Λ)-*lel*	0.033	−1.48		[5]
fac-(Δ+Λ)-*ob*	0.96	−0.018		[5]
mer-(Δ+Λ)-*ob*	1.00	0		[5]
MEN-MePYsar	1.44	0.16		[135]
MEPYsar	2.4	0.38		[135]
Dm$_3$(BF)$_2$	86	1.93		[41]
Dm$_3$(BC$_6$H$_5$)$_2$	118	2.07		[41]
Dm$_3$(Bn-C$_4$H$_9$)$_2$	546	2.47		[41]
Nx$_3$(BF)$_2$	200	2.30		[41]
Nx$_3$(BC$_6$H$_5$)$_2$	272	2.43		[41]
Nx$_3$(Bn-C$_4$H$_9$)$_2$	132	2.12		[41]
Bd$_3$(BC$_6$H$_5$)$_2$	634	2.80		[41]
azacapten	4500	3.65		[354]
	7.3×10^4	3.86		[355]
	2.2×10^4	4.34		[146]
diMEsar-S$_6$	2.8×10^4	4.45		[146]
AMHMEsar-N$_4$S$_2$	7.8×10^2	2.86		[226]
MEazasar-N$_4$S$_2$	1.12×10^3	3.05		[226]
MEsar-N$_4$S$_2$	1.84×10^3	3.26		[226]
diMEabcapten	1.3×10^4	4.11		[356]

For most cobalt N$_6$-sarcophaginates, the Log k_{11} values decrease with increasing E magnitudes (Fig. 55). For the [Co(sep)]$^{3+/2+}$ couple increasing the magnitude of Log k_{11} may be attributed to a small
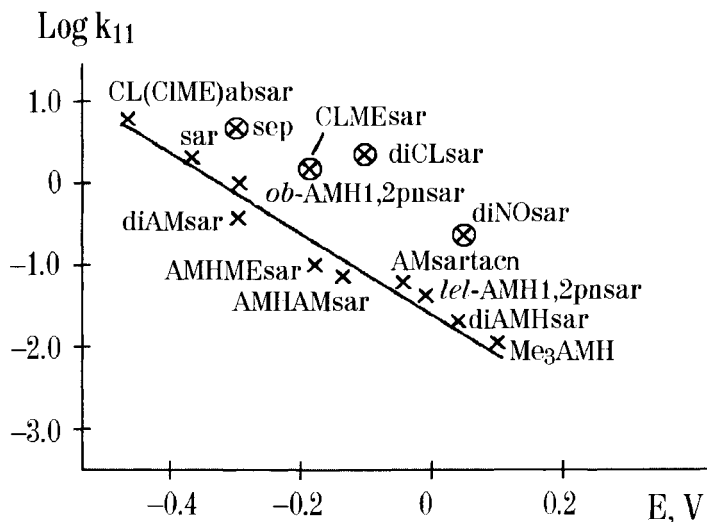
Fig. 55. Correlation between Log k_{11} and E for N_6-sarcophaginates.

change in the distortion angle φ from cobalt(III) sepulchrate to the cobalt(II) analogue ($\Delta\varphi = 14.3°$ instead of $24°$ for $[Co(sar)]^{3+/2+}$ couple). The complexes with apical chlorine, methyl and nitro substituents drop out of the correlation curve but complete structural data for these clathrochelates are absent.

The Log k_{11} value for a given substituted sarcophaginate cobalt(III)/cobalt(II) pair can also be described by an equation analogous in form to Eq. (90):

$$\text{Log}\,k_{11} = \text{Log}\,k_{11}(sar) + \sum_i a_i \qquad (100)$$

where a_i is the contribution of a given substituent. Optimal a_i values [-0.5(AM), -1.0(AMH), -0.05(ME), 0.09(CL), 0.20(aza), and 0.30 in passing from sar to $char$] were calculated from data listed in Table 51 and satisfactorily describe the experimental results.

A good agreement between the a_i values and Hammet's constants is observed in some cases (Fig. 56). For sepulchrate and sarcophaginate cobalt(III)/cobalt(II) pairs with apical amino, methyl, and chlorine substituents, the Log k_{11} values correlate with inductive constants of these substituents (Fig. 56).

The k_{11} constants for macrobicyclic dioximates are higher than those of N_6-sarcophaginates (Table 52); this is caused by an increase in the ligand field force and α-dioxime fragment rigidity compared
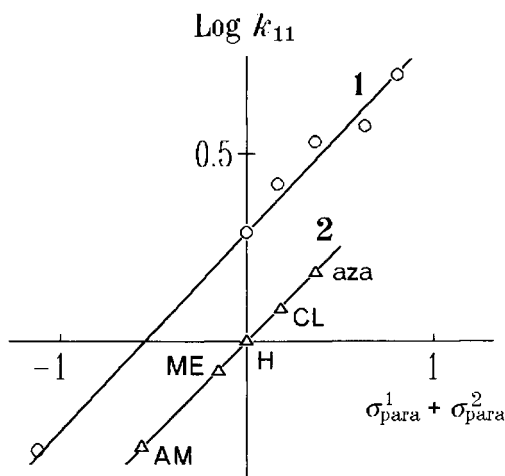
Fig. 56. Plot of Log k_{11} (1) and a_i values (2) *versus* the Hammet's σ_{para} constants of apical substituents.

with those of the ethylendiamine moiety, as well as by low-spin complex formation in both oxidation states [41, 357].

The highest k_{11} values for the [Co(azacapten)]$^{3+/2+}$ couple and cobalt(III)/cobalt(II) S_6-sarcophaginates are determined by a smaller Franck-Condon barrier, as a result of the low-spin state for both cobalt(II) and cobalt(III) complexes. The low-spin state of the encapsulated cobalt(II) ion corresponds to the reduced Co(II)–N and Co(II)–S distances in [Co(azacapten)]$^{2+}$ cation (see Table 20, Section 3.1); therefore, this cation undergoes a much smaller compression in the transition state than that of the [Co(sep)]$^{2+}$ cation.

The k_{11} values for most macrobicyclic tris-dioximes and $N_{6-n}S_n$-sarcophaginates $(n = 2, 3)$ increase with decreasing E values. The cobalt S_6-sarcophaginates and boron-capped tris-benzyldioximes drop out of linear correlation for both low-spin cobalt(II) and cobalt(III) complexes. The lack of this correlation in the first case may be attributed to the absence of structural changes in passing from the cobalt(III) complex to the cobalt(II) complex. In the second case, an increased k_{11} value may be attributed to the special rigidity of hexaphenyl-substituted cobalt clathrochelates.

The most commonly employed electron transfer theory was proposed by Marcus and Hush [358, 359]. In their approach, the electron transfer rate constant is expressed as

$$k = pZe^{-G^*/RT} \tag{101}$$

where Z is the collision rate, equal approximately to 10^{11} mol^{-1}s^{-1}, and p is the correction factor introduced in order to take account of a feasible nonadiabaticity of the reaction and is smaller than 1. The activation energy G^* is determined by the energy variations governed by electron transfer:

$$G^* = \frac{z_1 z_2 e^2}{D(a_1 + a_2)} + me^2 \frac{z_1 - z_2 - 1}{D(a_1 + a_2)} + mG^\circ - m(1 - m)(\lambda_0 + \lambda_i) \qquad (102)$$

The first and second terms in this equation describe the energy that is necessary for convergence of the charged species and for a change in their charges to a critical value, respectively. The last terms describe the energy variations required for the rearrangement of both the complex and the molecules of the solvent. Even approximate theoretical evaluation of these parameters presents difficulties. A somewhat simpler picture is observed in the case of isotopic exchange reactions (e.g., Co(III) ⇆ Co(II)) for which the transition state must be symmetric. Therefore, Eq. (102) is simplified to

$$G^* = \frac{z_1 z_2 e^2}{D(a_1 + a_2)} - \frac{(\lambda_0 + \lambda_i)}{2} \qquad (103)$$

Yet in this case, it is also difficult to perform exact calculations. So far, only rare calculations done according to the Marcus-Hush theory correlate with the experimental results.

It should be noted that most of the Co(III) ⇆ Co(II) exchange reactions are unsatisfactorily described by the adiabatic theory. This may be attributed partly to the fact that the spin state of the complex depends on its oxidation state: Co^{2+} ion possesses a high spin $t_{2g}^5 e_g^2$ configuration, whereas Co^{3+} ion has a low-spin t_{2g}^6 configuration. It is evident that one-electron transfer in this case must be accompanied by the transfer of one more electron from the e_g level to the t_{2g} level, or *vice versa,* i.e., either one of the initial complexes or the products must be in the excited state. As mentioned above, in some cases the correlation factor p (Eq. (101)) is employed for a quantitative evaluation of nonadiabaticity.

Since the charge of the complex during protonation becomes greater, it naturally leads to a lowering of the electron self-exchange rate. Actually, the term in Eq. (102) describing the

convergence energy for two charged species is expressed as $z_1z_2e^2/Da$, where z_1 and z_2 are the charges of these species, a is the distance between their centres, and D is the permittivity. With allowance for the ionic radius values for aqueous solutions in passing from a complex 2+/3+ pair to a 4+/3+ one, the electron transfer rate constant should decrease by approximately three orders of magnitude. The observed effect is substantially lower. When the charge increases by unity, the reaction rate drops approximately fivefold (Log k_{11} value decreases by 0.7). Therefore, the increase in charge is compensated by some other factors.

The Marcus-Hush theory was adapted to calculation of the volumes of activation for self-exchange $[Co(en)_3]^{3+/2+}$, $[Co(sep)]^{3+/2+}$, $[Co(diAMsar)]^{3+/2+}$, $[Co(diAMHsar)]^{5+/4+}$, $[CoD_3(BR)_2]^{3+/2+}$, and $[Co([9]aneS_3)_2]^{3+/2+}$ reactions [301, 333, 342, 355]. A plot of the calculated and observed mean volumes of activation for these reactions in aqueous solution is shown in Fig. 57. The Marcus-Hush theory is quantitatively successful in the description of aqueous systems for a variety of self-exchange reactions including the
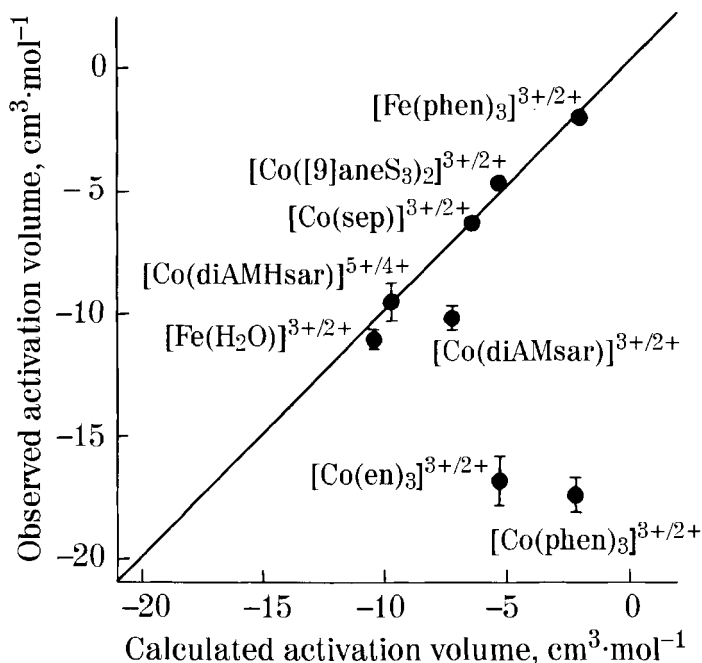
Fig. 57. Calculated and observed mean volumes of activation, 0.1÷200 MPa, for self-exchange reactions in aqueous solution [342].

macrocyclic ls/ls [Co([9]aneS$_3$)$_2$]$^{3+/2+}$ couple and ls/hs clathrochelate couples regardless of charge. For the [Co(diAMsar)]$^{3+/2+}$ couple, the ΔV_{ex} value is somewhat more negative than the calculated one but is acceptably close, but there is no correlation between the calculated and observed mean volumes of activation for the nonmacrocyclic cobalt chelates.

This is attributed to structural changes associated with a Co(II)(ls)/Co(II)(hs) spin equilibrium preceding electron transfer in these nonmacrocyclic chelates, which are suppressed in the clathrochelate complexes.

The effect of geometric isomerization of the sarcophaginate [Co(diAMH1,2pnsar)]$^{5+/4+}$ couple on the electron self-exchange rate constants was reported in Refs. 5 and 360 (Table 52). The rate constants for the lel_3-conformer of this cation are slightly higher than those for a regular ethylenediamine $diAMHsar$ ligand complex. At the same time, in passing to its ob_3-conformer, a 30-fold increases in the electron self-exchange rate was observed. This fact was attributed to the rearrangement energies of the ground and transition states of the complex [5, 360].

The formation of the outer-sphere complexes between macrobicyclic cobalt cations and the relevant counter-ions must also be taken into account. Actually, for single-charged anions, the stability constants of such complexes with di-, three-, four- and five-charged cations were found to be about 10, 30, 100, and 300, respectively [358]. The experimental rate constants are usually determined at $\mu = 0.1$–0.2 mol·l^{-1}, and under these conditions even three charged complexes exist in solution mainly as ion pairs. Thus, the true charge of a reactive species is lower at least by unity. Moreover, as the cation complex charge becomes greater, the concentration of ion pairs also grows, which compensates the effect of charge enhancement. In passing from a complex $+1/+2$ couple to a $+2/+3$ one, the Log k_{11} value should be lowered by approximately 1.8 (at the expense of the $z_1 z_2 e^2/Da$ term in the equation for free activation energy). With allowance for the formation of the ion pairs, the Log k_{11} values for complexes with protonated amino groups agree fairly well with those obtained from the correlation relationship (Fig. 56).

5.2.5 Electron-transfer cross-reactions of macrobicyclic cobalt complexes

The Marcus-Hush theory proved to be most advantage in describing of a cross-reactions:

$$Ox_1 + Red_2 \Leftrightarrow Ox_2 + Red_1$$

In this case, a fairly simple equation was obtained:

$$k_{12} = \sqrt{k_{11}k_{22}K_{12}f} \tag{104}$$

where k_{ii} is the rate constant of the corresponding isotopic exchange reaction; $K_{12} = e^{E_0/RT}$ is the equilibrium constant for the redox reaction, and $\mathrm{Log}\, f = (\mathrm{Log}\, K_{12})^2/4\, \mathrm{Log}\, (k_{11}k_{22}/z^2)$. In the framework of a more precise theory, the equation incorporates several additional terms, such as

$$k_{12} = W_{12}\sqrt{k_{11}k_{22}K_{12}f} \tag{105}$$

$$\ln f_{12} = (\ln K_{12} + (w_{12} - w_{21})/RT)^2/4(\ln(k_{11}k_{22}/z^2) + (w_{11} + w_{22})/RT) \tag{106}$$

$$W_{12} = \exp(w_{11} + w_{22} - w_{21} - w_{12})/2RT \tag{107}$$

$$w_{ij} = z_i z_j e^2/Da(1 + \beta a \mu^{1/2}) \tag{108}$$

where z_i and z_j are the charges of the interacting species, μ is the ionic strength, $\beta = 3.285 \times 10^9$ m^{-1}l$^{1/2}$mol$^{-1/2}$, and w_{ij} is a work term.

In the case of rapid electron transfer reactions, one should take account of diffusion control limiting the utmost feasible reaction rate:

$$k_{dif} = 7.4 \times 10^9 b/(e^b - 1) \tag{109}$$

$$k = k_0 \times 10^c \tag{110}$$

where $b = 14\, z_1 z_2/a$; $c = z_1 z_2\, \mu^{1/2}/(1 + \mu^{1/2})$; k_0 is the second-order rate constant at the ionic strength μ equal to zero. Correction for diffusion control has a final form [361]:

$$k_{cor} = k\, k_{dif}/(k + k_{dif}) \tag{111}$$

It is obvious that the allowance for diffusion control should be made for all rapid reactions.

An additional obstacle that may be encountered is the reaction nonadiabaticity. Therefore, to take into account nonadiabaticity effects for the exchange and the resulting redox reactions, the correction factor $p_{12}/(p_{11}p_{22})^{1/2}$ was introduced into Eq. (111). It should be noted that this factor may appear to approach unity not only when all terms p equal 1 but also at a certain combination ensuring the equality of the nume-

rator and dominator. Thus, the fact that the correction factor is equal to 1 cannot be accepted as evidence of the reaction's adiabaticity.

The measured rate constants for cross-reactions and those calculated from Eq. (104) are listed in Tables 53-55. A comparison of the calculated and observed constants indicates that Eq. (104) is solved with an accuracy of an order of magnitude. An attempt to solve this equation by introducing several adjusted z values was made in Ref. 364. Eqs. (105-108) are justified at appreciable differences in the charges of the reacting species. But in this case, the correction makes no marked contribution to the improvement in data coincidence [106]. Even for the structurally very similar complexes with close properties, i.e., various isomers of sarcophaginate $[Co(diAMHl,2pnsar)]^{5+}$ cation, the experimental rate constants differ from those calculated from Eq. (104) by a factor of 5–7. Sargeson attributed this difference to the

Table 53.

Cross-reaction electron-transfer rates for the macrobicyclic cobalt(III) complexes.

Reductant	Oxidant	Log k_{12} experimental	Log k_{12} calcd from Eq. (104)	Reference
	$[Co(sep)]^{3+}$			
$[Co(sar)]^{2+}$		1.30	1.5	[362]
Cr^{2+}		−3.06	−1	[362]
Eu^{2+}		−0.92	−0.7	[362]
U^{2+}		1.20		[362]
DQ		4.08	4.77	[353]
mv		4.85	5.55	[353]
MDQ		5.0	6.2	[353]
BDQ		4.04	6.35	[353]
	$[Co(diNOsar)]^{3+}$			
$[Co(sep)]^{2+}$		2.9	2.75	[353]
DQ		5.97	6.6	[353]
MDQ		6.76	7.5	[353]
	$[Co(diAMHsar)]^{5+}$			
$[Co(sep)]^{2+}$		2.16	2.17	[362]
Cr^{2+}		−2.09	0.6	[362]
Eu^{2+}		−0.88	0.7	[362]
V^{2+}		−0.40	0.7	[362]
	$[Co(MEazasar)]^{3+}$			
$[Co(sar)]^{2+}$		1.00	1.14	[362]
Cr^{2+}		−3.83	−1.5	[362]
Eu^{2+}		−1.82	−1.8	[362]
	$[Co(AMHMEsar)]^{4+}$			
Cr^{2+}		−3.31	1.1	[362]
Eu^{2+}		−1.52	−1	[362]

Table 54.
Cross-reaction electron-transfer rates for the cobalt(II) clathrochelates.

Oxidant	Reductant	Log k_{12} experim.	Log k_{12} calcd from Eq.(104)	Reference
	[Co(sep)]²⁺			
[Co(NH₃)₆]³⁺		−0.05	−0.25	[343]
[Co(en₃)]³⁺		−1.33	−0.97	[343]
I₂		4.8	−5.56	[98]
I₃⁻		4.6		[98]
[Fe(H₂O)₆]³⁺		5.2	−7.6	[364]
[Cr([15]aneN₄)]³⁺		−2.81		[365]
[V(pic)]³⁺		3.75	2.79	[365]
[2Fe - 2S]³⁺		2.45		[365]
[Co([19]aneN₃)₂]³⁺		−0.96	−0.88	[365]
[Co(DmH)₂(C₆H₅NH)₂]		2.88		[365]
cytochrome C(III)		5.49		[365]
[Co(terpy)₂]³⁺		5.17	6.48	[365]
[Co(cydta)]-		4.92		[365]
[Co(edta)]-		4.92	2.68	[365]
O₂		1.63		[142]
rac-[Co(bzo₃[12]hexaneN₃)₂]		2.71		[366,367]
mezo-[Co(bzo[12]hexaneN₃)₂]		2.0		[366]
[Co(phen)₃]³⁺		3.68		[366,367]
[Co(5-nitrophen)₃]³⁺		4.04		[363]
[Co(Me₄phen)₃]³⁺		3.38		[363]
[Ru(NH₃)₆]³⁺		4.55		[97]
[Co(bipy)₃]³⁺		4.0		[97]
[Ru(NH₃)₄(phen)]³⁺		5		[97]
[Co(NH₃)₅(cha)]³⁺		−0.85		[366]
[Co(NH₃)₅(aniline)]³⁺		−0.22		[366]
[Co(NH₃)₅CN]²⁺		−0.24		[366]
[Co(NH₃)₅Cl]²⁺		1.76		[366]
[Co(NH₃)₅Br]²⁺		3.2		[366]
[Co(NH₃)₅I]²⁺		4.1		[366]
[Co(NH₃)₅N₃]²⁺		0.87		[366]
[Co(NH₃)₅NO₂]²⁺		3.32		[366]
[Co(NH₃)₄(aniline)₂]³⁺		−0.22		[368]
[Co(NH₃)₄(NO₂aniline)₂]³⁺		0.32		[368]
cis-[Co(en)₂(cha)Cl]²⁺		−0.09		[366]
cis-[Co(en)₂(aniline)Cl]²⁺		0.52		[366]
cis-[Co(en)₂(benzylamine)Cl]²⁺		1.93		[366]
cis-[Co(en)₂CNCl]²⁺		0.08		[366]
cis-[Co(en)₂(NO₂aniline)Cl]²⁺		1.96		[368]
cis-[Co(phen)₂CN]²⁺		1.38		[366]

Table 54. (continued)

Oxidant	Reductant	Log k_{12} experim.	Log k_{12} calcd from Eq.(104)	Reference
[Co([14]aneN₄)(NH₃)₂]²⁺		−1.0		[366]
[Co(Me₄[14]tetraeneN₄)(NH₃)₂]		1.56		[366]
[Co([14]aneN₄)(H₂O)₂]		3.2(3.0)		[369]
[Co(Me₄[14]tetraeneN₄)(H₂O)₂]		4.23(4.8)		[366,369]
[Co(Me₂pyo[14]trieneN₄)(H₂O)₂]		4.7		[369]
[Co(Me₂[H]1,11-diene-13-oneN₄(H₂O)₂]		4.5		[369]
CBr₄		−1.4		[370,371]
C₂Br₄Cl₄		−1.05		[371]
CBr₂Cl₂		−1.85		[371]
CBrCl₃		−2.3		[371]
[Co(phen)₂(chn)]³⁺		2.55		[363]
[Co(diNOsar)]		2.9		[354]
[Co(diAMHsar)]⁵⁺		2.16	2.17	[362]
(−)-[Co(diAMHsar)]⁵⁺		2.15 [with(+)-Co(sep)]		[362]
		2.19 [with(−)-Co(sep)]		[362]
[Co(sar)]²⁺				
[Co(NH₃)₆]³⁺		0.36	0.5	[343]
[Co(en)₃]³⁺		0.04	0.1	[362]
[Co(sep)]³⁺		1.30	1.5	[362]
[Co(MEazasar)]³⁺		1.00	1.14	[362]
[Co(diAMHsar)]⁴⁺				
[Co(bipy)₃]³⁺		1.51	2.3	[362]

Table 55.

Cross-reaction electron-transfer rates (mol⁻¹·l·s⁻¹) for the [Co(diAMH1,2pnsar)]⁴⁺/⁵⁺ isomer couples ($\mu = 0.2$ mol·l⁻¹) [5].

System	k_{12} experim.	k_{12} calcd from Eq.(104)	System	k_{12} experim.	k_{12} calcd from Eq.(104)
mer-Λ-*lel*+*fac*-Δ-*ob*	54	90	*mer*-Λ-*lel*+*mer*-Δ-*ob*	17	75
mer-Δ-*lel*+*fac*-Δ-*ob*	45	90	*mer*-Λ-*lel*+*mer*-Δ-*ob*	14	75
fac-Δ-*lel*+*fac*-Δ-*ob*	40	77	*fac*-Λ-*lel*+*mer*-Δ-*ob*	13	64
fac-Λ-*lel*+*fac*-Δ-*ob*	32	77	*fac*-Δ-*lel*+*mer*-Δ-*ob*	10	64

stereochemistry of these complexes, namely, to the repulsion of the bulky methyl substituents in "inconvenient" ion pairs [5].

At the same time, several authors have given much attention to the deviations from Eq. (104). Endicott and Ramasami have studied in detail the nonadiabaticity of the electron-transfer cross-reactions with the participation of macrobicyclic cobalt complexes [363, 366, 367, 372].

It was shown that the rate of electron-transfer reactions substantially changes *via* the introduction of an additional electrolyte into solution [363, 367]. The variation of reaction rate constants depends on the type of anion added. Thus, this effect is not caused by ionic strength variations and is related to the formation of the outer-sphere complexes.

In fact, a comparison of the observed cross-reaction rate constants and those calculated from the Marcus-Hush's Eq. (104) indicates that in most cases the amount of nonadiabaticity cannot be neglected. The observed rate constant values are much smaller than the calculated ones even for structurally very similar complexes. Thus, the correction factor $p = p_{12}/(p_{11}p_{12})^{1/2}$ is substantially smaller than 1. This result has been interpreted in terms of metal-ligand charge transfer in the ion pairs formed in solution [363, 367]: the Log p correlates with $E(CT)$, where $E(CT)$ is the expected energy of a $[CoL]^{3+}...X \rightarrow [CoL]^{2+}...X$ transfer in the ion pair. The effect of various anions on the cross-reaction rates for cobalt(II) sepulchrate are shown in Table 56.

Table 56.
Effect of the anions on the cross-reaction electron-transfer rates for the macrobicyclic $[Co(sep)]^{2+}$ cation.

Oxidant	Anion	$k_e(X)$, mol·s^{-1}	k_x mol^{-1}	Reference
$[Co(phen)_3]^{3+}$	I$^-$	1.8×10^4	30	[363]
	NO$_2^-$	7.5×10^4	8	[363]
	ascorbat	2.23×10^5	35	[363]
	NCS$^-$	2.0×10^4	45	[363]
	CH$_3$COO$^-$	2.6×10^4	29	[363]
$[Co(NO_2phen)_3]^{3+}$	NO$_2^-$	1.2×10^5	7	[363]
	ascorbat	3.4×10^5	22	[363]
$[Co(MEphen)_3]^{3+}$	NO$_2^-$	1.35×10^4	10	[363]
	ascorbat	6.4×10^4	17	[363]
$[Co(Bzo_3[12]hexaeneN_3)_2]^{3+}$	I$^-$	2.5×10^3	2	[367]
	NO$_2^-$	2.3×10^4	2	[367]
	ascorbat	5.0×10^4	1.7	[367]

When the experimental results were evaluated [156], it was assumed that no ion pairs are formed in the presence of trifluoromethylsulfonate and perchlorate anions, and, therefore, an electron-transfer reaction results from the interaction of the cationic species. This conclusion contradicts an empirical equation for the outer-sphere complex stability constant and presumably needs more evidence.

An effect similar in nature may be exerted by coordinated ligands (for instance, $[Co(NH_3)_5X]$), Table 54. The correlation between p and the $(1/E(CT) + 1/E^*(CT))$ sum, where $E(CT)$ and $E^*(CT)$ are the lowest excited state energies for the initial complex and the resulting one, respectively, was reported in Ref. 366.

Nevertheless, no marked deviation from Eq. (104) was observed for many reactions (Table 57). As with k_{11}, the absence of spin forbiddenness allows one to employ the Marcus-Hush theory for a quantitative description.

Table 57.

Cross-reaction electron-transfer rates constants for the transition metal sarcophaginates [324].

Oxidant	Reductant	Log k_{12} experimental	Log k_{12} calcd from Eq.(104)
$[Ru(NH_3)_5Py]^{3+}$	$[Ru(sar)]^{2+}$	5.02	5.15
$[Ru(NH_3)_5nic]^{3+}$	$[Ru(sar)]^{2+}$	5.45	5.64
$[Ru(NH_3)_5isn]^{3+}$	$[Ru(sar)]^{2+}$	5.72	5.81
$[Ru(tacn)_2]^{3+}$	$[Ru(sar)]^{2+}$	5.85	5.53
$[Mn(sar)]^{3+}$	$[Ru(NH_3)_5Py]^{2+}$	4.57	4.85
$[Mn(sar)]^{3+}$	$[Ru(NH_3)_5isn]^{2+}$	4.15	4.20
$[Mn(sar)]^{3+}$	$[Ru(tacn)_2]^{2+}$	4.46	4.20
$[Ni(tacn)_2]^{3+}$	$[Mn(sar)]^{2+}$	5.08	5.41
$[Ni(tacn)_2]^{3+}$	$[Ni(sar)]^{2+}$	3.59	3.95
$[Ru(NH_3)_5Py]^{3+}$	$[Fe(sar)]^{2+}$	5.8	5.8
$[Ru(NH_3)_5isn]^{3+}$	$[Fe(sar)]^{2+}$	6.3	6.36
$[Fe(sar)]^{3+}$	$[Ru(NH_3)_6]^{2+}$	3.91	4.04
$[Fe(sar)]^{3+}$	$[Co(azacapten)]^{2+}$	4.66	4.73
$[Mn(sar)]^{3+}$	$[Ru(sar)]^{2+}$	5.23	4.95
$[Ni(sar)]^{3+}$	$[Mn(sar)]^{2+}$	5.0	4.82
$[Mn(sar)]^{3+}$	$[Fe(sar)]^{2+}$	≈ 6	5.43
$[Fe(H_2O)_6]^{3+}$	$[Ru(sar)]^{2+}$	4.86	4.83
$[Fe(H_2O)_6]^{3+}$	$[Mn(sar)]^{2+}$	1.08	1.3
$[Ni(sar)]^{3+}$	$[Fe(H_2O)_6]^{2+}$	1.63	1.45

5.3 PHOTOCHEMICAL PROPERTIES OF MACROBICYCLIC COMPLEXES

For realization of photochemical processes (Fig. 58) and their practical application, there is a need to use molecules that, when photoexcited, are able to luminesce (luminophores) and/or to transfer the energy of electrons (photosensitizers) without undergoing photodecomposition.

The main requirements needed for luminophores and photosensitizers were formulated in Ref. 373:
(a) absorption of light in a suitable spectral region;
(b) stability in the ground and excited states;
(c) highly efficient population of the excited states;
(d) suitable reduction (oxidation) potential;
(e) appropriate kinetic factors;
(f) reasonably long excited state lifetime.

From a spectral and photophysical point of view, clathrochelate complexes would be quite suitable to play these roles [340, 373-380].

5.3.1. Cobalt complexes

Most of the investigations in this field have focused on the use of cobalt sepulchrate and sarcophaginates as electron-transfer sensitizers in photocatalytic cyclic solar energy conversion processes [340, 375-378]. This is mainly due to their specific redox behaviour stipulated by peculiarities of the cobalt ion electronic structure and screening of this ion by an encapsulating ligand.
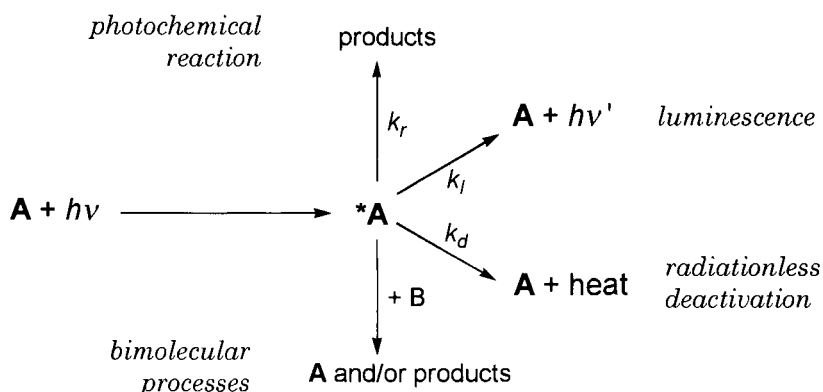
Fig. 58. Schematic representation of a photochemical process. *A represents an electronically excited state [373].

Since both $E_{1/2}$ values and electron-transfer rates are responsible for the photochemical and photocatalytical behaviour of cobalt clathrochelates, their variation by the introduction of substituents makes these compounds especially promising as photosensitizers.

Photolysis of the cobalt sepulchrate as well as their ion pairs with some anions has been studied in detail using mercury lamp irradiation at 39 370, 33 333, and 25 000 cm^{-1}. The decrease in the initial complex concentration and the appearance of the photolysis products have been used as parameters to evaluate the photolysis process. The $[Co(sep)]^{3+}$...H$_2$O, $[Co(sep)]^{3+}$...I$^-$, $[Co(sep)]^{3+}$...Br$^-$ [299, 300], and $[Co(sep)]^{3+}$...HC$_2$O$_4^-$ [306] systems have been examined in aqueous solutions. The resultant complexes show the ligand-metal CTB in the UV spectral region and the d-d transition bands in the visible one. Light irradiation at the CTB wavelength induces the reduction of the $[Co(sep)]^{3+}$ cation to the $[Co(sep)]^{2+}$ cation, which then either decomposes to give Co^{2+} aqua ion or oxidizes to the initial complex. The photoeffect observed in the first case has not been detected in the second one.

The $[Co(sep)]^{3+}$...H$_2$O system absorbs light at 40 000 cm^{-1}, but this excitation has not caused any spectral changes, and no photochemical reaction has been observed. The reactions occurring in this system may be represented by the following equations:

$$[Co^{III}(sep)]^{3+} \xrightarrow{\ hv\ } [Co^{II}(sep^+)]^{3+} \tag{112}$$

$$[Co^{II}(sep^+)]^{3+} \xrightarrow{\ fast\ } [Co^{III}(sep)]^{3+} \tag{113}$$

$$[Co^{II}(sep^+)]^{3+} \xrightarrow{\ slow\ } Co_{aq}^{2+} + decomposition\ products \tag{114}$$
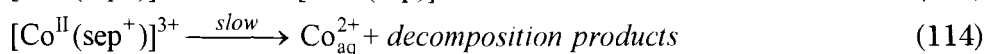
Since the cobalt(II) complex is inert, its decomposition (114) even in acidic medium ($k = 1.2 \times 10^{-2}$ mol^{-1}l·s^{-1}) is slow compared with the electron-transfer rate ($k = 5.0$ mol^{-1}l·s^{-1}). Therefore, process (113) dominates, and no photoeffect has been observed. The inertness of the $[Co(sep)]^{3+}$ cation in photochemical processes is caused by complete encapsulation of the cobalt ion. In the system with the nonmacrocyclic hexamine $[Co(NH_3)_6]^{3+}$ trication, photoreduction was found to occur in relatively high quantum yield ($\Phi = 0.16$). In this case, the photocomposition rate of $[Co^{II}(NH_3)_5(NH_3)^+]^{3+}$ cation formed on irradiation ($k > 10^6$ s^{-1}) is higher than that of electron transfer ($k = 10^{-5}$ mol^{-1}l·s^{-1}).

The addition of iodine anion (NaI) to an aqueous solution of $[Co(sep)]^{3+}$ cation led to spectral changes: the CTB shifted to the

Table 58.

Photochemistry of $[Co^{III}(sep)]^{3+}...I^-$ system in aqueous solution [299].

Test number	$[Co(sep)^{3+}] \times 10^3$, mol·l^{-1}	[I⁻]	pH	[a] Φ	Test number	$[Co(sep)^{3+}] \times 10^3$, mol·l^{-1}	[I⁻]	pH	[a] Φ
1	5.0	0.1	3.0	[b] 10^{-6}	10	2.0	0.1	5.5	1.1×10^{-3}
2	1.0	0.1	5.5	10^{-6}	11	5.0	0.1	4.5	5.4×10^{-3}
3	1.0	0.1	1.0	[c] 3.4×10^{-3}	12	5.0	0.1	4.0	5.6×10^{-3}
4	1.0	0.1	5.5	0.6×10^{-3}	13	5.0	0.1	3.8	7.2×10^{-3}
5	5.0	0.1	5.5	0.5×10^{-3}	14	5.0	0.1	3.0	8.8×10^{-3}
6	5.0	0.1	3.0	3.2×10^{-3}	15	5.0	0.1	1.5	1.5×10^{-2}
7	5.0	0.1	1.0	9.6×10^{-3}	16	5.0	0.1	1.0	[e] 5.1×10^{-2}
8	5.0	0.02	5.5	0.2×10^{-3}	17	2.0	0.02	1.0	1.8×10^{-2}
9	5.0	0.1	5.5	[d] 2.4×10^{-3}	18	2.0	0.1	1.0	4.3×10^{-2}

[a] The quantum yield of 1/2 I_3^- anion formation. Solutions 2 and 3 are deoxygenated, solutions 1 and 4÷7 are saturated with air and solutions 8÷18 are saturated with oxygen. [b] The quantum yield of $[Co(sep)]^{3+}$ cation disappearance and Co^{2+} aqua ion formation. [c] $\Phi_{Co_{aq}^{2+}} = \Phi_{1/2\,I_3^-}$ [d] TON > 40 [e] TON > 20

longwave region, and new bands at 27 777 and 20 833 cm^{-1} appeared owing to the formation of a $[Co(sep)]^{3+}...I^-$ ion pair. On light excitation of this ion pair, the electron is promoted from the outer-sphere coordinated anion onto encapsulated cobalt(III) ion. The resultant $[Co^{II}(sep)]^{2+}...I$ ion pair is kinetically inert in neutral solutions. Its conversion may take place in two directions: either a reverse electron transfer inside the solvate shell (116), or the production of the primary photoproducts (117):

$$[Co^{III}(sep)]^{3+}...I^- \xrightarrow{\;h\nu\;} [Co^{II}(sep)]^{2+}...I \qquad (115)$$

$$[Co^{II}(sep)]^{2+}...I \longrightarrow [Co^{III}(sep)]^{3+}...I^- \qquad (116)$$

$$[Co^{II}(sep)]^{2+}...I \longrightarrow [Co^{II}(sep)]^{2+} + I^\bullet \qquad (117)$$
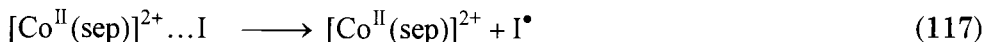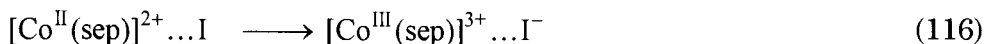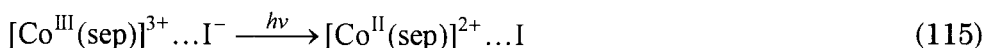
The reaction direction is determined by a higher rate of recombination of the $I^\bullet$ radical. The latter can react with I^- anion to produce the I_2^- species, which disproportionates to I^- and I_3^- anions ($k = 7.7 \times 10^9$ mol·l^{-1}·s^{-1}). Both I_2^- and I_3^- anions oxidize $[Co^{II}(sep)]^{2+}$ cation to $[Co^{III}(sep)]^{3+}$ cation. As a consequence, no photochemical reaction is detected (Table 58).

In acid medium, the quantum yield increases up to 3.4×10^{-3} (Table 58), indicating the occurrence of reaction

$$[Co^{II}(sep)]^{2+} \longrightarrow Co_{aq}^{2+} + decomposition\ products \qquad (118)$$
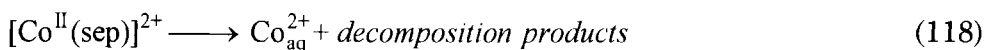
to give Co^{2+} aqua ion, which oxidizes to Co^{3+} ion by either I_2^- or I_3^- anions. The quantum yield of Co^{3+} ion formation coincides with that of 1/2 I_3^- anion formation. In the presence of oxygen, the reaction proceeds as follows:

$$[Co^{II}(sep)]^{2+} + 1/2\ O_2 \xrightarrow{\ H^+\ } [Co^{III}(sep)]^{3+} + 1/2\ H_2O_2 \tag{119}$$
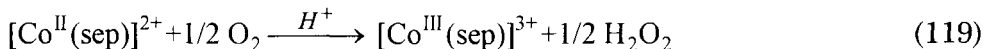
The hydrogen peroxide formed in this reaction also oxidizes $[Co^{II}(sep)]^{2+}$ cation, and $[Co^{III}(sep)]^{3+}$ cation regenerates, but I_3^- anion accumulates (Table 58).

The resulting photoreaction is the oxidation of I^- anion to I_3^- anion by oxygen, wherein $[Co^{III}(sep)]^{3+}$ cation acts as a photosensitizer. The quantum yield of I_3^- anion formation enhances with increasing oxygen concentration. The turnover number (TON) for $[Co(sep)]^{3+}$ cation is higher in neutral medium than in acid one, which may be attributed to partial acidic decomposition of $[Co^{II}(sep)]^{2+}$ cation by Reaction (118).

In acid medium the secondary reaction

$$H_2O_2 + 3I^- + 2H^+ \rightarrow I_3^- + 2H_2O \tag{120}$$

can also take place. It accounts for some facts:
(a) the formation of I_3^- after irradiation ceases,
(b) the growth in the quantum yield of the I_3^- species with increasing light excitation times,
(c) the dependence of the quantum yield of this species on the concentration of I^- anion. However, these effects may also be attributed to the increase in the concentration of the ion pair.

The oxidation of I^- anion by oxygen, in which $[Co(sep)]^{3+}$ cation serves as a photosensitizer, may be represented by the Scheme 119.

The photolysis data obtained for the $[Co^{III}(sep)]^{3+} ... Br^-$ ion pair on light excitation indicate that a photochemical reaction is not detected in deoxygenated aqueous solutions ($\Phi < 10^{-6}$). Unlike the $[Co(sep)]^{3+} ... I^-$ system, the photochemical reaction for the
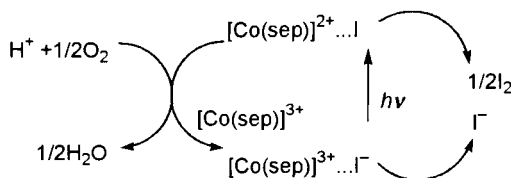
Scheme 119
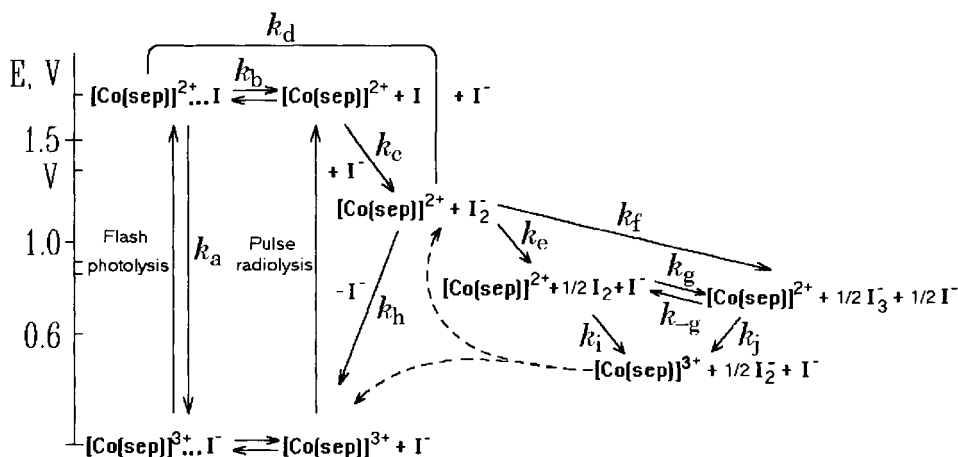
Fig. 59. The complete scheme of the reactions in the $[Co(sep)]^{3+}...I^-$ system follow flash photolysis or pulse radiolysis exitation [300].

$[Co(sep)]^{3+}...Br^-$ system does not take place either in oxygen-saturated or in aerated aqueous solutions.

More complete information on photochemical and concomitant processes occurring in the $[Co(sep)]^{3+}...I^-$ and $[Co(sep)]^{3+}...Br^-$ systems was obtained from flash photolysis and pulse radiolysis data [300].

These experiments confirm the formation of I_2^- anion in the $[Co(sep)]^{3+}...I^-$ system, its conversion to I_3^- ion within 50 μs, and simultaneous occurrence of the reactions

$$I_2^- + [Co(sep)]^{2+} \rightarrow 2I^- + [Co(sep)]^{3+} \qquad (121)$$

$$I_2 + [Co(sep)]^{2+} \rightarrow I_2^- + [Co(sep)]^{3+} \qquad (122)$$

$$I_3^- + [Co(sep)]^{2+} \rightarrow I_2^- + I^- + [Co(sep)]^{3+} \qquad (123)$$
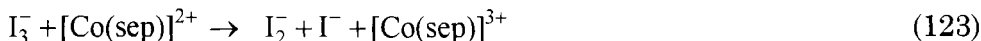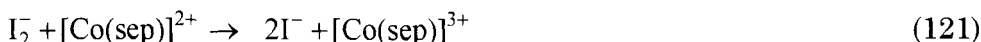
The complete scheme of reactions proceeding in the $[Co(sep)]^{3+}...I^-$ system is shown in Fig. 59.

For the $[Co(sep)]^{3+}...Br^-$ system, the flash photolysis experiment showed the formation of Br_2^- anion, and no Br_3^- species was observed.

The hydrated electrons and $OH^\bullet$ radicals produced in a 1:1 stoichiometric ratio under pulse radiolysis conditions in aqueous solutions reacted very rapidly with $[Co(sep)]^{3+}$ and X^- ions, respectively, to form the $[Co(sep)]^{2+}$ and $X^\bullet$ products in the equivalent concentrations

$$[Co(sep)]^{3+} + e_{aq}^{-} \rightarrow [Co(sep)]^{2+} \tag{124}$$

$$OH^{\bullet} + X^{-} \rightarrow OH^{-} + X^{\bullet} \tag{125}$$
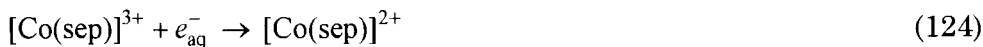
$X = Br^{-}$ or I^{-}

For the $[Co(sep)]^{3+}...I^{-}$ system, intermediate I_2^{-} anion decay with mixed-order kinetics was found and accounted for by the concurrent reactions:

$$2I_2^{-} \rightarrow I_2 + 2I^{-} \tag{126}$$

$$2I_2^{-} \rightarrow I_3^{-} + I^{-} \tag{127}$$

With the relatively long light pulse, Reaction 121 becomes predominant with kinetics close to first-order. The rate constant for Reaction (121) was found to be 5.0×10^9 $mol^{-1}l\cdot s^{-1}$ using the known rate constants for Reactions 126 and 127.

The similar rate constant $k = 1.4\times10^{10}$ $mol^{-1}l\cdot s^{-1}$ was calculated for the $[Co(sep)]^{3+}...Br^{-}$ system. More than 80% of the initial bromine disappears *via* $[Co(sep)]^{2+}$ cation oxidation, but partial formation of Br_3^{-} anion in this system cannot be excluded, although in much less quantity than that of the I_3^{-} anion in the $[Co(sep)]^{3+}...I^{-}$ system.

A photocatalytic cycle based on the $[Co(sep)]^{3+}...I^{-}$ system, in which substrates easily oxidized by iodine are oxidized by oxygen, is described in Ref. 374. By this process, the two $[Co(sep)]^{3+}$ and I^{-} components act not only as photosensitizers but also as relays. The O_2 oxidation is activated as follows:

$$\frac{1}{2}O_2 + substrate + 2H^{+} \xrightarrow[{[Co(sep)]^{3+}...I^{-}}]{h\nu} substrate\ (oxidized) + H_2O \tag{128}$$
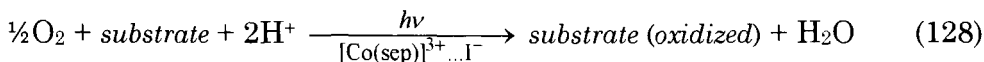
The cycle with SO_3^{2-} to SO_4^{2-} oxidation by O_2, photosensitized by the $[Co(sep)]^{3+}...I^{-}$ ion pairs, is represented in Scheme 120.

The $[Co(sep)]^{3+}$ cation in aqueous solution forms an ion pair with the oxalate anion that exhibits a CTB in the near-UV and visible regions. Light excitation ($\nu = 31\ 949$ cm^{-1}) causes the reduction of this cation to $[Co(sep)]^{2+}$ cation and the oxidation of the oxalate anion to
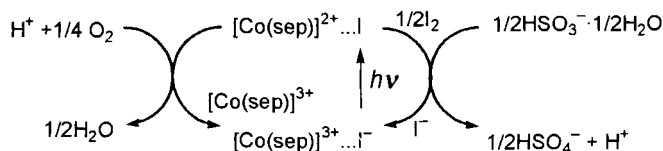
Scheme 120

Table 59.
Photochemistry of the $[Co(sep)]^{3+}...HC_2O_4^-$ system [306].

$[Co(sep)^{3+}] \times 10^2$, mol·l^{-1}	$[(NH_4)_2C_2O_4]$, mol·l^{-1}	pH	$[Pt] \times 10^5$, mol·l^{-1}	a $\Phi_{Co^{3+}}$	Φ_{CO_2}	Φ_{H_2}
5.0	0.1	0.5		$< 10^{-3}$		
5.0	0.1	3.0		0.13	0.13	
5.0	0.1	5.5		0.29	0.28	
5.0	0.01	3.0		0.03		
1.0	0.1	3.0		0.08		
5.0	0.1	3.0	5.0	$<10^{-3}$	0.14	0.07
5.0	0.1	5.5	5.0	$< 10^{-3}$	0.24	0.1
5.0 b	0.1	3.0		$< 10^{-3}$	0.17	

a $\Phi = 0.16$ for $[Co(en_3)]^{3+}$ cation; $\Phi = 0.13$ for $[Co(NH_3)_6]^{3+}$ cation.
b Oxygen-saturated solution.

carbon dioxide. The photoeffect (or its absence) and the quantum yield of the photochemical reaction depend on the pH of the solution, the concentration of oxalate anion, and the presence or absence of oxygen in solution (Table 59) [306].

Light irradiation of deoxygenated aqueous solution of $[Co(sep)]^{3+}$ cation and $(NH_4)_2C_2O_4$ at pH 0.5 caused neither spectral changes nor carbon dioxide evolution. At higher pH values, however, the concentration of sarcophaginate cation (and absorbance of the solution in the near-UV and visible region) decreases and carbon dioxide evolves from the solution. Bubbling oxygen or air into such reduced solutions causes a fast recovery of absorbance leading to a final spectrum that is exactly the same as that of the solution before irradiation in the visible region but is somewhat more intense in the UV region. This absorption increase was more noticeable at pH 5.5 than at pH 3.0.

It follows from these data that the ion pairing is necessary for a photoeffect to manifest itself in aqueous solutions. Since ion pairs are not formed at pH 0.5, no photoeffect is detected. At pH 3.0 and 5.5, ion pairs arise (bands at 36 364 and 20 833 cm^{-1}) and the photoeffect was observed.

In this case, the photochemical reaction may be represented by the equations

$$[Co^{III}(sep)]^{3+}...HC_2O_4^- \xrightarrow{hv} [Co^{II}(sep)]^{2+}...HC_2O_4 \tag{129}$$

$$[Co^{II}(sep)]^{2+}...HC_2O_4 \xrightarrow{hv} [Co^{II}(sep)]^{2+} + CO_2 + CO_2^{\bullet} + H^+ \tag{130}$$
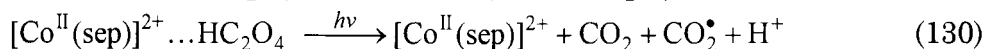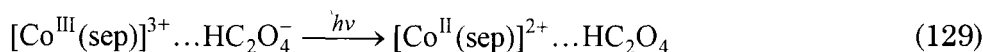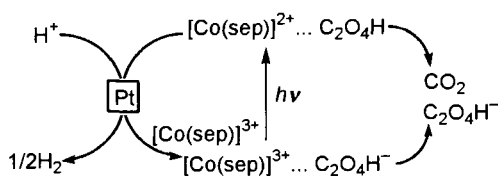
Scheme 121

Then the $CO_2^{\bullet}$ radical reduces another $[Co^{III}(sep)]^{3+}$ cation:

$$[Co^{III}(sep)]^{3+} + CO_2^{\bullet} \xrightarrow{h\nu} [Co^{II}(sep)]^{2+} + CO_2 \qquad (131)$$

with $k = 4.3 \times 10^8$ mol^{-1}·l·s^{-1}. The overall reaction

$$2[Co^{III}(sep)]^{3+} + HC_2O_4^- \xrightarrow{h\nu} 2[Co^{II}(sep)]^{2+} + 2CO_2 + H^+ \qquad (132)$$
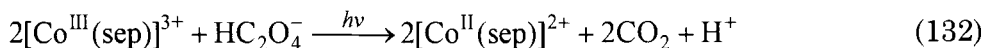
corresponds to data on the equal quantum yields of $[Co(sep)]^{2+}$ and CO_2 reaction products, Table 59. The $[Co^{II}(sep)]^{2+}$ cation is a strong reductant (E = –280 mV) and reduces the H^+ ions to hydrogen at both pH 3 and pH 5.5. When a platinum catalyst is present in the solution, such a reaction indeed occurs (Table 59) and a stoichiometric amount of H_2 evolves. Under such conditions, the overall reaction is

$$HC_2O_4^- + H^+ \xrightarrow[\text{[Co(sep)]}^{3+}...I^-]{h\nu} 2CO_2 + H_2 \qquad (133)$$
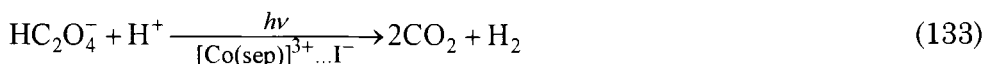
and $[Co(sep)]^{3+}$ cation plays the role of a photosensitizer (Scheme 121).

The turnover number of this cation is higher than 700 at pH 3 and the quantum yield for hydrogen production is *ca* 0.1 [306].

When the platinum catalyst is not present and the solution is oxygen-saturated, the $[Co(sep)]^{2+}$ complex produced on excitation is reoxidized to $[Co(sep)]^{3+}$ cation by oxygen. Such a reaction, thoroughly studied by Sargeson and coworkers, is known to proceed by the steps

$$[Co^{II}(sep)]^{2+} + O_2 \xrightarrow{H^+} [Co^{III}(sep)]^{3+} + HO_2/O_2^- \qquad (134)$$

$$HO_2 \rightleftharpoons O_2^- + H^+ \qquad (135)$$

$$HO_2 + [Co^{II}(sep)]^{2+} \xrightarrow{H^+} [Co^{III}(sep)]^{3+} + H_2O_2 \qquad (136)$$

$$O_2^- + [Co^{II}(sep)]^{2+} \xrightarrow{2H^+} [Co^{III}(sep)]^{3+} + H_2O_2 \qquad (137)$$

$$2HO_2/O_2^- \xrightarrow{H^+} H_2O_2 + O_2 \qquad (138)$$
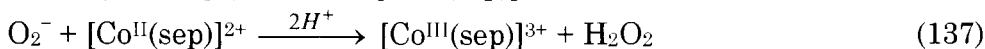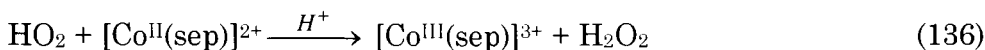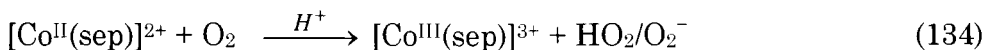
The electron transfer from oxygen to the sarcophaginate cation (Reaction (134)) is the rate-determining stage. The next fast step may be either the oxidation of $[Co(sep)]^{2+}$ cation with the superoxide radical (Reactions 136 and 137) or disproportionation (Reaction 138).

Since the stoichiometry and the final products in both cases are identical, they cannot be distinguished either by their kinetics or by analysis of the products.

The use of Co^{2+} ions as a radical trap and the flash photolysis data obtained for such a system [381] indicate that during the oxidation of $[Co(sep)]^{2+}$ cation the superoxide radical O_2^- anion is formed as an intermediate and its reduction even in acidic media (Reaction 137) is more favourable than disproportionation (Reaction 138).

By the mechanism proposed for the $[Co(sep)]^{2+}$ cation oxidation, the O_2^- anion reacts with one of the ligand coordinated amino groups, with the hydrogen atom abstraction followed by rapid protonation of the products:

$$[Co^{II}(sep)]^{2+} + O_2^- \longrightarrow [Co^{III}(sep-H)]^{2+} + HO_2^- \qquad (139)$$

$$HO_2^- + H^+ \longrightarrow H_2O_2 \qquad (140)$$

$$[Co^{III}(sep-H)]^{2+} + H^+ \longrightarrow [Co^{III}(sep)]^{3+} \qquad (141)$$
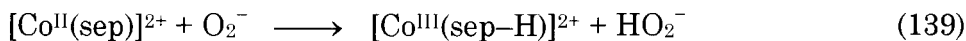
A similar hydrogen atom transfer mechanism for the oxidation of some transition-metal complexes by C-centred radicals was proposed in Ref. 382.

The reaction reversibility stipulated by the sepulchrate $[Co(sep)]^{2+}$ cation stability reduces the quantum yield (calculated from the decrease in the initial compound concentration) compared with nonmacrocyclic $[Co(NH_3)_6]^{3+}$ and $[Co(en)_3]^{3+}$ cations. The Φ values obtained from CO_2 production retain the same order.

The photochemistry of the water-insoluble $[Co(sep)](B(C_6H_5)_4)_3$ complex was studied in aprotic solvents (THF, AN, and DMF) [309]. When THF solution was irradiated with visible light, the cobalt(III) complex has been reduced by the tetraphenylborate anion to give a white $[Co(sep)](B(C_6H_5)_4)_2$ precipitate. From the residual solution biphenyl and phenol were isolated as the main products. This photoreaction proceeded much slower in DMF solution.

When the solution of colourless cobalt(II) complex that appears in AN was exposed to air, it gradually assumes a purple colour and on addition of THF precipitated a purple complex, identified as a diamagnetic cobalt (III) $[Co(sep-H)](B(C_6H_5)_4)_2$ complex with a deprotonated ligand. The quantum yield of $[Co(sep)](B(C_6H_5)_4)_3$ photolysis in aprotic solvents was not reported [309].

The photolysis of the clathrochelate cobalt(III) $[Co(sep)]^{3+}$ (I), $[Co(diNOsar)]^{3+}$ (II), $[Co(diNOsar-H)]^{2+}$ (III), $[Co(diAMsar)]^{3+}$ (IV),

ε, mol^{-1}·l·cm^{-1}
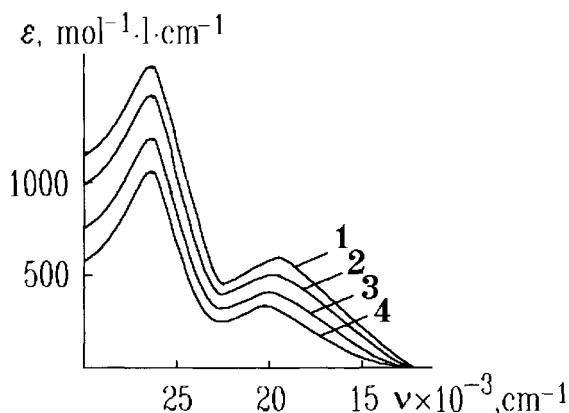
Fig. 60. Spectral changes in the photolysis of [Co(diNOsar–H)]$^{2+}$ cation after 10 (2), 20 (3), and 30 (4) min irradiation [383].

and [Co(diAMHsar)]$^{5+}$ (V) cations was reported in Ref. 383. In aqueous and aqueous-methanol solutions, these compounds demonstrated a CTB at ca 40 000 cm^{-1} and, in addition, the d-d transition band at ca 20 000 cm^{-1} was observed for complexes I, II, IV, and V. Protonation of apical amino groups occurs in acidic media (pK$_1$ = 3.3, pK$_2$ = 2.7) and does not affect the spectra. Deprotonation of the coordinated secondary amino group in [Co(diNOsar)]$^{3+}$ cation (pK = 8.7) causes no changes in the UV region, but the bands in the visible region are broadened and more intense. A new CTB due to charge transfer from the deprotonated nitrogen atom to the cobalt ion appears at ca 27 777 cm^{-1} (Fig. 60).

Photolysis of these solutions was performed at 39 370 cm^{-1}. The quantum yields of disappearance of the initial complexes were determined from the UV-vis absorbence decrease. The concentration of the resultant formaldehyde was also measured (Table 60).

In aqueous solutions, photolysis of cobalt(III) sarcophaginates causes practically no spectral changes, except for [Co(diNOsar–H)]$^{2+}$ cation. Similar data were obtained for [Co(sep)]$^{3+}$ cation [299].

Light irradiation of the deoxygenated aqueous-methanol solutions of complexes I and II causes an absorbence decrease due to the reduction of encapsulated cobalt(III) ion to cobalt(II) ion. In this reaction, formaldehyde accumulates, the pH values decrease (Table 60), and the quantum yield increases with the methanol concentration. The ratio of the quantum yields of disappearance of the initial complex and the formation of formaldehyde was approximately 2:1. The EPR spectrum

Table 60.
Photolysis of cobalt(III) sepulchrate and sarcophaginates in aqueous-methanol solutions [383].

Cation		Medium	pH	$\Phi_{Co^{3+}}\times10^3$		$\Phi_{CH_2O}\times10^3$	
				O_2-free	with O_2	O_2-free	with O_2
[Co(sep)]$^{3+}$	(I)	50% CH$_3$OH	4.5	2	2	2	2
[Co(diNOsar)]$^{3+}$	(II)	H$_2$O	4.5	2	2		
		33% CH$_3$OH	4.5	19	2		
		50% CH$_3$OH	4.5	30	2	16	13
		50% CH$_3$OH	1.5	29			
[Co(diNOsar–H)]$^{2+}$	(III)	H$_2$O	9.4	5	5		
		50% CH$_3$OH	9.4	58	23	22	19
[Co(diAMsar)]$^{3+}$	(IV)	H$_2$O	8.0	2	2		
		33% CH$_3$OH	8.0	3	3	2	2
[Co(diAMHsar)]$^{5+}$	(V)	H$_2$O	1.5	2	2		
		33% CH$_3$OH	1.5	22	2	8	6

of the frozen and irradiated (at 77K) aqueous-methanol solution of complex II contained a signal from the $^\bullet$CH$_2$OH radical.

Using the results obtained for complexes II, III, and V, the sequence of reactions occurring in deoxygenated aqueous-methanol solutions was proposed (for simplicity, only one ligand nitrogen atom is given):

$$Co^{III} - NH \xrightarrow{h\nu} Co^{II} - N^+H \tag{142}$$

$$Co^{II} - N^+H \longrightarrow Co^{III} - NH \tag{143}$$

$$Co^{II} - N^+H \longrightarrow Co^{II} - N + H^+ \tag{144}$$

$$Co^{II} - N + CH_3OH \longrightarrow Co^{II} - NH + {}^\bullet CH_2OH \tag{145}$$

$$Co^{III} - NH + {}^\bullet CH_2OH \longrightarrow Co^{II} - NH + CH_2O + H^+ \tag{146}$$
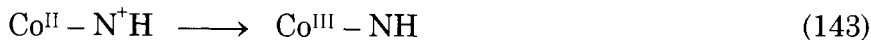
The overall reaction is as follows

$$2Co^{III}NH \xrightarrow{h\nu,\ CH_3OH} 2Co^{II}NH + CH_2O + 2H^+ \tag{147}$$
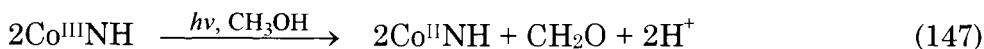
Since the resultant cobalt(II) complex undergoes two types of conversions, one of which (Reaction 143) results in the initial product, the quantum yield of the photocatalytic reaction is lower than those of nonmacrocyclic complexes. The quantum yields of the irradiated [Co(sep)]$^{3+}$ cation in 50% methanol and the irradiated [Co(diAMsar)]$^{3+}$ cation in water and 33% methanol are of the same order of magnitude as that for the [Co(sep)]$^{3+}$...I$^-$ ion pair in water. The quantum yields of the complexes examined markedly change. The [Co(diNOsar)]$^{3+}$, [Co(diAMHsar)]$^{5+}$, and [Co(diNOsar–H)]$^{2+}$ cations proved to be the

most photochemically active: for the first two with the highest redox potentials, the quantum yields are approximately equal; for the last cation, the yield is higher [383].

The formaldehyde formation quantum yields for complexes II and V are nearly the same as those for deoxygenated complexes, which may be attributed to a rapid oxidation ($k = 44$ mol^{-1}·l·s^{-1} for [Co(diNOsar)]$^{2+}$ cation and 22 mol^{-1}·l·s^{-1} for [Co(diAMHsar)]$^{4+}$ cation) of complex cations by oxygen:

$$Co^{II}NH + O_2 \longrightarrow Co^{III}NH + O_2^- \tag{148}$$

$$Co^{II}NH + O_2^- \longrightarrow Co^{II}N^\bullet + HO_2^- \tag{149}$$

$$Co^{II}N^\bullet \rightleftarrows Co^{III}N: \tag{150}$$

$$Co^{III}N: + H^+ \rightleftarrows Co^{III}NH \tag{151}$$

$$HO_2^- + H^+ \longrightarrow H_2O_2 \tag{152}$$

$$2Co^{II}NH + H_2O_2 + 2H^+ \longrightarrow 2Co^{III}NH + 2H_2O \tag{153}$$
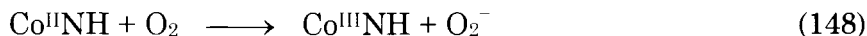
The rate of last reaction is relatively low.

When the irradiated solutions are exposed to air, the initial solution spectra for the cobalt(III) complexes are re-established. A slight increase in the intensity and the appearance of a longwave band in the UV range were attributed to the formation of a deprotonated complex [383].

The reactions induced by irradiation of aqueous-methanol solutions of the macrobicyclic cobalt(III) complexes occur by Scheme 122. The resulting effect is the photocatalytic oxidation of methanol by oxygen.

Substituents in the macrobicyclic cobalt complexes affect their photochemical properties. These effects are more pronounced for solutions of the complexes exhibiting high redox potentials and low electron-transfer rates (Tables 42 and 52). Clathrochelates with lower redox potentials and higher electron-transfer rates are less photochemically active. As mentioned above, the [Co(diNOsar–H)]$^{2+}$ cation displays the highest photochemical activity among the other complexes studied: spectral changes are observed on its irradiation

$$H^+ + O_2 \quad [CoL]^{2+} \quad CH_2O + H^+$$
$$hv$$
$$H_2O \quad [CoL]^{3+} \quad CH_3OH$$
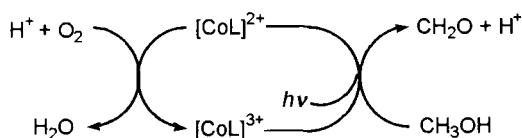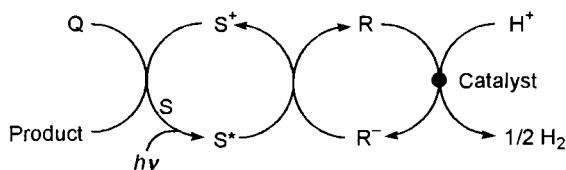
Scheme 122

Scheme 123

in aqueous and aqueous-methanol solutions in both the presence and the absence of oxygen. The correlation between the redox potentials and the photochemical behaviour suggests that the potential for the $[Co(diNOsar-H)]^{2+}$ cation is higher than that of the $[Co(diNOsar)]^{3+}$ cation [383]. It is consistent with the assumption that the potential becomes higher with CoN_6 coordination polyhedron distortion. The E values, however, are expected to decrease with a decrease in the charge of the complex. The growth in the photochemical activity of the $[Co(diNOsar-H)]^{2+}$ cation can also be due to the solvation of the deprotonated nitrogen atom by methanol.

For the macrobicyclic $[Co(sep)]^{3+}$ cation in different solvents and with various anions, the photoeffect enhances in the order $H_2O < CH_3OH < Br^- < I^- < HC_2O_4^-$. For the $[Co(sep)](B(C_6H_5)_4)_3$ complex, the photoeffect increases with decreasing solvent polarity that makes the bond between the cation and the anion or a solvent more stable.

The scheme of the photochemical reactions that occur in the presence of oxygen indicates that macrobicyclic cobalt complexes can be employed as efficient catalysts for photochemical electron-transfer processes.

In this respect, much interest may be focused on the photo-reduction cycle of water decomposition to produce hydrogen [384]; this is represented by Scheme 123, in which S is a sensitizer and R is an electron-transfer agent (ETA), Q is an electron donor. The macrobicyclic complexes in this cycle act as ETAs. Such a cycle, in which $[Ru(bpy)_3]^{2+}$ cation is used as a sensitizer and mv^{2+} cation as an ETA, has already been implemented.

The reaction that occur in such systems is as follows:

$$[Ru(bpy)_3]^{2+} + h\upsilon \longrightarrow [Ru^*(bpy)_3]^{2+} \tag{154}$$

$$[Ru^*(bpy)_3]^{2+} \longrightarrow [Ru(bpy)_3]^{2+} \tag{155}$$

$$[Ru^*(bpy)_3]^{2+} + R \longrightarrow [Ru(bpy)_3]^{3+} + R^- \tag{156}$$

$$[Ru^*(bpy)_3]^{2+} + R \longrightarrow [Ru(bpy)_3]^{2+} + R^* \tag{157}$$

$$[Ru(bpy)_3]^{3+} + R^- \longrightarrow [Ru(bpy)_3]^{2+} + R \tag{158}$$

$$R^- + H^+ \xrightarrow{\quad Pt(PVA) \quad} \tfrac{1}{2} H_2 + R \tag{159}$$
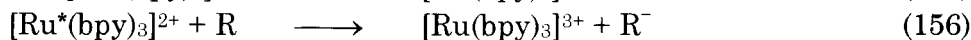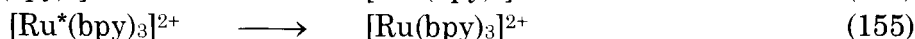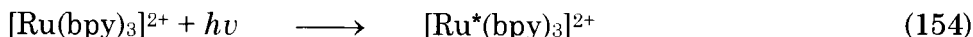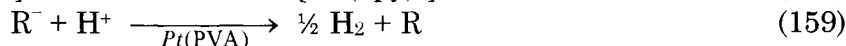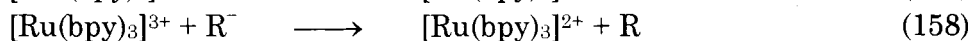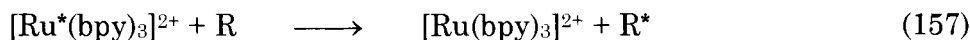
Reaction 159 proceeds in the presence of Pt(PVA) as a catalyst. To perform a closed cycle, one should introduce a sacrificial electron donor Q to remove $[Ru(bpy)_3]^{3+}$ cation:

$$[Ru(bpy)_3]^{3+} + Q \longrightarrow [Ru(bpy)_3]^{2+} + Q^+ \tag{160}$$

$$Q^+ \longrightarrow \textit{decomposition products} \tag{161}$$
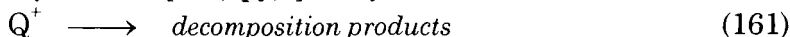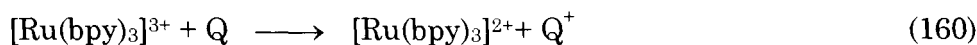
ETA should possesses the following properties: (a) very high stability in the two oxidation states; (b) photochemical inertness to solar radiation in both oxidation states; (c) redox reversibility at negative potentials ($-800 < E < 200$ mV); (d) a high electron-transfer rate; (e) thermal stability; (f) stability toward hydrogenation.

Methylviologen meets all these requirements except the last one. It is hydrogenated with hydrogen in the presence of a platinum catalyst:

$$H_3C-\overset{+}{N}\!\!-\!\!\langle\bigcirc\rangle\!\!-\!\!\langle\bigcirc\rangle\!\!-\!\!\overset{+}{N}\!\!-\!\!CH_3 \xrightarrow[Pt]{+H_2} H_3C-\overset{+}{N}\!\!-\!\!\langle\bigcirc\rangle\!\!-\!\!\langle\bigcirc\rangle\!\!-\!\!\overset{+}{N}\!\!-\!\!CH_3 \tag{162}$$
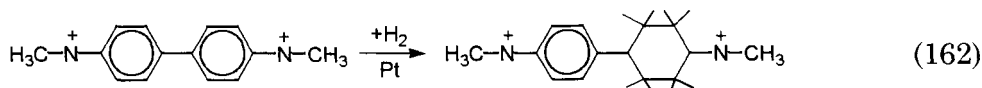
Attempts to utilize coordination compounds and inorganic ions (Eu^{3+}_{aq}, V^{3+}_{aq}, and $[Co(en)_3]^{3+}$) as ETA have not been successful because of a low electron-transfer rate and decomposition in the photochemical or hydrogenation processes.

Macrobicyclic cobalt compounds satisfy all these requirements. Their additional advantage is that the redox potentials and electron-transfer rates may be varied on introduction of different apical substituents, by changing the charge of the complexes *via* protonation or deprotonation, or by altering steric factors. This allows one to select the most suitable complexes as ETAs.

Data on the photocatalytic hydrogen-production cycles in systems including different macrobicyclic complexes are systematized in Ref. 384. $[Ru(bpy)_3]^{2+}$, $[Ru(4,4'\text{-}Me_2bpy)_3]^{2+}$, and $[Ru(bpy)_2L]^+$ (L^- is a carboxylic acid or its derivatives) cations were chosen as sensitizers and EDTA as a sacrificial electron donor. Dependences of hydrogen-production rates and hydrogen yields on the redox potential magnitude, as well as on the concentrations of ETA, sensitizer, and platinum catalyst; the irradiation time; and the pH of the solution have been studied.
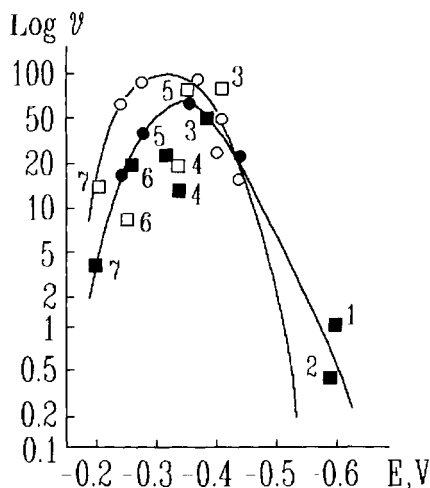
Fig. 61. Plot of the Log (maximum hydrogen-production rate) *versus* the potential of Co$^{3+/2+}$ couple with both [Ru(bpy)$_3$]$^{2+}$ (open symbols) and [Ru(4,4'-Me$_2$bpy)$_3$]$^{2+}$ (closed symbols) cations as sensitizers at pH 5.0. (1) [Co(ClMEMEabsar)]$^{3+}$; (2) [Co(EFMEoxosar–H)]$^{2+}$; (3) [Co(diazachar)]$^{3+}$; (4) [Co(AMMEsar)]$^{3+}$; (5) [Co(sep)]$^{3+}$; (6) [Co(diAMchar)]$^{3+}$; (7) [Co(diAMsar)]$^{3+}$ [384].

The dependence of the maximum hydrogen-production rate on the redox potential of the clathrochelate Co$^{3+/2+}$ couple is shown in Fig. 61 and Table 61. The most efficient ETA for systems with both sensitizers proved to be [Co(CLsar)]$^{3+}$ cation. Similar values of maximum rates of hydrogen production and hydrogen yields were obtained for [Co(CLHOsar)]$^{3+}$/[Co(sep)]$^{3+}$ and *lel*$_3$-[Co(diazachar)]$^{3+}$/ [Ru(bpy)$_3$]$^{2+}$ systems. Plots of maximum rates of hydrogen production *versus* the concentration of ETA (*mv*$^{2+}$ or [Co(CLSar)]$^{3+}$ cations) for the two ruthenium complexes are shown in Fig. 62 at a constant concentration of Pt(PVA) (*ca* 5 × 10^{-5} mol·l^{-1}) as catalyst. For both sensitizers the hydrogen-production rates attain their maximal values at 4 × 10^{-3} mol·l^{-1} for the cobalt complexes and at 2 × 10^{-3} mol·l^{-1} for methylviologen. Plots of the maximum rate of hydrogen production and the volume of the hydrogen produced *versus* the Pt(PVA) concentration are shown in Fig. 63. With [Co(CLsar)]$^{3+}$ cation, optimal conditions for hydrogen production were attained at a Pt(PVA) concentration close to 5 × 10^{-5} mol·l^{-1}.

The pH dependencies of hydrogen production with [Ru(bpy)$_3$]$^{2+}$ cation as a sensitizer for the three complexes are listed in Table 62.

Table 61.

Hydrogen production in cyclic systems with $[Ru(bpy)_3]^{2+}$ and $[Ru(4,4'-Me_2bpy)_3]^{2+}$ cations as sensitizers at pH = 5.0 [384].

Cation	$^a E$, mV	$[Ru(bpy)_3]^{2+}$		$[Ru(4,4'-Me_2bpy)_3]^{2+}$	
		^{b}Relative rate	Yield, μmol/ml	^{b}Relative rate	Yield, μmol/ml
$[Co(HYMEoxosar–H)]^{2+}$	–590				
$[Co((ClME)MEabsar)]^{3+}$	–510			0.27	0.07
$[Co(EFMEoxosar–H)]^{2+}$	–510			0.12	0.03
$[Co(sar)]^{3+}$	–400	3.2	0.9	4.6	1.3
$[Co(MEazasar)]^{3+}$	–350	13	3.0	6.4	1.8
$[Co(AMMEsar)]^{3+}$	–340	9	2.4	6	1.5
lel_3-$[Co(diazachar)]^{3+}$	–400	33	7.5	15	4.3
$[Co(CLsar)]^{3+}$	–260	36	8.2	26	7.4
$[Co(sep)]^{3+}$	–260	31	7.1	9.8	2.4
$[Co(MENOsar)]^{3+}$	–190	4.2	0.78	0.45	0.01
$[Co(CLHOsar)]^{3+}$	–160	31	6.8	12	3.6
$[Co(diCLsar)]^{3+}$	–130	22	5.0	5.5	1.4
lel_3-$[Co(diAMchar)]^{3+}$	–350	3.9	1.0	6	1.4
$[Co(diAMsar)]^{3+}$	–300	4.7	0.7	1.3	0.2
$[Co(CLNOsar)]^{3+}$	–60	14.2	2.5		
$[Co(diNOsar)]^{3+}$	40				
$[Co(azacapten)]^{3+}$	–10				
$[Co(AMcapten)]^{3+}$	60				
mv^{2+}	–440	100	19.6	13	4.5

^{a} Redox potential was measured under photolysis conditions. ^{b} Relative rate of the initial hydrogen production *versus* 100% for methylviologen.

Table 62.

Hydrogen production with $[Ru(bpy)_3]^{2+}$ cation as sensitizer at different pH values [384].

Cation	pH	Relative rate	Volume of H_2, ml
$[Co(sep)]^{3+}$	2.6	0.33	0.0026
	3.7	6.2	0.10
	5.0	31	0.80
	6.65	11	0.18
	7.6	2.3	0.04
$[Co(sar)]^{3+}$	3.7	0.65	0.0059
	5.0	3.2	0.03
	6.65	6.1	0.06
	7.8	0.34	0.02
$[Co(AMMEsar)]^{3+}$	3.7	4.4	0.07
	5.0	9.0	0.15
	6.65	6.0	0.09
	7.80	1.0	0.01
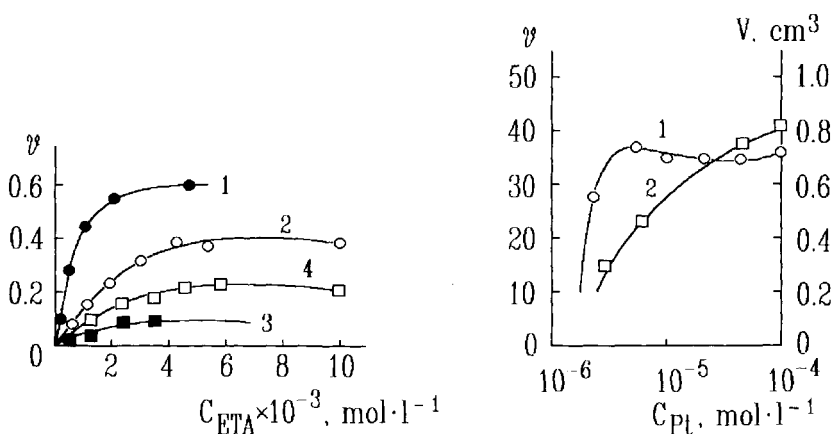
Fig. 62. ETA concentration dependencies of the maximum hydrogen-production rates for the $[Ru(bpy)_3]^{2+}/mv^{2+}$ **(1)**, $[Ru(bpy)_3]^{2+}/[Co(CLsar)]^{3+}$ **(2)**, $[Ru(4,4'-Me_2bpy)_3]^{2+}/mv^{2+}$ **(3)** and $[Ru(4,4'-Me_2bpy)_3]^{2+}/[Co(CLsar)]^{3+}$ **(4)** systems [384].

Fig. 63. Effect of Pt(PVA) concentration on the hydrogen-production rates **(1)** and hydrogen yields **(2)** for the $[Co(CLsar)]^{3+}$ / $[Ru(bpy)_3]^{2+}$ system [384].

Optimal conditions for H_2 production are achieved in the systems with $[Co(sep)]^{3+}$ and $[Co(AMMEsar)]^{3+}$ cations at pH 5 and in the system with the $[Co(sar)]^{3+}$ cation at pH 6.65. However, the hydrogen-production rate and the hydrogen yield in the last system are lower than those of the two former systems, Fig. 64 [340].

A plot of the hydrogen-production rate *versus* the irradiation time in systems with $[Ru(bpy)_3]^{2+}$ cation as sensitizer and sarcophaginate $[Co(diAMsar)]^{3+}$, $[Co(diCLsar)]^{3+}$, and $[Co(Clsar)]^{3+}$ cations as ETAs are shown in Fig. 65.

The hydrogen-production rate increases in the systems with $[Co(CLsar)]^{3+}$ and $[Co(diCLsar)]^{3+}$ cations for the first 10 min and then remains constant. In the system with $[Co(diAMsar)]^{3+}$ cation, the hydrogen-production rate is small and increases linearly for 20 min. During prolonged irradiation at pH 5.0, the rate of H_2 production decreases more rapidly for macrobicyclic complexes than for methylviologen. Neither the dependence of this rate on the concentration of $[Co(CLsar)]^{3+}$ cation nor substantial decomposition of this cation even after 10 hours of irradiation were observed. The extrapolated turnover numbers (> 5000) derived from experimental data for $[Co(CLsar)]^{3+}$ and $[Co(sep)]^{3+}$ cations are at least two orders of magnitude greater than those observed for methylviologen (TON *ca* 55).
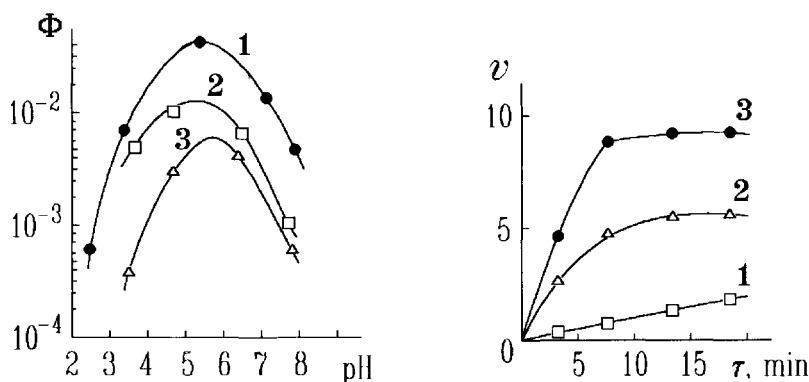
Fig. 64. Plots of the hydrogen quantum yields *versus* pH of the solution for [Ru(bpy)₃]²⁺/[Co(sep)]³⁺ **(1)**, [Ru(bpy)₃]²⁺/[Co(AMMEsar)]³⁺ **(2)** and [Ru(bpy)₃]²⁺/[Co(sar)]³⁺ **(3)** systems [340].

Fig. 65. Plot of hydrogen-production rates *versus* the irradiation time for [Co(diAMsar)]³⁺ **(1)**, [Co(diCLsar)]³⁺ **(2)**, and [Co(CLsar)]³⁺ **(3)** cations with [Ru(bpy)₃]²⁺ cation as sensitizer [384].

Thus, the data on photochemical hydrogen production indicate that macrobicyclic complexes can be effective ETAs only in a narrow redox potential range (−400 mV < E < −260 mV). Special experiments demonstrated that cage complexes with such potentials are efficient for quenching of [Ru(bpy)₃]²⁺ and [Ru(4,4'-Me₂bpy)₃]²⁺ cations (Table 63).

The relative rate of hydrogen production drastically drops when potentials are lower than −380 mV, since cobalt(II) ions with such potentials can only partially reduce water at pH 5.0. To achieve hydrogen maximal yields with these complexes, much more time is required. There is no agreement between the hydrogen-production rate and hydrogen yields for such complexes. With macrobicyclic complexes whose potentials are lower than −340 mV, the rate of hydrogen production is determined by the cobalt(II) formation rate, whereas the hydrogen yield is quantitatively related to the cobalt(II) quantum yields.

Table 64 lists the redox potentials of several sensitizers and complexes, acting as ETAs, under photolysis conditions. The cobalt(II) formation quantum yields and the relative rates of hydrogen production were determined experimentally and normalized to the cobalt(II) quantum yield [385]. The efficiency of hydrogen production is determined as the product $\Phi_e C_e$, where Φ_e is the quantum yield of

Table 63.
Quenching the excited states of the $[Ru(bpy)_3]^{2+}$ and $[Ru(4,4'-Me_2bpy)]^{2+}$ cations (T = 293K) [384].

Complex	[a] E, mV	$\Phi_{Co(III)}$ System with $[Ru(bpy)_3]^{2+}$	System with $[Ru(4,4'-Me_2bpy)_3]^{2+}$
$[Co(HYMEoxosar-H)]^{2+}$	−630	10^{-4}	
$[Co((ClME)MEabsar)]^{3+}$	−590	10^{-4}	10^{-4}
$[Co(EFMEoxosar-H)]^{2+}$	−580	10^{-4}	10^{-4}
$[Co(sar)]^{3+}$	−460	4×10^{-4}	0.002
$[Co(MEazasar)]^{3+}$	−430	0.017	0.008
$[Co(AMMEsar)]^{3+}$	−360	0.01	0.005
lel_3-$[Co(diazachar)]^{3+}$	−400	0.027	0.017
$[Co(CLsar)]^{3+}$	−360	0.052	0.035
$[Co(sep)]^{3+}$	−350	0.040	0.014
$[Co(MENOsar)]^{3+}$	−290	0.056^b	0.004^b
$[Co(CLHOsar)]^{3+}$	−280	0.19	0.039
$[Co(diCLsar)]^{3+}$	−250	0.24	0.043
$[Co(diAMsar)]^{3+}$	−210	0.033	0.012
lel_3-$[Co(diAMchar)]^{3+}$	−260	0.040	0.047
$[Co(CLNOsar)]^{3+}$	−170	0.41	0.05
$[Co(diNOsar)]^{3+}$	−70	0.40	0.07
$[Co(azacapten)]^{3+}$	−20	0.6	
$[Co(AMcapten)]^{3+}$	430	0.31	0.06
mv^{2+}	−440	0.1	0.07

[a] Redox potential was measured under photolysis conditions.
[b] This value may be lower than the actual value due to reaction of the apical nitro group with cobalt(II) ion.

quenching S^* by electron transfer and C_e is the efficiency of formation of the resulting ions from the cage complex. The $\Phi_e C_e$ value can be obtained by dividing the relative rates of hydrogen production by $\Phi_{Co(II)}$. The normalized rates are represented in Table 64. These rates of hydrogen production in systems with $[Ru(bpy)_3]^{2+}$ cation increase in the series mv^{2+} < $[Co(sep)]^{3+}$ < $[Co(CLsar)]^{3+}$.

Since the early 1990s, ruthenium (II) polypyridine complexes have been used as mediators in the interconversion of light and chemical energy. A quite important property for photosensitizers is their stability toward photodecomposition. For $[Ru(bpy)_3]^{2+}$ cation in aqueous solution, the quantum yield of photodecomposition is from 10^{-5} to 10^{-3}, depending on the pH and temperature. In the solution containing X^- anions (Cl^-, Br^-, and NCS^-), this quantum yield can be as high as 0.1 for solvents with a low dielectric constant [386]. A way

Table 64.
Quantum yields of cobalt(II) complex formation and rates of hydrogen production [385].

E, mV (Ru^{3+}/Ru^{2+} couple)	Electron carrier	E, mV (Co^{3+}/Co^{2+} couple)	$\Phi_{Co(II)}$	Rate of H$_2$ production	
				relative	normalized
sensitizer: diethyl ester of 2,2'-bipyridine-4,4'-dicarboxylic acid					
−730	mv^{2+}	−280	0.08	20	250
	[Co(sep)]$^{3+}$	−380	0.07	0.9	13
	[Co(CLsar)]$^{3+}$	−370	0.07	1.0	14
sensitizer: ethyl ester of 4'-methyl-2,2'-bipyridine-4-carboxylic acid					
−740	mv^{2+}	−290	0.12	22	183
	[Co(sep)]$^{3+}$	−390	0.05	0.8	16
	[Co(CLsar)]$^{3+}$	−380	0.05	0.8	16
sensitizer: methylbipyridinecarboxylate anion					
−780	mv^{2+}	−310	0.50	73	146
	[Co(sep)]$^{3+}$	−410	0.46	29	63
	[Co(CLsar)]$^{3+}$	−400	0.43	32	74
sensitizer: bipyridinecarboxylate anion					
−780	mv^{2+}	−330	0.65	68	104
	[Co(sep)]$^{3+}$	−430	0.28	12	43
	[Co(CLsar)]$^{3+}$	−420	0.25	11	44
sensitizer: [Ru(bpy)$_3$]$^{2+}$					
−840	mv^{2+}	−390	0.54	100	185
	[Co(sep)]$^{3+}$	−490	0.15	31	207
	[Co(CLsar)]$^{3+}$	−480	0.15	36	240

to prevent ligand photodissociation without changing other properties is cross-linking by covalent bonds (i.e., cage formation). The extraordinary (about 10^4 times higher than that of [Ru(bpy)$_3$]$^{3+}$ cation) stability of the macrobicyclic ruthenium bipyridinate toward photodecomposition is described in Ref. 386.

The ionic pair of [Co(AMMEsar)]$^{3+}$ cation with an anthracene carboxylate anion (A–Co(III)) was used as both a photosensitizer and an ETA in the photodecomposition of water to produce hydrogen [387]. The photoreduction of encapsulated cobalt(III) ion to cobalt(II) ion occurs on excitation of anthracene chromophore ($\nu < 25\,000$ cm^{-1}). The A–Co(III) complex shows almost no fluorescence ($\Phi \leq 2 \times 10^{-4}$), whereas the A–Co(II) complex produces specific violet fluorescence (Fig. 66). The cobalt(II) complex is formed in the presence of EDTA on light irradiation of the A–Co(III) solution ($\nu > 25\,641$ cm^{-1}). The visible band at 21 276 cm^{-1} disappeared, and violet fluorescence was observed. The quantum yield of cobalt(II) complex formation was
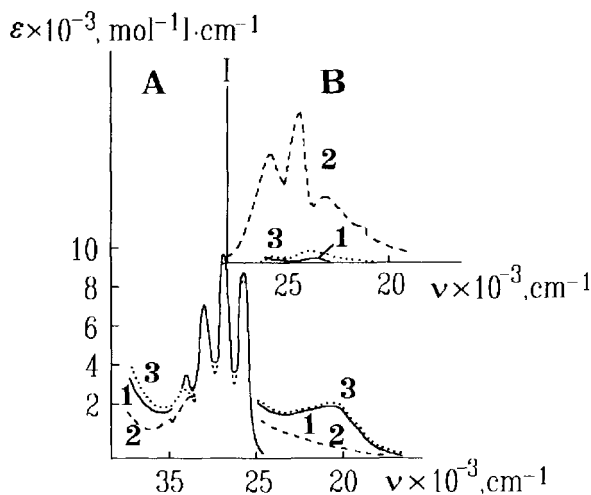
Fig. 66. Absorption (**A**) and fluorescence (**B**) spectra of cobalt diaminosarco-phaginates...anthracene carboxylate ion pairs [387]. (**1**) Cobalt(III) complex; (**2**) cobalt(II) complex; (**3**) after cobalt(II) complex oxidation.

small ($\Phi \leq 0.01$). After cobalt(II) complex oxidation to cobalt(III) complex with air oxygen, the fluorescence disappeared (Fig. 66).

Since the cobalt (III) complex undergoes rapid one-electron reduction at −400 mV (pH 5), it may be utilized as an ETA in water decomposition:

$$A\text{–}Co(II) + H^+ \xrightarrow{\;Pt(PVA)\;} A\text{–}Co(III) + \tfrac{1}{2}\,H_2 \qquad (163)$$
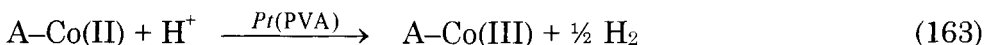
Actually, hydrogen was produced in quantum yields 0.01 and 0.03 at pH 8 and 5, respectively, on light irradiation (at 25 641 cm^{-1}) of A–Co(III) (2×10^{-3} mol·l^{-1}), EDTA (0.1 mol·l^{-1}) and Pt(PVA) (5×10^{-3} mol·l^{-1}) aqueous solutions. In this reaction, the A–Co(III) complex serves not only as an ETA but also as a sensitizer. When this complex was replaced by [Co(AMMEsar)]$^{3+}$ cation, no hydrogen production was observed.

Two cobalt cage complexes with covalently linked anthracene chromophore (Scheme 124) have been studied as coupled photo-sensitizers (anthracene substituent) and electron relays (cage fragment) to produce hydrogen [305].
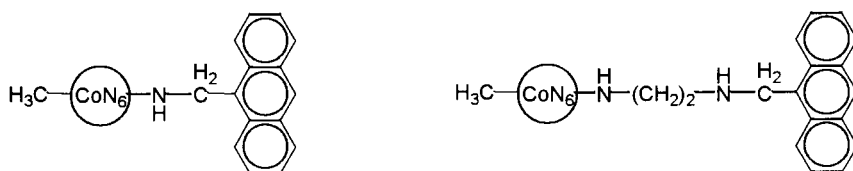
Scheme 124

It was shown that the efficiency of energy transfer from the anthracene singlet excited state to the cobalt cage decreases with increasing length of the bridge.

A contracted sarcophaginate $[Co((ClME)abcapten)]^{3+}$ cation ($E_{1/2} = -200$ mV, $k_{11} = 1.3 \times 10^4$ mol^{-1}s^{-1}) was examined as an ETA in photocatalytic systems for hydrogen production [356]. The rate of photoinduced hydrogen formation is controlled by the generation of the excited state S* and three processes of the electron transfer:

$$S + h\upsilon \longrightarrow S^* \tag{164}$$

$$S^* + [Co^{III}((ClME)abcapten)]^{3+} \longrightarrow S^+ + [Co^{II}((ClME)abcapten)]^{2+} \tag{165}$$

$$[Co^{II}((ClME)abcapten)]^{2+} + H^+ \xrightarrow{\ Pt(PVA)\ } \tfrac{1}{2}H_2 + [Co^{III}((ClME)abcapten)]^{3+} \tag{166}$$

$$[Co^{II}((ClME)abcapten)]^{2+} + S^+ \longrightarrow S + [Co^{III}((ClME)abcapten)]^{3+} \tag{167}$$
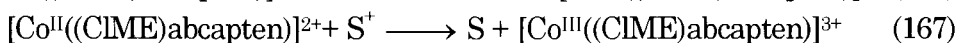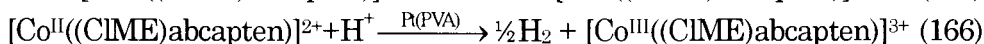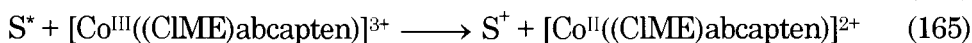
Excited-state quenching reactions were studied with both [Ru(bpy)$_3$]$^{2+}$ dication and anthracene carboxylate anion as sensitizers. Both the excited states of **AA**$^-$ (^{1}**AA**$^-$, $E(^1$**AA**$^\bullet$–**AA**$^-) = -2200$ mV and ^{3}**AA**$^-$, $E(^3$**AA**$^\bullet$–**AA**$^-) = -880$ mV) are capable of reducing the cobalt(III) sarcophaginate (Reaction 165). The cobalt(II) complex should reduce protons in the presence of Pt(PVA) (Reaction 166) and together with the high electron self-exchange rate, this made it a promising candidate for use as an ETA for light-induced hydrogen formation.

Energy and electron transfer processes between **AA**$^-$ and [Co((ClME)abcapten)]$^{3+/2+}$ are shown in Fig. 67. Antenna molecules, which absorb a large part of the solar spectrum, can be used to transfer light energy efficiently to anthracene. An assembly consisting of an antenna molecule, anthracene, and a stable cobalt N$_3$S$_3$-sarcophaginate has the potential for the efficient conversion of light energy to chemical energy [356].

The electrochemical data for cobalt(III) sarcophaginates with pendant aromatic substituents [137] showed that the reduction potential of the anthraquinone-containing complex is more positive than that of Co$^{3+/2+}$ couples in these complexes. Hence, they may be
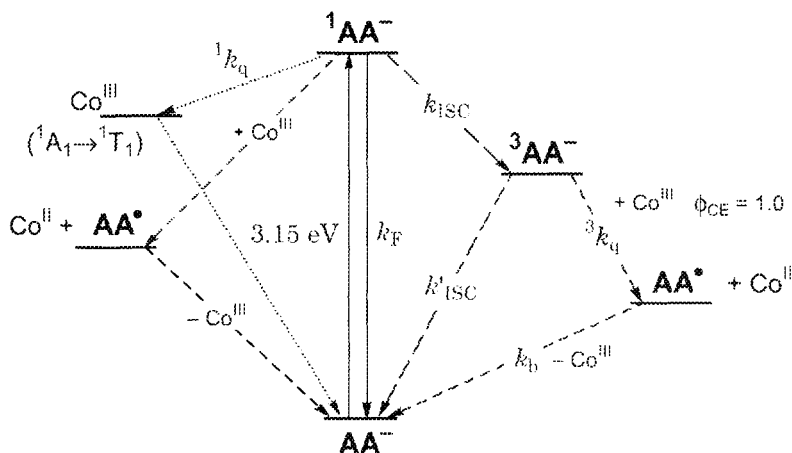
Fig. 67. Energy and electron transfer processes between AA^- and a $[Co((ClME)abcapten)]^{3+/2+}$ pair. Radiative transitions (——), nonradiative transitions (– – – –), electron transfer processes (- - - - -), energy transfer processes (············) [356].

used to intercalate anthracene or phenanthrene pendant substituents with DNA and have the ability to participate in reactions centred on the aromatic substituent, such as photochemical reactions. Photochemical cleavage of DNA following binding of polycyclic aromatic-functionalized cobalt(III) sarcophaginates (Scheme 117) was examined in Ref. 315.

Attempts have been made [4] to employ cobalt(III) clathrochelates for the photosynthesis of unusual compounds, e.g., to obtain a dimer head-to-head clathrochelate starting from the $[Co(MECAsar)]^{3+}$ cation. It was assumed that on UV irradiation at CTB wavelength, the encapsulated cobalt(III) ion would reduce to cobalt(II) ion, or a carboxyl ligand radical would be formed, which eliminate CO_2 forming decarboxylated ligand radical. The coupling of two such radicals would give the desired dimer. However, this dimer was not obtained in this manner since the encapsulated cobalt(II) ion was rapidly oxidized, primarily back to $[Co(MEsar)]^{3+}$ cation plus some cage framework opening to give olefin complexes (Scheme 125). The head-to-head dimer was obtained in a small yield by photoreduction of modified $[Co(MECAsar)]^{3+}$ cation, wherein the carboxyl group hydrogen was replaced by the readily reducible $[Co(NH_3)_5]^{3+}$ cation. It was suggested that the cobalt(III) ion of the latter complex would be reduced before the sarcophaginate fragment, but that turned out to be only partly successful. About 75% of the photolysis occurred by the
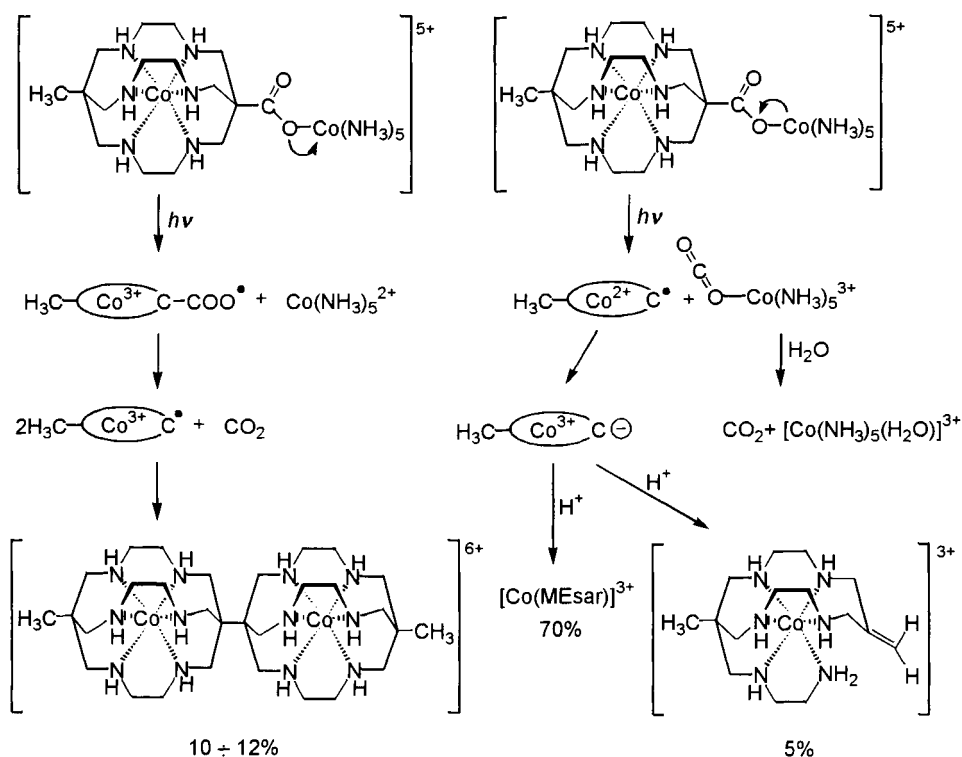
Scheme 125

initial reduction of the clathrochelate fragment, and only 10÷12% of this process resulted in reduction of the $[Co(NH_3)_5]^{3+}$ cation to give the carboxyl ligand radical, which then eliminated CO_2 and dimerized to yield the head-to-head dimer.

5.3.2. Chromium complexes

Several papers deal with the photochemical, photophysical, and related spectral characteristics of macrobicyclic chromium complexes [4, 158, 159, 374, 388, 389]. The spectra of these complexes differ from those of nonmacrocyclic $[Cr(NH_3)_6]^{3+}$ and $[Cr(en)_3]^{3+}$ cations by (a) the high intensity of the low-energy spin-allowed quartet-quartet transition, (b) a resolved splitting in the longwave region (aqueous solution, 298K), and (c) an increased line width and decreased energy for the spin-forbidden transition to the doublet ^2E state.

Photochemical experiments have been carried out at 22 222 cm^{-1} using a xenon lamp irradiation dispersed by a monochromator. The $[Cr(diAMsar)]^{3+}$ and $[Cr(sar)]^{3+}$ cations showed no detectable

phosphorescence from the doublet states at 273 K in aqueous solution. Emission for the $[Cr(diAMsar)]^{3+}$ cation was detected neither in various solvents such as D_2O, CH_3OH, CD_3OD, AN, and DMF nor in solid matrixes such as polystyrene at the same temperature. The $[Cr(sep)]^{3+}$ and $[Cr(en)_3]^{3+}$ cations exhibited phosphorescence at room temperature in aqueous solution. Very weak phosphorescence ($\Phi \sim 10^{-4}$) was observed for $[Cr(diAMsar)]Cl_3 \cdot H_2O$ and $[Cr(diAMsar-d_{10})]Cl_3 \cdot D_2O$ crystalline powders at 298K. Both $[Cr(sar)]^{3+}$ and $[Cr(diAMsar)]^{3+}$ sarcophaginates emit rather strongly at 77K ($\Phi \sim 0.02$). Under these conditions, the phosphorescence lifetimes for the $[Cr(diAMsar)]^{3+}$ cation are longer than those of the $[Cr(en)_3]^{3+}$ cation in both H_2O and D_2O matrixes, and the excited state lifetimes increase by deuteration. Since phosphorescence appears simultaneously with the laser excitation pulse (excitation time 2 ns), it was concluded [158] that intercombination conversion is a rapid process with a rate constant approximately 10^9 s^{-1}. The phosphorescence intensities and the lifetimes (τ) decrease with temperature increases. The change in phosphorescence lifetimes for the $[Cr(diAMsar)]^{3+}$ cation in the temperature range from 77 to 298K in H_2O, D_2O, and crystals is shown in Fig. 68.

The phosphorescence lifetimes in solution are strongly dependent (about 3 orders of magnitude) on temperature from 150 to 230 K, and for deuterated samples are four times longer than that for the
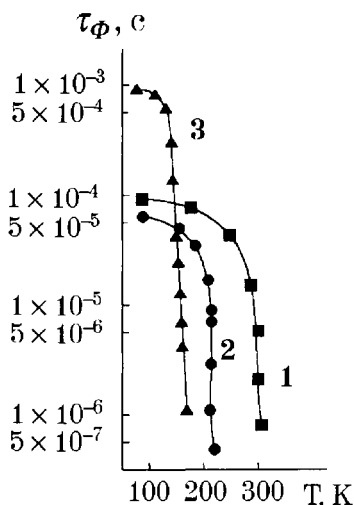
Fig. 68. Phosphorescence lifetime as a function of temperature for the $[Cr(diAMsar)]^{3+}$ cation doublet state: in crystal (1), H_2O (2), and D_2O (3) [4].

nondeuterated species. The lifetimes of the excited states are much longer in deuterated solvents. In methanol-water (3:1) mixture, the change in phosphorescence lifetimes with temperature for [Cr(diAMsar)]$^{3+}$ and [Cr(en)$_3$]$^{3+}$ cations differs dramatically: at 130 K they have essentially the same lifetime (100 µs), but at 200 K the lifetimes differ by 2 orders of magnitude.

The photodecomposition of the [Cr(diAMsar)]$^{3+}$ cation and the other amine complexes was monitored by HPLC. Quantum yields of these processes in aqueous solutions as well as doublet state lifetimes are listed in Table 65.

The quantum yields increase from 2×10^{-5} to 0.45 in the [Cr(sar)]$^{3+}$ < [Cr(diAMsar)]$^{3+}$ < [Cr(sep)]$^{3+}$ < [Cr(en)$_3$]$^{3+}$ < [Cr(NH$_3$)$_6$]$^{3+}$ series. Clathrochelate complexes demonstrated the minimal photo-decomposition quantum yields. The lifetime of the [Cr(sar)]$^{3+}$ cation at room temperature in aqueous solutions is less than 10 ns, approaches that of the [Cr(diAMsar)]$^{3+}$ cation, and is in sharp contrast to those of nonmacrocyclic [Cr(en)$_3$]$^{3+}$ and [Cr(NH$_3$)$_6$]$^{3+}$ cations in DMF (17 and 6 µs, respectively). The lifetime of the [Cr(sep)]$^{3+}$ cation was found to be about the same (10 µs) [4, 158]. At 77K, the excited state lifetimes are longer and little different for clathrochelates and nonmacrocyclic complexes (22÷60 µs).

The pathway for the relaxation of the excited doublet state is described in Ref. 159. Three models for the relaxation of the lowest-energy exited states were employed: (a) the quenching of the excited state by direct chemical reaction; (b) the back-intersystem crossing to excited quartet state; (c) would account for the

Table 65.
Photophysical Properties of Hexamine Chromium Complexes [4].

Parameter	Ligand				
	diAMsar	sar	sep	en	NH$_3$
^2E, cm^{-1}	14500	15630	15000	15000	15200
$^4T_2$, cm^{-1}	21950	21860	21740	21930	21790
	22350	22250			
$^4T_1$, cm^{-1}	28940	28820	28990	28330	28490
τ, µs (297 K)	< 0.1	< 0.1	10	6	17
τ, µs (77 K)	65	60		22	
Φ (77 K)	0.02	0.02			
Φ (298 K)	2×10^{-5}	2×10^{-5}	3×10^{-2}	0.37	0.45
E (Cr$^{3+/2+}$ couple), mV	−1100		−1100	−1100	
Cr–N, Å	2.07			2.07	2.06
Distortion angle φ, deg	49			51	60

behaviour of the ^2E state in terms of a surface crossing to a reactive ground-state intermediate.

The first model implies the rupture of the coordination bonds. This is inconsistent with the inertness of the macrobicyclic complex because its decomposition causes the rupture not only of M–N bonds, but also of C–C and C–H bonds. Therefore, this model predicts a relatively long lifetime of the ^2E state for the $[Cr(sep)]^{3+}$ cation. In fact, the ^2E states for $[Cr(en)_3]^{3+}$ and $[Cr(sep)]^{3+}$ cations have very similar lifetimes (of the order of 10^{-5} µs) in DMF at 0°C and similar spectral characteristics (both of them show an intense band at 15 151 cm^{-1} and possess a quantitatively similar low-intensity vibronic structure). The macrobicyclic ligand ensures that ligand dissociation will have a large activation barrier, even in metal-centred electronic exited states. Neither the first model nor the second one adequately accounts for the photolytic similarities of $[Cr(sep)]^{3+}$, $[Cr(en)_3]^{3+}$ and $[Cr(NH_3)_6]^{3+}$ cations. The third model seems the most realistic alternative [159].

5.3.3. Lanthanide complexes

Photoluminescence of tris-bipyridine europium and terbium(III) clathrochelates in aqueous solutions and in the solid state has been studied in the temperature range from 4.2 to 300 K [212, 374, 390-394]. It has been assumed that luminescence is favoured by (a) the inertness of clathrochelates; (b) the complete encapsulation of the rare earth metal ion in macrobicyclic ligand cavities, preventing deactivation of these luminescent ions owing to interaction with the solvent molecules; and (c) the possibility of energy transfer from the ligand chromophore to the luminescent ion.

Low-temperature studies of solid tris-bipyridine europium, terbium, lanthanum(III), and sodium clathrochelates were performed on UV excitation [390]. The lanthanum(III) and sodium clathro-chelates were examined to get more information on the luminescent properties of the ligand. These clathrochelates showed luminescence at temperatures below 100 K upon longwave UV excitation corresponding to ligand-centred absorption. The quantum yield of the ligand phosphorescence is ca 0.02. An increase of temperature results in a drastic decrease in the luminescence intensity, and at 100 K it becomes equal to zero (Fig. 69).
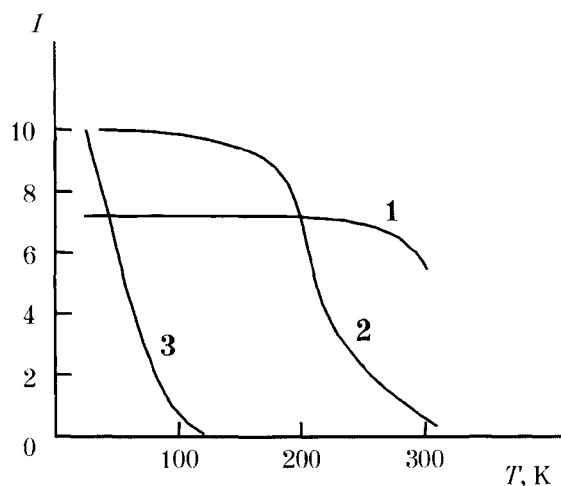
Fig. 69. Temperature dependence of luminescence intensities for clathrochelate europium (1) and terbium(III) (2) tris-bipyridinates and the initial macrobicyclic ligand (3).

The low quantum yield is caused by migration of the $^3(\pi\text{-}\pi^*)$ excited state yield among the three *bpy* fragments. This migration increases with temperature and reduces the luminescence yield.

The excitation spectra of europium and terbium(III) clathrochelates contain a strong dominant band at 27 000 cm^{-1}. The CTB at 23 809 cm^{-1} (4.2 K) is mirror-symmetric to the luminescence band. The red emission is detected for the exited europium(III) clathrochelate. The emission spectrum of this complex (Fig. 70) also contains a set of lines corresponding to the $^5D_0 \rightarrow \, ^7F_J$ transitions, which indicates the C_3 symmetry of the clathrochelate molecule.

The luminescence quantum yield for the europium complex (0.65 ± 0.10 and 0.50 ± 0.10 at 4.2 and 300 K, respectively) decreases starting from 250 K.

Terbium clathrochelate showed green emission of very high intensity. The emission spectrum contains the $^5D_4 \rightarrow \, ^7F_J$ transition bands of the encapsulated terbium ion. The same but less intense emission spectrum was observed at higher temperatures. The luminescence quantum yield is close to 1 at 4.4 K and is approximately 0.05 at room temperature [390]. The decrease in intensity of the terbium(III) ion luminescence starts at 100 K (higher than that of free macrobicyclic tris-bipyridine ligand and lower than that of the corresponding europium(III) compound, Fig. 69). It may be
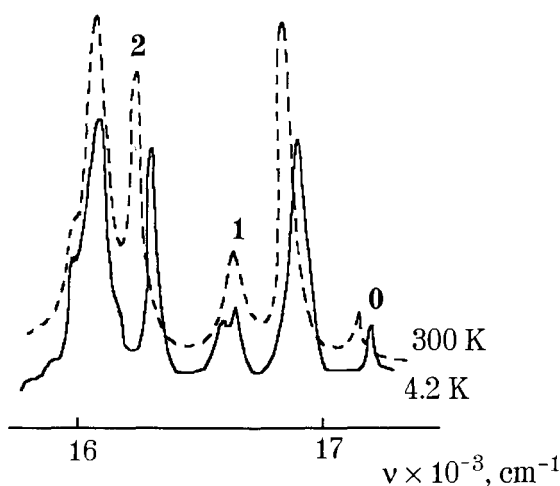
Fig. 70. Emission spectrum of tris-bipyridine europium(III) clathrochelate at 300 and 4.2K ($^5D_0 \to {}^7F_J$ (0,1,2) transitions) [212].

assumed that at T > 100 K, the migration rate of the triplet excited state of *bpy* fragments in the terbium(III) clathrochelate competes with the *clathrochelate ligand* → Tb^{3+} energy-transfer rate. As result, the Tb^{3+} emission intensity starts to decrease. The decrease in the luminescence quantum yield of the europium(III) clathrochelate at higher temperatures compared with the terbium(III) yield may be accounted for by a higher *clathrochelate ligand* → Eu^{3+} energy-transfer rate [390].

The differences observed in the temperature dependences of luminescence for europium and terbium(III) clathrochelates can also be due to the absence of back energy transfer from encapsulated Eu^{3+} cation to the clathrochelate ligand. The expression for the rate constant of metal-to-ligand back transfer contains the ΔE value, which is the energy difference between the triplet level of the bipyridine fragment and the metal ion phosphorescence level. The back transfer rate for the europium(III) ion is much less than that for the terbium(III) ion. This process is essential for the terbium(III) ion, and this is confirmed by differences in the temperature dependence of excited-state lifetimes for europium and terbium(III) clathrochelates in D_2O: the luminescence of the terbium(III) complex at 77 K is approximately an order of magnitude higher than that at 300 K, whereas for the europium(III) complex, it does not depend on temperature.

The luminescence of the bipyridine europium and terbium(III) clathrochelates in aqueous and D_2O solutions has been reported in several papers [212, 391, 393].

Europium and terbium(III) clathrochelates in aqueous solution exhibit a strong ligand-centered (LC) absorption band, $10^4 - 10^5$ times more intense than the metal-centered (MC) $f-f$ bands characteristic of the lanthanide ions. The luminescent emission wavelength is almost unaffected by the central ion arrengement (water, coordinated nitrogen atoms), whereas the excited-state lifetime is affected: for the europium(III) ion it increases and for the terbium(III) ion it decreases as mentioned above. The luminescence quantum yield for aqueous solutions of these clathrochelates enhances with respect to the aqua ion and drastically drops compared with the solid samples (Table 66). A relatively small luminescence quantum yield is attributed to a low-efficiency intramolecular ligand-to-metal energy transfer due to intraligand radiationless processes (excitation state → ground state) [393]. The radiationless deactivation of lanthanide ions cannot also be excluded.

Table 66.
Absorption and emission of europium (I) and terbium(III) aqua ions and clathrochelates in aqueous solution and in the solid state [380, 390, 391, 393].

Cation	T, K	Absorption		Emission				Φ	n
		$\nu_{max}\times10^{-3}$, cm^{-1}	ε, mol^{-1}·l·cm^{-1}	$\nu_{max}\times10^{-3}$, cm^{-1}	τ, ms				
					H$_2$O	D$_2$O			
[Eu(bpy.bpy.bpy)]$^{3+}$$_{aq}$	300	32.9(LC)	25 000	[a] 16.3	0.34	1.7		0.02	2.5
	77					1.7			
Eu^{3+}$_{aq}$	300	25.4(f-f)	3	[a] 16.2	0.11	3.2		0.006	9.6
	77					3.3			
[Eu(bpy.bpy.bpy)]$^{3+}$ (powder)	4.2				1.13			0.65	0.3
	300				0.95			0.50	0.5
[Eu(bpy.bpy.bpz)]$^{3+}$$_{aq}$	300	32.7	20 000	[a] 16.2	0.87			0.035	
[Eu(bpy.bpy.bpz)]$^{3+}$$_{D_2O}$	300	33.0	20 000	[a] 16.2		1.6		0.10	
[Eu(bpy.bpy.bpz)]$^{3+}$$_{CH_3OH}$	300	33.0	46 000	[a] 16.2	1.1(CH$_3$OH)			0.07	
[Tb(bpy.bpy.bpy)]$^{3+}$$_{aq}$	300	32.9(LC)	29 000	[b] 18.5	0.33	0.43		0.03	3.0
	77					3.8			
Tb^{3+}$_{aq}$	300	32.5(f-f)	0.3	[b] 18.4	0.40	3.8		0.08	9.0
	77					3.8			
[Tb(bpy.bpy.bpy)]$^{3+}$ (powder)	4.2							1	
	300							0.05	

[a] $^5D_0 \to {}^7F_2$ transition   [b] $^5D_4 \to {}^7F_5$ transition

The mean number of coordinated water molecules (n) for aqua ions and clathrochelates in aqueous solution and in the solid state was calculated from the excited-state lifetimes (Table 66).

The powder contains 0.5 and 0.3 water molecule per europium(III) clathrochelate molecule at 300 K and 4.2 K, respectively, and the quantum yields were calculated to be 0.56 and 0.65, respectively. These values practically coincide with the experimental data. The observed deviation of the quantum yield from 100% for this solid sample is caused by the presence of solvate water molecules [391]. The decrease in the luminescence quantum yield in aqueous solutions is also largely caused by an increase in the number of water molecules around the clathrochelate complex. Close to unity luminescence yield for terbium(III) clathrochelate powder may be attributed to the absence of water in this sample. The scheme of the light conversion process: *absorption – energy transfer – emission* (A–ET–E) is shown in Fig. 71.

A theoretical model of the energy-transfer process in clathrochelate [Eu(bpy.bpy.bpy)]$^{3+}$ and [Eu(bpy.bpy.bpy)]$^{3+}$·2 H$_2$O cations taking into account a ligand-to-metal charge transfer (LMCT) state was proposed in Ref. 379. This model includes the calculation of the molecular structure of the complexes and the ligand electronic structure as well as the ligand-lanthanide energy transfer and the temporal dependence of the populations of the ligand and the lanthanide ion; the quantum yield and the relative intensity of emission; the lifetime of the emitting state. The diagram of the most probable states involved in the ET process of the [Eu(bpy.bpy.bpy)]$^{3+}$ and [Eu(bpy.bpy.bpy)]$^{3+}$·2 H$_2$O cations is also discussed in Ref. 379.
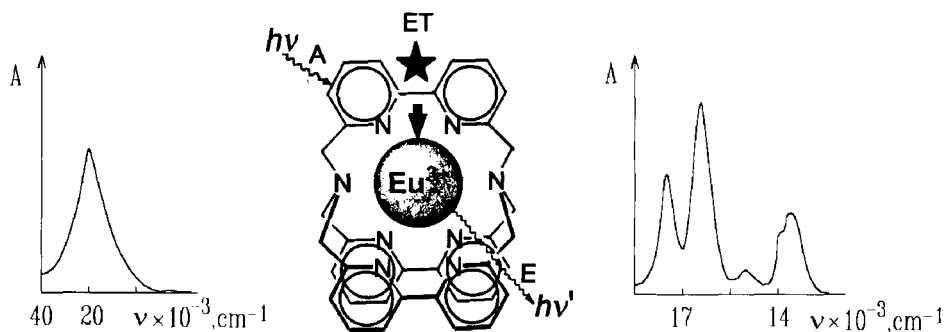
Fig. 71. The light conversion process: *absorbtion – energy transfer – emission* (A–ET–E) performed by the tris-bipyridine europium(III) clathrochelate [212].

The luminescence properties of macrobicyclic mixed bipyridine-bipyrazine and macrocyclic polybipyrazine europium(III) complexes were reported in Ref. 380. A noticeable enhancement in the lifetime and fluorescence quantum yield for the macrobicyclic $[Eu(bpy.bpy.bpz)]^{3+}$ cation was observed in comparison with other europium(III) clathrochelates and attributed to the introduction of the *bpz* fragment. Among the four studied europium(III) complexes, only the macrobicyclic one is stable in dilute aqueous solution [380].

5.3.4. Ruthenium complexes

The unique complication of ground- and excited-state properties of the macrobicyclic ruthenium(II) tris-bipyridinates is very useful for photochemistry. The prototype of these complexes is $[Ru(bpy)_3]^{2+}$ cation, which is used as a luminescent compound and sensitizer in photochemical processes [373, 374, 395-401]. Comparison with the requirements needed for photosensitizers and luminophores shows that the main disadvantages of $[Ru(bpy)_3]^{2+}$ cation are a relatively short excited-state lifetime, a small luminescence efficiency, and the occurrence of a photodestruction reaction [374]. The formation of cage structures, in which *bpy* fragments are cross-linked, should remove all these disadvantages. However, the cage ligand should allow the encapsulated ruthenium(II) ion to be in octahedral coordination with a suitable Ru–N bond distance. The macrobicyclic *bpy.bpy.bpy* ligand is too rigid to create the coordination required by ruthenium(II) ion. This is confirmed by the lack of luminescence of $[Ru(bpy.bpy.bpy)]^{2+}$ cation at room temperature. Molecular modelling showed that the cage cavity and the coordination polyhedron symmetry can be "tuned" using different capping groups [374].

The spectral characteristics of $[Ru(bpy.bpy.bpy)]^{2+}$ cation are quite similar to those of $[Ru(bpy)_3]^{2+}$ cation, but a longer excited-state lifetime and much larger stability toward ligand photosubstitution were observed. This should ensure a reasonably high turnover number when this clathrochelate is used as a photosensitizer [373, 374, 401].

The corresponding monocapped ruthenium(II) semiclathrochelate can be used to obtain dinuclear and trinuclear polypyridine clathrochelates with interesting photochemical properties [374, 400].

Chapter 6

Application possibilities of clathrochelate chemistry

Because of their unique redox properties (Chapter 5), clathrochelates have been applied to several interesting areas of investigation. The use of these compounds as electron transfer agents for the photocatalytic generation of hydrogen from water has been amply described in Refs. 4, 158, 340, 378, 384, 385, 402, and 403. The remarkable successes achieved in this field have demonstrated a lot of advantages of clathrochelates over available electron transfer agents (in particular, over methylviologen), such as high stability of the complexes in the reduced form, their photochemical stability in both oxidation states, and their stability toward hydrogenation and hydrogenolysis, as well as a lower platinum catalyst concentration compared with systems with methylviologen, to attain the same rate of hydrogen production. The high efficiency displayed by systems with macrobicyclic complexes also contributes to their attractiveness as electron transfer agents.

Disadvantages of clathrochelates include comparable rates of electron and energy transfers that imply higher concentrations of cobalt complexes for equivalent hydrogen production; light absorption in the visible region for cobalt complexes, which results in light filtering in the maximum of the absorption spectrum of the sensitizer; and shorter lifetimes of the excited states. The application of unsaturated and other types of clathrochelates to improve the electron-transfer rate constants in such systems is now under study.

With a platinum catalyst, methylviologen is undoubtedly a better electron transfer agent than macrobicyclic cobalt complexes. To the contrary, when colloidal Ru_2O_3 (5×10^{-5} mol·l^{-1}) deposited on silicon surface is employed as a catalyst, the rate of hydrogen production in the case of $[Co(Clsar)]^{3+}$ cation is 55 μmol·min^{-1}, whereas for methylviologen it is 11 μmol·min^{-1} under the same experimental conditions.

The oxidation of oxygen to hydrogen peroxide is one of the significant reactions in which macrobicyclic complexes can be used [94]. This reaction occurs as follows: anthraquinone is catalytically hydrogenated to form anthraquinol, which is oxidized by a macrobicyclic complex to yield anthraquinone and hydrogen peroxide. Such processes involve systems with hydrophobic organic solvents capable of dissolving anthraquinone and anthraquinol. The resultant hydrogen peroxide is isolated by aqueous extraction. This method for hydrogen peroxide production is profitable because the initial substance is regenerated in the course of reaction and the process may be cyclic provided the redox agent undergoes a reverse reaction and does not decompose. The procedure of the hydrogen peroxide production in which macrobicyclic rhodium, platinum, and cobalt complexes act as redox agents has been covered by a patent [94].

The unique luminescent properties of rare earth metal clathrochelates have been used in the development of luminescent materials (luminophores and laser materials). The luminescence of these clathrochelates in solution makes their application as biological probes and concentrators of the luminescence (i.e., the "antenna effect") promising. These complexes can also serve as efficient molecular devices to convert UV light absorbed by the ligand to lanthanide ion luminescence in the visible region. Even in very dilute (10^{-5} mol·l^{-1}) solutions, the conversion of irradiated photons to luminescent ones has been observed to occur at a rate of approximately 1%. For rare earth metal aqua ions at the same concentration, the efficiency of conversion is equal to 4×10^{-5} % [212, 390-392].

A still greater effect can be achieved if structural modifications, exhibiting more efficient central ion isolation and more efficient energy transfer from ligand to metal can be found (for example, as described in Ref. 380, the C_3-nonsymmetric clathrochelate [Eu(bpy.bpy.bpz)]$^{3+}$ cation demonstrated substantial increases in both lifetime and quantum yield compared with other complexes of this type).

The redox reactions of cobalt sarcophaginates with hemerythrin and cytochrome C have aroused particular interest for biochemists [316, 320, 404-406]. The kinetics of the redox reactions and relaxation dynamics of the clathrochelate cobalt tris-dioximates have been discussed in Refs. 407-409.

Optically active macrobicyclic complexes may be employed as chiral eluents for the separation of optically active anions (Section 5.1) and as chirality probes for biological objects [307, 310, 312].

The immobilization of the cage complexes on the surface through apical groups offers interesting application possibilities. This approach enables one to obtain ion-exchange resins especially selective for metal ions. The immobilized optically active cations allow one to obtain ion-exchange resins for the separation of optical isomers, such as racemic amino acids or optically active complexes.

When immobilized on polymer surfaces, cage complexes may be utilized for modifications of electrodes. The increase in the electron-transfer rate on such surfaces is governed by two factors: a high rate of electron transfer in cobalt clathrochelates and the regular disposition of these complexes on the surface. The properties of immobilized macrobicyclic complexes have been considered in Refs. 94, 410, and 411. Cyclic voltammetry has been used to characterize the incorporation of a range of structurally different d-metal sarcophaginates and sepulchrates into Nafion polymer [412].

An unusual clathrochelate species $\{[Na^+(bpy.bpy.bpy)]\cdot e^-\}^\bullet \cdot AN$ formed by electroreductive crystallization from [Na(bpy.bpy.bpy)]Br acetonitrile solution was characterized by X-ray crystallography [413].

The reduction of apical nitro substituents to amino groups is a precursor to the synthesis of a large variety of sarcophaginate complexes. The redox behaviour of these nitro substituents is very diverse and complexes with nitro radical anions, nitroso, hydroxylamine and amine substituents were obtained as primary products from such reductions, depending on the type of reductant, pH, solvent, and the amount of reductant supplied [414].

Cobalt(II,III) sepulchrates have been used in the chemical education [415] and considerable number of the chemical and physicochemical studies: as efficient quencher of the phosphorescence [416] and electronic excited states [417, 418], as a reductant in kinetic studies of redox reactions [419, 420], as a model for study of magnetodynamic [421], solvent [422] and pressure [423] effects on the outer-sphere electron-transfer reactions. Transfer chemical potentials (from solubility measurements) [424], electrochemical reduction potentials [425] and ligand-field parameters [426] for cobalt sepulchrates have been calculated. Solvent effect on ^{59}Co chemical shift of cobalt(III) ion encapsulated in the sepulchrate cavity [427]

and the influence of anions on the crystal structure of cobalt(III) sepulchrate have also been studied [428].

It was reported in Ref. 392 that rare earth metal clathrochelates are deposited onto porous glass. If the size of these complexes is slightly smaller than that of glass pores, they are anchored onto the glass surface through apical groups along the threefold axis perpendicular to the glass surface. Since such clathrochelates demonstrate intense luminescence, this can be useful in creating new luminescent materials.

The inplane packing of pillars in smectites as a function of relative pillar charge has been measured in Ref. 429 using $[Ir(diAMsar)]^{3+}$, $[Hg(diAMHsar)]^{4+}$, and $[Hg(diAMsar)]^{2+}$ cations.

An extremely selective synthesis reaction of the boron-capped macrobicyclic iron dioximates was proposed for the analysis and purification of extra-pure materials [54]. The extraction-photometric procedure reported for iron determination enables one to detect iron at a concentration down to 10^{-6} % and, additionally, to purify these materials. The extraction-photometric procedure is unaffected by the presence of other metal ions even in great amounts (from 10- to 100-fold excess).

The clathrochelate $[CoPcc(BF)]^+$ cation has been used as a paramagmetic phosphine shift reagent for the elucidation of the structures of transition metal complexes (in particular, (substituted-allyl)-palladium ones, Scheme 126) in solution [430, 431]. The resonance in the NMR spectra of the complexes obtained was assigned and applied to isomers and cyclic allyls identification. The reproducibility and transferability of NMR chemical shifts as well the

$R^1 \div R^5 = H$
$R^1 = R^2 = R^3 = R^4 = H, \ R^5 = CH_3$
$R^1 = R^2 = R^3 = R^5 = H, \ R^4 = CH_3$
$R^1 = R^2 = R^3 = H, \ R^4 = R^5 = CH_3$
$R^1 = R^3 = R^5 = H, \ R^2 = R^4 = CH_3$
$R^1 = R^2 = R^5 = H, \ R^3 = CH_3, \ R^4 = COCH_3$
$R^1 = R^2 = R^4 = H, \ R^3 = CH_3, \ R^5 = COCH_3$

Scheme 126

384
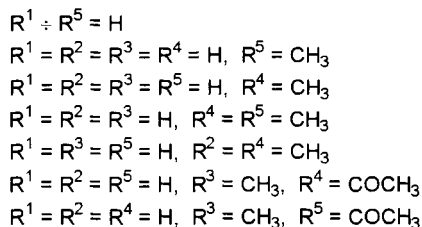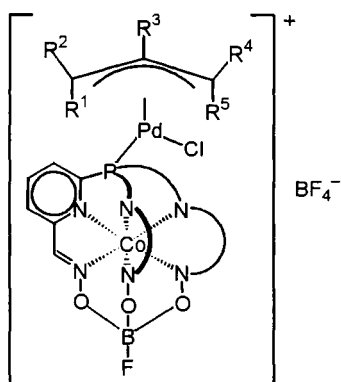
X, Y = CR^2, N, P, C-Z
Z = functionalizing group
R^2 = H, Hal, OH, NO_2, NO, NH_2,
  Alk, Ar, ArAlk, CN, COOR',
  COCOOR', $NHCOCH_2Br$,
  NHCOCH=CHCOOR'
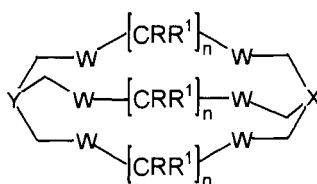
R^1 = H, Alk
W = NH, S, O
R, R^1 = H, CH_3, COOH,
  NO_2, CH_2OH, H_2PO_4,
  HSO_3, CN, $C=ONH_2$

Scheme 127

correlations of NMR data to structure in solution have also been discussed [430, 431].

The perspectives of the application of cage complexes with *sar*, *diAMsar*, and *AMcapten* ligands, modified by attaching peptides, cholestane, and paraffin tails, as detergents and their antiparasitic properties have been discussed in detail [6, 110, 141] as well as the ability of these ligands to capture transition metal ions in detoxifying biological systems [6]. The manganese(II) sarcophaginates are potentially interesting as imaging and therapeutic agents. The intercalation and electrostatic binding to DNA of aromatic-substituted sarcophaginates (e.g. anthracenyl-containing), bis- and tris-sarcophaginates are also described in Ref. 6.

The functionalized macrobicyclic compounds (Scheme 127) have also been proposed for the diagnosis and therapy of a disease [432]. These compounds are capable of being radiolabeled. For example, the 1-(4-aminophenylmethylamino)-8-aminosarcophagine was incubated with an antibody and then the immunoconjugate obtained was complexed with $^{64/67}Cu^{2+}$ ions. The biodistribution of this complex has also been studied [432].

Prospective use of ruthenium(II) clathrochelates includes use as luminescent probes and DNA-cleaving agents, combining a high specificity of intercalation with DNA sites and an opportunity for easy chemical modification of the conjugate. Easy and directed functionalization of reactive clathrochelates (see Chapter 2) and kinetic control of their destruction in various media gives one an opportunity for prolonged and controllable input of the metal ions (including radioactivity) in a desired type of cells.

Chapter 7

New types of clathrochelates: perspectives of synthesis

Among the diverse possible strategies for the synthesis of compounds with an encapsulated metal ion, the most promising, in our opinion, are those that can be implemented the soonest.

7.1. RIBBED-FUNCTIONALIZED *d*-METAL TRIS-DIOXIMATES

The synthesis of mono- and trisubstituted ribbed-functionalized *d*-metal tris-dioximates starting from the initial monohalogen-dioximes can be realized by Scheme 128. An alternative pathway of halogenation of the monosubstituted glyoxime derivatives is complicated because of side reactions of the clathrochelate framework destruction and halogenation of the substituents in α-dioximate fragments and at the boron atom, as well as by the fact that the products of partial halogenation (in the case of trisubstituted clathrochelates) may predominate.

Attempts to implement the solid-phase synthesis of *mer*-isomers of trihalogenide precursors on the element-oxide matrix surface seem to be promising with allowance for the fact that monohalogendioximes demonstrate the drastically different affinities for the surface their alkyl-, aryloxime, and halogenoxime groups (Scheme 129).

The mono- and trihalogendioximate precursors can readily be functionalized by nucleophilic substitution reactions (Scheme 128).

Monoribbed-functionalized C_3-nonsymmetric diamino- and dithioclathrochelates can be prepared starting from the dichloride precursor by Scheme 130. The complexing capabilities of such clathrochelates as *cis*-ligands should first be studied with respect to Pt^{2+} and Pd^{2+} ions. In this case, both 1:1 and 2:1 complexes can be isolated (Scheme 130).

R^1, R^2 = C_6H_5, CH_3;   R = F, n-C_4H_9, C_6H_5; M^{n+} = Fe, Ru(II), Co(II,III)

R^3 = –SAlk, –S—⟨C₆H₅⟩, –NH—(CH₂)₄—NH₂, –NH—CH₂CH₂—OH, –O—⟨C₆H₅⟩, –N⟨

Scheme 128

R^2 = H, CH$_3$, C$_6$H$_5$
X, Y = Lewis acid

Scheme 129

R = C$_6$H$_5$, F, n-C$_4$H$_9$
R^1 = Alk, Ar, H
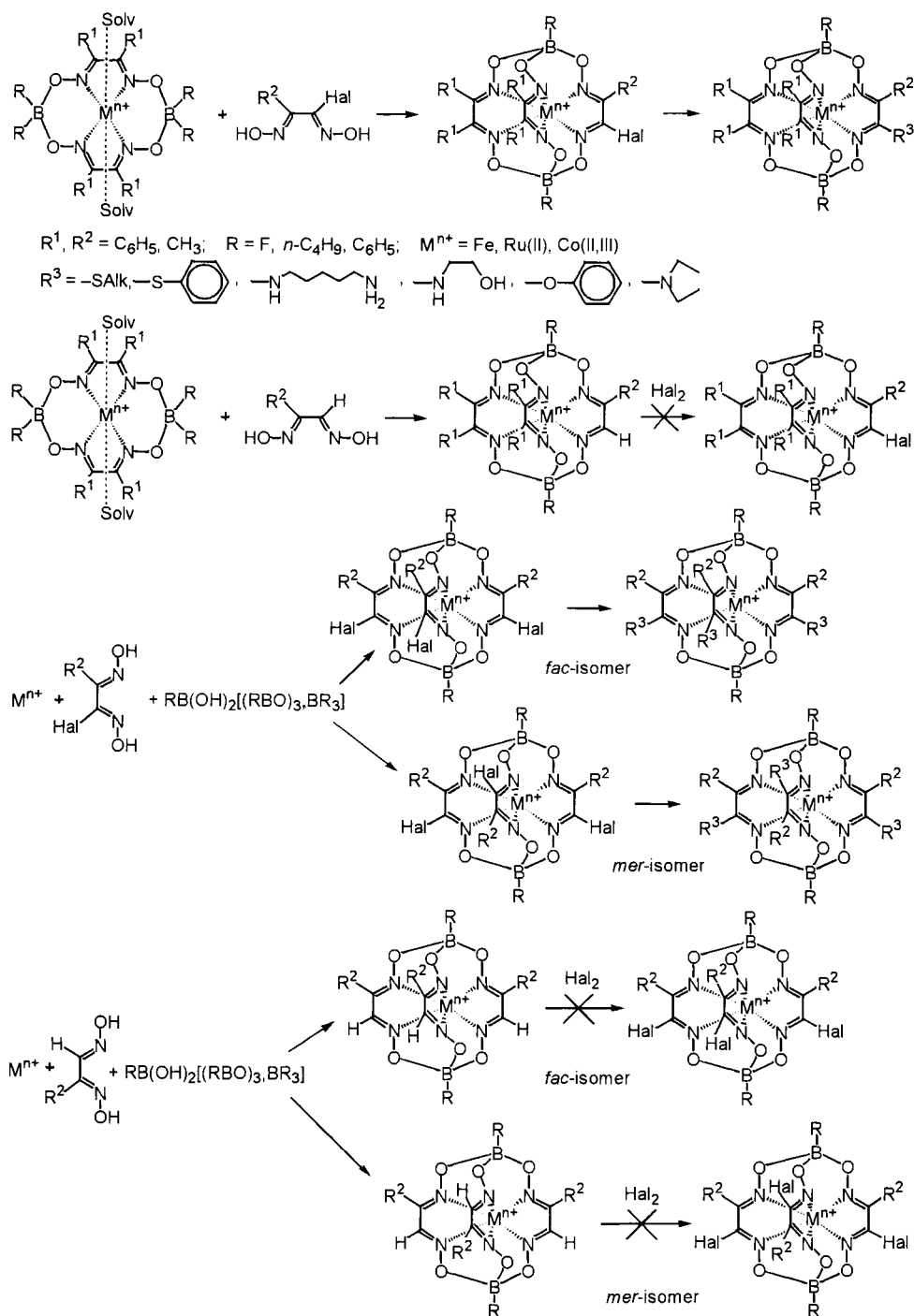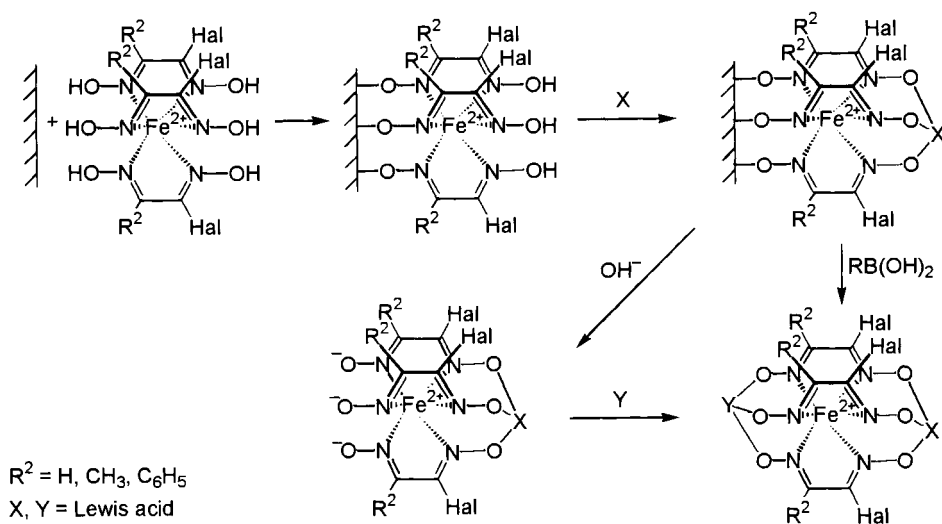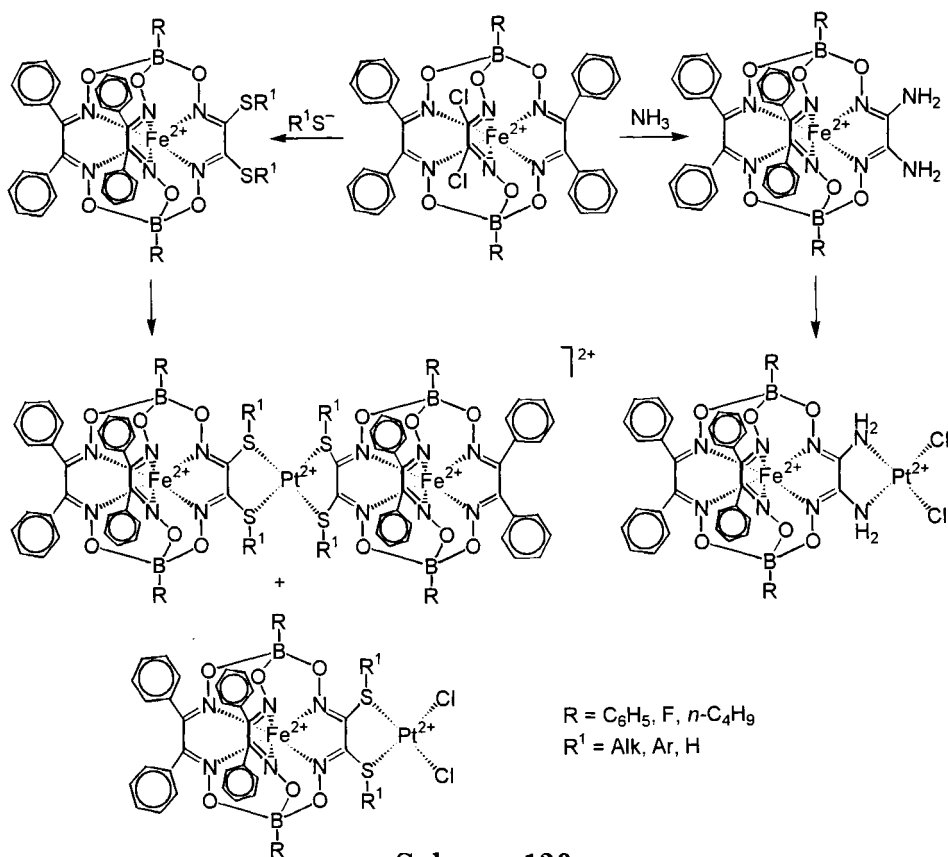
Scheme 130

The synthesis of thiocrown ether clathrochelates can be implemented both by a direct template reaction on an appropriate metal ion (for instance, in the presence of Cd^{2+} ions) and by a stepwise procedure, as shown in Scheme 131.

The hexachloride cobalt(II) tris-dioximates resulting from a direct template reaction have proved to be suitable precursors for the synthesis of triribbed-functionalized cobalt clathrochelates in different oxidation states. The reduction of these precursors can lead to the formation of cobalt(I) clathrochelates, the stability of which is accounted for by the effect of six acceptor chloride substituents in the clathrochelate framework.

The nucleophilic substitution reactions of reactive chlorine atoms in hexachloride cobalt precursors in the presence or absence of an oxidizing agent can be employed to obtain the thioalkyl, thioaryl,
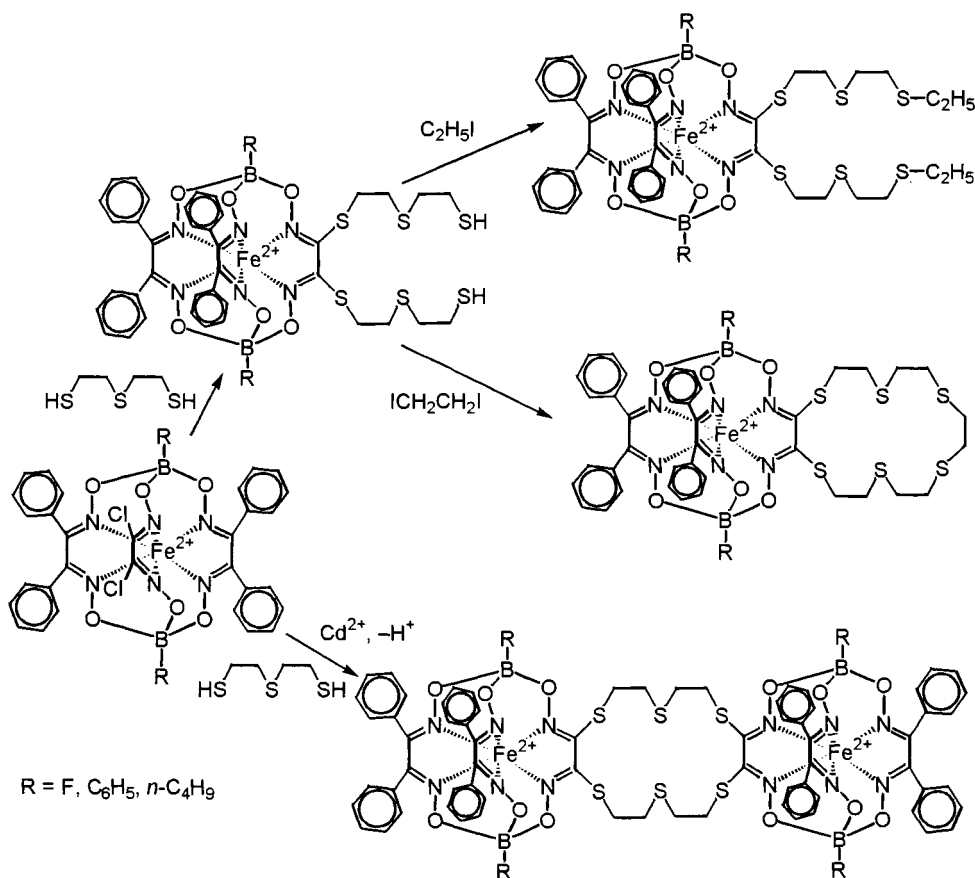
Scheme 131

amine, and aroyl cobalt(III) and cobalt(II) clathrochelates, respectively (Scheme 132).

Ribbed-functionalized clathrochelates with a TAP geometry can be obtained starting from the tin-, germanium-, and antimony-capped chloride precursors (Scheme 133).

Scheme 132

R^1 = NHAlk, NAlk$_2$, SAlk, SAr, OAr
R^2 = C$_6$H$_5$, CH$_3$

Q = SnHal$_3$, SbAlk$_3$, SbAr$_3$, Ge(CF$_3$)$_3$
M^{n+} = Fe, Ru(II), Co(II,III)
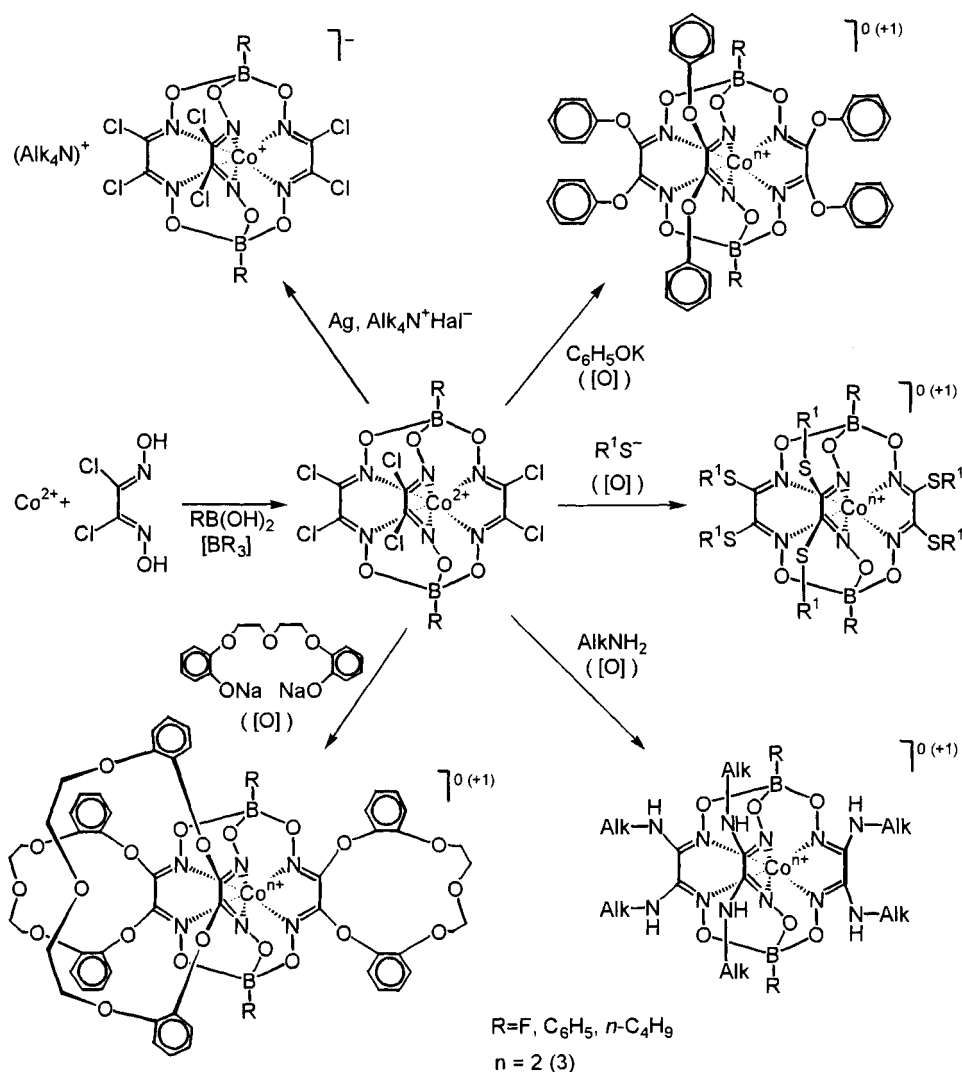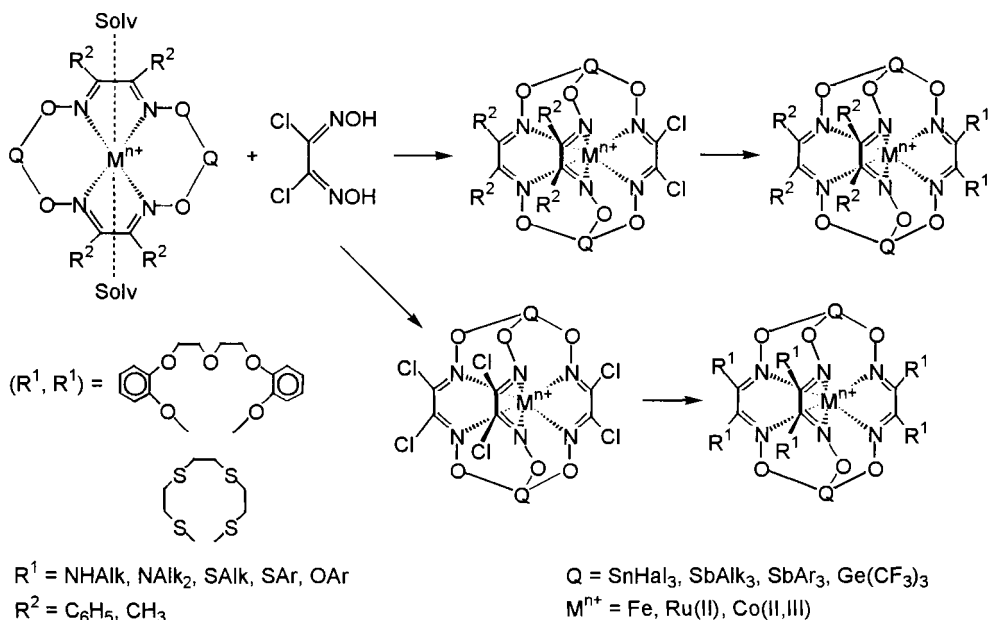
Scheme 133

7.2. MONONUCLEAR AND POLYNUCLEAR α-DIOXIMATES AND α-OXIMEHYDRAZONATES OBTAINED BY CAPPING WITH SEVERAL *p*-BLOCK ELEMENTS (ARSENIC, BISMUTH, AND SOME OTHERS), *d*- AND *f*-ELEMENTS

In many cases the possibility of the synthesis of such complexes are limited by their tendency to form polymers. Therefore, with tris-dioximate compounds, the methods involving the protection of one of the two triangular bases formed by the three oxygen atoms of three dioximate fragments are thought to be the most promising. As described above, the protection can be implemented by functiona-lization of one of the two oxime groups of the initial α-dioxime or by immobilizing of the tris-complex on the sorbent surface (see Chapter 2, Scheme 11). The subsequent capping with a Lewis acid makes it possible to obtain a semiclathrochelate complex that can readily be cross-linked with *p*-element (arsenic, bismuth, and others) compounds (Lewis acids). In these cases both mono- and binuclear clathrochelates (Scheme 88) can be formed [433].
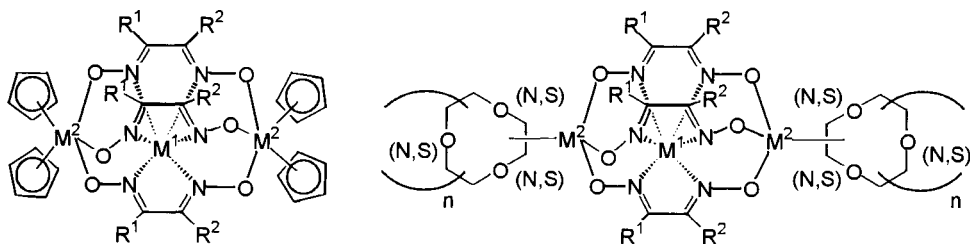
Scheme 134
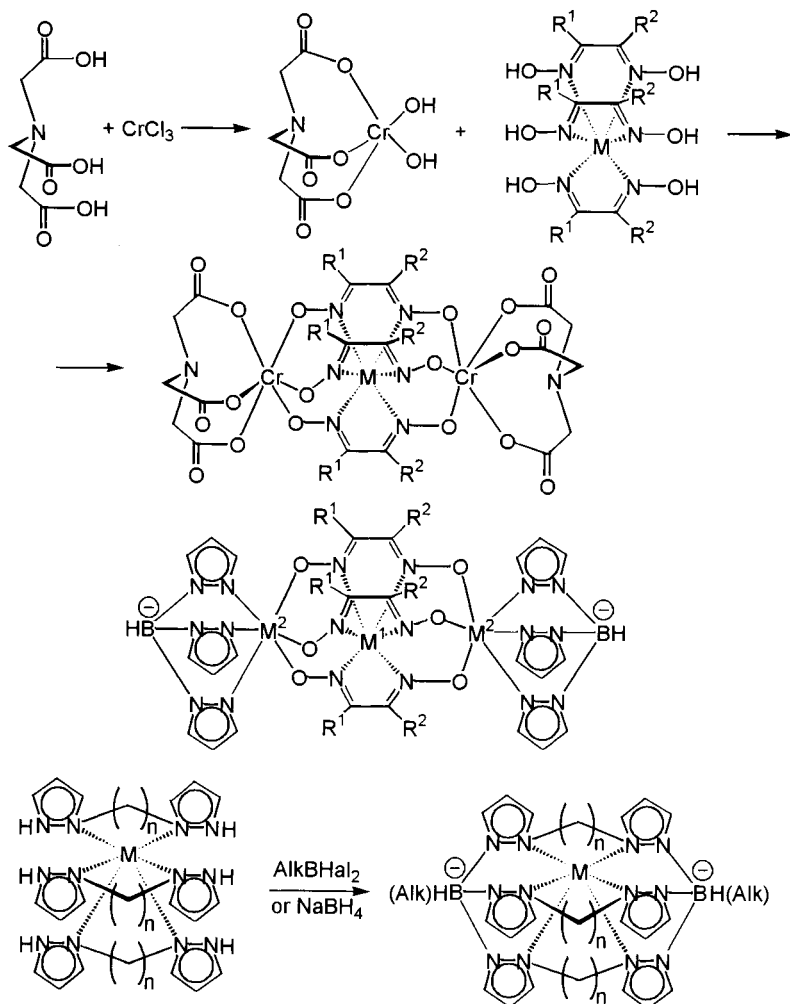
Scheme 135

An alternative method allows one to obtain mononuclear compounds with p-, d- and f-elements as caps using their organyls or coordinately unsaturated complexes as capping agents. The use of metallocenes and p-, d-, and f-metal coordinately-unsaturated crown ether and polythioazamacrocyclic complexes is thought to be especially promising (Scheme 134).

Tripodal coordinating systems of the atrane and tris-pyrazolborate types seem to be rather attractive as initial semi-clathrochelate precursors or cross-linking agents (Scheme 135). The former are thought to be very promising for the encapsulation of d-metal ions, displaying a high affinity to donor nitrogen atoms. In this case, ions larger than those in the case of tris-dioximates can be encapsulated [433].

Mixed polyclathrochelate α-dioximato-oximehydrazonates can be obtained from the initial mononuclear complexes by Scheme 136.

Bi- and trinucleating azineoxime tetra- and hexadentate ligands have generally been synthesized preliminarily (see Chapter 2), though in several cases, their stepwise construction can be used until the desired structure is obtained (Schemes 87 and 137). In the latter case, the initial mononuclear complex undergoes a template condensation to give a binucleating semiclathrochelate, capable of encapsulating the second metal ion followed by capping. This stepwise formation allows one to obtain not only heteronuclear compounds but also complexes with a vacant cavity, which are
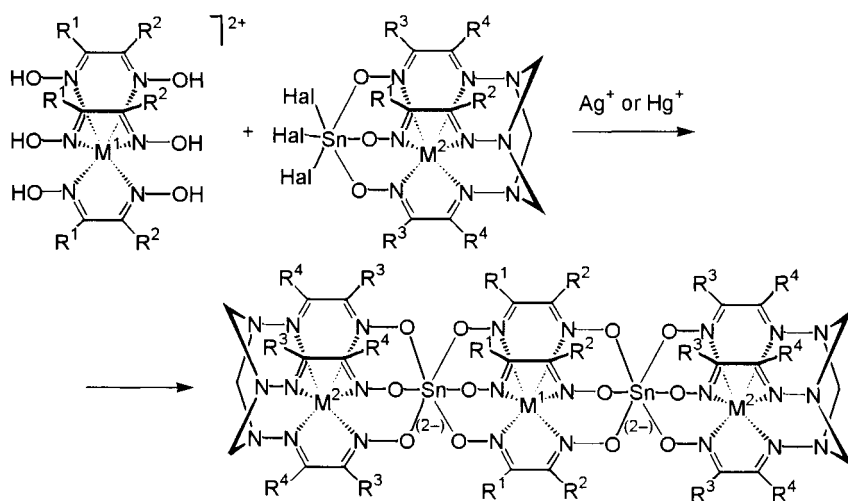
Scheme 136
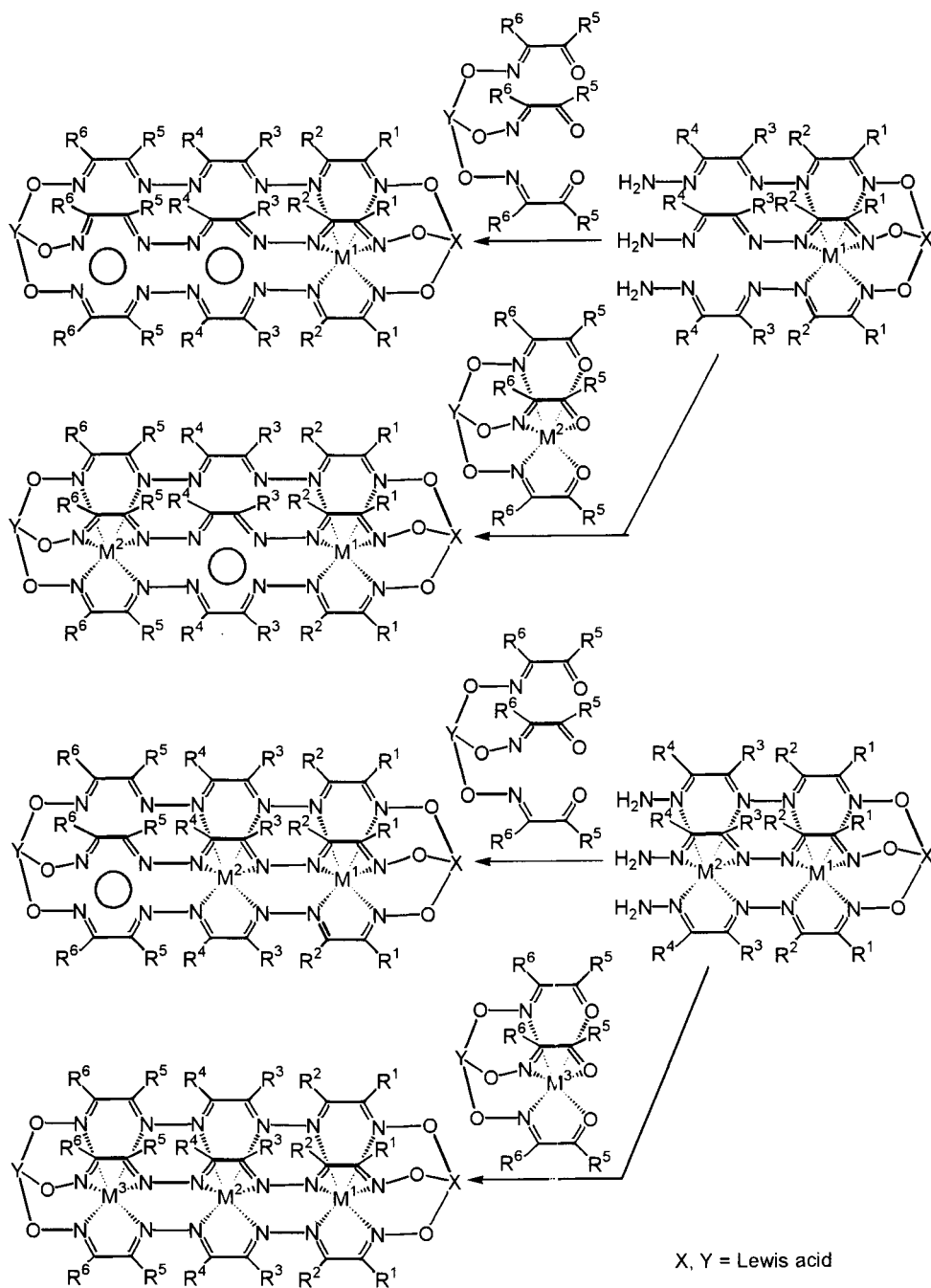
Scheme 137
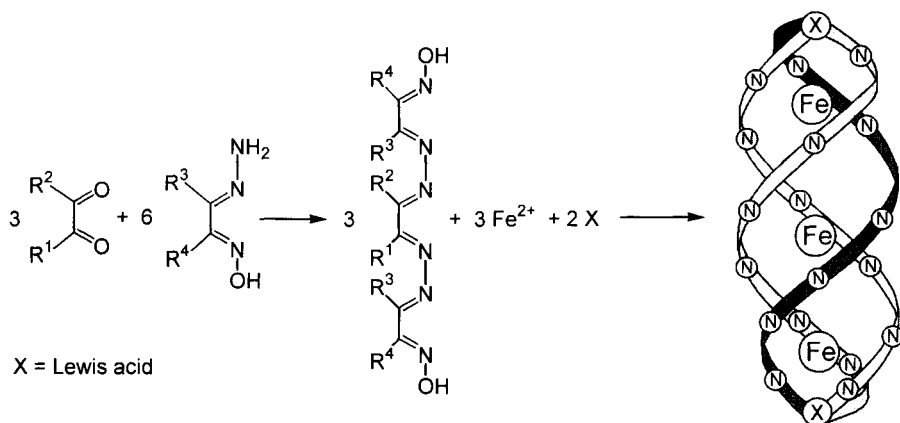
Scheme 138

attractive as potential molecular switches. In the case of nonsymmetric azineoxime ligands, a stepwise approach allows one to isolate sole *fac-* or *mer-*isomer instead of their mixture. Binuclear and trinuclear clathrochelates can be obtained starting from the initial tetra- and hexadentate ligands by the main pathways employed for the synthesis of such types of compounds: direct template condensation on the metal ion, capping of the initial nonmacrocyclic tris-complex, the capping group substitution reaction, and modification of ligand peripheral substituents.

In particular, starting from the potentially hexadentate azineoxime ligands, one can synthesize trinuclear clathrochelates possessing a triple helix geometry (Scheme 138).

7.3. MACROBICYCLIC SCHIFF BASES FORMED BY CAPPING WITH LEWIS ACIDS

The template condensation of tripodal amines or carbonyls with ketoximes and aminoximes, respectively, in the presence of alkaline-earth metal ions is assumed to be the most obvious pathway for the synthesis of semiclathrochelate oxime-containing ligands capable of coordinating transition metal ions followed by capping with Lewis acids (Scheme 139).

A rigid dihydrazinophthalazine ligand may turn out to be a fairly selective precursor of binuclear clathrochelates (Scheme 140).

Substituted and unsubstituted mono- and dihydrazones, as well as their tetradentate analogs, can interact on the metal ion with tripodal
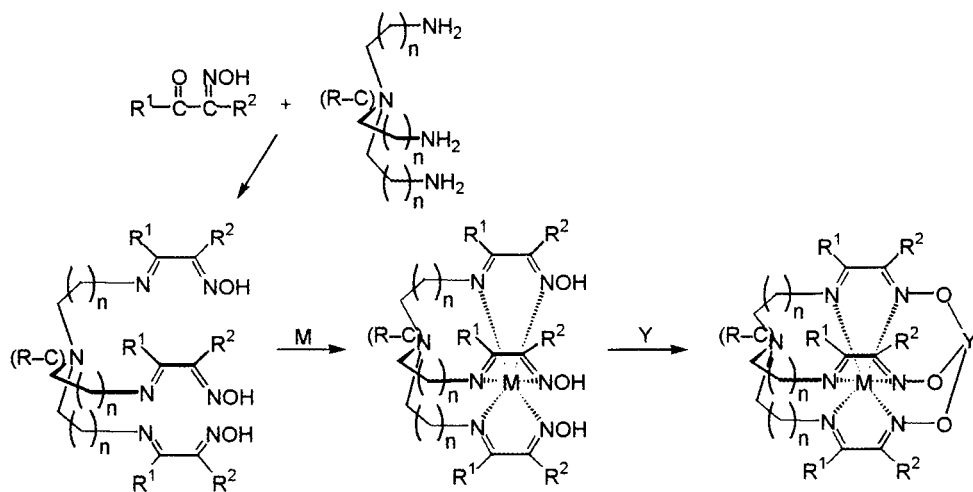
Scheme 139
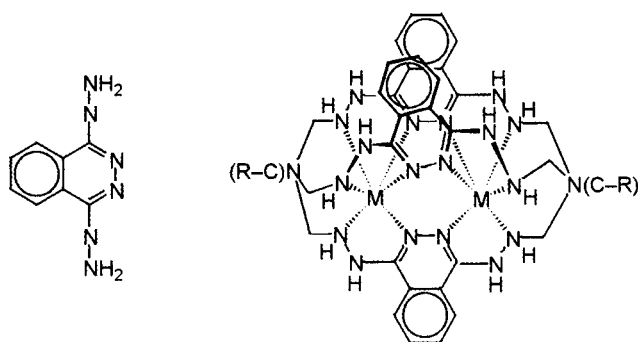
Scheme 140
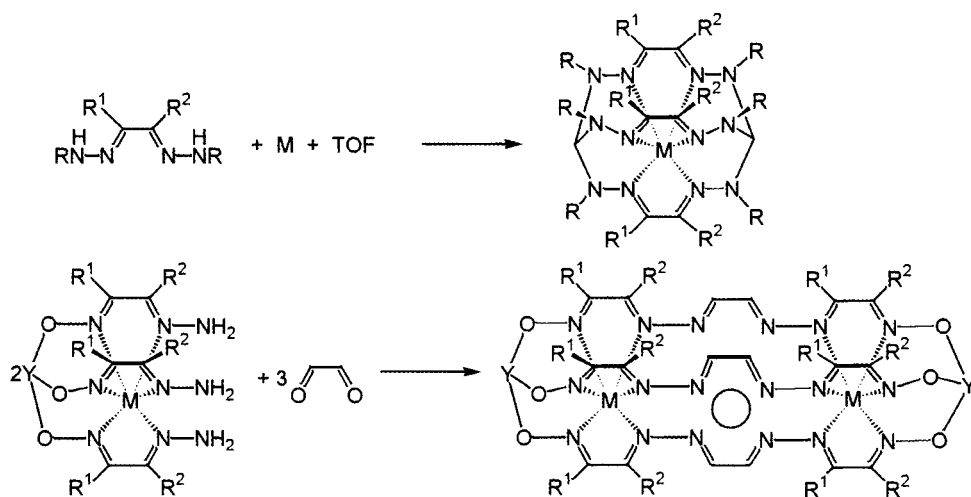
Scheme 141

cross-linking agents of the triethyl orthoformate type and with active dicarbonyl compounds of the glyoxal type to yield mono- and binuclear trinucleating compounds (in the latter case, with a vacant cavity), respectively, Scheme 141) [433].

7.4. CLATHROCHELATE COMPLEXES FORMED BY THE ANALOGS OF α-DIOXIMES AND α-OXIMEHYDRAZONES

Polynuclear clathrochelate hydrazonates can be synthesized by the same reaction pathways as those described for oximehydrazonates (Schemes 88 and 137) using formaldehyde, triethyl orthoformate, chloral, and others as cross-linking agents. Scheme 142 represents the formation of a binuclear double-decker complex.

The α-azadioximines, being in a tautomeric equilibrium with N-nitrozoamidoximes, have proved to be analogs of α-dioximes:

(168)

The expected macrobicyclic ligands with a contracted cavity and high delocalizing ability can stabilize metal ions in the high oxidation states. In this case, one should expect the formation of a mixture of *fac*- and *mer*-isomers because of the initial ligand C_2-nonsymmetry.

The mixed pyrazoloxime ligands can also form clathrochelates by Scheme 143 [433].

The hydrophosphoryl ligands have coordination properties similar to those of oximes and form the stable complexes represented in Scheme 144. This Scheme shows the pathway of synthesis of the phosphorus-containing analogs of clathrochelate tris-dioximates.
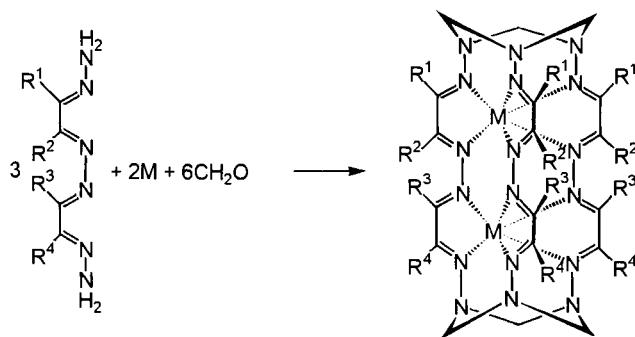
Scheme 142
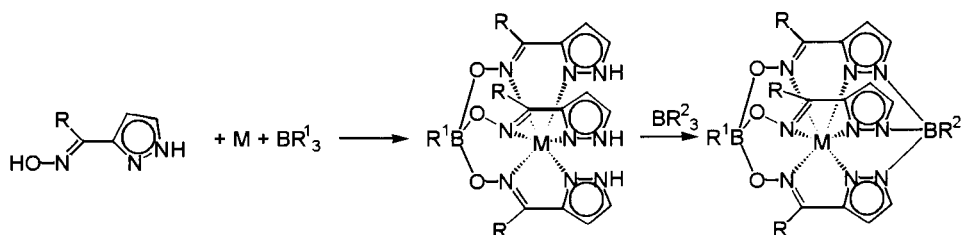
Scheme 143
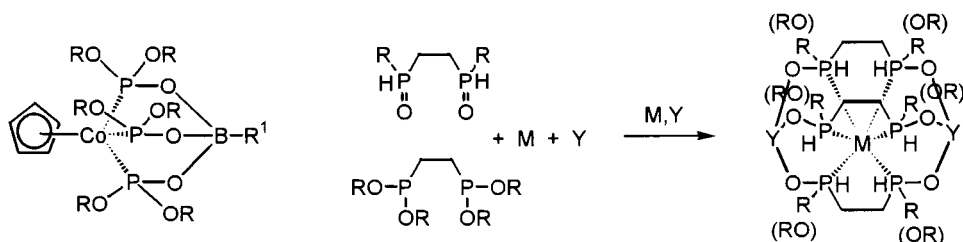
Scheme 144

The 1,3-dioximes have proved to be not quite successful complexing agents owing to a lack of conjugation between the azomethine fragments and the ease of their rearrangement to aromatic oxazoline. The sulphur-containing 1,3-dioximes that are apt to encapsulate metal ions with big size, as well as 2-butyne-1,4-dioximes and cyclopropane derivatives (Scheme 145), may prove to be more promising.

Adamantanetriontrioxime may be regarded as an analog of tripodal amines in the synthesis of macrobicyclic Schiff bases and is promising in the formation of rigid clathrochelates with expanded cavity (Scheme 146).

Dicarboxylic compounds with orientation of substituents, suitable for cross-linking with Lewis acids, have significant potential in the synthesis of the clathrochelate complexes with encapsulated metal ions, being Pearson's hard acids and preferring coordination with oxygen atoms (Scheme 147).

Scheme 148 represents feasible routes for the formation of several tetra- and pentacoordinate clathrochelate complexes. Such ligands are essential in complexing metal ions, in particular cooper and zinc(II) ions, that form stable tetragonal and square-pyramidal complexes.
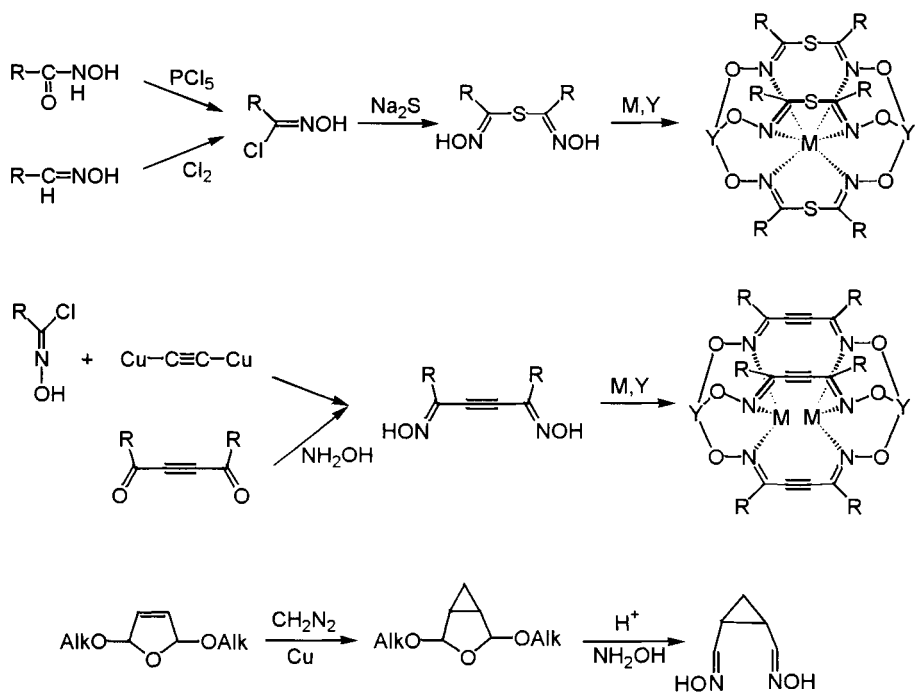
Scheme 145
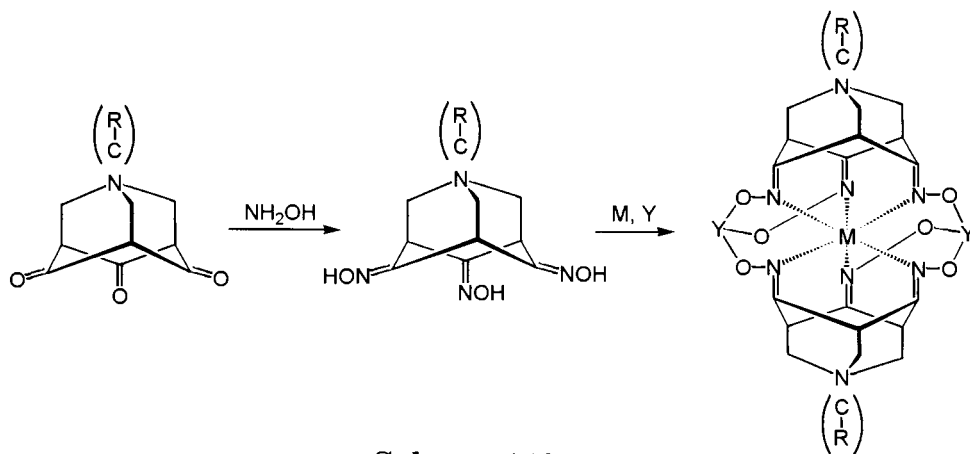
Scheme 146

Scheme 147

Z = halogen,
N(CH₃)₂, OCH₃
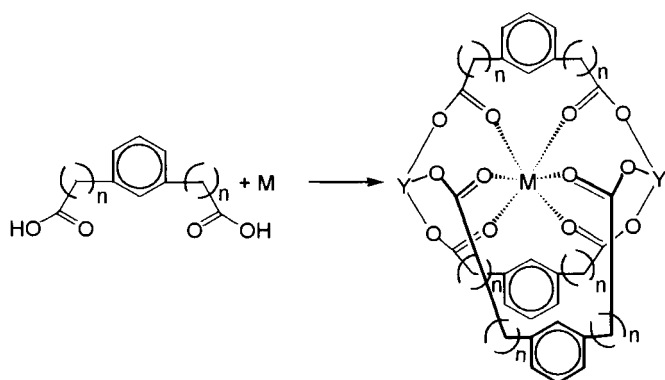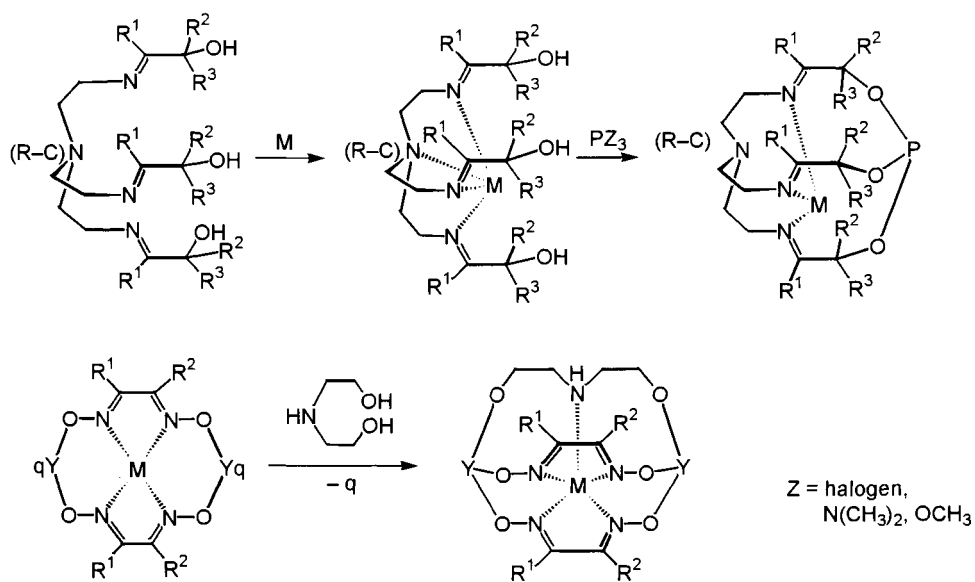
Scheme 148

7.5. SUPERCLATHROCHELATE STRUCTURES

Compounds **1** and **2**, represented in Scheme 149, contain a second "shell" that completely excludes the extrusion of the metal ion without rupture of the clathrochelate framework and enforces a cage by additional covalent bonds. The first ligand of this type with a partially formed "secondary" structure was synthesized (see Chapter 2, Scheme 73). In this case, the encapsulated metal ion, exerting no influence on the number of physical characteristics of the complex such as solubility, volatility, and others, can be regarded only as the matrix that forms the macropolycyclic system [433].
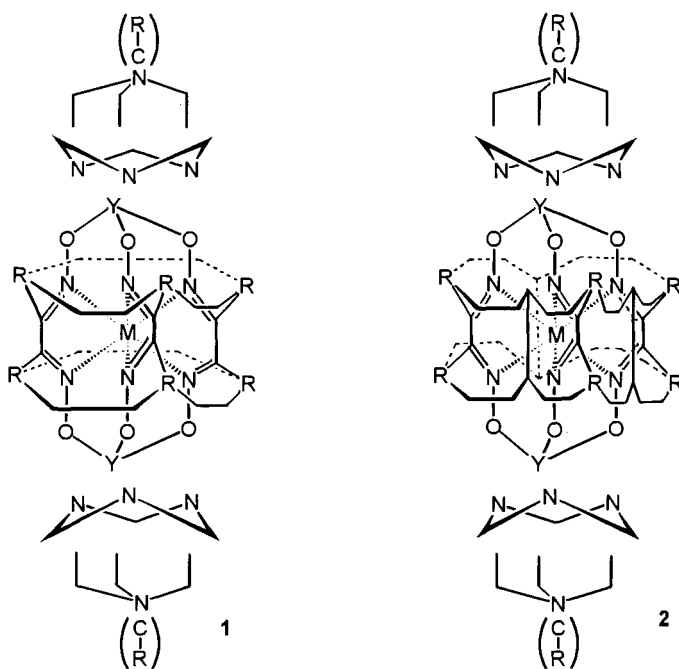
Scheme 149

References

[1]   D.H. Busch, Rec. Chem. Progr., 25 (1964) 107.

[2]   D.R. Boston and N.J. Rose, J. Am. Chem. Soc., 90 (1968) 6859.

[3]   A.M. Sargeson, Chem. Brit., 15 (1979) 23.

[4]   A.M. Sargeson, Pure Appl. Chem., 56 (1984) 1603.

[5]   A.M. Sargeson, Ibid., 58 (1986) 1511.

[6]   A.M. Sargeson, Coord. Chem. Rev. 151 (1996) 89.

[7]   G.W. Gokel and S.H. Korzeniowski, Macrocyclic Polyether Chemistry, Springer Verlag, Berlin, 1982.

[8]   Synthesis of Macrocycles. The Design of Selective Complexing Agents / Ed. by R.M.Izatt and J.J.Christensen, Wiley-Interscience, New York, 1987.

[9]   Coordination Chemistry of Macrocyclic Compounds / Ed. by G.A. Melson, Plenum Press, New York, 1980.

[10]   K.B. Yatsimirskii and Y.D. Lampeka. Physicochemistry of Metal Complexes with Macrocyclic Ligands, Naukova Dumka, Kiev, 1985.

[11]   K.B. Yatsimirskii, A.G. Kolchinskii, V.V. Pavlischuk and G.G. Talanova. Synthesis of Macrocyclic Compounds. Naukova Dumka, Kiev, 1987.

[12]   M.Hiraoka. Crown Compounds: Their Characteristics and Applications, Elsevier, Amsterdam, 1982.

[13]   Host-Guest Complex Chemistry: Macrocycles. Synthesis, Structures, Application / Ed. by F.Vögtle and E. Weber, Springer Verlag, Heidelberg, 1985.

[14]   G.W. Gokel, Crown Ethers and Cryptands, The Royal Society of Chemistry, Cambridge, 1991.

[15]   Macrocycle Synthesis: A Practical Approach / Ed. by D. Parker, Oxford University Press, Oxford, 1996.

[16]   J.-M. Lehn, Supramolecular Chemistry, VCH, Weinheim, 1995.

[17]   N.V. Gerbeleu, V.B. Arion and F.J. Burgess, Template Synthesis of Macrocyclic Compounds, Wiley-VCH, Weinheim, 2000.

[18]   N.A. Kostromina, Y.Z. Voloshin and A.Y. Nazarenko, Clathrochelates: Synthesis, Structure, Properties, Naukova Dumka, Kiev, 1992.

[19]   D.H. Busch, Chem.Rev., 93 (1993) 847.

[20]   V.L. Goedken, P.H. Merell and D.H. Busch, J. Am. Chem. Soc., 94 (1972) 3397.

[21]   Y.Z. Voloshin, Dr. Sc.(Prof.) Thesis, Institute of Solution, Ivanovo, 1993.

[22]   B. Dietrich, M.W. Hosseini, J.-M. Lehn and R.B. Sessions, Helv. Chim. Acta, 68 (1985) 289.

[23]   H. Christopherson and E.B. Sandell, Anal. Chim. Acta, 10 (1954) 1.

[24]   G.N. Schrayzer, Chem.Ber., (1962)1438.

402

[25] F. Umland and D. Thierig, Angew. Chem., 74 (1962) 388.
[26] F. Umland and D. Thierig, Z. Anal. Chem., 197 (1963) 151.
[27] J. Chakrabarty and B. Sahoo, Indian J. Chem. A., 21 (1982) 48.
[28] W. Fedder, H.G. von Schnering and F. Umland, Z. Anorg. Allg. Chem., 382 (1971) 123.
[29] J. Chakrabarty, K.B. Naik and B. Sahoo, Indian J. Chem., A21 (1982) 370.
[30] W. Fedder, F. Umland and E. Hohaus, Monatsheft. Chem., 111 (1980) 971.
[31] W. Fedder, F. Umland and E. Hohaus, Z. Anorg. Allg. Chem., 471 (1980) 77.
[32] D. Dorn, D. Linke and E. Uhlig, Ibid., 468 (1980) 153.
[32] M.L. Bowers and C.L. Hill, Inorg. Chim. Acta, 72 (1983) 149.
[34] J. Chakrabarty, K.B. Naik and B. Sahoo, Indian J. Chem., A21 (1982) 1103.
[35] D.W. Thompson and D.V. Stynes, Inorg. Chem., 29 (1990) 3815.
[36] D.V. Stynes, D.B. Leznoff and D.G.A. Harshani de Silva, Inorg. Chem., 32 (1993) 3989.
[37] A.S. Abushamleh and M.M. El-Abadelah, J. Chem. Soc. Pak., 22 (2000) 293.
[38] F. Umland, W. Fedder, H.G. von Schnering and D. Thierig, Proc.of 12th Intern.Conf.Coord. Chem. Sydney, (1969) 46.
[39] D.R. Boston and N.J. Rose, J. Am. Chem. Soc., 95 (1973) 4163.
[40] S.C. Jackels, J. Zektzer and N.J. Rose, Inorg. Synth., 17 (1978) 139.
[41] D. Borchardt and S. Wherland, Inorg. Chem., 25 (1986) 901.
[42] Y.Z. Voloshin, N.A. Kostromina and A.Y. Nazarenko, Teor. Eksp. Khim., 26 (1990) 375.
[43] M.A. Murguia, D. Borchardt and S. Wherland, Inorg. Chem., 29 (1990) 1982.
[44] Y.Z. Voloshin and V.V. Trachevskii, J. Coord. Chem., 31 (1994) 147.
[45] Y.Z. Voloshin, V.K. Belsky and V.V. Trachevskii, Polyhedron, 11 (1992) 1939.
[46] R.S. Drago and J.H.Elias, J. Am. Chem. Soc., 99 (1977) 6570.
[47] S.C. Jackels and N.J. Rose, Inorg. Chem., 12 (1972) 1232.
[48] S.C. Jackels, D.S. Dierdorf and N.J. Rose, J. Chem. Soc., Chem. Commun., (1972) 1291.
[49] A.Y. Nazarenko and Y.Z. Voloshin, Zh. Neorg. Khim., 28 (1984) 1776.
[50] Y.Z. Voloshin, A.Y. Nazarenko and V.V. Trachevskii, Ukr. Khim. Zh., 51 (1985) 121.
[51] H.C. Rai, A.K. Jena and B.Sahoo, Inorg. Chim. Acta, 35, (1979) 29.
[52] M.K. Robbins, D.W. Naser, J.L. Heiland and J.J. Grzybowski, Inorg. Chem., 24 (1985) 3381.
[53] M. Verhage, G.A. Hoogwater and H. van Bekkum, Rec. trav. chim. Pays-Bas, 101 (1982) 351.
[54] A.Y. Nazarenko and Y.Z. Voloshin, Zh. Anal. Khim., 37 (1982) 1469.
[55] Y.Z. Voloshin. Ph.D. Thesis, Institute of Generale and Inorganic Chemistry, Kiev, 1988.
[56] Y.Z. Voloshin, N.A. Kostromina and A.Y. Nazarenko, Inorg. Chim. Acta, 170 (1990) 181.
[57] J.N. Johnson and N.J. Rose, Inorg. Synth., 21 (1982) 112.
[58] J.J. Grzybowski, Inorg. Chem., 24 (1985) 1125.
[59] Y.Z. Voloshin, A.Y. Nazarenko, E.V. Polshin, S.I. Tyukhtenko and N.A. Kostromina, Teor. Eksp. Khim., 25 (1989) 382.

[60] Y.Z. Voloshin, N.A. Kostromina, A.Y. Nazarenko and E.V. Polshin, Ukr. Khim. Zh., 55 (1989) 7.

[61] Y.Z. Voloshin, N.A. Kostromina, A.Y. Nazarenko, and V.N. Shuman, Ibid., 56 (1990) 443.

[62] Y.Z. Voloshin, N.A. Kostromina and A.Y. Nazarenko, Ibid., 56 (1990) 451.

[63] S.V. Lindeman, Y.Z. Voloshin and Y.T Struchkov, Koord. Khim., 18 (1990) 1367.

[64] Y.Z. Voloshin, O.A. Varzatskii, A.V. Palchik, E.V. Polshin, Y.A. Maletin and N.G. Strizhakova, Polyhedron, 17 (1998) 4315.

[65] Y.Z. Voloshin, O.A. Varzatskii, T.E. Kron, V.K. Belsky, V.E. Zavodnik, and A.V. Palchik, Inorg. Chem., 39 (2000) 1907.

[66] Y.Z. Voloshin, T.E. Kron, V.K. Belsky, V.E. Zavodnik, Y.A. Maletin and S.G. Kozachkov, J. Organomet. Chem., 536/537 (1997) 207.

[67] Y.Z. Voloshin, O.A. Varzatskii, A.I. Stash, V.K. Belsky, Y.N. Bubnov, I.I. Vorontsov, K.A. Potekhin, M.Y. Antipin, and E.V. Polshin, Polyhedron 20 (2001) 2721.

[68] Y.Z. Voloshin, V.E. Zavodnik, O.A. Varzatskii, V.K. Belsky, A.V. Palchik, N.G. Strizhakova, I.I. Vorontsov and M.Y. Antipin, J. Chem. Soc., Dalton Trans., (2002) 1193.

[69] Y.Z. Voloshin, V.E. Zavodnik, O.A. Varzatskii, V.K. Belsky, I.I. Vorontsov and M.Y. Antipin, Inorg. Chim. Acta, 321 (2001) 116.

[70] Y.Z. Voloshin, V.V. Trachevskii and E. V. Polshin, Polish J. Chem., 71 (1997) 428.

[71] Y.Z. Voloshin, N.A. Kostromina, A.Y. Nazarenko and E.V. Polshin, Inorg. Chim. Acta, 185 (1991) 83.

[72] Y.Z. Voloshin and E.V. Polshin, Polyhedron, 11 (1992) 457.

[73] Y.Z. Voloshin, O.A. Varzatskii, N.G. Strizhakova and E.Y. Tkachenko, Inorg.Chim. Acta, 299 (2000) 104.

[74] Y.Z. Voloshin, O.A. Varzatskii, S.V. Korobko and Y.A. Maletin, Inorg. Chem. Commun., 1 (1998) 328.

[75] Y.Z. Voloshin, O.A. Varzatskii, S.V. Korobko, M.Yu. Antipin, I.I. Vorontsov, K.A. Lysenko, D.I. Kochubey, S.G. Nikitenko and N.G. Strizhakova, J. Chem. Soc., Dalton Trans., submitted.

[76] J.G. Muller, J.J. Grzybowski and K.J. Takeuchi, Inorg. Chem., 25 (1986) 2665.

[77] J.G. Muller, K.J. Takeuchi and J.J. Grzybowski, Polyhedron, 8 (1989) 1391.

[78] Y.Z. Voloshin, O.A. Varzatskii, T.E. Kron, V.K. Belsky, V.E. Zavodnik, N.G. Strizhakova, V.A. Nadtochenko and V.A. Smirnov, J. Chem. Soc., Dalton Trans., (2002) 1203.

[79] P. Chaudhuri, M. Winter, P. Fleischhauer, W. Haase, U. Flörke and H.-J. Haupt, J. Chem. Soc., Chem. Commun., (1990) 1728.

[80] P. Chaudhuri, M. Winter, B.P.C. Della Védova, P. Fleischhauer, W. Haase, U. Flörke and H-J. Haupt, Inorg. Chem., 30 (1991) 4777.

[81] P. Chaudhuri, M. Winter, F.Birkelbach, P. Fleischhauer, W. Haase, U. Flörke and H-J. Haupt, Inorg. Chem., 30 (1991) 4291.

[82] F. Birkelbach, U. Flörke, H.-J. Haupt, C. Butzlaff, A.X. Trautwein, K. Wieghardt and P. Chaudhuri, Inorg. Chem., 37 (1998) 2000.

404

[83] F. Birkelbach, T. Weyhermüller, M. Lengen, M. Gerdan, A.X. Trautwein, K. Wieghardt and P. Chaudhuri, J. Chem. Soc., Dalton Trans., (1997) 4529.

[84] D. Burdinski, F. Birkelbach, M. Gerdan, A.X. Trautwein, K. Wieghardt and P. Chaudhuri, J. Chem. Soc., Chem. Commun., (1995) 963.

[85] D. Burdinski, F. Birkelbach, T. Weyhermüller, U. Flörke, H.-J. Haupt, M. Lengen, A.X. Trautwein, E. Bill, K. Wieghardt and P. Chaudhuri, Inorg. Chem., 37 (1998) 1009.

[86] D. Burdinski, E. Bill, F. Birkelbach, K. Wieghardt and P. Chaudhuri, Inorg. Chem., 40 (2001) 1160.

[87] E.N. Treher, J. Gougoutas, M. Malley, A.D. Nunn and S.E. Unger, J. Labelled Compounds and Radiopharmaceuticals, 23 (1986) 1118.

[88] E.N. Treher, L.C. Francesconi, J.Z. Gougoutas, M.M. Maley and A.D. Nunn, Inorg. Chem., 28 (1989) 3411.

[89] K.E. Linder, M. Malley, J. Gougoutas, S. Unger and A.D. Nunn, J. Labelled Compd. Radiopharm., 26 (1989) 54.

[90] K.E. Linder, M.F. Malley, J.Z. Gougoutas, S.E. Unger and A.D. Nunn, Inorg. Chem., 29 (1990) 2428.

[91] J.E. Parks, B.E. Wagner and R.H. Holm, J. Am. Chem. Soc., 92 (1970) 3500.

[92] J.E. Parks, B.E. Wagner and R.H. Holm, Inorg. Chem., 10 (1971) 2472.

[93] E. Larsen, G.N. La Mar, E.B. Wagner and R.H Holm, Inorg. Chem., 11 (1972) 2652.

[94] Pat. 525243 Australia, IC3 C 07 D 487/08, C 07 B 15/022, C 07 F 9/022. Metal complexes and their use for hydrogen peroxide production / A.J. Hertl, A.M. Sargeson and J.M. Harrowfield. Publ. 28.10.1982.

[95] J.M. Harrowfield, A.J. Hertl and A.M. Sargeson, Inorg. Synth., 20 (1980) 85.

[96] I.I. Greaser, R.J. Geue, J.M. Harrowfield, A.J. Hertl, A.M. Sargeson, M.R. Snow and J. Springbore, J. Am. Chem. Soc., 104 (1982) 6016.

[97] J.F. Endicott, G.R. Brubaker, T. Ramasami, K. Kumar, K. Duarakanath, J. Gassei and D. Jonhson, Inorg. Chem., 22 (1983) 3754.

[98] N. Rudgewick-Brown and R.D.Cannon, J. Chem. Soc., Dalton Trans., (1984) 479.

[99] L.R. Gahan, P.C. Healy and G.J. Patch, J. Chem. Educ., 66 (1989) 445.

[100] M.A. Rampi-Scandola, F. Scandola and A. Indelli, J. Chem. Soc., Faradey Trans. 1, 81 (1985) 2967.

[101] R.J. Geue, T.W. Hambley, J.M. Harrowfield, A.M. Sargeson and M.R. Snow, J. Am. Chem. Soc., 106 (1984) 5478.

[102] J.M. Harrowfield, G.A. Lawrance and A.M. Sargeson, J. Chem. Educ., 62 (1985) 804.

[103] R. Balahura, G. Ferguson, B. Ruhl and G. Wilkins, Inorg. Chem., 22 (1983) 3990.

[104] K. Tsukahara, Bull. Chem. Soc. Jpn., 59 (1986) 1709.

[105] J.K. Bashkin, L.A. Bass, S.M. Sondhi, K.D. Robinson and A.M. Beatty, Inorg. Chim. Acta, 253 (1996) 91.

[106] R.J. Gene, P. Osvath, A.M. Sargeson, K.R. Acharya, S.B. Noor, T.N.G. Row and K. Venkatesan, Aust. J. Chem., 47 (1994) 511.

[107] R.J. Geue, M.G. McCartny and A.M. Sargeson, J. Am. Chem. Soc., 106, 8282(1984).

[108] D.J. Bull, I.I. Greaser, A.M. Sargeson, B.W. Skelton and A.H. White, Inorg. Chem., 26, 3040(1987).

[109] S. Burnet, M.-H. Choi, P.S. Donnelly, J.M. Harrowfield, I. Ivanova, S.-H. Jeong, Y. Kim, M. Mocerino, B.W. Skelton, A.H. White, C.C. Williams and Z.-L. Zeng, Eur. J. Inorg. Chem., (2001) 1869.

[110] C.A. Behm, P.F.L. Boreham, I.I. Greaser, B. Korybut-Daszkiewicz, D.J. Maddalena, A.M. Sargeson and G.M. Snowdon, Aust. J. Chem., 48 (1995) 1009.

[111] Y. Kim, S.H. Jeong, J.M. Harrowfield, B.W. Skelton and A.H. White, Abstr. of the XXII Int. Symp. Macrocyclic Chem., August 3-8, 1997, Seoul, Korea, (1997) 119.

[112] P.V. Bernhardt and A.M. Sargeson, Abstr. of the 30th Inter. Conf. Coord. Chem., July 24-29, Kyoto, Japan, 1994, (1994) S2-16.

[113] P.V. Bernhardt, J.M. Harrowfield, D.C.R. Hockless and A.M. Sargeson, Inorg. Chem., 33 (1994) 5659.

[114] J.M. Harrowfield, A.M. Sargeson, B.W. Skelton and A.H. White, Aust. J. Chem., 47 (1994) 181.

[115] J.M. Bottomley, L.J. Clark, I.I. Creaser, L.M. Engelhardt, R.J. Geue, K.S. Hagen, J.M. Harrowfield, G.A. Lawrence, P.A. Lay, A.M. Sargeson, A.J. See, B.W. Skelton, A.H. White and F.R. Wilner, Ibid., 47 (1994) 143.

[116] P.V. Bernhardt, A.M.T. Bygott, R.J. Geue, A.J. Hendry, B.R. Korybut-Daszkiewicz, P.A. Lay, J.R. Pladziewicz, A.M. Sargeson and A.C. Willis, Inorg. Chem., 33 (1994) 4553.

[117] P.S. Donnelly, J.M. Harrowfield, B.W. Skelton and A.H. White, Ibid., 39 (2000) 5817.

[118] U. Sakaguchi, S. Tamaki and K. Tomioka, Ibid., 24 (1985) 1624.

[119] L.J. Clark, R.J. Geue, L.M. Engelhardt, J.M. Harrowfield, A.M. Sargeson and A.H. White, Aust. J. Chem., 46 (1993) 1485.

[120] I.I. Creaser, J.D. Lydon, A.M. Sargeson and E. Horn, J. Am. Chem. Soc., 106 (1984) 5729.

[121] L.R. Gahan, G.A. Lawrence and A.M. Sargeson, Inorg. Chem., 21 (1982) 2699.

[122] L.R. Gahan and A.M. Sargeson, Aust. J. Chem., 34 (1981) 2499.

[123] P.A. Lay, J. Lydon, A.W-H. Mau, P. Osvath, A.M. Sargeson and W.H.F. Sasse, Ibid., 46 (1993) 641.

[124] P. Osvath, A.M. Sargeson, A. McAuley, R.E. Mendelez, S. Subramanian, M.J. Zaworotko and L. Broge, Inorg. Chem., 38 (1999) 3634.

[125] R. Bhula, A.P. Arnold, G.J. Gainsford and W.G. Tackson, J. Chem. Soc., Chem. Commun., (1996) 143.

[126] P.M. Angus, A.M. Sargeson and A.C. Willis, Ibid., (1999) 1975.

[127] J.I. Bruce, L.R. Gahan, T.W. Hambley and R. Stranger, Inorg. Chem., 32 (1993) 5997.

[128] T.M. Donlevy, L.R. Gahan, T.W. Hambley and R. Stranger, Ibid., 31, (1992) 4376.

[129] A.P. Arnold,R. Bhula, X. Chen, R.J. Geue and W.G. Jackson, Ibid., 38 (1999) 1966.

[130] T. Konno, K. Tokuda, T. Suzuki and K. Okamoto, Bull. Chem. Soc. Jpn., 71 (1998) 1049.

[131] K. Tokuda, K. Okamoto and T. Konno, Inorg. Chem., 39 (2000) 333.

[132] B. Korybut-Daszkiewicz, R.M. Hartshorn and A.M. Sargeson, J. Chem. Soc., Chem. Commun., (1989) 1375.

[133] R.J. Geue, W.R. Petri, A.M. Sargeson and M.R. Snow, Aust. J. Chem., 45 (1992) 1681.

[134] P.M. Angus, A.J. Elliott, A.M. Sargeson and A.C. Willis, J. Chem. Soc., Dalton Trans. (2000) 2933.

[135] R.J. Geue, B. Korybut-Daszkiewicz and A.M. Sargeson, J. Chem. Soc., Chem. Commun., (1993) 1454.

[136] R.J. Geue, B. Korybut-Daszkiewicz and A.M. Sargeson, Ibid., (1996) 1569.

[137] P.M. Angus, A.M.T. Bygott, R.J. Geue, B. Korybut-Daszkiewicz, A.W.H. Mau, A.M. Sargeson, M.M. Sheil and A.C. Willis, Chem. Eur. J., 3 (1997) 1283.

[138] A. Hohn, R.J. Geue, A.M. Sargeson and A.C. Willis, J. Chem. Soc., Chem. Commun., (1989) 1644.

[139] A. Hohn, R.J. Geue, A.M. Sargeson and A.C. Willis, Ibid., (1989) 1648.

[140] A. Hohn, RJ. Geue and A.M. Sargeson, Ibid., (1990) 1473.

[141] C.A. Behm, I.I. Creaser, B. Korybut-Daszkiewicz, R.J. Geue, A.M. Sargeson and G.W. Walker, Ibid., (1993) 1844.

[142] A. Hammershoi and A.M. Sargeson, Inorg. Chem., 22 (1983) 3554.

[143] A.A. Achilleos, L.R. Gahan and K.A. Nicolaidis, Aust. J. Chem., 42 (1989) 649.

[144] L.R. Gahan, T.M. Donlevy and T.W. Hambley, Inorg. Chem., 29 (1990) 1451.

[145] B. Dietrich, J.-M. Lehn and J.-P. Sauvage, J. Chem. Soc., Chem. Commun., (1970) 1055.

[146] P. Osvath, A.M. Sargeson, B.W. Skelton and A.H. White, Ibid., (1991) 1036.

[147] P. Osvath and A.M. Sargeson, Ibid., (1993) 40.

[148] R.J. Geue, M.G. McCartny, A.M. Sargeson, B.W. Skelton and A.H White, Inorg. Chem., 24 (1985) 1607.

[149] G.J. Gainsford, R.J. Geue and A.M.Sargeson, J. Chem. Soc., Chem. Commun., (1982) 233.

[150] A.M. Sargeson, Research School of Chemistry. The Australian National University. Annual Reports 1989. (1989) 138.

[151] R.J. Geue, C. Jin Qin, S.F. Ralph, A.M.Sargeson, B.W. Skelton, A.H White and A.C. Willis, J. Chem. Soc., Chem. Commun., (1999) 2351.

[152] R.J. Geue, A.Hohn, S.F. Ralph and A.C. Willis, Ibid., 1513(1994).

[153] K.N. Brown, R.J. Geue, G. Moran, S.F. Ralph, H. Riesen and A.M. Sargeson, Ibid., (1998) 2291.

[154] K.N. Brown, R.J. Geue, T.W. Hambley, A.M. Sargeson and A.C. Willis, Ibid., (1996) 567.

[155] R.J. Geue, M.G. McCartney, A.M. Sargeson, E. Horn and M.R. Snow, Ibid., (1986) 848.

[156] H.A. Boucher, A. Lawrence, P.A. Lay, A.M. Sargeson, A.M. Bond, D.F. Sangsten and J.C. Sullivan, J. Am. Chem. Soc., 105 (1983) 4652.

[157] J.M. Harrowfield, A.J. Herlt, A.P. Lay and A.M. Sargeson, Ibid., 105 (1983) 5503.

[158] P. Comba, I.I. Creaser, L.R. Gahan, J.M. Harrowfield, G.A. Lawrence, L.L. Martin, A.W.H. Mau, A.M. Sargeson, W.H. Sasse and M.R. Snow, Inorg. Chem., 25 (1986) 384.

[159] T. Ramasami, J.F. Endicott and G.R. Brubaker, J. Phys. Chem., 87 (1983) 5057.

[160] M.P. Suh, W. Shin, D. Kim and S. Kim, Inorg. Chem., 23 (1984) 618.

[161] A. Arkowska, E. Grazynska and R. Kubiak, Inorg. Chim. Acta, 159 (1989) 153.

[162] P. Comba, N.F. Curtis, G.A. Lawrence, A.M. Sargeson, B.W. Skelton and A.H. White, Inorg. Chem, 25 (1986) 4260.

[163] P.V. Bernhardt, L.S. Curtis, N.F. Curtis, G.A. Lawrence, B.W. Skelton and A.H. White, Aust. J. Chem., 42 (1989) 767.

[164] R.J. Geue, M.B. McDonnell, A.W.H. Mau, A.M. Sargeson and A.C. Willis, J. Chem. Soc., Chem. Commun., (1994) 667.

[165] P.H. Smith, Z.E. Reyes, C.W. Lee and K.R. Raymond, Inorg. Chem., 27 (1988) 4154.

[166] J.I. Bruce, L.R. Gahan, T.W. Hambley and R. Stranger, J. Chem. Soc., Chem. Commun., (1993) 702.

[167] P. Comba, L.M. Engelhardt, J.M. Harrowfield, G.A. Lawrence, L.L. Martin, A.M. Sargeson and A.H. White, J. Chem. Soc., Chem. Commun., (1985) 174.

[168] P.V. Bernhardt and A.M. Sargeson, Ibid., (1985) 1516.

[169] P.V. Bernhardt, A.M. Sargeson and F.G. Anson, Inorg. Chem., 27 (1988) 2754.

[170] T.M. Donlevy, L.R. Gahan, R.Stranger, S.E. Kennedy, K.A. Byriel and C.H.L. Kennard, Ibid., 32 (1993) 6023.

[171] T.M. Donlevy, L.R. Gahan, T.W. Hambley, G.R. Hanson, K.L. McMahon and R. Stranger, Ibid., 33 (1994) 5131.

[172] L.M. Engelhardt, J.M. Harrowfield, A.M. Sargeson and A.H. White, Aust. J. Chem., 46 (1993) 127.

[173] P.V. Bernhardt, R. Bramlay, L.M. Engelhardt, J.M. Harrowfield, D.C.R. Hockless, B. Korybit-Daszkiewicz, E.R. Krausz, T. Morgan, A.M. Sargeson, B.W. Skelton and A.H. White, Inorg. Chem., 34 (1995) 3589.

[174] L. Grondahl, A. Hammershoi, A.M. Sargeson and V.J. Tröm, Inorg. Chem., 36 (1997) 5396.

[175] N.M. Di Bartolo, A.M. Sargeson, T.M. Donlevy and S.V. Smith, J. Chem. Soc., Dalton Trans., (2001) 2303.

[176] J. Mrozinski, A. Skorupa, A. Pochaba, Y. Dromzee, M. Verdaguer, E. Goovaerts, H. Varcammen and B. Korybut-Daszkiewicz, J. Mol. Str., 559 (2001) 107.

[177] A.S. El-Tabl., Trans. Met. Chem., 21 (1996) 428.

[178] P. Comba, A.M Sargeson and L.M, Engelhardt, Inorg. Chem., 24 (1985) 2325.

[179] P.A. Anderson, I.I. Greaser, C. Dean, J.M. Harrowfield, E. Horn, L.L. Martin, A.M. Sargeson, M.R. Snow and E.R.T. Tickink, Aust. J. Chem., 46 (1993) 449.

[180] I.I. Creaser, L.M. Engelhardt, J.M. Harrowfield, A.M. Sargeson, B.W. Skelton and A.H. White, Ibid., 46 (1993) 465.

408

[181] B. Korybut-Daszkiewicz and J. Klimkiewicz, J. Chem. Soc., Chem.Commun, (1996) 1175.

[182] L.M. Engelhardt, J.M. Harrowfield, S.J. McNiven, B.W. Skelton and A.H. White, Aust. J. Chem., 43 (1990) 1803.

[183] U.L. Goedken and S.-M. Peng, J. Chem. Soc., Chem. Commun., (1973) 62.

[184] M.J. Blandamer, J. Burgess, J. Fawcett, S. Radulović and D.R. Russell, Trans. Met. Chem., 13 (1988) 120.

[185] J.A. Belinski, M.E. Squires, J.M. Kuchna, B.A. Bennet and J.J. Grzybowski, J. Coord. Chem., 19 (1988) 159.

[186] J.J. Grzybowski, R.D. Alien, J.A. Belinski, K.L. Bieda, T.A. Bish, P.A. Finnegan, M.L. Hartenstein, G.S. Regitz, D.M. Ryalls, M.E. Squires and HJ. Thomas, Inorg. Chem., 32 (1993) 5266.

[187] K.L. Bieda, A.L. Kranitz and J.J. Grzybowski, Ibid., 32 (1993) 4209.

[188] Y.Z. Voloshin, A.I. Stash, O.A. Varzatskii, V.K. Belsky, Y.A. Maletin and N.G. Strizhakova, Inorg. Chim. Acta, 284 (1999) 180.

[189] C. Engtrakul, W.J. Shoemaker and J.J. Grzybowski, Inorg. Chem., 39 (2000) 5161.

[190] P. Beizer, L. De Cola and von A. Zelewsky, J. Chem. Soc., Chem. Commun., (1988) 1057.

[191] S. Grammenudi and F. Vögtle, Angew. Chem. Int. Ed. Engl, 25 (1986) 1122.

[192] M. Timken, W.A. Marritt, D.N. Hendrickson, K.A. Gagne and E. Sinn, Inorg. Chem., 24 (1985) 4202.

[193] Y.Z. Voloshin, O.A. Varzatskii, E.Y. Tkachenko, Y.A. Maletin, S.P. Degtyarov and D.I. Kochubey, Inorg. Chim. Acta, 255 (1997) 255.

[194] Y.Z. Voloshin, O.A. Varzatskii, I.I. Vorontsov, M.Y. Antipin and E.Y. Tkachemko, Russ. Chem. Bull., Int. Ed., 51 (2002), accepted. (TAO.doc)

[195] J.De Mendoza, E. Mesa, J.-C. Rodriquez-Ubis, P. Vazquez, F. Vögtle, P.-M. Windscheif, K. Rissanen, J.-M. Lehn, D. Lilienbaum and R. Ziessel, Angew. Chem. Int. Ed. Engl., 30 (1991) 1331.

[196] J. Hunter, J. Nelson, C. Harding, M. McKann and V. McKee, J. Chem. Soc., Chem. Commun., (1990) 1148.

[197] C. Harding, V. McKee and J. Nelson, J.Am.Chem.Soc., 113 (1991) 9684.

[198] A. Al-Obaidi, G. Baranovič, J. Coyle, C.G. Coates, J.J. McGarvey, V. McKee and J. Nelson, Inorg. Chem., 37 (1998) 3567.

[199] K.G. Ragunathan and P.K. Bunadwaj, J. Chem. Soc., Dalton Trans., (1992) 1653.

[200] P.H. Smith, M.E. Barr, J.R. Brainard, D.K. Ford, H. Freiser, S. Muralidharan, S.D. Reilly, R.R. Ryan, L.A. Silks,III, and W. Yu, J. Org. Chem., 58 (1993), 7939.

[201] S.W. Annie Bligh, M.G.B. Drew, N. Martin, B. Maubert and J. Nelson, J. Chem. Soc., Dalton Trans., (1998) 3711.

[202] D.C. Apperley, W. Clegg, S. Coles, J.L. Coyle, N. Martin, B. Maubert, V. McKee and J. Nelson, J. Chem. Soc., Dalton Trans., (1999) 229.

[203] J. Coyle, M.G.B. Drew, C.J. Harding, J. Nelson and R.M. Town, J. Chem. Soc., Dalton Trans., (1997) 1123.

[204] M. Ciampolini, M. Micheloni, F. Vizza, F. Zanobini, S. Chimichi and P. Dapporto, Ibid., (1986) 505.

[205] M. Ciampolini, M. Formica, V. Fusi, A. Saint-Mauricec, M. Micheloni, N. Nardi, R. Pontellini, F. Pina, P. Romani, A.M. Sabatini and B. Valtancoli, Eur. J. Inorg. Chem., 12 (1999) 2261.

[206] A. Bianchi, E. Garcia-Espana, M. Micheloni, N. Nardi and F. Vizza, Inorg. Chem., 25, (1986) 4379.

[207] M. Micheloni, J. Coord. Chem., 18 (1988) 3.

[208] A. Bencini, A. Biachi, M. Ciampolini, E. Garcia-Espana, P. Dapporto, M. Micheloni, P. Paoli, J.A. Ramirez and B. Valtankoli, J. Chem. Soc., Chem. Commun., (1989) 701.

[209] A. Bencini, A. Biachi, A. Baselli, M. Ciampolini, E. Garsia-Espana, P. Dapporto, M. Micheloni, P.Padi, J.A. Ramirez and B. Valtancoli, Inorg. Chem., 28 (1989) 4279.

[210] P. Dapporto, P. Paoli, C. Bazzicalupi, A. Bencini, N. Nardi, B. Valtancoli and V. Fusi, Supramol. Chem., 7 (1996) 195.

[211] J.-C. Rodriguez-Ubis, B. Alpha, D. Plancherei and J.-M. Lehn, Helv. Chim. Acta., 67 (1984) 2264.

[212] B. Alpha, J.-M. Lenh and G. Mathis, Angew. Chem. Int. Ed. Engl, 26 (1987) 266.

[213] H. Durr, K. Zengerle and H.-P. Trierweiler, Z. Naturforsch., B43 (1988) 361.

[214] O. Juanez, J. de Mendoza and J.-C. Rodriguez-Ubis, J. Chem. Soc., Chem. Commun., (1985) 1765.

[215] N. Herron, J.J. Grzybowsky, N. Matsumoto, L.L. Zimmen, G.G. Crysten and D.H. Busch, J. Am. Chem. Soc., 104 (1982) 1999.

[216] K.B. Mertes, P. Corfield and D.H. Busch, Inorg. Chem., 16 (1977) 3227.

[217] M.L. Caste, C.J. Cairns, J. Church, W.-K. Lin, J.C. Gallucy and D.H. Busch, Ibid., 26 (1987) 78.

[218] S.G. Taylor, M.R. Snow and T.W. Hambley, Aust. J. Chem., 36 (1983) 2359.

[219] T.W. Hambley and M.R. Snow, Inorg. Chem., 25 (1986) 1378.

[220] I.I. Creaser, J.M. Harrowfield, A.J. Herlt, A.M. Sargeson and J.M. Springborg, J. Am. Chem. Soc., 99 (1977) 3181.

[221] U. Sakaguchi and T. Ito, Bull. Chem. Soc. Jpn., 59 (1986) 635.

[222] A.A. Ashilleos, L.R. Gahan, K.A. Nicolaidis and T.W. Hambley, J. Chem. Soc., Chem. Commun., (1988) 912.

[223] A.A. Achilleos, L.R. Gahan, T.W. Hambley, P.C. Healy and D.M. Weedor, Inorg. Chim. Acta, 157 (1989) 209.

[224] M. Mikami, M. Konno and Y. Saito, Acta Crystallorg., B35 (1979) 3096.

[225] K.S. Hagen, P.A. Lay and A.M. Sargeson, Inorg. Chem., 27 (1988) 3424.

[226] T.M. Donlevy, L.R. Gahan and T.W. Hambley, Ibid., 33 (1994) 2668.

[227] L.J. Clark, I.I. Creaser, L.M. Engelhardt, J.M. Harrowfield, E.R. Krausz, G.M. Moran, A.M. Sargeson and A.H. White, Aust. J. Chem., 46 (1993) 111.

[228] K.J. Haller, A.D. Rae, A.M.T. Bygott, D.C.R. Hockless, S.F. Ralph, R.J. Geue and A.M. Sargeson, Acta Crystallogr., B55 (1999) 380.

[229] P.V. Bernhardt, D.J. Bull, W.T. Rabinson and A.M. Sargeson, Aust. J. Chem., 45 (1992) 1241.

[230] P. Comba, Inorg. Chem., 28 (1989) 426.

[231] A.M. Bond, T.W. Hambley and M.R. Snow, Ibid., 24 (1985) 1920.

[232] P.S. Donnelly, J.M. Harrowfield, B.W. Skelton and A.H. White, Ibid., 40 (2001) 5645.

[233] P.S. Donnelly, J.M. Harrowfield, B.W. Skelton and A.H. White, J. Chem. Soc., Dalton Trans., (2001) 3078.

[234] R. Castro, L.A. Godínez, C.M. Criss, S.G. Bott and A.E. Kaifer, J. Chem. Soc., Chem. Commun., 10 (1997) 935.

[235] P.A. Lay and A.M. Sargeson, Ibid., 25 (1986) 4801.

[236] A.B.P. Lever, Inorganic Electronic Spectroscopy, Amsterdam, Elsevier, 1984.

[237] P. Comba and A.F. Sickmüller, Inorg. Chem., 36 (1997) 4500.

[238] T.M. Donlevy, L.R. Gahan, T.W. Hambley, K.L. McMahon and R. Stranger, Aust. J. Chem. 46 (1993) 1799.

[239] R. Stranger, K.L. McMahon, L.R. Gahan, J.I. Bruce and T.W. Hambley, Inorg. Chem., 36 (1997) 3466.

[240] P.V. Bernhardt and P. Comba, Ibid., 32 (1993) 2798.

[241] L.L. Martin, K.S. Hagen, A. Hauser, R.L. Martin and A.M. Sargeson, J. Chem. Soc., Chem. Commun., (1988) 1313.

[242] L.L. Martin, R.L. Martin, K.S. Murray and A.M. Sargeson, Inorg. Chem., 29 (1990) 1387.

[243] L.L. Martin, R.L. Martin and A.M. Sargeson, Polyhedron, 13 (1994) 1969.

[244] P. Comba and A.M. Sargeson, Aust. J. Chem., 39 (1986) 1029.

[245] T.K. Kundu and P.T. Manoharan, Mol. Phys., 97 (1999) 709.

[246] K. Padmakumar and P.T. Manoharan, Pramana, 53 (1999) 353.

[247] T.K. Kundu, R. Bruyndonckx, C. Daul and P.T. Manoharan, Inorg. Chem., 38 (1999) 3931.

[248] M.R. Churchill and A.H. Reis, Inorg. Chem., 11 (1972) 2299.

[249] M.R. Churchill and A.H. Reis, J. Chem. Soc., Dalton Trans., (1973) 1570.

[250] M.R. Churchill and A.H. Reis, Inorg. Chem., 11 (1972) 1811.

[251] M.R. Churchill and A.H. Reis, Ibid., 12 (1973) 2280.

[252] E.B. Fleischer, A.E. Gebala and D.R. Swift, J. Chem. Soc., Chem. Commun., (1971) 1280.

[253] W.O. Gillum, J.C. Huffman, W.E. Streib and R.A.D. Wentworth, Ibid., (1969) 843.

[254] E.B. Fleischer, A.E. Gebala, D.R. Swift and P.A. Tasker, Inorg. Chem., 11 (1972) 2775.

[255] E.B. Fleischer, A.E. Gebala and P.A. Tasker, J. Am. Chem. Soc., 92 (1970) 6365.

[256] C. Mealli and E.C. Lingafelter, J. Chem. Soc., Chem. Commun., (1970) 885.

[257] W.M. Reiff, J. Am. Chem. Soc., 95 (1973) 3048.

[258] G.A. Zakrzewski, C.A. Chilardi and E.C. Lingafelter, Ibid., 93 (1971) 4411.

[259] S.A. Kubow, K.J. Takeuchi, J.J. Grzybowski, A.J. Jircitano and V.L. Goedken, Inorg. Chim. Acta, 241 (1996) 21.

[260] S.V. Lindeman, V.T. Struchkov and Y.Z. Voloshin, J. Coord. Chem., 34, (1995) 203.

[261] Y. Sasaki and T. Shigematsu, Bull. Chem. Soc. Jpn., 46 (1973) 3590.

[262] K.I. Turta, R.A. Stukan, J.J. Bulgak, D.J. Batyr and L.D. Ozol, Koord. Khim., 4 (1978) 1391.

[263] E.V. Polshin, V.V. Trachevskii, S.I. Tyukhtenko, A.Y. Nazarenko and Y.Z. Voloshin, Koord. Khim., 13 (1987) 96.

[264] A.Y. Nazarenko, E.V. Polshin and Y.Z. Voloshin, Mendeleev Commun., (1993) 45.

[265] Y.Z. Voloshin, E.V. Polshin and A.Y. Nazarenko, Hyperfine Inter., (2002) accepted.

[266] V.E. Zavodnik, V.K. Belsky, Y.Z. Voloshin and O.A. Varzatsky, J. Coord. Chem., 28 (1993) 97.

[267] S.V. Lindeman, Y.T. Struchkov and Y.Z. Voloshin, Inorg. Chim. Acta, 184 (1991) 107.

[268] S.V. Lindeman, Y.T. Struchkov and Y.Z. Voloshin, Polish J. Chem., 67 (1993) 1575.

[269] V.E. Zavodnik, V.K. Belsky and Y.Z. Voloshin, Polish J. Chem., 67 (1993) 1567.

[270] I.I. Vorontsov, K.A. Lysenko, K.A. Potekhin, M.Y. Antipin, Y.Z. Voloshin, E.V. Polshin and O.A. Varzatskii, Rus. Chem. Bull., Int. Ed., 49 (2000) 2018.

[271] Y.Z. Voloshin, M.I. Terekhova, Y.G. Noskov, V.E. Zavodnik and V.K. Belsky, Anales de Química Int. Ed., 94 (1998) 142.

[272] Y.Z. Voloshin, *unpublished results*.

[273] Y.Z. Voloshin, O.A. Varzatskii, A.V. Palchik, A.I. Stash and V.K. Belsky, New J. Chem., 23 (1999) 355.

[274] S.V. Lindeman, Yu.T. Struchkov and Ya.Z. Voloshin, J. Coord. Chem., 28 (1993) 319.

[275] G.M. Bancroft, Coord. Chem. Rev., 11 (1973) 247.

[276] G.M. Bancroft, Mössbauer Spectroscopy – An Introduction for Inorganic Chemists and Geochemists, McGraw-Hill, New York, 1973.

[277] R.V. Parish, Structure and Bonding in Tin Compounds. In "Mossbauer Spectroscopy Applied to Inorganic Chemistry", Vol.1, Plenum Press, NY, 1984.

[278] M.Y. Antipin, V.G. Tsirelson, M.P. Flugge, Y.T. Struchkov, R.P. Ozerov, Koord. Khim., 13 (1987) 121 [Sov. J. Coord. Chem. (Engl. Trans.), 13 (1987) 67].

[279] M. Iwata and Y. Saito, Acta Crystallogr., B29 (1973) 822.

[280] B.K. Vainshtein, V.M. Fridkin and V.L. Idenbom, Comprehensive Crystallography, Nauka, Moscow, vol. 2, 1979.

[281] I.I. Vorontsov, K.A. Potekhin, M.Y. Antipin, Y.Z. Voloshin, A.I. Stash, V.K. Belskii, I.I. Dubovik and V.S. Papkov, Krystallographya, 46 (2001) 833.

[282] I.I. Vorontsov, Y.Z. Voloshin, M.Y. Antipin, K.A. Potekhin, O.A. Varzatskii, E.V. Polshin, I.I. Dubovik and V.S. Papkov, Koord. Khim., 27 (2001) 299.

[283] Chemical Applications of Mössbauer Spectroscopy / Ed. by V.I. Goldanskii and R.H. Herber, Academic Press, New York, 1968.

[284] R.G. Pearson, J. Am. Chem. Soc., 85 (1963) 3533.

[285] R.E. Marsh and W.P. Schaefer, Inorg. Chem., 25 (1986) 3661.

[286] Y.Z. Voloshin and A.Y. Nazarenko, Dokl. AN UkrSSR Ser.B, (1985) 34.

[287] Y.Z. Voloshin, N.A. Kostromona and A.Y. Nazarenko, Zh. Obsch. Khim., 60 (1990) 1481.

[288] Y.Z. Voloshin, Y.G. Noskov, M.I. Terekhova and T.E. Kron, Ukr. Khim. Zh., 59 (1993) 231.

[289] Y.Z. Voloshin and Y.G. Noskov, Ibid., 59 (1993) 347.

[290] Y.Z. Voloshin, Y.G. Noskov, M.I. Terekhova and T.E. Kron, Polish J. Chem., 70(1996) 1229.

[291] R. Shmidt and V.N. Sapunov. Non-formal Kinetics, Verlag Chemie, Weinheim, 1982.

[292] Y.Z. Voloshin, V.V. Mosin and E.N. Korol, Inorg. Chim. Acta, 180 (1991) 189.

[293] I.I. Creaser, J.M. Harrowfield, G.A. Lawrence, W. Mulac, D. Sangster, A.M. Sargeson, K. Schmidt and J.C. Sullivan, J. Coord. Chem., 23 (1991) 389.

[294] N.R. Streltsova, V.K. Belsky and Y.Z. Voloshin, Acta Crystallogr., C49 (1993) 635.

[295] S.F. Ralph, M.M. Sheil, L.A. Hick, R.J. Geue and A.M. Sargeson, J. Chem. Soc., Dalton. Trans., (1996) 4417.

[296] P. Osvath and A.M. Sargeson, Aust. J. Chem., 47 (1994) 807.

[297] A. Indelli, A. Duatti and P. Lanza, J. Chem. Soc., Faraday Trans. 1, 85 (1989) 3107.

[298] L. Dubicki, J. Ferguson and B. Williamson, J. Phys. Chem., 88 (1984) 4254.

[299] F. Pino, M. Ciano, L. Moggi and V. Balzani, Inorg. Chem., 24 (1985) 844.

[300] F. Pino, M. Maestri, R. Ballardini, Q.G. Mulazzani, M.D'Agelantonio and V. Balzani, Ibid., 25 (1986) 4249.

[301] N.A. Lewis, W.I. Purcell and D.V. Taveras, Ibid., 28 (1989) 133.

[302] J. Sotomayor, H. Santos and F. Pina, Can. J. Chem., 69 (1991) 567.

[303] A. Indelly and A. Duatti, J. Chem. Soc., Faraday Trans. 1, 82 (1986) 1429.

[304] C.R.M. Martinez, C.M.D. Graciani, F. Ferranti and A. Indelli, An. quim. Real Soc. exp. fis. y quim., A80 (1984) 89.

[305] I.I. Creaser, A. Hammershøi, A. Launikonis, A.W.H. Mau, A.M. Sargeson and W.H.F. Sasse, Photochemistry and Photobiology, 49 (1989) 19.

[306] F. Pina, Q.G. Mulazzani, M. Venturi, M. Ciano and V. Balzani, Inorg. Chem., 24 (1985) 848.

[307] U. Sakaguchi, A. Tsuge and H. Yoneda, Ibid., 22 (1983) 1630.

[308] R.A. Marusak, P. Osvath, M. Kemper and A.G. Lappin, Inorg. Chem, 28 (1989) 1542.

[309] H. Sugimoto, H. Hataoka and M. Mori, J. Chem. Soc., Chem. Commun., (1982) 1301.

[310] U. Sakaguchi, A. Tsuge and H. Yoneda, Inorg. Chem., 22 (1983) 3745.

[311] K. Miyoshi, S. Izumoto, K. Nakai and H. Yoneda, Ibid., 25 (1986) 4654.

[312] S. Izumoto, K. Miyoshi and H. Yoneda, Bull. Chem. Soc. Jpn., 60 (1987) 3199.

[313] K. Miyoshi, Y. Sakamoto, A. Ohguni and H. Yoneda, Ibid., 58 (1985) 2239.

[314] K. Miyoshi, Y. Sakamoto, Y. H. Toda and H. Yoneda, Ibid., 58 (1985) 1837.

[315] S. Moghaddas, P. Hendry, R.J. Geue, C. Qin, A.M.T. Bygott, A.M. Sargeson and N.E. Dixon, J. Chem. Soc., Dalton Trans., (2000) 2085.

[316] G.D. Armstrong, J.A. Chambers and A.G. Sykes, Ibid., (1986) 755.

[317] D.W. Conrad and R.A. Scott, J. Am. Chem. Soc., 111 (1989) 3461.

[318] P.L. Drake, R.T. Hartshorn, J. McGinnis and A.G. Sykes, Inorg. Chem., 28 (1989) 1361.

[319] J.R. Pladziewicz, M.A. Accola, P. Osvath and A.M. Sargeson, Ibid., 32 (1993) 2525.

[320] D.W. Conrad, H. Zhang, D.E. Stewart and R.A. Scott, J. Am. Chem. Soc., 114 (1992) 9909.

[321] R.S.K. Chia, L.F. Linday, G.W. Walkes, G.W. Evesett, Ibid., 113 (1991) 2533.

[322] B.S. Brunschwig, S. Ehrenson and N. Sutin, J. Phys. Chem., 90 (1986) 3657.

[323] M.C. Ball and A.H. Norbury, Physical data for inorganic chemists, Longman, London, 1974.

[324] P. Bernhardt and A.M. Sargeson, Inorg. Chem., 26 (1987) 4122.

[325] P. Bernhardt and F.C. Anson, Ibid., 27 (1988) 4574.

[326] M.H. Jensen, P. Osvath, A.M. Sargesson and J. Ulstrup, J. Electroanal. Chem., 377 (1994) 131.

[327] P. Bernhard and A.M. Sargeson, J. Am. Chem. Soc., 111 (1989) 597.

[328] R. Shankar, A.K. Rout and B. Sahoo, Indian J. Chem., 26A (1987) 156.

[329] T.V. Magdesieva and K.P. Butin, Uspehi Khimii, 62 (1993) 387.

[330] V.V. Strelets, S.V. Kukharenko and Y.Z. Voloshin, Polish J. Chem., 69, (1995) 1520.

[331] M.A. Murguia and S. Wherland, Inorg. Chem., 30 (1991) 139.

[332] K.A. Anderson and S. Wherland, Ibid., 30 (1991) 624.

[333] D. Tran, J.P. Hunt and S. Wherland, Ibid., 31 (1992) 2460.

[334] B. Xie, T. Elder, L.J. Wilson and D.M. Stanbury, Ibid., 38 (1999) 12.

[335] A.J. Bard and L.R. Faulkner, Electrochemical methods: fundamentals and applications, 2nd ed., Wiley, New York, 2001.

[336] R.W. Taft and R.D. Topson, Prog. Phys. Org. Chem., 16 (1987) 1.

[337] L.P. Hammet, Physical Organic Chemistry: Reaction Rates, Equilibria and Mechanisms, 2nd ed., McGraw-Hill, New York, 1970.

[338] A.M. Bond, G.A. Lawrance, P.A. Lay and A.M. Sargeson, Inorg. Chem., 22 (1983) 2010.

[339] L.R. Gahan, G.A. Lawrance and A.M. Sargeson, Ibid., 23 (1984) 4369.

[340] P.A. Lay, A.W.H. Mau, W.H. Sasse, I.I. Greaser and A.M. Sargeson, Ibid., 22 (1983) 2347.

[341] C.-Y. Mok, A.W. Zanella, C. Creutz and N. Sutin, Ibid., 23 (1984) 2891.

[342] R.D. Shalders and T.W. Swaddle, Ibid., 34 (1995) 4815.

[343] K. Zahir, W. Bottcher and A. Haim, Ibid., 24 (1985) 1966.

[344] T.W. Hambley, Ibid., 27 (1988) 2496.

[345] D.A. Geselowitz, Ibid., 20 (1981) 4457.

[346] A.Y. Nazarenko, Y.Z. Voloshin and N.A. Kostromina, Ukr. Khim. Zh., 56 (1990) 1281.

[347] A.T. Gordon and R.A. Ford, The Chemist's Companion, Wiley-Interscience, New York, 1972.

[348] H. Becker, Rinführung in die Elektronen theorie organisch chemischer Reactionen, Berlin, DVW, 1964.

[349] J. March, Advanced Organic Chemistry, Wiley-Interscience, New York, Vol. 1, 1985.

[350] J.A. Streeky, D.G. Pillsburg and D.H. Busch, Inorg. Chem., 19 (1980) 3148.

[351] R.G. Goel, P.M. Henry and P.C. Polyzou, Ibid., 18 (1979) 2148.

[352] G.A. Lawrance, P.A. Lay and A.M. Sargesson, Ibid., 29 (1990) 4808.

414

[353] K. Tsukahara and R.G. Wilkins, Ibid., 24 (1985) 3399.
[354] R.V. Dubs, L.R. Gahan and A.M. Sargeson, Ibid., 22 (1983) 2523.
[355] P.D. Metelski, Y. Fu, K. Khan and T.W. Swaddle, Ibid., 38 (1999) 3103.
[356] C. Königstein, A.W.H. Mau, P. Osvath and A.M. Sargeson, J. Chem. Soc., Chem. Commun., (1997) 423.
[357] D. Borchardt, K. Pool and S. Wherland, Inorg. Chem., 21 (1982) 93.
[358] F. Basolo and R.G. Pearson, Mechanism of Inorganic Reactions, Wiley, New York, 1967.
[359] Inorganic Biochemistry / Ed. by L. Eichehorn, Elsevier, Amsterdam, Vol.1, 1973, Vol.2, 1975.
[360] R.J. Geue, A.J. Hendry and A.M. Sargeson, J. Chem. Soc., Chem. Commun., 21 (1989) 1646.
[361] K.R. Howes, C.G. Pippin, J.C. Sullivan, D. Meisel, J.H. Espenson and A. Bakac, Inorg. Chem., 27 (1988) 2932.
[362] I.I. Creaser, A.M. Sargeson and A.W. Zanella, Ibid., 22 (1983) 4022.
[363] J.F. Endicott, T. Ramasami, D.C. Gaswick, R. Tamilarasan, M.J. Hug, G.R. Brubaker and S.C. Pyke, J. Am. Chem. Soc., 105 (1983) 5301.
[364] N. Rudgewick-Brown and R.D. Cannon, Inorg. Chem., 24 (1985) 2463.
[365] G.D. Armstrong, J.D. Sinclair-Day and A.G. Sykes, J. Phys. Chem., 90, (1986) 3805.
[366] J.F. Endicott and T. Ramasami, J. Phys. Chem., 90 (1986) 3740.
[367] T. Ramasami and J.F. Endicott, Inorg. Chem., 23 (1984) 3324.
[368] T. Ramasami and J.F. Endicott, Ibid., 23 (1984) 2917.
[369] F.Endicott, B. Durham, M.D. Glick, T.J. Anderson, J.M. Kuszaj, G. Sohmonsels and K.P. Balakushnan, J. Am. Chem. Soc., 103 (1981) 1431.
[370] L. Eberson and M. Ekstrom, Acta Chim.Scand., B41 (1987) 41.
[371] L. Eberson and M. Ekstrom, Ibid., B42 (1988) 113.
[372] F. Endicott and T. Ramasami, J. Am. Chem. Soc., 104 (1982) 5252.
[373] V. Balzani, Gazz. Chim. Ital., 119 (1989) 311.
[374] V. Balzani and F. Scandola, Supramolecular Photochemistry, 1991, Ellis Horwood, Ch. 11, pp. 319-354.
[375] P. Figuereido and F. Pina, J.Photochem. Photobiol., A44 (1988) 57.
[376] V. Houlding, T. Geiger, U. Kolle and M. Cratzel, J. Chem. Soc., Chem. Commun., (1982) 681.
[377] M.A.Rampi-Scandola, F. Scandola, A. Indelli and V. Balzani, Inorg. Chim. Acta., 76 (1983) L67.
[378] T. Geiger, R. Nottenberg, M.-L. Pélaprat and M. Crätsel, Helv. Chim. Acta, 65 (1982) 2507.
[379] R. Longo, F.R. Gonçalves e Silva and O.L. Malta, Chem. Phys. Letters, 328 (2000) 67.
[380] F. Bodar-Houillon and A. Marsura, New J. Chem, 20 (1996) 1041.
[381] A. Bakac, J.H. Espenson, I.I. Creaser and A.M. Sargeson, J. Am. Chem. Soc., 105 (1983) 7624.
[382] J.T. Chen and J.H. Espenson, Inorg. Chem., 22 (1983) 1651.
[383] Y.D. Lampeka and S.V. Rossokha, Zh. Neorg. Khim., 33 (1988) 937.

[384] I.I. Creaser, L.R. Gahan, R.J. Geue, A. Launikonis, P.A. Lay, J.D. Lydon, M.G. McCarthy, A.W.H. Mau, A.M. Sargeson and W.H.F. Sasse, Inorg. Chem., 24 (1985) 2671.

[385] A. Launikonis, P.A. Lay, A.W.H. Mau, A.M. Sargeson and W.H.F. Sasse, Aust. J. Chem., 39 (1986) 1053.

[386] L. De Cola, F. Barigelleti, V. Balzani, P. Belser, A. von Zelewsky, F. Vogtle, F. Ebmeyer and S. Grammenudi, J. Am. Chem. Soc., 110 (1988) 7210.

[387] A.W.H. Mau, W.H. Sasse, I.I. Creaser and A.M. Sargeson, New J. Chem., 10 (1986) 589.

[388] P. Comba, A.W.H. Mau and A.M. Sargeson, J. Phys. Chem., 89 (1985) 394.

[389] S.J. Strach and R. Bramley, J. Chem. Phys., 88 (1988) 7380.

[390] G. Blasse, G.J. Dirksen, N. Sabbatini, S. Peratoner, J.-M. Lehn and B. Alpha, J. Phys. Chem., 92 (1988) 2419.

[391] G. Blasse, G.J. Dirksen, D.Var Der Voort, S. Perathoner, J.-M. Lehn and B. Alpha, Chem. Phys. Letters, 146 (1988) 347.

[392] N. Sabbatini, S. Perathoner, V. Balzani, M. Ventuty,B. Alpha and J.-M. Lehn, Proc. NATO Adv. Res. Workshop Photoinduced. Charge Separ. and Energy Charge Migr. Supramol. Species, (1987) 187.

[393] B. Alpha, V. Balzani, J.-M. Lehn, S. Perathoner and N. Sabbatini, Angew. Chem. Int. Ed. Engl, 26 (1987) 1266.

[394] N. Sabbatini, S. Dellonte and G. Blasse, Chem. Phys. Letters, 129 (1986) 541.

[395] K. Kalyanasundaram, Coord. Chem. Rev., 46 (1982) 159.

[396] T.J. Meyer, Pure Appl. Chem., 58 (1986) 1193.

[397] R.A. Krause, Structure and Bonding, 67 (1987) 1.

[398] A. Juris, V. Balzani, F. Barigelletti, S. Campagna, P. Belser and A. von Zelewsky, Coord. Chem. Rev., 84 (1988) 85.

[399] V. Balzani, F. Barigelletti and L. De Cola, Topics Curr. Chem., 158 (1990) 31.

[400] L. De Cola, P. Belser, F. Ebmeyer, F. Barigelletti, F. Vögtle, A. von Zelewsky and V. Balzani, Inorg. Chem., 29 (1990) 495.

[401] F. Barigelletti, L. De Cola, V. Balzani, P. Belser, A. von Zelewsky, F. Vögtle, F. Ebmeyer and S. Grammenudi, J. Am. Chem. Soc., 111 (1989) 4662.

[402] F. Pina, M. Ciano, Q.G. Mulazzani, V. Balzani and L. Moggi, Sci Pap. Inst. Phys. and Chem. Res., 78 (1984) 166.

[403] O. Johansen, A. Launikonis and J.W. Loder, Aust. J. Chem., 34 (1981) 2347.

[404] G.D. Armstrong, T. Ramasami and A.G. Sykes, Inorg. Chem., 24 (1985) 3230.

[405] G.D. Armstrong, T. Ramasami and A.G. Sykes, J. Chem. Soc., Chem. Commun., (1984) 1017.

[406] H.E. Toma and R.A. Mukakami, Inorg. Chim. Acta, 93 (1984) L33.

[407] D. Borchardt and S. Wherland, Inorg. Chem., 23 (1984) 2537.

[408] J. Gribble and S. Wherland, Ibid., 28 (1989) 2859.

[409] R.M. Nielson and M.J. Weaver, J. Electroanal. Chem., 260 (1989) 15.

[410] J.T. Hupp, H.Y. Liu, P.A. Lay, W.H.F. Petry, A.M. Sargeson and M.J. Weawer, Ibid., 163 (1984) 371.

[411] A.M. Timonov, K.P. Balasheev, G.A. Shagisultanova, V.N. Fateev, V.P. Pakhomov and P.H. Tchekmarev, Electrokhimiya, 23 (1987) 1061.

[412] H.D. Dewald and J. Chen, Microchem. J., 56 (1997) 197.

[413] L. Echegoyen, A. DeCian, J. Fischer and J.-M. Lehn, Angew. Chem. Int. Ed. Engl., 30 (1991) 838.

[414] P.A. Lay and A.M. Sargeson, Inorg. Chem., 29 (1990) 2762.

[415] D.E. Hamilton, J. Chem. Educ., 68 (1991) A144.

[416] P. Riccieri and E. Zinato, Inorg. Chem., 29 (1990) 5035.

[417] J.F. Endicott, M.J. Heeg, D.C. Gaswick and S.C. Pyke, J. Phys. Chem., 85 (1981) 1777.

[418] G.J. Ferraudi and J.F. Endicott, Inorg. Chim. Acta, 37 (1979) 219.

[419] M.J. Sisley and R.B. Jordan, Inorg. Chem., 31 (1992) 2880.

[420] J.F. Endicott, B. Durham and K. Kumar, Ibid., 21 (1982) 2437.

[421] S. Ronco and G. Ferraudi, Ibid., 29 (1990) 3961.

[422] P.A. Lay, N.S. McAlpine, J.T. Hupp, M.J. Weaver and A.M. Sargeson, Ibid., 29 (1990) 4322.

[423] H. Doine and T.W. Swaddle, Ibid., 30 (1991) 1858.

[424] M.J. Blandamer, J. Burgess, B. Clark, P.P. Duce, A.W. Hakin, N. Gosal, S. Radulovic, P. Guardado, F. Sanches, C.D. Hubbard and E.-E.A. Abu-Gharib, J. Chem. Soc., Faraday Trans. 1, 82 (1986) 1471.

[425] R. Billing, R. Benedix, G. Stich and H. Hennig, Z. Anorg. Allg. Chem., 583 (1990) 157.

[426] D.A. Geselowitz, Inorg. Chim. Acta, 163 (1989) 79.

[427] Y. Mizuno, A. Yokote and M. Iida, Bull. Chem. Soc. Jpn., 70 (1997) 2437.

[428] A. Bacchi, F. Ferranti and G. Pelizzi, Acta Cryst., C49 (1993) 1163.

[429] F. Tsvetkov and J. White, J. Am. Chem. Soc., 110 (1988) 3183.

[430] J.W. Faller, C. Blankenship and S. Sena, Ibid., 106 (1984) 793.

[431] J.W. Faller, C. Blankenship, B. Whitmore and S. Sena, Inorg. Chem., 24 (1985) 4483.

[432] S.V. Smith, J.M. Harrowfield, N.M. Di Bartolo and A.M. Sargeson, Cryptate compounds and methods for diagnosis and therapy, PCT Int. Appl. WO 00 40,585 (Cl. C07D487/08) Publ. 13.07.2000.

[433] Y.Z. Voloshin, Russ. J. Chem., 42 (1998) 5.

Subject index

This Page Intentionally Left Blank